AFWAL-TR-80-3019

AD A090553

SONIC FATIGUE DESIGN TECHNIQUES FOR ADVANCED COMPOSITE AIRCRAFT STRUCTURES

FINAL REPORT

Ian Holehouse

Rohr Industries
P.O. Box 878
Chula Vista, California 92012

April 1980

Technical Report AFFDL-TR-80-3019

Final Report
August 1977 - December 1979

Approved for public release; distribution unlimited.

OCT 1 4 1980

A

80 10 14 197

NOTICE

When Government drawings, specifications, or other data are used for any purpose other than in connection with a definitely related Government procurement operation, the United States Government thereby incurs no responsibility nor any obligation whatsoever; and the fact that the government may have formulated, furnished, or in any way supplied the said drawings, specifications, or other data, is not to be regarded by implication or otherwise as in any manner licensing the holder or any other person or corporation, or conveying any rights or permission to manufacture, use, or sell any patented invention that may in any way be related thereto.

This report has been reviewed by the Office of Public Affairs (ASD/PA) and is releasable to the National Technical Information Service (NTIS) At NTIS, it will be available to the general public, including foreign nations.

This technical report has been reviewed and is approved for publication.

KENNETH R. WENTZ
PROJECT ENGINEER

FRANK D. ADAMS, Acting Chief
Structural Integrity Branch
Structures and Dynamics Division

FOR THE COMMANDER

RALPH L. KUSTER, JR., COL, USAF
Chief, Structures & Dynamics Division

"If your address has changed, if you wish to be removed from our mailing list, or if the addressee is no longer employed by your organization please notify _AFWAL/FIBED_ W-PAFB, OH 45433 to help us maintain a current mailing list."

Copies of this report should not be returned unless return is required by security considerations, contractual obligations, or notice on a specific document.

REPORT DOCUMENTATION PAGE	READ INSTRUCTIONS BEFORE COMPLETING FORM

1. REPORT NUMBER	2. GOVT ACCESSION NO.	3. RECIPIENT'S CATALOG NUMBER
AFWAL-TR-80-3019	AD-A090 553	RHR-80-019

4. TITLE (and Subtitle)

Sonic Fatigue Design Techniques for Advanced Composite Aircraft Structures.

5. TYPE OF REPORT & PERIOD COVERED

Final Technical Report
August 1977-December 1979

6. PERFORMING ORG. REPORT NUMBER

7. AUTHOR(s)

Ian Holehouse

8. CONTRACT OR GRANT NUMBER(s)

F33615-77-C-3033

9. PERFORMING ORGANIZATION NAME AND ADDRESS

Rohr Industries
P. O. Box 878
Chula Vista, California 92012

10. PROGRAM ELEMENT, PROJECT, TASK AREA & WORK UNIT NUMBERS

11. CONTROLLING OFFICE NAME AND ADDRESS

Air Force Wright Aeronautical Laboratory
Air Force Systems Command
Wright-Patterson Air Force Base, Ohio 45433

12. REPORT DATE

April 1980

13. NUMBER OF PAGES

14. MONITORING AGENCY NAME & ADDRESS(if different from Controlling Office)

343

15. SECURITY CLASS. (of this report)

Unclassified

15a. DECLASSIFICATION/DOWNGRADING SCHEDULE

16. DISTRIBUTION STATEMENT (of this Report)

Approved for public release; distribution unlimited.

17. DISTRIBUTION STATEMENT (of the abstract entered in Block 20, if different from Report)

18. SUPPLEMENTARY NOTES

19. KEY WORDS (Continue on reverse side if necessary and identify by block number)

Acoustic Fatigue
Sonic Fatigue
Composites
Graphite

20. ABSTRACT (Continue on reverse side if necessary and identify by block number)

A combined analytical and experimental program was conducted in order to develop a semi-empirical sonic fatigue design method for curved and flat graphite-epoxy skin-stringer panels. A range of multi-bay panels was subjected to high intensity noise environments in a progressive-wave tube. Shaker tests were also performed in order to provide additional random

(Continued)

DD FORM 1473 (1 JAN 73) EDITION OF 1 NOV 65 IS OBSOLETE

fatigue data. Finite-element analyses were carried out on the test panel designs, generating static strains and frequencies. Multiple stepwise regression analysis was used to develop the sonic fatigue design method. Design equations and a nomograph are presented. Comparisons of sonic fatigue resistance between graphite and aluminum panels were also carried out. The design method developed is presented as a self-contained section in this report and is suitable for practical design use.

FOREWORD

iii

TABLE OF CONTENTS

LIST OF ILLUSTRATIONS

LIST OF ILLUSTRATIONS - Continued

ix

LIST OF ILLUSTRATIONS - Continued

LIST OF ILLUSTRATIONS - Continued

LIST OF ILLUSTRATIONS - Continued

LIST OF ILLUSTRATIONS - Concluded

LIST OF TABLES

SECTION I
INTRODUCTION

Sonic fatigue has become a recognizable and persistent structural design problem over the past twenty-five years. Although not usually a catastrophic problem in terms of human lives, it has resulted in structural failures adversely affecting maintenance costs, mission effectivity and often requiring major structural redesigns. Sonic fatigue problems have been characterized by a significant degree of inherent unpredictability that has so far denied the structural designer the precise analytical tools that are available in other areas of structural analysis. These limitations have been accompanied by the need for minimum weight designs in increasingly severe and varied acoustic environments. This situation has led to the development and application of semi-empirical design techniques based on Miles'[1] single degree-of-freedom approach in combination with experimental data from full-scale airplane tests and laboratory sonic fatigue tests. References 2, 3 and 4 have used such techniques to develop design nomographs for various types of structures. References 5 and 6 present much of this work as part of overall sonic fatigue design guides.

These existing design methods have been developed for metal structures. However, recent advanced composite materials development has led to a wide-spread aerospace application of nonmetallic structures, in the interests of cost and/or weight savings. The most notable of these materials to date is graphite-epoxy. Although there have been

1

investigations into the sonic fatigue resistance of graphite structures[7], there are no sonic fatigue design methods available for these materials that are comparable to those currently available for most metal structures. Consequently, it is difficult for the designer to translate the potential weight savings of graphite structures into a practical reality with the necessary level of assurance against sonic fatigue failures. The primary purpose of the program described in this report was to remedy this by developing a semi-empirical sonic fatigue design method for both flat and curved graphite-epoxy stiffened-skin panels.

The program comprised three phases: analytical, experimental and the development of a design method. The analytical approach consisted of incorporating composite laminate analyses into finite-element computer methods in order to determine the static and dynamic response characteristics of a range of graphite-epoxy stiffened-skin panels. These panels were 3 x 3, 4 x 3 and 6 x 3 arrays, with various laminate thicknesses, stiffener spacings, radii of curvature and ply orientations represented. The experimental phase consisted of fabricating and sonic fatigue testing a range of test panel configurations corresponding to those subjected to analysis. Sonic fatigue testing was carried out in a "progressive-wave tube" with the panels being subjected to random acoustic loading at grazing incidence. The panels were instrumented with strain gauges and flush-mounted microphones, and data taken over a wide range of sound pressure levels. The sonic fatigue test program was augmented by performing shaker tests, with random loading, on sections of skin-laminates in order to develop random fatigue curves.

The design method phase of the program attempts to relate the analytical results and the test data in order to provide a semi-empirical design method. Measured random strains are compared to those calculated from Miles' equation, using the analytically determined static strains and frequencies as inputs. The test results were also compared to values obtained from the AGARD nomographs[5], with density and elastic modulus

2

values modified to reflect the graphite-epoxy laminates. Finally, "multiple stepwise-regression" analysis techniques were used to develop empirical relationships between the measured strains and frequencies, and various combinations of panel configuration parameters and finite element analysis results. From these regression analyses, a set of design equations was developed and a design nomograph constructed. The design method is presented as a self-contained unit (Section IV.5), allowing it to be utilized independently of the remainder of this report. A worked example is also presented. Figure 1 shows the program phase/task flow diagram.

PHASE I - ANALYSIS

PHASE II - EXPERIMENTAL

PHASE III - DEVELOPMENT OF DESIGN METHOD

DELIVERY OF ORAL AND WRITTEN REPORTS

COMPOSITE LAMINATE ANALYSIS

FINITE ELEMENT MODELING AND COMPUTER SOLUTIONS

SONIC FATIGUE ANALYSIS

COMPARISON ANALYTICAL AND TEST RESULTS

ANALYSIS CHANGES

MULTIPLE REGRESSION ANALYSIS

DESIGN NOMOGRAPHS

DESIGN METHOD AND EQUATIONS

PRELIMINARY ANALYSIS

FATIGUE ANALYSIS

TEST SPECIMEN/FIXTURE DESIGN AND FABRICATION

TEST PLAN AND INSTRUMENTATION DETAILS

SHAKER TESTS

PROGRESSIVE-WAVE TUBE TESTS

TEST RESULTS

PRESENT TEST PLAN TO AFFDL PROJECT ENGINEER FOR APPROVAL

MONTHLY R&D STATUS REPORTS

FOUR INFORMAL ORAL REPORTS

ABSTRACT OF NEW TECHNOLOGY (ANT)

FINAL PROGRAM REPORT

FINAL ORAL REPORT

Figure 1. Program Phase/Task Flow Diagram

4

SECTION II
ANALYTICAL

1. INTRODUCTION

This section describes the analytical work performed in support of the program. A description of general sonic fatigue theory is given in Section II.2. The analytical approach consisted of generating a complete set of elastic properties for each composite laminate used in the program; these properties were then used as inputs to both the preliminary analyses and the finite-element solutions. The preliminary analysis consisted of using Miles' equation and Reference 5 to calculate natural frequencies and dynamic stresses for each of the proposed test panel configurations. This was done in order to ensure that their expected response characteristics were compatible with the expected sonic fatigue test envelope. The finite-element analysis consisted of constructing a series of coarse and fine grid finite-element models, and using the NASTRAN computer program to generate a set of natural frequencies and static strains to be used as inputs in determining acoustically induced dynamic strains. An additional set of natural frequencies was generated using equations developed by Lin[8].

Table 1 lists the panel configurations used in this program. An analytical comparison was also made between Z and J type stiffeners. Figure 2 presents a flow chart of the analytical work.

TABLE 1

TEST PANEL CONFIGURATIONS

Configuration and Number of Bays		Number of Panels	Skin Laminate		Stringer Spacing (in.)	Stiffener Type	Radius of Curvature (in.)
			No.of Plies	Ply Orientation			
a	(3 x 3)	2	6	$(0, \pm45)_s$	8	Zee	Flat
b	(3 x 3)	2	8	$(0, \pm45,90)_s$	8	Zee	Flat
bj	(3 x 3)	1	8	$(0, \pm45,90)_s$	8	J	Flat
c	(3 x 3)	2	8	$(0_2, \pm45)_s$	8	Zee	Flat
cj	(3 x 3)	1	8	$(0_2, \pm45)_s$	8	J	Flat
d	(3 x 3)	1	12	$(0, \pm45)_{2s}$	8	Zee	Flat
e	(3 x 3)	2	8	Same as (b)	8	Honeycomb	Flat
f	(3 x 3)	2	8	Same as (b)	8	Zee	30
g	(3 x 3)	2	8	Same as (b)	8	Zee	60
h	(3 x 3)	1	8	Same as (b)	8	Zee	90
i	(6 x 3)	1	8	Same as (b)	4	Zee	Flat
j	(6 x 3)	1	8	Same as (b)	4	Zee	90
k	(4 x 3)	2	8	Same as (b)	6	Zee	Flat
l	(4 x 3)	1	12	Same as (d)	6	Zee	90
m	(8 x 1)	1	8	Same as (b)	4.5	Zee	Flat
n	(3 x 3)	1	4	$(0, 90)_s$	8	Zee	Flat
p	(3 x 3)	1	4	Same as (n)	8	Zee	90
q	(6 x 3)	1	4	Same as (n)	4	Zee	Flat
r	(6 x 3)	1	6	Same as (a)	4	Zee	60
s	(4 x 3)	1	4	Same as (n)	6	Zee	30
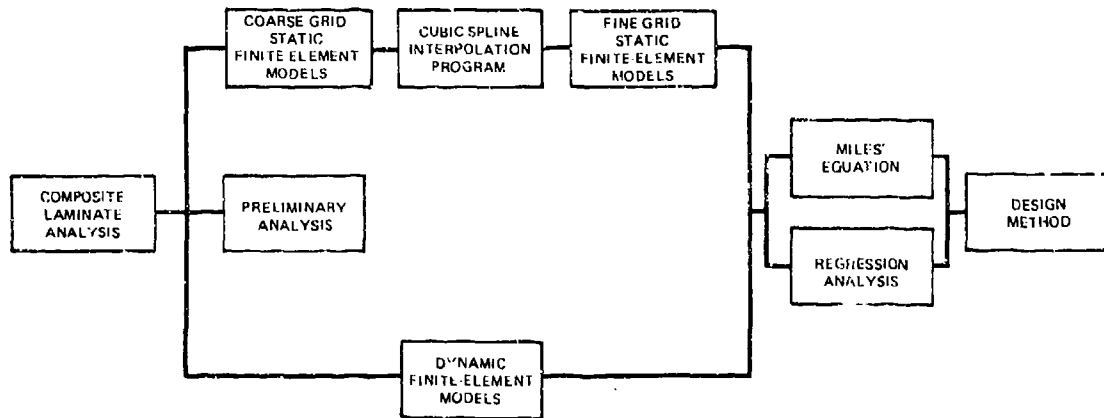
Figure 2. Flow Chart of Analytical Work

2. GENERAL SONIC FATIGUE THEORY

The central problem in sonic fatigue analysis is the calculation of the vibratory stress levels in structural panels subjected to the random acoustic excitation associated with jet engine noise, and then to predict the resulting fatigue life. Since the structural loading is random (Gaussian), the structural response is also random and multimodal in nature. It also follows that the amplitude distribution of the random response must be taken into account in order to determine corresponding fatigue lives.

The complete response of a complex structure to a random noise field can be fully described by an equation developed by Powell[9]. However, Powell's theory is too cumbersome to be used in everyday design and requires input data that is never available in the design stage of a vehicle. In order to simplify the theory to the level of practical use, the following assumptions are made:

7

(1) Only one mode of vibration contributes to fatigue failure, and that this mode is the fundamental mode of the individual panel bays. This mode is usually assumed to be the fundamental fully-fixed mode or the fundamental in-phase mode, in which adjacent bays vibrate in-phase with each other, putting the panel stiffeners into bending. Full scale tests on aircraft have shown this assumption to be generally true.

(2) The vibratory mode shape is identical with the static deflected shape of the panel when subjected to a uniform static pressure.

(3) The acoustic pressure is exactly in-phase over the whole panel. This assumption is reasonable for jet noise excitation of typically sized aircraft panels. It may not be valid for boundary-layer excitation.

(4) The power spectral density of the acoustic pressure is constant over the frequency range near the fundamental natural frequency of the panel. It is also assumed that the whole of the energy represented by the acoustic spectrum level at the frequency of the assumed mode of vibration is used to excite that mode.

These assumptions simplify the structural response equation to the form developed by Miles[1]:

$$\text{Mean square stress}\quad \sigma^2(t) = \frac{\pi}{4\zeta}\ f_n \cdot G(f_n)\sigma_o^2 \tag{1}$$

where ζ is the damping ratio of the fundamental mode, often assumed to be typically 0.017 (Reference 5).

         f_n is the natural frequency of the assumed fundamental mode in Hz.

         $G(f_n)$ is the spectral density of the acoustic pressure at the frequency f_n.

σ_0 is the static pressure at the point of interest due
to a unit uniform static pressure over the whole
of the panel.

This equation forms the basis of most design oriented sonic fatigue work
to date, including the nomographs presented in Reference 5. Many of the
simplified sonic fatigue design methods assume fully-fixed panel edges in
the calculation of f_n and σ_0. In this program, these values were to be
determined from the finite-element solutions, using actual boundary
conditions.

The usual estimating procedure, using Miles' equation is as follows:

    a. Estimate the fundamental natural frequency of the panel,
usually assuming fixed edges. Reference 5 provides an appropriate
nomograph for this purpose.

    b. Obtain the acoustic spectrum level at the estimated frequency.
NOTE: The spectrum level, $L(f_n)$, is the square root of the
spectral density $G(f_n)$. Since the acoustic spectrum
level corresponds to the acoustic energy in a 1-Hz
bandwidth, acoustic data expressed in other bandwidth form
must be converted to the spectrum level using the following
relationship

$$L = \text{Sound Pressure Level} - 10 \log_{10} (f_2 - f_1) \qquad (2)$$

where f_2 and f_1 are the upper and lower frequency limits, respectively, of
the given bandwidth.

    c. Calculate σ_0. Reference 10 gives a simplified equation for
the maximum static stress in a fully-fixed panel.

d. Calculate $\sigma(t)$ using Equation 1, assuming $\zeta = 0.017$.

e. Determine sonic fatigue life using specially generated random fatigue curves. Reference 6 contains examples of random S-N curves.

NOTE: Random fatigue curves can be developed from conventional cyclic fully-reversed flexural fatigue curves. This is accomplished by applying Miner's[11] cumulative damage law to the Rayleigh distribution function for peak amplitudes in a Gaussian process.

3. COMPOSITE LAMINATE ANALYSIS

Rohr has several computer programs available for analysis of composite laminates. These analytical techniques range from large general purpose programs down to simplified procedures used on the desk computers.

The primary general purpose program developed for laminate property analysis, called COMPOSITE, calculates the laminate elastic and strength properties for a specified laminate layup. The program may also analyze a laminate with up to five different materials in the layup, hence, is useful in determining the properties of hybrid laminates. Options for three failure criteria are also included within the program and can be used to assist in determining laminate failure modes. The laminate analysis can be performed for combinations of in-plane and bending loads.

The COMPOSITE program was developed with several additional features for the analysis of laminate properties. If the laminate fails under the specified load, one program feature will remove the failed plies from the layup and recalculate the laminate elastic and strength properties. This feature is useful in evaluating nonlinearities due to ply failure and determining to what degree the laminate with the failed plies removed can sustain the load. The laminate stiffness matrix, suitable for direct input into the NASTRAN finite-element program, is also computed and is part of the output.

10

The program can also calculate the buckling coefficients for flat laminate panels. By selecting the options and inputting panel size, the buckling coefficient can be determined and displayed either in tabular or graphical printout. A material data bank is also incorporated into the COMPOSITE program. Material laminate properties are stored within the program and may be called by identification number for a laminate analysis. This feature saves time in setting up the computer deck and provides consistent properties for use on a regular basis. The laminate properties in the data bank may be updated as necessary to reflect current data.

Material property data for all the skin and stiffener laminates were calculated and tabulated based on carpet plots in Reference 12. Rohr has used its "COMPOSITE" computer program and performed laminate property tests to confirm selected data points in Reference 12. Tables 2 through 6 list the laminate properties generated and used as inputs for the finite element analyses. Values shown in parentheses are computer generated values used to check those obtained from Reference 12. Elastic properties were computed for the skin, skin/stiffener attach flange, stiffener web, and the stiffener free flange with unidirectional reinforcement. Modulus values are times 10^6 (1b/in^2).

Effect of Stacking Order

One of the advantages of composite materials is the capability to tailor structural properties by dictating the number and orientation of plies. The in-plane strength and elastic properties (E_x, E_y, G_{xy}) of the laminate can be readily determined for specified orientation patterns through the use of computer programs or "carpet plots." These procedures are documented in the Air Force Composite Design Guide[12] and other sources.

The elastic properties are customarily used in the structural finite-element programs, such as NASTRAN (see Section II.5).

11

TABLE 2

LAMINATE PROPERTIES FOR SHAKER SPECIMEN 1 AND PANELS a, j AND r

Laminate	E_y	E_x	G_{yx}	ν_{yx}	ν_{xy}	G11 $\dfrac{E_y}{1-\nu_{xy}\,\nu_{yx}}$	G22 $\dfrac{E_y}{1-\nu_{xy}\,\nu_{yx}}$	G21 = G12 $\dfrac{\nu_{xy}\,E_y}{1-\nu_{xy}\,\nu_{yx}}$	G33 G_{yx}
Skin - $(0, +45)_s$	7.5 (7.3)	3.3 (3.3)	3.4 (3.2)	.69 (.69)	.31	9.54	4.2	2.96	3.4 (3.2)
Skin + attached stiffener flange -	4.5	3.1	3.9	.73	.50	7.09	4.88	3.54	3.9
Stiffener, web -	2.4 (2.3)	2.4 (2.3)	4.5 (4.5)	.76 (.76)	.76	5.68	5.68	4.32	4.5 (4.5)
Stiffener, free-flange -	10.2	3.0	2.4	.61	.17	11.38	3.35	1.93	2.4

NOTE: Modulus values are in units of 10^6 lb/in.^{2}.

TABLE 3

LAMINATE PROPERTIES FOR SHAKER SPECIMENS 2, 5 AND 6 AND PANELS b, e, f, g, h, i, k AND m

Laminate	E_y	E_x	G_{yx}	ν_{yx}	ν_{xy}	G11 $\dfrac{E_y}{1-\nu_{xy}\,\nu_{yx}}$	G22 $\dfrac{E_y}{1-\nu_{xy}\,\nu_{yx}}$	G21 = G12 $\dfrac{\nu_{xy}\,E_y}{1-\nu_{xy}\,\nu_{yx}}$	G33 G_{yx}
Skin - $(0, \pm 45, 90)_s$	6.7 (6.8)	6.7 (6.8)	2.6 (2.6)	.31 (.31)	.31	7.41	7.41	2.3	2.6 (2.6)
Skin + attached stiffener flange -	4.75	4.75	3.6	.49	.49	6.25	6.25	3.06	3.6
Stiffener, web -	2.4 (2.3)	2.4 (2.3)	4.5 (4.5)	.76 (.76)	.76	5.68	5.68	4.32	4.5 (4.5)
Stiffener, free-flange -	9.3	3.2	2.7	.64	.21	10.74	3.7	2.26	2.7

NOTE: Modulus values are in units of 10^6 lb/in.^{2}.

TABLE 4
LAMINATE PROPERTIES FOR SHAKER SPECIMEN 3 AND PANEL c

Laminate	E_y	E_x	G_{yx}	ν_{yx}	ν_{xy}	G11 $\dfrac{E_y}{1-\nu_{xy}\nu_{yx}}$	G22 $\dfrac{E_y}{1-\nu_{xy}\nu_{yx}}$	G21 = G12 $\dfrac{\nu_{xy}E_y}{1-\nu_{xy}\nu_{yx}}$	G33 G_{yx}
Skin - $(0_2, \pm 45)_s$	9.7 (9.8)	3.2 (3.2)	2.6 (2.6)	.63 (.63)	.21	11.18	3.69	2.35	2.6 (2.6)
Skin + attached stiffener flange -	6.0	3.3	3.6	.71	.39	8.3	4.56	3.24	3.6
Stiffener, web -	2.4 (2.3)	2.4 (2.3)	4.5 (4.5)	.76 (.76)	.76	5.68	5.68	4.32	4.5 (4.5)
Stiffener, free-flange -	9.3	3.2	2.7	.64	.21	10.74	3.7	2.26	2.7

NOTE: Modulus values are in units of 10^6 lb/in.^{2}.

TABLE 5
LAMINATE PROPERTIES FOR SHAKER SPECIMEN 4 AND PANELS d AND 1

Laminate	E_y	E_x	G_{yx}	ν_{yx}	ν_{xy}	G11 $\dfrac{E_y}{1-\nu_{xy}\nu_{yx}}$	G22 $\dfrac{E_y}{1-\nu_{xy}\nu_{yx}}$	G21 = G12 $\dfrac{\nu_{xy}E_y}{1-\nu_{xy}\nu_{yx}}$	G33 G_{yx}
Skin - $(0, \pm 45)_{2s}$	7.5	3.3	3.4	.69	.31	9.54	4.2	2.96	3.4
Skin + attached stiffener flange -	4.5	3.1	3.9	.73	.5	7.09	4.88	3.54	3.9
Stiffener, web -	2.4	2.4	4.5	.76	.76	5.68	5.68	4.32	4.5
Stiffener, free-flange -	6.2	3.3	3.5	.73	.39	8.67	4.61	3.38	3.5

NOTE: Modulus values are in units of 10^6 lb/in.^{2}.

TABLE 6

LAMINATE PROPERTIES FOR SHAKER SPECIMEN 7 AND PANELS n, p, q AND ٬

Laminate	E_y	E_x	G_{yx}	ν_{yx}	ν_{xy}	G11 $\dfrac{E_y}{1-\nu_{xy}\nu_{yx}}$	G22 $\dfrac{E_y}{1-\nu_{xy}\nu_{yx}}$	G21 = G12 $\dfrac{\nu_{xy}\,E_y}{1-\nu_{xy}\nu_{yx}}$	G33 G_{yx}
Skin – $(0, 90)_s$	9.4 (9.4)	9.4 (9.4)	.65 (.65)	.05 (.04)	.05	9.42	9.42	.47	.65 (.65)
Skin + attached stiffener flange –	4.8	4.8	3.25	.4	.4	5.71	5.71	2.29	3.25
Stiffener, web –	2.4 (2.3)	2.4 (2.3)	4.5. (4.5)	.76 (.76)	.76	5.68	5.68	4.32	4.5 (4.5)
Stiffener, free-flange –	10.2	3.0	2.4	.61	.17	11.38	3.35	1.93	2.4

NOTE: Modulus values are in units of 10^6 ib/in.^{2}.

However, for this investigation where composite structures are exposed to a sonic environment, additional composite properties are desired. A laminated structure subjected to a bending load whether applied by a sonic or structural source requires the use of the inertia or bending stiffness properties. For laminates, the bending stiffness is defined by the "D_{ij}" matrix. The D_{ij} matrix is computed from the individual ply properties transformed from the specified orientation to the desired stiffness direction. The ply location from the center of the laminate is also taken into consideration. The D_{ij} matrix is therefore written in short notation as:

$$D_{ij} = \frac{1}{3} \sum_{K=1}^{n} (\overline{Q}_{ij})_K (h^3_k - h_{K-1}{}^3) \qquad (3)$$

The $\overline{Q}_{ij}$ matrix is the in-plane stiffness of each ply and h_K, h_{K-1} provides the geometric location. The summation provides the bending stiffness of

the laminate. The position of the ply in the laminate therefore will dictate the stiffness.

The effect of ply position or "stacking order" on the laminate stiffness, (D_{ij}), can be determined by using the COMPOSITE computer program. The D_{ij} matrix results for different ply stacking orders are shown in Table 7. In the table, the D_{11} stiffness is in the laminate 0 degree direction, the d_{12} is the Poisson effect, D_{22} is the laminate 90° stiffness and D_{66} is the in-plane shear stiffness. Even the quasi-isotropic layup ($\pm 45°/90°/0°)_{2s}$ has different values in the laminate orthogonal directions.

The variability of the D_{ij} factors indicates that stacking order has an effect upon the performance of composite panels subjected to an acoustic environment. As an example of the stacking order effect, the natural frequency of simply supported composite plate is of the form

$$W = \frac{\pi}{\rho_1}^2 K \qquad (4)$$

where $K = D_{11} \left(\frac{m}{a}\right)^4 + 2 (D_{12} + 2 D_{66}) \left(\frac{mn}{ab}\right)^2 + D_{22} \left(\frac{n}{b}\right)^4$ and

ρ_1 = mass density.

Since the stacking order affects only the factor "K", its value was tabulated for various laminate layups in Table 8. For a sixteen ply laminate, the stiffness factor has a 12 percent variation depending upon the stacking order.

Complications arose in trying to quantify the effects of stacking order on panel response. This is discussed in Paragraph II.5.a.

15

TABLE 7

EFFECTS OF STACKING ORDER AND PLY ORIENTATION ON BENDING STIFFNESS MATRIX

LAMINATE "D_{ij}" MATRIX

GR/EP 3501/AS TYPE

$$E_1 = 17 \times 10^6 \qquad E_2 = 1.7 \times 10^6 \qquad G = .65 \times 10^6$$

Orientation	No. Plies	D_{11}	D_{22}	D_{12}	D_{66}
$(\pm 45/90_2)_{2s}$	16	246.01	518.74	171.32	187.87
$(\pm 45/0_2)_{2s}$	16	518.74	246.01	171.32	187.87
$(\pm 45/90/0)_{2s}$	16	351.7	413.06	171.32	187.87
$(\pm 45/0_2)_4$	16	549.49	235.85	161.03	177.58
$(0/90/\pm 45)_s$	8	66.407	40.48	5.051	6.80
$(0/90/\pm 45)_{3s}$	24	1793.1	1093.0	136.4	183.6
$(\pm 45)_{8s}$	16	265.17	265.17	202.78	216.76
$(0_2/\pm 45_8)_s$	20	1046.3	343.28	219.18	246.5

$$D_{16} = D_{26} = 0$$

$$D_{ij} = \frac{1}{3} \sum_{K=1}^{n} (\overline{Q}_{ij})_K (h_K^3 - h_{K-1}^3)$$

Where $\overline{Q}_{ij}$ is the transformed ply property

and h_K, h_{K-1} is the distance of the ply surfaces

from the reference.

TABLE 8

EFFECTS OF STACKING ORDER ON NATURAL FREQUENCY FACTORS

Layup	K	Number of Plies
$(\pm 45/90_2)_{2s}$	.4514	16
$(\pm 45/0_2)_{2s}$	.5072	16
$(\pm 45/90/0)_{2s}$	.4738	16
$(\pm 45/0_2)_4$	.5075	16
$(0/90/\pm 45)_s$	.149	8
$(0/90/\pm 45)_{3s}$	.7745	24
$(\pm 45)_{8s}$	.4643	16
$(0_2/\pm 45_8)_s$	.6531	20

(1)   Where $\omega = \left(\dfrac{\pi}{\rho_1}\right)^2 K$

17

4. PRELIMINARY SONIC FATIGUE ANALYSIS

Preliminary sonic fatigue analyses were performed in support of the design of the sonic fatigue test panels, given in Table 1. These analyses were made to ensure that the application of these panels in acoustic environments appropriately spanned the full range of aircraft application. It was also necessary to ensure that the sonic fatigue resistance of the test panels was within the available progressive-wave tube test envelope. It is important in a sonic fatigue test program to obtain a good spread of response characteristics, and to obtain some sonic fatigue failures out in the 10^6 to 10^7 cycle range, without having too many panels fail either too quickly or not at all. The AGARD[5] sonic fatigue design nomographs were used in this analysis, with the results being modified to take account of the elastic modulus and density values for the appropriate skin laminates. The results are shown in Table 9. A pre-test evaluation of the progressive-wave tube indicated that endurance testing would be best carried out in the 160 to 165 dB overall sound pressure level range, corresponding to acoustic spectrum levels in the 130 to 150 dB/Hz range. The results show a good spread in both predicted frequencies and rms stresses. They also show that almost all of the panels could be expected to fail at an acoustic spectrum level of 150 dB/Hz.

5. FINITE ELEMENT SOLUTIONS

The general sonic fatigue theory described in Section 11.2 utilizes as inputs the static stresses or strains due to a uniform unit pressure load and the natural frequency of the fundamental in-phase stringer-bending mode. These stress and frequency inputs were determined for each of the panel configurations given in Table 1, using a variety of finite-element models in conjunction with the NASTRAN computer program. NASTRAN is a general purpose finite-element digital computer program especially suited for the analysis of large complex structures. Its ability to handle a large range of problems has resulted in its adoption throughout the aerospace industry. This wide acceptance and versatility are the primary reasons for the selection of NASTRAN as the fundamental analytical tool in this program. The uniform pressure load condition is widely used in sonic

TABLE 9

PRELIMINARY SONIC FATIGUE ANALYSIS RESULTS

Panel Config- uration	Acoustic Spectrum Level dB/Hz	Stringer Spacing b (in)	Skin Thickness t (in)	Radius of Curvature R (in)	Fully- Fixed Frequency (Hz)	RMS Stress (lb/in^2)	Laminate F_{tu} (lb/in^2)
a	130 140 150	8	.033	Flat	160	20,900 66,200 209,000	70,000
b&e	130 140 150	8	.044	Flat	202	12,800 40,400 128,000	64,000
c	130 140 150	8	.044	Flat	247	14,200 44,800 142,000	96,000
d	130 140 150	8	.066	Flat	308	7,400 23,400 74,000	70,000
f	130 140 150	8	.044	30	825	1,700 5,400 17,000	64,000
g	130 140 150	8	.044	60	510	3,250 11,000 32,500	64,000
h	130 140 150	8	.044	90	.375	4,750 17,500 47,500	64,000
i	130 140 150	4	.044	Flat	674	6,600 20,900 66,000	64,000
j	130 140 150	4	.044	90	824	6,000 18,000 60,000	64,000
k	130 140 150	6	.044	Flat	312	10,500 31,700 100,000	64,000
l	130 140 150	6	.066	90	631	4,100 13,000 41,000	70,000
n	130 140 150	8	.022	Flat	120	38,400 121,000 384,000	88,000
p	130 140 150	8	.022	90	377	7,800 23,000 78,000	88,000
q	130 140 150	4	.022	Flat	409	19,800 62,600 198,000	88,000
r	130 140 150	4	.033	60	782	6,400 22,000 69,000	70,000
s	130 140 150	6	.022	30	828	3,500 11,000 35,000	88,000

Note: $\rho = 0.055$ lb/in^3

19

fatigue work since its resulting displacement field closely resembles the fundamental in-phase mode shape.

The accuracy of finite-element solutions is highly dependent upon the element size and the applied boundary conditions. Consequently, considerable effort was put forth in the determination of each. This involved many iterations before arriving at optimum model configurations. Due to the nature of the test panel designs, i.e., relatively massive stiffeners interfacing with thin plates, some difficulty was experienced in generating the in-phase mode from the dynamic models. Eventually, well defined stringer-bending in phase modes were obtained for all but two of the panel configurations (the two 30-inch curved panels, f and s, being the exceptions). However, the mode shapes for the stiffer panels exhibited excessive substructure deflections, resulting in low frequency estimates. This conditioning problem was successfully overcome in the static analysis.

Finite element models were also constructed for the shaker specimens described in Section III.4. Computed natural frequencies gave good agreement with the shaker test results, and are given in Paragraph II.5.d.

  a. Analytical Approach - In order to provide static and dynamic analyses in sufficient detail to support the development of a semi-empirical sonic fatigue design method, finite-element models were constructed to represent each of the panel configurations shown in Table 1. Initially it was believed that relatively coarse grid models would be sufficient for the dynamic analysis. Consequently, models comprising 2-inch plate elements, with bar elements representing the stringers and frames, were constructed. These models were used to generate a set of static and dynamic solutions. Although primarily intended as dynamic models, they also provided a good starting point for the static analysis. The material properties used in these and subsequent models were determined from the Rohr composite laminate properties program "COMPOSITE," described in Section II.3.

20

The dynamic results from the 2-inch grid models appeared to be satisfactory for the 3 x 3 panel arrays; however, it was decided to use a finer grid for the panels with smaller bays (4 x 3 and 6 x 3 panel arrays). Models comprising 1-inch plate elements were therefore constructed and a second set of results was generated. The mode shapes and natural frequencies generated by the 1-inch and the 2-inch models were in close agreement. However, some difficulties were encountered with both sets of models in identifying the desired in-phase stringer-bending mode. Further modeling refinements did not result in significant improvements in the dynamic solutions, consequently the 1-inch coarse grid quarter models were used for the dynamic analyses.

As expected, neither the 2-inch nor the 1-inch coarse grid models provided the necessary detail for the static analysis, particularly in high stress gradient areas. A set of 1/2-inch models was constructed and another set of static solutions obtained. Accuracy at the skin-stiffener interfaces was still considered inadequate. All of these coarse grid models represented a quarter of each panel array, as shown in Figure 3.

It was then decided to represent the center bay portion of each panel with a fine grid model, also shown in Figure 3. Because of the lack of symmetry of zee stiffeners, these fine-grid models included the stringers on both of the long sides. The maximum stress in stiffened skin panels occurs at the center of, and normal to, the longer edges. Detailed accuracy is therefore of great importance in these areas. This was accomplished by representing the zee stiffeners as a series of plates (thereby creating three-dimensional models) rather than as simple bar elements. In addition, the grid size was optimized by computing the bending moment distributions from three specially constructed small plate (6 in. by 4 in.) models employing, in turn, 1-inch, 1/2-inch and 1/4-inch grid sizes. The results were then compared with hand calculations using Timoshenko[13]. Figure 4 shows the results of the comparison. It can be seen that 1/2-inch grid size provides accurate results at the panel center. Even the 1-inch grid has reasonable accuracy at the center of the

21
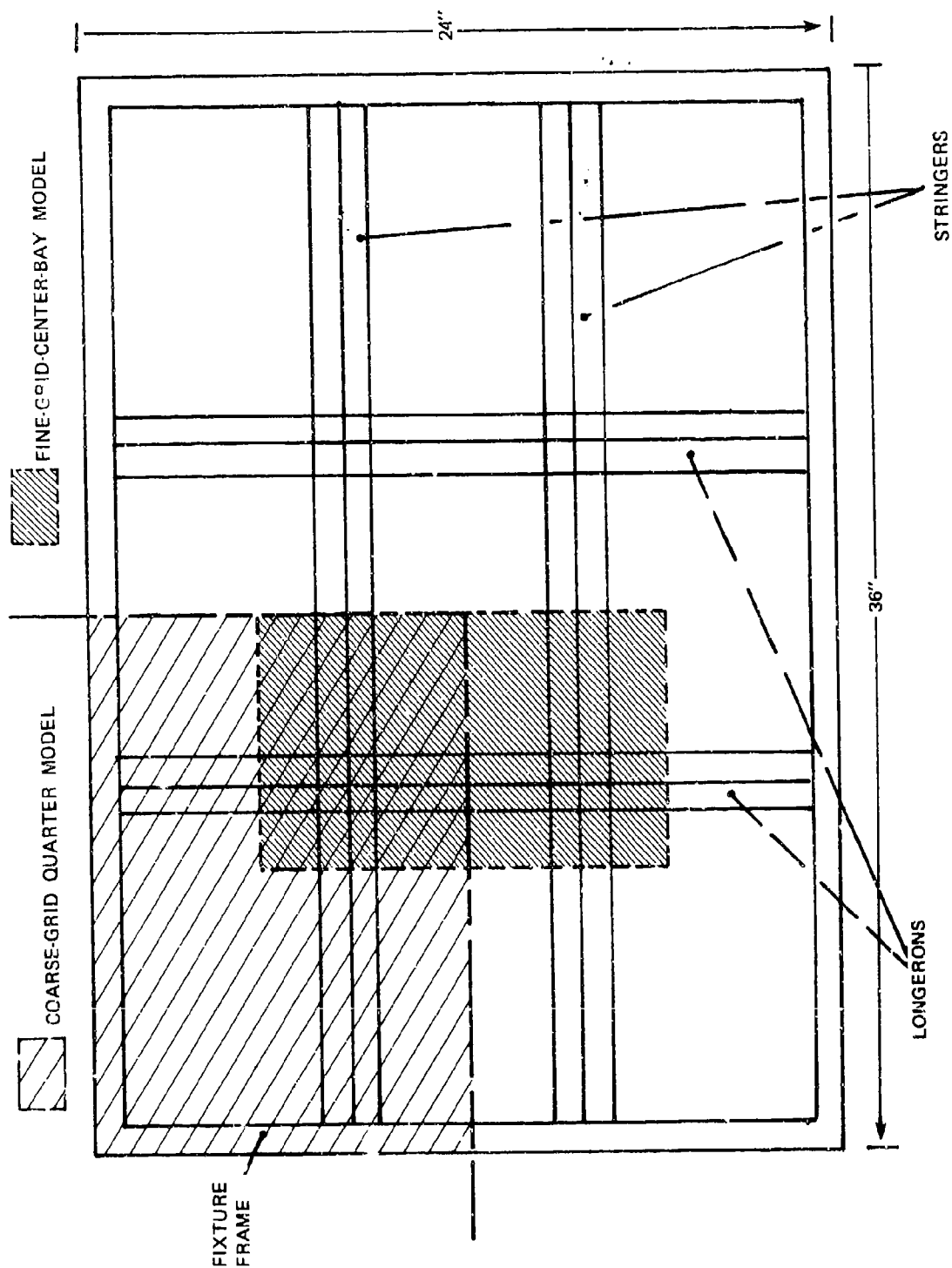
Figure 3. Location of Finite Element Models Relative to Entire Panel

24"

36"

STRINGERS

LONGERONS

FIXTURE FRAME

FINE-GRID-CENTER-BAY MODEL

COARSE-GRID QUARTER MODEL

22
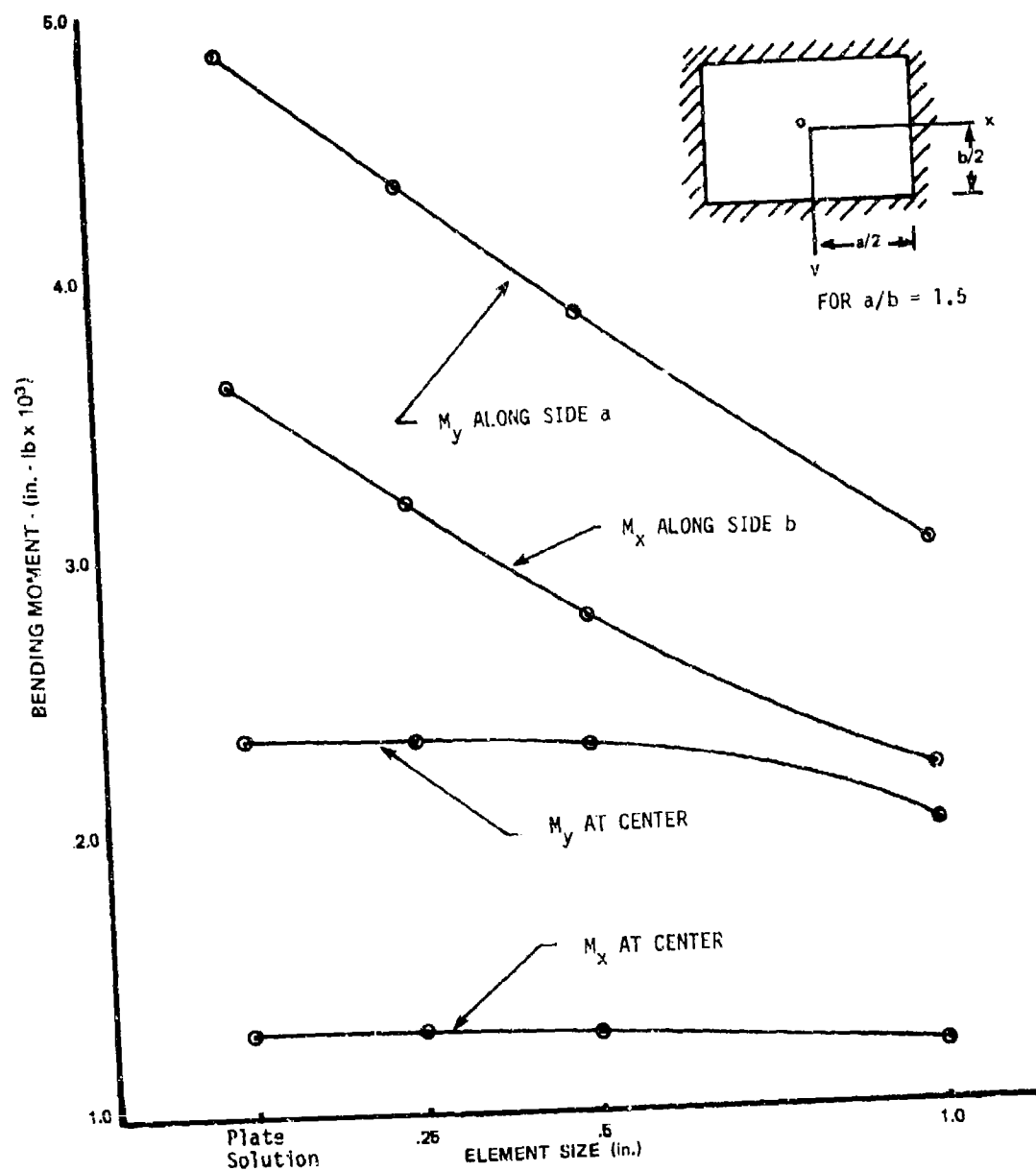
Figure 4. Comparison of Bending Moment Distributions Using Different Size Elements and Plate Solution Taken from Timoshenko (13)

23

panel. However, the gradient at the panel edges requires a very fine grid in order to achieve reasonable accuracy. A compromise between structural accuracy and practical constraints, such as computer size limitations, resulted in 1/4-inch elements being selected to represent the skin-stiffener interface regions. This results in an 11-14 percent underestimate in computed bending moments at the panel edges, compared to the values calculated using Timoshenko. Although a maximum grid size of 0.875-inch was used in some non-critical skin areas, all strains used in the development of the design method (Section IV) were taken from 1/4-inch elements. There are practical limitations in combining radically different element sizes within one model. In order to limit the number of grid points to within manageable proportions, the smaller elements (1/4-inch) must have higher aspect ratios than the larger elements (1/2-inch). Unfortunately, analytical accuracy deteriorates with increased aspect ratio (above unity). An element aspect ratio of 3:1 is considered the maximum for reasonable accuracy.

In order to obtain boundary conditions for the fine grid center bay models, a cubic-spline computer program was written to interpolate the displacement and rotation fields along the interfaces with the 2-inch coarse grid quarter models. This method assumes the deflected shape which minimizes potential (strain) energy. Conventional "beam theory" shows this energy to be proportional to the integral, with respect to the arc length, of the square of the curvature of the spline. The accuracy of this approach was verified using the previous 1/2-inch grid model. Displacement data at 2-inch intervals on the 1/2-inch model were interpolated to obtain intermediate displacements at 1/2-inch intervals. These interpolated displacements were within 1 percent of the actual results from the 1/2-inch model. Initially it was thought that the fine-grid boundary conditions could be adequately described using displacement data only. However, when this was attempted with the 1/2-inch model, it was found that resultant stress and displacement fields were not sufficiently accurate. Consequently, it was decided to also include the interpolated values of the two components of rotation along the boundary.

24

This improved the accuracy of the interpolated stresses to within 2 percent of the 1/2-inch model results.

During the subsequent static analysis of the curved panels, it was determined that additional in-plane displacements were needed in order to fully define the boundary conditions. Flat panels, under normal loading, do not undergo axial displacements and all the load is taken in pure bending. However curved panels, under normal loading, experience both hoop and bending stresses, requiring the application of in-plane displacement boundary conditions. A further refinement was evaluated, which was to apply rotation and displacement boundary conditions to the out-of-plane zee stiffener elements, in addition to the skin elements. The effects of this refinement on one flat and one curved panel was less than 10 percent and have not been included in the results in Paragraph II.5.c.

A comparison was made in both the static and dynamic analyses, between Z and J stiffener designs. A sample calculation using one of the dynamic quarter models showed no significant differences in natural frequencies nor mode shapes between the Z and the J stiffened panels. No further dynamic analysis of the J stiffeners was performed. Significant differences between the Z and the J stiffened panels did occur in the static analysis results, and are given in Paragraph II.5.c.

b. Effects of Skin Ply Stacking Order - Attempts were made to evaluate the significance of these effects on the computed static stresses. The previous analyses utilized Rohr's "COMPOSITE" computer program to generate laminate elastic properties, which are not dependent upon stacking order, leaving the bending stiffness (EI) to be computed by NASTRAN in the usual manner.

25

Because laminated composite materials exhibit orthotropic properties, it is necessary to input the total plate constitutive equation

$$\begin{bmatrix} N \\ M \end{bmatrix} = \begin{bmatrix} A & \vdots & B \\ B & \vdots & D \end{bmatrix} \begin{bmatrix} \epsilon \\ k \end{bmatrix} \tag{5}$$

in matrix form to fully describe the behavior of a general orthotropic plate. Where N and M are the applied loads and ϵ and k are the resultant strains. The A and D matrices define the extensional and bending stiffnesses respectively. The "B" matrix defines the bending-extensional coupling for the laminate. From a practical standpoint this term is nearly always zero, because ply orientation and stacking orders are selected to give a "balanced symmetric" layup which eliminates bending-extensional coupling. The bending and extensional constitutive equations can therefore be shown below:

$$[N] = [A] [\epsilon] \text{ and } [M] = [D] [k] \tag{6}$$

For the isotropic extensional case, NASTRAN computes the constitutive equations

$$A_{11} = A_{22} = (\frac{E}{1-\nu^2}) t \tag{7}$$

$$A_{12} = \nu A_{11} \tag{8}$$

$$A_{66} = (\frac{E}{2(1+\nu)}) t \tag{9}$$

from the data supplied on the PQUAD quadrilateral plate element card (thickness, t) and on the MAT1 material card (E and ν). The remaining matrix terms are zero.

26

If an orthotropic material is to be analyzed for axial loading, the MAT2 card is utilized to input the material property matrix "G" terms

$$\left(\frac{E_x}{(1-\nu_{xy}\nu_{yx})}, \frac{E_y}{1-\nu_{xy}\nu_{yx}}, \text{etc.}\right). \tag{10}$$

The complete constitutive equations are obtained by the product of this matrix and the material thickness which is again input on the appropriate PQUAD card.

For the isotropic bending case, NASTRAN computes the constitutive equations

$$D_{11} = D_{22} = \frac{E\,t^3}{12(1-\nu^2)} \tag{11}$$

$$D_{12} = \nu D_{11} = D_{21} \tag{12}$$

$$D_{66} = \frac{E\,t^3}{24(1+\nu)} \tag{13}$$

from the same data supplied for the extensional case. If no additional information is supplied, NASTRAN will also compute the orthotropic bending constitutive equations in the same manner (multiplying the "G" matrix terms by the appropriate $t^3/12$ term).

However, the true bending stiffness of an orthotropic laminate is a function of the laminate stacking order in addition to the laminate elastic properties.

The constitutive equation for bending (the "D" matrix) can be input into NASTRAN using the MAT2 card. In this case the "D" matrix must be factored by the $t^3/12$ term because NASTRAN is programmed to multiply the "G" matrix by the $t^3/12$ term.

27

The Cosmic version of NASTRAN does not have the capability to accept the complete orthotropic constitutive equation matrix for plate elements.

In many cases, where loading is primarily axial or the laminate has a large number of plies, the inaccuracies introduced by using the extensional "G" matrix to compute the bending constitutive equations is small and this approach has been used with reasonable accuracy. Conversely, if the panel has a small number of plies and the loading is primarily in bending, then the bending "G" matrix can be used.

The Rohr laminate analysis program COMPOSITE outputs the extensional "G" matrix directly in addition to the "A," "B" and "D" matrices.

In the case of the structural analysis of the sonic fatigue panels, an attempt has been made to input both the extensional and bending constitutive equation matrices. This was done using the "PQUAD 1" general quadrilateral element property card which is primarily utilized for the analysis of sandwich structures. This property card allows for separate input of membrane (extensional), bending and shear properties.

The extensional information required is the material identification and plate thickness. The extensional constitutive matrix can be input by identifying a "MAT2" material property card containing the appropriate "G" matrix.

The input data defining the bending properties are the material identification and the area moment of inertia per unit width (I) of the quadrilateral element. NASTRAN is programmed to calculate the isotropic constitutive bending equations using the input values of I ($t^3/12$), the elastic constants and the appropriate numerical values. NASTRAN is also programmed to utilize the "I" value in the computation of the bending stresses.

To obtain the orthotropic constitutive bending equations, the bending
material was defined on a "MAT2" material property card containing the "D"
matrix factored by $1/I$ $(12/t^3)$. The complete "D" matrix was then obtained
internally in NASTRAN using the computational procedure defined above.
The results of this investigation were inconclusive, requiring further
study beyond the schedule of this program. No correlation was established
between the stacking order and the effect on computed stresses.

c. Static Analysis - The analysis of the sonic fatigue panel
configurations in this program required the construction of detailed
finite-element models to accurately predict the panel responses to a
uniform 1 lb/in^2 applied pressure load. The iterations involved in
arriving at optimum model designs are discussed in Paragraph II.5.a. The
panel configurations are given in Table 1, and the location of the finite-
element models relative to the entire panel arrays is given in Figure 2.

Although there are 20 panel configurations in Table 1, the final analysis
results in this section are limited to 18 configurations. Panels "e" and
"m" were eliminated prior to the final computer runs. Because of the many
iterations involved in obtaining the final analytical results and the
consequent effects that this had on program schedule, it became necessary
to limit the final analysis to those panels to be used in the development
of the design method. Panel "e" was intended to evaluate honeycomb beam
stiffeners and panel "m" was primarily intended as a data link to sonic
fatigue test panels, comprising a single row of bays, typically used in
previous sonic fatigue programs. This program utilizes panels comprising
three rows of bays. Geometric similarities allowed the remaining 16
configurations to be represented by 10 fine grid center bay models.
Figures A-1 through A-6 in Appendix A show six of these models. The
three-dimensional modeling of the stiffeners is clearly seen, as is the
smaller grid spacing at the panel edges and along the center line of the
center bay.

29

The 2-inch coarse grid models were used to generate boundary conditions
for the fine grid center bay model, utilizing the cubic spline program
described in Paragraph II.5.a. The unit uniform pressure load was then
applied to the fine grid models, generating a series of stress
distributions. Although the subsequent design method would be based on
maximum edge stresses and/or center bay stresses, it is desirable to know
the displacement patterns and stress distributions over the entire
surface. This was accomplished by plotting isopleths of the desired
quantities. These are shown in Figures A-7 through A-18 in Appendix A.
Static deformations, out-of-plane displacements (Z direction) and stresses
in the "y" and "x" directions are given for panels "b," "d" and "f." The
plots are consistent with expected structural behavior and show the
stiffeners to provide good edge restraint. The stress contours show the
high gradients that exist at the skin-stringer interfaces, demonstrating
the need for accurate modeling in these areas. These plots were generated
prior to some model corrections and the introduction of in-plane boundary
conditions (see Paragraph II.5.a); consequently, the stress magnitudes on
the plots do not all correspond to the tablulated stresses shown later in
this section.

In determining stress magnitudes at critical locations, it was noticed
that the curved panels exhibited large stress differences on opposite
faces of the skin elements, indicative of significant axial stresses.
This is logical following the application of the in-plane boundary
conditions to the skin elements, described in Paragraph II.5.a. Figure 5
shows the locations of the stresses given in Table 10. Stresses on both
skin faces are given for all the curved panels. They are also given for
the flat panels at locations 5 and 6. Location 5 is at the center of the
center bay and location 6 is the maximum edge stress. The "y" direction
is across the narrow span and is therefore the critical direction. The
results show the flat panels to be in pure bending and also show the
extent of axial stresses occurring on the curved panels. However, during
sonic fatigue testing, back-to-back strain gauges gave equal and opposite
readings, indicative of pure bending on both curved and flat panels.

30
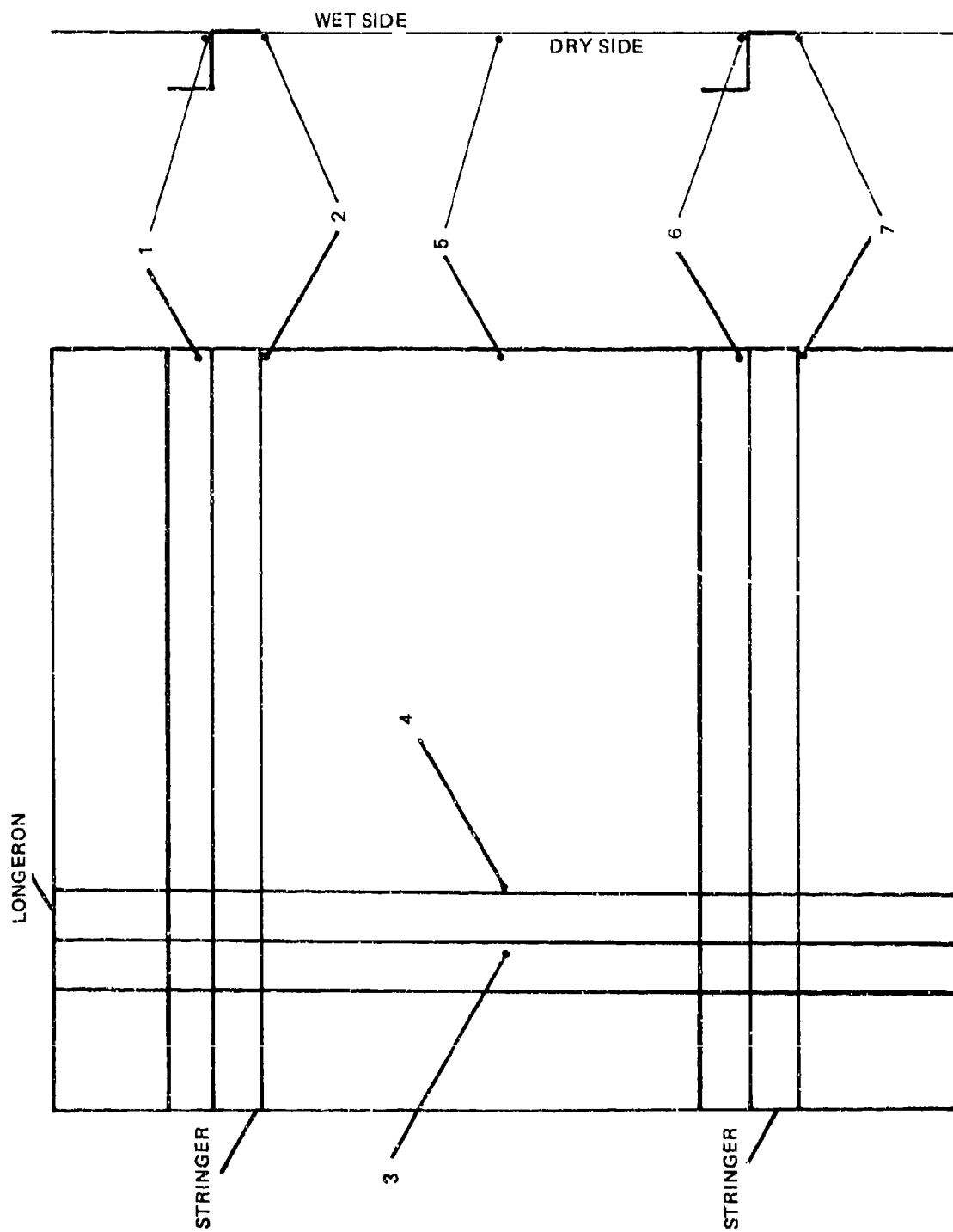
Figure 5. Location of Points Used in Table 10

31

TABLE 10

STATIC STRESS LEVELS FOR ZEE STIFFENED PANELS (KSI)

Panel		Point 1 σx	Point 1 σy	Point 2 σx	Point 2 σy	Point 3 σx	Point 3 σy	Point 4 σx	Point 4 σy	Point 5 σx	Point 5 σy	Point 6 σx	Point 6 σy	Point 7 σx	Point 7 σy
a	Wet	-7.82	-26.31	-4.52	-16.07	-11.12	-6.97	-6.18	-3.35	4.49	10.90	-7.72	-26.63	-5.93	-20.81
	Dry									-3.62	-10.68	8.65	25.20		
b	Wet	-3.98	-14.35	-2.21	-9.81	-11.80	-3.00	-6.00	-1.18	3.52	5.87	-3.76	-14.35	-3.03	-12.18
	Dry									-2.78	-5.69	4.99	14.02		
c	Wet	-3.23	-17.18	-1.68	-9.92	-5.91	-3.04	-2.79	-0.95	1.85	6.10	-2.92	-16.41	-1.94	-11.60
	Dry									-1.17	-6.00	3.86	16.03		
d	Wet	-2.15	-8.13	-0.98	-4.43	-3.98	-2.29	-1.30	-0.47	1.29	2.54	-1.76	-7.32	-1.04	-4.80
	Dry									-0.53	-2.36	2.60	7.05		
f	Wet	-0.25	-0.49	-0.27	-0.54	0.04	-0.32	-0.14	-0.45	-1.36	-0.76	-0.25	-0.49	-0.24	-0.48
	Dry	-0.36	-0.86	-0.35	-0.82	-0.65	-0.53	-0.47	-0.53	-0.30	-0.58	-0.37	-0.87	-0.36	-0.89
g	Wet	-0.04	0.36	-0.21	-0.11	1.19	0.02	0.60	-0.81	-0.03	-1.97	-0.02	0.49	-0.17	-0.10
	Dry	-0.96	-2.72	-0.88	-2.31	-2.07	-0.96	-1.51	-0.29	-0.35	-0.49	-1.06	-2.91	-0.84	-2.33
h	Wet	1.36	4.54	0.65	2.15	7.31	2.31	3.06	1.09	-1.34	-3.49	1.27	4.34	0.97	3.24
	Dry	-2.21	-6.99	-1.46	-4.80	7.93	-2.21	-3.46	-0.74	0.45	0.69	-2.19	-6.90	-1.86	-5.77
i	Wet	-0.89	-3.76	-0.26	-1.53	-2.68	-0.80	-0.52	0.01	0.50	1.03	-0.84	-3.78	-0.17	-1.39
	Dry									-0.19	-0.92	1.41	3.81		
j	Wet	-0.27	0.28	-0.52	-0.61	0.56	-0.70	-0.21	-1.04	-0.85	-1.71	-0.19	0.49	-0.47	-0.71
	Dry	-1.10	-2.55	-0.80	-1.69	-1.42	-1.24	-0.82	-1.08	-0.43	-0.57	-1.13	-2.69	-0.66	-1.53
k	Wet	-2.33	-8.40	-1.16	-4.54	-6.57	-1.89	-2.74	-0.61	1.36	3.28	-2.34	-8.71	-1.42	-5.81
	Dry									-1.14	-3.15	2.99	8.68		
l	Wet	0.07	0.97	-0.22	0.09	0.27	-0.27	-0.10	-0.53	-0.71	-1.45	0.08	1.07	-0.16	0.09
	Dry	-1.01	-2.48	-0.73	-1.59	-1.09	-1.15	-0.73	-0.84	-0.22	-0.02	-0.97	-2.45	-0.61	-1.54
n	Wet	-1.89	-60.77	-1.10	-41.84	-43.52	-0.51	-27.68	0.72	9.50	26.05	-0.83	-58.54	-1.58	-79.79
	Dry									-8.94	-26.45	4.90	57.13		
p	Wet	-0.04	-0.55	-0.28	-0.15	3.30	-0.45	4.66	-1.09	-1.01	-6.53	-0.07	1.16	-0.14	-1.40
	Dry	-0.42	-7.11	-0.65	-7.43	-4.09	-0.82	-5.74	-1.12	-0.64	-1.07	-0.60	-8.80	-0.38	-6.32
q	Wet	-0.17	-13.37	0.26	-5.22	-9.09	-0.40	-3.83	0.43	0.55	5.19	0.09	-13.54	0.20	-8.13
	Dry									-0.19	-5.06	1.37	13.58		
r	Wet	-0.25	-0.23	-0.50	-1.05	0.12	-0.75	-0.32	-1.15	-0.80	-2.02	-0.10	0.21	-0.45	-1.11
	Dry	-0.95	-2.53	-0.70	-1.74	-1.04	-1.47	-0.73	-1.27	-0.38	-0.74	-1.06	-2.92	-0.61	-1.62
s	Wet	-0.10	-0.85	-0.12	-0.86	1.60	-0.25	0.46	-0.78	-0.18	-1.69	-0.09	-0.55	-0.06	-0.68
	Dry	-0.15	-1.81	-0.16	-1.80	-1.73	-0.38	-0.68	-0.71	-0.13	-0.97	-0.16	-2.11	-0.12	-2.50

Consequently, it was decided to separate out the bending and axial stress components in the analytical results, and to use only the bending stress component in the development of the design method. Table 11 lists the results. Since the design method will utilize strain values rather than stress values, the corresponding bending strains are also shown in Table 11.

In order to provide a direct experimental comparison to the analytical static stresses, a static test was performed on panel "d." The panel was mounted in the same fixture that was used during sonic fatigue testing and that was also used to generate boundary conditions for the coarse grid models. A uniform pressure loading was incrementally applied, from 1 to $7\text{-}lb/in^2$ using an air bag. Strains were measured at each load increment using strain gauges. Back-to-back gauges were used at the panel center to measure axial strains in addition to bending strains. The strain response appeared to be nonlinear, with stresses increasing approximately 50 percent for a doubling of load. However, the back-to-back strain gauges gave readings within 2 percent of each other, indicating pure bending. It had been anticipated that any nonlinearities in structural response would show up as membrane (axial) stresses. No explanation is offered for this occurrence, and no evidence of nonlinear response occurred during sonic fatigue testing. Because of the nonlinear response, the comparison with the analytical results varied depending upon which load magnitude was used. At $7\ lb/in^2$ the center bay stresses were within 20 percent of the analytical value. The higher the load the better the comparison. Figure 6 compares the analytical results with the one $1\ lb/in^2$ and $7\ lb/in^2$ test values. Although the results from the $7\ lb/in^2$ load correspond more closely to the analytical results at the panel center, than do the $1\ lb/in^2$ results; the reverse is true at the panel edges. Another puzzling aspect of this static test was that the biaxial strain relationship at the panel center was markedly different during the static test from both the analytical results and from the sonic fatigue test results. In the static test, the strains in the long direction were very small (10 percent) compared to the strains in the short direction.

33

TABLE 11

STATIC STRESSES AND BENDING STRAINS FOR REGRESSION

Panel Configuration	Elastic Modulus E (10⁶ lb/in.²)	Center Stress (ksi)				Edge Stress (ksi)			
		Wet a	Dry b	Bending Stress	Bending Strain (μin./in.)	Wet a	Dry b	Bending Stress	Bending Strain (μin./in.)
a	7.5	+10.9	-10.68	10.79	1,439	-26.63	+26.2	-26.415	3,522
b	6.7	+ 5.87	- 5.69	5.78	863	-14.35	+14.02	-14.185	2,117
d	7.5	+ 2.54	- 2.36	2.45	327	- 7.32	+ 7.05	- 7.185	958
f	6.7	- 0.76	- 0.58	-.09	13	- 0.49	- 0.87	.19	28
g	6.7	- 1.97	- 0.49	-.74	110	+ 0.49	- 2.91	1.7	254
h	6.7	- 3.49	+ 0.69	-2.09	312	+ 4.34	- 6.9	5.62	839
i	6.7	+ 1.03	- 0.92	.975	146	- 3.78	+ 3.81	-3.795	566
j	7.5	- 1.71	- 0.57	-.57	76	+ 0.49	- 2.69	1.59	212
k	6.7	+ 3.28	- 3.15	3.215	480	- 8.71	+ 8.68	-8.695	1,298
l	7.5	- 1.46	- 0.02	-.72	96	+ 1.07	- 2.45	1.76	235
n	9.4	+26.05	-26.45	26.25	2,793	-58.54	+57.13	-57.835	6,153
p	9.4	- 6.53	- 1.07	-2.73	290	+ 1.16	- 8.8	4.98	530
q	9.4	+ 5.19	- 5.06	5.125	545	-13.54	+13.58	-13.56	1,443
r	7.5	- 2.02	- 0.74	-.64	85	+ 0.21	- 2.92	1.565	209
s	9.4	- 1.69	- 0.97	-.36	38	- 0.55	- 2.11	.78	83

34
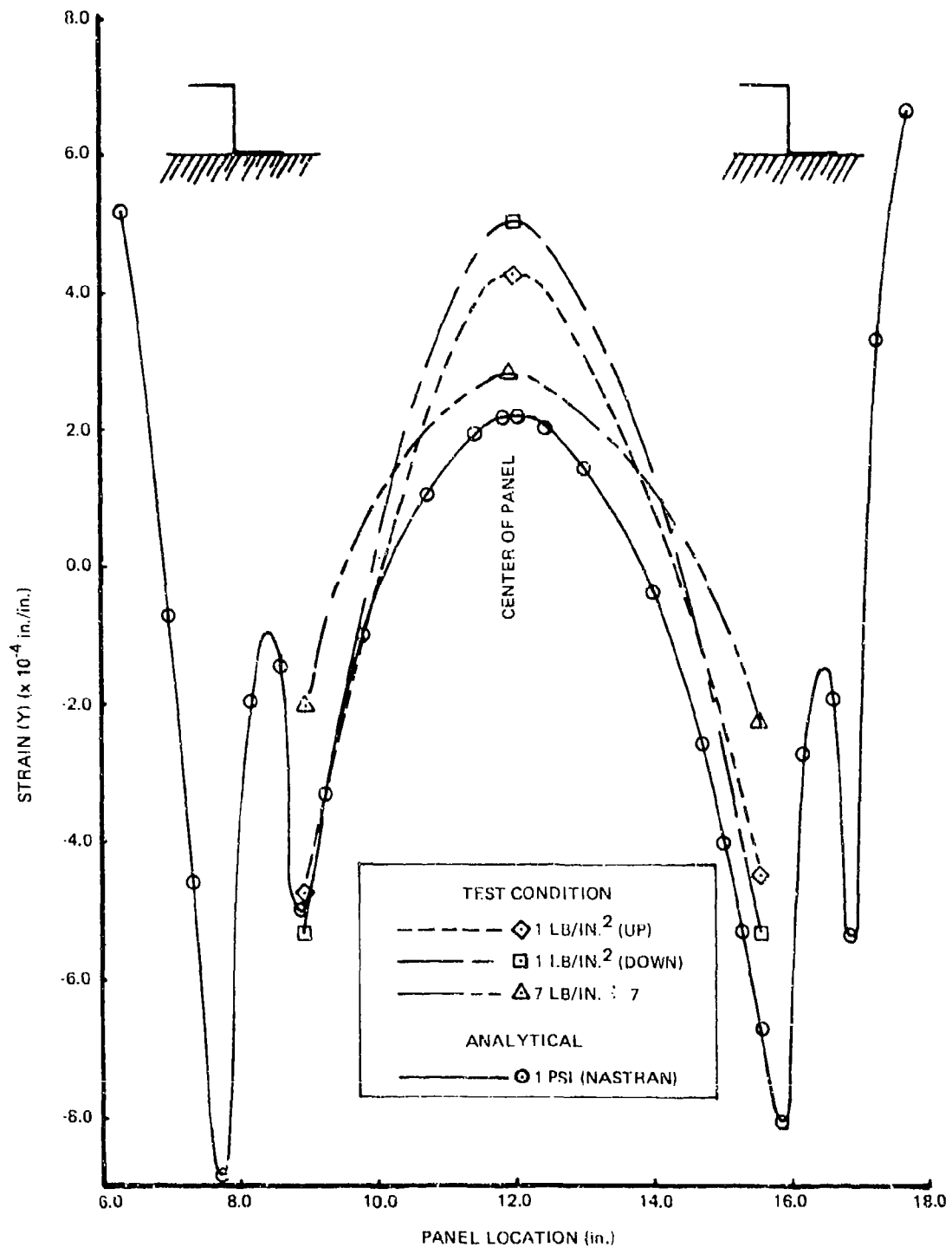
Figure 6. Comparison of Test and Analytical Static Strain (y)
Distributions for Panel d (Z Type Stiffeners)

35

The analytical results gave a corresponding ratio of 2:1, which is a more reasonable ratio. The sonic fatigue test results gave ratios a little less than 2:1. Thus, the static result seems inconsistent with both the analytical and the sonic fat_ue test results, in addition to appearing to be less logical. Conversely, the static test results showed the edge stresses to be approximately 85 percent to 90 percent of the center bay stresses, whereas the analytical results showed the same edge stress to be approximately three times the corresponding center stress.

Under fully-fixed edge conditions, the edge stress should be twice the center stress, thus the static test result appears more logical. The sonic fatigue test results showed a corresponding ratio very close to the static test results. It is surprising that the analytical results would produce a higher stress ratio between the edge and center stresses than one would obtain under fully fixed edge conditions. In summary, the static test gave a logical relationship between center and edge stresses, but an unexplained relationship between biaxial stresses at the panel center; whereas the finite-element results gave a logical relationship between the center panel biaxial stresses, but a surprising relationship between center and edge stresses. The sonic fatigue test results, which are more typically plagued with inconsistencies, gave logical relationships for both biaxial and center-to-edge stress ratios.

A set of analytical results was generated using a J type stiffener in place of the Z stiffeners, for stiffener design comparison purposes. Since the stiffeners in this program were adhesively bonded to the skins, the J configuration offers twice the bonded footprint area on the skin than does the Z configuration.

The static analysis utilizing the J stiffeners was accomplished in much the same way as with the Z stiffeners. Portions of the previous finite-element models were utilized, except for areas near the stiffeners which were modified to incorporate the additional flange of the J design. Identical boundary conditions from _he 2-inch coarse grid model were used

36

and a unit pressure load was again applied. The results for panel "b" are
shown in Figure 7. As expected, the stress distributions for the two
stiffener designs are quite similar across the majority of the panel, with
the J stiffener effecting a 20 percent stress reduction at the panel
center. The major difference occurs at the panel edge, where the
additional attach flange of the J stiffener significantly reduces the peak
stress by avoiding the abrupt stiffness change at the attach radius of the
Z stiffener.

    d. Dynamic Analysis - The dynamic analysis of the sonic fatigue
panel configurations in this program required the construction of finite-
element models to represent a quarter of each panel array. The primary
purpose of the analysis was to determine the natural frequency and
corresponding mode shape of the fundamental in-phase stringer-bending mode
for each panel configuration. The quarter model (shown in Figure 3)
limits modal solutions to those that are symmetric or antisymmetric about
the panel array center lines, thereby excluding certain intermediate modes
that are not of interest to this program. The quarter model does,
however, cover all the bays in one quadrant, thereby facilitating the
identification of a stringer-bending mode in which all bays vibrate
in-phase. Skin members were represented by the NASTRAN plate element
"CQUAD2." Stringer and frame members were intially represented by bar
elements.

Problems were encountered in identifying an in-phase stringer-bending mode
for certain panel configurations, particularly those panels having greater
stiffness due to curvature and/or close stringer spacing. In such cases,
the response was dominated by deflections of the substructure to the
extent that computed frequencies were not responsive to changes in skin
thickness. In addition, it was not possible to distinguish between
overall panel-array modes and coupled "bay" modes. Such structural
behavior would be typical of panels having inadequate stiffening members,
incapable of properly serving as panel breakers. However, both the static
model results and measurements made during sonic fatigue testing showed

37
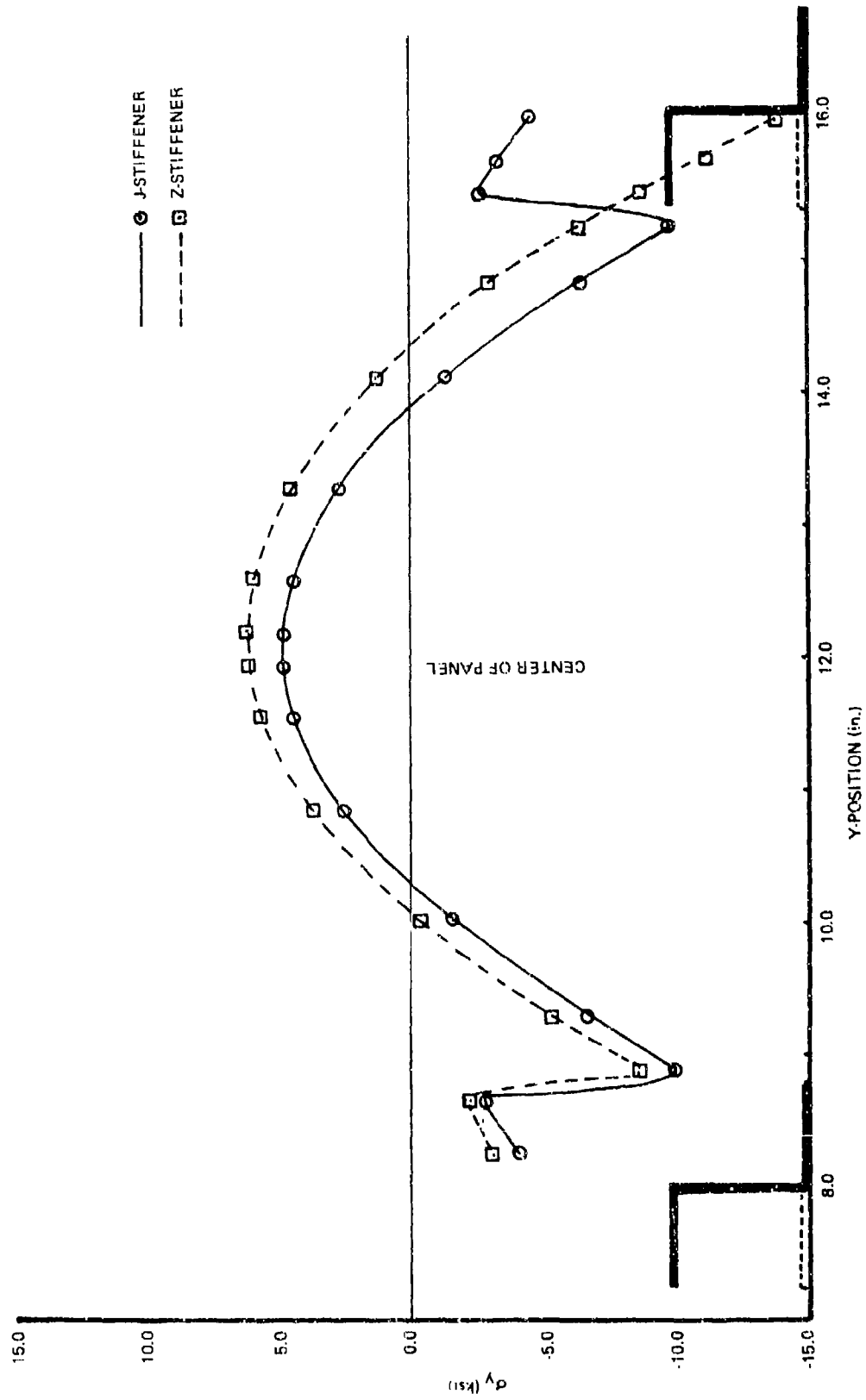
Figure 7. Comparison of Static Stress Results Between J and Z Type Stiffeners for Panel b

38

the stiffening members to be adequate and to properly break up the overall panel arrays into their individual bays. This modal identification problem was therefore assumed to be related to the finite-element models, the NASTRAN plate elements or even fundamental analytical problems associated with finite-element techniques. This type of problem is not confined to this program. Previous sonic fatigue programs have reported[2] similar difficulties regarding the dominant behavior of substructure in the dynamic analysis of skin stringer structures using finite-element techniques. The problem is compounded in curved panels by the inherent limitations of flat finite-elements to represent highly curved structures. NASTRAN does have available curved plate elements. However, advice from several sources, including AFFDL, cautioned against using them.

Various attempts to solve the problem were undertaken. NASTRAN has three dynamic solution methods available: "Inverse-Power," "Givens" and the "Determinant Method." The "Inverse-Power" method was being used when the modal identification problem was encountered. The other two methods were consequently tried; however, the results from all three methods were strikingly similar. Many of the mode shapes obtained during this exercise were observed to be similar to those generated in Reference 2.

Finite-element methods and computer programs such as NASTRAN are known to experience mass conditioning problems when analyzing thin sheets reinforced with relatively massive stiffeners. This aspect of the problem led to using dynamic models similar to the coarse grid quarter models used in the static analysis, combined with representing the stiffeners as plate elements as in the fine grid three-dimensional models used in the static analysis. This resulted in a significant improvement in the generation of the in-phase stringer-bending mode for all but the two 30-inch curved panels (f and s). These two panels failed to generate recognizable in-phase modes. Other panels that had previously failed to generate this mode (d, i, j, l and r) now produced an in-phase mode, but with excessive stiffener deflections and at unreasonably low frequencies. The

compatibility of test frequencies with fully fixed frequencies, calculated using Reference 5, confirmed that the problem was with the finite-element analysis results. Figures A-19 through A-24 in Appendix A show six of the ten models.

A further refinement of the model was then made. Previously, the stiffener skin interface had been modeled with a series of single elements whose properties were composed of an homogeneous superimposition of the individual skin and stiffener flange properties. It was thought that the interface between the massive stiffener element and the thin skin element could be the source of mass ill-conditioning. These areas were therefore remodeled with the frame and skin elements individually represented. Connection between the two was provided through the use of multipoint constraints (MPC) that enforce displacements of equal magnitude, normal to the panel, for pairs of adjacent grid points. This required some resequencing of grid points, which resulted in a significant increase in the stiffness matrix bandwidth. The problem was overcome by using a preprocessor program that resequenced the grid numbering. The results from this effort were disappointing, however, with no improvement in the dynamic response of the problem panels.

Another area of concern in the dynamic analysis was the sensitivity of the results to the boundary conditions applied to the test panel fixture frame. During sonic fatigue testing, both steel and aluminum frames were used on selected panels. Also, changes were made in the elastic restraining forces acting on the panel-fixture assembly. Neither of these variations influenced the dynamic response of the test panels. However, the analysis results were found to be highly dependent upon such variations. It was also noted that the fixture frame had much greater predicted deflections from the analysis than occurred during testing. The reasons for this inconsistency are not known. It was decided to reduce the influence of these boundary conditions and the fixture displacements by modifying the finite-element models to eliminate the out-of-plane motion of the fixture. This resulted in changes in response frequencies,

40

but did not clarify the modal identification problems. The final dynamic results were generated with this fixture motion eliminated.

Although some analytical difficulties remained unsolved, the majority of the panels produced well defined in-phase stringer-bending modes, many of them occurring in the expected frequency range. Figures A-25 through A-28 in Appendix A show the first four mode shapes for panel "b." The frequency progression of these four modes is interestingly consistent with the elastic properties of the panel and its boundary conditions. The bay having the maximum response is seen to shift in turn from that of least fixity (center bay), to that bay with one short side restrained, to that with one long side restrained and finally to that bay with two sides restrained (corner bay), with increasing frequency. It is also clear that Figure A-25 is the desired in-phase stringer-bending mode, occurring at 171 Hz. A list of the complete set of dynamic solutions is given in Table 12. No solutions are offered for panels "f" and "s." The first four modes obtained for panel "f" are shown in Figures A-29 through A-32 in Appendix A. The first modes are first order modes within each bay, but all contain a combination of in-phase and out-of-phase components. The fourth mode (Figure A-32) shows the first of the second-order modes. One last attempt was made to force a first-order in-phase mode by forcing an in-phase displacement at the center of each bay. Under this condition the model did not generate a solution (no roots were found). This confirmed that the desired mode was not simply being missed in the modal search procedure, but was actually nonexistent within the analytical framework presented here.

Early in the program, finite-element models were constructed to represent the shaker specimens. The purpose of these models was to ensure that the shaker specimens were designed to fall within the test envelope of the shaker to be used and to avoid having shaker test specimens with torsional and bending modes too close together. It was important in the shaker test program to avoid exciting torsional modes. This analysis also served as an indication of the accuracy with which NASTRAN, combined with the

TABLE 12
TABULATED RESULTS OF NATURAL FREQUENCY SOLUTIONS

Panel	Panel 1st Bending Frame Free (In-Phase)	Panel 1st Bending Frame Fixed (In-Phase)	Panel 1st Torsion Frame Free	Panel 1st Torsion Frame Fixed	Panel Description
a	139	-	-	-	3 x 3 Flat
b	171	-	177	-	3 x 3 Flat
c	179	-	187	-	3 x 3 Flat
d	-	246	271	275	3 x 3 Flat
f	-	-	464	463	3 x 3 R = 30
g	398	-	285	-	3 x 3 R = 60
h	318	-	236	-	3 x 3 R = 90
i	-	305*,332*	570	570	6 x 3 Flat
j	-	341	611	612	6 x 3 R = 90
k	302	276	312	312	4 x 3 Flat
l	347*	317*	520	520	4 x 3 R = 90
n	94	-	-	-	3 x 3 Flat
p	219	-	160	-	3 x 3 R = 90
q	-	299	330	353	6 x 3 Flat
r	-	348*	-	483	6 x 3 R = 60
s	-	-	372	350	4 x 3 R = 30

*Significant Stringer Movement

laminate properties generated by the COMPOSITE program, would represent the composite laminates used on this program for the sonic fatigue test panels. Figure 8 shows the finite-element model used to represent the shaker specimens. Table 13 gives the first four plate bending modes for the shaker specimens described in Section III. Hand calculated values using Den Hartog[14] are shown for comparison. The hand calculated values assume the zee stiffener to represent a fully-fixed support, resulting in slightly higher values than the first anti-phase mode. The fact that the first in-phase mode frequencies are higher than the hand calculated values is probably due to stiffening effects of the zee along its attach flange, which effectively shortens the length of cantilevered skin. Figure 9 shows the first six modes for shaker specimen type 2. In the shaker specimen analysis, the term "torsion" refers to the skins twisting out-of-plane and not to stringer torsion. These results show the torsion and bending modes well separated. Table 14 shows a comparison of the first four skin bending mode frequencies with measured values on the shaker table. The relatively close agreement between measured and calculated values even for the higher order modes is indicative of a sound analytical approach.

This early optimism turned out not to be fully justified when analyzing the more complex multi-bay panels, as discussed earlier in this section.

This concluded the dynamic analysis using the finite-element models. Because of the progressive underestimation of computed frequencies with increasing panel stiffness, these computed frequencies are thought to be unsuitable for use in developing a sonic fatigue design method. In order to present alternative frequency prediction techniques, some additional dynamic analysis was performed and the results are presented in Section II.6.
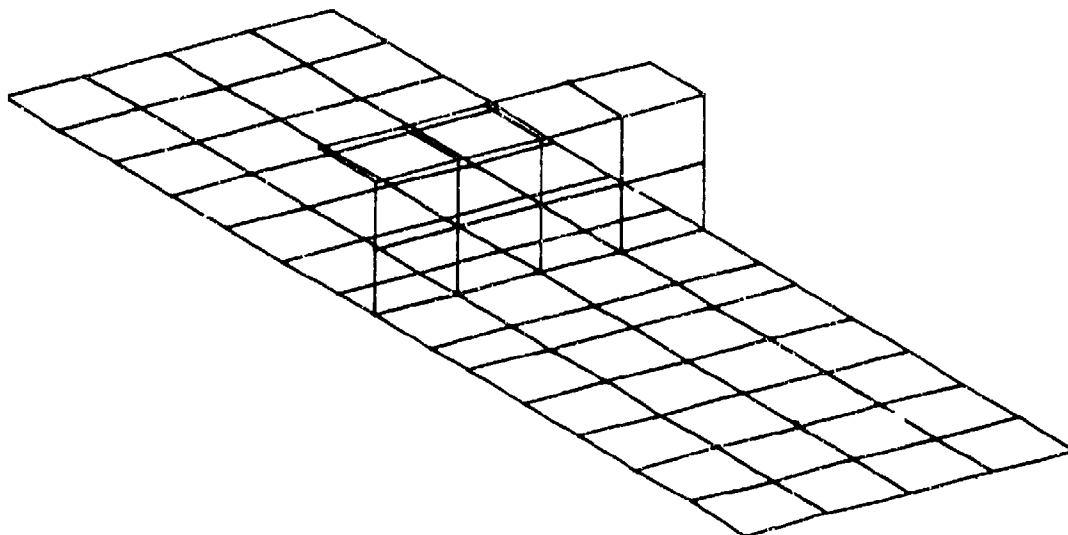
Figure 8. Finite Element Model for Shaker Specimens

TABLE 13

NATURAL FREQUENCIES OF SHAKER TEST SPECIMENS

Panel Number	NASTRAN Generated Frequencies (Hz)				Hand Calculated Frequencies (Den Hartog)
	Anti Phase Modes		In Phase Modes		
	First	Second	First	Second	
1	40	254	61	346	49
2 & 6	58	352	77	438	62
3	56	366	89	505	74
4	81	507	122	692	97
5	73	399	74	455	77
7	33	203	45	253	36

44

Panel Configuration (Not to Scale)

Mode Shapes (Not to Scale)

No. 1   Plate Bending (f = 58 Hz) - First Anti-Symmetric Mode
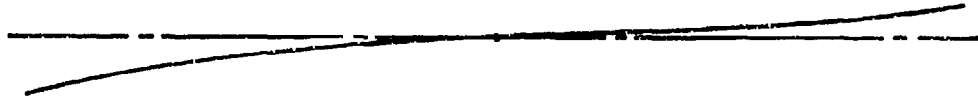
No. 2   Plate Bending (f = 77 Hz) - First Symmetric Mode

No. 3   Plate Torsion (f = 220.5 Hz)
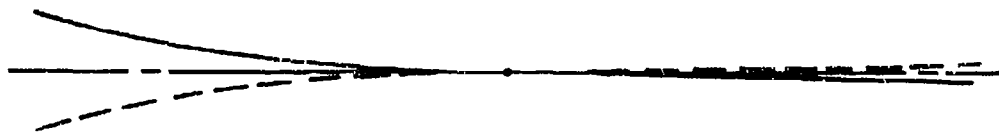
No. 4   Plate Torsion (f = 352 Hz)

No. 5   Plate Bending (f = 438 Hz) - Second Anti-Symmetric Mode
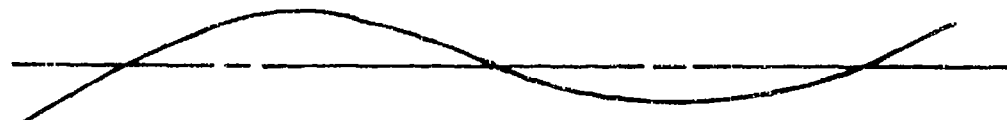
No. 6   Plate Bending (f = 423.4 Hz) - Second Symmetric Mode

Figure 9.   Mode Shapes of Shaker Specimen No. 2

45

TABLE 14

COMPARISON OF MEASURED AND CALCULATED FREQUENCIES
FOR SHAKER SPECIMEN TYPE 2

Mode Shape	Calculated Frequencies (Hz) Original Model	Measured Frequencies (Hz)
First anti-phase	58	65
First in-phase	77	91
Second anti-phase	352	443
Second in-phase	438	534

6. ADDITIONAL FREQUENCY ANALYSIS

Because of the unresolved difficulties with the dynamic analysis using finite-element techniques, it was decided to generate a set of solutions for the in-phase stringer-bending mode, using a set of equations developed by Lin[8]. Lin's approach utilizes differential equations applied to a row of continuous panels. By treating the skin and stringers as integral parts of the structure, the method utilizes stringer properties in addition to skin properties, thereby facilitating accurate comparisons between different stringer properties and designs. Differential equations are used to represent flat and curved panels. The flat panel equation is derived from a well known fourth order equation of motion, applying Levy's[15] solution and appropriate boundary conditions to develop the following equation for the frequency of the in-phase stringer-bending mode:

$$k_1 \sinh \frac{k_1}{2} \left\{ \left[E_b I_n \left(\frac{m\pi}{\ell} \right)^4 - p_b A \omega_m^2 \right] \cos \frac{k_2}{2} - 2 \frac{D}{b^3} k_2^3 \sin \frac{k_2}{2} \right\}$$

$$+ k_2 \sin \frac{k_2}{2} \left\{ \left[E_b I_n \left(\frac{m\pi}{\ell} \right)^4 - p_b A \omega_m^2 \right] \cosh \frac{k_1}{2} \right.$$

$$\left. - 2 \frac{D}{b^3} k_1^3 \sinh \frac{k_1}{2} \right\} = 0 \qquad (14)$$

46

where

$$k_{1_p} = b_p \left[\omega_m \left(\frac{h_p \rho_p}{D_p} \right)^{1/2} + \left(\frac{m\pi}{\ell} \right)^2 \right]^{1/2} \tag{15}$$

$$k_{2_p} = b_p \left[\omega_m \left(\frac{h_p \rho_p}{D_p} \right)^{1/2} - \left(\frac{m\pi}{\ell} \right)^2 \right]^{1/2} \tag{16}$$

and

A	=	cross-sectional area of stringer
D	=	bending stiffness for skin, $Eh^3/12(1 - \nu^2)$
E	=	modulus of elasticity of skin material
E_b	=	modulus of elasticity of stringer material
I_n	=	moment of inertia of stringer cross section
m, n	=	positive integers
ω_m	=	natural frequency for flat continuous panels, radians/sec
t	=	time, sec
b	=	width of individual panel
h	=	thickness of skin
ℓ	=	length of individual panel
ρ	=	mass density of skin material
ρ_b	=	mass density of stringer material

The curved panel solution is obtained by expressing the strain and kinetic energies in terms of generalized coordinates. The equations of motion are then derived by a Lagrangian formulation.

The results of this analysis are shown in Table 15. For convenience, frequencies calculated from AGARD design nomographs[5], the finite-element models, Lin's equations[8], and the sonic fatigue tests are all presented for comparison purposes. It is not known why Lin's equations failed to generate solutions for panels "j" and "l." It is interesting to note that Lin's equations gave unexpectedly high frequency values for the 30-inch curved panels (f and s); the same two panels for which the finite-element

47

TABLE 15
COMPUTED AND MEASURED NATURAL FREQUENCIES

				Frequencies (Hz)			
Configuration	Skin Thickness "t" (in.)	Stringer Spacing "b" (in.)	Radius of Curvature "R" (in.)	Agard[5] Fully Fixed	Nastran	Lin[8]	Test
a	.033	8	Flat	160	139	151	143
b	.044	8	Flat	202	171	177	170
d	.066	8	Flat	308	246	281	340
f	.044	8	30	825	-	1,208	505
g	.044	8	60	510	398	583	350
h	.044	8	90	375	318	363	290
i	.044	4	Flat	674	332	558	800
j	.044	4	90	824	340	-	950
k	.044	6	Flat	312	302	292	380
l	.066	6	90	631	347	-	680
n	.022	8	Flat	120	94	101	140
p	.022	8	90	377	219	447	180
q	.022	4	Flat	409	299	363	370
r	.033	4	60	782	348	442	780
s	.022	6	30	828	-	1,366	380

analysis failed to generate solutions. It is also interesting to note that of the three sets of calculated frequencies, the AGARD nomograph results showed the best correspondence to the test results.

SECTION III
EXPERIMENTAL

1. INTRODUCTION

The purpose of the experimental program was to provide the empirical data base for the design method described in Section IV. This phase of the program consisted of designing and fabricating a range of shaker test beam specimens and "progressive-wave tube" (PWT) multi-bay test panels. The multi-bay panels covered a range of stringer spacings, skin laminate thicknesses and radii of curvature typical for aircraft application. The configurations are shown in Table 1. They were instrumented with strain gauges and microphones and their response characteristics measured over a wide range of sound pressure levels, before being tested to failure. The shaker tests augmented the PWT tests by providing additional random fatigue data for the composite skin laminates used in the multi-bay panel designs.

2. TEST SPECIMEN AND FIXTURE DESIGN

a. Progressive-Wave Tube Test Panels — Twenty-seven multi-bay test panels, comprising eighteen configurations, were designed and fabricated for subsequent sonic fatigue testing in a progressive-wave tube. Seven of the configurations had duplicate panels and one configuration (m) was a reference panel. The reference panel provided a data link to a set of existing Rohr test panels, which were also tested in this program.

49

These existing panels included an aluminum skin-stringer panel to provide a data link between graphite and aluminum panels. The configurations of the new panels are listed in Table 1. They comprise flat and curved graphite-epoxy skins, ranging from 4 ply (.022") to 12 ply (.066"), stiffened with adhesively bonded graphite-epoxy Z stringers and longerons in 3 x 3, 4 x 3 and 6 x 3 panel arrays. One configuration (e) had honeycomb beam stiffeners and two configurations (b and c) had additional panels fabricated with J stiffeners, thus facilitating a comparison between different stiffener designs. Figure B-1 in Appendix B shows engineering drawings of the test panels.

The overall test panel size was kept constant (24-inch by 36-inch) in order to minimize tooling and test fixture costs. Ten of the configurations consisted of nine 8-inch by 12-inch equal size bays in 3 x 3 arrays. Ten configurations were flat and eight were curved, with radii of curvature of 30-inch, 60-inch and 90-inch. These curvatures encompass radii ranging from small aircraft nacelles through to wide body fuselages. Five different skin laminates were used, two of which (b and c) had the same number of plies but with different orientations. This served to isolate the effects of ply orientation for a given number of plies. With the exception of the reference panel (m); 4-inch, 6-inch and 8-inch stringer spacings were used in 6 x 3, 4 x 3 and 3 x 3 arrays respectively. Panel e had honeycomb beam stiffeners, utilizing a nonmetallic core material. This is a lightweight, low cost stiffening concept whose sonic fatigue resistance relative to the more conventional Z stiffeners is of considerable interest. Thus, with 27 panels, a comprehensive range of design parameters were covered, with duplicate panels of some configurations provided to check test repeatability and to provide more reliable fatigue data points. The panel parameters (stringer spacing "b," laminate thickness "t" and radius of curvature "R") were varied such that any two panel responses can be related by varying one parameter at a time, thereby facilitating a quantitive identification of the parametric cause of the difference in response.

50

The reference panel (m) comprised a single row of bays, duplicating the panel geometry of the five existing Rohr panels, shown in Figure B-2 in Appendix B. Panels 1 and 5 provide a direct comparison between aluminum and graphite multi-bay structures. Panels 2 and 3 are identical unstiffened graphite panels, representative of a current nacelle structure in commercial service on an experimental basis. Panel 4 had a single honeycomb stiffener.

b. Stiffener Design -- Three types of stiffeners were evaluated in this program; graphite epoxy Z and J section stiffeners and honeycomb beam stiffeners with graphite reinforced caps. The program concentrated on the Z stiffeners which are widely used on aircraft structures. The J stiffeners were included because of their ability to reduce edge stresses (compared to a Z) for minimal cost and weight increase. In aluminum structures, Z stiffeners are inexpensively formed, whereas J stiffeners have to be more expensively extruded or machined. In graphite structures, however, both stiffener types are similarly fabricated. Consequently, the J section is a more cost effective design in graphite than in aluminum. The honeycomb stiffeners, as mentioned earlier, were included for their low cost and low weight advantages.

Stiffener details are shown in Figure B-1. The Z and J stiffeners were constructed from $\pm$ 45 deg. graphite epoxy laminates with unidirectional fibers buried in the free flanges. The number of $\pm$ 45 deg. laminates were varied from configuration to configuration in order to provide the appropriate stiffnesses for their respective skins. The Z stringers were 1-inch deep and the longerons were 1-1/2-inch deep. Their stiffnesses were designed to ensure that they effectively served as panel breakers. This was accomplished by using Reference 8 to calculate their fundamental in-phase stringer-bending mode frequencies, and comparing the results with corresponding fully-fixed frequencies of individual bays calculated using Reference 5. If the stiffeners have adequate bending stiffness, the frequency of the stringer-bending mode will approach the fully-fixed value. The results of this comparison can be seen in Table 15, and show

51

the Z stiffeners to be effective. At stringer-longeron intersections, continuity of the attached and free flanges was maintained for both stringers and longerons. The webs of the stringers were also continuous and were clipped to the webs of the longerons, which were partially cut away. Titanium clips are shown in Figure B-1. These were later changed to steel following some clip failures during the first sonic fatigue tests. For the honeycomb stiffeners, the intersections consisted of honeycomb core splices with a foaming adhesive locally applied. The graphite caps were continuous. At the edges of the panels, the attach flanges of the stiffeners extended under the test fixture frame and the upstanding stiffener webs were clipped to the fixture web. Figure 10 shows a photograph of a honeycomb beam stiffened panel. Examples of zee stiffened panels are shown in Figures 29, 30 and 31. For cross reference purposes with Section II of this report, the stringers run in the X-direction and the longerons in the Y-direction.

c. Progressive-Wave Tube Fixture Design -- The test panels were terminated by relatively stiff channel sections, shown in Figure B-1. There were two fixturing approaches considered in this program. One was to bolt a picture frame/panel assembly rigidly to the progressive-wave tube (PWT). The other was to suspend a stiff picture frame/panel assembly on captive wires. The former approach more closely approximates fully-fixed edge conditions, which is more convenient when the test results are to be compared to simplified analyses where fixed edges are usually assumed. This approach has the disadvantage of the panel response being affected by vibrations in the PWT itself. The latter approach eliminates any response interference from the PWT and allows the fixture to be accurately represented in the finite-element models. Since the fixture is constrained only spatially in the PWT, its boundary conditions are able to be accurately represented in the analysis. The latter approach was chosen for this program. An additional advantage of this approach was that it was a relatively simple matter to remove a panel from its frame and thereby make response measurements under two different boundary conditions, in order to evaluate their effects. A set of steel frames was
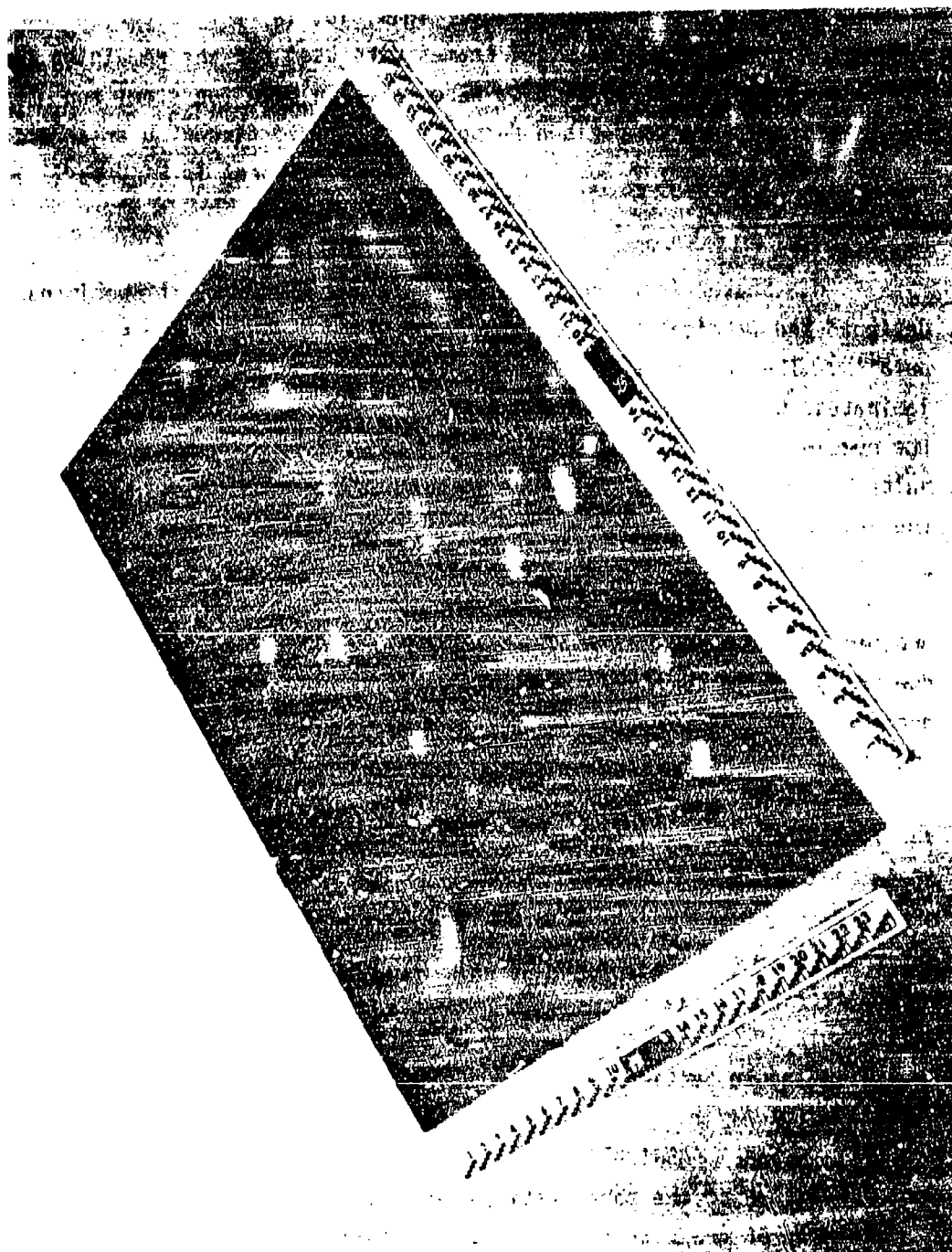
Figure 10. Honeycomb Beam Stiffened Panel (e)

53

added to the program as back-up fixturing should the aluminum frames experience any sonic fatigue damage. This did, in fact, occur on one of the curved panels, and the steel frames were used for the remaining curved panels. Some panel response data were taken in both tne steel and aluminum frames for comparison purposes. The test fixturing arrangement is discussed further in Section III.5, and can be seen in Figures 22 and 24.

d. Shaker-Test Specimens -- Eighty-one shaker test specimens were designed and fabricated. Figure B-3 in Appendix B shows the specimen details. The specimens consisted of 3-inch by 10-inch sections of skin laminates, with stringer sections attached across the short dimension. The specimens represented each skin-stiffener combination used on the multi-bay test panels. A set of specimens having the stringer riveted to the skin was included to provide for a fatigue life comparison with bonded joints. The shaker specimens were intended for fatigue testing the skin-stringer joints in order to develop fatigue curves to augment the progressive-wave tube test results. This objective was not fully realized due to some adhesive bonding quality problems encountered early in the program. These problems and their effects are discussed in Sections III.3 and III.4.

The fixturing for the shaker tests was originally a simple tee section, 15-in. long, accomodating five specimens at a time. The upstanding webs of the Z stringers were mechanically fastened to the upstanding leg to the tee. The assembly was then simply bolted to the shaker table for testing. This fixturing was later changed when the shaker test program was modified as a result of the adhesive bonding problems mentioned above. The changes are discussed in Section III.4.

3. TEST SPECIMEN FABRICATION

Fabrication of the sonic fatigue test panels involved the manufacture and assembly of graphite epoxy skins and stiffeners fabricated from Hercules AS-3501 Pre-Preg. The skins were laid up and cured, on a flat or

54

curved tool as appropriate, from 12-inch wide graphite tape. Each ply was oriented with respect to a reference direction in order to build up the desired panel stiffness properties. After cure of the skin, the stiffeners were attached in a secondary bond cycle using 3M's AF147 adhesive.

The Z and J stiffeners were laid up and cured on a separate tool. Layup of these stiffeners included $\pm$ 45 deg. plies, from the flanges through the web, for shear stiffness and strength. Additional unidirectional fibers were added to the free flanges of the stiffeners for bending stiffness and strength. Following adhesive bonding assembly with the skin, the stringer-longeron intersections were stabilized with angle clips, which were mechanically fastened in place.

For the sandwich stiffened panels, the stiffeners were fabricated in place on the skins by cocuring the core-to-skin and cap-to-core bonds simultaneously with the cure of the cap. Since the longerons utilized deeper core than did the stringers, the caps for both were continuous across the intersections. The only tie then required at the intersections was a foaming core splice adhesive, cocured with the remainder of the stiffeners as described above. Fiber orientation in the caps was primarily unidirectional.

All panels required an edge buildup to allow for mechanical fastening in the test fixture. This was accomplished as part of the layup and cure of the panel skins. Provisions were also made for attachment of the ends of the stiffener webs to the fixture.

Fabrication of the shaker specimens was basically the same as for the sonic fatigue test panels. For the shaker specimens, however, it was more efficient to fabricate several large panels and subsequently cut them into the required size for the individual specimens.

55

A quantity of 25 basic tools plus 2 rate tools were designed and fabricated. Tooling for the shaker specimens was minimal, with only two assembly bond jigs and one Z section layup tool required. The flat sonic fatigue panels required eight tools. The remaining 16 tools were for the curved panels.

Figures 11 through 17 show photographs of the tools and layup. Figure 11 shows the bond jig for the zee layup. The zees were made by cutting hat sections in half. The beam in the center of the tool is for the hat layup. Around the edge of the tool is a rubber tube bonded in place with RTV. This acted as a vacuum seal for the rubber bag (Figure 13). Figure 12 shows the same tool with the graphite-epoxy fabric laid down for the hat section. Figure 13 shows the tool with the silicone rubber bag in place. This was a reusable bag, which effects cost savings and improves laminate surface condition, as compared to using disposable bags. Figure 14 shows a pair of cured hat sections. Figure 15 is an assembly tool, which was used to locate the zees on a skin laminate. The two beams, when bolted down, locate the zee section. Figure 16 is the corresponding locating tool for the honeycomb stiffeners. Figure 17 shows a layup of graphite/epoxy prepreg for the skin elements.

Coupon tests were performed on each layup to determine resin content, density, fiber content and void content. Two 1-inch square coupons were used for each layup. Ultrasonic C-scans were performed on each specimen to check for bondline voids.

During specimen fabrication, problems were encountered in two areas. The first problem occurred in the layup of the zee stringers and longerons. The bond tool failed to generate adequate pressure in the zee radius to be adjacent to the skins. As a result, this radius had sporadic areas of surplus resin and resin starvation. This bond pressure deficiency resulted in inadequate interlaminar strength. In addition, excess resin areas are prone to surface cracking, which in turn can result in premature fatigue crack initiation under the kind of severe test conditions for

56

Figure 11. Bond Jig for Z Layup

Figure 12. Bond Jig with Hat Section in Place

58
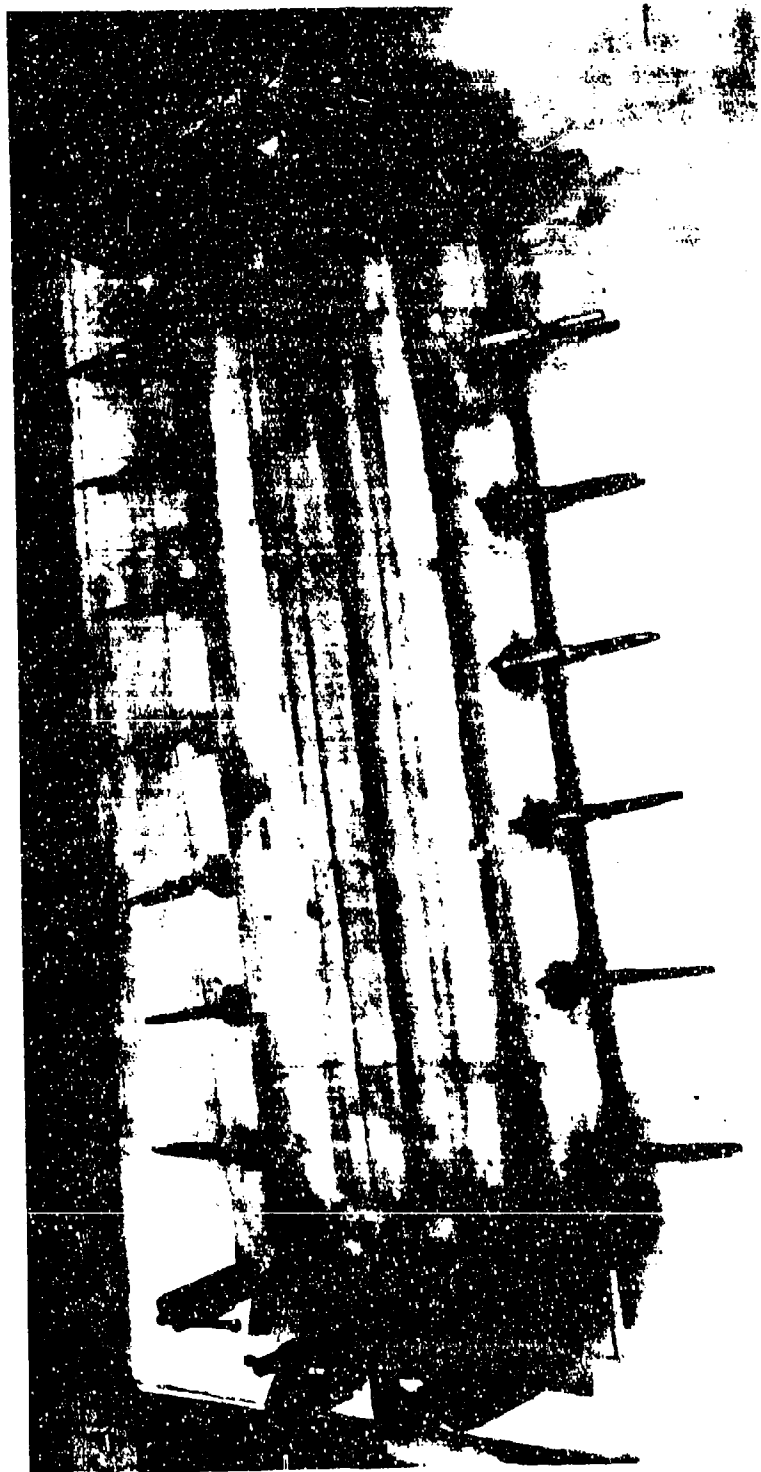
Figure 13. Bond Jig with Bag in Place

59

Figure 14. Cured Hat Sections

60
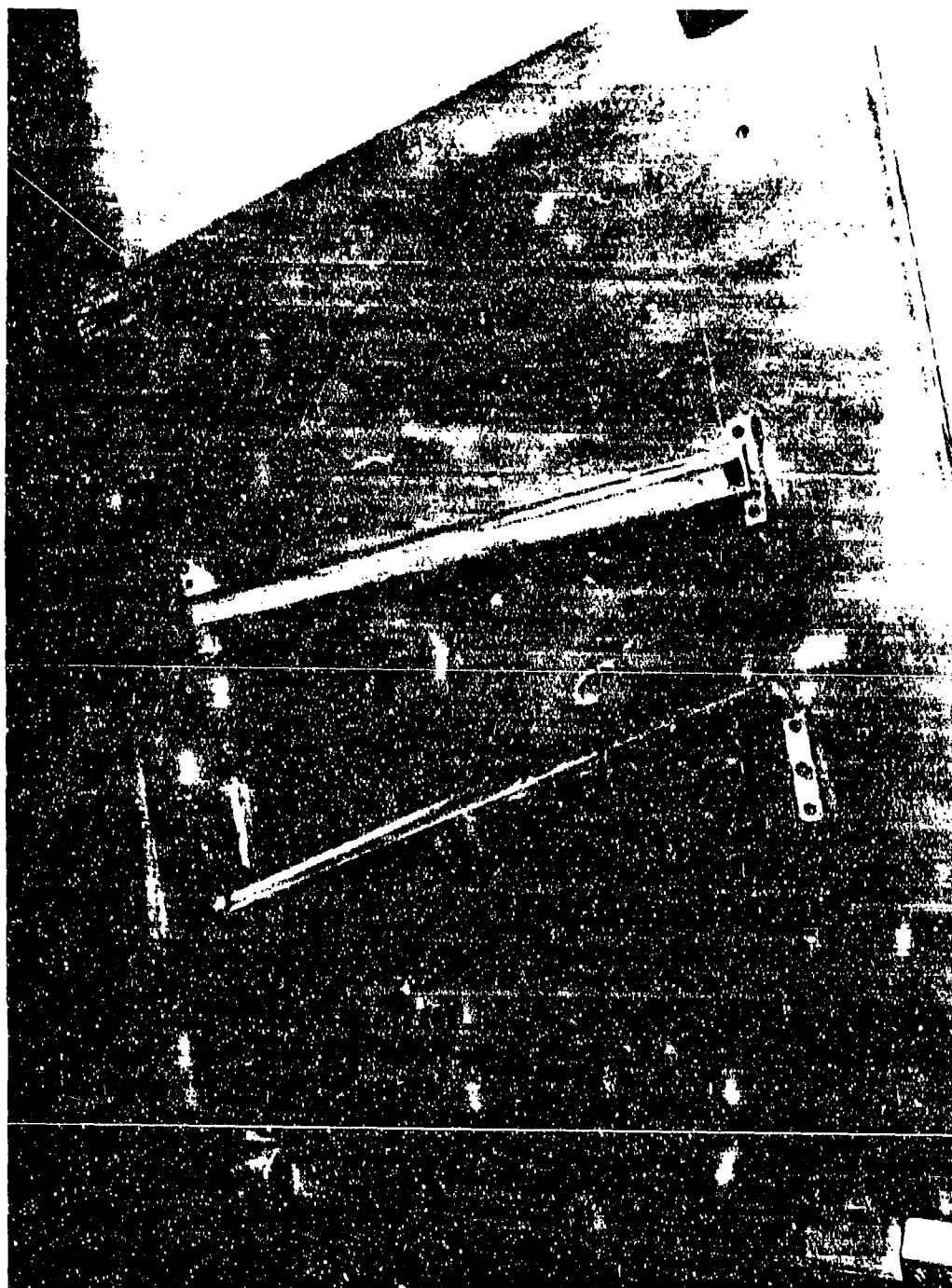
Figure 15. Locating Tool for Zee Stiffeners

Figure 16. Locating Tool for Honeycomb Stiffeners

Figure 17. Layup of Graphite Epoxy Skin

63

which these specimens were intended. Although there were no reliable
criteria for the strength requirements in the stiffener radii, the fact
that zee stiffeners are not symmetrical sections and can be expected to
experience some rotation under random acoustic loading conditions, led to
them being rejected as unsuitable for sonic fatigue testing. The bond
tool was then modified to provide more effective throw-in blocks in the
radii, and a set of good quality stiffeners was then fabricated. Although
this problem did not affect the sonic fatigue test panels, some of the
shaker specimens had already been completed before the problem was
discovered. The effects that this problem had on some of the shaker test
results are discussed in Section III.4.

A second, and more serious, problem was discovered during the early shaker
tests. The first specimens tested (see Section III.5) experienced
premature failure in the adhesive joint between the stiffeners and the
skins. This caused considerable concern, since the fabrication of the
shaker specimens had been completed, and fabrication of the multi-bay
panels was in progress, with some of them already completed. Visual
examination of the failed adhesive joints revealed excessive porosity in
the adhesive. This type of porosity, consisting of a large number of very
small voids, does not show up on ultrasonic C-scans. In addition, there
was no graphite fiber pull-out around the failed joints. Fabrication of
the multi-bay panels was then suspended, and a thorough investigation of
the adhesive bonding problem as initiated. The investigation centered on
an examination of the bonding process, but also included a reevaluation of
AF147, the adhesive selected for this program. AF147 is a tough,
elastomeric adhesive with high peel strength. It is used extensively on
he F16 airplane and has good strength properties over the temperature
range for which graphite-epoxy structures are considered suitable. It is,
however, an adhesive that is particularly susceptible to moisture during
fabrication

The initial investigation of the bonding process and the condition of the adhesive revealed a higher moisture content than was considered acceptable. An additional batch of shaker test specimens was fabricated after additional storing of the adhesive in a dessicator in order to eliminate any moisture. Some of these specimens were statically tested by simply pulling the skin and stringer sections apart. A 10 percent increase in static strength was obtained, compared to the original shaker specimens. Comparative shaker tests were then carried out. Some riveted specimens were added to this comparative test, in order to provide a reference to which the bonded specimens could be compared. The results of this comparative testing were disappointing. Although the "dried" adhesive produced significant fiber pull-out upon failure, the fatigue life did not significantly increase. Table 16 shows the results.

As a result of this adhesive problem, and also because of the extreme importance of stiffener and skin laminate quality, a thorough investigation was carried out to determine the history and quality of all the sonic fatigue panel components and assemblies, including additional assessments of adhesive bond quality. The following tasks were performed:

(1) The weight percent of resin and void percent by volume of all skins were determined and tabulated. The results are given in Table 17. Acceptance criteria for this program required a resin content of 27 percent. Consequently, skins b_1 and c_1 were rejected. q was considered marginal at 26 percent. However, the flatwise tension tests performed on the rejected c_1 skin (see Item 3 below) produced good results, indicating that q was an acceptable laminate.

(2) Sections of Z stiffeners were cut, mounted and photographed. The zees made on the original tool were found to be resin rich. However, the zees used for the sonic fatigue test panels were found to be representative of production quality.

65

TABLE 16
SHAKER TEST RESULTS FOR ADHESIVE EVALUATION

Specimen (All type 2)	Overall RMS Stress Level (1b/in²)	Cycles to Failure
Riveted	7,370	234,000
Bonded - dried	8,040	3,000
Bonded - dried	6,432	6,000
Bonded - original	Gauge Lost	5,400
Bonded - original	9,179	5,400

TABLE 17
VOID AND RESIN CONTENTS OF SKIN LAMINATES

Skin	No. Plies	Average Resin (%)	Average Void (%)	Average Density (%)
a-1	6	28	.64	1.61
a-2	6	29	.47	1.60
b-1	8	24	1.20	1.63
b-2	8	31	-0-	1.61
c-1	8	24	1.29	1.63
c-2	8	29	.175	1.60
d	12	27	.31	1.63
e-1	8	33	.26	1.58
e-2	8	30	.21	1.60
f-1	8	31	.57	1.59
f-2	8	31	.46	1.59
g-1	8	29	.575	1.61
g-2	8	27	.79	1.67
h	8	29	.11	1.61
i	8	33	.03	1.58
j	6	27	.155	1.63
k-1	8	31	-0-	1.60
k-2	8	31	.765	1.58
l	12	29	.224	1.61
m	8	28	.16	1.62
n	4	28	1.37	1.60
p	4	27	.63	1.63
q	4	26	.58	1.62
r	6	29	.36	1.62
s	4	27	1.595	1.59

66

(3) Flatwise t \ision tests were performed on the rejected cl skin laminat.· an-l on a specially fabricated d (12 ply) laminate. The results are given in Table 18. They show the c laminate to have comparable strength to the d laminate, indicating the percent resin content criterion to be conservative.

(4) A range of shaker specimens were fabricated using different adhesives and different processes, for comparison with the original specimens. The adhesives used were AF147, the current selection, and FM1000. FM1000 is an older adhesive that has excellent strength properties and is easy to use. However, it is environmentally susceptible and is not widely used in production. It is, however, an excellent reference adhesive. Using two plies of AF147 was also evaluated. Table 19 shows the results of the static tests and Table 20 shows the shaker test results. The AF147 was found to have superior static strength, but FM1000 did better in fatigue. It was also clear that a second ply of AF147 resulted in a significant improvement in fatigue life.

Following the above tests, the failed static and shaker test specimens bonded with AF147 were found to have porosity uniformly dispersed in the weave pattern of the knitted fabric in the bond line. Additional testing was then performed in order to determine the cause of this porosity.

These tests included the comparative evaluation of (1) solvent wiping subsequent to grit blasting, (2) no solvent, just dusting with a clean dry cloth, (3) an evaluation of the amount of vacuum used during bagging and curing, (4) oven drying of composite details and glass cloth (used as air bleeder) and (5) evaluation of weight loss during oven drying. All of the above were evaluated through lap shear testing and visual examination of failure mode. Volatile contents determinations were also made. The results are given in Table 21. In the lap shear tests, Process 2 gave the highest failing stress, but more importantly, the bond line porosity was

67

TABLE 18
FLATWISE TENSILE TEST RESULTS ON SKIN LAMINATES

Specimens from Panel c-1 (Flatwise Tensile)

Specimen No.	Failing Stress (psi)
c-1-1	3480
c-1-2	3200
c-1-3	3310

NOTES: 1. Resin content 23.6% by weight, voids 1.29% by volume.

2. Specimens c-1-1 and c-1-2 failed between surface plies, Specimen c-1-3 failed approximately in the center of the laminate.

Specimens from Panel d Noted in Item 3
(Flatwise Tensile)

Specimen No.	Failing Stress (psi)
d-1	3200
d-2	3340
d-3	3180

NOTES: 1. Resin content 32.8% by weight, voids 0.21% by volume.

2. All failures occurred at the approximate center of the laminate.

TABLE 19

COMPARATIVE ADHESIVE EVALUATION - STATIC RESULTS

Failing Load (Lbs.)	Adhesive
220	Original Lot AF-147, dried (48 hrs.)
205	Original Lot AF-147, as received
168	Second Lot AF-147, Dried (120 hrs.)
206	Second Lot AF-147, 1 ply, dried
242	Second Lot AF-147, 2 plies, dried
186	FM-1000
200	Original Lot AF-147, cut from Panel c-1
202	Original Lot AF-147, cut from Panel c-1
220	Original Lot AF-147, cut from Panel c-1

TABLE 20

COMPARATIVE ADHESIVE EVALUATION - SHAKER TEST RESULTS

Time To Failure (Minutes)	Adhesive
125	FM-1000
37	AF-147, 1 ply, dried
63	AF-147, 2 plies, dried
29	AF-147 - original group

TABLE 21

AF-147 ADHESIVE PROCESSING EVALUATION

1. One-half inch Overlap Lap Shear Specimens (Adherends cut from Panel c-1).

Process	Avg. Failing Stress (psi)
1	3240
2	3430
3	3065

Process

1   Adherends grit blasted, wiped with MEK and air dried 30 minutes; 25" Hg vacuum used during bag check and cure.

2   Adherends grit blasted and wiped with clean dry cloth. Adherends and glass breather cloth oven baked at 150°F for 45 minutes. 10" vacuum used during bag check and panel vented to atmosphere during cure.

3   Same as Process 2, except 25" Hg vacuum was applied to assembly throughout cure.

2. Volatile Content Determination

Four adhesive specimens were cut from the roll, placed in a 200°F oven, withdrawn at the noted intervals and weighed.

Spec. No.	Time at 200°F	% Weight Change (Decrease)
1	15 mins.	0.53
2	45 mins.	0.55
3	90 mins.	0.49
4	240 mins.	0.65

70

reduced by approximately 75 percent from the original specimens.
Processes 1 and 3 exhibited excessive porosity, similar to that of the
original specimens. Volatile content was determined to be within normal
limits for adhesive films. The major factor in the porosity problem was
concluded to be the amount of vacuum used during bag check and the lack of
subsequent venting to atmosphere during cure. The pulling of vacuum
during curing combined with the presence of slight moisture is what caused
the poor bond quality. All subsequent assemblies were then fabricated
with the AF147 adhesive system (single ply) using the optimized bonding
process. Subsequent sonic fatigue tests on joints utilizing Process 2
showed order-of-magnitude improvements in sonic fatigue life over joints
utilizing Process 1. It is interesting to note that a major improvement
in joint quality relative to porosity and random fatigue life corresponded
to a very modest improvement in static strength.

This adhesive evaluation underscores the crucial importance of bond
quality in a program of this type, and the need to rectify any problems
prior to fabricating a large number of expensive test structures.
Fortunately, in this program, the problem was discovered and rectified
prior to the fabrication of most of the multi-bay test panels. Those that
had already been fabricated were eventually subjected to sonic fatigue
testing (see Section III.5), and failed prematurely in the bonded joints.
They were subsequently replaced with new panels and successfully tested.
Unfortunately, the fabrication of the shaker specimens had already been
completed prior to the resolution of the bonding problem, and in addition,
many specimens were used in the process of achieving a solution. This
resulted in a major change in the objective of the shaker tests. It was
not now possible to use the existing specimens to evaluate the skin-
stiffener joint fatigue properties. Instead, they were used to evaluate
the skin laminate fatigue properties, which were unaffected by the bonding
problem.

NOTE: It was later learned that the manufacturer of the AF147 adhesive
had been having problems with air porosity in this adhesive, and
that this had been a contributing factor in the bonding problem
experienced by Rohr. The manufacturer, like Rohr, has now overcome
the problem.

4. SHAKER TESTS

The shaker test program was originally intended to provide additional
fatigue life and mode of failure data on the skin-stringer adhesively
bonded joints. The data was to augment the sonic fatigue test data from
the multi-bay panels. However, as a result of the adhesive bonding
problems, discussed in Section III.3, tests were redefined in objective
and scope.

Early shaker tests revealed poor bond quality between the skin and
stringer elements. The resulting investigation indicated that the
remaining specimens would be similarly deficient. Part of this resulting
investigation consisted of performing shaker tests on some of the original
specimens and comparing the results with those from a variety of new
specimens utilizing different adhesives and process parameters. In this
endeavor, the shaker tests proved to be a valuable aid in both discovering
the bond problem and in evaluating solutions.

One of the major justifications for shaker testing the skin-stringer
joints was the belief that the modes of failure and cycles to failure
would correlate with the sonic fatigue test results. This belief turned
out to be fully justified. The shaker tests that revealed the poor bond
quality were characterized by rapid failures, with stiffeners completely
delaminating from the skins, with virtually no graphite fibers being
pulled from the skin laminates and occurring at relatively low strain
levels. Some early sonic fatigue tests on panels made prior to the
resolution of the bonding problem displayed the same failure
characteristics. Subsequent testing of specimens having good bond quality
resulted in considerable skin laminate damage prior to and during skin-

72

stringer joint failure in both the shaker and the sonic fatigue tests. Additionally, shaker tests performed on the riveted specimens resulted in failures in the zee radius adjacent to the skin. This same mode of failure occurred during sonic fatigue testing of riveted multi-bay panels.

The specimens were ganged together in groups of five, mechanically fastened through the stringer webs to the upstanding leg of a horizontal tee bar, and subjected to 1/3 octave random loading centered around the specimen response frequency and tested on a Ling B290 shaker having a capacity of 1,500 force pounds. This method was specifically intended to primarily load the skin-stringer joint. Following the discovery and resolution of the bonding problem, it was decided to use the remaining shaker specimens to develop random fatigue data for the skin laminates. In order to accomplish this, the test fixture was modified to support the skin elements as cantilevers, making sure that the skin-stringer joint was well away from the point of maximum stress on the skin. The skins were mounted in tapered blocks in order to avoid abrupt changes in stiffness, and strain-gauged at the point of expected maximum strain. Testing was then carried out as before, with 1/3 octave random loading. Figure 18 shows the shaker test setup.

Complications arose during the early tests due to the high strains required to cause fatigue failures of the laminates. Conventional strain gauges do not have significant fatigue life at the strains required to fail the graphite laminates. To overcome this problem, the specimen holding fixture was strain-gauged and tests carried out to establish a relationship between the fixture gauge and the specimen gauges. This was done using static loading of up to 4,000 microinches/inch on the specimen, and noting the corresponding fixture gauge readings. Correspondence between the specimen and fixture strain gauges was also determined by apply a sinusoidal load up to a specimen strain of 3,000 microinches/inch. Finally, similar correspondence was also established using low level random excitation. The fixture gauge was found to read approximately 1/20 of the specimen gauges. Although there was little variation from specimen

73

Figure 18. Shaker Test Set-Up

74

to specimen, nevertheless strain conversion factors were measured for each test.

The remaining shaker specimens were then tested to failure. The results are shown in Figures 19 and 20. Figure 19 shows actual rms strains vs. cycles to failure. The curve drawn represents minimum values. The numbers in parentheses refer to the specimen types given in Figure B-3 in Appendix B. Since the elastic modulus varies between different specimen types, there are advantages in presenting data in strain form, allowing users to apply their own modulus values. Figure 20 shows the same fatigue data plotted as rms stress vs. cycles to failure. These curves are used in Section IV in conjunction with the progressive-wave tube test results.

5. PROGRESSIVE-WAVE TUBE TESTS

Sonic fatigue tests were performed on the twenty-seven panels shown in Table 1 and existing panels 1, 2, 4 and 5 shown on Figure B-2 in Appendix B. The tests were carried out in a progressive-wave tube (PWT) at the Acoustic Test Facility, Rockwell International (Los Angeles Aircraft Division), Los Angeles, California. The facility is powered by four Ling EPT 200 transducers, each capable of generating 10,000 acoustic watts. Sine and random inputs are available with frequency spectrum control from 50 Hz to 1,200 Hz. Indefinite endurance tests can be carried out at overall sound pressure levels of 167 to 168 dB. The main test section is in a 6-foot by 1-foot duct cross-section, capable of taking two panels simultaneously, one above the other. The PWT has an acoustic wedge termination into a reverberation room. Rockwell personnel operated the PWT. All instrumentation, data acquisition, signal conditioning and data reduction were performed by Rohr personnel using Rohr's mobile Vibro-Acoustic Laboratory. Figure 21 shows the Rockwell facility and the Rohr mobile laboratory. Figure 22 shows the test section with panels installed. The main purpose of the tests was to obtain strain and frequency response data for the test panels under random acoustic excitation at grazing incidence, and to test the panels to failure, using the data generated to develop a sonic fatigue design method.
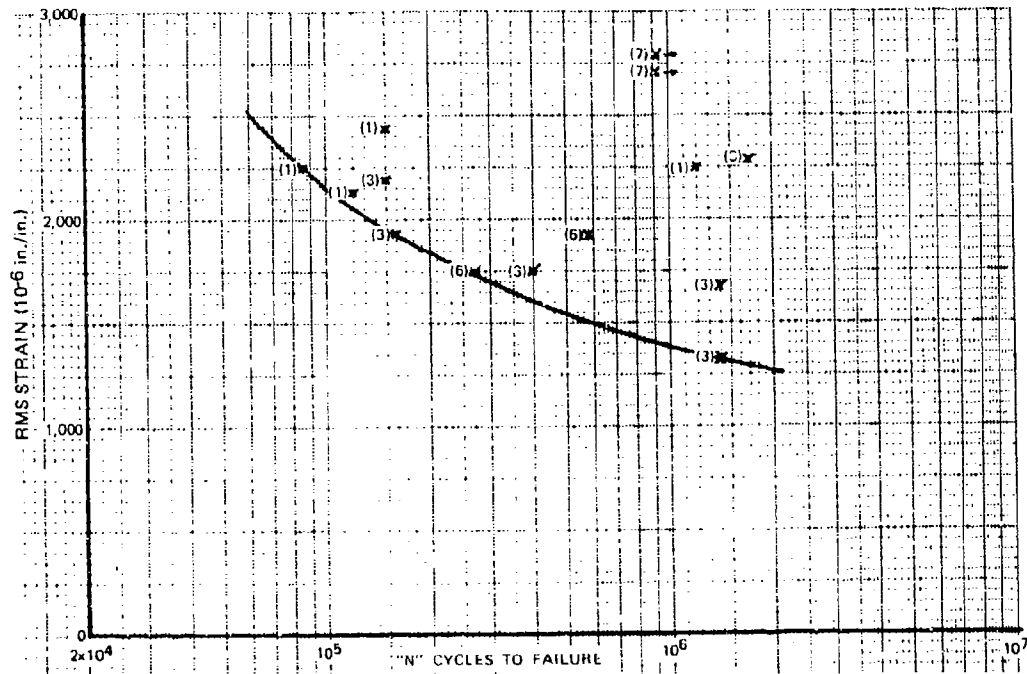
Figure 19.   Shaker Test Fatigue Curve: Strain v Cycles to Failure
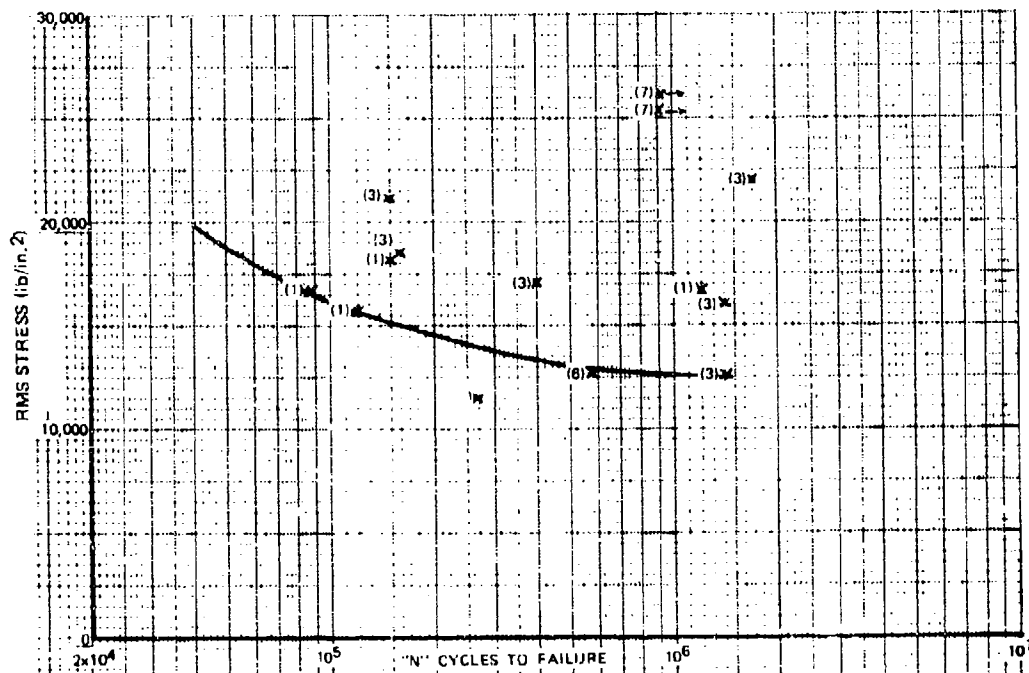
Figure 20.   Shaker Test Fatigue Curve: Stress v Cycles to Failure

Figure 21. Rockwell Facility and Rohr Mobile Laboratory

77
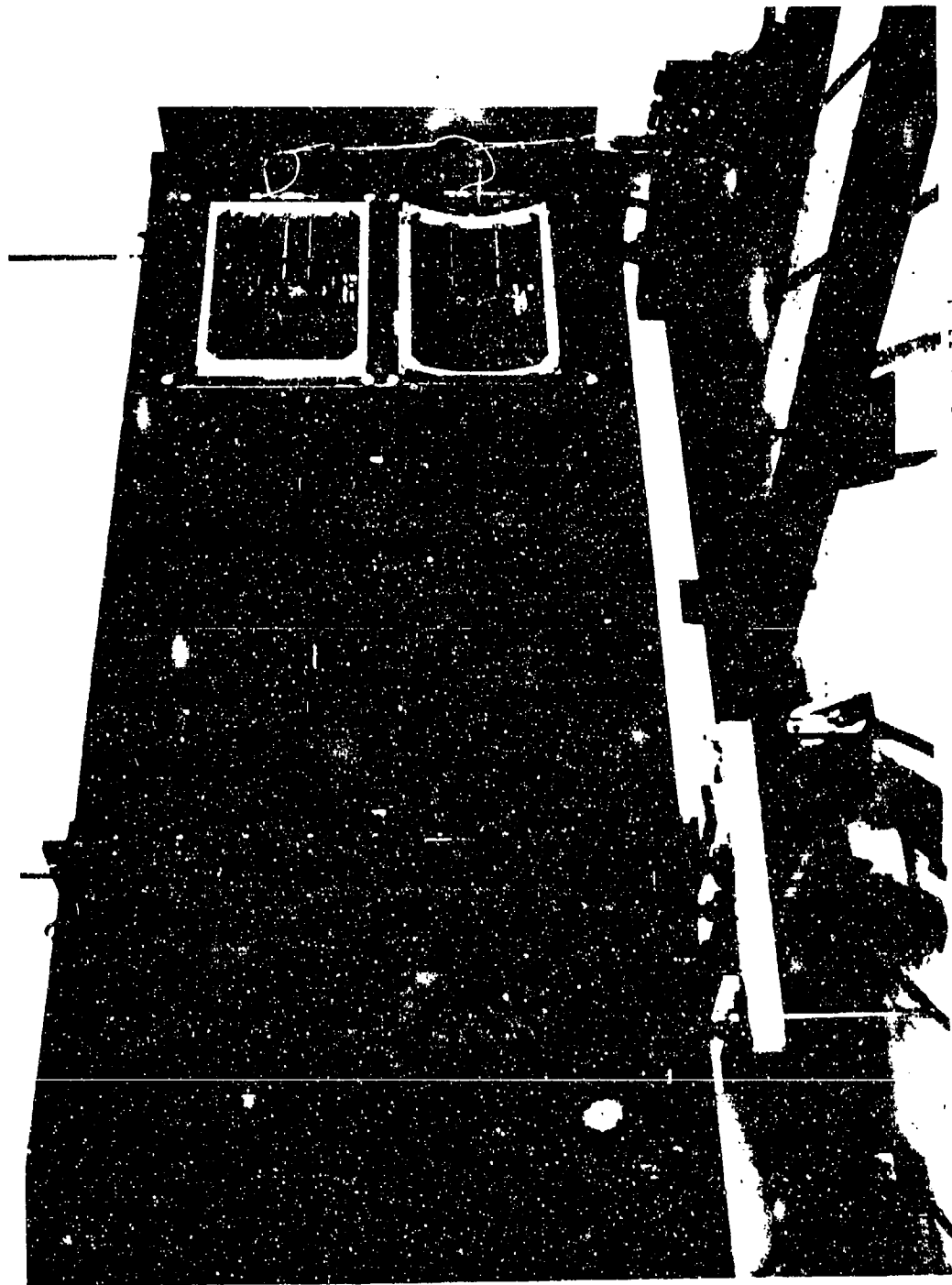
Figure 22. Progressive Wave Tube with Panels Installed

a. Evaluation of Progressive-Wave Tube (PWT) - Prior to the actual test program, a series of measurements were made in the Rockwell PWT in order to determine the maximum overall and spectrum acoustic levels available, without noticeable "clipping". Amplitude distribution plots were also made in order to determine if the acoustic field was reasonably Gaussian. Three microphones were used, in a vertical spread along the center line of the test panel openings. The results showed acoustic spectrum levels of around 140 to 145 dB/Hz to be attainable with broad-band loading. Reducing the acoustic loading spectrum to 1/3-octave showed an increase in maximum acoustic spectrum levels of approximately 8 to 10 dB. Figure 23 shows the amplitude distribution function for the center microphone with broad-band input. These data showed the Rockwell facility to be suitable for this program.

b. Instrumentation - All the test panels were instrumented with sufficient strain gauges and microphones to accurately identify dynamic strains, mode shapes and acoustic loading. The center bay of each panel was the most heavily strain-gauged. All panels had biaxial gauges at the center of the center bay and adjacent to both zees on the longer sides. Strain gauge and microphone locations are shown on Figure B-1 in Appendix B. Sheet 1 shows locations for panel "b." Referring to the numbering system for panel b, the other test panels were instrumented as follows:

Panels a, c, d, f, g, h, n. p had strain gauges at positions 3, 4, 7, 8, 10, 11, 18, 26 and 31. In addition, panels a, b, d, n and p had back-to-back gauges for positions 3, 4 and 10.

Panel e was gauged as per Figure B-1, sheet 2.

Panels i, j, q and r had gauges in positions 3 and 4 on each of the four center bays, plus positions 7, 8, 10 and 11 on one center bay, plus position 31.
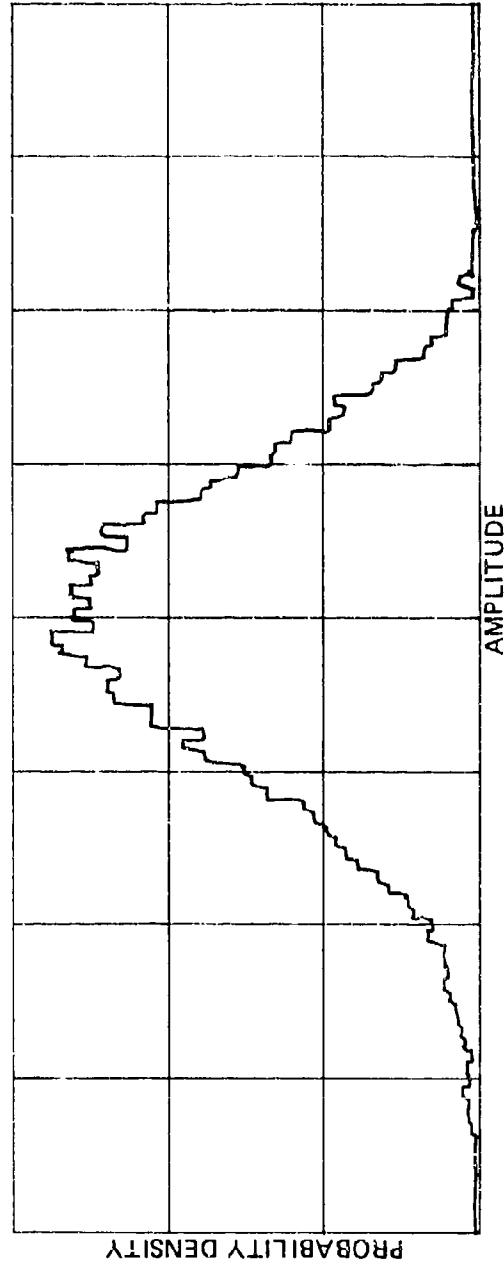
Figure 23. PWT Microphone Amplitude Distribution

Panels k, l and s had gauges at positions 3 and 4 on each of the two center bays, plus positions 7, 8, 10 and 11 on one center day, plus position 31.

Panel m had gauges at positions 1 through 13 on one of the center bays, plus a gauge corresponding to "4" on the remaining seven bays.

The J stiffened panels were instrumented as panel b.

Back-to-back gauges were used on selected panels in order to separate out membrane and flexural strains. Strain gauges were also installed on the test fixture to check for unwanted resonances.

Small (1/8-inch) strain gauges were used to provide for good resolution. Larger strain gauges result in excessive strain averaging, particularly near stiffeners and fixtures where there are high strain gradients. Since these locations are where maximum strains and fatigue failures occur, good resolution is of particular importance. Each panel had two flush-mounted microphones installed. "Kulite" pressure transducers were used. Several panel/fixture assemblies had extra microphone holes provided to facilitate acoustic measurements on all four panel sides. "Kulite" transducers are a strain gauge type microphone and therefore used compatible signal conditioning to that used for the strain gauges. Their high natural frequency (above 70 KHz) and low mass makes them especially suitable for mounting on vibrating structures. Three B&K condenser microphones were installed and monitored inside the PWT as part of the facility operation.

     c. Data Acquisition - The data acquisition consisted of twenty channels of strain gauge signal conditioners, coupled through a patch panel to a 14-track FM tape recorder. Two channels were set up for handling microphone (Kulite) signals. Prior to each test run, insertion calibrations for all data channels were recorded on magnetic tape. These insertion calibrations consist of applying a calibration resistor in parallel across each strain gauge to simulate a known compressive strain.

81

Post test calibrations were also performed as a check, and as a safeguard against neglecting gain changes made during test runs.

d. Test Procedure - Each panel was installed in the progressive-wave tube and subjected to acoustic loading at grazing incidence. The panel-fixture assemblies were suspended on wires, in order to isolate them from PWT vibrations and to achieve accurate boundary condition representation for comparison with the analytical results. Figure 24 shows a closeup view of the panel-fixture installation in the PWT. Load cells were incorporated into the wire harness supporting the panels. This allowed the wire tension to be adjusted identically for each test panel and also facilitated dynamic monitoring to ensure that there were no significant resonances in the panel suspension system. The turnbuckle-pulley arrangement, seen in Figure 24, automatically centered the test panels in the specimen windows.

The test procedure for each panel started with a sine sweep from 50 Hz to 1,200 Hz. The sine sweep was used to identify major panel resonances. This was followed by full spectrum (50 Hz to 1,200 Hz) random acoustic loading from 140 dB to 165 dB in 5 dB steps at 30 second intervals. All strain gauge and microphone outputs were recorded on magnetic tape throughout. In addition, real-time frequency response plots were made for one key strain gauge and microphone. Where the number of transducers for a given panel exceeded the 14 channels available on the tape recorder, these runs were repeated until all transducer outputs, including the fixture gauges and the load cell, had been recorded on magnetic tape. The overall strain levels from all the strain gauges were monitored throughout. When the strains reached levels suitable for endurance testing, the random response check would not proceed to the next acoustic load level. Careful response monitoring is of particular importance in setting the test levels for panel endurance runs. The strain and acoustic levels measured during these random response checks form the data base for the design method in Section IV. Endurance runs were then made at selected sound pressure levels until panel failure occurred. A target of

82
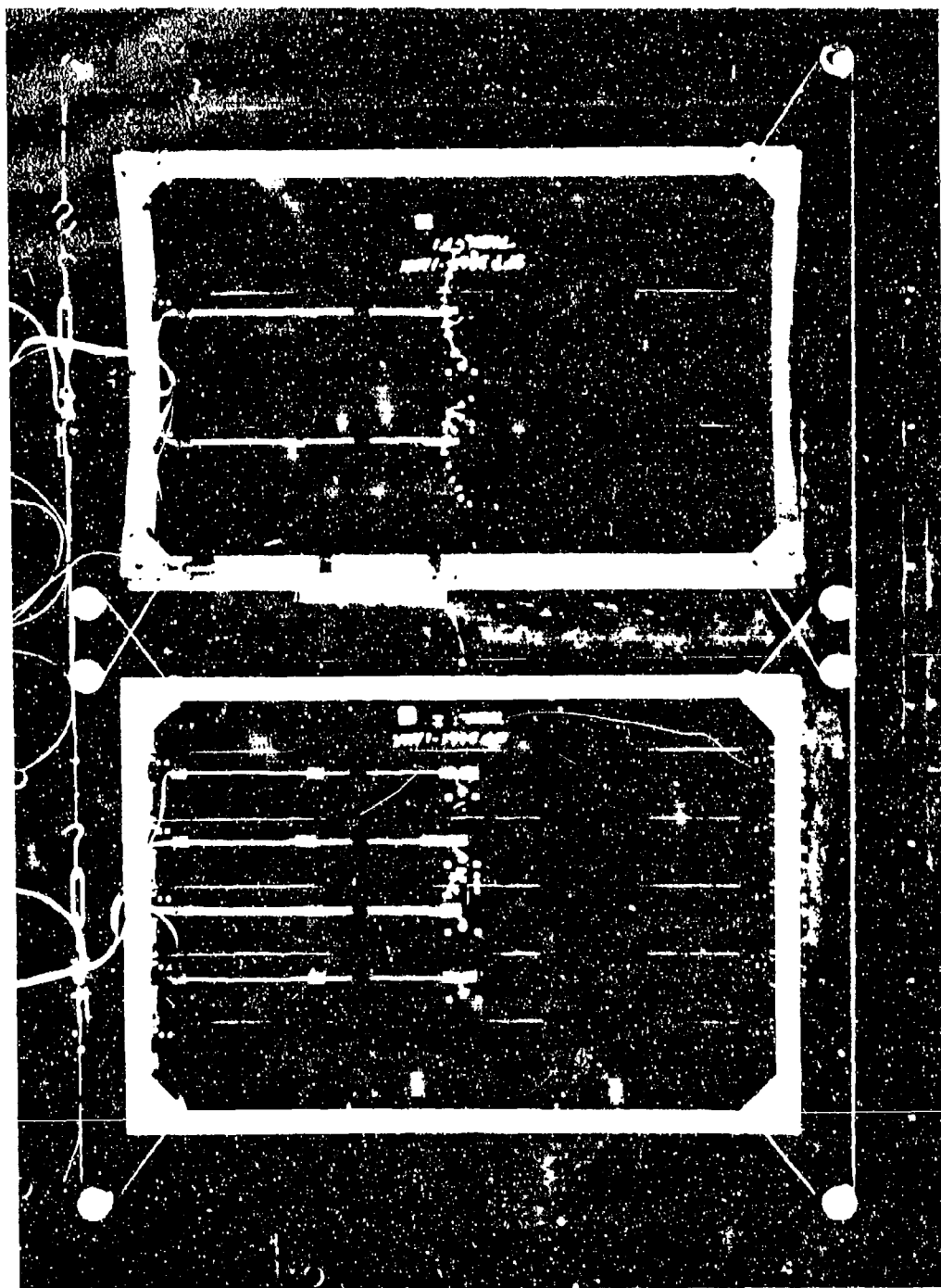
Figure 24. Closeup of Panel Installation in the PW!

83

10 hours exposure time was set as a maximum. The intention in the endurance runs was to avoid rapid or protracted failure times and to obtain a good spread of fatigue life data. Panels that could not be failed within 10 hours at 165 dB were subsequently subjected to reduced bandwidth testing, with correspondingly higher acoustic spectrum levels. During endurance runs, panel gauges were continually monitored for changes in response (frequency or strain levels) indicative of structural failure. In addition, periodic visual inspections of the panels were made. First signs of visual damage were noted.

The panels often had slow progressive fiber failures, where the time from first visual damage to major damage affecting panel response was several hours. In such cases, both times were noted. Major damage was defined as any skin damage extending through the laminate thickness or fracture or separation of stiffeners from the skin in one of the center bays.

In addition to the basic tests described above, the following additional tests were carried out:

(1) Testing identical panels in steel and aluminum fixture frames.

(2) Testing a panel without a fixture frame and also rigidly bolted to the PWT.

(3) Full depth vs. panned down closures on the honeycomb beam stiffeners.

(4) Testing with and without the stiffeners clipped to the fixture frame.

(5) Comparison between bonded and riveted skin to stiffener joints.

(6) Switching panel positions in the two test windows.

(7) Measuring response on one panel, with other test window open.

(8) Same as above with hard wall installed in other test window.

e. Data Reduction - A Spectral Dynamics Digital Signal Processor, Model SD360 was used to perform all spectral analyses. The SD360 is a self contained fast fourier transform analyzer, capable of displaying and plotting, in real-time, the complex relationship of two signals, both in the time domain and the frequency domain. An analysis range of 1.2 KHz was sel .cted, corresponding to a filter bandwidth of 2.16 Hz. The actual aliasing filter cutoff was 960 Hz. Overall sound pressure levels and rms strain levels were determined by converting the signal to a d.c. value proportional to its instantaneous rms value, integrating over a 20 second period, and reading the value on a digital voltmeter.

Frequency spectra were generated for all microphones and strain gauges at the endurance test sound pressure levels. Spectra were also generated at each sound pressure level (140 dB to 165 dB) for selected gauges. The strain gauges selected for spectral analysis over the full response range were the center biaxial pair (numbers 3 and 4) and the gauge near the zee radius (number 10). Overall rms levels were measured for all transducers at all sound pressure levels. Cross-spectral density measurements were made between corresponding strain gauges on adjacent bays. Integrated power spectral density plots were made for some panel gauges in order to determine the relative contributions of individual modes to the overall rms strain value.

f. Progressive-Wave Tube Test Results - The first panels to be tested were the existing panels, shown in Figure B-2. Tables 22 and 23 summarize the overall rms stress levels. Panels 1 and 5 have the same geometry, and offer a comparison between a graphite and an aluminum panel. The stresses on the graphite panel (5) ranged from 50-75 percent of the

85

TABLE 22

OVERALL RMS STRESS LEVELS FOR EXISTING PANELS 1, 5 and 4

OVERALL RMS STRESS LEVELS (LB/IN^2)

OASPL (dB) / Gauge Number	Panel 1 – Aluminum Skin-Stringer					Panel 5 – Graphite Skin-Stringer					Panel 4 – Single Stiffener				
	145	150	155	160	165	145	150	155	160	165	145	150	155	160	165
1	430	720	1180	2200	-	261	469	884	1608	2291	-	-	-	-	-
2	-	-	-	-	-	241	422	918	1461	2124	-	-	-	-	-
3	-	-	-	-	-	248	449	978	1515	2198	-	-	-	-	-
4	470	700	1070	2040	3200	168	275	670	1119	1749	657	1012	1642	2385	2874
5	-	-	-	-	-	-	-	-	-	-	1320	1836	2660	3464	4027
6	-	-	-	-	-	-	-	-	-	-	456	730	1112	1575	-
7	-	-	-	-	-	101	241	402	717	-	496	824	1273	1715	-
8	700	1250	1750	-	-	214	429	737	1253	978	429	737	1166	1575	-
9	-	-	-	-	-	121	208	342	570	1675	469	771	1186	1648	-
10	-	-	-	-	-	201	315	563	945	1608	-	-	-	-	-
11	500	900	1400	2150	3000	154	348	616	1079	1742	-	-	-	-	-
12	500	900	1350	1970	-	147	355	637	1092	871	1635	2111	3002	3933	4362
13	-	-	-	-	-	101	168	335	509	-	784	1186	1896	2767	3296
14	-	-	-	-	-	194	315	529	858	-	-	-	-	-	-
15	200	350	500	870	1350	121	295	469	824	1240	-	-	-	-	-
16	750	1300	2000	2920	3600	214	496	864	1407	2010	-	-	-	-	-
17	-	-	-	-	-	114	201	335	563	938	-	-	-	-	-
18	-	-	-	-	-	174	281	509	858	1575	-	-	-	-	-
19	-	-	-	-	-	147	302	677	1052	-	-	-	-	-	-
20	-	-	-	-	-	295	456	911	1474	1997	-	-	-	-	-
21	720	1200	1850	3400	4100	255	462	918	1508	2044	-	-	-	-	-
22	670	940	1700	3200	4700	188	348	697	1139	1983	-	-	-	-	-

TABLE 23

OVERALL RMS STRESS LEVELS FOR EXISTING PANEL 3, FLAT AND CURVED

OASPL (dB) / Gauge Number	Panel 3 - With 30 Inch Curvature					Panel 3 - Unstiffened Graphite				
	145	150	155	160	165	145	150	155	160	165
1	804	1474	2345	3390	-	1059	1575	-	-	-
2	315	526	905	1742	-	951	1387	-	-	-
3	369	670	1206	1843	2680	1106	1876	2613	3551	3015
4	670	1306	2077	3350	5079	-	-	-	-	-
5										
6										
7	362	610	1139	1943	-	-	-	-	-	-
8										
9	134	214	342	603	-	1039	1642	2278	3015	2144
10	174	275	570	1045	-	1642	2814	3886	4288	-

corresponding aluminum values (1) in the maximum stress direction (short direction). In the long direction (strain gauge 15) the stresses were comparable. Panel 4, which has four times the bay span as panel 5, shows a corresponding stress increase of from 2 to 4 times. The unstiffened panel (3) was tested both as a flat panel and with a curvature of 30-inches. The 165 dB data points may not be valid comparisons, since the panel was undergoing extremely large deflections at this high load. The 165 dB points may also represent the onset of failure. The center stresses were reduced to 1/3 to 1/2 of their original values due to curvature, whereas the edge stresses were reduced to 1/5 to 1/7 of their original values. The response of panels 1 and 5 were plotted against sound pressure levels in order to compare the degree of linear response between the aluminum and graphite panels. Figures 25 and 26 show the results. The dotted lines represent linear response. These graphs show both the aluminum and the graphite panels to be responding in a linear fashion. Figure 27 shows the graphite skin-stringer panel following sonic fatigue failure. Figure 28 shows sections of honeycomb stiffeners with skin laminate fibers still attached. The time to failure for panel 5 was 15 minutes at 165 dB. Panels 3 and 4 lasted for 5 minutes.

These photographs show the mode of failure to be in the skin laminate at the stiffener locations. This shows that the secondary bond between the skin and stringers is superior to the interlamina bond strength, as it should be. This is because the adhesive strength in the laminate comes from the epoxy matrix material, which is selected for criteria other than just pure strength. Flow characteristics, for example, are very important when laying up a large surface area. The adhesives used to bond the skin and stringers together are chosen primarily for strength. Consequently, extensive fiber pull-out on failure is indicative of good bond quality. This mode of failure also indicates that the flatwise tension strength of the laminate may be a critical parameter in sonic fatigue resistance. This is a property that is not commonly measured or quoted in structural property specifications of composite laminates. This conclusion has considerable logical appeal, since stress concentrations and extra inertia
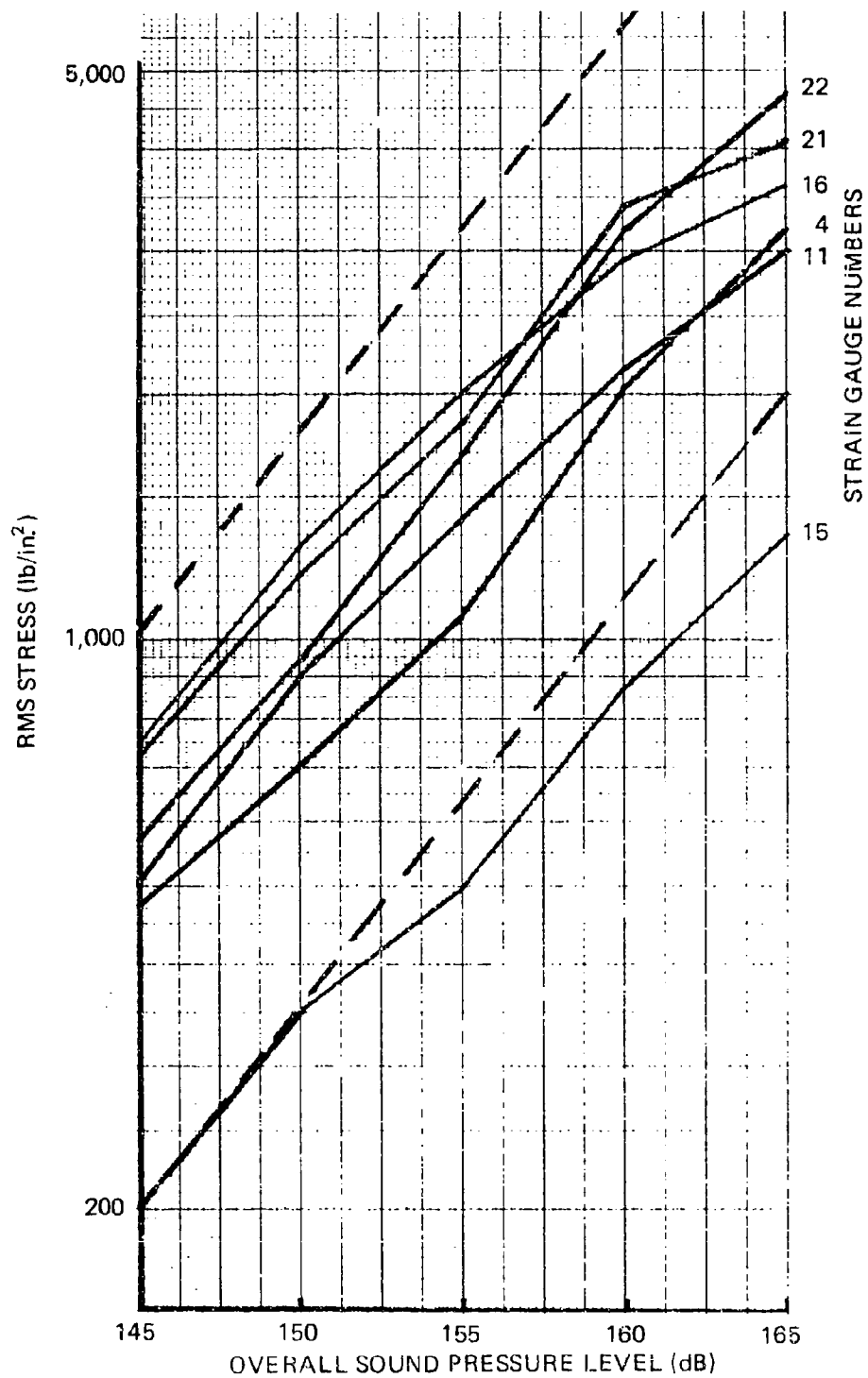
88

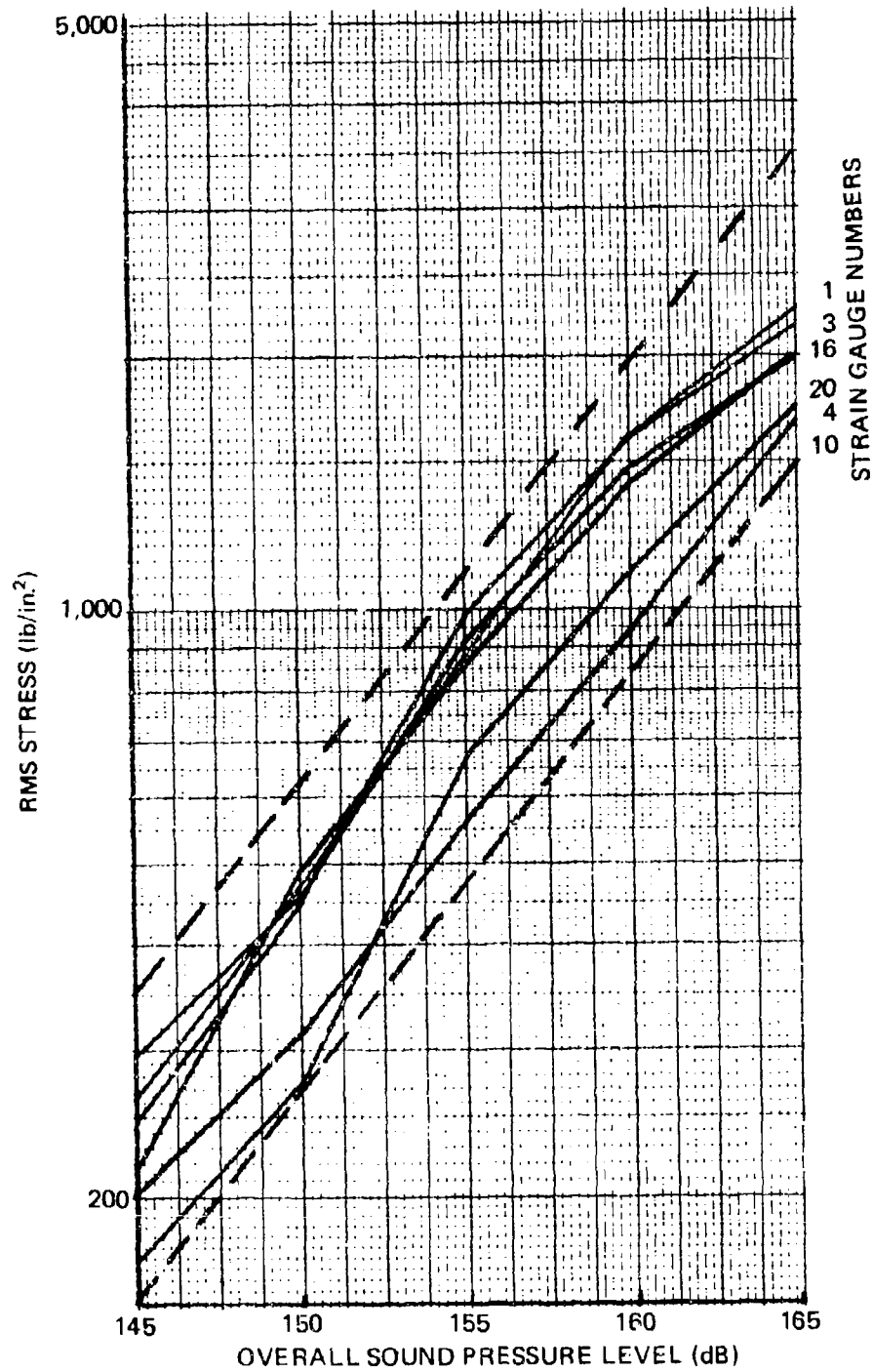Figure 25. Panel 1 - Linear Response of Aluminum Skin-Stringer Panel

89

Figure 26.   Panel 5 - Linear Response of Graphite Skin-Stringer Panel
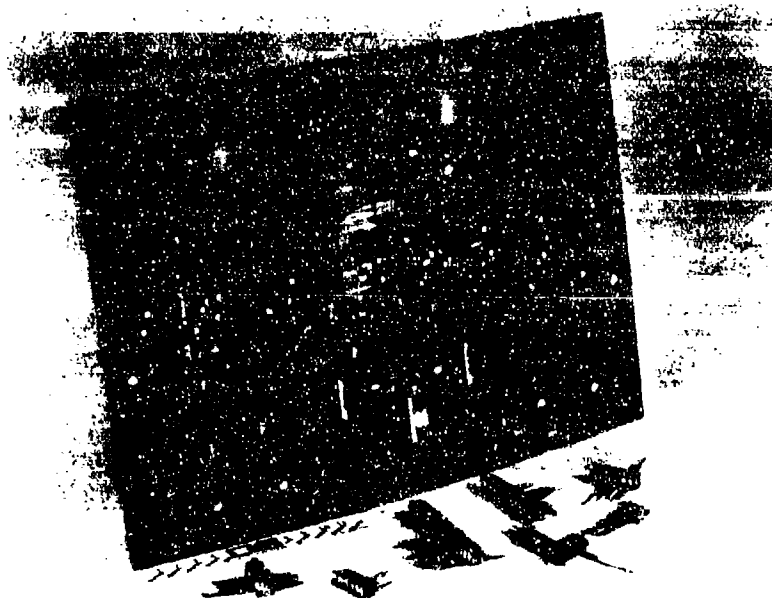
90

Figure 27. Rohr Panel No. 5 After Sonic
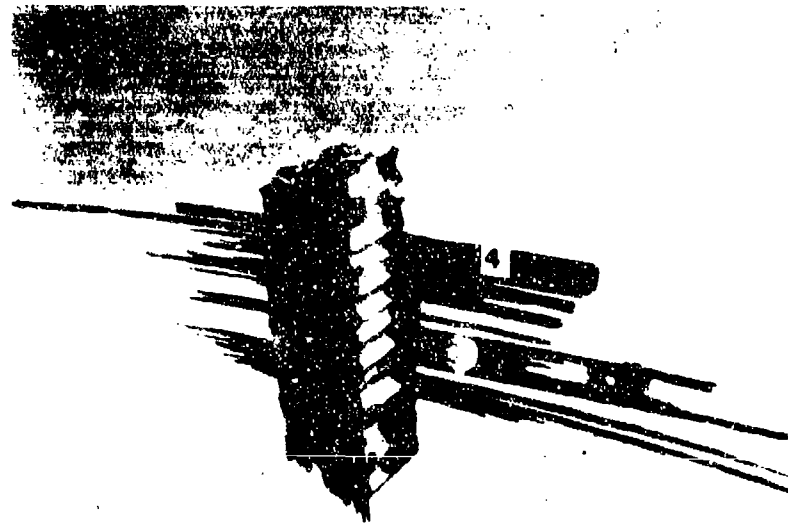Fatigue Failure

Figure 28.   Sections of Failed Honeycomb Stiffener from Panel No. 5

forces are experienced by the surface laminate underneath the stiffeners during dynamic behavior. Since the interlamina strength will be the same between each lamina, failure will occur at the first bonded interface. This mode of failure also indicates that mechanically fastening the stiffeners to the skins may result in longer sonic fatigue life than using bonded stiffeners. This is because fasteners will distribute stresses across the whole skin laminate, rather than just into the surface laminate. As a result of these findings, it is recommended that flatwise tension tests be performed on composite skin laminates in the future. Such tests may provide valuable information in selecting the best resin systems and adhesives for sonic fatigue critical applications of advanced composites structures.

The next, and most important phase in the sonic fatigue test program, was to test the multi-bay panels shown in Figure B-1. These are the panel tests upon which the design method in Section IV was based. The first of these panels were fabricated prior to the resolution of the adhesive bonding problems, discussed in Section III.3. Some of these panels failed prematurely, with the stiffeners delaminating from the skins, with no fiber pull-out occurring. The response data for these panels is unaffected by the weak bond, but the times to failure are not representative of the panel's fatigue lives. The panels that had been fabricated with suspect bonds were: al, cl, fl, gl, i, kl, n and q. Panel al gave good response data up to 160 dB, but failed prematurely at 165 dB, with very slight skin damage. Since this was a configuration for which there was a planned duplicate panel (a2) yet to be made, there was no need to refabricate al. Panels cl and gl also had duplicate panels scheduled, and it was decided to rivet the suspect skin-stringer joints on panel g in order to provide a comparison between bonded and riveted joints. Panels i and kl failed prematurely with no skin damage occurring. These panels were subsequently riveted back together and retested in order to provide additional response comparisons between bonded and riveted specimens. Panels n and q gave good response data and failed with significant fibers being pulled from the skin laminate. Panel fl gave

93

good response data and did not fail after 9 hours at 165 dB.
Figure 29 shows panel al following sonic fatigue failure. The
skin-stringer joint areas show a mixture of weak bonding (white
areas) with no attendant fiber pull-out and satisfactorily bond-
ed areas with fiber pull-out occurring. Figure 30 shows panel n
following sonic fatigue failure. Here the suspect bonding proc-
ess does not seem to have resulted in a weak joint, and the
failure shows extensive skin laminate damage. It should be
pointed out that skin laminate damage is a desired mode of
failure and represents a successful test. Figures 31 and 32
provide a good example of this desired mode of failure. They
show the front and back faces respectively of panel p follow-
ing sonic fatigue failure. In this case the skin-stiffener
bond strength and the skin laminate quality are well demon-
strated by the even distribution of the failure through the
entire thickness of the skin laminate.

Table 24 gives the overall rms strain levels for those panels
whose response data was subsequently used in the development
of the design method. Corresponding response spectra are
given in Appendix C. Omitted from this table are those panels
whose purpose was to investigate specific effects, outside the
main design method; such as the J stiffened panels, the honey-
comb stiffened panels (e), panel m - the 8 x 1 array and panel
c - which was designed to investigate the effects of ply ori-
entation. Strains are given in microinches/inch for the
following strain gauges: 3- center of bay, long direction;
4 - center of bay, short direction; and 10-edge, short direc-
tion, normal to longest side. Strain gauge 10 gave the high-
est measured strains for the majority of the panels, and
represents the location of maximum interest in this program.
At the panel centers, where the response strain magnitudes are
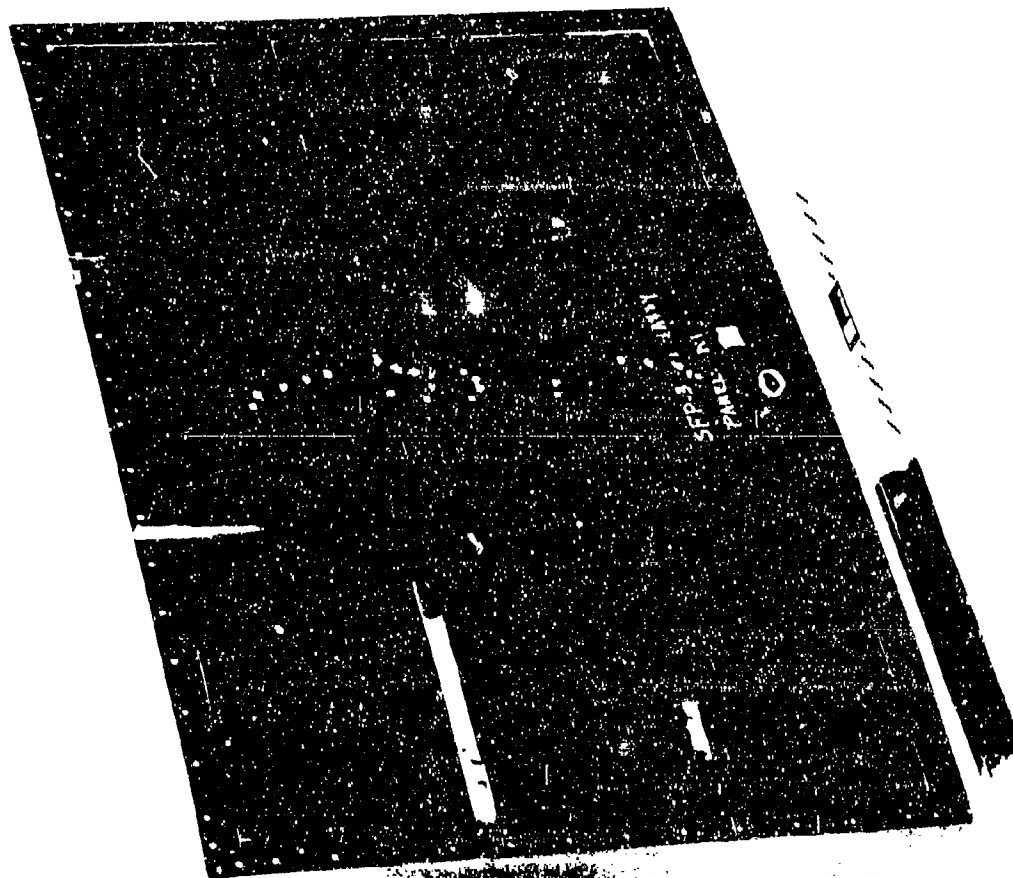
94

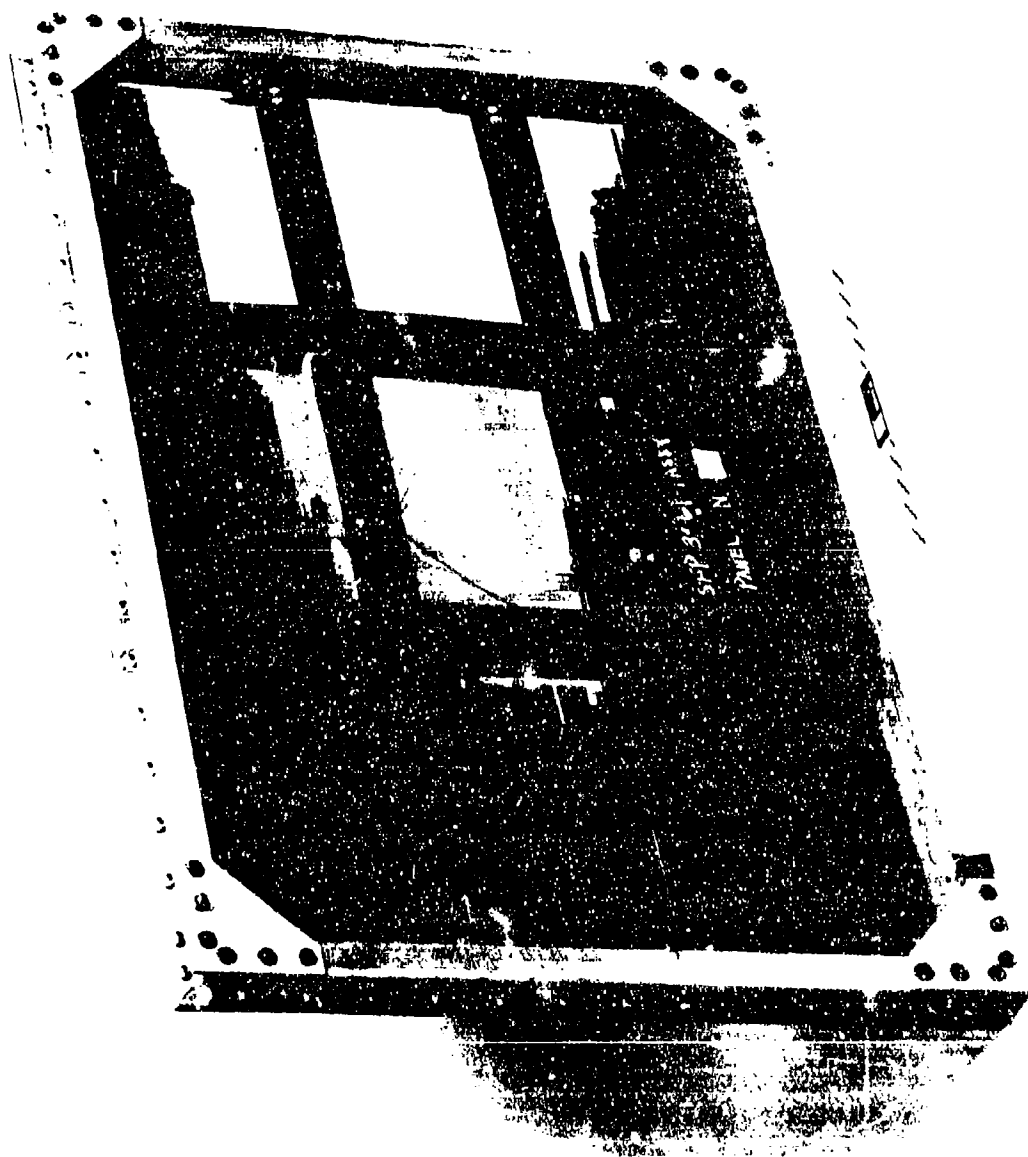Figure 29. Panel al after Sonic Fatigue Testing

95

Figure 30. Panel n after Sonic Fatigue Testing
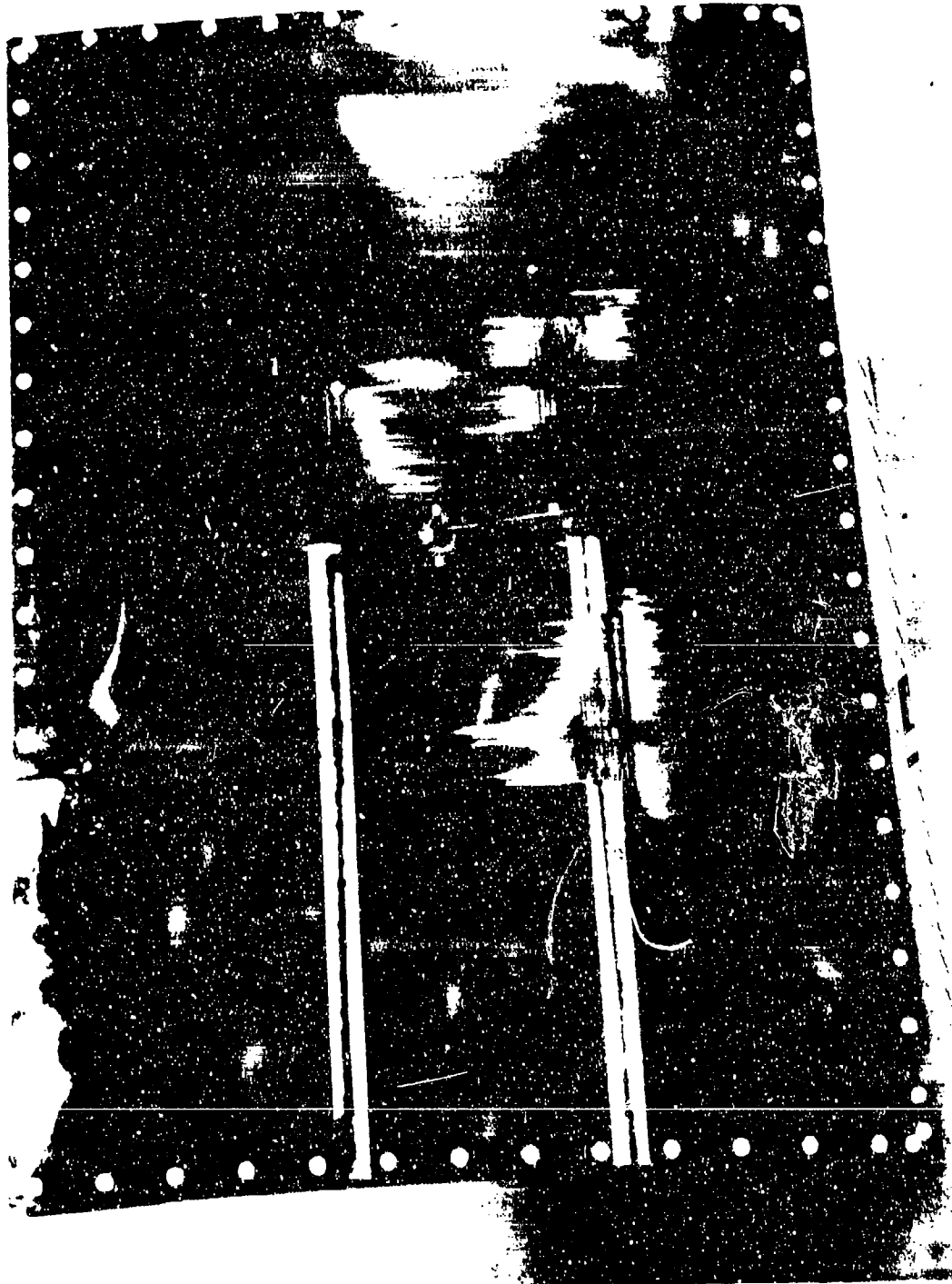
Figure 31. Panel p after Sonic Fatigue Testing -- Back Face

Figure 32. Panel p after Sonic Fatigue Testing -- Front Face

98

TABLE 24

OVERALL RMS STRAINS (MICROINCHES/INCH) USED IN THE DEVELOPMENT OF THE DESIGN METHOD

OVERALL SOUND PRESSURE LEVELS

Strain Location	140 dB				145 dB				150 dB				155 dB				160 dB				165 dB			
Panel Configuration	Center-3	Center-4	Center-B1	Edge-10	Center-3	Center-4	Center-B1	Edge-10	Center-3	Center-4	Center-B1	Center-10	Center-3	Center-4	Center-B1	Edge-10	Center-3	Center-4	Center-B1	Edge-10	Center-3	Center-4	Center-B1	Edge-10
a	69	90		102	113	148	144	161	149	199	95	225	-	275	-	342	221	338	343	411	-	-	-	-
b	49	65	55	77	85	114	96	147	135	190	164	267	199	261	221	358	249	357	288	482	334	412	342	-
d	26	33	32	34	39	58	58	57	67	109	112	101	113	183	148	174	183	284	290	274	285	416	417	425
f	22	21	15	22	27	25	18	30	39	34	24	49	61	52	36	78	96	103	81	154	141	152	120	247
g	31	29	21	51	42	44	31	93	73	70	53	151	149	120	81	250	280	205	130	400	368	299	204	555
h	39	36	27	54	62	61	45	101	101	93	68	150	187	167	121	286	276	276	210	466	194	-	-	721
i	25	31	26	26	42	64	56	47	75	120	107	84	117	192	172	133	140	226	201	168	169	325	293	258
j	24	37	37	41	31	47	48	59	47	70	70	86	71	101	100	137	110	151	148	216	-	209	200	312
k	44	53	44	50	71	90	75	84	133	144	113	142	189	227	187	211	254	322	269	295	227	197	161	283
l	24	23	20	28	34	33	28	43	53	50	42	68	97	79	66	109	140	124	102	179	-	-	-	-
n	141	131	124	187	161	185	177	266	181	209	201	307	208	234	224	355	244	249	238	408	-	-	-	-
p	45	72	70	96	57	86	83	116	124	198	192	253	213	354	344	455					-	-	-	-
q	54	85	83	58	105	136	132	93	127	203	198	141	168	256	248	202	220	381	370	312	-	-	-	-
r	31	36	34	44	46	57	53	62	78	91	85	108	118	129	118	160	183	208	190	265	278	348	333	446
s	37	36	35	48	63	68	65	91	107	112	107	149	190	193	184	262	279	315	302	444	-	-	-	-

comparable in both directions, it is necessary to combine their effects using the relationship

$$\varepsilon_{rms} = \frac{\varepsilon_y - \nu_{xy}\,\varepsilon_x}{1 - \nu_{yx}\,\nu_{xy}} \tag{17}$$

where ε_y is from strain gauge 4

ε_x is from strain gauge 3

and ν_{xy} and ν_{yx} are from Tables 2 through 6. The resulting biaxial strains are also given in Table 24.

A detailed discussion of the results in Table 24, as they relate to the development of a design method, is given in Section IV. In general, the results show basic logical trends, such as decreasing strains with increasing skin laminate thickness; and increasing strains with both increasing stringer spacing and increasing radii of curvature. There are, however, several inconsistencies in the data; panel a is identical to panel b except for having fewer skin plies, yet it has lower edge strains than does panel b at the higher sound pressure levels. Panel n, which has even fewer skin plies, also has lower strains at the higher sound pressure levels. However, it should be remembered that the different skin laminates have different ply orientations, and consequently, different elastic modulii. Panels a and d have an elastic modulus of 7.5×10^6 lb/in^2. Panel b has a value of 6.7×10^6 and panel n has 9.4×10^6. Although this program compared two different ply orientations for the same laminate thickness (panels b and c), this variable was not represented over a number of panels sufficient to permit its inclusion as a quantitative variable in the design method. Instead typical symmetric ply orientations were chosen, with the expectation that the resultant design method would be applicable to other similar laminates. This limitation should be remembered if radically different ply orientations are used in conjunction with the results of this program.

100

Although there were a few exceptions, the maximum strain response on the panels occurred at the center of, and normal to, the longest bay side, adjacent to the radius of the zee (strain gauge 10). This is as it should be, and also corresponds to the finite-element static analysis results.

The measured strains did not linearly increase with overall sound pressure level, but increased at a lower rate, which varied from panel to panel. It is not entirely clear whether or not this is indicative of nonlinear structural response. The response frequencies of the in-phase stringer-bending mode for the panels listed in Table 24 were given in Table 15, where they can be seen to correspond quite well to the fully-fixed frequencies calculated from Reference 5.

Fatigue lives, as expected, showed considerable scatter. Figure 33 shows the fatigue life data points for the multi-bay panels. The data points are shown superimposed on the shaker test fatigue data. The curve shows the strain endurance level to be approximately 400 microinches/inch. Taking a conservative line through the data, the curve for the skin-stiffener joint appears to be approximately 42 percent of the shaker test curve for the skin laminate. This ratio is similar to that for riveted aluminum skin-stiffener panels. The lowest strain at which a panel failure occured (excluding the defective panels) was 411 microinches/inch, and that appears to be an outlier compared to the other data points. The next lowest failure strains were 444/446 microinches/inch, occurring at approximately 10^7 cycles. Virtually all of the panels (again excluding the defective panels) displayed the same failure mechanism. The first signs of failure were isolated failed skin fibers at the skin-stiffener joints. The number of failed fibers would gradually increase, often over a period of several hours, without having any effect on the panel response. Only when the damaged skin fibers had extended across nearly all of the skin-stiffener joints was a change is response detected. This would usually be closely followed by a major failure of the skin laminate. This failure mechanism presents a problem in defining the effective fatigue lives of the panels. If the first visible sign of skin damage is the criterion
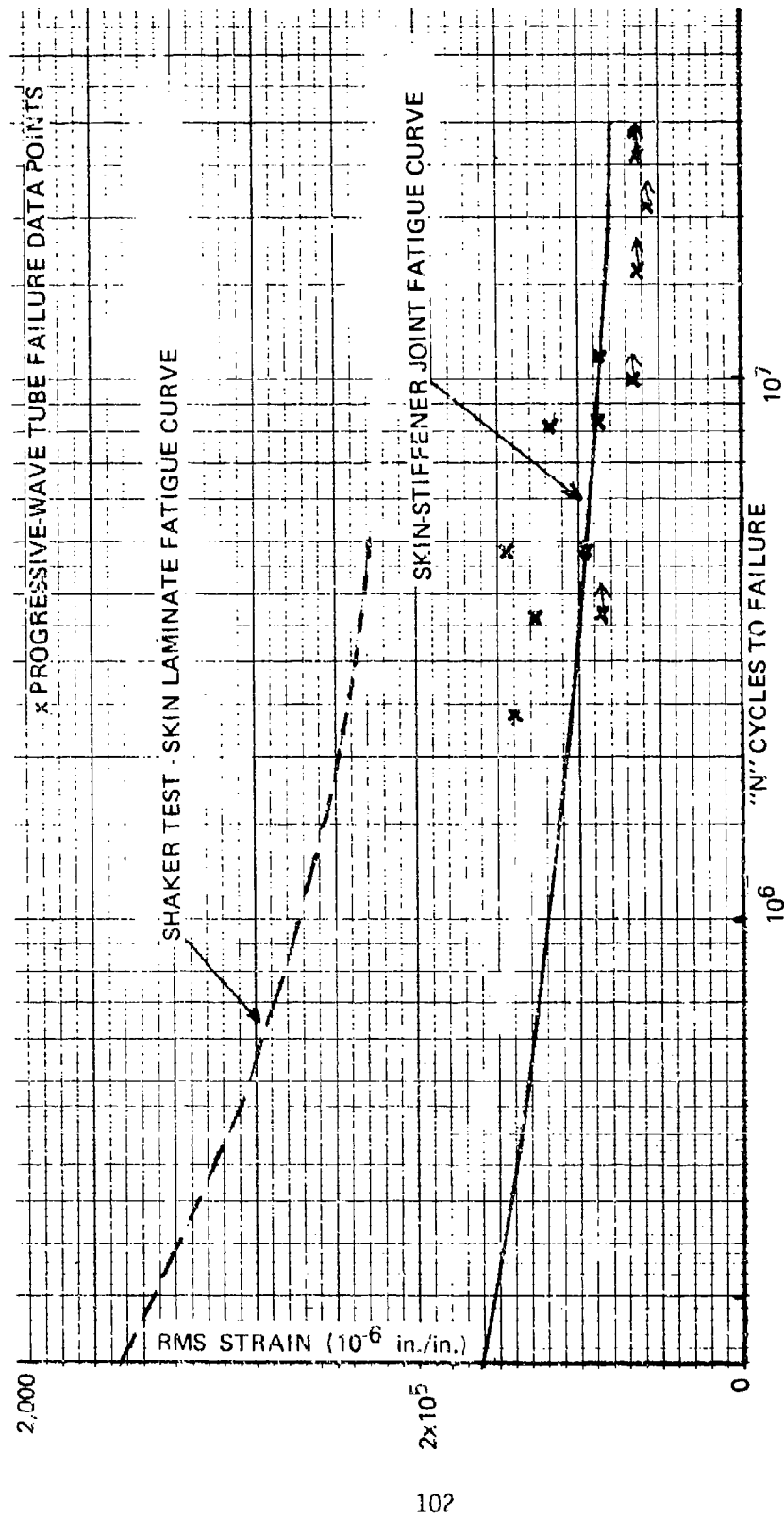
101

Figure 33. Sonic Fatigue Test Fatigue Curve: Strain vs. Cycles to Failure

for failure, then the cluster of fatigue data points shown on Figure 33 in the 10^6-10^7 range would occur in the 5×10^5 to 10^6 range. Also, some panel fatigue data points shown as run-outs had very slight fiber damage. These effects would cause the assumed endurance level to drop from 400 to 300 microinches/inch. From a structural point of view, failure should be defined in terms of significant damage or a reduction in load carrying capability. On an actual aircraft, however, it seems likely that any structural component showing visible signs of damage would be removed, even if the damage were unlikely to propagate. Several sonic fatigue test panels exhibited a small number of fiber failures early during testing, but did not experience any damage propagation, even after several million more cycles.

Phase and cross-spectral density functions were generated between corresponding strain gauges in adjacent bays in order to identify the stringer-bending, in-phase mode. Figures 34 through 37 are for panel r (6 x 3, 6 ply, 60-inch radius). Figure 34 shows the sine sweep at the center of the center bay. Figures 35 and 36 show the random response spectra for the centers of two adjacent center bays. From these spectra it can be seen that the major response modes occur at 350-430 Hz and at 750-800 Hz. Figure 37 shows the corresponding phase relationship between the adjacent bays (top plot) and the associated cross-spectral density function (bottom plot). From this figure, it can be seen that the response in these two bays is coupled at the major response peaks (shown by peaks in the cross-spectral density function) and that the coupled response peaks at 360 Hz and 400 Hz are 180 deg. out of phase, whereas the response at 760-780 Hz is the in-phase mode. The cross-spectral density plots also assist in more precisely defining the coupled mode frequencies.

Another example of the value of phase and cross-spectral density functions in identifying response modes is shown in Figures 38, 39 and 40. Figures 38 and 39 show response spectra for adjacent bays. Figure 38 shows two distinct response peaks, at 240 Hz and 400 Hz, but Figure 39 only shows one peak, at 215 Hz. From these two plots alone, modal
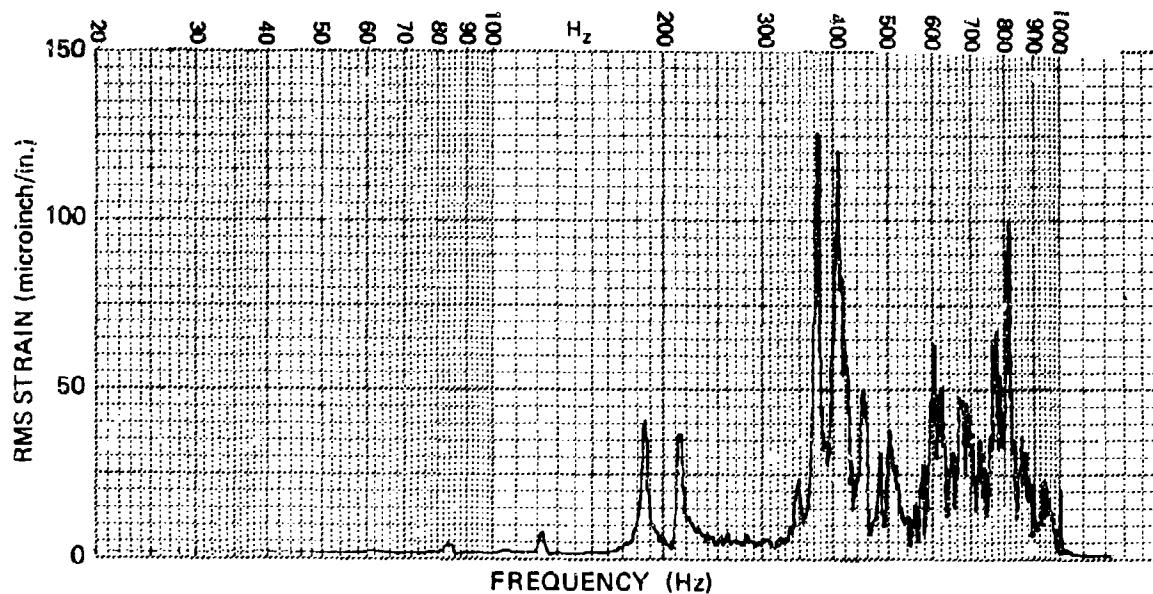
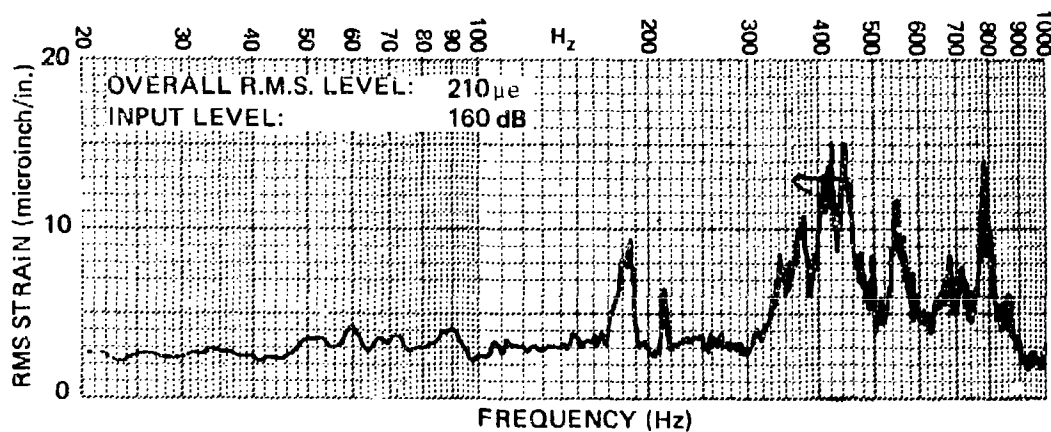103

Figure 34. Sine Sweep - Panel r, Gauge 4

OVERALL R.M.S. LEVEL: 210 μe
INPUT LEVEL: 160 dB

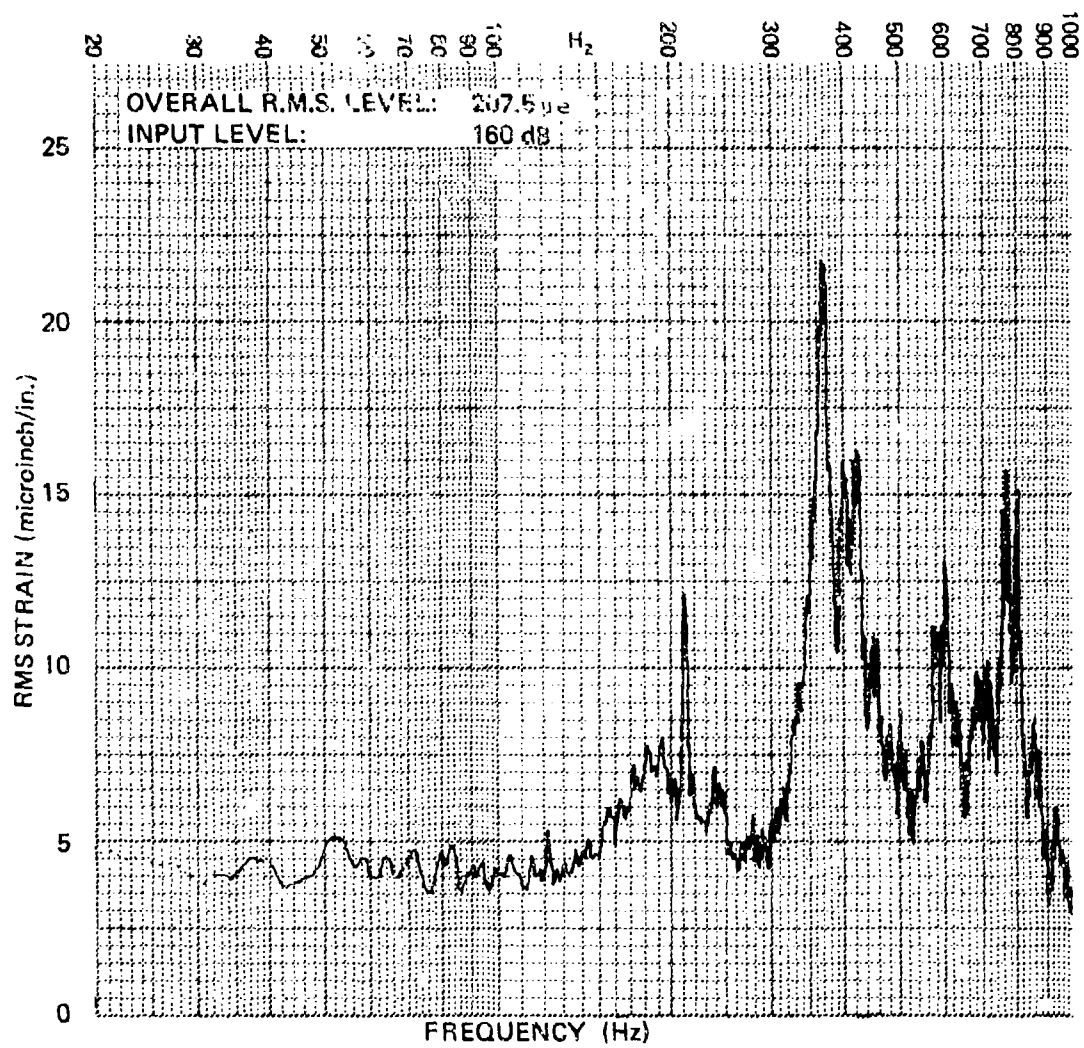Figure 35. Random Response - Panel r, Gauge 4-1

104

Figure 36. Random Response - Panel r, Gauge 4
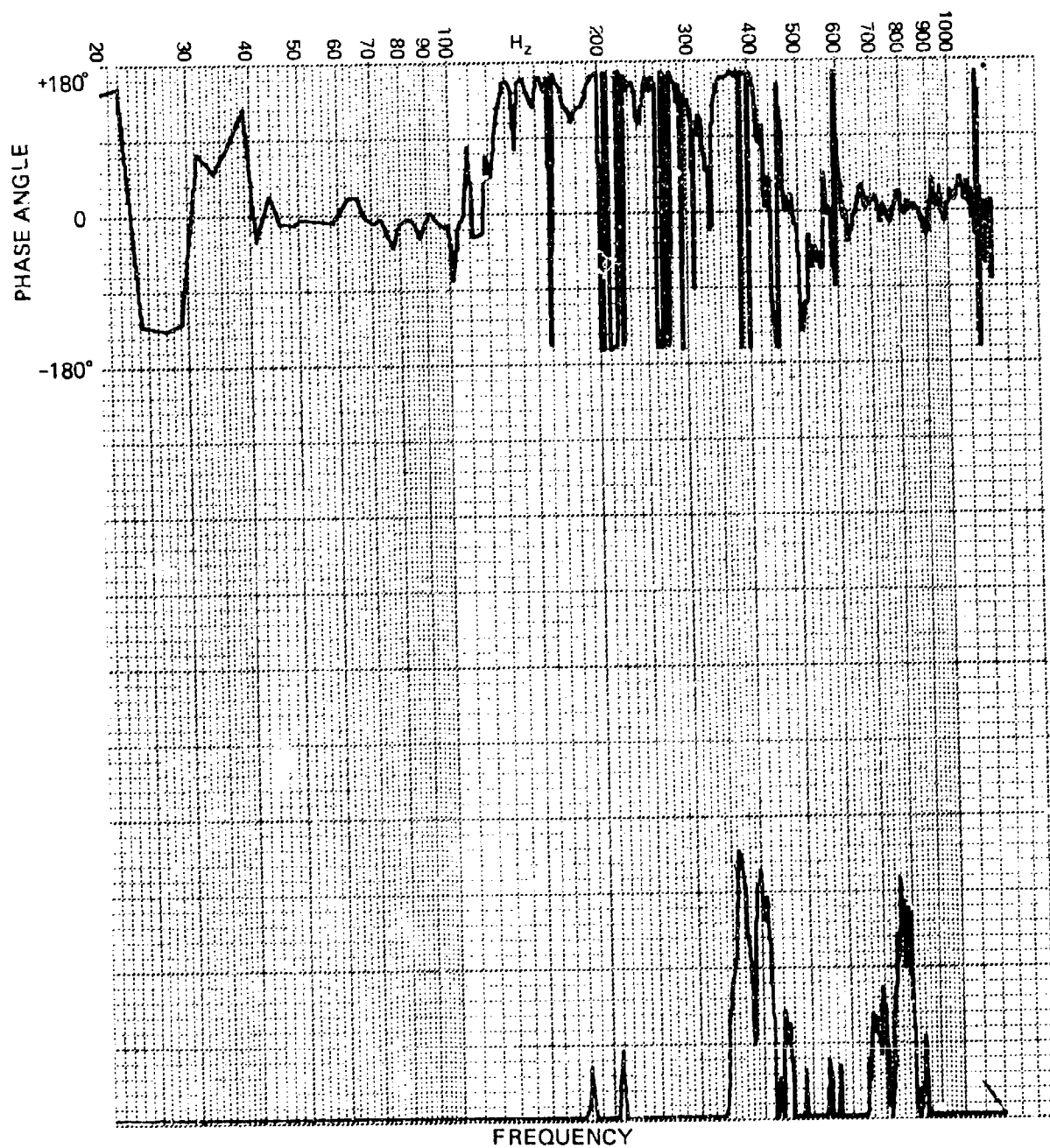
105

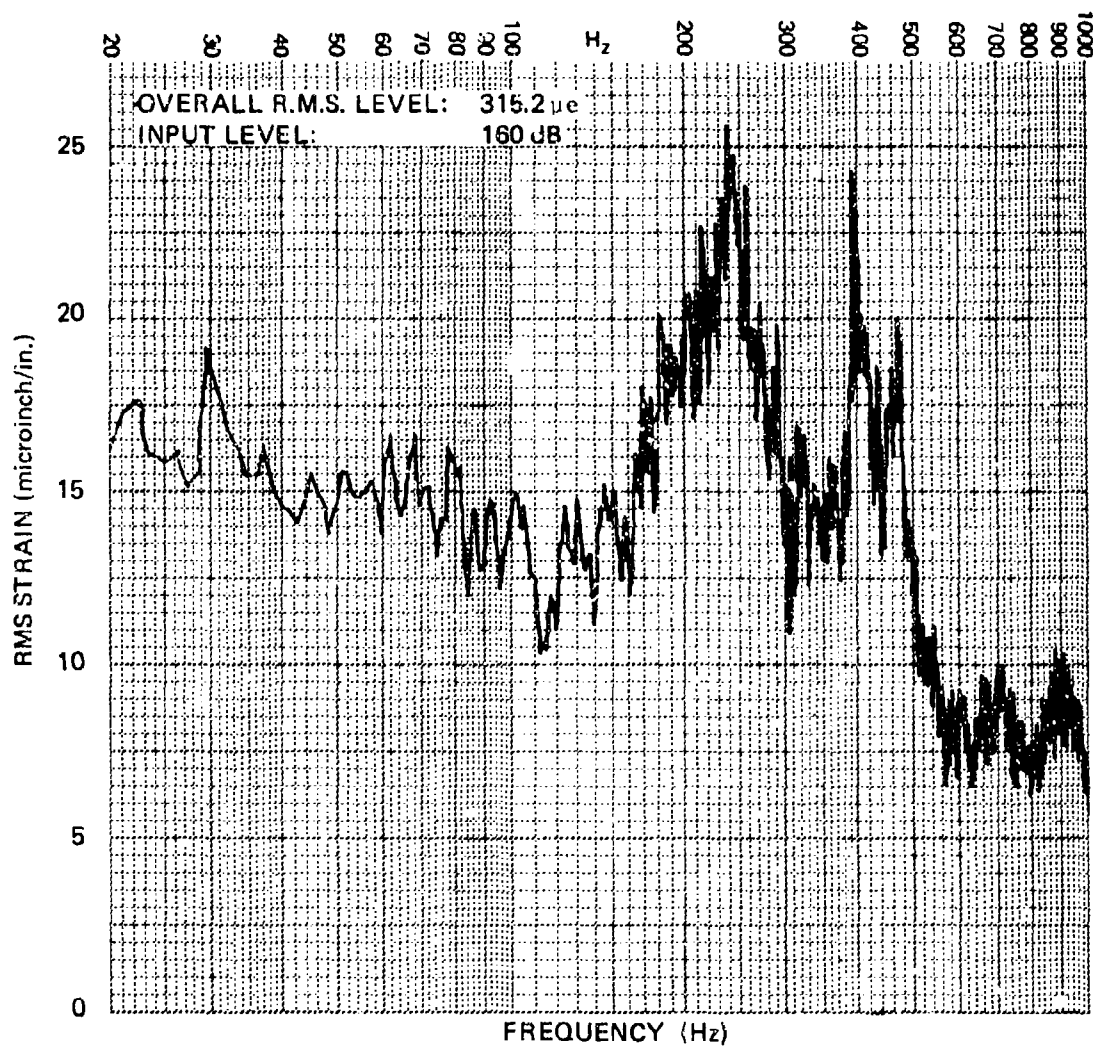Figure 37. Phase and Cross Spectral Density - Panel r,   Gauges 4 and 4-1
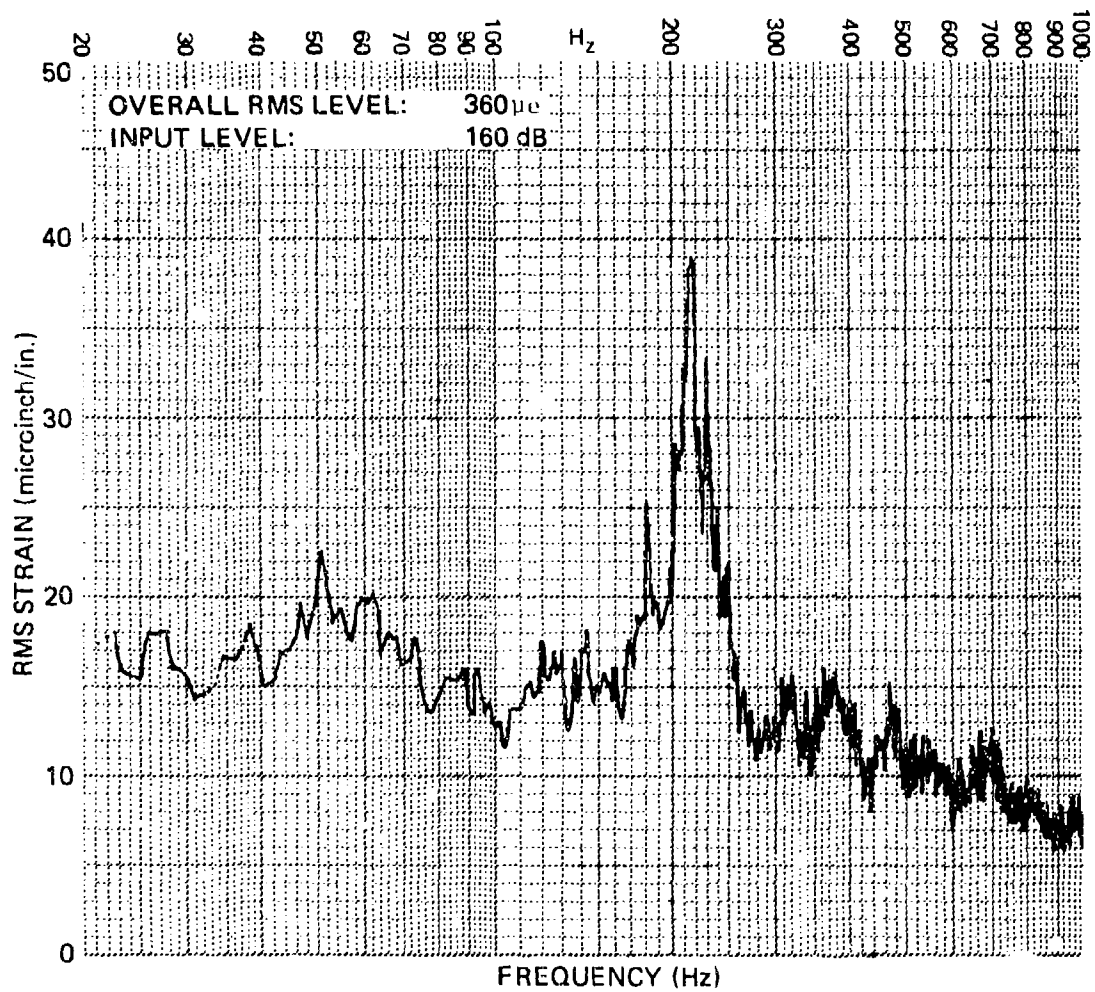
Figure 38. Random Response - Panel s, Gauge 4-1
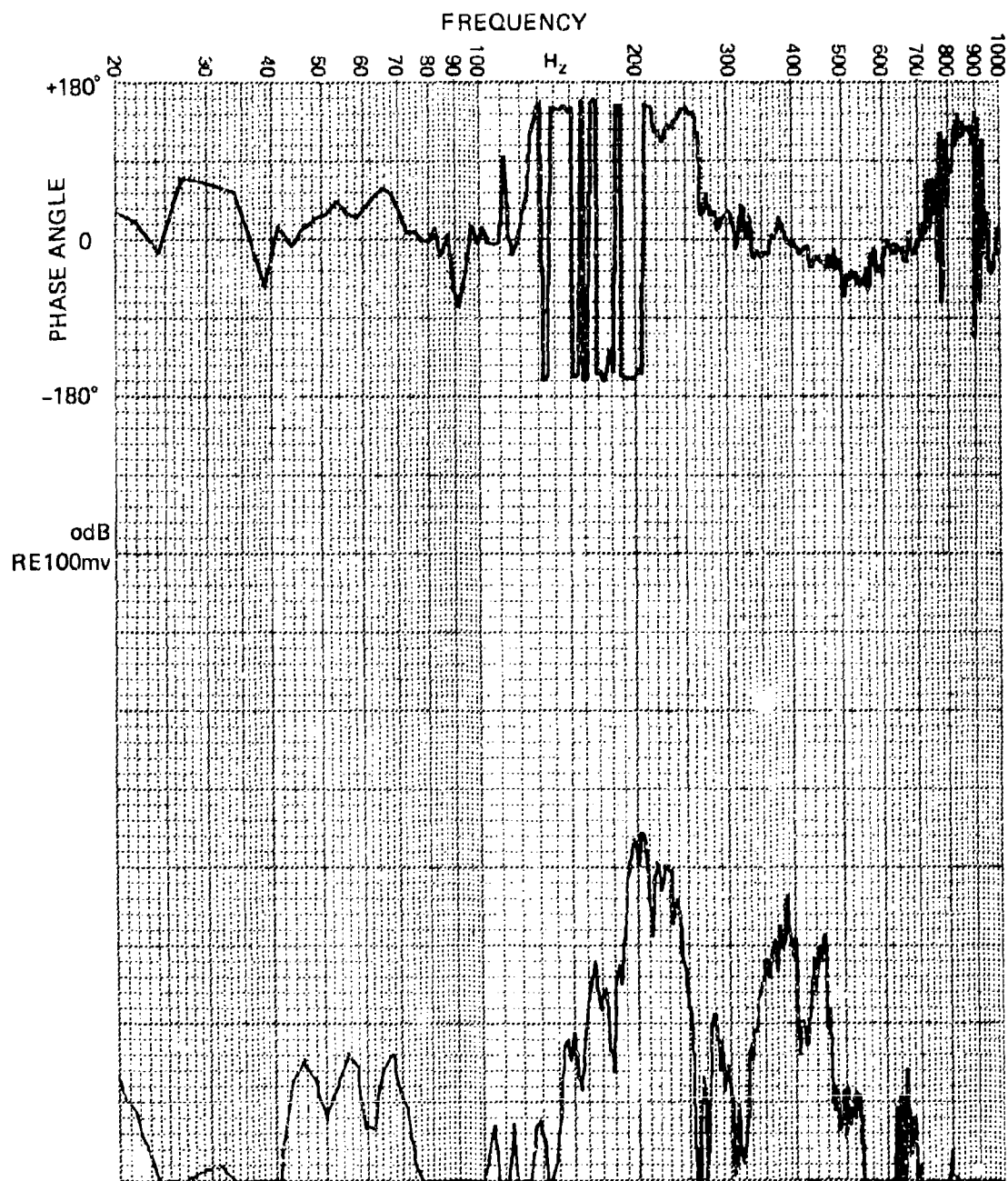
Figure 39.   Random Response – Panel s, Gauge 4-2

108

Figure 40. Phase and Cross Spectral Density - Panel s, Gauges 4-1 and 4-2

109

identification is not possible. Figure 40 shows the corresponding phase and cross-spectral density plots. The phase plot shows the 200 Hz region to be out-of-phase. But since the response spectra (Figures 38 and 39) do not show identical peak response frequencies, the cross-spectral density plot is required in order to identify the frequencies at which the response is coupled between the adjacent bays. Then it can be clearly seen that the out-of-phase mode occurs at 200 Hz and the in-phase mode occurs at 380 Hz.

Table 25 compares overall rms strain levels for Z and J stiffeners, and also between a quasi-isotropic laminate (b) and a more highly oriented laminate (c). Strains are given at the panel centers and at the edges, over a range of overall sound pressure levels. Figures 41 through 48 give corresponding strain spectra at 160 dB. The comparison between the Z and J stiffeners does not present a clear picture. At the panel centers, the strains are comparable for both stiffener types, although it can be seen that for the (b) panel at 160 dB and 165 dB, the J. stiffener resulted in higher strains than did the Z. Looking at the spectra on Figures 41 and 42 (note scale difference) it can be seen that the higher J stiffener strains are due primarily to the response peak at 275 Hz. The fundamental 170 Hz peak was reduced by the introduction of the J stiffener. The same comparison for panel c (Figures 43 and 44) also shows the J stiffener effecting a reduction in response at the fundamental mode frequency. In this case, without a significant increase in the amplitudes of the higher frequency modes. Corresponding comparisons of the edge strains show significant response reductions on panel b, but not on panel c. The corresponding spectra for panel b (Figures 45 and 46) show a 2:1 reduction in the peak response level due to the J stiffeners. Panel c also shows a reduction in the response of the first mode, but the increased response in the other modes results in an increase in the overall strain level. In general, it is clear that, compared to the Z stiffeners, the J stiffeners resulted in a lower response level for the fundamental stringer-bending mode, but had a tendency to stimulate the stringer-torsion mode at 280 Hz. Figure 49 shows the 160-170 Hz peak to be in-phase and the 270-280 Hz peak

110

TABLE 25

RESPONSE STRAIN COMPARISONS BETWEEN Z AND J STIFFENERS AND BETWEEN
$(0, \pm45, 90)_s$ AND $(0_2, \pm45)_s$ PLY ORIENTATIONS

Sound Pressure Level	Center Strain (Gauge 4)				Edge Strain (Gauge 10)			
	Panel b $(0, \pm45, 90)_s$		Panel c $(0_2, \pm45)_s$		Panel b $(0, \pm45, 90)_s$		Panel c $(0_2, \pm45)_s$	
	Z	J	Z	J	Z	J	Z	J
140	65	49	57	65	77	53	57	61
145	114	109	106	115	147	118	112	125
150	190	169	168	176	267	182	185	197
155	261	248	230	227	358	263	253	256
160	337	388	312	306	482	381	330	359
165	412	566	419	416	-	493	432	-

111

OVERALL R.M.S. LEVEL: 337.3 µe
INPUT LEVEL: 160 dB
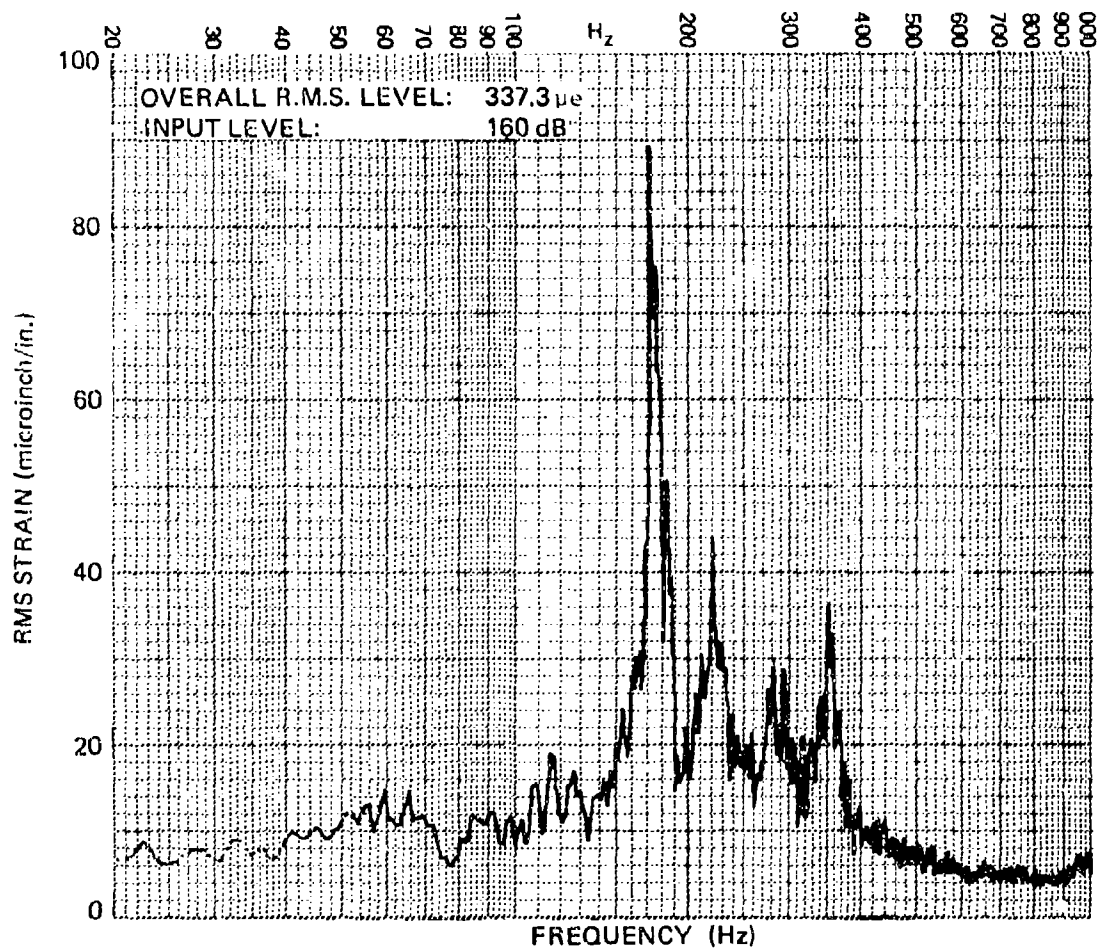
Figure 41. Center Strain - Panel b, Z Stiffener

112
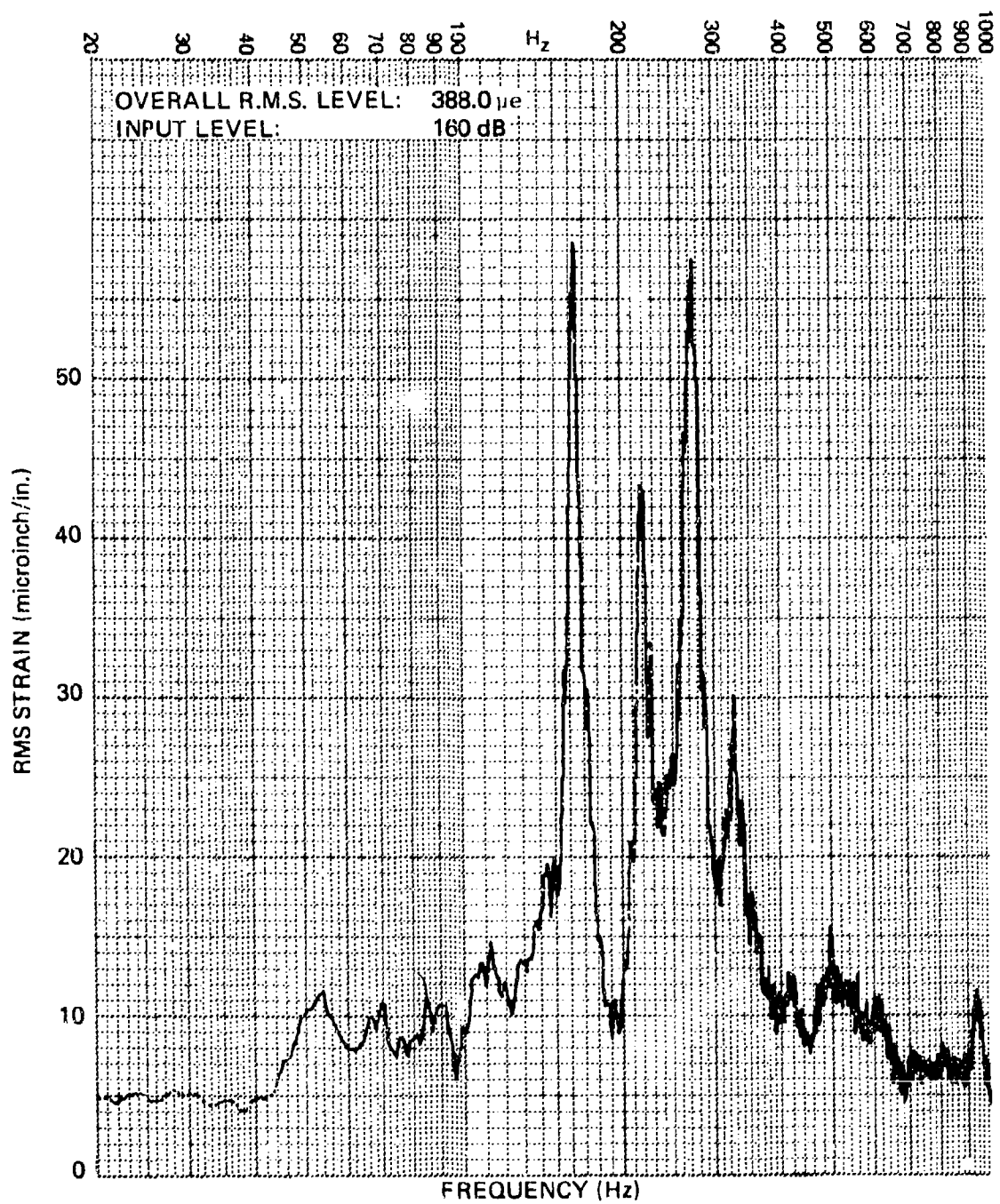
Figure 42. Center Strain - Panel b, J Stiffener

113
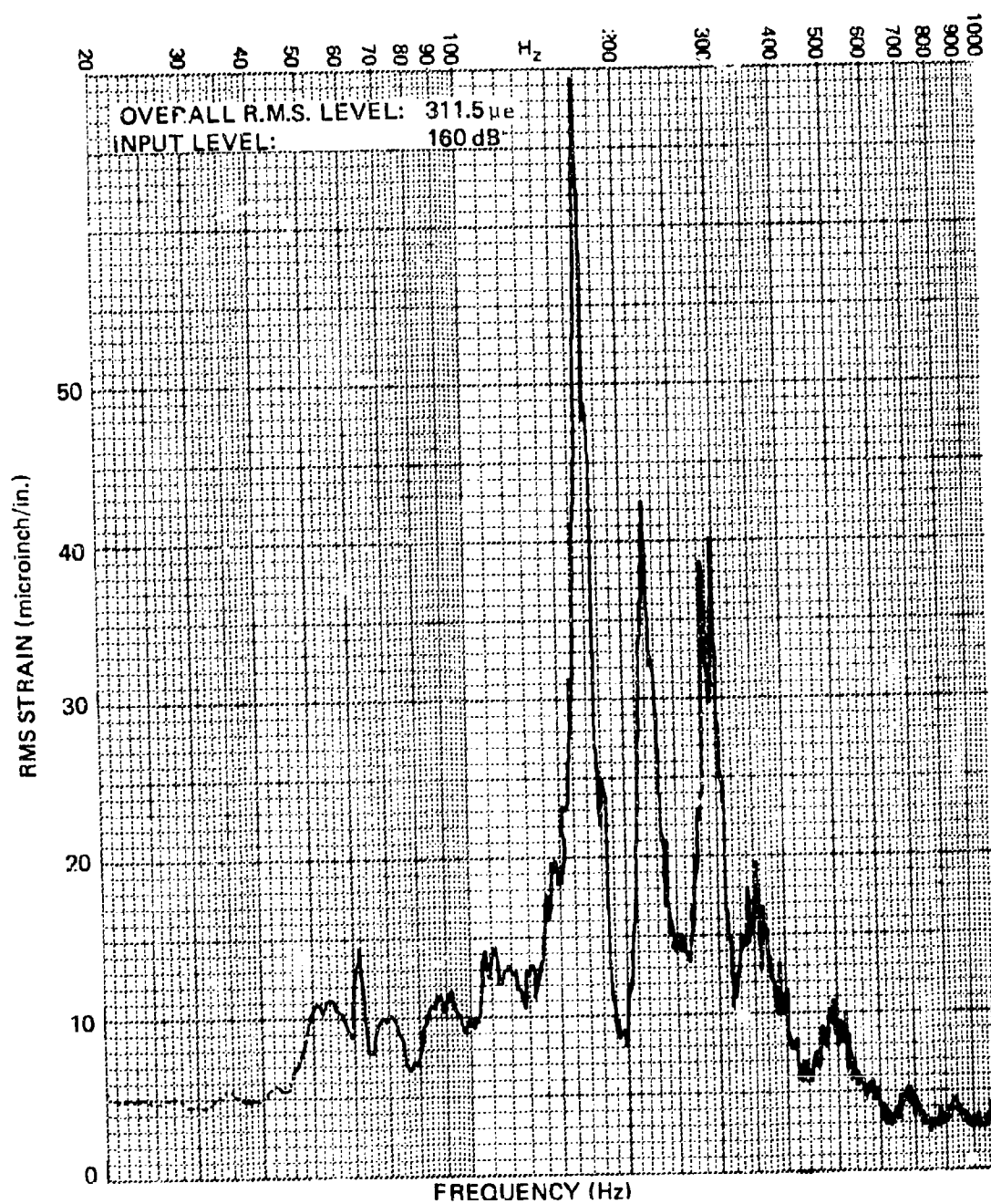
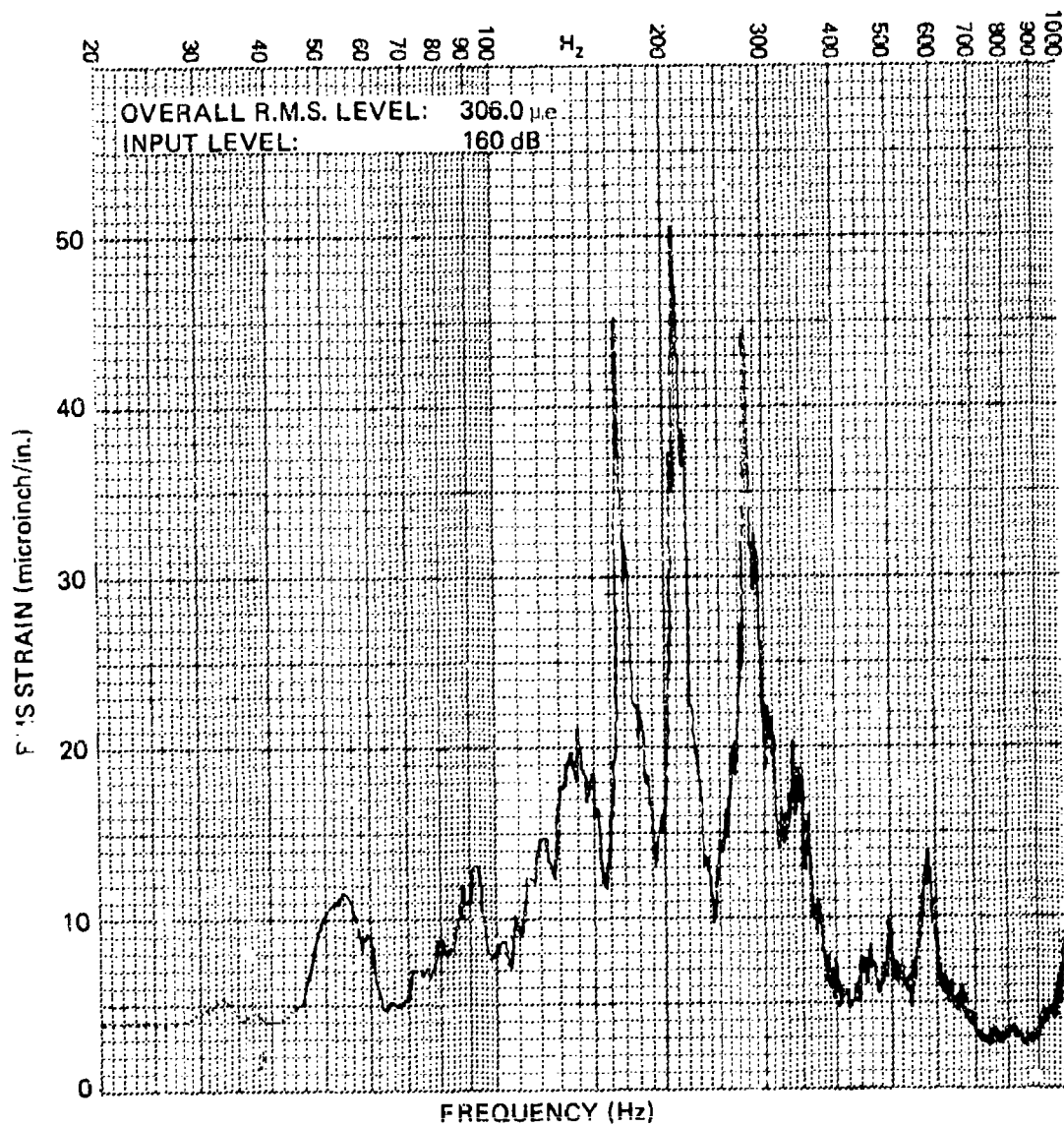Figure 43.   Center Strain - Panel c, Z Stiffener

114

OVERALL R.M.S. LEVEL: 306.0 µe
INPUT LEVEL: 160 dB

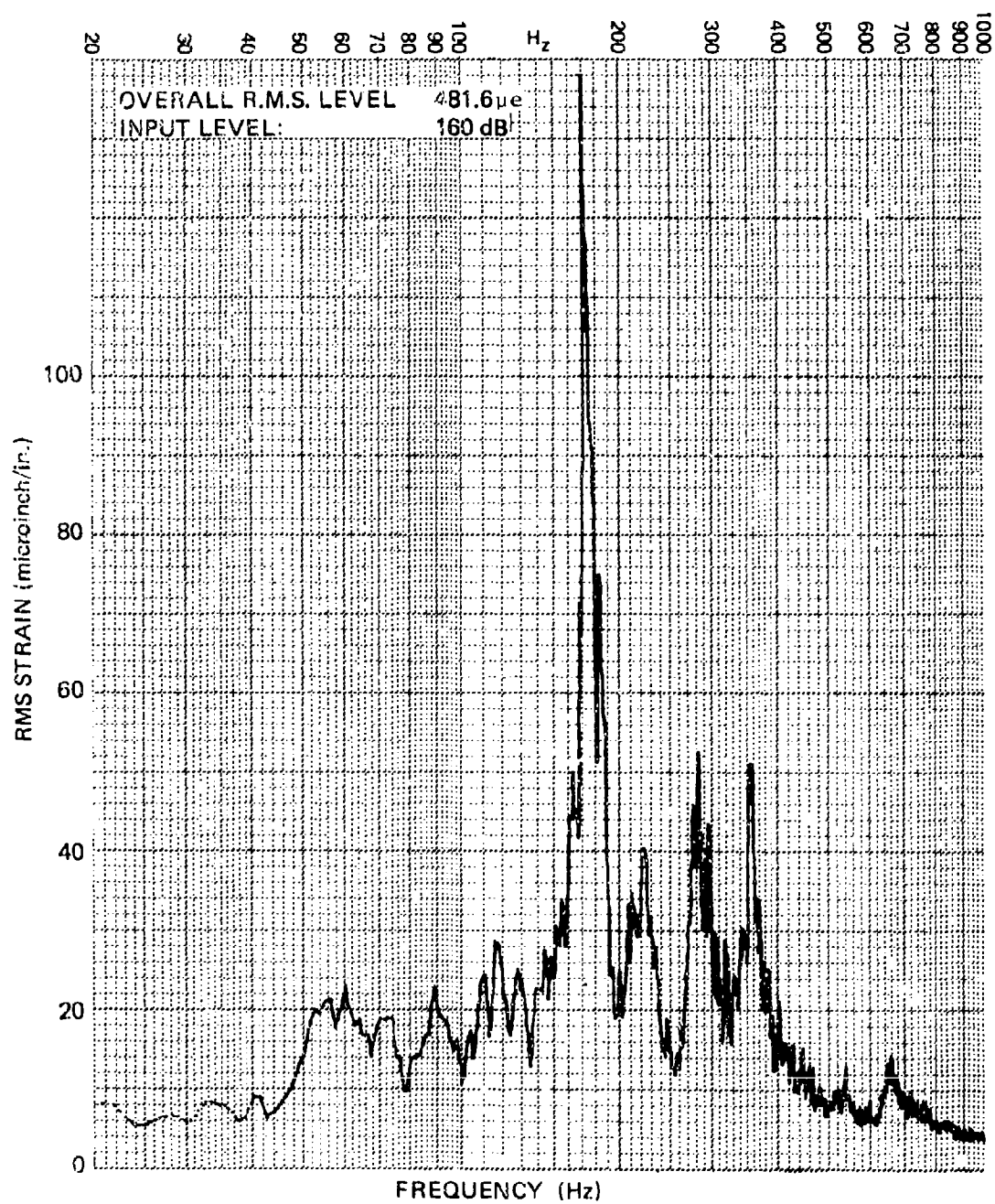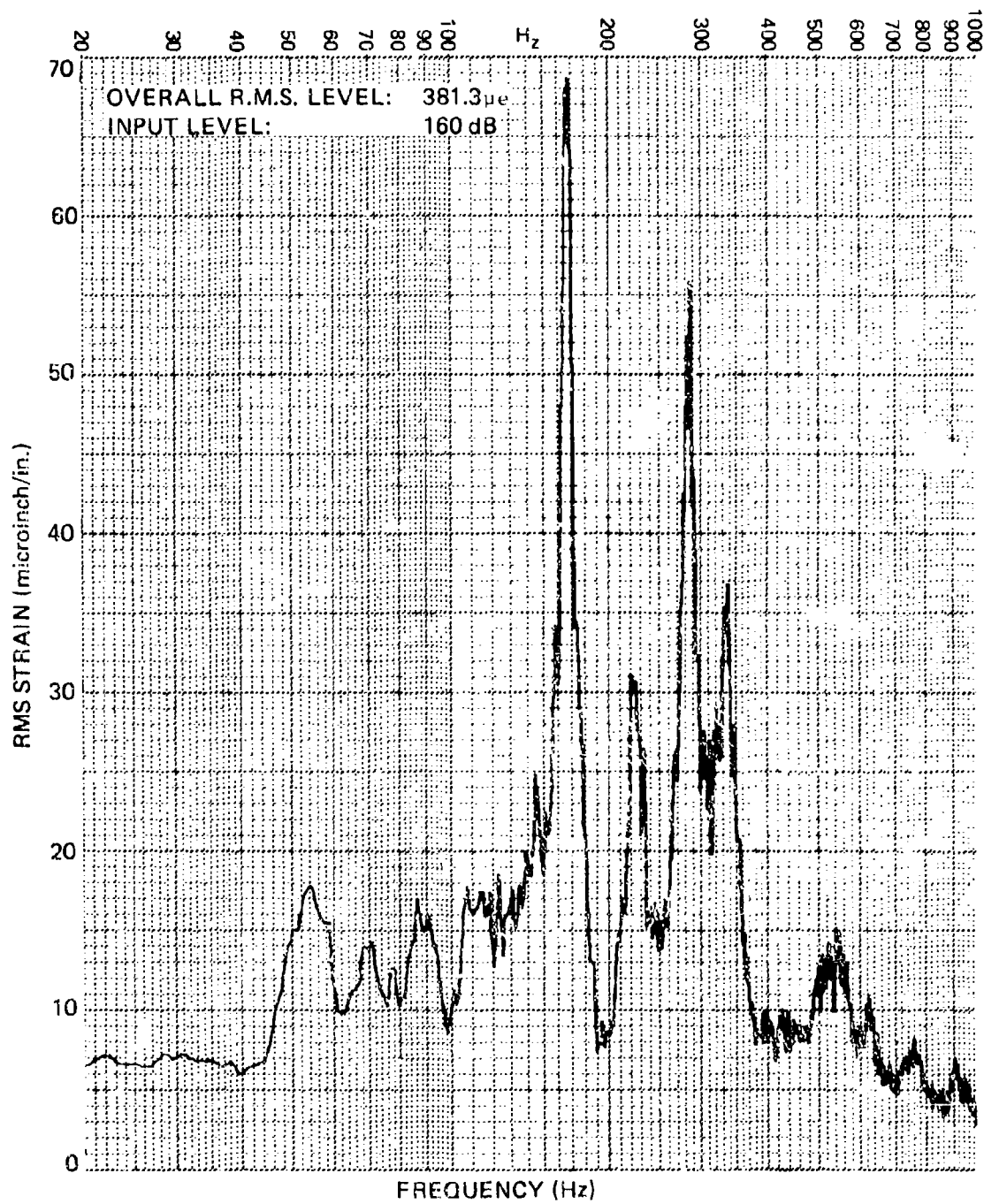Figure 44. Center Strain - Panel c, J Stiffener

115

Figure 45. Edge Strain - Panel b, Z Stiffener

116

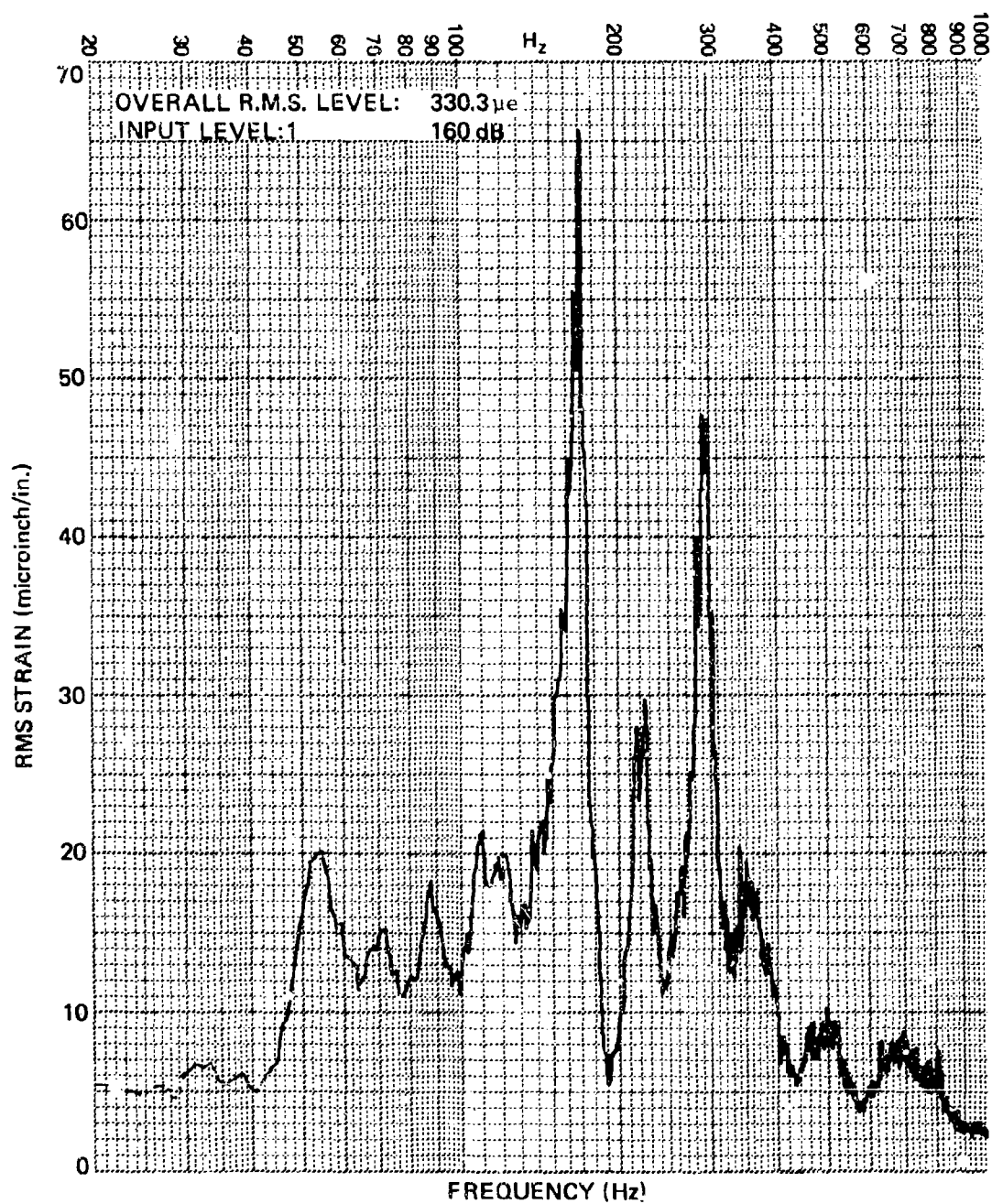Figure 46.   Edge Strain - Panel b, J Stiffener

117
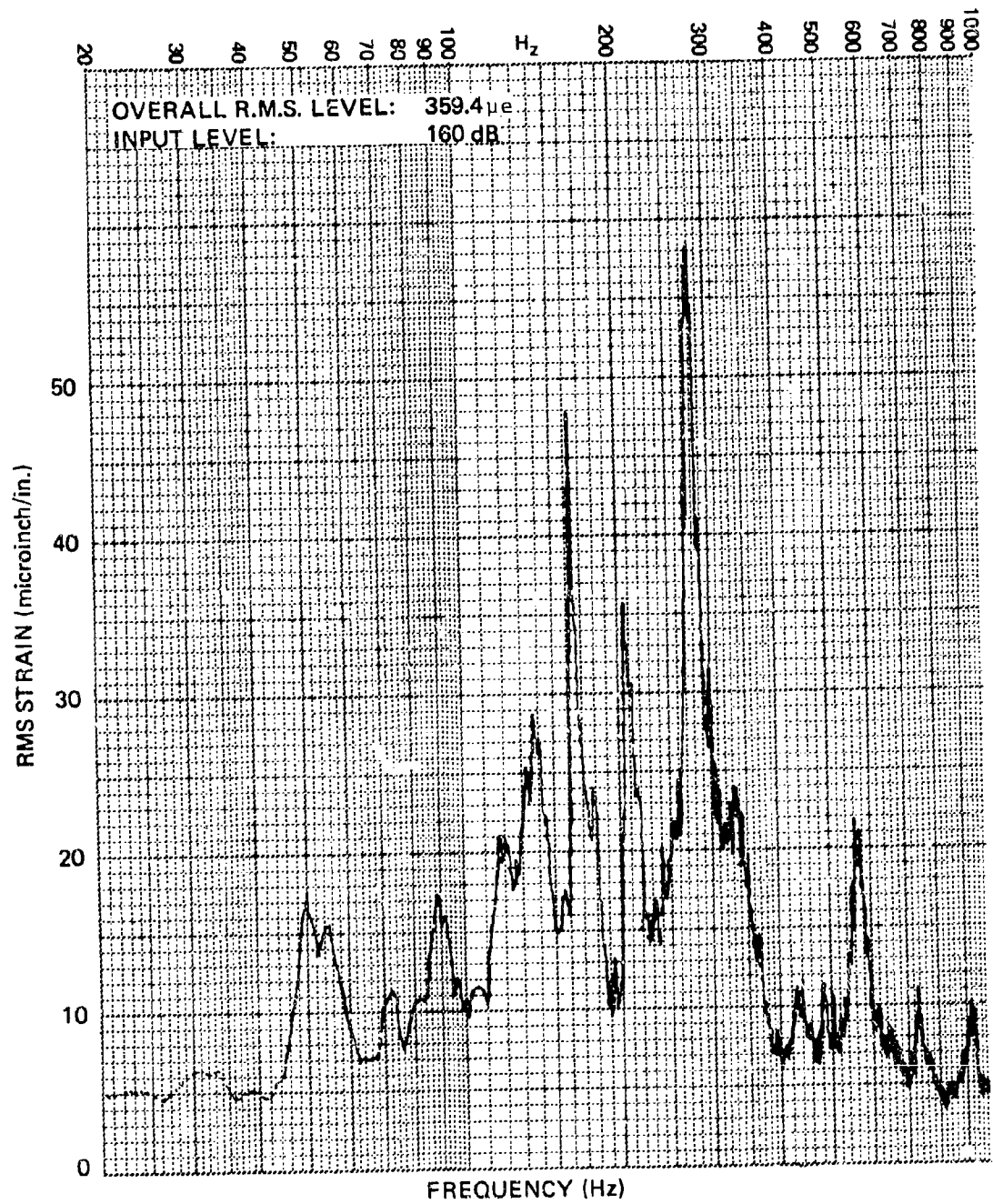
Figure 47. Edge Strain, Panel c, Z Stiffener

118

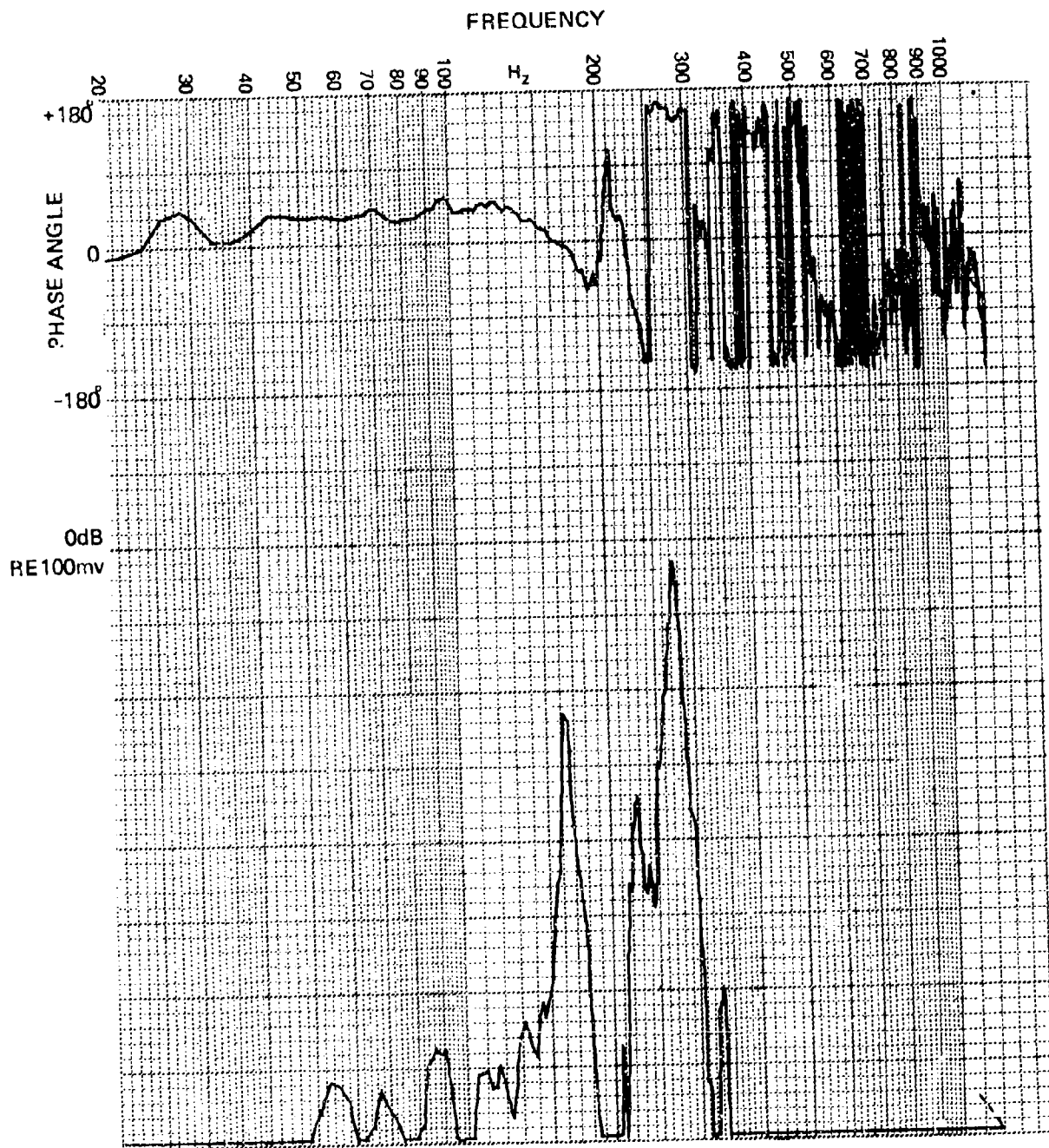Figure 48.   Edge Strain - Panel c, J Stiffener

119

Figure 49. Phase and Cross Spectral Density for Panel b, J Stiffener, Gauges 4 and 28

to be out-of-phase. The J-stiffened panels did, as expected, exhibit longer fatigue lives than did the Z-stiffened panels. For panel b, the J stiffener increased the fatigue life from 50 minutes (for the Z stiffener) to 7 hours. For panel c, the fatigue life increased from 1 hour to 17 hours. This large increase in fatigue life, without a major reduction in response was due to the increased bonded footprint area of the J compared to the Z. This results in more extensive fiber pull-out from the skin laminate upon failure, hence there is slower damage propagation and longer fatigue lives. Based on these results, the J configuration appears to be an attractive stiffener concept.

Table 25 and the corresponding spectra also provide for a comparison between the laminates used for panels b and c. The more highly oriented "c" laminate shows a significant reduction in response of the edge strains (approximately 25 percent). The center strains are similar for both laminates. However, the reduction in edge strain does not occur when using the J stiffener. The corresponding frequency spectra do not provide any additional information on the response difference between the two laminates. The difference between the two laminates involves taking two of the eight plies running in the long bay direction (90 deg., in the X direction) and running them in the short direction (0 deg., Y direction-between stringers). Looking at the overall results, it was concluded that these two laminates had comparable sonic fatigue resistance.

Three panel configurations (g, i and k) were used to compare the response of bonded and riveted joints. Table 26 summarizes the overall rms strain levels at the center and edge of the center bay of each panel. The differences between strains at the bay center do not appear to be significant. There is a tendency for the edge strains to be a little lower on the riveted panels than on the bonded panels, but the differences are neither large nor consistent. Figure 50 shows a comparison of response spectra for panel g at 160 dB. Although the overall levels differ (205 to 162 microinches/inch), the spectra are remarkably similar.

121

TABLE 26

COMPARISON OF OVERALL RMS STRAIN LEVELS FOR BONDED AND RIVETED PANELS

| Sound Pressure Level	Center Strain (Gauge 4)						Edge Strain (Gauge 10)					
	Panel g		Panel i		Panel k		Panel g		Panel i		Panel k	
	Bonded	Riveted	Bonded	Riveted	Bonded	Riveted	Bonded	Riveted	Bonded	Riveted	Bonded	Riveted
140	29	28	31	40	53	51	51	50	26	35	50	58
145	44	42	64	55	90	74	93	76	47	46	84	78
150	70	64	120	86	144	113	151	127	84	63	142	111
155	120	94	192	139	227	199	250	204	133	102	211	194
160	205	162	226	222	322	297	460	317	168	162	295	279
165	299	296	325	335	-	408	595	503	258	254	-	413
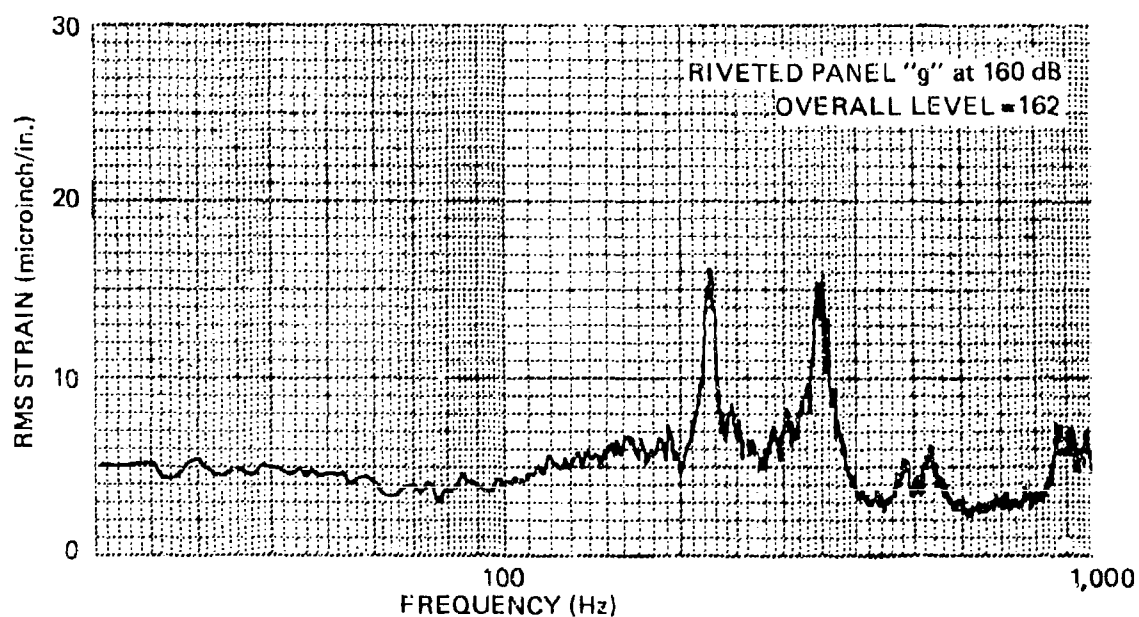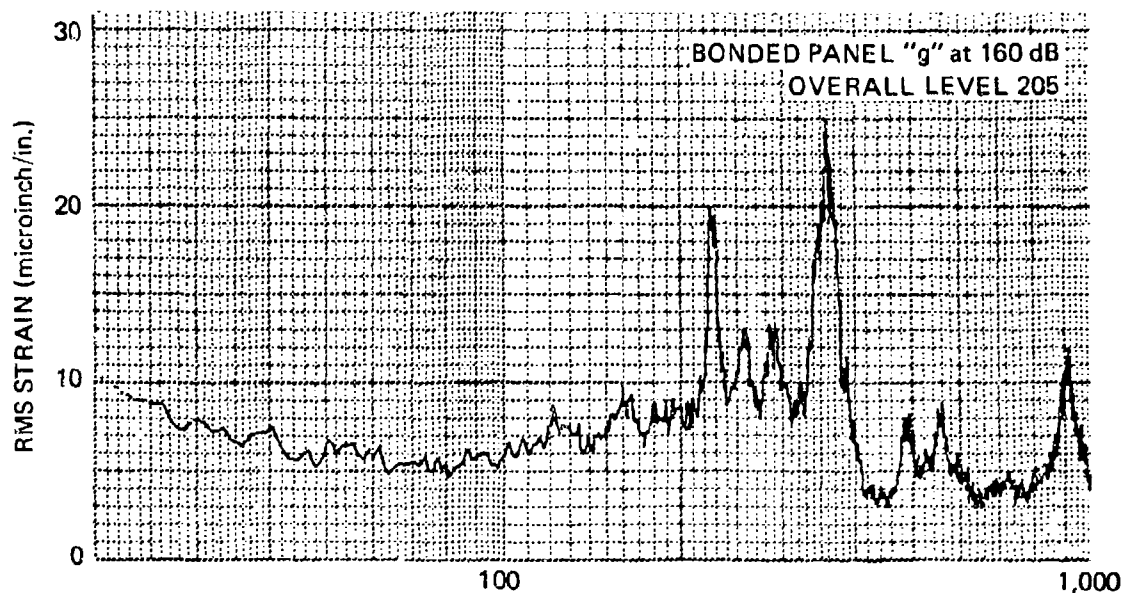
Figure 50. Comparison of Strain Spectrum for Bonded and Riveted Panels

123

Overall, it appears that the riveted joints do not significantly affect panel response. They do, however, affect the mode of failure. The riveted panels experienced partial failure in the Z radius adjacent to the skin, in addition to skin laminate failures. The fatigue lives of the riveted panels were not significantly longer than for the bonded panels with good quality joints. However, observations of damage propagation during testing indicated that heavier stiffeners and more rigid clipping at the stiffener intersections would result in longer fatigue life for the riveted panels. This is because the riveted panels experienced significant stiffener and clip damage prior to skin failure. This was not true of the bonded panels, where skin damage was the primary mode of failure. Another factor to bear in mind is that a slightly substandard bond is difficult to detect and may result in a highly premature f-tigue failure. A slightly substandard rivet joint is detectable and will have a less severe affect on fatigue life.

Figure 51 shows the strain spectrum corresponding to the top spectrum on Figure 50, without the stiffener webs clipped to the fixture frame. Although the overall strain level increased from 205 to 240 microinches/inch, due to removing the clips, the spectra show this increased strain to be predominantly below 200 Hz. This indicates that providing proper attachments at the panel boundaries is desirable and reduces the low frequency overall panel motion.

Early testing of a curved panel in an aluminum fixture resulted in a fixture failure. Steel backup fixtures had been fabricated for such an eventuality, and consequently, it became necessary to determine whether or not the steel versus the aluminum fixtures affected panel response. Figure 52 shows the results of this comparison. As expected, no significant panel response effects were observed.

Early in the test program, several side experiments were performed in order to ensure that testing two panels simultaneously would not produce any unwanted response interrelationships. One of the panels was
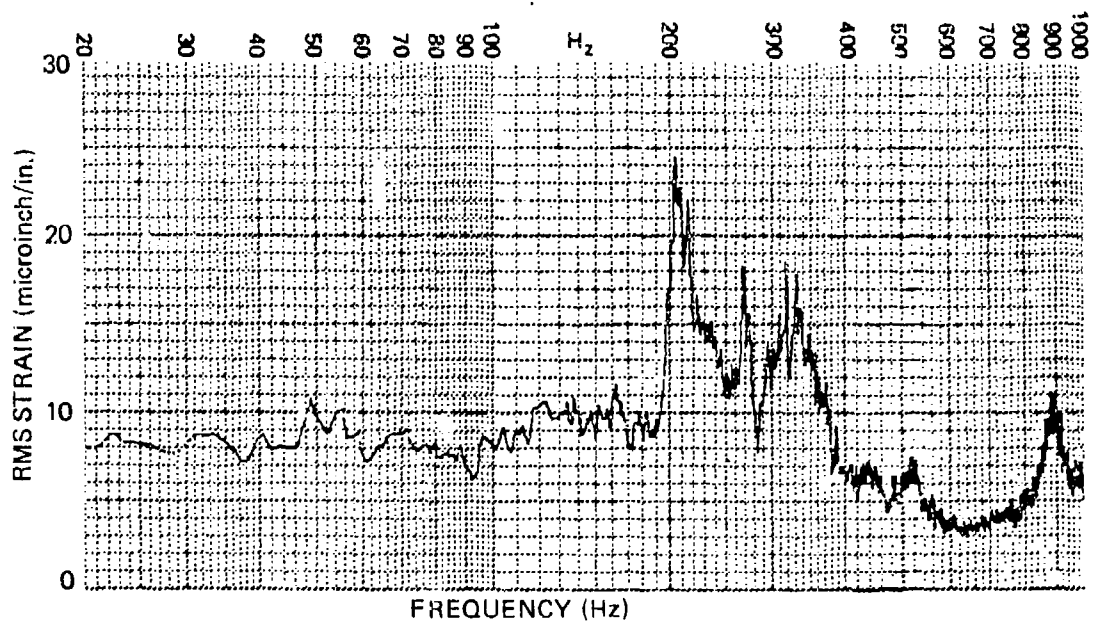
124

Figure 51. Strain Spectrum for Panel g-Stiffener Clips Not Attached, Gauge 4
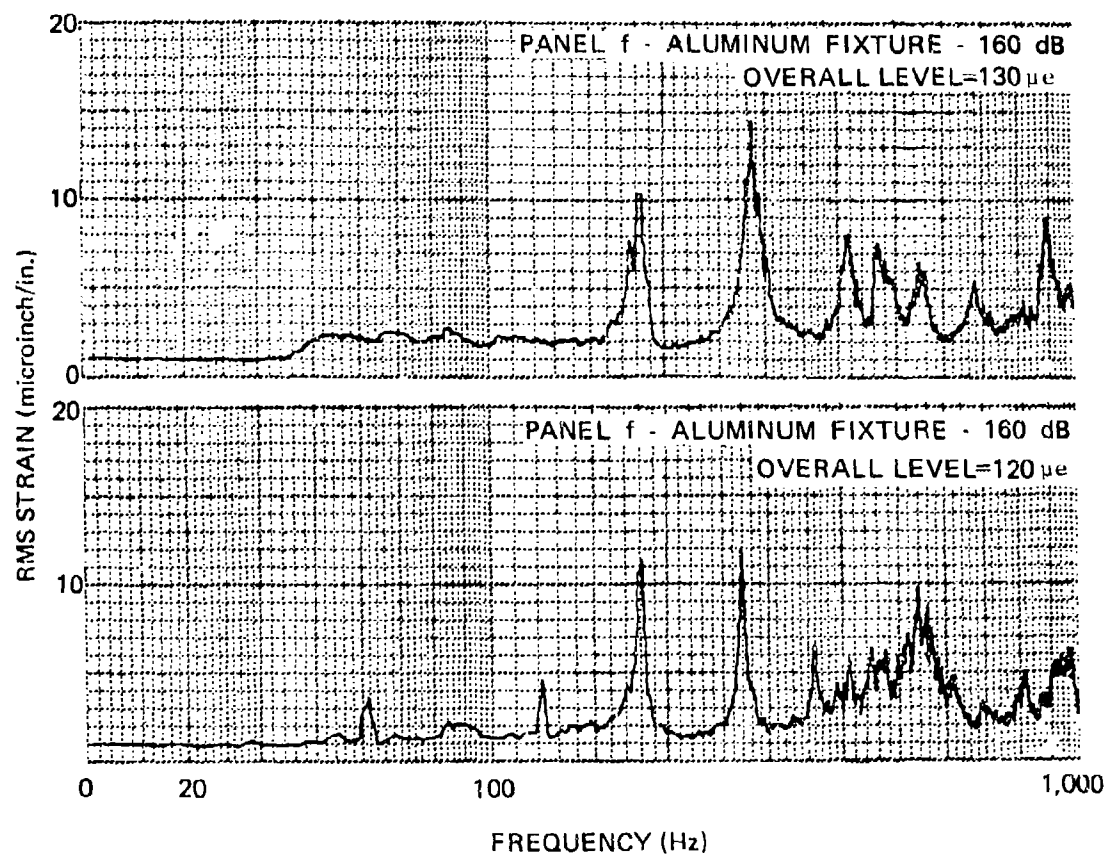
Figure 52. Comparison of Strain Spectrum for Aluminum and Steel Fixtures

126

concurrently tested in the top and bottom test windows, paired with different panels and also paired with a steel plate in the second test window. No significant effects on the panel responses were noted. The second test window was left open at one point and the only noticeable effect was a 2-3 dB drop in acoustic levels in the PWT. When the driver outputs were increased to bring up the acoustic level to that previously used, there was not noticeable change in the response characteristics of the test panels due to the open window.

In order to evaluate some boundary condition effects, panel d was tested for response under three different edge conditions. First, it was suspended in the test window without a fixture frame, i.e., with free edges. The fixture support wires supported the panel at the four corners only. Then the panel was bolted into the wall of the PWT, simulating fixed edge conditions. Finally, the panel was supported in the regular fixture frame and suspended on the fixture support wire, as used on the remaining panels. The effect of these different boundary conditions can be seen in Table 27. The overall rms strains show that the free edges result in lower response levels than when using the test fixture or fixed edges. When it was decided to perform the sonic fatigue tests using a picture-frame fixture, supported on wires, it was hoped that the response in the center bay would be the same as for fixed edges. The overall strains appear to confirm this. Figures 53, 54 and 55 show corresponding edge strain spectra at 165 dB for the three edge conditions. The stringer bending mode occurs at 340 Hz. This basic mode occurs with all three boundary conditions. The major response effects of the boundary conditions occur at 160-180 Hz and at 250 Hz. The modes at these frequencies do not occur when the panel is freely supported. If these extra modes were due to vibrations of the PWT wall, they would not occur when the panel is in the fixture frame, supported on wires unless the PWT vibrations were transmitted through the wire harness. If this were the case, the load-cell in the wire harness would detect them. Figure 56 shows the corresponding frequency spectrum for the load-cell. As can be clearly seen, there was no significant dynamic response occurring in the
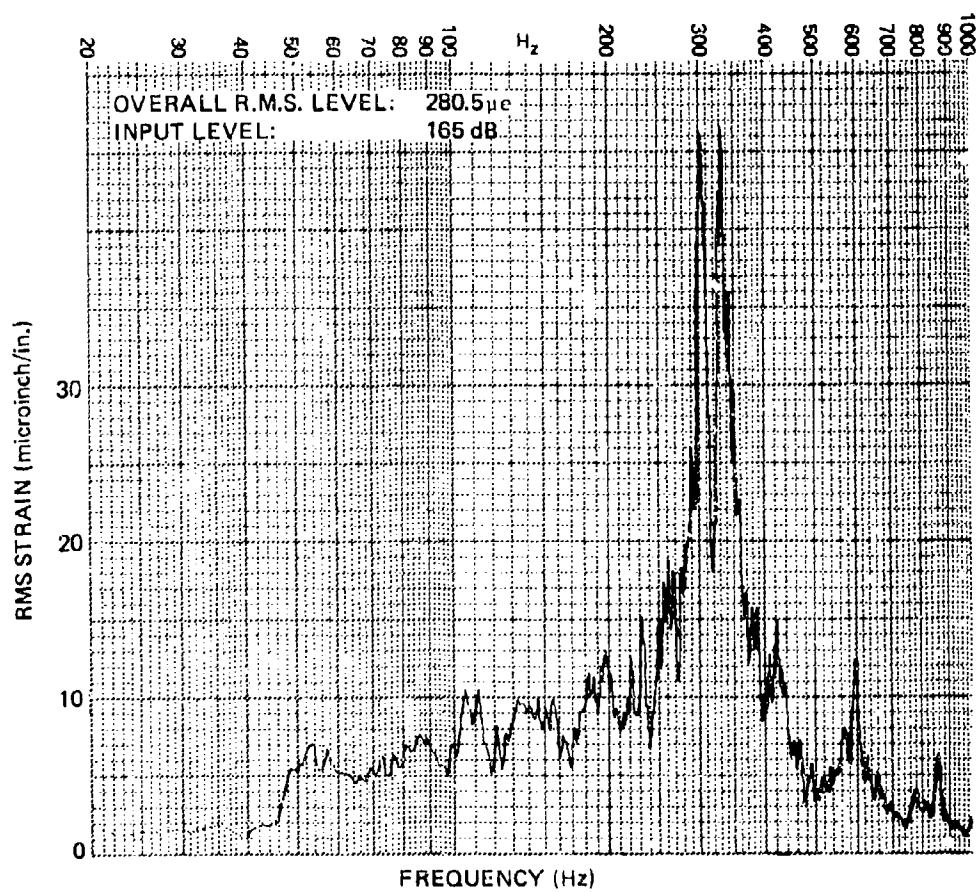
127

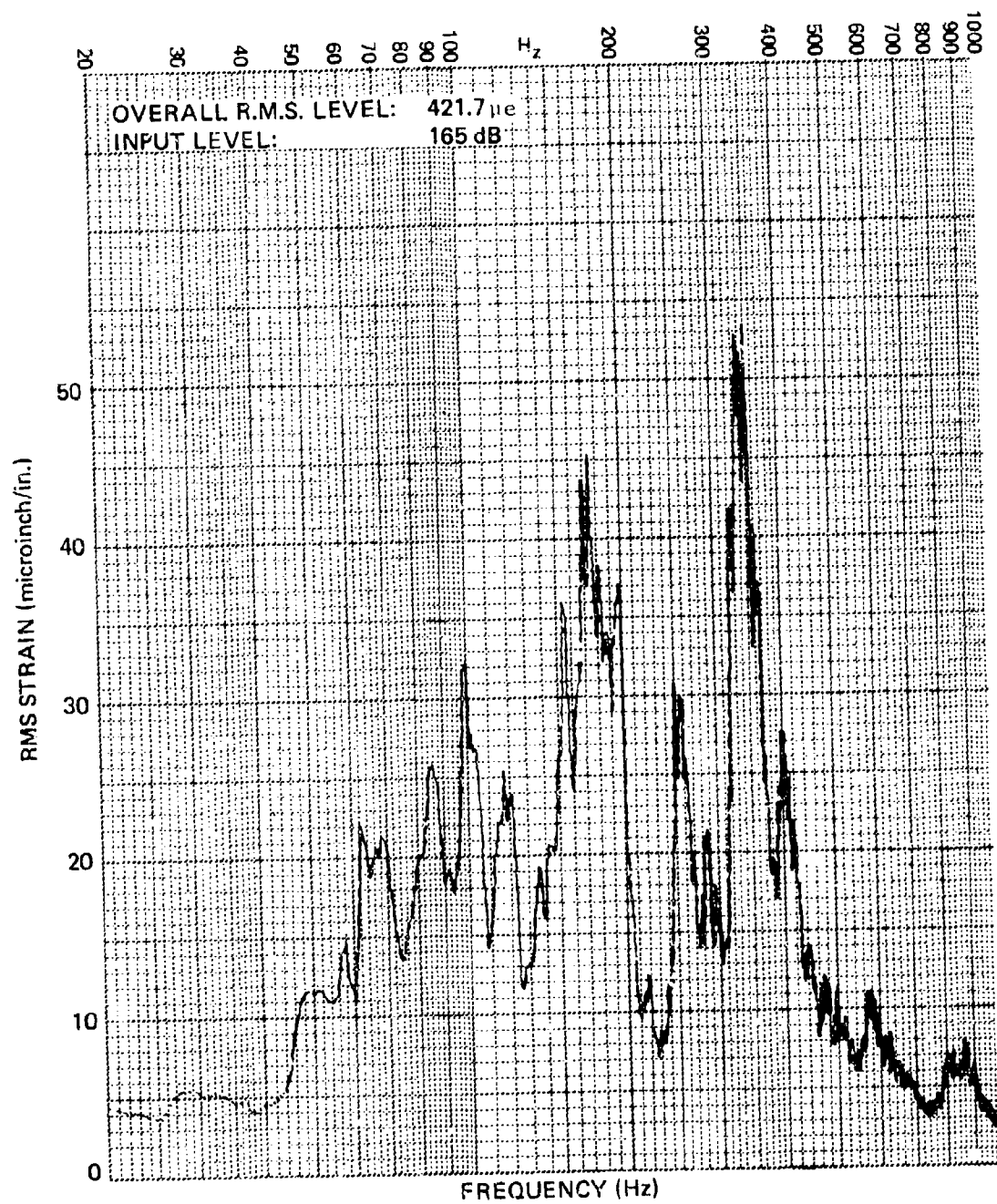Figure 53.   Response Spectrum for Panel d - Free Edges, Gauge 10

128

Figure 54. Response Spectrum for Panel d - Fixed Edges, Gauge 10
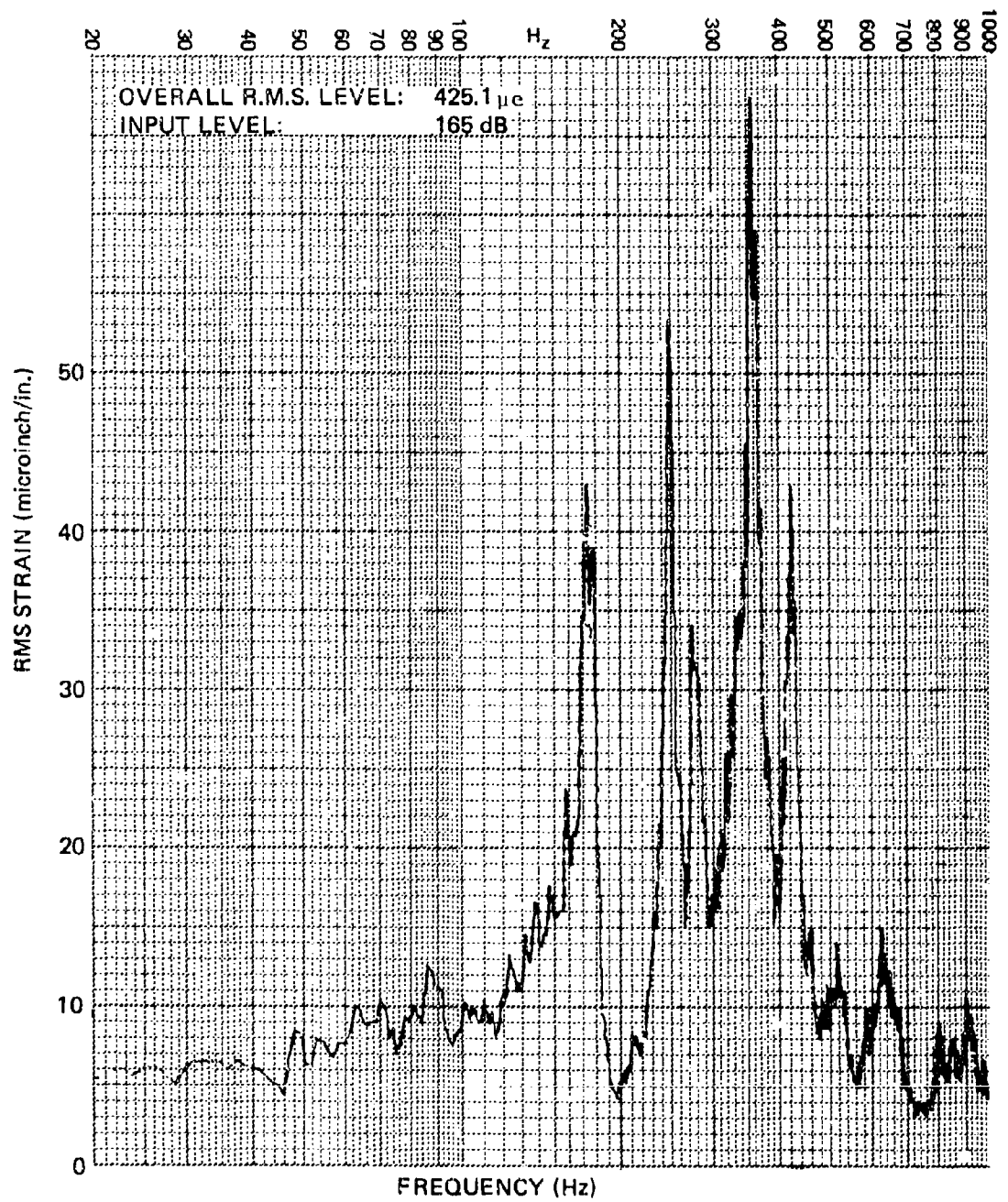
129

Figure 55.   Response Spectrum for Panel d - Regular Test Fixture, Gauge 10

130

TABLE 27

OVERALL RMS STRAIN LEVELS (MICROINCHES/INCH) FOR
PANEL "d" WITH DIFFERENT EDGE CONDITIONS

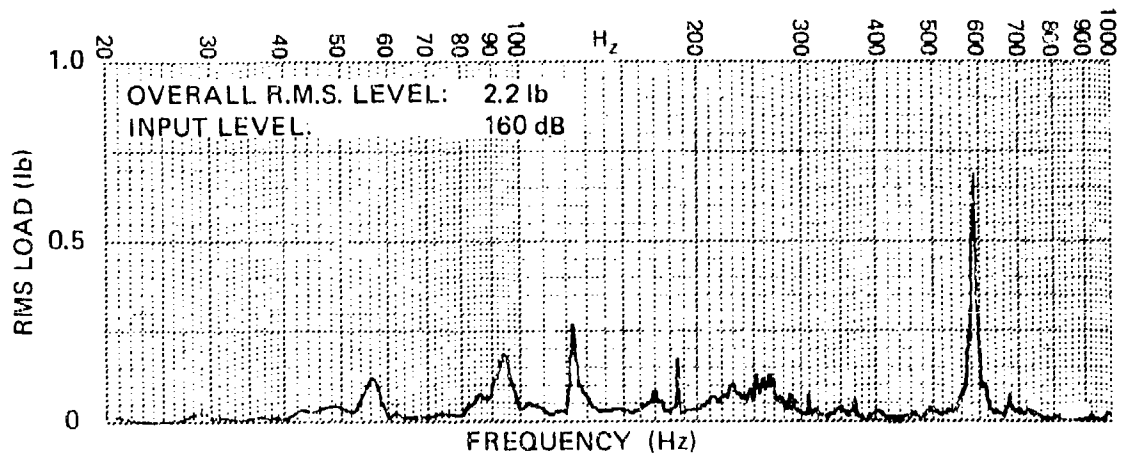| Sound Pressure Level (dB)	Center Strain (Gauge 4)			Edge Strain (Gauge 10)		
	Free Edges	Fixed Edges	Edges Supported in Test Fixture	Free Edges	Fixed Edges	Edges Supported in Test Fixture
140	23	34	33	24	37	34
145	31	55	58	35	59	57
150	49	119	109	56	124	101
155	88	171	183	107	186	174
160	140	261	284	190	296	274
165	226	372	416	281	422	425

Figure 56.   Load Cell Spectrum

131

wire harness supporting the panel fixture assembly. If the modes at the
160-180 Hz and 250 Hz were associated with the regular fixture frame, they
would not have occurred when the panel was bolted to the PWT wall (for
this test the panel was first removed f   s fixture frame and then
bolted directly to the PWT wall). The major response difference between
the fixed edge conditions and the regular test fixture occurs at 100 HZ
and below. The response peaks in this frequency region appear to be due
to the effects of the PWT wall. Thus, the panel support system chosen for
this test program appears to be structurally similar to the more typical
method of bolting the panel to the PWT wall, without picking up PWT
dynamic effects.

Two honeycomb beam stiffened panels, shown in Figure B-1, were tested and
the results compared to an equivalent panel with Z stiffeners - panel b.
The results are shown in Table 28. The first panel (el) had panned down
closures for the honeycomb stiffeners, as shown in Figure B-1. This panel
failed in these closures after 1-1/2 minutes at 165 dB. The second panel
(e2) was subsequently modified, replacing the existing panned down
closures with full depth closures, clipped to the fixture in a similar
fashion as the Z stiffener attachments. This panel failed after 5-10
minutes at 165 dB.

Although these times to failure seem short, the maximum strains on both
panels were high, such that if superimposed on the fatigue curve on
Figure 33, both panels appear to be on, or slightly above, the curve drawn
for the Z-stiffened panels. The maximum strains on both el and e2 were
higher than those shown in Table 28 (which are presented for comparison
purposes), and occurred at the center of the shorter sides. It is not
known why the honeycomb stiffened panels had different maximum reponse
locations compared to the Z-stiffened panels. In any event, the
comparison between the honeycomb and zee stiffeners was inconclusive. It
does seem probable that the honeycomb stiffeners would have been more
effective if the core material had had greater shear strength.

132

TABLE 28

COMPARISON OF OVERALL RMS STRAINS (MICROINCHES/INCH) FOR HONEYCOMB
AND Z STIFFENED PANELS

Sound Pressure Level (dB)	Center Strain (Gauge 4)			Edge Strain (Gauge 10)		
		Stiffener Type			Stiffener Type	
	Z (b)	Honeycomb-Panned Down Closure (e1)	Honeycomb-Full Depth Closure (e2)	Z (b)	Honeycomb-Panned Down Closure (e1)	Honeycomb-Full Depth Closure (e2)
140	65	56	74	77	65	94
145	114	103	129	147	134	166
150	190	189	207	267	245	287
155	261	262	261	358	343	382
160	337	350	385	482	455	521
165	412	440		-		-

Ideally, a sonic fatigue design method should be based on using acoustic spectrum levels to predict strain spectrum levels at corresponding frequencies. However, individual response spectrum levels usually vary inconsistently, compared to overall response levels, making them unsuitable for analysis purposes. An example of this is shown in Figure 57. The spectra shown are for the same strain gauge at 160 dB (top) and 165 dB (bottom). The overall rms strain level increased from 310 to 435 microinches/inch due to the 5 dB increase in acoustic load. However, the strain spectrum level at the major response mode (170 Hz) actually decreased slightly (from 82 to 68 microinches/inch). The increased overall strain level was due to increases in the strain response at other frequencies. Inconsistencies of this type make it impractical to use the strain spectrum levels in the development of the design method. This leads to a dilemma in the treatment of random strain data. Spectrum levels, with their narrow bandwidth, often vary unpredictably; whereas overall levels, with their wide bandwidth, include response that does not contribute to fatigue. It has been suggested that 1/3-octave or 1-octave bandwidth measurements may provide the necessary stability without being influenced by superfluous data. Again referring to Figure 57, it can be seen that some of the increase in overall rms strain was due to the low amplitude strains in the 250-1,000 Hz region. This is quantitatively demonstrated in Figure 58. Superimposed on the power spectral density function, is the integrated power spectral density. From this plot it can be seen that the major response peak at 170 Hz contributes only about 20 percent of total power spectral density (mean square). Whereas the low amplitude response above 250 Hz accounts for 40 percent of the total spectral density. Based on this data, it might be thought that increasing the sound pressure level from 160 to 165 dB would not necessarily bring about a more rapid sonic fatigue failure. However, data taken during the test program clearly pointed to a definite relationship between the overall rms strains and fatigue failures, leading to the conclusion that some low amplitude strains that might be thought of as not contributing to fatigue failure do, in fact, make a significant contribution. As a
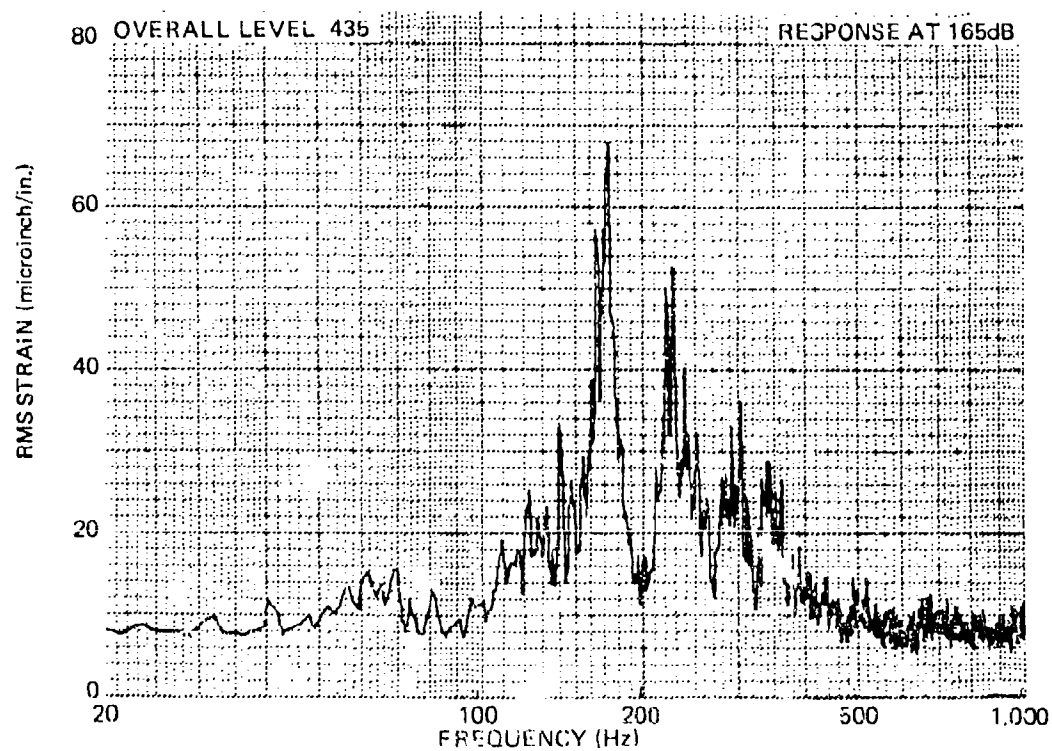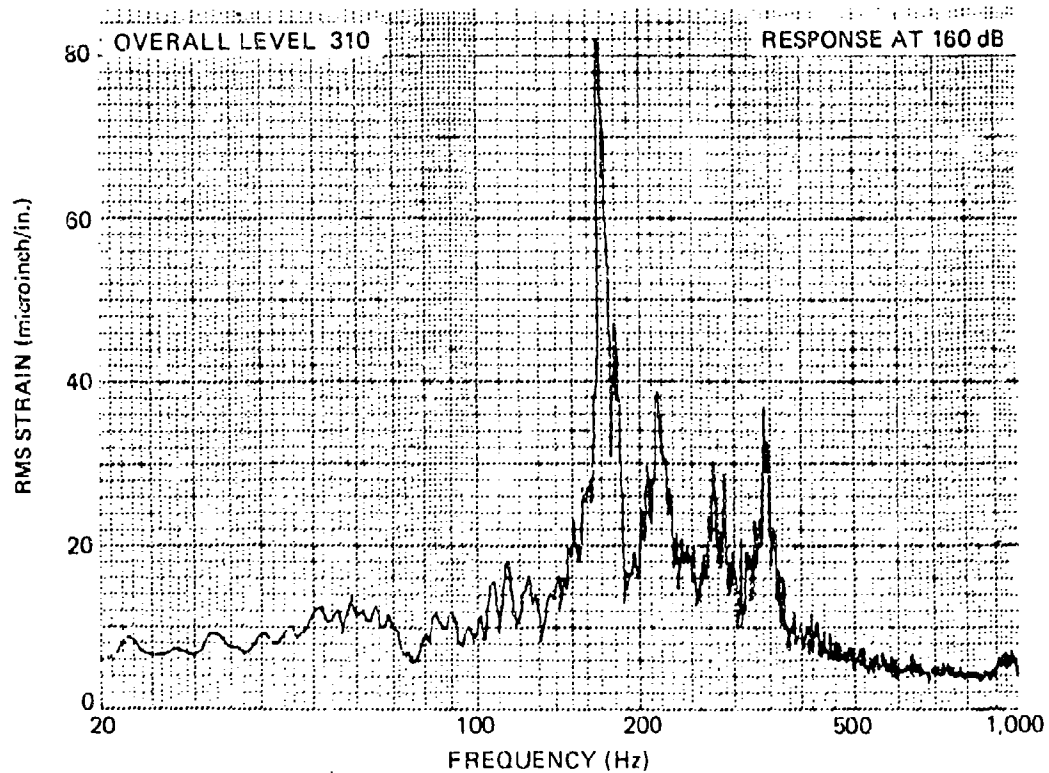
134

Figure 57. Comparison of Strain Spectrum at 150 dB and 165 dB (Panel b)
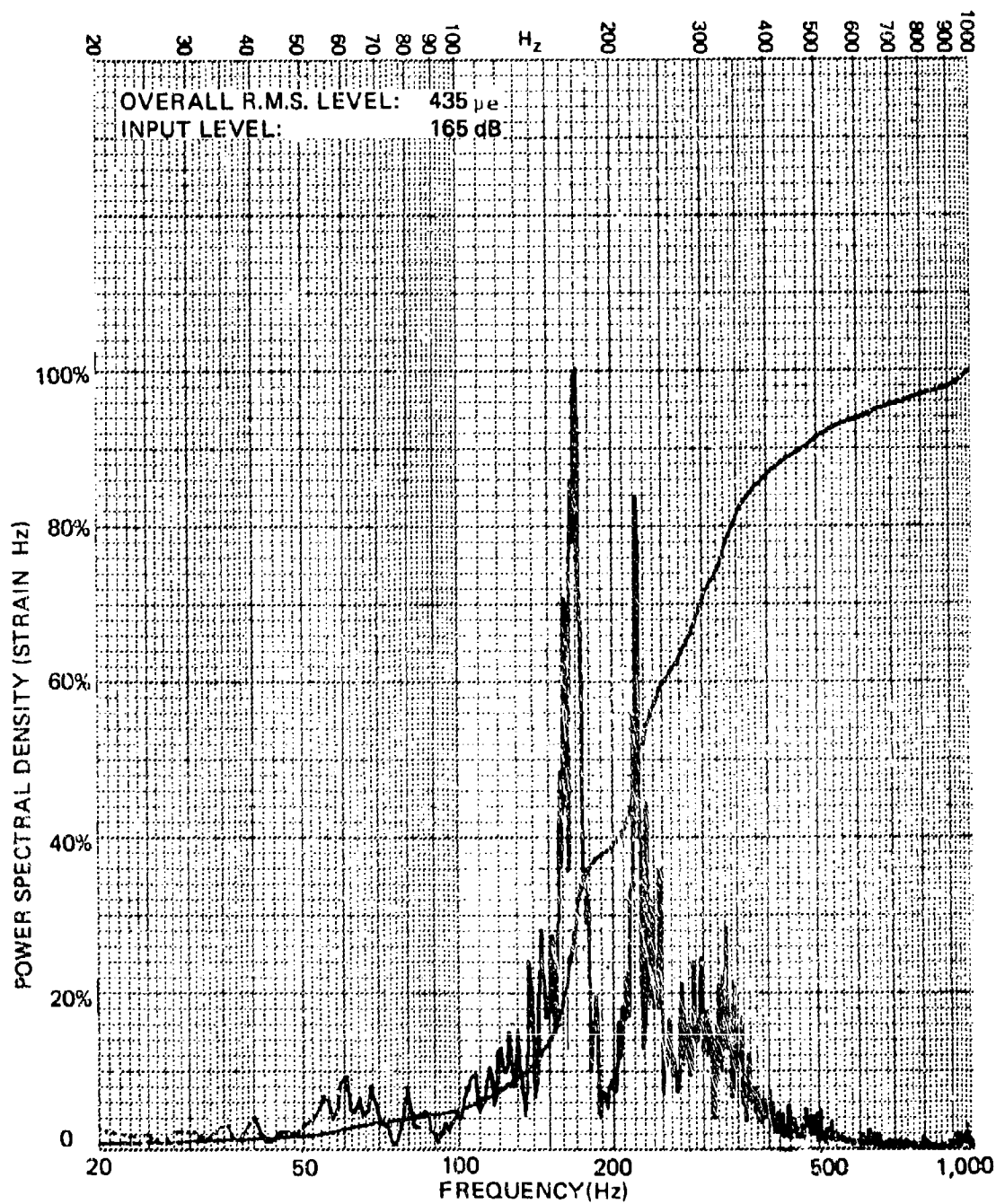
135

Figure 58.   Integrated Power Spectral Density for Strain Response, for Panel b, Gauge 4

136

result, overall rms strains generated in the PWT test program were used in the development of the design method, described in Section IV.

Integrated power spectral density functions were generated for another purpose. The PWT had a tendency to generate an acoustic peak in the 150-180 Hz region (see Figures C-1 through C-6). It was found that this peak could be satisfactorily controlled by adjusting the bias voltage in the EPT 200 acoustic drivers. In most cases the peak did not significantly affect panel response; where it did, integrated PSD functions were used to quantify the effects. Figure 59 shows a situation where the response spectrum makes it appear as if the acoustic peak has produced a major response peak at 180 Hz. However, the integrated PSD curve shows that only 14 percent cf the energy is contained within that peak. When converted to rms levels, this unwanted peak accounted for less than 10 percent of the overall rms strain level. In a situation where spurious peaks have a major effect on response levels, the integrated PSD function provides a quantitative tool for subtracting the effects out.

The strain spectra generated during the progressive-wave tube tests (contained in Appendix C) were used to determine damping ratios for various panels, using the "half power-point bandwidth" method. The damping ratio is found from the following relationship:

$$\zeta = \frac{\Delta f}{2f}$$

where
ζ = Damping ratio

Δf = Frequency bandwidth (Hz) at the half-amplitude point of major strain reponse peak

f = Center frequency of major strain response peak

The values obtained showed considerable scatter and did not show any significant correlation with strain response levels. Consequently, damping was not included as a design parameter in Section IV. Instead, the use of a typical value was recommended.
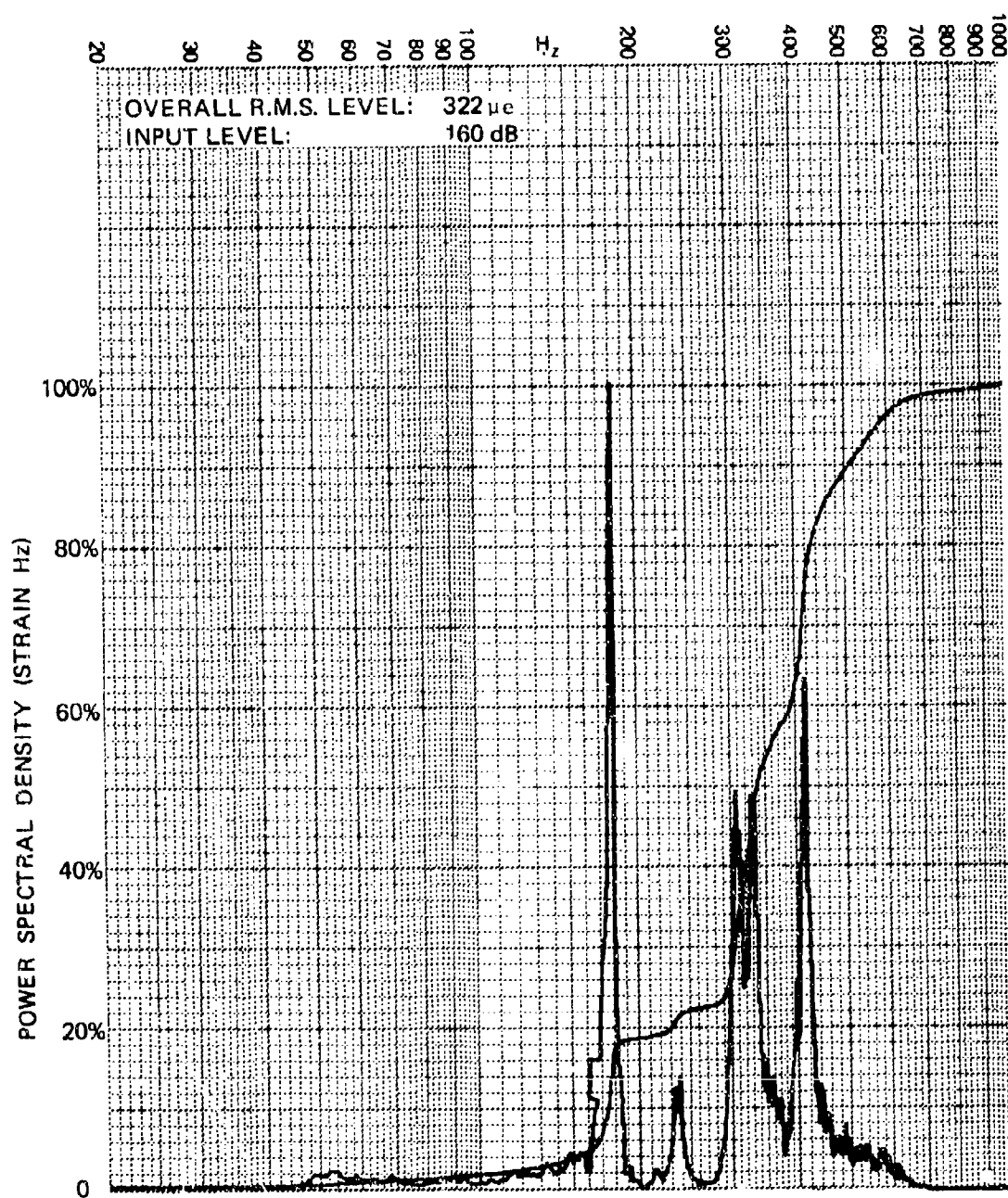
137

Figure 59. Integrated Power Spectral Density for Panel k, Gauge 4-1

138

Damping ratio values obtained ranged from 0.02 to 0.08. However, the higher values occurred when more than one response mode appeared to be contained within the major response peak. In those cases where the response peak was clearly a single mode only, damping ratio values were typically 0.02 to 0.03. These damping values were compared to values obtained in Reference 2 for aluminum skin-stringer structures. Reference 2 quotes values of 0.010 to 0.018 using the "logarithmic decrement" method. However, when the "half power-point" method was used on response spectra in Reference 2, values in the region of 0.05 were obtained. Based on these observations, it was concluded that the damping characteristics of graphite and aluminum panels do not significantly differ.

Some further discussion of the progressive-wave tube test results, as they relate to the development of the design method, is contained in Section IV.

SECTION IV
DEVELOPMENT OF DESIGN METHOD

1. INTRODUCTION

The primary objective of this phase of the program was to utilize the analytical and experimental results to develop a practical semi-empirical sonic fatigue design method for graphite-epoxy skin-stringer panels. Measured random strains from the sonic fatigue tests were compared to those calculated from Miles' equation[1], using as inputs the static strains calculated from the finite-element analyses. The test results were also compared to values determined from the AGARD nomographs[5] for fully-fixed edge conditions. Finally, multiple stepwise regression analyses were performed to develop empirical relationships between the measured strains and frequencies and various combinations of panel configuration parameters and finite-element analysis results. From these regression analyses, design equations were developed and a design nomograph constructed. A worked example is also presented. Section IV.5 presents the design method and nomographs as a self-contained unit, capable of being used independently of the remainder of this report. Appendix C contains the test data (overall acoustic and strain levels and spectra) used in the development of the design method.

An early problem encountered in the development of the design method involved the use of acoustic spectrum levels as loads. In Paragraph III.5.f, reasons for not using strain spectrum levels were given. The main reason is that although the response spectrum levels show

logical overall trends, the individual variations from one data point to another are too large and unpredictable for use in developing a design method. Acoustic spectrum levels, however, while exhibiting a certain degree of unpredictable variation, are sometimes consistent enough to facilitate their use as the load function. However, in this program the acoustic spectrum levels varied in such a way as to invalidate their use as a regression variable. Figures C-2 through C-7 show the test acoustic spectra. These spectra correspond to flat, 1/3-octave spectra. Consequently, the spectrum levels (1 Hz bandwidths) decrease with increasing frequency. Since panel frequencies increase with panel stiffness, the stiffer panels were effectively tested at lower acoustic spectrum levels. This resulted in a high degree of interdependence between the acoustic spectrum levels and the panel configuration parameters, thereby violating the necessary assumption of independent variables. A problem similar to this was encountered in Reference 3. In that case the problem was overcome by dividing the load into the dependent variable (measured rms strain). When that was attempted in this program, the resulting regression equations showed good accuracy and satisfied all the usual statistical requirements (F-values, t-values, Durbin-Watson statistics, etc.). However, when these equations were used on combinations of panel configurations other than those used in the test program, it was found that the equations were numerically dominated by changes in the acoustic spectrum levels, and were not sufficiently responsive to changes in panel dimensions. When comparing responses between two very different panels, the stiffer panel had a much lower response and a lower acoustic spectrum level at the major response frequency than did the less stiff panel. The regression analysis largely attributed the lower response to the reduced acoustic spectrum level, rather than to the increased panel stiffness. However, a review of the integrated power spectral density plots showed that the major response peaks, associated with the pertinent acoustic spectrum levels, usually accounted for less than 25 percent of the overall strain response. Thus, since the overall sound pressure levels did not vary from panel to panel, as did the acoustic spectrum levels, the reduced response of the stiffer

141

panels was, in fact, due largely to the changes in panel configuration paramenters. Consequently, regression analyses using the overall sound pressure levels as the load function, resulted in acceptable design equations.

2. SUMMARY OF ANALYTICAL AND EXPERIMENTAL RESULTS

RMS stresses and frequencies calculated using the AGARD nomographs[5] were given in Table 9. The static strains and stringer-bending mode frequencies, analytically determined from the finite-element models and the NASTRAN computer program, were given in Tables 11 and 15, respectively. Table 15 also listed frequencies calculated from the AGARD nomograph, Lin's equations[8] and those measured during the progressive-wave tube tests. The rms strains measured during the progressive-wave tube tests that are pertinent to the design method were given in Table 24. Table 29 contains calculated and measured frequencies, static strains, rms strains calculated using Miles' equation and measured rms strains. These are the data subsequently used in the regression analyses. For the reasons given in Paragraph II.5.d, the frequencies computed from the finite-element models were not used for the design method. The strains calculated using Miles' equation have very high values, compared to the test strains. This was expected and is due to using the overall sound pressure level rather than the spectrum level as the load, for the reasons given in Section IV.1. The only purpose of generating these calculated strains was to determine if there was a consistent relationship between them and the measured strains.

3. REGRESSION ANALYSIS

Regression analysis is a statistical method for investigating functional relationships between variables, based on sample data. It is particularly suitable when the data are imprecise and there is a need to determine optimum relationships. The basic approach is to use samples of data to calculate an estimate of a proposed relationship and then to evaluate the fit using statistics such as "F" and "T."

TABLE 29

SUMMARY OF ANALYTICAL AND EXPERIMENTAL RESULTS

Panel Configuration	Frequencies (Hz)		Static Strains*		Overall Sound Pressure Level dB	Calculated RMS Strains †*	Measured Overall RMS Strains*	
	Calculated (AGARD)	Measured (PWT)	Center	Edge			Center	Edge
a	160	143	1,439	3,522	140	8,785	87	102
					145	15,753	144	161
					150	27,871	195	225
					155	49,379	-	342
					160	87,852	343	411
b	202	170	863	2,117	140	5,933	55	77
					145	10,639	96	147
					150	18,823	164	267
					155	33,349	221	358
					160	59,334	288	482
					165	105,574	342	-
d	308	340	327	958	140	3,315	32	34
					145	5,945	58	57
					150	10,518	112	101
					155	18,635	148	174
					160	33,154	290	274
					165	58,993	417	425

* Microinches/inch

† RMS strains calculated from Miles' Equation using computed static strains and fully fixed frequencies.

143

TABLE 29

SUMMARY OF ANALYTICAL AND EXPERIMENTAL RESULTS - Continued

Panel Configuration	Frequencies (Hz) Calculated (AGARD)	Measured (PWT)	Static Strains* Center	Edge	Overall Sound Pressure Level dB	Calculated RMS Strains +*	Measured Overall RMS Strains* Center	Edge
f	825	505	13	28	140	158	15	22
					145	284	18	30
					150	503	24	49
					155	891	36	78
					160	1,585	81	154
					165	2,821	120	247
g	510	350	110	254	140	1,131	21	51
					145	2,028	31	93
					150	3,588	53	151
					155	6,357	81	250
					160	11,311	130	400
					165	20,126	204	595
h	375	390	312	839	140	3,203	27	54
					145	5,745	46	101
					150	10,164	68	150
					155	18,008	121	286
					160	32,039	210	466
					165	57,008		721
i	674	800	146	566	140	2,897	26	26
					145	5,195	56	47
					150	9,192	107	84
					155	16,287	172	133
					160	28,976	201	168
					165	51,559	293	258

TABLE 29

SUMMARY OF ANALYTICAL AND EXPERIMENTAL RESULTS - Continued

Panel Configuration	Frequencies (Hz)		Static Strains*		Overall Sound Pressure Level dB	Calculated RMS Strains ÷ *	Measured Overall RMS Strains*	
	Calculated (AGARD)	Measured (PWT)	Center	Edge			Center	Edge
j	824	950	76	212	140	1,200	37	41
					145	2,151	48	59
					150	3,807	70	86
					155	6,745	100	137
					160	12,000	148	216
					165	21,352	200	312
k	312	380	480	1,298	140	4,521	44	50
					145	8,107	75	34
					150	14,343	113	142
					155	25,412	187	211
					160	45,212	269	295
l	631	680	96	235	140	1,164	20	28
					145	2,087	28	43
					150	3,693	42	68
					155	6,543	66	109
					160	11,640	102	179
					165	20,712	161	283
n	120	140	2,793	6,153	140	13,291	124	187
					145	23,833	177	266
					150	42,167	201	307
					155	74,709	224	355
					160	132,918	238	408

TABLE 29

SUMMARY OF ANALYTICAL AND EXPERIMENTAL RESULTS - Concluded

Panel Configur-ation	Frequencies (Hz) Calculated (AGARD)	Frequencies (Hz) Measured (PWT)	Static Strains* Center	Static Strains* Edge	Overall Sound Pressure Level dB	Calculated RMS Strains +*	Measured Overall RMS Strains* Center	Measured Overall RMS Strains* Edge
p	377	180	290	530	140	2,029	70	96
					145	3,639	83	116
					150	6,438	192	253
					155	11,406	344	455
q	409	370	545	1,443	140	5,754	83	58
					145	10,319	132	93
					150	18,256	198	141
					155	32,346	248	202
					160	57,548	370	312
r	782	780	85	209	140	1,152	34	44
					145	2,066	53	62
					150	3,656	85	108
					155	6,478	118	160
					160	11,525	190	265
					165	20,507	333	446
s	828	380	38	83	140	470	35	48
					145	844	65	91
					150	1,494	107	149
					155	2,647	184	262
					160	4,709	302	444

The regression analyses performed in this section utilized a modified multiple-stepwise regression computer program. Stepwise regression involves a forward selection procedure for the independent variables, with the provision for eliminating variables, as in backward elimination procedures. The program analyzes the relationship between a dependent variable (measured overall rms strains) and a set of independent variables (panel configuration parameters). The independent variables are selected in order of importance for entering into the regression, based on the reduction of sums of squares. The user can override this feature and enter the independent variables in any chosen sequence. The program has six algebraic transformations available, as follows:

$$\text{Linear } y = a + b_1 x_1 + b_2 x_2 + \ldots \ldots b_n x_n$$

$$\text{Log } y = a + b_n x_n$$

$$\text{Log } y = a + b_n \text{ Log } x_n$$

$$y = a + b_n x_n + c_n x_n^2$$

$$1/y = a + b_n x_n$$

$$y = a + b_n \text{ Log } x_n$$

$$y = a + b_n / x_n$$

where y is the dependent variable and x_1, and $x_2 \ldots x_n$ are the independent variables.

For each variable entered the program computes the mean values, standard deviations and cross-correlation coefficients. For each step in the regression analysis, the program computes and lists the following:

147

Sum of Squares Reduced: This is an indication of the amount of points summed around a mean value line for a certain step.

Proportion Reduced: Indication of how well a variable explains the regression at a certain step.

Cumulative Sum of Squares Reduced: Indication of how much the dependent variable correlates with the independent variables entered at that point.

Cumulative Proportion Reduced: Indication of how well the independent variables explain the regression at that step.

Multiple Correlation Coefficient: Indication of how much the dependent variable correlates with the independent variables entered at that point.

F-Value: A measure of the scattering of values about the mean accounted for by the regression. It is used in conjunction with F-tables to determine the degree of fit of the regression equation.

Standard Error of Estimate: A measure of the dispersion of the observed points about the regression equation. It is in fact the "standard deviation of the residuals."

148

Regression Coefficients:	Coefficients of the regression equation.
Standard Error of Regression Coefficients:	Indication of the confidence level for the regression coefficients.
T-Values:	Ratio of intercept to standard error of regression coefficient. It is used in conjunction with T-tables to determine the accuracy of the corresponding regression coefficient.
Table of Residuals:	Difference between actual and estimated values for the dependent variable.
Durbin-Watson Statistic:	Test for lack of autocorrelation between error terms. A bad statistic is indicative of an independent variable being omitted.
Von-Neumann's Ratio:	The ratio of the mean-square successive difference to the variance.

The following is a description of the sequence of regression operations with examples of computer program outputs used to develop the rms strain nomograph in Section IV.5:

The input data were of the form

$$\left(\frac{\epsilon_{rms}}{SPL}\right) = F\ (b,\ t,\ R) \tag{18}$$

where ε_{rms} is the overall rms strain from strain gauge 10, i.e., the maximum edge strain.

       SPL   is the test overall sound pressure level in lb/in^2 corresponding to the strain value.

       b   is the stringer spacing in inches.

       t   is the skin laminate thickness in thousandths of an inch, and

       R   is the radius of curvature in inches.

Table 30 lists the input data in the order (left to right) b, t, R and $\left(\dfrac{\varepsilon_{rms}}{SPL}\right)$. At the bottom of the table are the means and standard deviations of the input data. An explanation of the R = 150 value is given later in this section.

The program then computes the cross-correlation coefficients between the variables, giving the output in the form of a correlation matrix. This is shown at the top of Table 31. Regression then proceeds with the linear form of the regression equation: $y = a + b_n x_n$. Each variable is entered in turn and a corresponding regression coefficient determined. The program also computes at each stage the parameters shown on the remainder of Table 31. Three sets of statistics are shown, one for each of the independent variables. The bottom set represents the final linear equation, which may be written:

$$\left(\frac{\varepsilon_{rms}}{SPL}\right) = 224.0 + 358.2\ b - 51.65\ t + 11.22R \qquad (19)$$

The program then used this equation to calculate a set of estimated values for the dependent variable $\left(\dfrac{\varepsilon_{rms}}{SPL}\right)$. The results are shown in Table 32. As can be clearly seen from the percent deviation column, the linear equation does not have acceptable accuracy. The average deviation is given as 40 percent.

150

TABLE 30

REGRESSION INPUT DATA

```
TRANSFORMATION CODE = 0
LINEAR TYPE CURVE. GENERAL EQUATION FORM IS   Y = A + BX.
INPUT CARD #  1    8.000    33.000   150.000  3506.800
INPUT CARD #  2    8.000    44.000   150.000  2665.500
INPUT CARD #  3    8.000    44.000   150.000  2828.800
INPUT CARD #  4    8.000    44.000   150.000  2900.000
INPUT CARD #  5    8.000    44.000   150.000  2194.500
INPUT CARD #  6    8.000    66.000   150.000  1155.200
INPUT CARD #  7    8.000    66.000   150.000  1094.200
INPUT CARD #  8    8.000    66.000   150.000  1097.800
INPUT CARD #  9    8.000    66.000   150.000  1068.100
INPUT CARD # 10    8.000    66.000   150.000   945.500
INPUT CARD # 11    8.000    66.000   150.000   823.800
INPUT CARD # 12    4.000    44.000   150.000   686.200
INPUT    ARD # 13    4.000    44.000   150.000   909.600
INPUT CARD # 14    4.000    44.000   150.000   918.300
INPUT CARD # 15    4.000    44.000   150.000   810.500
INPUT CARD # 16    4.000    44.000   150.000   560.000
INPUT CARD # 17    6.000    44.000   150.000  1731.000
INPUT CARD # 18    6.000    44.000   150.000  1605.700
INPUT CARD # 19    6.000    44.000   150.000  1547.800
INPUT CARD # 20    6.000    44.000   150.000  1292.000
INPUT CARD # 21    6.000    44.000   150.000  1017.200
INPUT CARD # 22    8.000    22.000   150.000  6444.800
INPUT CARD # 23    8.000    22.000   150.000  5111.560
INPUT CARD # 24    8.000    22.000   150.000  3336.900
INPUT CARD # 25    4.000    22.000   150.000  1982.700
INPUT CARD # 26    4.000    22.000   150.000  1782.700
INPUT CARD # 27    4.000    22.000   150.000  1534.800
INPUT CARD # 28    4.000    22.000   150.000  1236.200
INPUT CARD # 29    8.000    44.000    30.000   768.900
INPUT CARD # 30    8.000    44.000    30.000   576.900
INPUT CARD # 31    8.000    44.000    30.000   527.200
INPUT CARD # 32    8.000    44.000    30.000   476.100
INPUT CARD # 33    8.000    44.000    30.000   529.600
INPUT CARD # 34    8.000    44.000    30.000   479.400
INPUT CARD # 35    8.000    44.000    60.000  1738.600
INPUT CARD # 36    8.000    44.000    60.000  1786.500
INPUT CARD # 37    8.000    44.000    60.000  1645.600
INPUT CARD # 38    8.000    44.000    60.000  1533.700
INPUT CARD # 39    8.000    44.000    60.000  1379.600
INPUT CARD # 40    8.000    44.000    60.000  1153.900
INPUT CARD # 41    8.000    44.000    90.000  1865.500
INPUT CARD # 42    8.000    44.000    90.000  1752.700
INPUT CARD # 43    8.000    44.000    90.000  1605.200
INPUT CARD # 44    8.000    44.000    90.000  1396.500
INPUT CARD # 45    6.000    66.000    90.000   905.500
INPUT CARD # 46    6.000    66.000    90.000   828.800
INPUT CARD # 47    6.000    66.000    90.000   742.400
INPUT CARD # 48    6.000    66.000    90.000   667.500
INPUT CARD # 49    6.000    66.000    90.000   618.300
INPUT CARD # 50    6.000    66.000    90.000   549.000
INPUT CARD # 51    8.000    22.000    90.000  3317.200
INPUT CARD # 52    8.000    22.000    90.000  2226.900
INPUT CARD # 53    8.000    22.000    90.000  2746.700


INPUT CARD # 54    4.000    33.000    60.000  1186.300
INPUT CARD # 55    4.000    33.000    60.000  1172.800
INPUT CARD # 56    4.000    33.000    60.000   980.300
INPUT CARD # 57    4.000    33.000    60.000   915.200
INPUT CARD # 58    4.000    33.000    60.000   865.500
INPUT CARD # 59    6.000    22.000    30.000  1744.200
INPUT CARD # 60    6.000    22.000    30.000  1619.500
INPUT CARD # 61    6.000    22.000    30.000  1006.100
INPUT CARD # 62    6.000    22.000    30.000  1532.400

VARIABLE     MEAN       STANDARD
  NO.                   DEVIATION
   1        6.61290      1.64322
   2       42.22581     14.66279
   3      102.09677     47.49934
   4     1556.95806   1079.09814
```

151

TABLE 31

REGRESSION RESULTS FOR LINEAR EQUATION

CORRELATION MATRIX

		b	t	R	$\left(\frac{\epsilon_{RMS}}{SPL}\right)$
ROW 1		1.00000	0.22549	-0.13435	0.32089
ROW 2		0.22549	1.00000	0.14763	-0.50589
ROW 3		-0.13435	0.14763	1.00000	0.31608
ROW 4		0.32089	-0.50589	0.31668	1.00000

VARIABLE ENTERED..... 2

SUM OF SQUARES REDUCED IN THIS STEP.... 18178738.145
PROPORTION REDUCED IN THIS STEP........ 0.256

CUMULATIVE SUM OF SQUARES REDUCED...... 18178738.145
CUMULATIVE PROPORTION REDUCED.......... 0.256   OF 71031620.831

FOR 1 VARIABLES ENTERED
  MULTIPLE CORRELATION COEFFICIENT...   0.506
     (ADJUSTED FOR D.F.)............   0.506
  F-VALUE FOR ANALYSIS OF VARIANCE...   20.637
  STANDARD ERROR OF ESTIMATE.........   958.553
     (ADJUSTED FOR D.F.)............   958.553

VARIABLE NUMBER	REGRESSION COEFFICIENT	STD. ERROR OF REG. COEFF.	COMPUTED T-VALUE
2	-37.23063041	8.19553	-4.543
INTERCEPT	3129.55145833		

VARIABLE ENTERED..... 1

SUM OF SQUARES REDUCED IN THIS STEP.... 14158919.601
PROPORTION REDUCED IN THIS STEP........ 0.199

CUMULATIVE SUM OF SQUARES REDUCED...... 32337657.746
CUMULATIVE PROPORTION REDUCED.......... 0.455   OF 71031620.831

FOR 2 VARIABLES ENTERED
  MULTIPLE CORRELATION COEFFICIENT...   0.675
     (ADJUSTED FOR D.F.)............   0.668
  F-VALUE FOR ANALYSIS OF VARIANCE...   24.654
  STANDARD ERROR OF ESTIMATE.........   809.633
     (ADJUSTED FOR D.F.)............   816.554

VARIABLE NUMBER	REGRESSION COEFFICIENT	STD. ERROR OF REG. COEFF.	COMPUTED T-VALUE
2	-44.83568830	7.25849	-6.177
1	300.94533129	64.76914	4.648
INTERCEPT	1460.65080857		

VARIABLE ENTERED..... 3

SUM OF SQUARES REDUCED IN THIS STEP.... 16423886.655
PROPORTION REDUCED IN THIS STEP........ 0.231

CUMULATIVE SUM OF SQUARES REDUCED...... 48761544.401
CUMULATIVE PROPORTION REDUCED.......... 0.686   OF 71031620.831

FOR 3 VARIABLES ENTERED
  MULTIPLE CORRELATION COEFFICIENT...   0.829
     (ADJUSTED FOR D.F.)............   0.822
  F-VALUE FOR ANALYSIS OF VARIANCE...   42.331
  STANDARD ERROR OF ESTIMATE.........   619.651
     (ADJUSTED FOR D.F.)............   630.060

VARIABLE NUMBER	REGRESSION COEFFICIENT	STD. ERROR OF REG. COEFF.	COMPUTED T-VALUE
2	-51.65485640	5.65092	-9.141
1	356.22811376	50.32665	7.118
3	11.21662906	1.71303	6.540
INTERCEPT	224.01654015		

152

TABLE 32

TABLE OF RESIDUALS FOR LINEAR REGRESSION EQUATION

TABLE OF RESIDUALS

CASE NO.	Y VALUE	Y ESTIMATE	RESIDUAL	% DEVIATION
1	3506.80000	3067.72555	+39.07445	12.52000
2	2605.50000	2499.52213	165.97787	6.22689
3	2828.80000	2499.52213	329.27787	11.64020
4	2900.00000	2499.52213	400.47787	13.80958
5	2194.50000	2499.52213	-305.02213	-13.89939
6	1155.20000	1363.11529	-207.91529	-17.99821
7	1094.20000	1363.11529	-268.91529	-24.57643
8	1097.80000	1363.11529	-265.31529	-24.16791
9	1068.10000	1363.11529	-295.01529	-27.62057
10	945.50000	1363.11529	-417.61529	-44.16872
11	823.80000	1363.11529	-539.31529	-65.46677
12	886.20000	1066.60967	-180.40967	-20.35767
13	909.60000	1066.60967	-157.00967	-17.26140
14	916.30000	1066.60967	-150.30967	-16.40398
15	816.50000	1066.60967	-250.10967	-30.63193
16	580.00000	1066.60967	-486.60967	-83.89822
17	1731.00000	1783.06590	-52.06590	-3.00785
18	1605.70000	1783.06590	-177.36590	-11.04502
19	1547.80000	1783.06590	-235.26590	-15.20002
20	1292.60000	1783.06590	-490.46590	-37.94414
21	1017.20000	1783.06590	-765.86590	-75.29157
22	6444.80000	3635.92897	2808.87103	43.58353
23	5111.50000	3635.92897	1475.57103	28.86767
24	3356.90000	3635.92897	-99.02897	-8.95128
25	1982.70000	2203.01651	-220.31651	-11.11194
26	1782.70000	2203.01651	-420.31651	-23.57752
27	1534.80000	2203.01651	-668.21651	-43.53769
28	1236.20000	2203.01651	-966.81651	-78.20875
29	768.90000	1153.52664	-384.62664	-50.02297
30	576.90000	1153.52664	-576.62664	-99.95262
31	527.20000	1153.52664	-626.32664	-118.80247
32	476.10000	1153.52664	-677.42664	-142.28663
33	529.60000	1153.52664	-623.92664	-117.81692
34	479.40000	1153.52664	-674.12664	-140.61882
35	1756.60000	1490.02551	266.57449	15.27206
36	1786.50000	1490.02551	296.47449	16.59527
37	1645.60000	1490.02551	155.57449	9.45397
38	1533.70000	1490.02551	43.67449	2.84766
39	1379.60000	1490.02551	-110.42551	-8.00417
40	1153.90000	1490.02551	-336.12551	-29.12952
41	1665.50000	1626.52438	38.97562	2.04929
42	1752.70000	1626.52438	-73.82438	-4.21204
43	1605.20000	1626.52438	-221.32438	-13.78796
44	1396.50000	1626.52438	-430.02438	-30.79301
45	965.50000	-26.33868	991.83868	102.72796
46	828.80000	-26.33868	855.13868	103.17793
47	742.40000	-26.33868	768.73868	103.54778
48	667.50000	-26.33868	693.83868	103.94587
49	610.30000	-26.33868	644.63868	104.25986
50	549.00000	-26.33868	575.33868	104.79757
51	3317.20000	2962.93122	354.26876	10.67975
52	2226.90000	2962.93122	-736.03122	-33.05183
53	2746.70000	2962.93122	-216.23122	-7.87240
54	1186.50000	625.31648	561.18352	47.29739
55	1172.80000	625.31648	547.48352	46.68175
56	980.30000	625.31648	354.96352	36.21172
57	915.20000	625.31648	289.88352	31.67434
58	863.50000	625.31648	238.18352	27.58350
59	1744.20000	1573.47125	170.72275	9.78803
60	1619.50000	1573.47725	46.02275	2.84179
61	1606.10000	1573.47725	32.62275	2.03118
62	1532.40000	1573.47725	-41.07725	-2.66058

AVERAGE % DEVIATION IS   40.21802

DURBIN-WATSON STATISTIC IS   1.11983

VON NEUMANN'S RATIO IS   1.13019

The program repeats this analysis procedure for each of the algebraic transformations listed above. They can then be compared with each other and the best one selected. In this case, the best transformation was the Log-Log form:

$$Log\ y = a + b_n\ Log\ x_n$$

Table 33 gives the mean and standard deviations of the transformed variables and also the cross-correlation matrix.

Table 34 gives the statistical parameters calculated as each variable is entered. At the bottom of the table are the coefficients for the final regression equation:

$$Log\ \left(\frac{\varepsilon_{rms}}{SPL}\right) = 3.0806 + 1.1045\ Log\ (b) - 1.2069\ Log\ (t) + 0.5519\ Log\ (R) \quad (20)$$

Where ε_{rms} is in microinches/inch, b is in inches, t is in thousandths of inches, R is in inches and SPL is in lb/in^2.

This is the equation used to generate the rms strain nomograph in Section IV.5.

Table 35 gives the corresponding residuals, showing an average deviation of 23 percent.

There are many aspects of the regression analysis that can be observed from the data contained in Tables 30 through 35. The emphasis in this program is not on the formal statistical tests, but on relating the regression results to what is known about the data.

Referring to Table 34, it is seen that as each successive variable is entered, the multiple correlation coefficient and F-value increased, while the standard error decreased. The T-values also increased. If by adding one of these variables (b, t or R), or an extra variable, the statistics

154

TABLE 33

CROSS-CORRELATION MATRIX FOR VARIABLES USED IN FINAL REGRESSION EQUATION

TRANSFORMATION CODE = 2
LOGARITHMIC TYPE CURVE. GENERAL EQUATION FORM IS $\log Y = A + B(\log X)$.

VARIABLE NO.	MEAN	STANDARD DEVIATION
1	0.80489	0.12180
2	1.59747	0.16212
3	1.94624	0.25581
4	3.11562	0.25085

CORRELATION MATRIX

	b	t	R	$\left(\dfrac{\varepsilon_{rms}}{SPL}\right)$
ROW 1	1.00000	0.23993	-0.14990	0.26480
ROW 2	0.23993	1.00000	0.15846	-0.56220
ROW 3	-0.14990	0.15846	1.00000	0.35886
ROW 4	0.26480	-0.56220	0.35886	1.00000

TABLE 34

REGRESSION ANALYSIS RESULTS FOR FINAL REGRESSION EQUATION

VARIABLE ENTERED..... 2

SUM OF SQUARES REDUCED IN THIS STEP....	1.213	
PROPORTION REDUCED IN THIS STEP.........	0.316	
CUMULATIVE SUM OF SQUARES REDUCED......	1.213	
CUMULATIVE PROPORTION REDUCED..........	0.316 OF	3.838

FOR 1 VARIABLES ENTERED
    MULTIPLE CORRELATION COEFFICIENT... 0.562
        (ADJUSTED FOR D.F.)............ 0.562
    F-VALUE FOR ANALYSIS OF VARIANCE... 27.729
    STANDARD ERROR OF ESTIMATE......... 0.209
        (ADJUSTED FOR D.F.)............ 0.209

VARIABLE NUMBER	REGRESSION COEFFICIENT	STD. ERROR OF REG. COEFF.	COMPUTED T-VALUE
2	-0.86981534	0.16518	-5.266
INTERCEPT	4.50532512		

VARIABLE ENTERED..... 3

SUM OF SQUARES REDUCED IN THIS STEP....	0.790	
PROPORTION REDUCED IN THIS STEP.........	0.206	
CUMULATIVE SUM OF SQUARES REDUCED......	2.003	
CUMULATIVE PROPORTION REDUCED..........	0.522 OF	3.838

FOR 2 VARIABLES ENTERED
    MULTIPLE CORRELATION COEFFICIENT... 0.722
        (ADJUSTED FOR D.F.)............ 0.717
    F-VALUE FOR ANALYSIS OF VARIANCE... 32.202
    STANDARD ERROR OF ESTIMATE......... 0.176
        (ADJUSTED FOR D.F.)............ 0.178

VARIABLE NUMBER	REGRESSION COEFFICIENT	STD. ERROR OF REG. COEFF.	COMPUTED T-VALUE
2	-0.98246594	0.14106	-6.965
3	0.45054767	0.08940	5.040
INTERCEPT	3.80640976		

VARIABLE ENTERED..... 1

SUM OF SQUARES REDUCED IN THIS STEP....	1.000	
PROPORTION REDUCED IN THIS STEP.........	0.261	
CUMULATIVE SUM OF SQUARES REDUCED......	3.003	
CUMULATIVE PROPORTION REDUCED..........	0.783 OF	3.838

FOR 3 VARIABLES ENTERED
    MULTIPLE CORRELATION COEFFICIENT... 0.885
        (ADJUSTED FOR D.F.)............ 0.880
    F-VALUE FOR ANALYSIS OF VARIANCE... 69.566
    STANDARD ERROR OF ESTIMATE......... 0.120
        (ADJUSTED FOR D.F.)............ 0.122

VARIABLE NUMBER	REGRESSION COEFFICIENT	STD. ERROR OF REG. COEFF.	COMPUTED T-VALUE
2	-1.20060298	0.09964	-12.112
3	0.55172533	0.06201	6.901
1	1.10453300	0.13245	8.339
INTERCEPT	3.06061391		

TABLE 35

TABLE OF RESIDUALS FOR FINAL REGRESSION EQUATION

SELECTION..... 3

TABLE OF RESIDUALS

CASE NO.	Y VALUE	Y ESTIMATE	RESIDUAL	% DEVIATION
1	3506.80000	2795.39504	711.40496	20.28044
2	2665.50000	1975.39640	690.10360	25.89021
3	2828.80000	1975.39640	853.40360	30.16840
4	2900.00000	1975.39640	924.60360	31.88288
5	2194.50000	1975.39640	219.10360	9.98422
6	1155.20000	1210.95831	-55.75831	-4.82672
7	1094.20000	1210.95831	-116.75831	-10.67066
8	1097.60000	1210.95831	-113.15831	-10.30773
9	1068.10000	1210.95831	-142.85831	-13.37499
10	945.50000	1210.95831	-265.45831	-28.07597
11	823.80000	1210.95831	-387.15831	-46.99684
12	886.20000	918.66396	-32.46396	-3.66328
13	909.60000	918.66396	-9.06396	-0.99648
14	916.30000	918.66396	-2.36396	-0.25799
15	816.50000	918.66396	-102.16396	-12.51243
16	580.00000	918.66396	-338.66396	-58.39034
17	1731.00000	1437.65703	293.34297	16.94645
18	1605.70000	1437.65703	168.04297	10.46540
19	1547.80000	1437.65703	110.14297	7.11610
20	1292.60000	1437.65703	-145.05703	-11.22211
21	1017.20000	1437.65703	-420.45703	-41.33475
22	6444.80000	4560.03583	1884.76417	29.24473
23	5111.50000	4560.03583	551.46417	10.78870
24	3336.90000	4560.03583	-1223.13583	-36.65485
25	1982.70000	2120.65819	-137.95819	-6.95816
26	1782.70000	2120.65819	-337.95819	-18.95766
27	1534.80000	2120.65819	-585.85819	-38.17163
28	1236.20000	2120.65819	-884.45819	-71.54653
29	768.90000	812.59923	-43.69923	-5.68334
30	576.90000	812.59923	-235.69923	-40.85617
31	527.20000	812.59923	-285.39923	-54.13491
32	476.10000	812.59923	-336.49923	-70.67627
33	529.60000	812.59923	-282.99923	-53.43641
34	477.40000	812.59923	-335.19923	-69.50339
35	1755.60000	1191.30204	564.29796	32.25850
36	1786.50000	1191.30204	595.19796	33.31643
37	1645.60000	1191.30204	454.29796	27.60683
38	1533.70000	1191.30204	342.39796	22.32496
39	1379.60000	1191.30204	188.29796	13.64874
40	1153.90000	1191.30204	-37.40204	-3.24136
41	1865.50000	1490.08402	375.41598	20.12415
42	1752.70000	1490.08402	262.61598	14.98351
43	1605.20000	1490.08402	115.11598	7.17144
44	1396.50000	1490.08402	-93.58402	-6.70133
45	965.50000	664.79345	300.70655	31.14516
46	828.80000	664.79345	164.00655	19.78844
47	742.40000	664.79345	77.60655	10.45347
48	667.50000	664.79345	2.70655	0.40558
49	618.30000	664.79345	-46.49345	-7.51956
50	549.00000	664.79345	-115.79345	-21.09170
51	3317.20000	3439.73318	-122.53318	-3.69387
52	2226.90000	3439.73318	-1212.83318	-54.46285
53	2746.70000	3439.73318	-693.03318	-25.23148
54	1186.50000	783.99490	402.50510	33.92373
55	1172.80000	783.99490	388.80510	33.15187
56	980.30000	783.99490	196.30510	20.02500
57	915.20000	783.99490	131.20510	14.33622
58	863.50000	783.99490	79.50510	9.20731
59	1744.20000	1365.18479	379.01521	21.73003
60	1619.50000	1365.18479	254.31521	15.70332
61	1606.10000	1365.18479	240.91521	15.00001
62	1532.40000	1365.18479	167.21521	10.91198

AVERAGE % DEVIATION IS   23.08296

DURBIN-WATSON STATISTIC IS   1.24243

VON NEUMANN'S RATIO IS   1.26280

deteriorated, it would indicate that that variable was unwanted. The regression would then probably be repeated with that variable deleted.

The final F-value is used to check the statistical accuracy with which the regression equation represents the data. Referring to F-tables, for 62 observations and three independent variables, an F-value of greater than five corresponds to a better than 1 percent level of significance. T-values are similarly evaluated. Here a T-value of 2.4 corresponds to a 1 percent level of significance. Although F and T values are important, it was found that in this program many completely unsatisfactory regression results met high levels of statistical significance. Consequently, F and T values were not used to evaluate the effectiveness of a particular regression analysis, but only to ensure that high levels of significance were being met. What was found to be desirable was that the T values for each variable be comparable in magnitude. If, for example, one variable had ten times the T-value of another variable, it would follow that the numerical contribution of the variable having the lower T value to the estimated value of the dependent variable would be so small as to render its presence useless.

The tables of residuals provide a good comparison between different regression equations. Table 35 shows the Log:Log equation to be a much more accurate predictor of the test data than the linear equation, whose residuals are shown in Table 32.

Elimination of Outliers

Tables of residuals are often used to reject data points as outliers. Data points having the largest percent deviations are rejected and the regression analysis is repeated. This invariably results in a more "accurate" equation. However, this is a more effective procedure when dealing with data about which little or nothing is known quantitatively, such as public opinion type surveys. In this program, however, a great deal is known about the data. In such cases, apparent regression outliers must be evaluated against the actual test data. An illustration of the

importance of this is given in Figure 60. The four points a, b, c and d represent response strain values for four different skin thicknesses. The line drawn (1) ---- (1) represents a computed regression relationship showing strain increasing with skin thickness. Based on a table of residuals, data point "d" appeared to be an outlier. Elimination of point "d" resulted in a new regression line (2) ---- (2), which had greater statistical accuracy than the first line. Since it is known that strain decreases with increasing thickness, it can be seen that the regression analysis resulted in an illogical relationship. In addition, by removing an outlier on the basis of statistical accuracy, the incorrect trend of the regression was worsened. By plotting the data prior to regression, and knowing that strains decrease with increasing skin thickness, it is obvious that data point "a' is the main outlier and not point "d". When point a was removed, the new regression line was (3) --- (3), which shows a more reasonable relationship. This example illustrates the importance of checking data for technical inconsistencies prior to regression analysis, preferably by graphical means; and also demonstrates the danger in allowing statistical decisions to replace technical ones.

Figures 61, 62 and 63 show graphical representations of measured rms strains versus stringer spacing, skin thickness and radius of curvature for each test sound pressure level. The only imposition made on the data prior to regression was that response strain must increase with increasing sound pressure level, stringer spacing and radius of curvature; and must decrease with increasing skin thickness. No prior limitation was placed on the rate of change. This is a sensible and practical approach when dealing with sonic fatigue test data, where isolated illogical data points are not unusual. Referring to Figure 61, there were no inconsistencies in the data presented. On Figure 62, however, both panels a (6 ply) and n (4 ply) had lower strains than panel b (8 ply). In order to determine whether panel b response was too high or that for panels a and n were too low, Figures 61 and 63 were referred to. From these graphs, it does not appear as if the response for panel b was too high. In fact, Figure 63

159
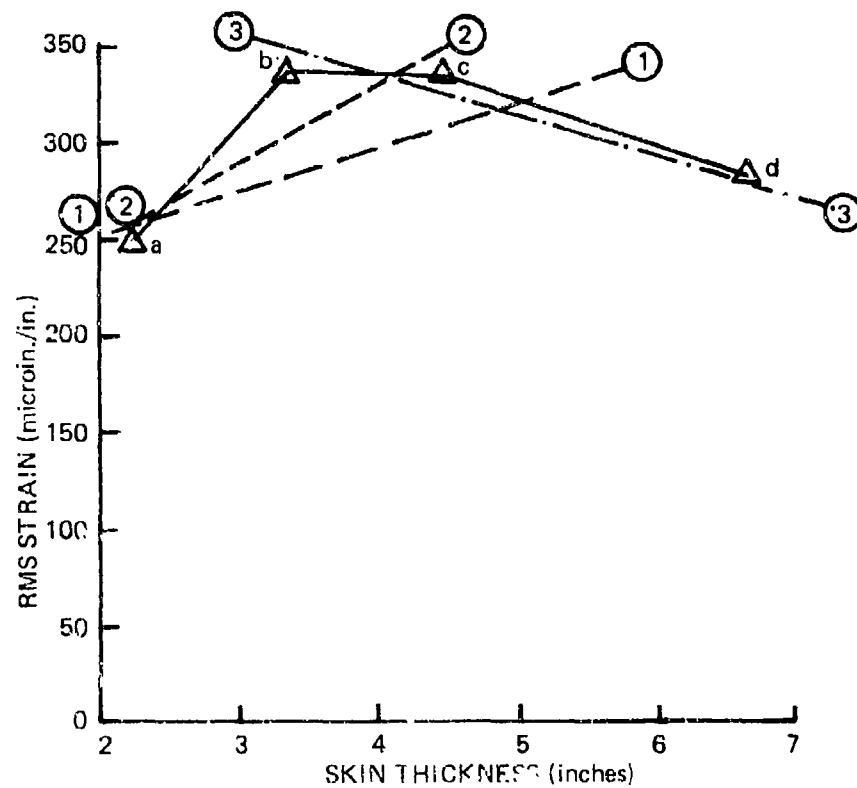
Figure 60. Graphic Illustration of Regression Error
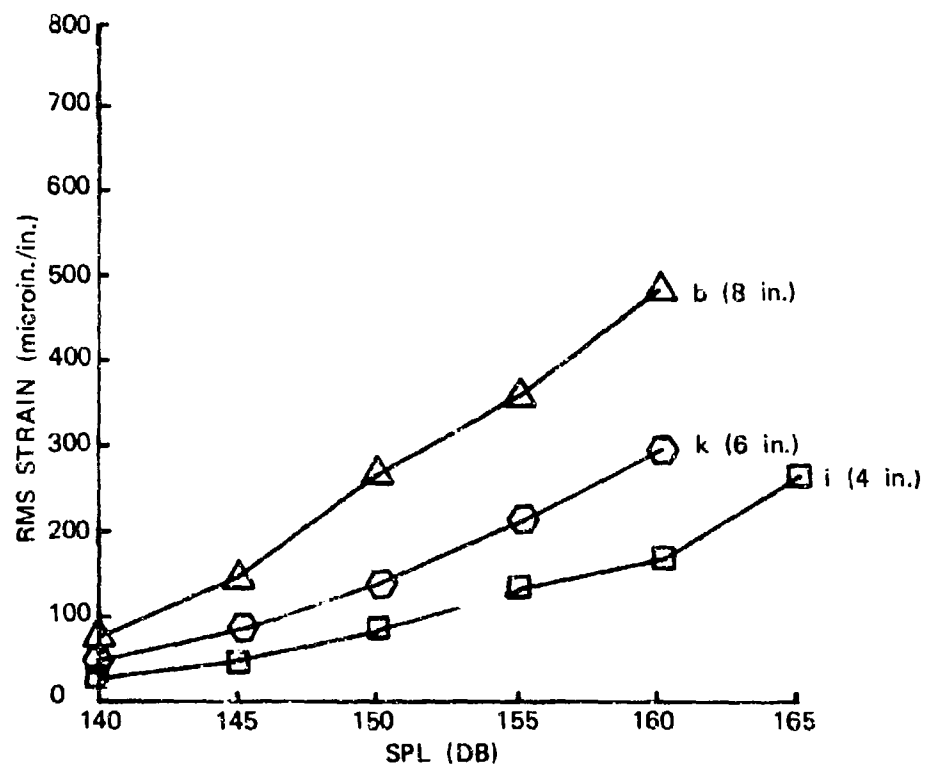
Figure 61.   Response Comparisons for Different Stringer Spacings
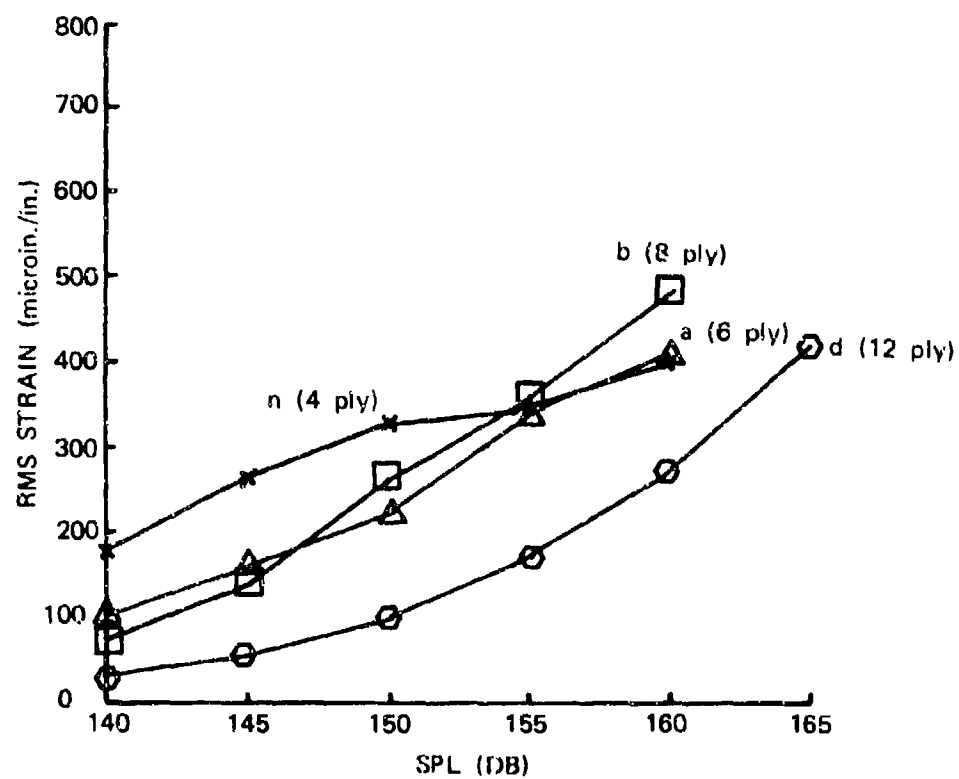
Figure 62. Response Comparisons for Different Skin Thicknesses
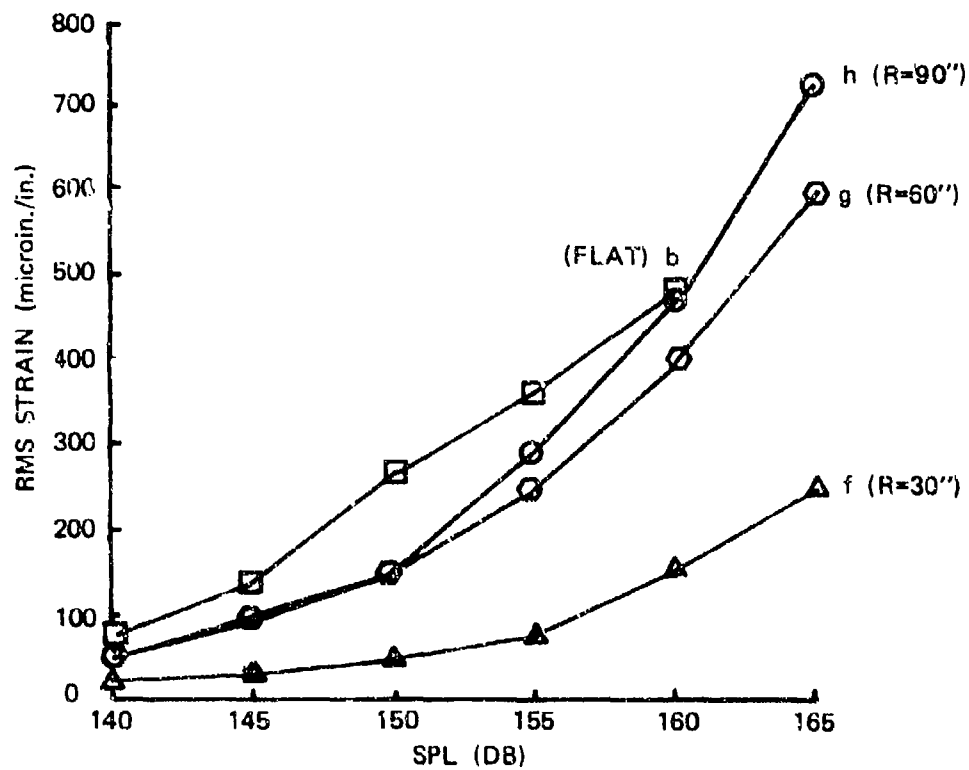
Figure 63.   Response Comparisons for Different Radii of Curvature

indicates that at 160 dB, the response for panel b was too low. Based on this observation, referring back to Figure 62, the following data points were rejected: panel a at 150, 155 and 160 dB; and panel n at 155 and 160 dB. Referring now to Figure 63; panel b at 160 dB was rejected, as was panel h at 145 and 150. S ne other data points were similarly rejected, based on comparisons that did not lend themselves to graphical representation. They were:

panel g @ 160 dB
panel i @ 165 dB
panel j @ 140 dB through 165 dB
panel p @ 155 dB
panel r @ 140 dB
panel s @ 140 dB

There was a tendency for data at 140 dB to be generally inconsistent due to the low response levels. With the possible exception of panel n, the data points rejected did not interfere with observations regarding the nonlinearity of the panel responses.

In developing a design method for both flat and curved panels, using regression analysis, it was necessary to determine a numerical value for the radius of curvature of a flat panel. Since regression analysis deals entirely with numerical values, using a very high value to represent an infinite radius of curvature must be avoided. Orginally, a value of R = 10,000 inches was used, resulting in a very small regression coefficient for this variable. Since the response differences between the flat and the R = 90-inch curved panels was much less than between the R = 30-inch and the R = 60-inch panels, it seemed likely that a much lower number than 10,000 inches would be appropriate. Various numbers were tried, and also a graphical review of the data was performed. It was determined that R = 150 inches was a satisfactory number to represent the flat panel radius.

NOTE: The following important observation was made during these regression analyses. The signs (+ or -) of the regression coefficients of the independent variables were determined within the computer program, based on the sign of the cross-correlation coefficient between the independent variables and the dependent variable. When using a Log function to represent an independent variable having values of less than unity, the program fails to take account of the logarithm of the value changing sign. To overcome this, the values of independent variables were adjusted to be always greater than unity. In this program, the skin thicknesses were entered $\times 10^3$.

Durbin-Watson Statistic

It will be noticed that the tables of residuals quote the Durbin-Watson statistic. In regression analysis it is assumed that the residual errors are an independent random variable. If the error terms are not independent, but show serial correlation, this indicates that the best possible curve fit may not have been obtained. It also means that the F and T tests may not accurately reflect the true confidence levels of the regression results. The Durbin-Watson statistic is used to check for serial correlation in the error terms. In the regression analyses performed here, the Durbin-Watson statistic indicated that there was some serial correlation in the error terms. However, this is not critical for the regression analysis performed in this section. As mentioned earlier, the emphasis here was more on uncovering patterns in the data than on formal tests. The best possible curve fit was sacrificed partially in order to ensure a technically acceptable result. Also, the F and T values obtained here were considerably in excess of those values required to assure good statistical accuracy, and therefore, the validity of these regression results is not affected by small changes in their values.

Many regression analyses were performed prior to selecting one for the final design method. Some resulted in unacceptable equations, others yielded results that may be used as alternatives to the one chosen here.

165

A major effort was made to use nondimensional independent variables, of the form used in AGARD[5] nomographs. Regression equations do not usually balance dimensionally, and therefore, care must be taken if using units other than those used in developing the equations. Nondimensional parameters overcome this objection. However, by imposing certain fixed relationships between variables, the accuracy of the equation usually suffers.

Other regression analyses performed included using as an independent variable rms strains calculated from Miles' equation, with the frequency component estimated from the AGARD nomograph and the static strain component computed from the finite-element models. These estimated strain values are given in Table 29. The following equation was obtained:

$$\text{Log } \varepsilon_{rms} = 0.33 + 0.47 \text{ Log } \varepsilon_{rms} \text{ calculated} \qquad (21)$$

The calculated and measured rms strains had a cross-correlation coefficient of 0.73 and satisfied the F and T tests. However, the average error was 50 percent with maximum errors exceeding 2:1. Table 36 shows the residuals.

Since the above regression yielded unacceptable results, the next step was to regress directly on the frequency and static strain components used in the preceding regression. The calculated frequency had a cross-correlation coefficient of -0.64 with the measured strains. The computed static strains had a corresponding correlation coefficient of 0.83. The average error was 32 percent. Table 37 shows the residuals for the following regression equation:

$$\varepsilon_{rms} = \frac{(1,825.3)\ 1.193^{\varepsilon_o}}{1.001^{f}} \qquad (22)$$

166

TABLE 36

TABLE OF RESIDUALS FOR REGRESSION OF MILES' EQUATION

TABLE OF RESIDUALS

NO.	Y VALUE	Y ESTIMATE	RESIDUAL	% DEVIATION
1	101.70000	151.96771	-50.26771	-49.42744
2	77.30000	126.38478	-49.08478	-63.49906
3	147.10000	166.26670	-19.16670	-13.02970
4	265.80000	217.35712	49.44288	18.55181
5	357.70000	284.33285	73.36715	20.51080
6	33.50000	96.15607	-62.65607	-187.03304
7	56.90000	126.50476	-69.60476	-122.32822
8	101.00000	165.37593	-64.37593	-63.73855
9	174.10000	216.33488	-42.23488	-24.25898
10	274.20000	283.55085	-9.35085	-3.41023
11	425.10000	371.67438	53.42564	12.56778
12	22.30000	23.02543	-0.72543	-3.25306
13	30.00000	30.32524	-0.32524	-1.08414
14	48.50000	39.66338	8.83662	18.21984
15	77.60000	51.88040	25.71960	33.14382
16	153.60000	67.99577	85.60423	55.73192
17	247.40000	89.15324	158.24676	63.96393
18	51.00000	58.02963	-7.02963	-13.78359
19	92.90000	76.33969	16.56031	17.82595
20	151.40000	99.79697	51.60303	34.08390
21	250.00000	130.54891	119.45109	47.78044
22	400.10000	171.11871	228.98129	57.23101
23	595.40000	224.30321	371.09679	62.32731
24	54.10000	94.61647	-40.51647	-74.89181
25	285.70000	212.88547	72.81453	25.48636
26	465.50000	279.03178	186.46822	40.05762
27	720.60000	365.74779	354.85221	49.24399
28	25.70000	90.25825	-64.55825	-251.19942
29	47.30000	118.74146	-71.44146	-151.03903
30	84.30000	155.23445	-70.93445	-84.14525
31	133.10000	203.07605	-69.97605	-52.57404
32	168.20000	266.16961	-97.96961	-58.24602
33	50.20000	111.23969	-61.03969	-121.59300
34	63.50000	146.34230	-62.84230	-75.26024
35	142.40000	191.30666	-48.90666	-34.34597
36	210.70000	250.25923	-39.55923	-18.77514
37	295.00000	328.01856	-33.01856	-11.19273
38	28.00000	58.81873	-30.81873	-110.06691
39	43.10000	77.37478	-34.27478	-79.52385
40	68.30000	101.15803	-32.85803	-48.10838
41	108.80000	132.32906	-23.52906	-21.62597
42	179.30000	173.43843	5.86157	3.26914
43	283.30000	227.34685	55.95315	19.75049
44	186.90000	184.58576	2.31424	1.23823
45	265.80000	242.83213	22.96787	8.64103
46	307.00000	317.45163	-10.45163	-3.40444
47	96.20000	76.35737	19.84263	20.62643
48	113.80000	100.46066	13.33934	11.72641
49	252.70000	131.32749	121.37251	48.03028
50	57.50000	124.58967	-67.08967	-116.67768
51	92.70000	163.89906	-71.19906	-76.80589
52	141.20000	214.25733	-73.05733	-51.74032
53	201.50000	280.29647	-78.79647	-39.10495
54	61.70000	77.00816	-15.30816	-24.81063
55	107.90000	100.68079	7.21921	6.69065
56	159.60000	131.51005	28.08995	17.57819
57	265.40000	172.65269	92.74731	34.94624
58	445.60000	226.28217	219.31783	49.21654
59	90.70000	50.57669	40.12331	44.23738
60	149.00000	66.13364	82.86636	55.61501
61	261.80000	86.51272	175.28728	66.95465
62	444.40000	113.39993	331.00007	74.48246

AVERAGE % DEVIATION IS 49.53563

DURBIN-WATSON STATISTIC IS 0.89991

VON NEUMANN'S RATIO IS 0.91466

TABLE 37

TABLE OF RESIDUALS FOR REGRESSION USING CALCULATED FREQUENCIES
AND STATIC STRAINS

TABLE OF RESIDUALS

CASE NO.	Y VALUE	Y ESTIMATE	RESIDUAL	% DEVIATION
1	3506.90300	2908.72965	598.17035	17.05695
2	2665.50000	2165.16459	500.33541	18.77079
3	2828.80000	2165.16459	663.63541	23.45996
4	2900.00000	2165.16459	734.83541	25.33913
5	2194.50000	2165.16459	29.33541	1.33677
6	1155.20000	1586.85772	-431.65772	-37.36649
7	1094.20000	1586.85772	-492.65772	-45.02447
8	1097.80000	1586.85772	-489.05772	-44.54869
9	1068.10000	1586.85772	-518.75772	-48.56827
10	945.50000	1586.85772	-641.35772	-67.83265
11	823.80000	1586.85772	-763.05772	-92.62657
12	768.90000	801.82038	-32.92038	-4.28149
13	576.90000	801.82038	-224.92038	-38.98776
14	527.10000	801.82038	-274.72038	-52.11922
15	476.10000	801.82038	-325.72038	-68.41428
16	529.70000	801.82038	-272.12038	-51.37255
17	479.50000	801.82038	-322.32038	-67.22010
18	1758.60000	1144.49731	614.10269	34.91998
19	1786.50000	1144.49731	642.00269	35.93634
20	1645.60000	1144.49731	501.10269	30.45106
21	1533.70000	1144.49731	389.20269	25.37672
22	1379.60000	1144.49731	235.10269	17.04137
23	1153.90000	1144.49731	9.40269	0.81486
24	1865.50000	1452.89788	412.60212	22.11751
25	1752.70000	1452.89788	299.80212	17.10516
26	1605.20000	1452.89788	152.30212	9.48805
27	1396.50000	1452.89788	-56.39788	-4.03852
28	886.20000	1025.81169	-139.61169	-15.75397
29	909.60000	1025.81169	-116.21169	-12.77613
30	916.30000	1025.81169	-109.51169	-11.95151
31	816.50000	1025.81169	-209.31169	-25.63523
32	580.00000	1025.81169	-445.81169	-76.86408
33	1731.00000	1678.17839	52.82161	3.05151
34	1605.70000	1678.17839	-72.47839	-4.51382
35	1547.80000	1678.17839	-130.37839	-8.42348
36	1292.60000	1678.17839	-385.57839	-29.82968
37	1017.20000	1678.17839	-660.97839	-64.98018
38	965.50000	1010.29191	-44.79191	-4.63925
39	828.80000	1010.29191	-181.49191	-21.89816
40	742.40000	1010.29191	-267.89191	-36.08458
41	667.50000	1010.29191	-342.79191	-51.35459
42	618.30000	1010.29191	-391.99191	-63.39834
43	549.00000	1010.29191	-461.29191	-84.02403
44	6444.80000	4790.22223	1654.57777	25.67307
45	5111.50000	4790.22223	321.27777	6.28539
46	3336.90000	4790.22223	-1453.32223	-43.55307
47	3317.20000	1373.80590	1943.39410	58.58538
48	2226.90000	1373.80590	853.09410	38.30859
49	2746.70000	1373.80590	1372.89410	49.98340
50	1982.70000	1562.02285	420.67715	21.21739
51	1782.70000	1562.02285	220.67715	12.37882
52	1534.80000	1562.02285	-27.22285	-1.77371
53	1236.20000	1562.02285	-325.82285	-26.35681
54	1186.50000	864.31802	322.18198	27.15398
55	1172.80000	864.31802	308.48198	26.30303
56	980.40000	864.31802	116.08198	11.84027
57	915.20000	864.31802	50.88198	5.55966
58	863.50000	864.31802	-0.81802	-0.09473
59	1744.20000	807.20336	936.99664	53.72071
60	1619.50000	807.20336	812.29664	50.15725
61	1606.10000	807.20336	798.89664	49.74140
62	1532.40000	807.20336	725.19664	47.32424

AVERAGE % DEVIATION IS   31.81944

DURBIN-WATSON STATISTIC IS   1.31602

VON NEUMANN'S RATIO IS   1.33760

168

This equation also results in major differences from many of the test data points, and is not recommended for design use. It is, however, significantly better than using Miles' equation. It may be used as a design guide for irregularly shaped structures for which there are no simple dimensions such as b, t and R; but for which computed static strains and frequencies are available.

A regression analysis was performed, combining c_0 and f with b, t and R as independent variables. However, the results were no better than using only b, t and R.

Effects of Nonlinear Structural Response
The regression analyses described thus far have all used $\left(\frac{c_{rms}}{SPL}\right)$ as the dependent variable. This imposes the assumption of linear response. However, although some panels show linear response, there was a general tendency for strains to not quite increase linearly with sound pressure level. This does not necessarily mean that the structural reponse is truly nonlinear. Several test panels had back-to-back strain gauges installed, and none detected any in-plane (membrane) strains. There are, however, aspects of sonic fatigue testing that can give the appearance of nonlinearity, such as "clipping" at high sound pressure levels, overall panel and fixture motion which may not be fully responsive to changing sound pressure levels. For these reasons, and because the degree of nonlinearity was not excessive, the design method proposed in Section IV.5 is based on linear response. However, in order to provide quantitative information on the degree of nonlinearity, and thereby make an alternative design equation for those who may wish to use it, a regression analysis was performed with overall sound pressure level as an independent variable. It should be remembered that some of the less stiff panels were not tested at the high sound pressure levels that the stiffer panels were subjected to, and as a result, there will be a slight bias in the regression equation. The bias, however, will be small. The following equation was obtained:

$$\text{Log } \varepsilon_{rms} = 0.3528 + 1.0458 \text{ Log } b - 1.1241 \text{ Log } t \tag{23}$$

$$+ 0.4994 \text{ Log } R + 0.873 \text{ Log } (SPL \times 10^{3})$$

(SPL was entered times 10^{3} in order to keep its value
above unity and prevent the logarithm from changing sign)

This equation had an average accuracy of 22 percent, slightly better than
the equation selected for the design nomograph. The residuals are shown
in Table 38. Table 39 shows the corresponding correlation matrix and
statistics for the above equation. A comparison between Tables 35 and 38
show the nonlinear regression to have significantly lower residuals.
Comparing the cross-correlation matrices for the linear and nonlinear
regressions (Tables 33 and 39) shows much lower correlation between ε_{rms}
and the panel dimensions (b, t and R) than between $\left(\dfrac{\varepsilon_{rms}}{SPL}\right)$ and the same
panel dimensions. This would indicate that there was significant
correlation between SPL and the panel dimensions. The correlation matrix
in Table 39 shows significant correlation between t, R and SPL. In fact,
t and R show higher correlation with SPL than with ε_{rms}. This lack of
independence between the "independent" variables is called multi-
collinearity, and is a condition of deficient data. The presence of
multicollinearity does not necessarily invalidate the regression, but it
is a signal for caution. Performing comparative calculations using the
linear and nonlinear equations indicated that the degree of multi-
collinearity was not excessive. In order to illustrate the degree of
nonlinearity, the change in strain due to 6 dB increase in sound pressure
level was found to be times 1.83. The linear equation would produce a
ratio of times 2.

It should be pointed out that the nonlinear equation is the most accurate
representation of the test data in this program, and may be quite
acceptable for design use. However, since the degree of nonlinearity was
not high, and in the interests of some conservatism, the linear equation
was used to develop the design nomograph in Section IV.5.

170

TABLE 38

TABLE OF RESIDUALS FOR NONLINEAR REGRESSION

TABLE OF RESIDUALS

CASE NO.	Y VALUE	Y ESTIMATE	RESIDUAL	% DEVIATION
1	101.78000	89.88492	11.81508	11.61758
2	77.30000	65.05009	12.24991	15.84724
3	147.10000	108.30686	38.79314	26.37195
4	260.80000	178.23057	88.56943	33.19694
5	357.70000	293.66055	64.03945	17.90312
6	33.50000	41.23920	-7.73920	-23.10210
7	56.90000	68.66230	-11.76230	-20.67188
8	101.00000	112.99119	-11.99119	-11.87246
9	174.10000	186.16927	-12.06027	-6.93238
10	274.20000	307.85920	-33.65920	-12.27542
11	425.10000	509.13430	-84.03430	-19.76613
12	22.30000	29.12132	-6.82132	-30.58887
13	30.00000	48.48631	-18.48631	-61.62103
14	48.50000	79.78943	-31.28043	-64.51429
15	77.60000	131.46458	-53.86458	-69.41312
16	153.60000	217.39669	-63.79669	-41.53430
17	247.40000	359.52835	-112.12835	-45.32269
18	51.00000	41.16546	9.83454	19.28340
19	92.90000	68.53953	24.36047	26.22225
20	151.40000	114.76915	36.61085	25.50254
21	250.00000	185.83630	64.16361	25.66545
22	400.10000	307.30873	92.79127	23.19202
23	595.40000	508.22395	87.17605	14.64159
24	54.10000	50.40609	3.69501	6.83163
25	285.70000	227.54300	58.15700	20.35597
26	465.50000	376.27696	89.22304	19.16714
27	720.60000	622.28287	98.31713	13.64370
28	25.70000	31.50944	-5.80944	-22.60483
29	47.30000	52.46248	-5.16248	-10.91432
30	84.30000	86.33264	-2.03264	-2.41120
31	133.10000	142.24546	-9.14546	-6.87112
32	168.20000	235.22451	-67.02451	-39.84810
33	50.20000	48.14942	2.05058	4.08481
34	83.50000	80.16765	3.33235	3.99083
35	142.40000	131.92449	10.47551	7.35640
36	210.70000	217.36450	-6.66450	-3.16308
37	295.00000	359.44544	-64.44544	-21.84591
38	28.00000	23.65219	4.34781	15.52790
39	43.10000	39.38034	3.71966	8.63031
40	68.30000	64.80457	3.49543	5.11775
41	108.80000	106.77487	2.02513	1.86133
42	179.30000	176.56850	2.73150	1.52343
43	283.30000	292.00712	-8.70712	-3.07346
44	186.90000	141.76310	45.11690	24.13459
45	265.80000	236.06552	29.73448	11.18670
46	307.00000	388.47117	-81.47117	-26.53784
47	96.20000	109.86069	-13.66069	-14.20031
48	115.80000	182.91547	-67.11547	-57.95800
49	252.70000	301.00705	-48.30705	-19.11636
50	57.50000	68.67794	-11.17794	-19.43990
51	92.70000	114.34714	-21.64714	-23.35184
52	141.20000	188.17053	-46.97053	-33.26525
53	201.50000	310.03406	-108.53406	-53.86504
54	61.70000	45.87466	15.82534	25.64884
55	107.90000	75.49169	32.40831	30.03551
56	159.80000	124.38343	35.41657	22.16306
57	265.40000	205.68693	59.71307	22.49927
58	445.60000	340.16288	105.43712	23.66183
59	90.70000	78.22380	12.47620	13.75545
60	149.00000	128.72567	20.27433	13.60693
61	261.80000	212.09409	49.70591	18.98621
62	444.40000	350.72985	93.67015	21.07769

AVERAGE % DEVIATION IS 21.61903

DURBIN-WATSON STATISTIC IS 0.86877

VON NEUMANN'S RATIO IS 0.88301

171

TABLE 39

REGRESSION ANALYSIS RESULTS FOR NONLINEAR REGRESSION

CORRELATION MATRIX

	b	t	R	SPL.	ϵ_{rms}
ROW 1	1.00000	0.23993	-0.14990	-0.03749	0.14109
ROW 2	0.23993	1.00000	0.15846	0.18721	-0.18026
ROW 3	-0.14990	0.15846	1.00000	-0.20010	0.02567
ROW 4	-0.03749	0.18721	-0.20010	1.00000	0.79075
ROW 5	0.14109	-0.18026	0.02567	0.79075	1.00000

VARIABLE ENTERED...... 3

SUM OF SQUARES REDUCED IN THIS STEP....	0.870
PROPORTION REDUCED IN THIS STEP.........	0.108
CUMULATIVE SUM OF SQUARES REDUCED......	7.373
CUMULATIVE PROPORTION REDUCED...........	0.914 OF 8.065

FOR 4 VARIABLES ENTERED
MULTIPLE CORRELATION COEFFICIENT...	0.956
(ADJUSTED FOR D.F.)............	0.954
F-VALUE FOR ANALYSIS OF VARIANCE...	151.895
STANDARD ERROR OF ESTIMATE..........	0.110
(ADJUSTED FOR D.F.)..........	0.113

VARIABLE NUMBER	REGRESSION COEFFICIENT	STD. ERROR OF REG. COEFF.	COMPUTED T-VALUE
4	0.8730418B	0.03702	23.583
2	-1.1240627Z	0.09465	-11.874
1	1.0457608 3	0.12285	8.513
3	0.4043508B3	0.05897	8.467
INTERCEPT	0.3527051 1		

172

Regression analyses were also performed on the test frequencies and the static strains computed from the finite-element models; against the panel dimensions b, t and R. It was originally hoped that simplified regression equations could be developed for frequencies and static strains, which in turn could be used as inputs to a regression equation for rms strain. However, the regression equation for rms strain which utilized frequencies and static strains as inputs was not particularly accurate. In addition, it was not possible to obtain a satisfactory regression equation for static strains on the curved panels. For the flat panels only, however, a regression equation between the computed static strains and the panel dimensions produced an equation with an average accuracy of 5 percent:

$$\epsilon_o = \frac{(921)(1.4105^b)}{(10^{18})^t} \tag{24}$$

Regression analysis on the test frequencies against the panel dimensions gave satisfactory results, but since the existing AGARD nomograph also gave satisfactory results, there was no point in using a regression equation in the design method.

4. DESIGN EQUATIONS

Before proceeding with the final design method, it seems useful to fully describe the regression equation used, and to present those alternatives that are viable.

The basic design method utilizes overall sound pressure levels rather than spectrum levels as applied loads. Consequently, it is not necessary to determine the natural frequency in order to determine rms strain. Response frequency estimates, however, are required in order to estimate fatigue lives.

a. Calculation of RMS Strains - Acceptable equations developed in
Section IV.3 follow:

(i) Equation for rms strain, used to develop the design
nomograph in Section IV.5 is:

$$\text{Log } \frac{\varepsilon_{rms}}{SPL} = 3.080614 + 1.104533 \text{ Log } b \hspace{2cm} (20)$$
$$-1.206903 \text{ Log } (10^3.t) + 0.551923 \text{ Log } R$$

where ε_{rms} is in microinches/inch
$\hspace{0.9cm}$ SPL $\hspace{0.2cm}$ is in lb/in^2
$\hspace{1.1cm}$ b $\hspace{0.4cm}$ is in inches
$\hspace{1.1cm}$ t $\hspace{0.4cm}$ is in inches
$\hspace{1.0cm}$ R $\hspace{0.4cm}$ is in inches

and where R = 150 inches for a flat panel, i.e., for
$150 < R \leq \infty$, use 150.

NOTE: (1) Because the equation is in Log:Log form, six
significant figures are required in order to
maintain reasonable accuracy.
(2) This equation assumes linear response, i.e.,
6 dB represents a doubling of strain.
(3) Strain levels were quoted rather than stress
levels in order to allow elastic modulus
values for alternative skin laminates to be
used in determining stress levels.

(4) All logarithms are to the base 10.

174

This equation may be written in the form:

$$\varepsilon_{rms} = \frac{(8.3234 \times 10^{-10}) \, 10^{(SPL/20)} \, b^{1.1045} \, R^{0.5519}}{t^{1.2069}} \qquad (25)$$

where SPL is in decibels (dB).

(ii) Nonlinear Response Equation (from equation 23):

$$\varepsilon_{rms} = \frac{(1.394 \times 10^{-8}) \, b^{1.0458} \, R^{0.4994} \, 10^{0.04365.SPL}}{t^{1.1241}} \qquad (26)$$

where the variables are defined as in (i) above.

NOTE: This equation is slightly more accurate than (i), but may be slightly unconservative at very high sound pressure levels

Effects of Aspect Ratio

In this program, the long side of the individual bays was kept constant at $\cdot$ = 12 inches. The short side varied from 4-inches to 8-inches, thus the aspect ratio varied from 1.5 to 3. In order to include the effects of varying aspect ratio, the stress nomograph in Reference 5 was used. RMS stresses for various aspect ratios were calculated, and the ratio effects applied to the strains calculated in this program. Within the levels of accuracy of the AGARD stress nomograph, and also considering the accuracies of the regression equations; there were no significant changes in strain response at aspect ratios above 1.5. Based on the combined effects of aspect ratio on static strains and frequencies, the dynamic strains at a/b = 1.5 and a/b = ∞ are within approximately 5 percent of each other. Consequently, the design nomograph was constructed assuming a common response for all aspect ratios above 1.5. Aspect ratio lines for

175

a/b = 1.2 and 1.0 were then superimposed based on stress ratios determined from the AGARD rms stress nomograph.

Effects of J Stiffeners

The static analysis showed that J stiffeners resulted in significantly lower edge strains, compared to using Z stiffeners. The ratio of J to Z being 0.71. The measured data gave a corresponding ratio of 0.7 to 0.8 for configuration b. Configuration c did not show any strain reduction due to the J stiffeners, but it did show a major increase in fatigue life. Based on these observations, it is recommended that the calculated strains in this design method be factored by 0.8 when using J stiffeners. This is believed to be a slightly conservative factor.

b. Calculation of Natural Frequencies - Reference 5 was used to calculate the fundamental fully-fixed panel frequencies. The equations and nomograph are included in Section IV.5.

This method was derived for typical metals, and assumes typical values for elastic modulus (E) and material density (ρ). It is necessary to modify these values when using composite materials. Graphite/expoxy laminates have a density of 0.055 lb/in^3. The elastic modulus varies with ply orientation. In this program, elastic modulus values are given in Tables 2 through 6.

Reference 8 is recommended for use if stiffener properties are to be used, rather than assuming fully-fixed edges. For flat panels only, Reference 5 contains a simplified method based on Reference 8. However, both the flat and curved panel equations in Reference 8 lend themselves to programming on modern desk top computers.

5. DESIGN METHOD

This section contains a semi-empirical method for estimating rms strains and natural frequencies for curved and flat graphite-epoxy skin-stringer panels, in order to predict their sonic fatigue lives. A random rms strain versus cycles to failure curve is presented for bonded skin-stiffener joints. A worked example is also presented.

The design equation and corresponding nomograph for rms strain was based on Z stiffeners. However, they can be readily factored to allow for the use of J stiffeners.

 a. Estimation of RMS Strain - The RMS strain nomograph is shown in Figure 64. It is based on equation 25 from Paragraph IV.4.a:

$$\epsilon_{rms} = \frac{(8.3234 \times 10^{-10}) \ 10^{(SPL/20)} \ b^{1.1045} \ R^{0.5519}}{t^{1.2069}} \quad (25)$$

where ϵ_{rms} = Maximum rms strain at panel edge due to random
  acoustic loading (10^{-6} in/in)

  SPL = Overall sound pressure level (dB)

  a = Panel length, between longerons (inches)

  b = Panel width, between stringers (inches)

  t = Skin laminate thickness (inches) (also given on nomograph as number of plies)

  R = Radius of curvature in "b" direction (inches).
  R = 150 in. is the maximum value to be used in the response equation, and is valid for flat panels and all R > 150 in.

Equation is valid for a/b $\geq$ 1.5.
For a/b = 1.2, factor equation by x 0.849.
For a/b = 1.0, factor equation by x 0.744.

177
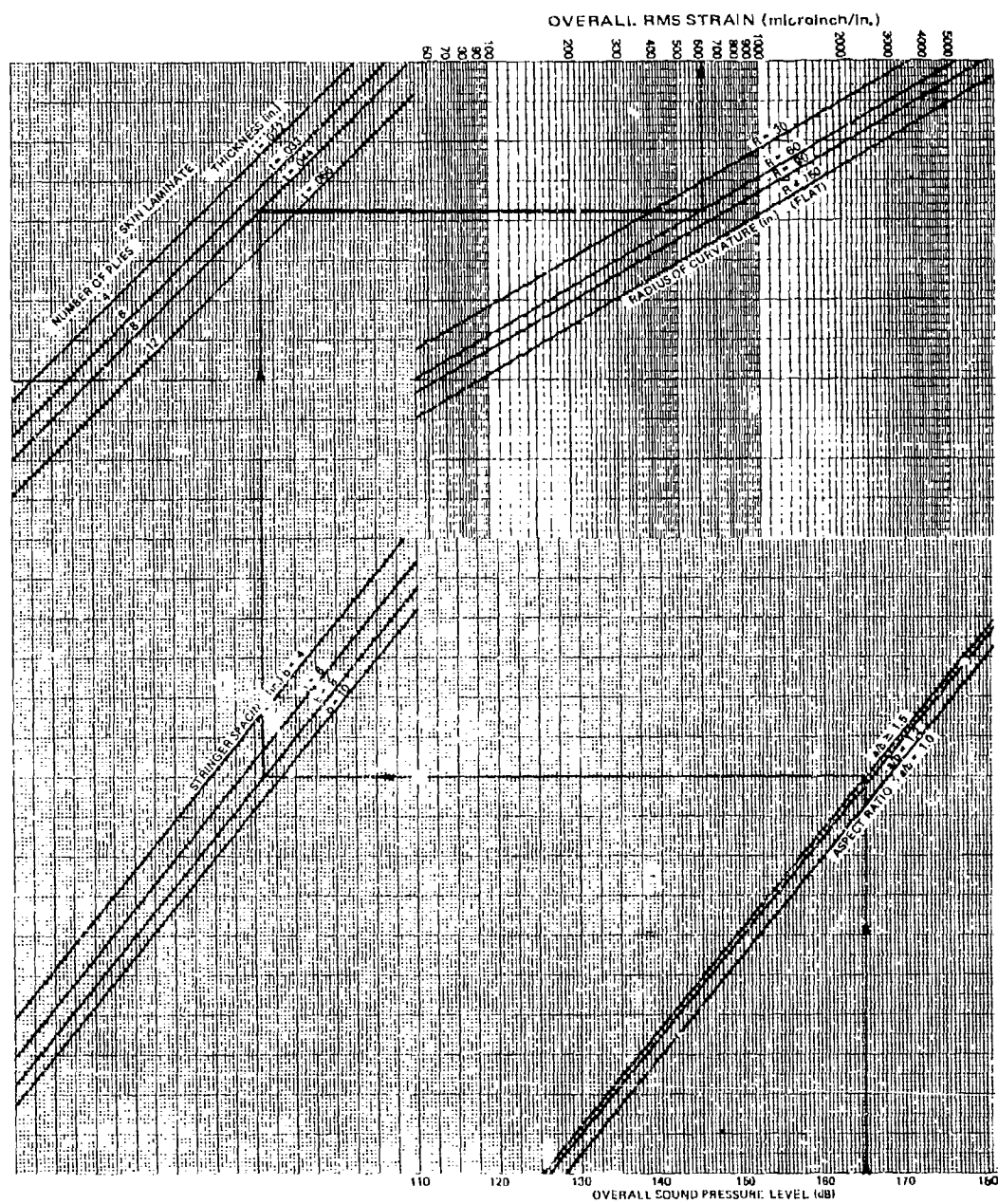
Figure 64. RMS Strain Nomograph

178

b. Estimation of Fully-Fixed Natural Frequency

From Reference 5,

$$f = V.K.\frac{t}{b^2} \tag{27}$$

where f = frequency of fundamental fully-fixed natural frequency (Hz).

$$V = (E_y/\rho)^{1/2}/200,000 \tag{28}$$

where　　　　E_y is the elastic modulus in the "y" direction, i.e., "b" direction (lb/in^2). Obtained from Tables 2 through 6 for laminates used in this program. For other laminates, Reference 12 may be used.

ρ = density of skin laminate. If expressed in units of lb/in^3, it must be divided by 386.4. For graphite-epoxy laminates,

$$\rho = \left(\frac{0.055}{386.4}\right)$$

K is obtained from Figure 65 for given b, t and R.

b,t and R are defined as in Paragraph IV.5.a, except that true values are to be used for all R, including ∞ for flat panels.

c. Estimation of Fatigue Life - Estimated sonic fatigue life is obtained by reading number of cycles to failure (N) from Figure 66 for rms strain (ϵ_{rms}) calculated in Paragraph IV.5.a. The number of cycles to failure is converted to life in hours by the relationship $\left(\frac{N}{3,600f}\right)$.

179
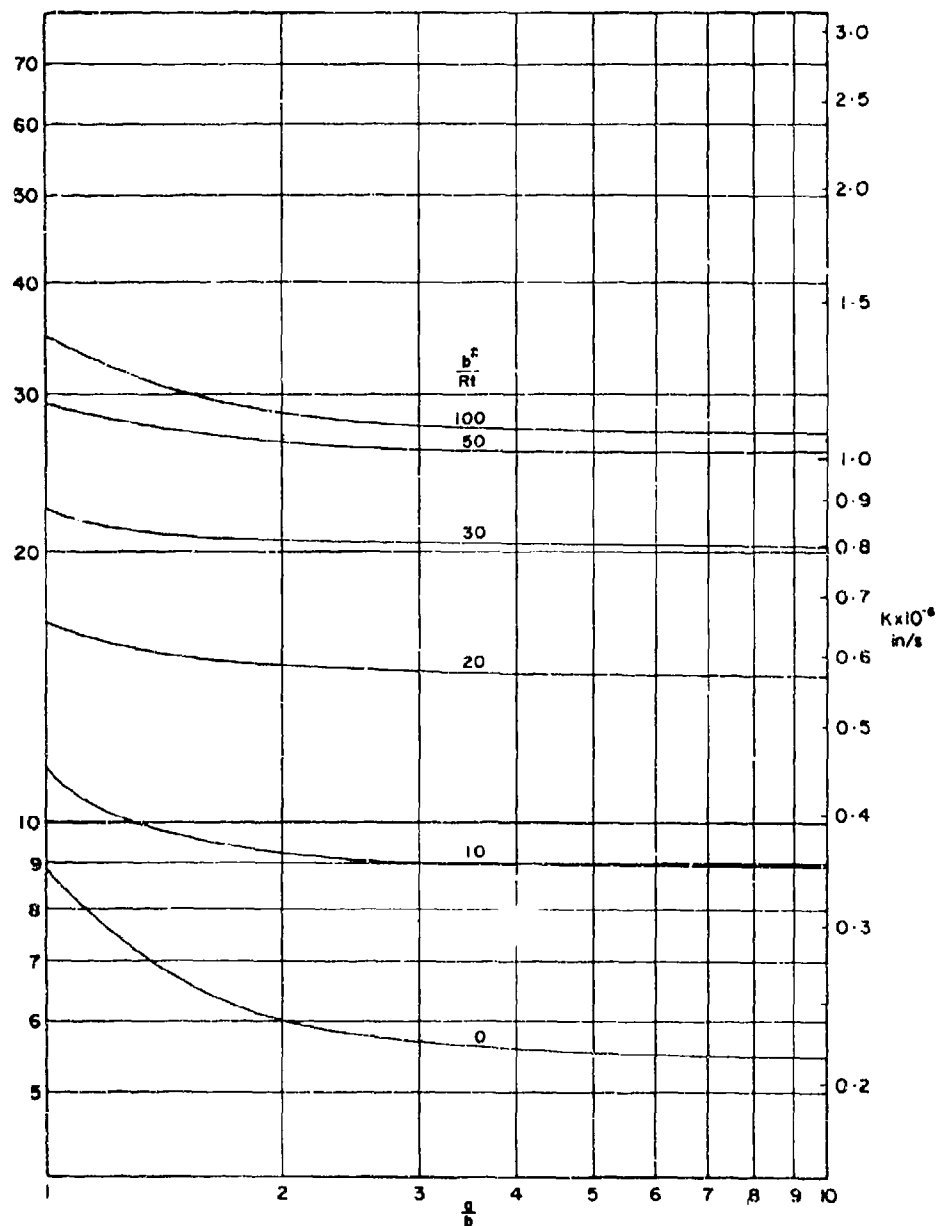
Figure 65. Natural Frequency Nomograph for Panel with Fixed Edges (Reference 5)

180
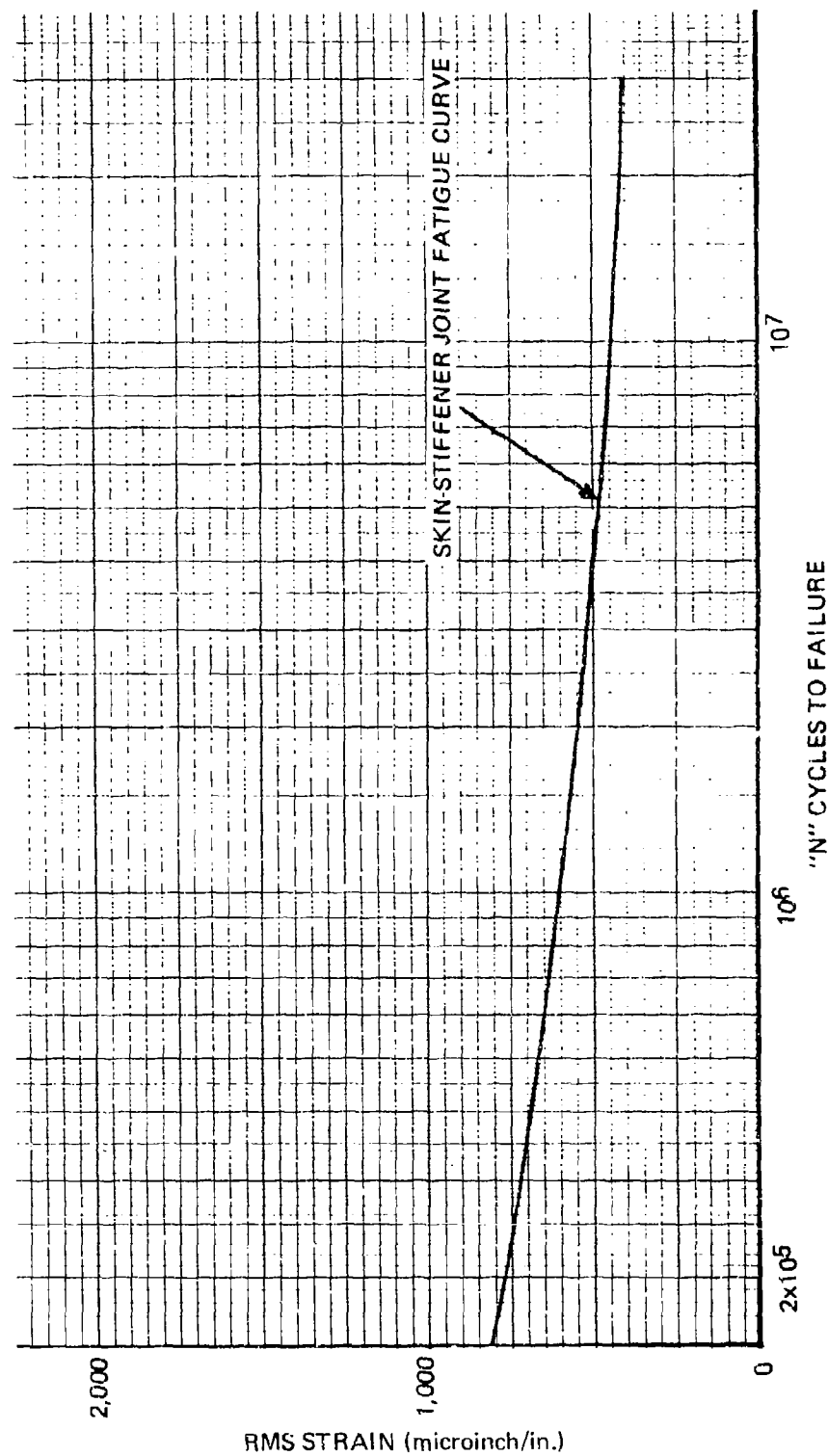
Figure 66. Random Fatigue Curve for Bonded Skin-Stiffener Joint — RMS Strain vs. Cycles to Failure

181

d. Calculation Procedure

   (1) Estimate rms strain (ε_{rms}) from Figure 64 or from equation 25, for given SPL (dB), b, t and R. (For flat panels and other R > 150, put R = 150-in.).

   If J stiffeners are used, multiply ε_{rms} by 0.8.

   (2) Calculate V from equation 28.

   (3) Estimate K from Figure 65 for given b, t and R. Use R = ∞ for flat panels.

   (4) Calculate frequency (f) from equation 27.

   (5) Estimate number of cycles to failure (N) from Figure 66 for estimated ε_{rms} from (1).

   (6) Convert cycles to failure to fatigue life in hours, using calculated frequency from (4).

e. Worked Example - A curved panel is made up from an 8 ply skin laminate, having a ply orientation of $(0, \pm 45, 90)_s$, which corresponds to t = .044 in. and E_y = 6.7 x 10^6 lb/in.^{2}. The panel has Z section stiffeners, with bay dimensions of a = 12 in. and b = 8 in. The radius of curvature is 60 in. The overall sound pressure level is 165 dB.

   (i) From Figure 64, the corresponding rms strain ε_{rms} = 615 microinches/inch.

   (ii) $V = (E_y/\rho)^{1/2}/200,000$, $\rho = \dfrac{.055}{386.4} = .000142$

   $= \left(\dfrac{6.7 \times 10^6}{.000142}\right)^{1/2} /200,000 = 1.0861$

(iii)   In order to determine K from Figure 65, first calculate:

$$a/b = \frac{12}{8} = 1.5$$

$$\frac{b^2}{Rt} = \frac{8^2}{(60)(.044)} = 24$$

From Figure 65, K = 0.68×10^6.

(iv)   From equation 27:

$$f = V.K.\frac{t}{b^2}$$

$$f = (1.0861)(0.68 \times 10^6)\frac{(.044)}{8^2}$$

$$= 508 \text{ Hz}$$

(v)   From Figure 66,

Cycles to failure N = 8×10^5

for ε_{rms} = 615.

(vi)   Fatigue life = $\frac{N}{3.600\ f}$

$$= \underline{0.44 \text{ hours}}$$

NOTE: The estimated rms strain of 615 μ in./in. corresponds to
a measured value of 595 μ in./in. The estimated
frequency of 508 Hz corresponds to a measured value of
350 Hz.

f. Fan Noise as Acoustic Load - The design method presented here
utilizes the overall sound pressure level as the design load. While this
is adequate for the broad-band spectra that typify jet exhaust noise, it
does not automatically lend itself to designing for the inlet and fan exit

183

acoustic spectra that occur due to fan noise on high bypass ratio engines. These spectra often have overall sound pressure levels that are dominated by very high acoustic spectrum levels occurring at the blade passage frequency and some of its harmonics. Since the blade passage frequency (typically 2-4 KHz) is usually well above the frequency range of interest for structural reponse (typically 50-1,000 Hz), including it in the overall sound pressure level to be used in this design method may result in overly conservative designs. In order to deal with this type of acoustic load it is necessary to eliminate these high frequency peaks, and develop an estimate for the overall sound pressure level from 50 Hz-1,000 Hz. This can be accomplished in one of the following ways. (1) If the actual measured acoustic data are available (e.g., on magnetic tape), reanalyze the data to measure the overall sound pressure level with a 1,000 Hz cutoff filter applied. (2) If only the acoustic spectrum plot is available, then sum together in sequence all the significant peaks between 50 Hz and 1,000 Hz in the following way:

If the difference (in dB) between two peaks is (any bandwidth):

	0	1	2	3	4	5	6	7	8	9	10	>10
then add to the larger peak (dB)	3	2.5	2.1	1.8	1.5	1.2	1.0	0.8	0.6	0.5	0.4	0

Example: If there were four peaks with the following levels (dB):

140, 134,   139 and 139,   then
    \ /   \ /
     difference = 6 dB   difference = 0 dB
     add 140 + 1.0   then add 139 + 3
     = 141dB   = 142 dB
              \   /
               difference + 1 dB
               add 142 + 2.5
               = 144.5 dB

This 144.5 dB is the overall sound pressure level to be used as the design load.

6. DESIGN METHOD COMPARISONS

Graphite-epoxy skin-stringer structures, of the type evaluated in this program, are primarily in competition with similarly configured aluminum structures for application on both military and civil aircraft. Cost/weight tradeoffs between graphite and aluminum structures having comparable sonic fatigue resistance are, therefore, of interest to potential users of the design method in Section IV.5. In order to provide an estimate of the sonic fatigue resistance of graphite relative to aluminum, comparisons were made between the method in Section IV.5 and those in References 2 and 5. One difficulty in making these direct comparisons is that References 2 and 5 utilize acoustic spectrum levels, whereas Section IV.5 here utilizes overall sound pressure levels. In order to overcome this, a typical broad band sonic fatigue design load spectrum was used which had an overall sound pressure level of 157 dB and a corresponding acoustic spectrum level of 132 dB/Hz in the frequency range of interest. This 25 dB difference between overall and spectrum levels is compatible with the acoustic load in this program.

The following example problem was used for comparison:

Required life = 10^7 cycles (using the -50% confidence level from Reference 2).

$$b = 8$$
$$a/b = 2$$
$$\zeta = .02$$

Calculate required skin thicknesses.

The following results were obtained:

Reference 2 - Riveted Aluminum Skin-Stringer: t = .05-in.

Reference 5 - Riveted Aluminum Skin-Stringer: t = .076-in.

Section IV.5 - Bonded Graphite Skin-Stringer: t = .041-in.

Paragraph IV.4.a. - Using the nonlinear
response equation: t = .037-in.

Comparisons of sonic fatigue resistance using References 2 and 5 yield similar results for some configurations and very different results for others. Where differences do occur, Reference 5 is the more conservative.

Since the density of graphite is approximately half that of aluminum, the potential weight saving of graphite over aluminum for equivalent sonic fatigue resistance is significantly large. Comparing values generated in this program with those in Reference 2, the weight of graphite is slightly less than half that of the equivalent aluminum structure.

186

SECTION V
CONCLUSIONS

A satisfactory sonic fatigue design method was developed for curved and
flat graphite-epoxy skin-stringer panels. The design method is presented
as a self-contained section suitable for application to aircraft
structural design. Design trade-offs with aluminum structures indicated
that graphite offers a 2:1 weight saving over aluminum, for comparable
sonic fatigue resistance.

Analytical results indicated that ply stacking order may have an effect on
sonic fatigue life. However, the effects were not quantified sufficiently
to facilitate the inclusion of this variable in the design method. This
is an area requiring further work.

The finite-element analyses gave good static strain distributions for the
test panel configurations. These computed strains displayed high
statistical correlation with measured dynamic strains. Element grid size
was found to be critically important at panel edges. Representing panel
stiffeners as plates in three-dimensional models resulted in more accurate
computed strains than when representing stiffeners as beams in two-
dimensional models.

The finite-element analyses did not result in satisfactory frequency
estimates for all the test panel configurations. On the stiffer panels,
mode shapes were dominated by motion of the substructure, resulting in low
frequency estimates. Test data contradicted this response behavior. The

best analytical comparisons with measured frequencies were obtained using simple frequency calculations assuming fully-fixed edges.

Adhesive bonding problems encountered during the early stages of test specimen fabrication demonstrated the importance of assuring good bond and laminate quality prior to fabricating expensive sonic fatigue test panels. Shaker testing of small coupons was found to be an excellent method of evaluating specimen quality. The modes of failure during shaker testing showed good correlation with progressive-wave tube failures.

The sonic fatigue data obtained during the progressive-wave tube tests showed good correlation with variations in panel configuration parameters. The data also displayed some inconsistencies, characteristic of sonic fatigue testing. Sonic fatigue failures were generally observed to occur over long periods of time, often over several million cycles. The first signs of fatigue damage were fractured skin laminate fibers in the stiffener-skin joint areas. Isolated fiber failures would continue to occur until the extent of the skin damage resulted in separation from the stiffeners. This type of slow progressive failure presents problems in defining time to failure. The mode of sonic fatigue failure was indicative of good quality structural panels. The fatigue lives of bonded and riveted joints were compared. Riveted joints displayed slower rates of progressive damage.

Slight variations in ply orientation did not appear to affect panel response or fatigue life. However, it is expected that major variations in ply orientation would have significant effects.

J stiffeners were observed to result in significantly longer fatigue lives than did Z stiffeners.

Panel responses showed some degree of nonlinearity, however, back-to-back strain measurement did not reveal any membrane strains.

188

Multiple stepwise regression analysis, relating rms strains to panel
configuration parameters, provided the basis for the recommended design
method. Miles' equation did not show good correlation with the test data.
Linear and nonlinear equations were developed to predict panel response.
Emphasis was placed on the importance of critically reviewing the test
data prior to regression analysis. The potential hazards of using
regression analysis were discussed in some detail. A design nomograph to
predict rms strains was constructed and presented as part of a sonic fatigue
design method. A worked example was also presented.

REFERENCES

1.   Miles, J. W., "On Structural Fatigue Under Random Loading," Journal of Aeronautical Sciences, Vol. 21, November 1954.

2.   Ballentine, J. R. et al. "Refinement of Sonic Fatigue Structural Design Criteria," AFFDL-TR-67-156, January 1968.

3.   Holehouse, I., "Sonic Fatigue of Diffusion Bonded Titanium Sandwich Structures," Paper No. 15, AGARD-CP-113, Advisory Group for Aerospace Research and Development, North Atlantic Treaty Organization, 1972.

4.   Schneider, C. W., "Acoustic Fatigue of Aircraft Structures at Elevated Temperatures," AFFDL-TR-73-155.

5.   Thompson, A.G.R. and Lambert, R. F., "Acoustic Fatigue Design Data," AGARD-AG-162, Advisory Group for Aerospace Research and Development, North Atlantic Treaty Organization, November 1972.

6.   Rudder, F. F. and Plumblee, H. E., "Sonic Fatigue Design Guide for Military Aircraft," AFFDL-TR-74-112, May 1975.

7.   Jacobson, J. J., "Acoustic Fatigue Design Information for Fiber Reinforced Structures," AFFDL-TR-68-107, October 1968.

8.   Lin, Y. K., "Free Vibrations of Continuous Skin-Stringer Panels," Journal of Applied Mechanics, December 1960.

9.   Powell, A., "On the Fatigue Failure of Structures Due to Vibrations Excited by Random Pressure Fields," Journal of the Acoustical Society of America, Vol. 30, No. 12, December 1958.

10. Roark, J. R., "Formulas for Stress and Strain," McGraw Hill.

11. Miner, M. A., "Cumulative Damage in Fatigue," Journal of Applied Mechanics. Vol. 12, 1954.

12. Lackman, L. M., et al. "Advanced Composites Data for Aircraft Structural Design, Volume IV," AFML-TR-70-58, September 1972.

13. Timoshenko, S. P., "Theory of Plates and Shells," McGraw Hill.

14. Den Hartog, J. P., "Mechanical Vibrations," McGraw Hill.

15. Levy, M., "Compt. rend., Vol. 129," Paris 1900.

APPENDIX A

FINITE ELEMENT MODELS AND RESULTS

Figures A-1 through A-32 are computer generated plots of the following:

- Finite element models used in the static and dynamic analyses
- Static deflections and stresses for panels b, d and f
- Mode shapes for panels b and f
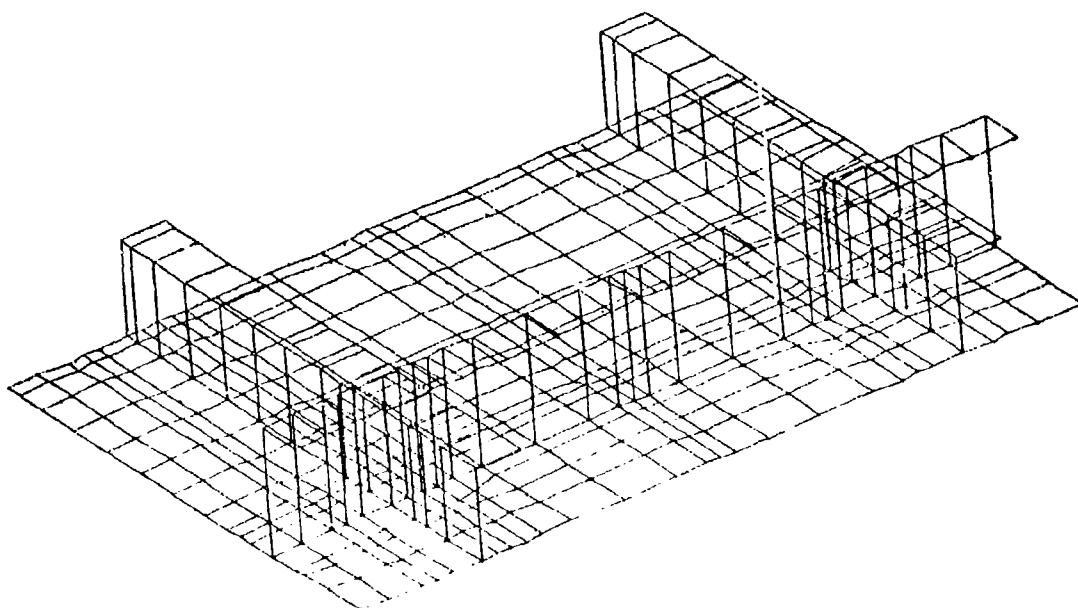
Figure A-1. Finite Element Model of 3 x 3 Center Panel - Flat
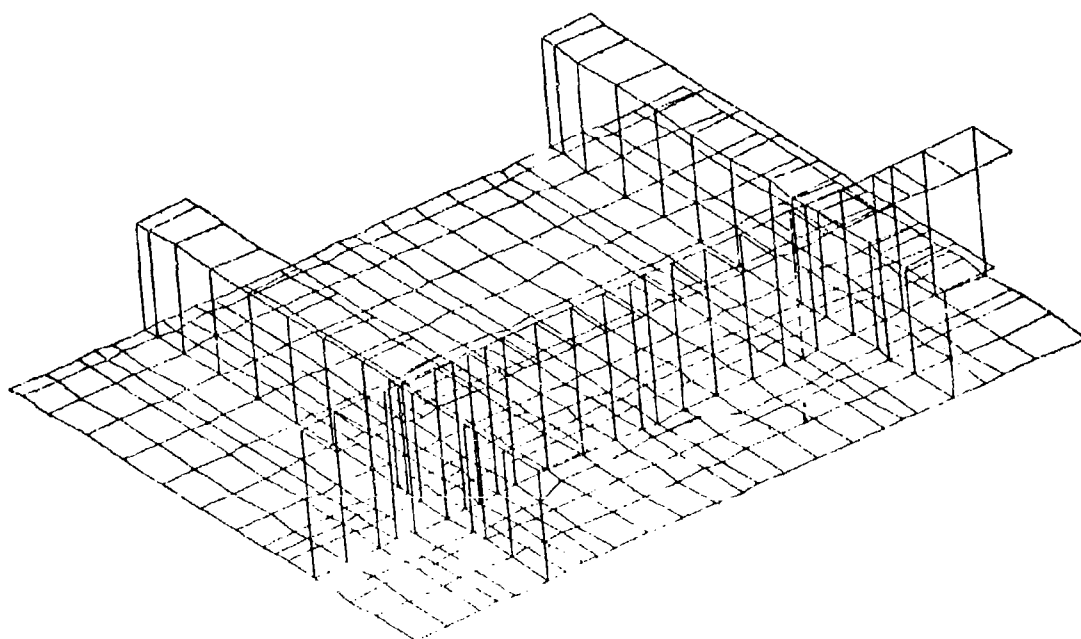
Figure A-2. Finite Element Model of 4 x 3 Center Panel - Flat
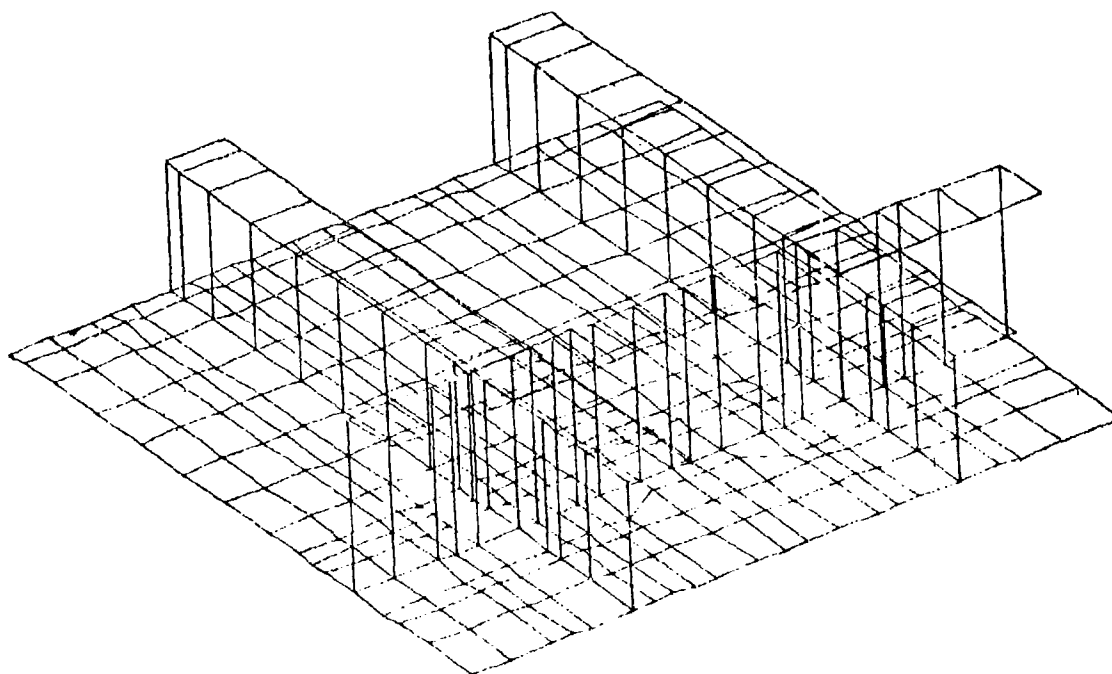
Figure A-3. Finite Element Model of 6 x 3 Center Panel - Flat
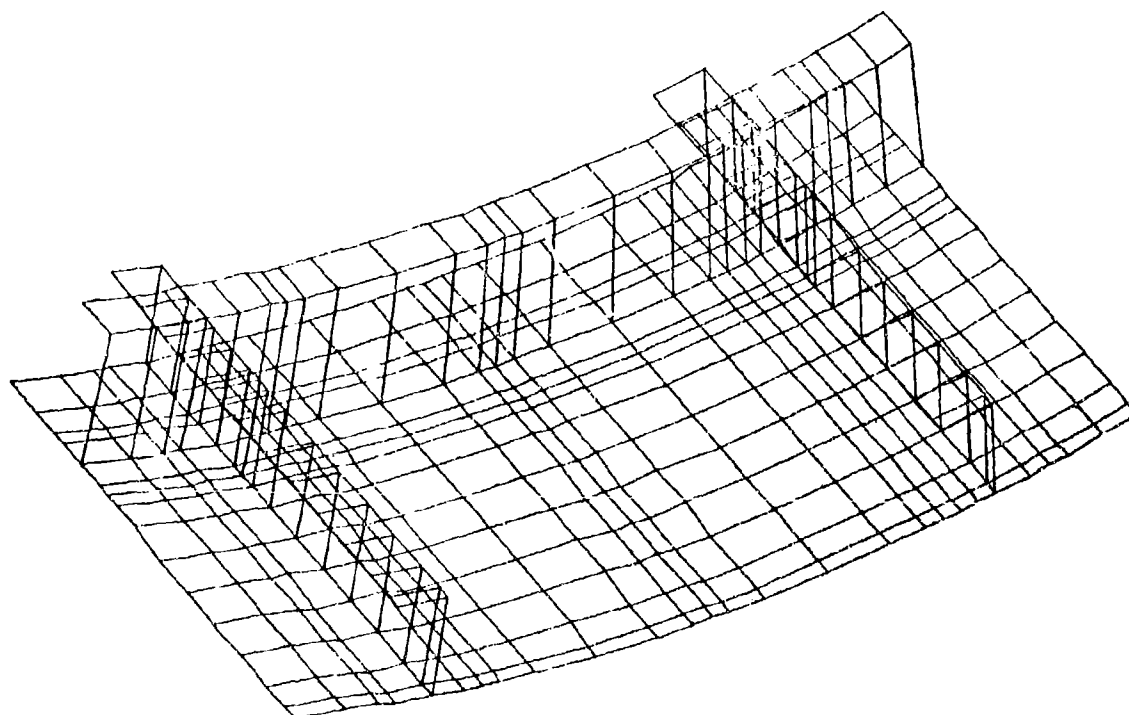
Figure A-4. Finite Element Model of 3 x 3 Center Panel
(Radius of Curvature = 30 In.)

A-3
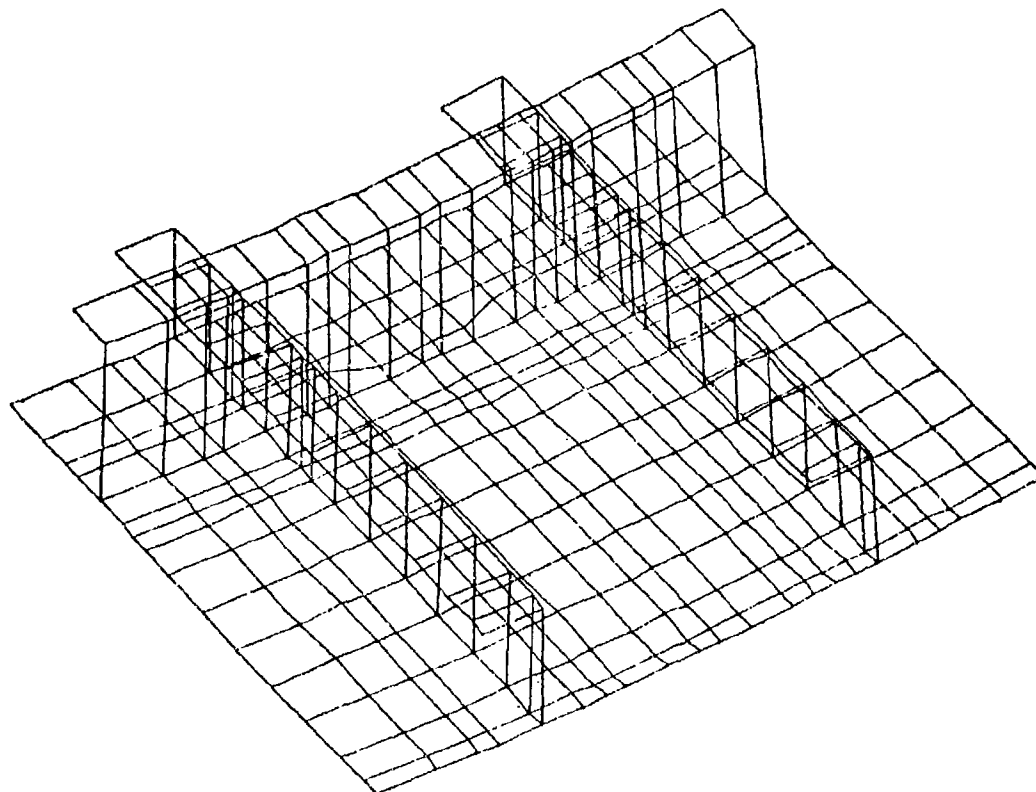
Figure A-5. Finite Element Model of 6 x 3 Center Panel
(Radius of Curvature = 60 In.)
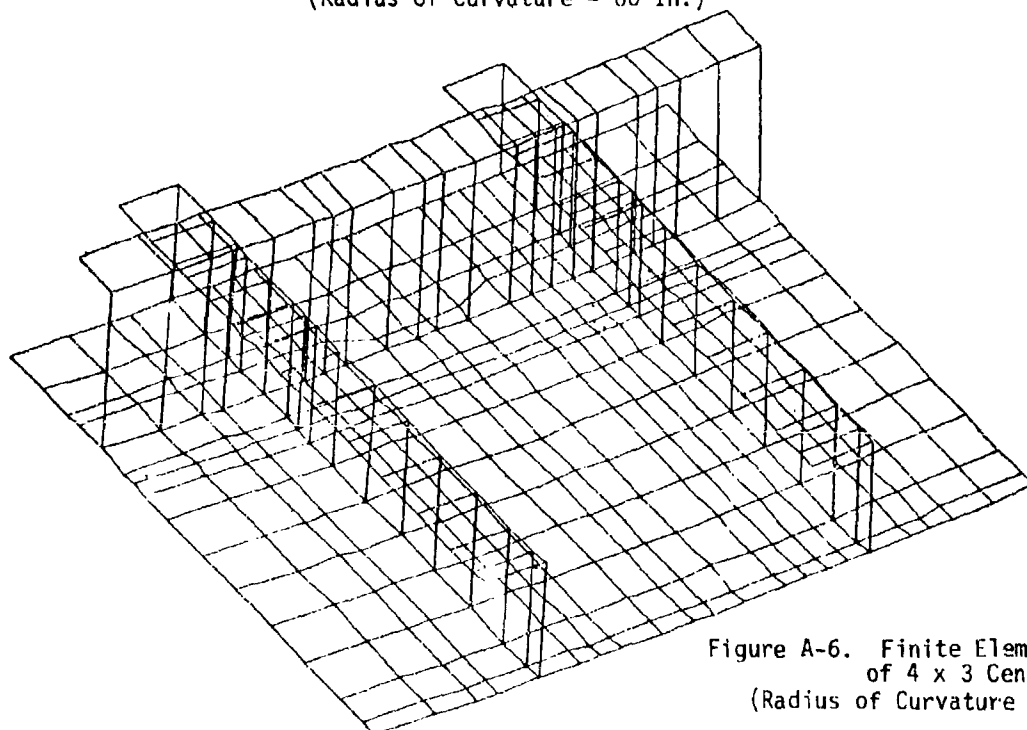
Figure A-6. Finite Element Model
of 4 x 3 Center Panel
(Radius of Curvature = 90 In.)
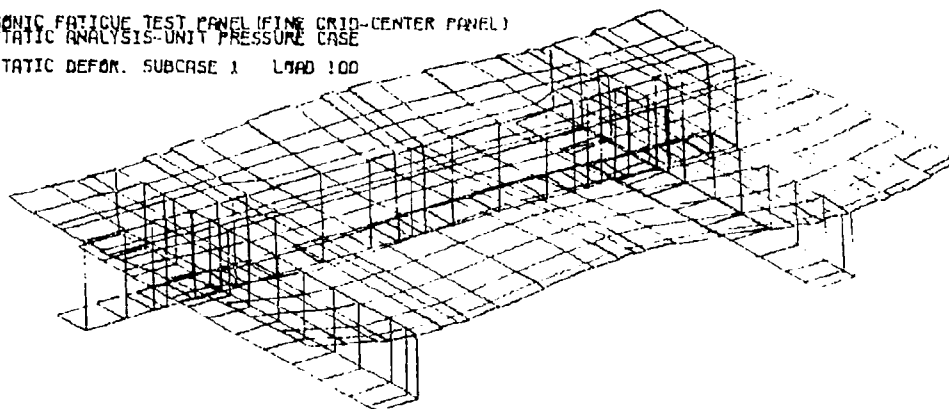
Figure A-7.   Static Deformation for Configuration b

SYMBOL	VALUE (IN.)
1	1.21372 0E-01
2	1.33321 6E-01
3	1.46271 6E-01
4	1.54721 3E-01
5	1.71171 1E-01
6	1.83620 9E-01
7	1.96070 7E-01
8	2.08520 4E-01
9	2.20970 2E-01
10	2.33420 0E-01

1/10/79   MAX-DEF. = 0.23341999
Z-DISPLACEMENT PLOT
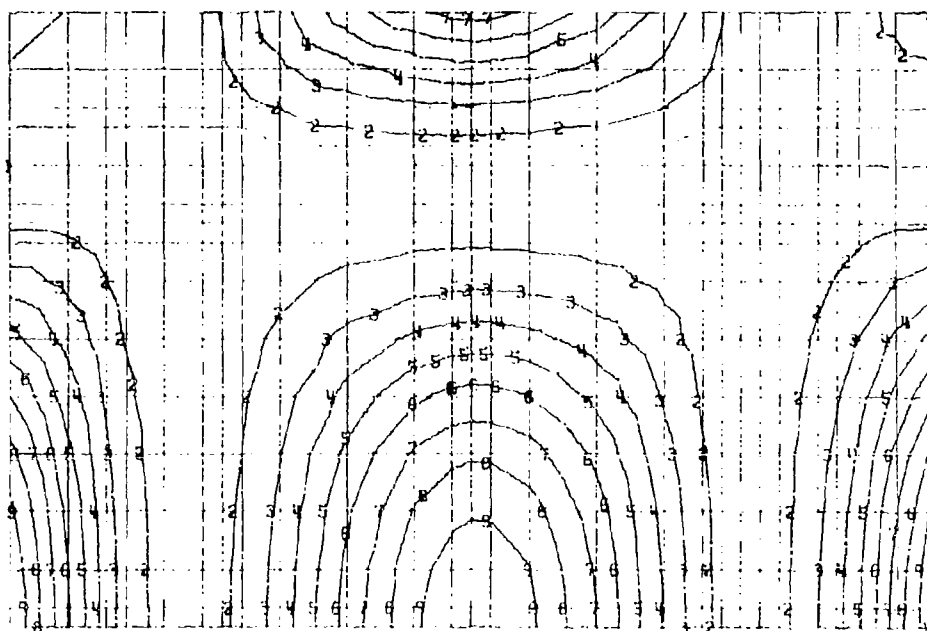
Figure A-8.   Z-Displacement for Configuration b

A-5

SYMBOL   VALUE (PSI)
1   -1.428621E+04
2   -1.204323E+04
3   -9.800246E+03
4   -7.557261E+03
5   -5.314277E+03
6   -3.071293E+03
7   -8.282080E+02
8   1.414676E+03
9   3.657661E+03
10   5.900645E+03

1/10/79   MAX-DEF. = 0.23941999
YNORMAL STRESS PLOT
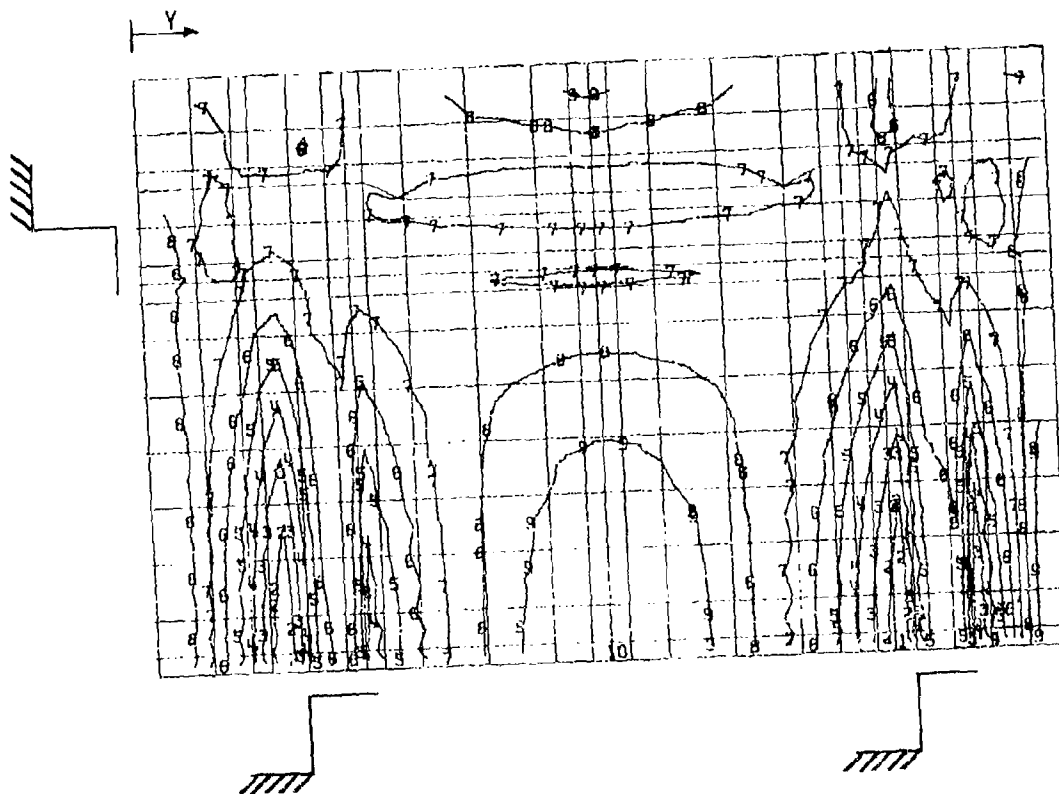
Figure A-9.   Normal Stress (y) for Configuration b

A-6

1/10/79   MAX-DEF. = 0.23341999
XNORMAL STRESS PLOT
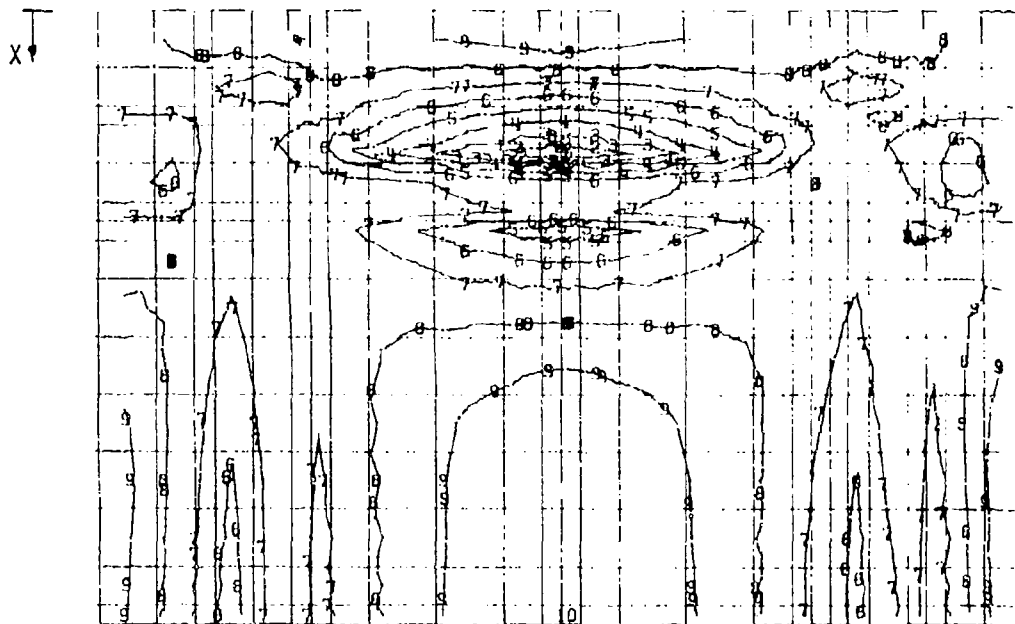
Figure A-10.   Normal Stress (x) for Configuration b

A-7
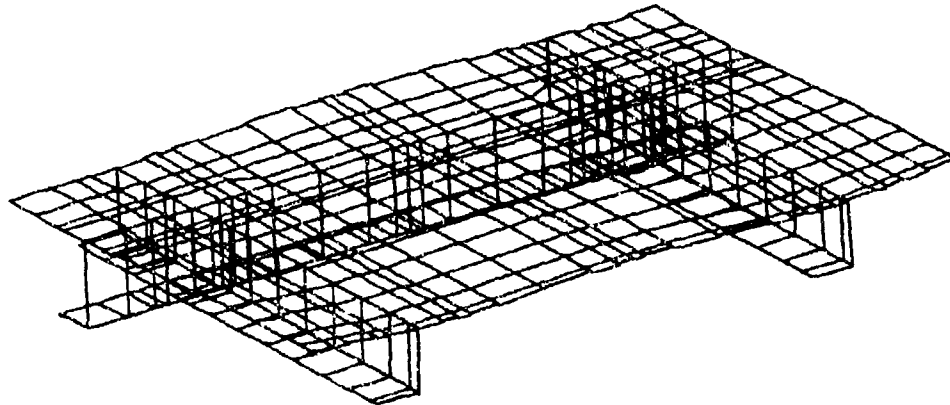
Figure A-11. Static Deformation for Configuration d

SYMBOL	VALUE (IN.)
1	1.050580E-01
2	1.096771E-01
3	1.142962E-01
4	1.189153E-01
5	1.235344E-01
6	1.281536E-01
7	1.327727E-01
8	1.373918E-01
9	1.420109E-01
10	1.466300E-01

1/18/79   MAX-DEF. = 0.14662999
Z-DISPLACEMENT PLOT
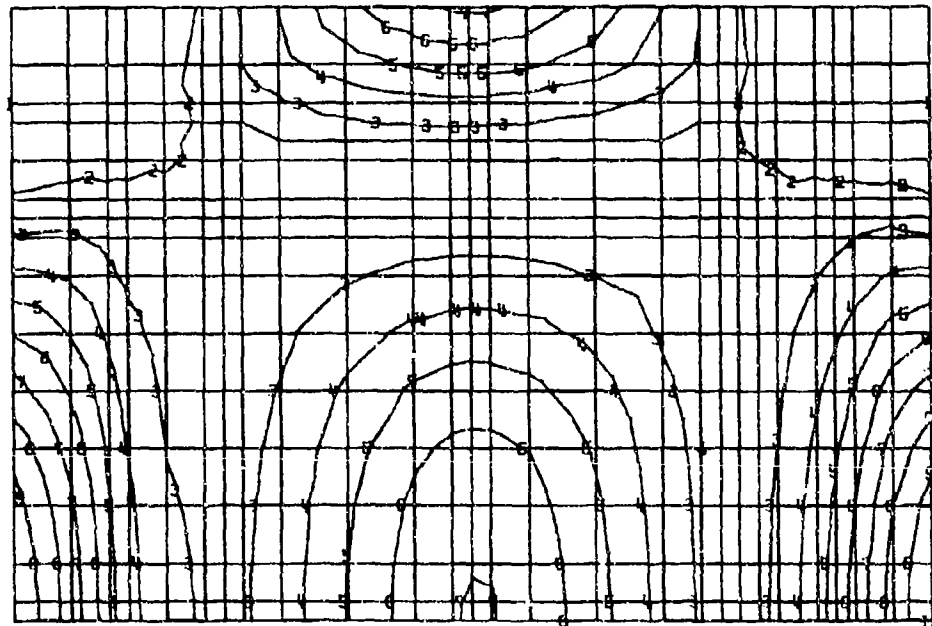
Figure A-12. Z-Displacement for Configuration d

A-8

SYMBOL   VALUE (PSI)

1	-8.147581E+03
2	-6.495972E+03
3	-4.844363E+03
4	-3.192754E+03
5	-1.541146E+03
6	1.104631E+02
7	1.762072E+03
8	3.413681E+03
9	5.065289E+03
10	6.716898E+03

YNORMAL STRESS PLOT   1/16/79   MAX-DEF. = 0.14662999
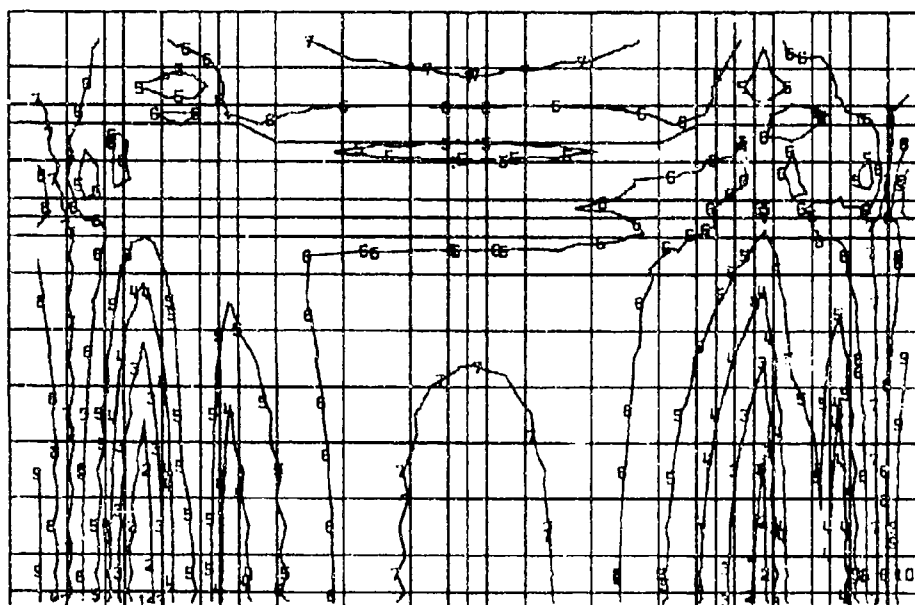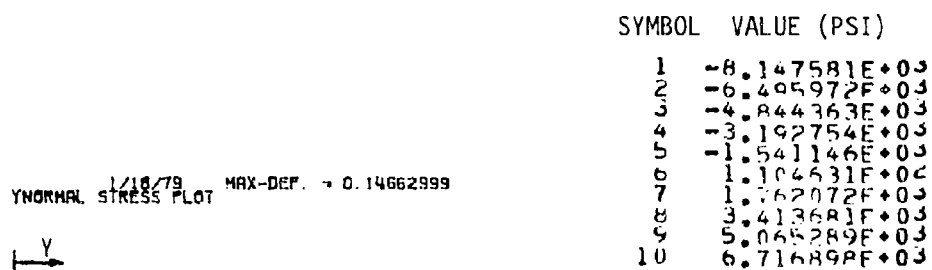
Figure A-13.   Normal Stress (y) for Configuration d

A-9

1/18/79   MAX-DEF. = 0.14682999
XNORMAL STRESS PLOT

X
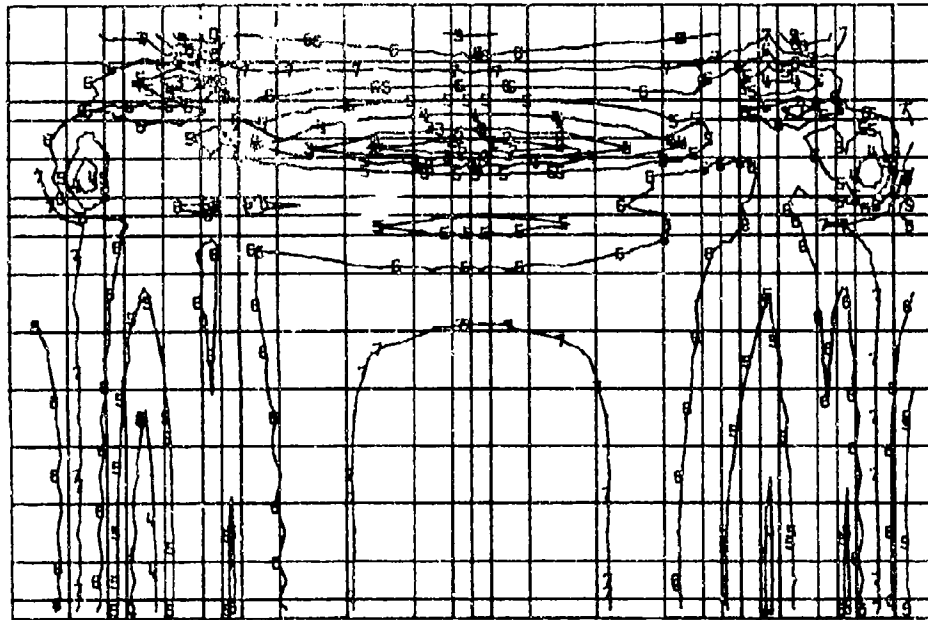
Figure A-14.   Normal Stress (x) for Configuration d

A-10
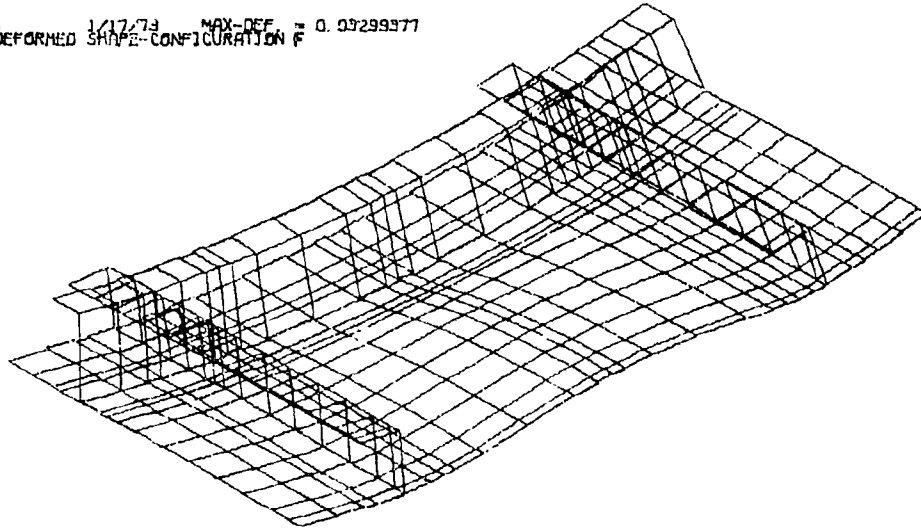
Figure A-15.   Static Deformation for Configuration f

SYMBOL	VALUE
1	5.075326E-03
2	8.177376E-03
3	1.127943E-02
4	1.438148E-02
5	1.748353E-02
6	2.058558E-02
7	2.368763E-02
8	2.678968E-02
9	2.989173E-02
10	3.299378E-02

1/17/79   MAX-DEF. = 0.03299377
Z-DISPLACEMENT PLOT
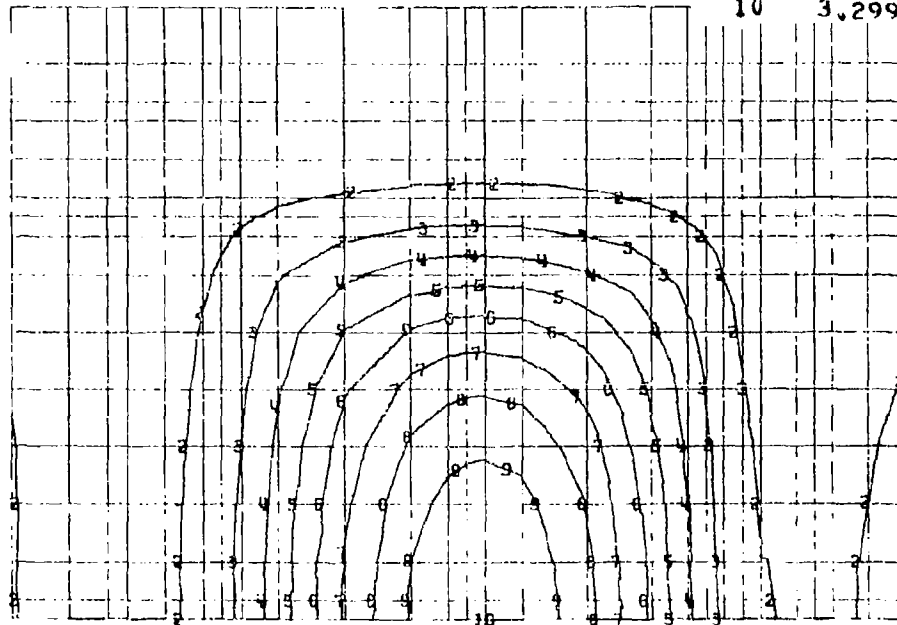
Figure A-16.   Z-Displacement for Configuration f

A-11

Figure A-17. Normal Stress (y) for Configuration f

A-12

1/17/79   MAX-DEF. = 0.09299.371
XNORMAL STRESS PLOT
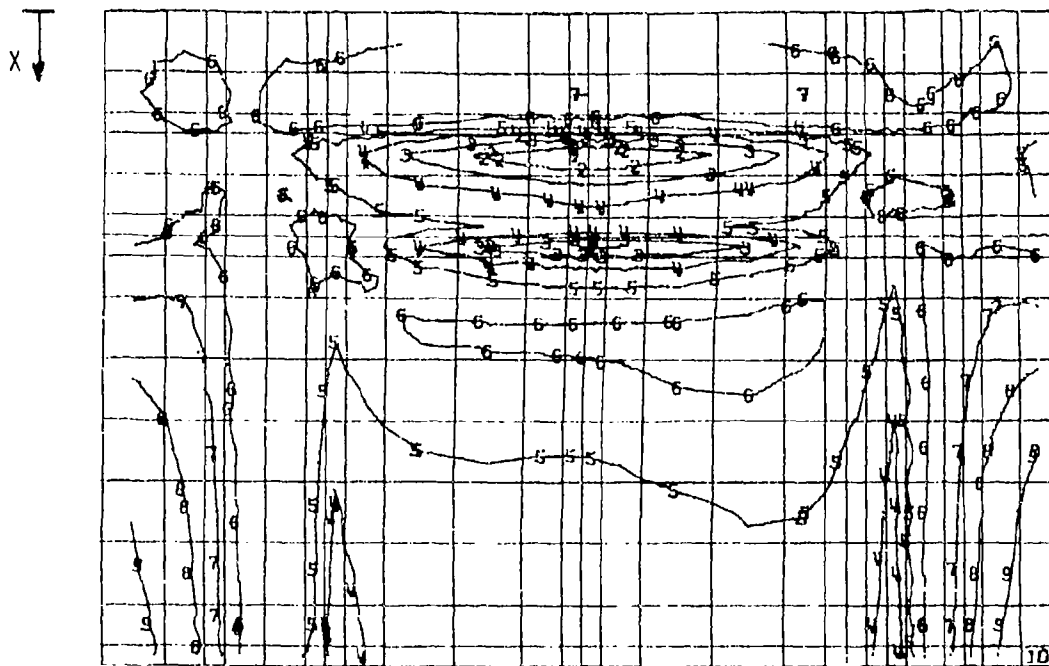
Figure A-18.   Normal Stress (x) for Configuration f

A-13
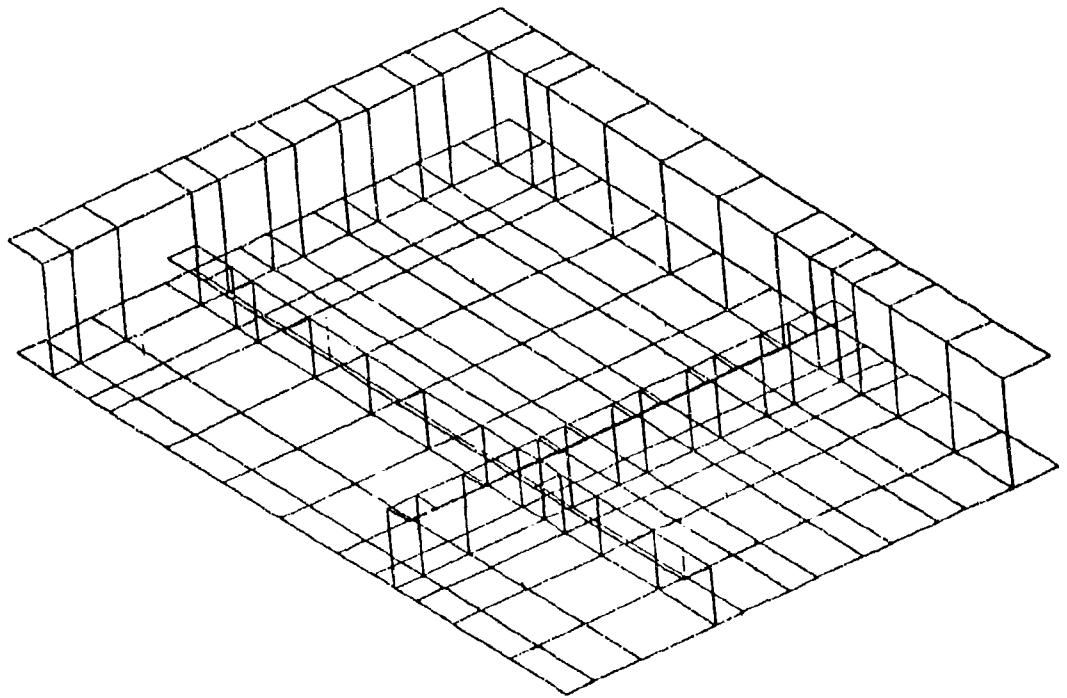
Figure A-19. Flat 3 x 3 Finite Element Model for Dynamic Analysis
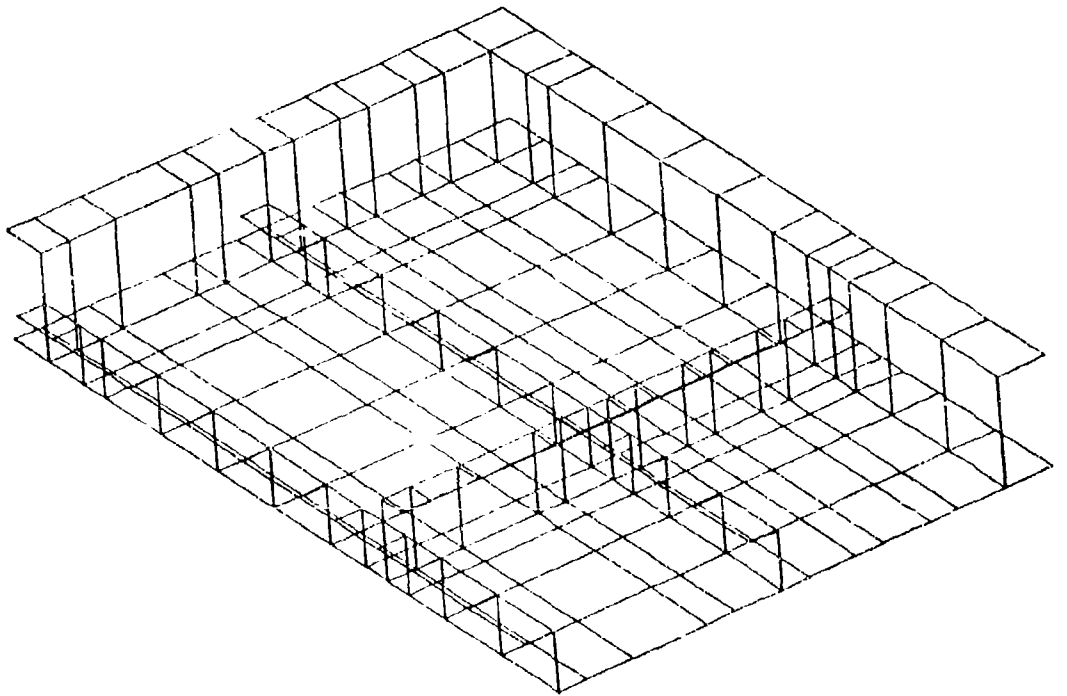
Figure A-20. Flat 4 x 3 Finite Element Model for Dynamic Analysis
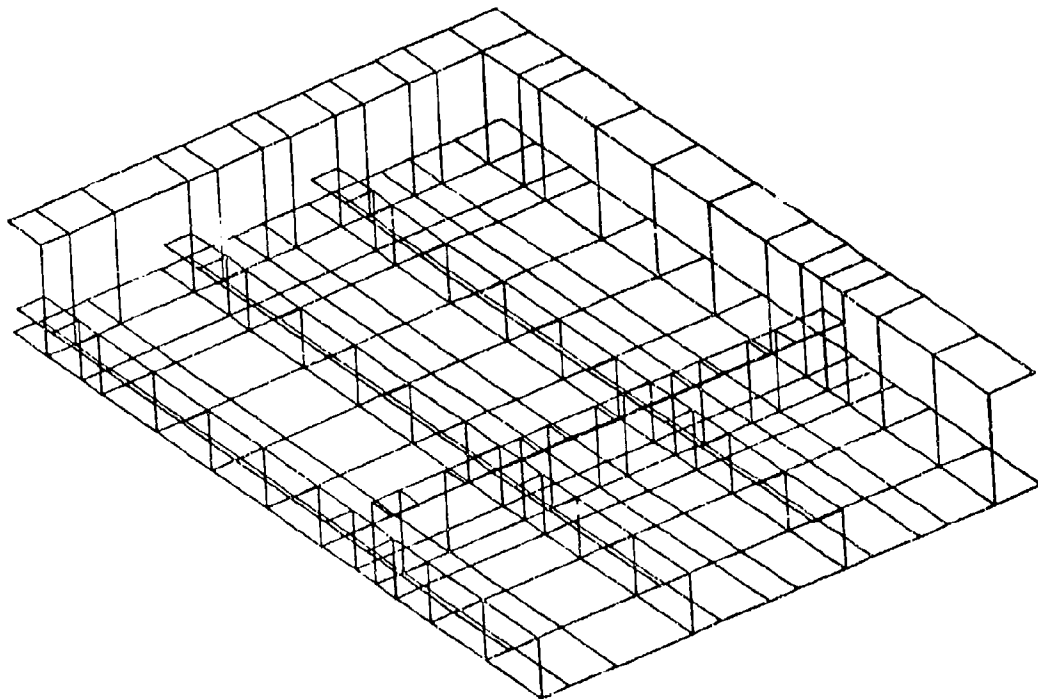
Figure A-21.   Flat 6 x 3 Finite Element Model for Dynamic Analysis
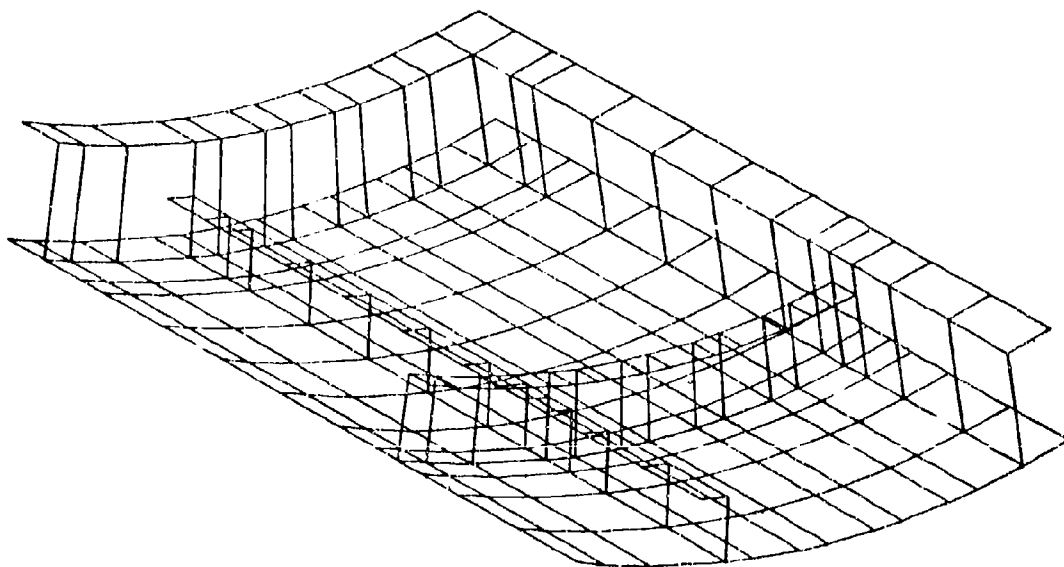
Figure A-22.   Curved (R=30) 3 x 3 Finite Element Model for Dynamic Analysi
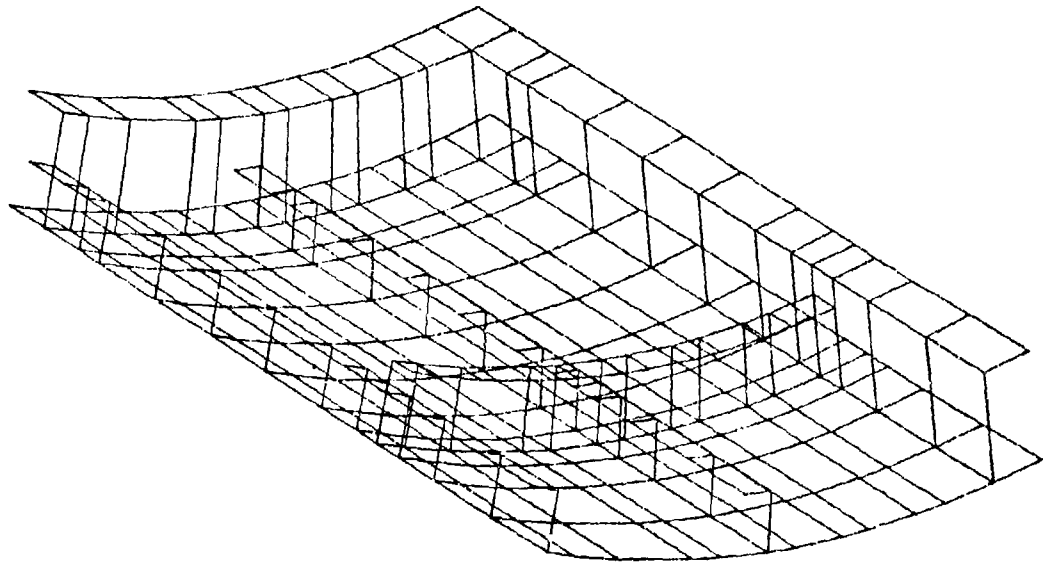
Figure A-23. Curved (R=30) 4 x 3 Finite Element Model for Dynamic Analysis
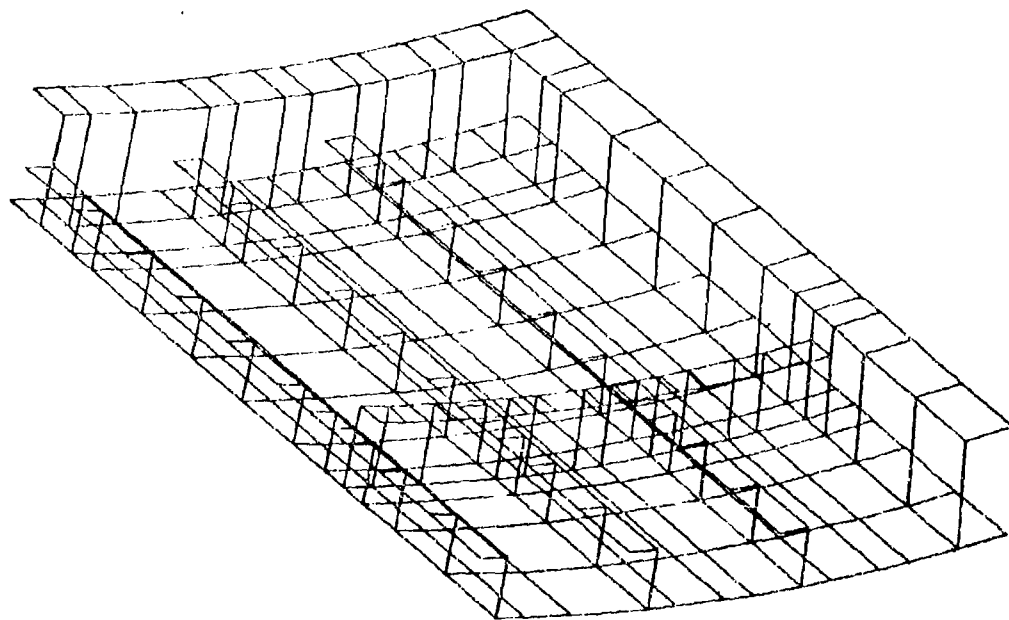
Figure A-24. Curved (R=60) 6 x 3 Finite Element Model for Dynamic Analysis
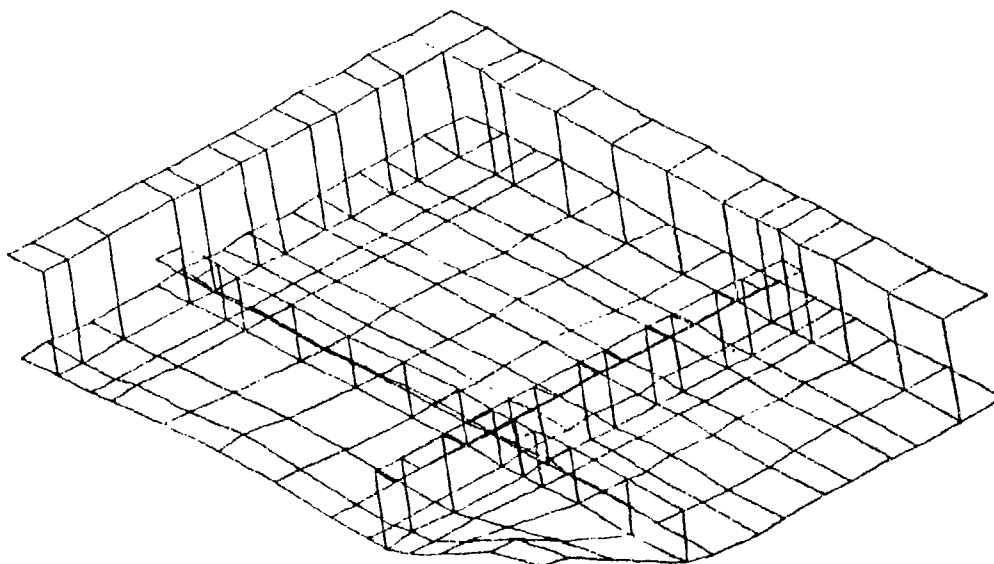
Figure A-25. First (Fundamental) Harmonic for Panel b (f_1 = 171 Hz)
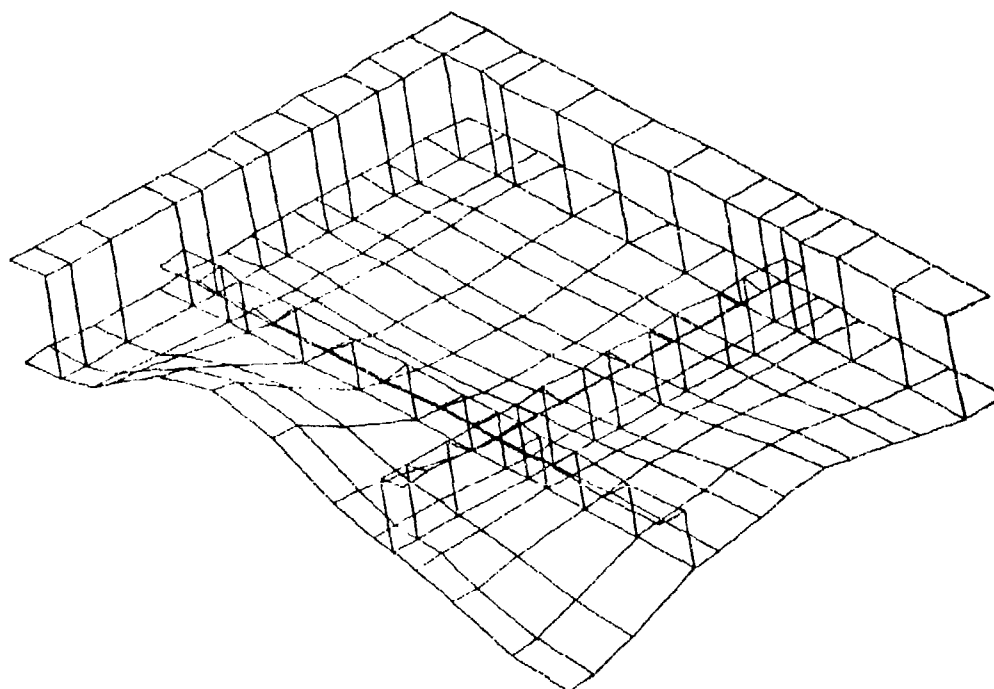
Figure A-26. Second Harmonic for Panel b (f_2 = 177 Hz)
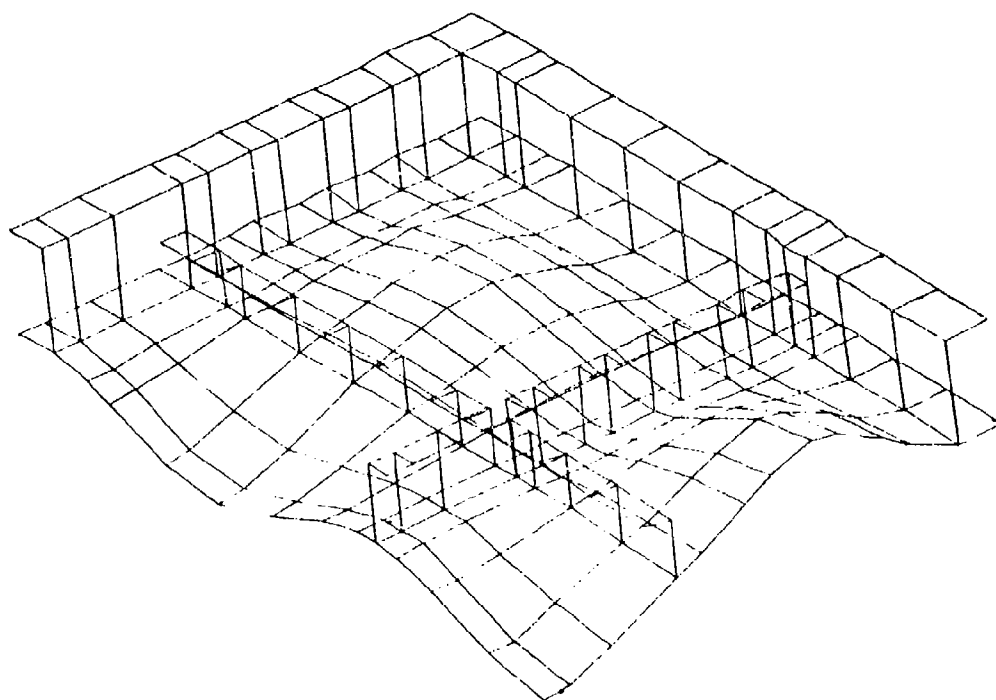
Figure A-27. Third Harmonic for Panel b (f_2 = 189 Hz)
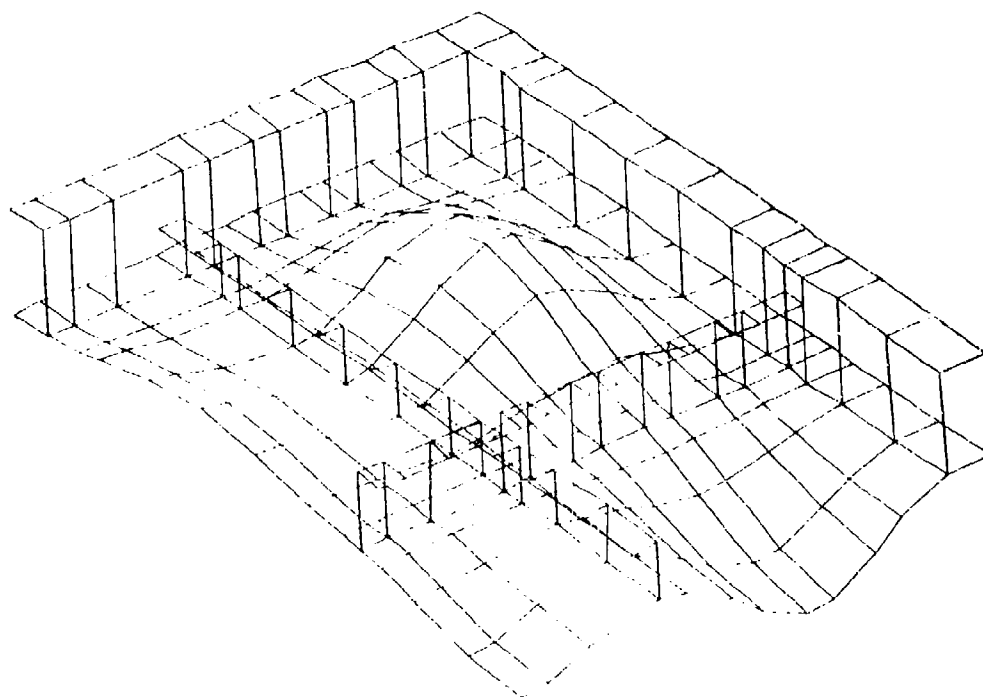
Figure A-28. Fourth Harmonic for Panel b (f_4 = 213 Hz)

A-18
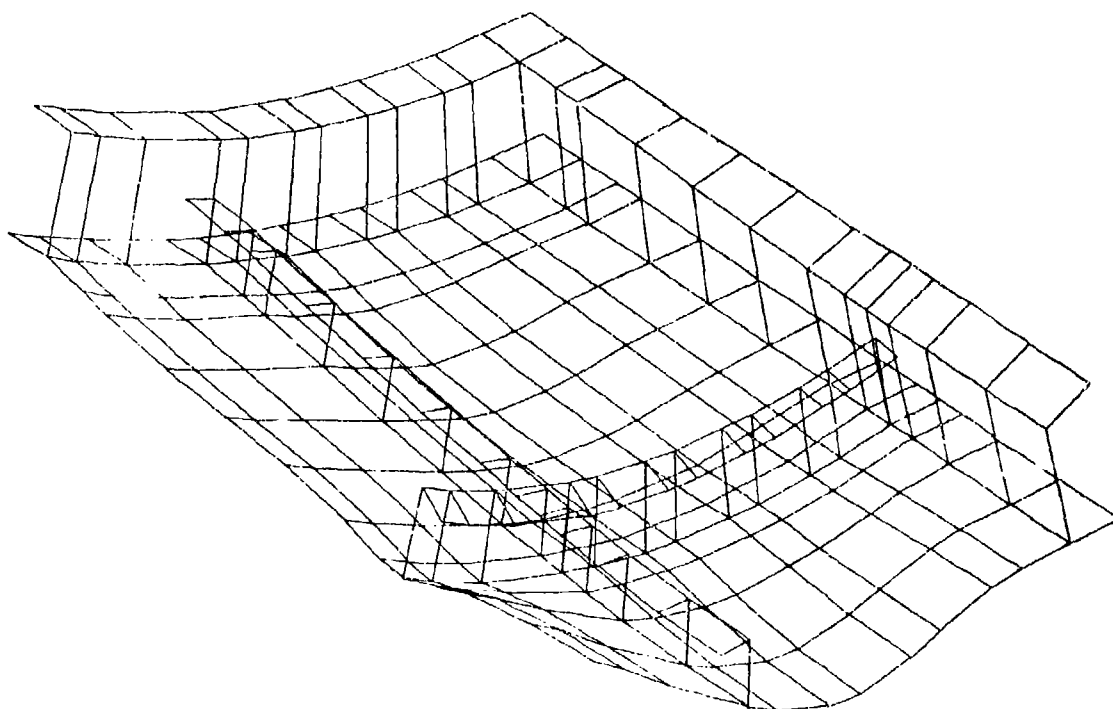
Figure A-29. First (Fundamental) Harmonic for Panel f (f_1 = 343 Hz)
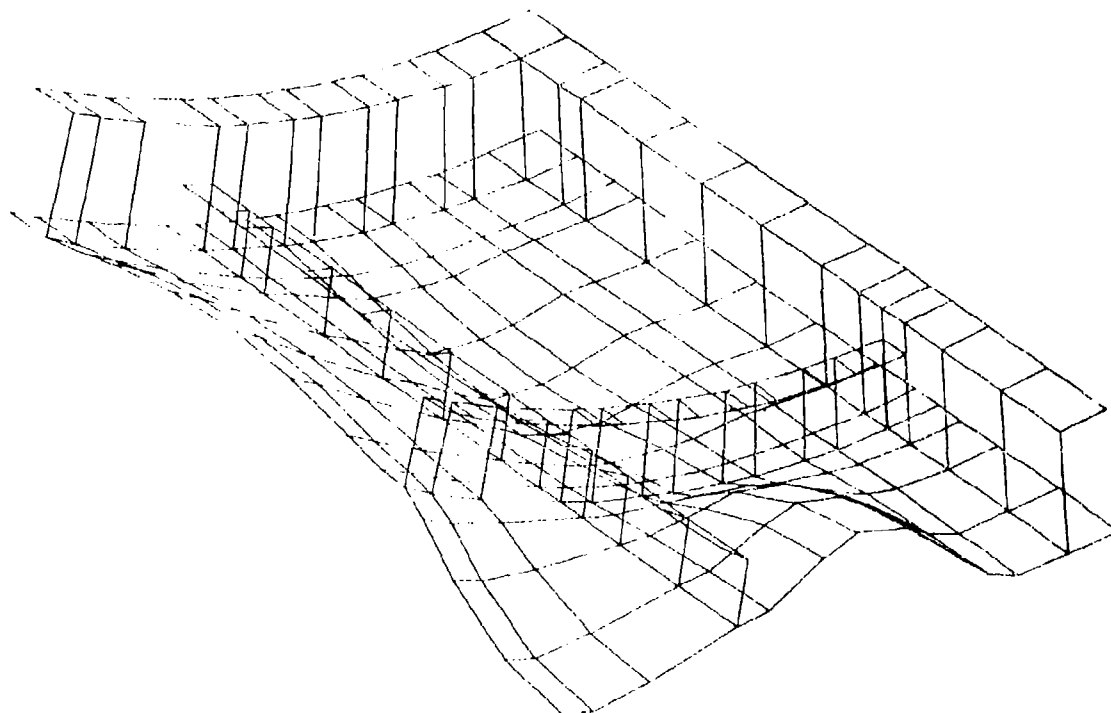
Figure A-30. Second Harmonic for Panel f (f_2 = 463 Hz)
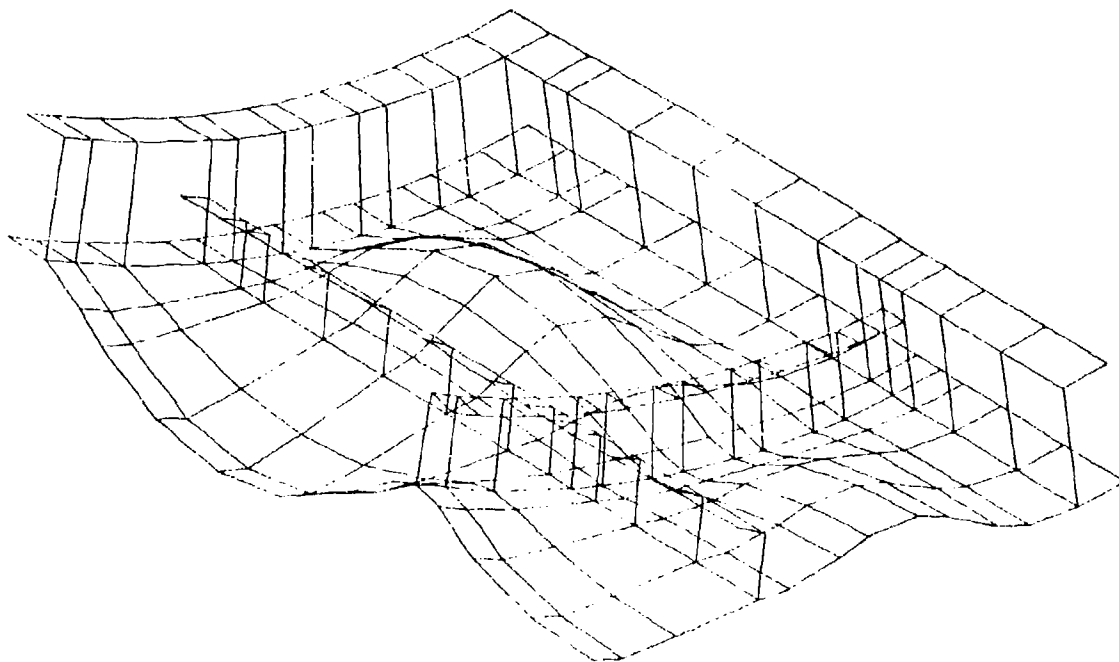
Figure A-31. Third Harmonic for Panel f (f_3 = 483 Hz)
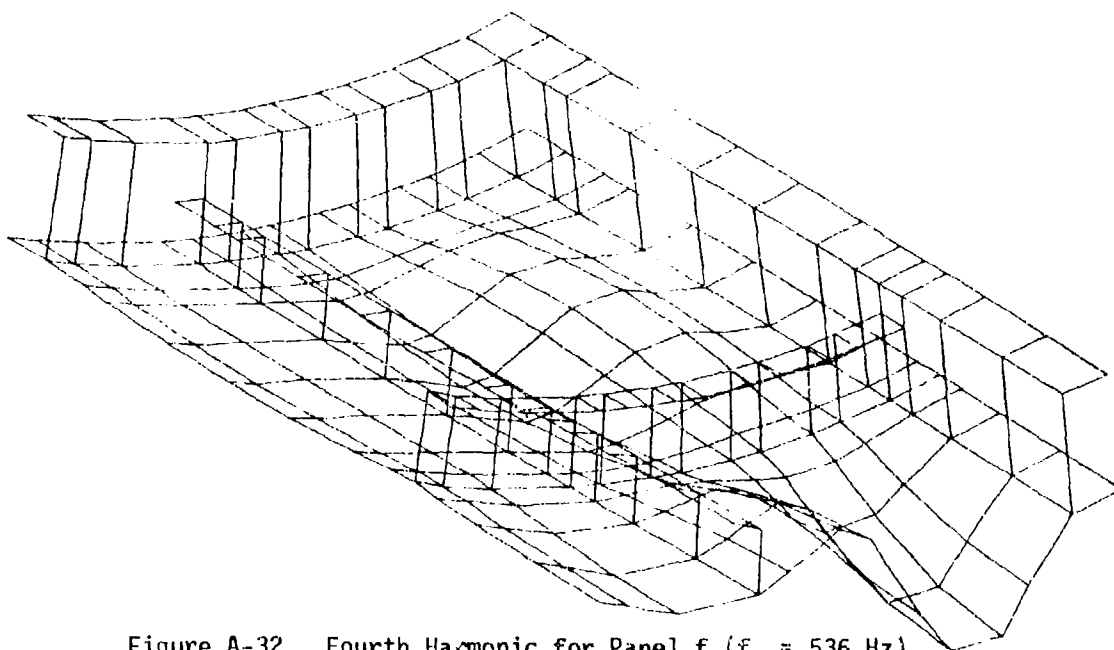
Figure A-32. Fourth Harmonic for Panel f (f_4 = 536 Hz)

A-20

APPENDIX B

ENGINEERING DRAWINGS OF TEST STRUCTURES

Figures B-1 through B-3 are engineering drawings for the sonic fatigue
test panels and the shaker test specimens. The test panel drawings show
strain gauge locations and their corresponding numbers. Hercules 3501
graphite/epoxy system was used for the laminates. Stiffener-skin bonds
utilized the 3M AF147 adhesive.

Figure B-1. Fatigue Test Panels (Sheet 1 of 3)

INSULATE GR/EP FROM ALUM WITH 1 PLY F/GLASS CLOTH

1.25

X

26.50

X

TITANIUM CLIPS
MONEL FASTENERS
(TYP)

X

FRAME
MAKE FROM
AND 10137-2008
ALUMINUM EXTRU.

SECTION A-A
SCALE 1/2

.044 REF
8 PLIES UNIDIRECTIONAL
GR/EP

t SKIN (REF)

.50

.75

t STIFFENER
(SEE TABLE)

.75

.110

SECTION C-C
SCALE 1/1

(STRINGER)

PANEL	NUMBER OF BAYS	STRINGER SPACING X	t SKIN *			t STIFFENER †		
			PLIES	ORIENTATION	t REF	PLIES	ORIENTATION	t REF
a	3x3	8	6	$(0,\pm45)_s$	.033	3	$(\pm45)_{REF}$	.039
b	3x3	8	8	$(0,\pm45,90)_s$	.044	4	↕	.052
c	3x3	8	8	$(0_2,\pm45)_s$	.044	4		.052
d	3x3	8	12	$(0,\pm45)_{2s}$	.066	6		.078
i	6x3	4	8	$(0,\pm45,90)_s$	.044	4	↕	.052
k	4x3	6	8	$(0,\pm45,90)_s$	.044	4	$(\pm45)_{REF}$	.052

* GR/EP TAPE
† GR/EP FABRIC (HERCULES 2501)

n	3x3	8	4	$(0,90)_s$	.022	3	$(\pm45)_{REF}$	.039
q	6x3	4	4	$(0,90)_s$	.022	3	$(\pm45)_{REF}$	.039

Figure B-1. Fatigue Test Panels (Sheet 1 of 3) - Continued

B-3

Figure B-1. Fatigue Test Panels (Sheet 2 of 3)

F/GLASS
CLOTH
(TYP)

1.25
TYP

8.00

8.00

26.50

FRAME
MAKE FROM
AND. 10137-2008
ALUM. EXTRUSION

SECTION A-A
SCALE 1/2

CAP (.066 REF)
12 PLIES UNIDIRECTIONAL
GR/EP

.044 (REF)

1.00

1.00

HFT-1/8-5.5
CORE

SECTION C-C
SCALE 1/1

TEST PANEL					
PANEL	NUMBER OF BAYS	STRINGER SPACING (REF)	t SKIN *		
			PLIES	ORIENTATION	t REF
e	3×3	8	8	$(0, \pm45, 90)_S$	.044

* GR/EP TAPE

" FABRIC (HERCULES)
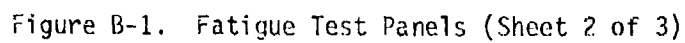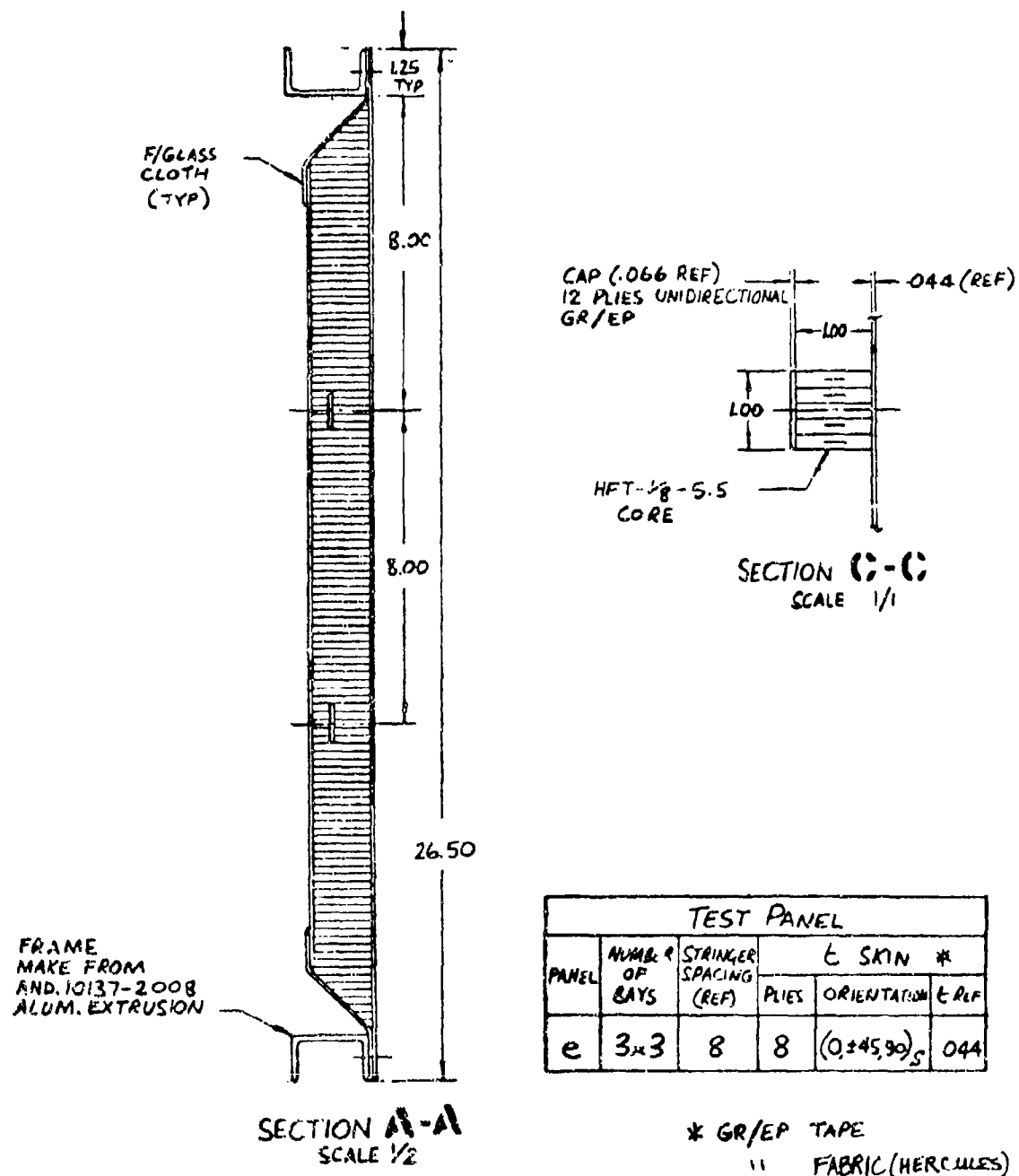
Figure B-1. Fatigue Test Panels (Sheet 2 of 3) - Continued

Figure B-1. Fatigue Test Panels (Sheet 3 of 3)

SECTION C-C
SCALE 1/1

(STRINGER)

SECTION A-A
SCALE 1/2

TEST PANELS									
PANEL	NUMBER OF BAYS	STRINGER SPACING X	t SKIN *			t STIFFENER †			RADIUS OF CURVATURE R
			PLIES	ORIENTATION	t REF	PLIES	ORIENTATION	t REF	
f	3x3	8	8	(0,±45,90)s	.044	4	(±45) REF	.052	30
g	3x3	8							60
h	3x3	8							90
j	6x3	4	8	(0,±45,90)s	.044	4	(±45) REF	.052	90
l	4x3	6	12	(0,±45)2.5	.066	6	(±45) REF	.078	90
P	3x3	8	4	(0,90)s	.022	3	(±45)REF	.039	90
r	6x3	4	6	(0±45)s	.033	3	(±45)REF	.039	60
s	4x3	6	4	(0,90)s	.022	3	(±45)REF	.039	30

* GR/EP TAPE
† GR/EP FABRIC (HERCULES 3501)

Figure B-1. Fatigue Test Panels (Sheet 3 of 3) - Concluded

Figure B-2. Existing Rohr Test Panel Configurations
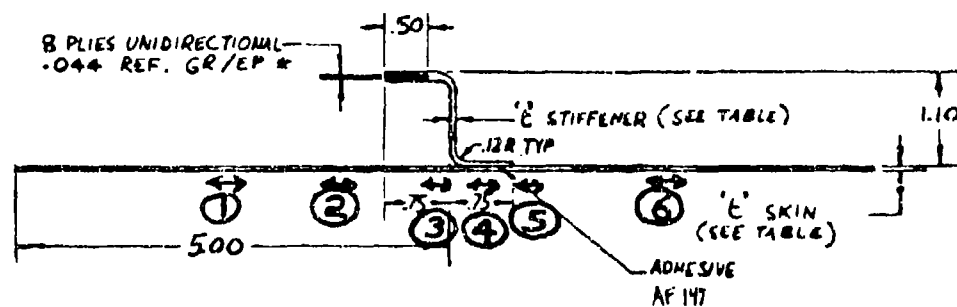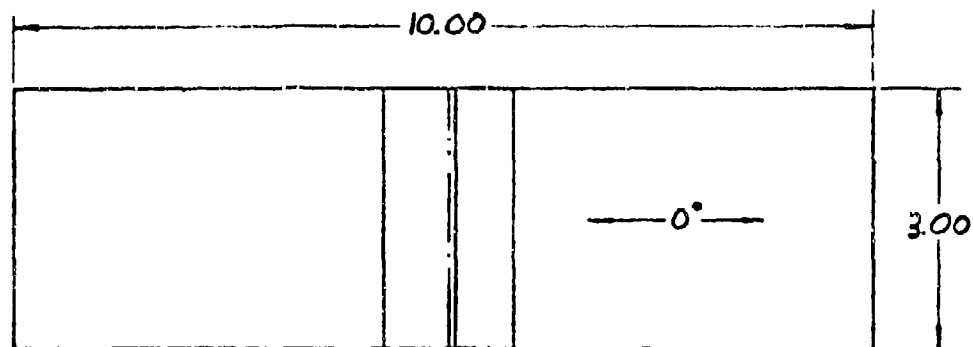
TYPE A

STRAIN GAUGE NUMBERS & LOCATIONS

Figure B-3. Shaker Test Specimens (Sheet 1 of 3)
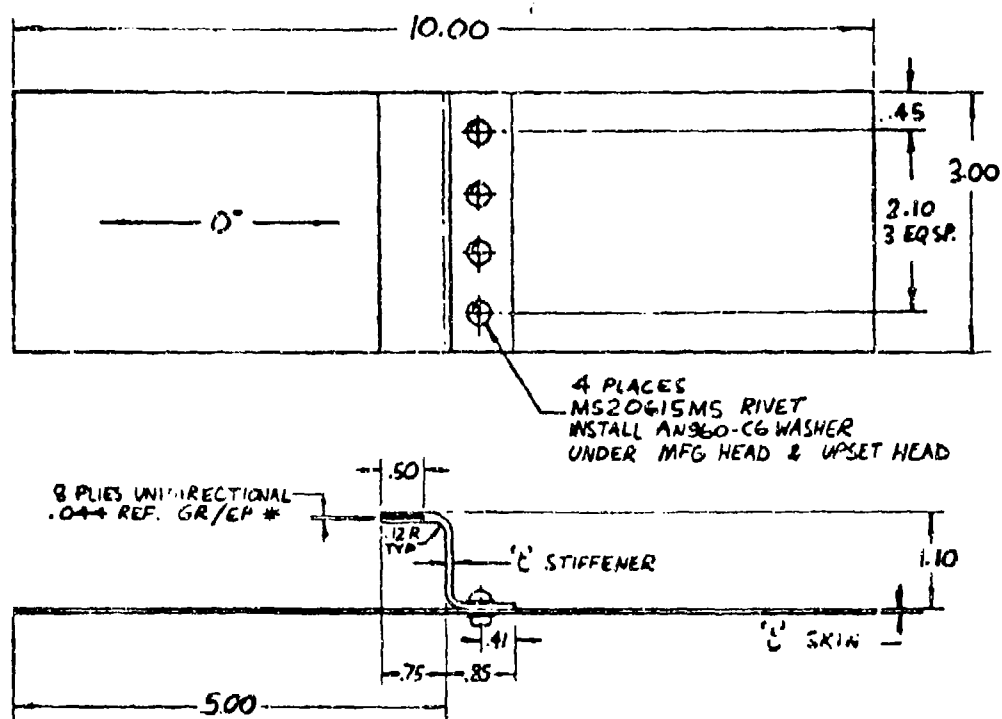
TYPE B

			'T' SKIN		*	'C' STIFFENER †		
SPECIMEN	SPECIMEN TYPE	NUMBER SPECIMENS	PLIES	ORIENTATION	t REF	PLIES	ORIENTATION	t REF
1	A	15	6	$(0, \pm45)_s$	.033	3	$(\pm45)_{RF}$	.039
2	A	15	8	$(0,\pm45,90)_s$	.044	4	$(\pm45)_{RF}$	.052
3	A	10	8	$(0_2, \pm45)_s$	.044	4	$(\pm45)_{REF}$	.052
4	A	15	12	$(0, \pm45)_{2s}$	.066	6	$(\pm45)_{RF}$	.078
5	C	10	8	$(0,\pm45,90)_s$	.044	NOT APPLICABLE		
6	B	6	8	$(0,\pm45,90)_s$	.044	4	$(\pm45)_{RF}$	.052
			* GR/EP TAPE — 3501 AS					
			† GR/EP FABRIC—					
7	A	10	4	$(0,90)_s$	.022	SAME AS 1		

SHAKER SPECIMENS

Figure B-3.   Shaker Test Specimens (Sheet 2 of 3)

TYPE C
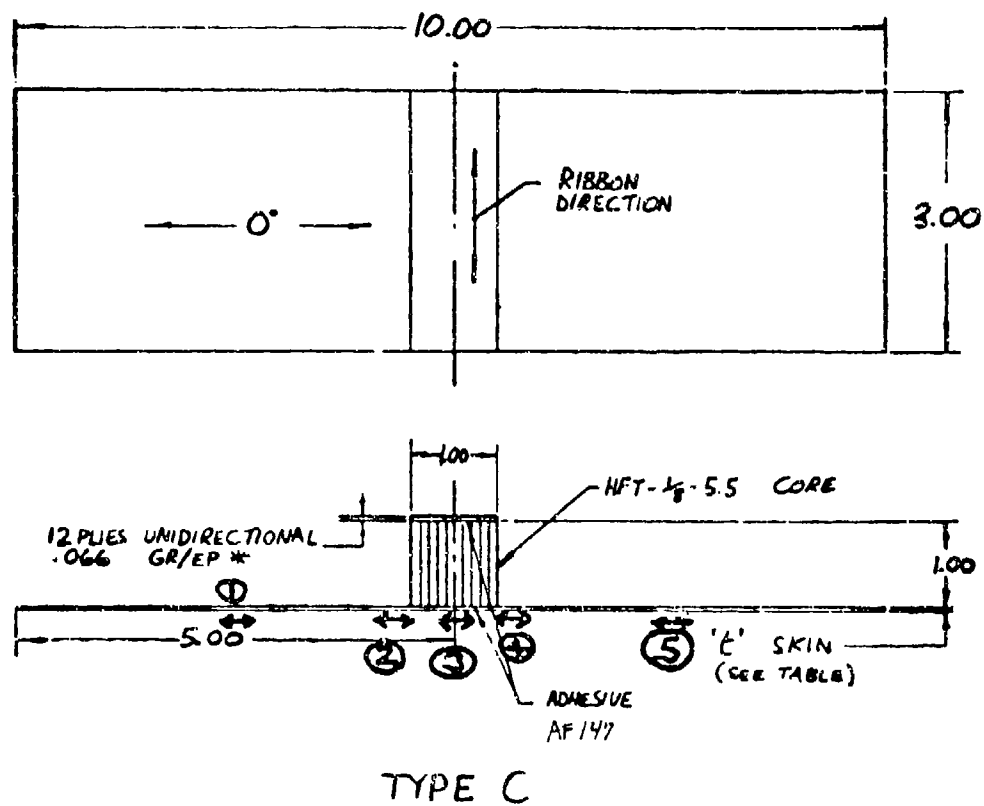
Figure B-3. Shaker Test Specimens (Sheet 3 of 3)

APPENDIX C
TEST DATA USED IN THE DEVELOPMENT OF THE DESIGN METHOD

This section contains acoustic and strain spectra and associated overall rms levels that are pertinent to the development of the design method. Figures C-1 through C-7 show microphone spectra for a sine sweep and for each test acoustic load level. Figures C-8 through C-101 show strain spectra and their corresponding overall rms strain levels for strain gauge number 10 (located at the center of, and normal to, the longest side of the center bay -- see Figure B-1). Spectra are shown for sine sweeps and broadband random acoustic loading from 140 dB up to (in most cases) 165 dB in 5 dB increments for the following panel configurations: a1, b2, d, f2, g2, h, i, j, k1, l, n, o, p, q, r and s.

All spectra have an effective filter bandwidth of 2·16 Hz with an aliasing filter cutoff of 960 Hz. Twenty-second samples were used for all spectral analysis.
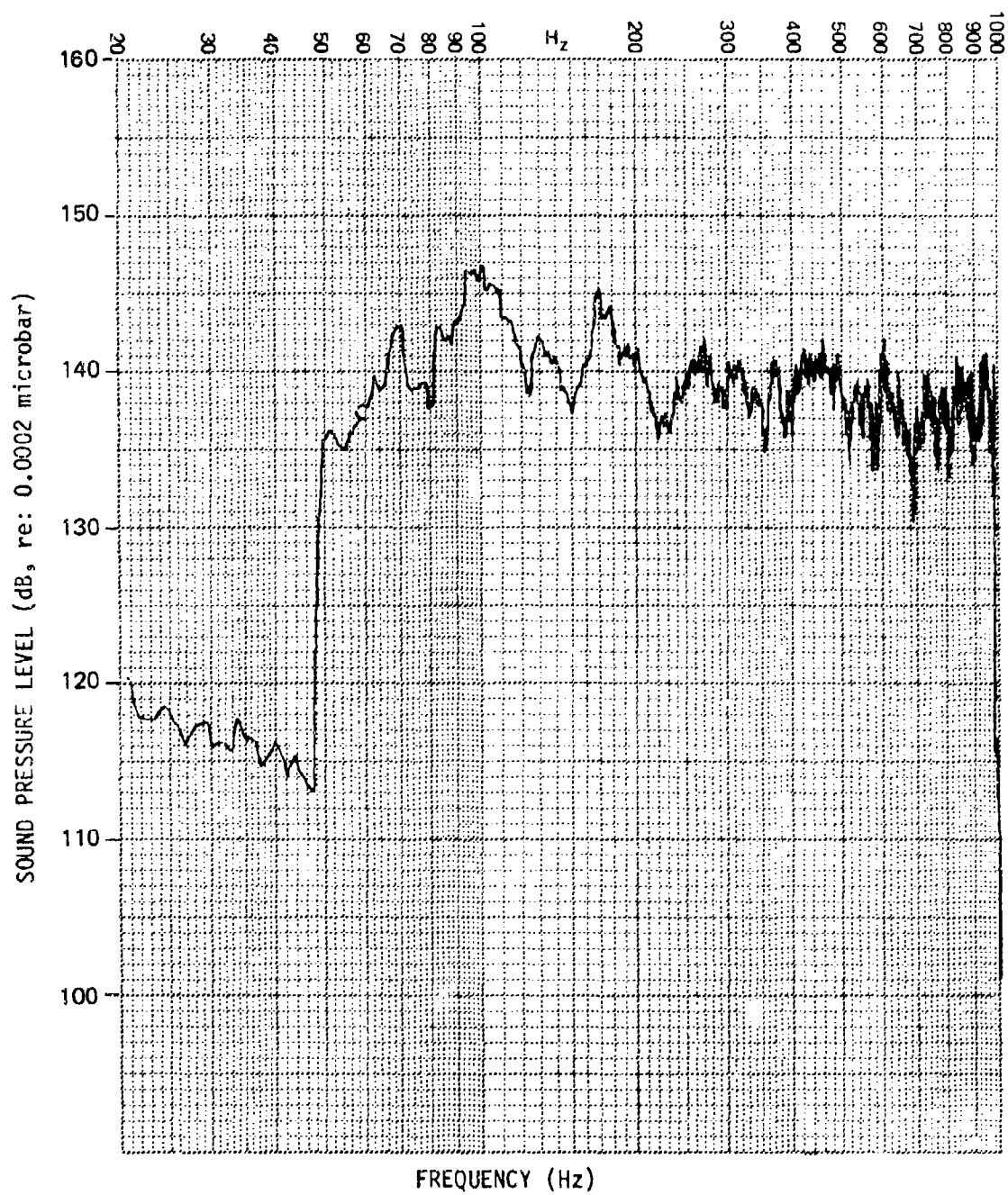
Figure C-1. Microphone Spectrum - Sine

C-2
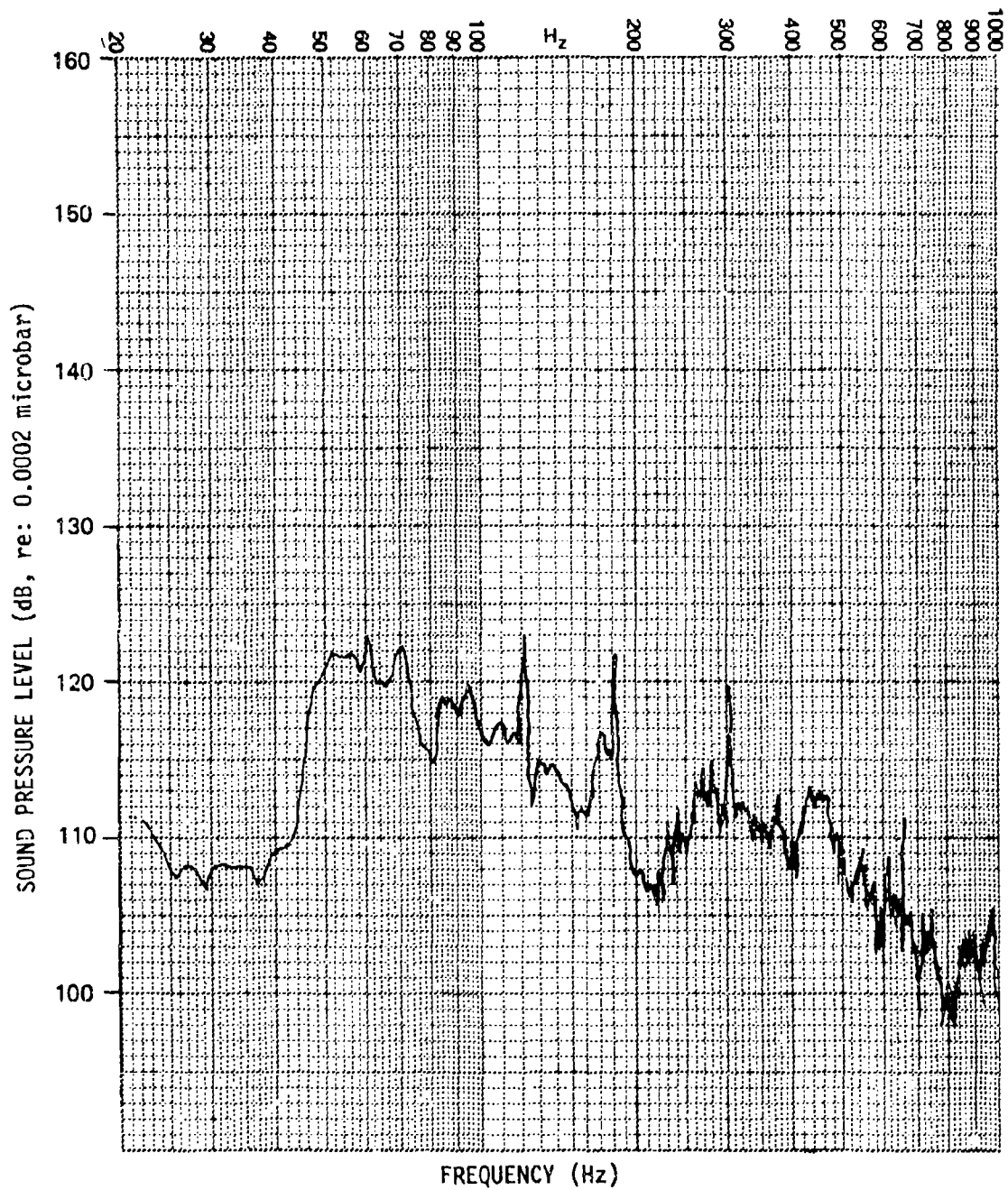
Figure C-2. Microphone Spectrum - 140 dB Random
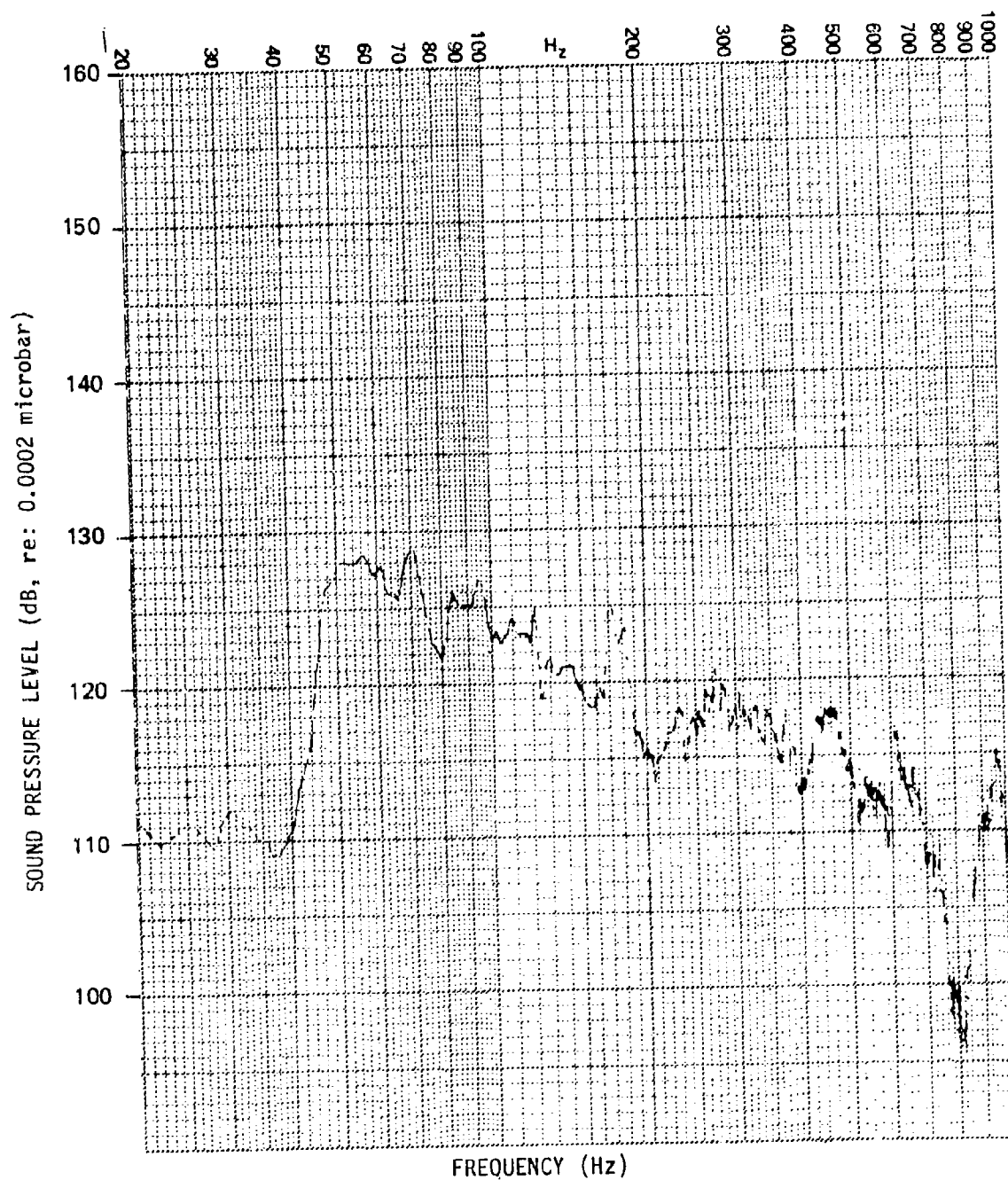
Figure C-3. Microphone Spectrum - 145 dB Random

C-4
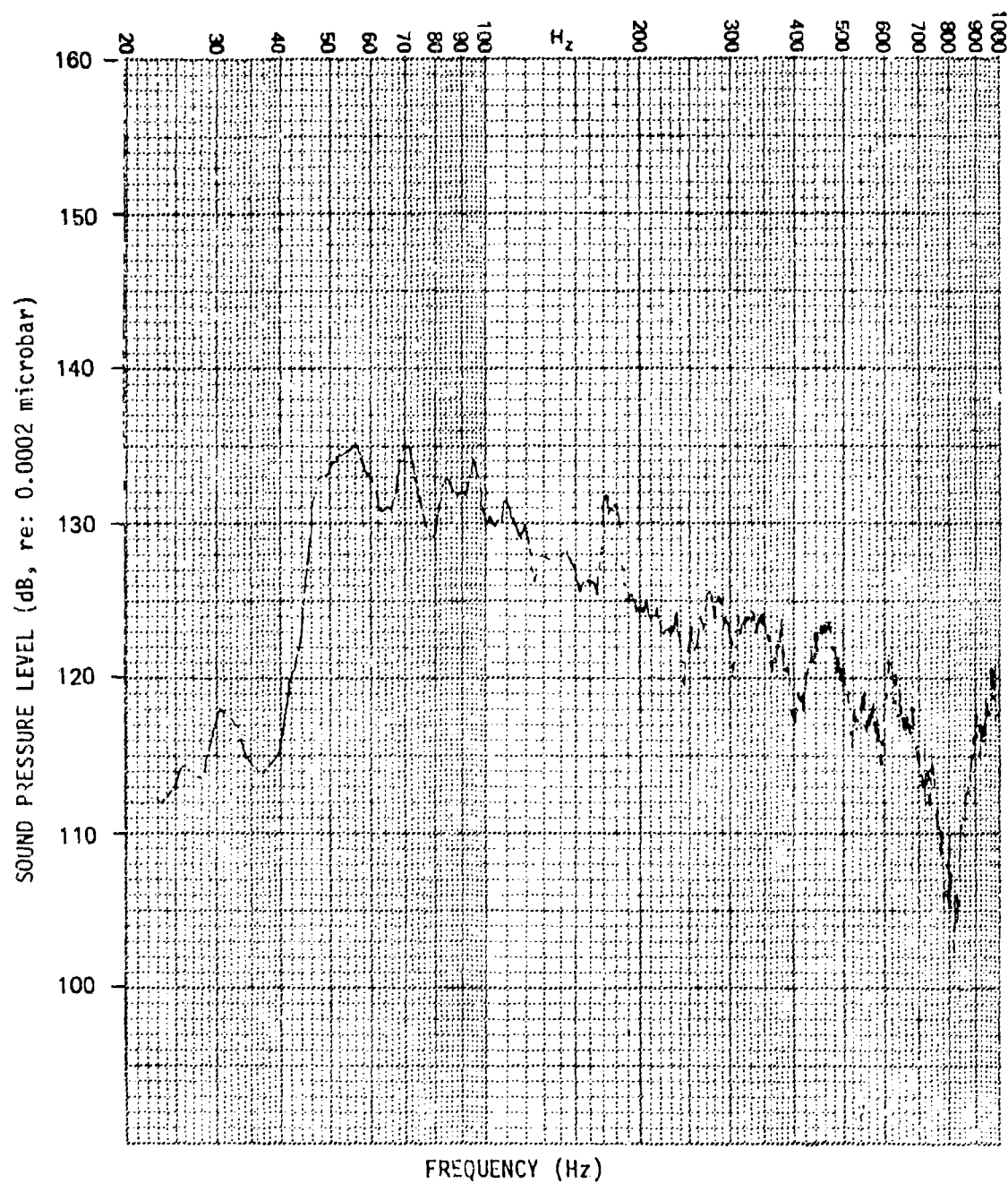
Figure C-4.   Microphone Spectrum - 150 dB Random

C-5
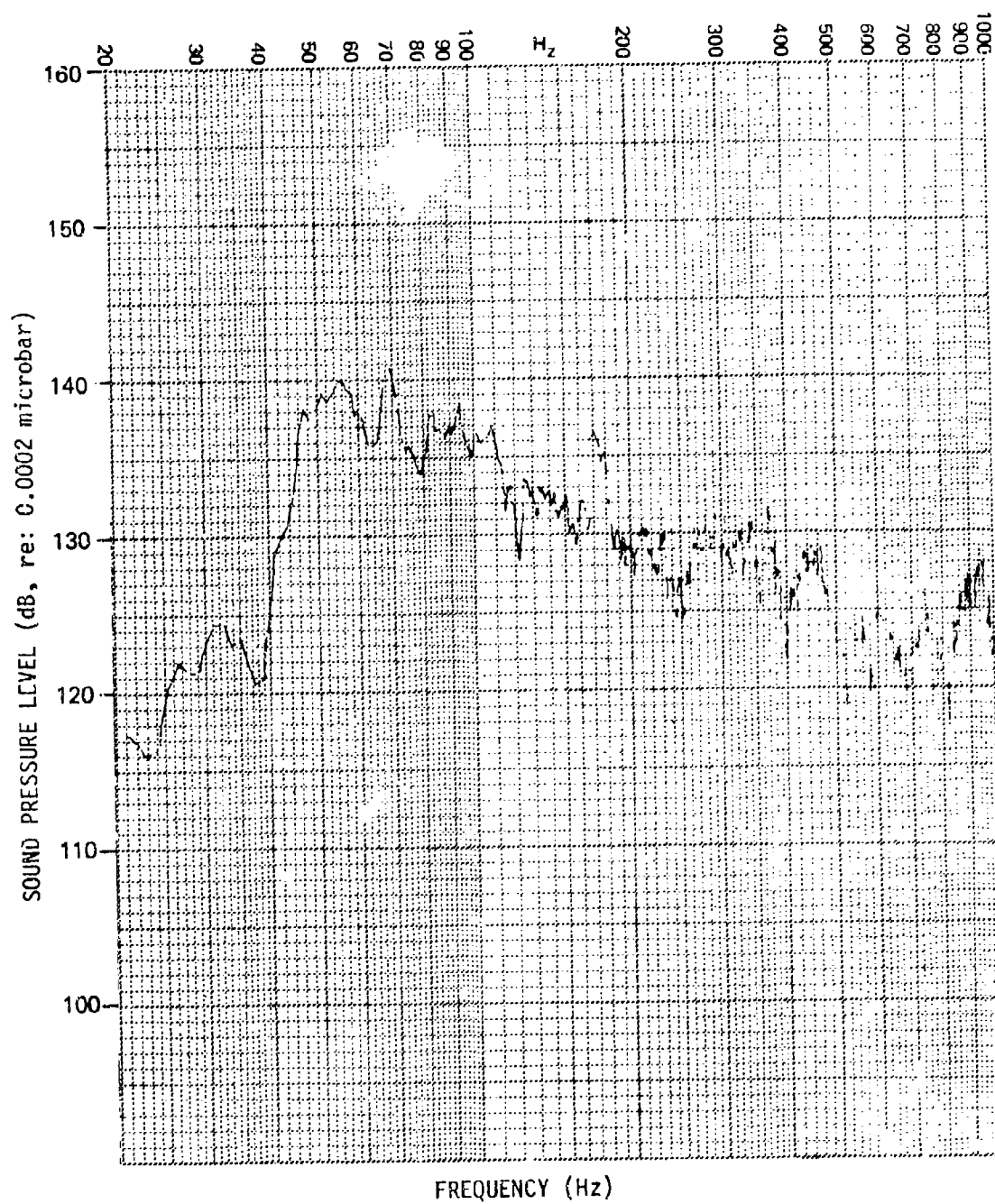
Figure C-5.   Microphone Spectrum - 155 dB Random

C-6
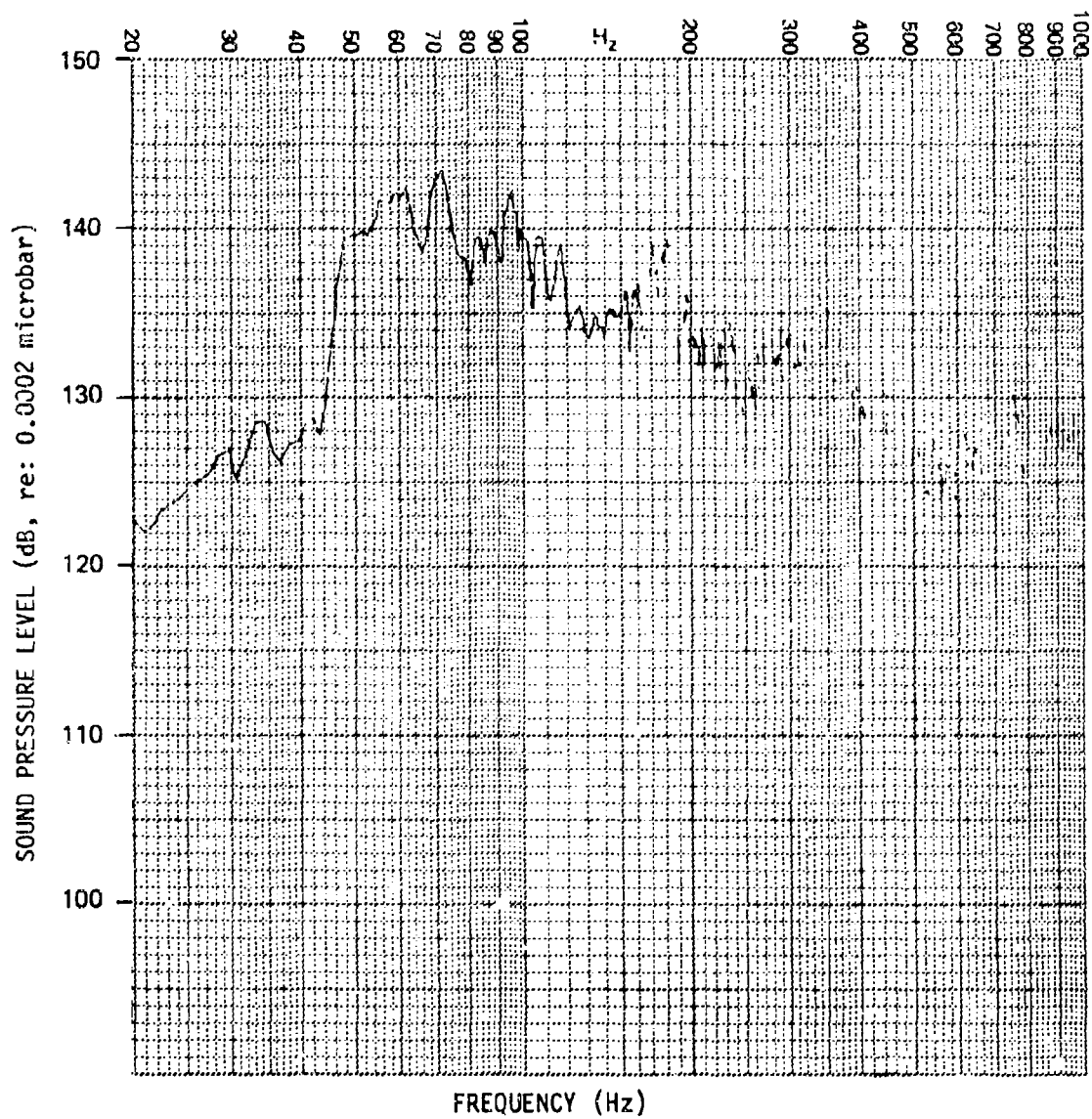
Figure C-6. Microphone Spectrum - 160 dB Random
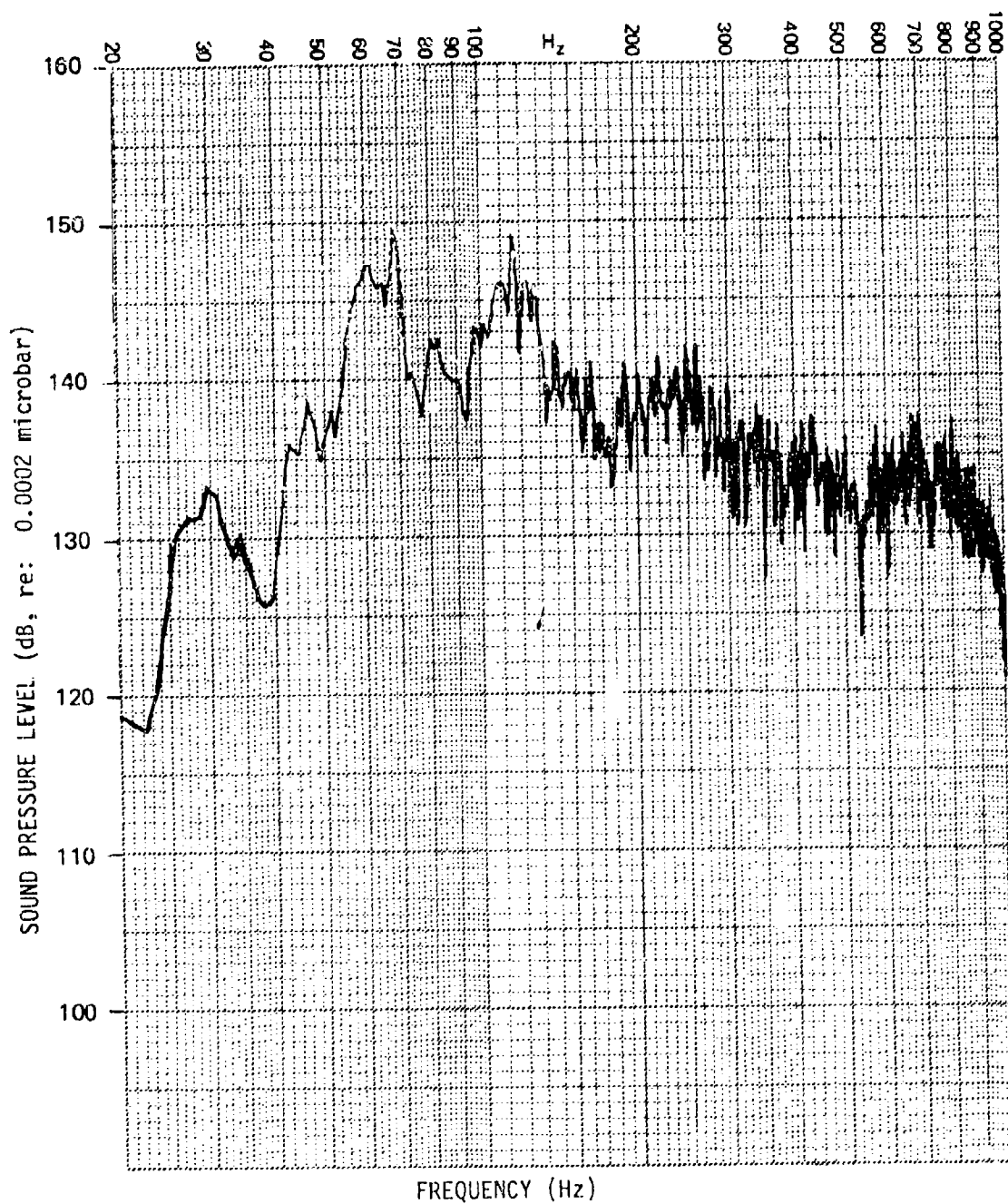
Figure C-7.   Microphone Spectrum - 165 dB Random

C-8

PANEL CONFIGURATION: a1
TRANSDUCER: G10
OVERALL R.M.S. LEVEL:
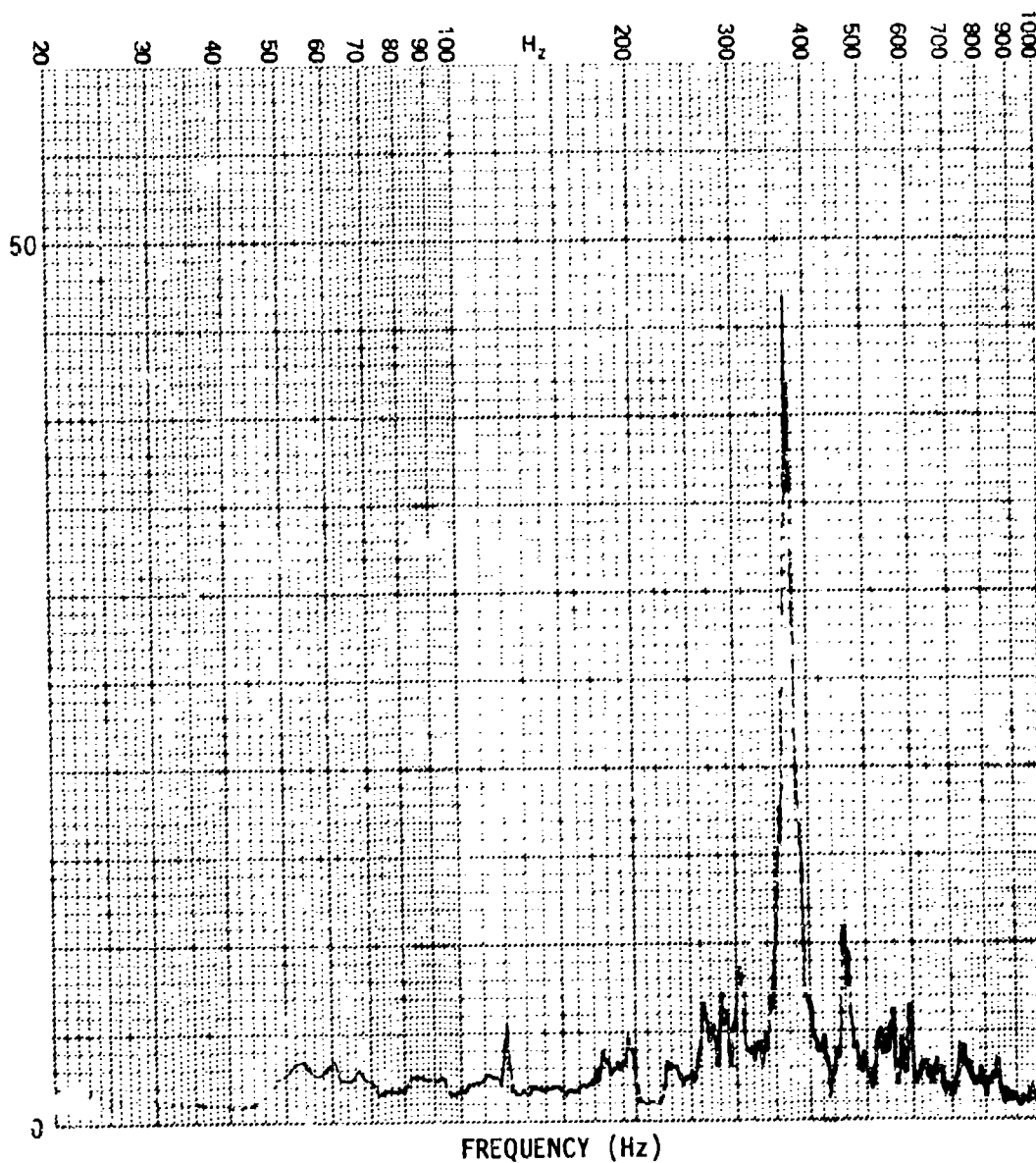INPUT SPECTRUM: SINE
INPUT LEVEL: 130 dB
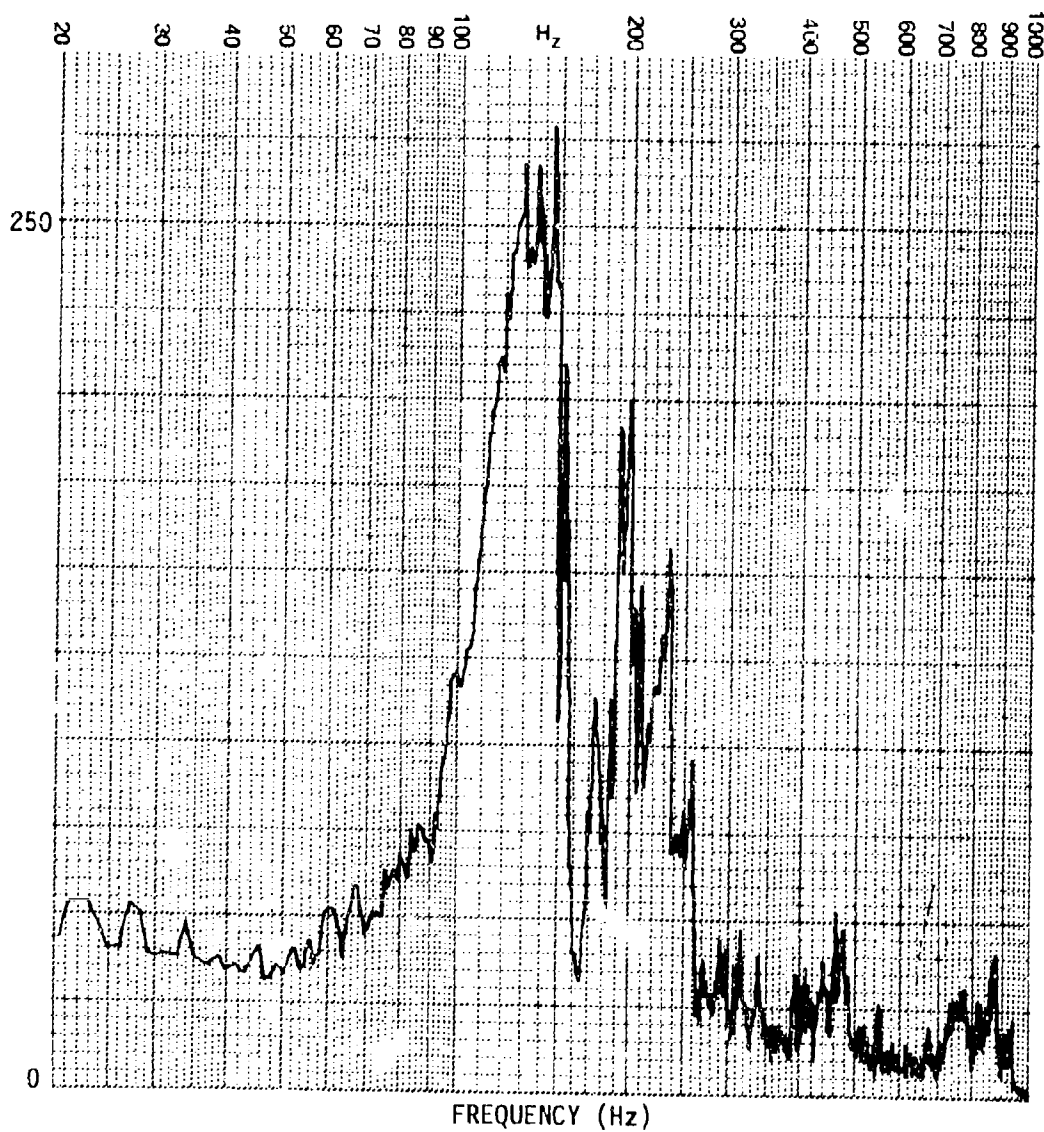
Figure C-8.   Strain Spectrum for Panel a1

C-9

PANEL CONFIGURATION: a1
TRANSDUCER: G10
OVERALL R.M.S. LEVEL: 101.7µe
INPUT SPECTRUM: RANDOM
INPUT LEVEL: 140 dB
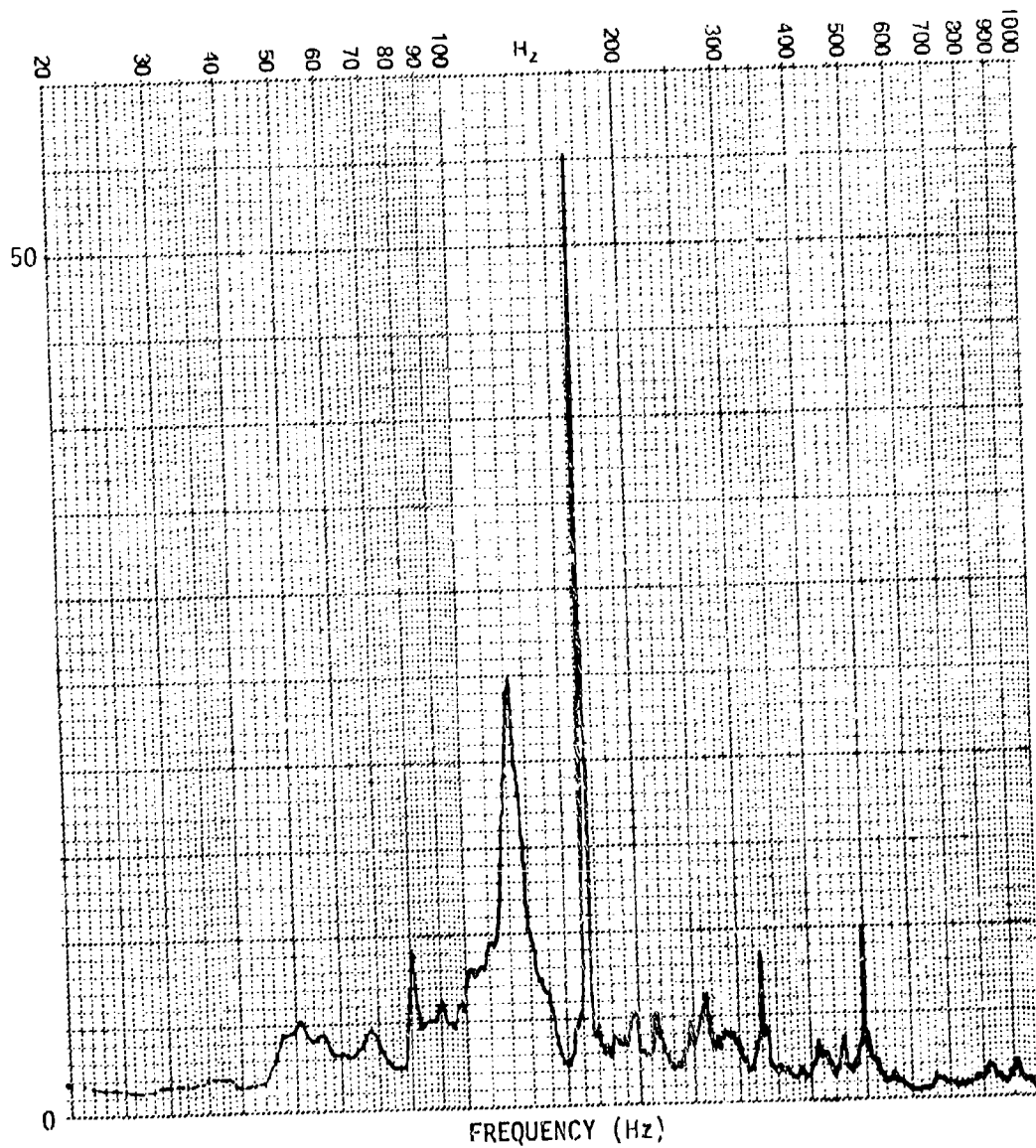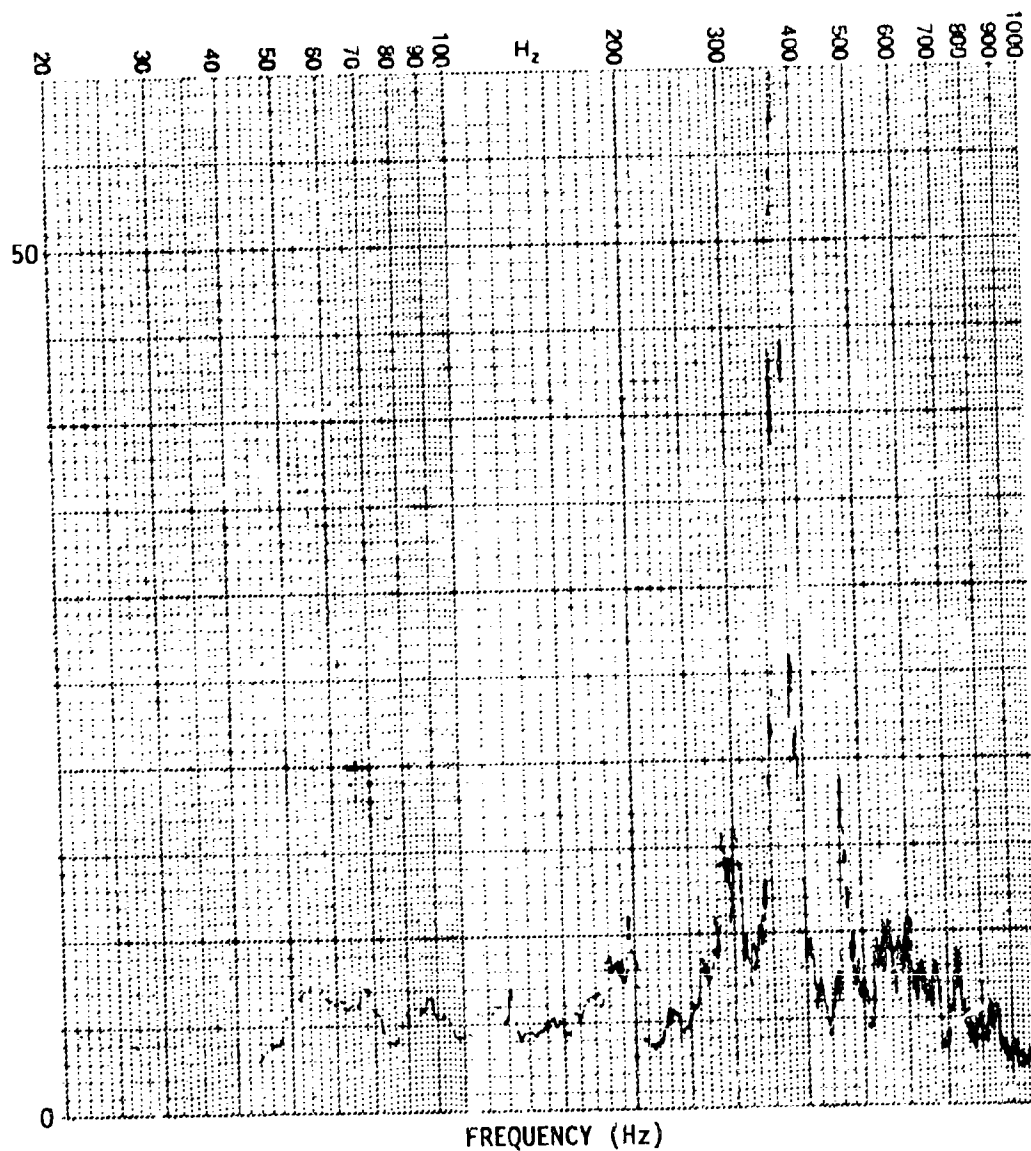

Figure C-9. Strain Spectrum for Panel a1

C-10

PANEL CONFIGURATION: a1
TRANSDUCER: G10
OVERALL R.M.S. LEVEL: 161.1μe
INPUT SPECTRUM: RANDOM
INPUT LEVEL: 145 dB
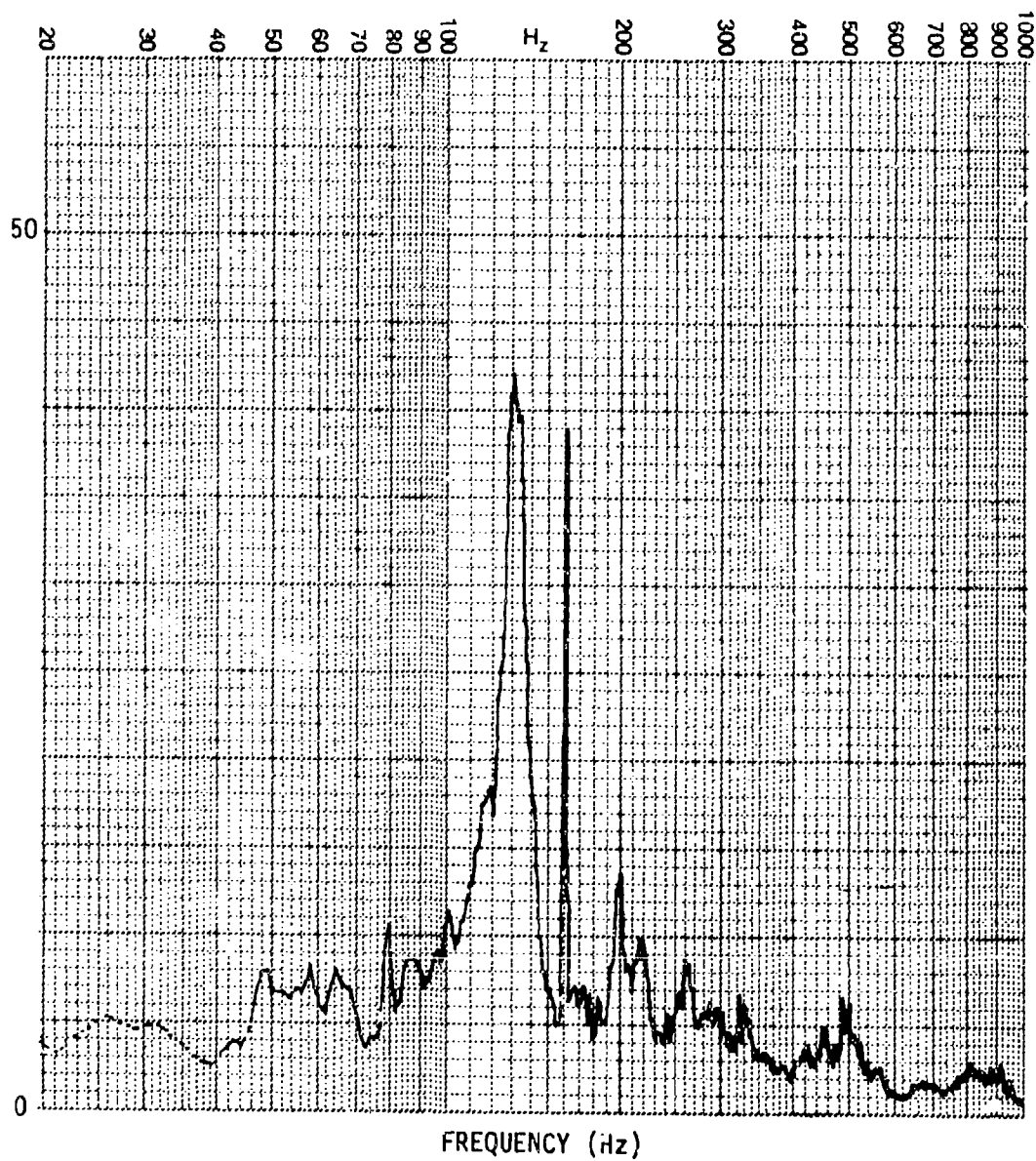
Figure C-10.   Strain Spectrum for Panel a1

C-11

PANEL CONFIGURATION: a1
TRANSDUCER: G10
OVERALL R.M.S. LEVEL: 224.7μe
INPUT SPECTRUM: RANDOM
INPUT LEVEL: 150 dB
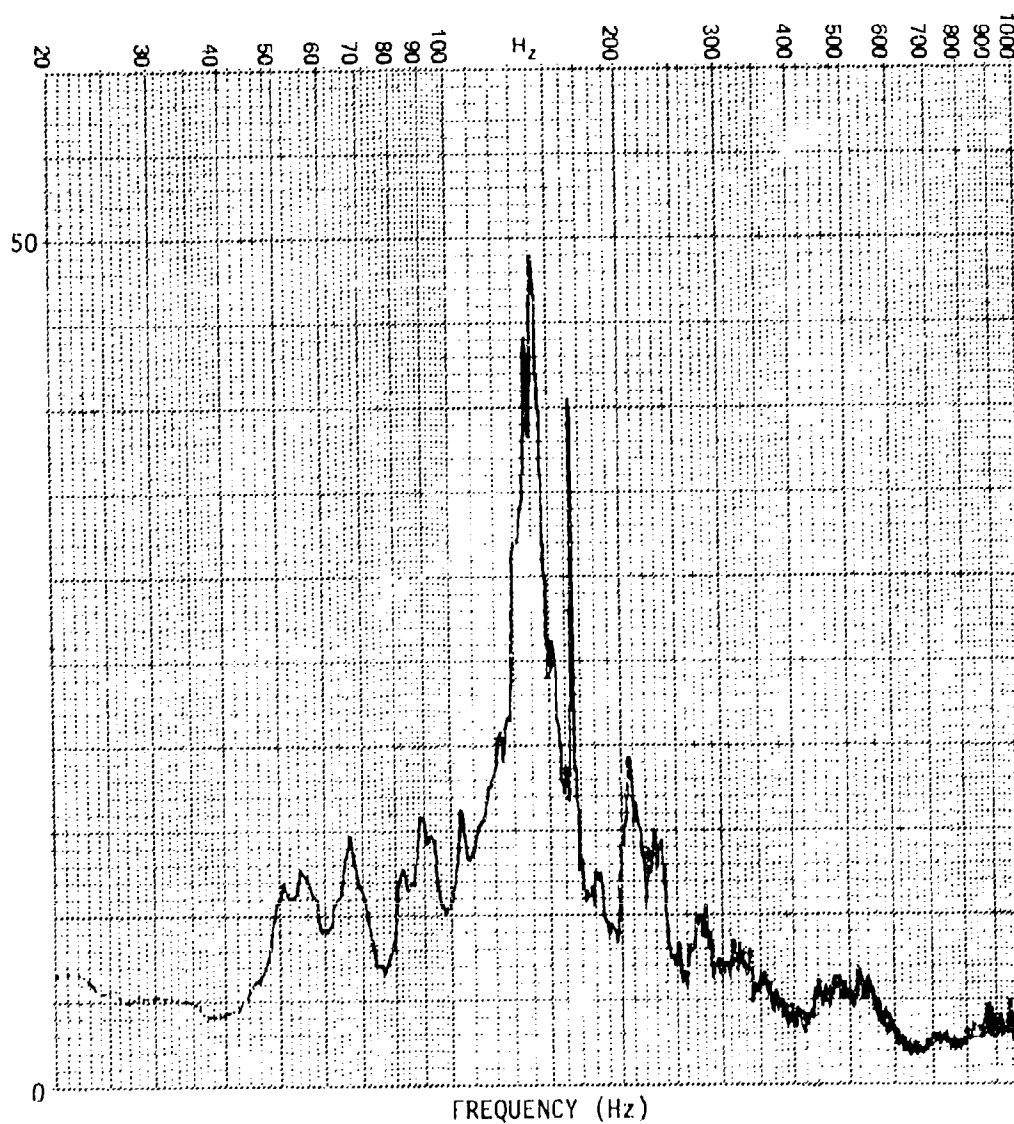
Figure C-11.   Strain Spectrum for Panel a1

C-12

PANEL CONFIGURATION: a1
TRANSDUCER: G10
OVERALL R.M.S. LEVEL: 410.8µe
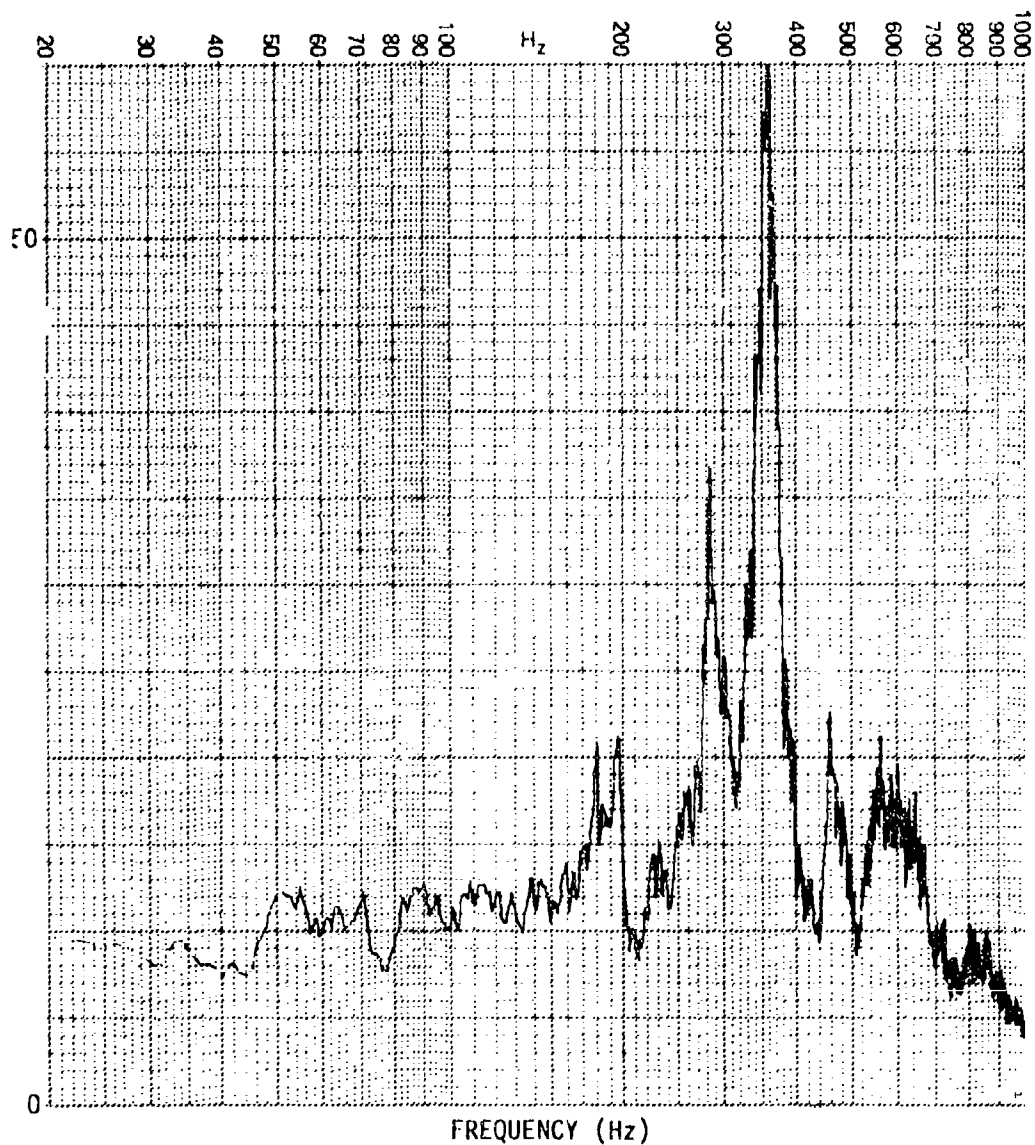INPUT SPECTRUM: RANDOM
INPUT LEVEL: 160 dB

FREQUENCY (Hz)
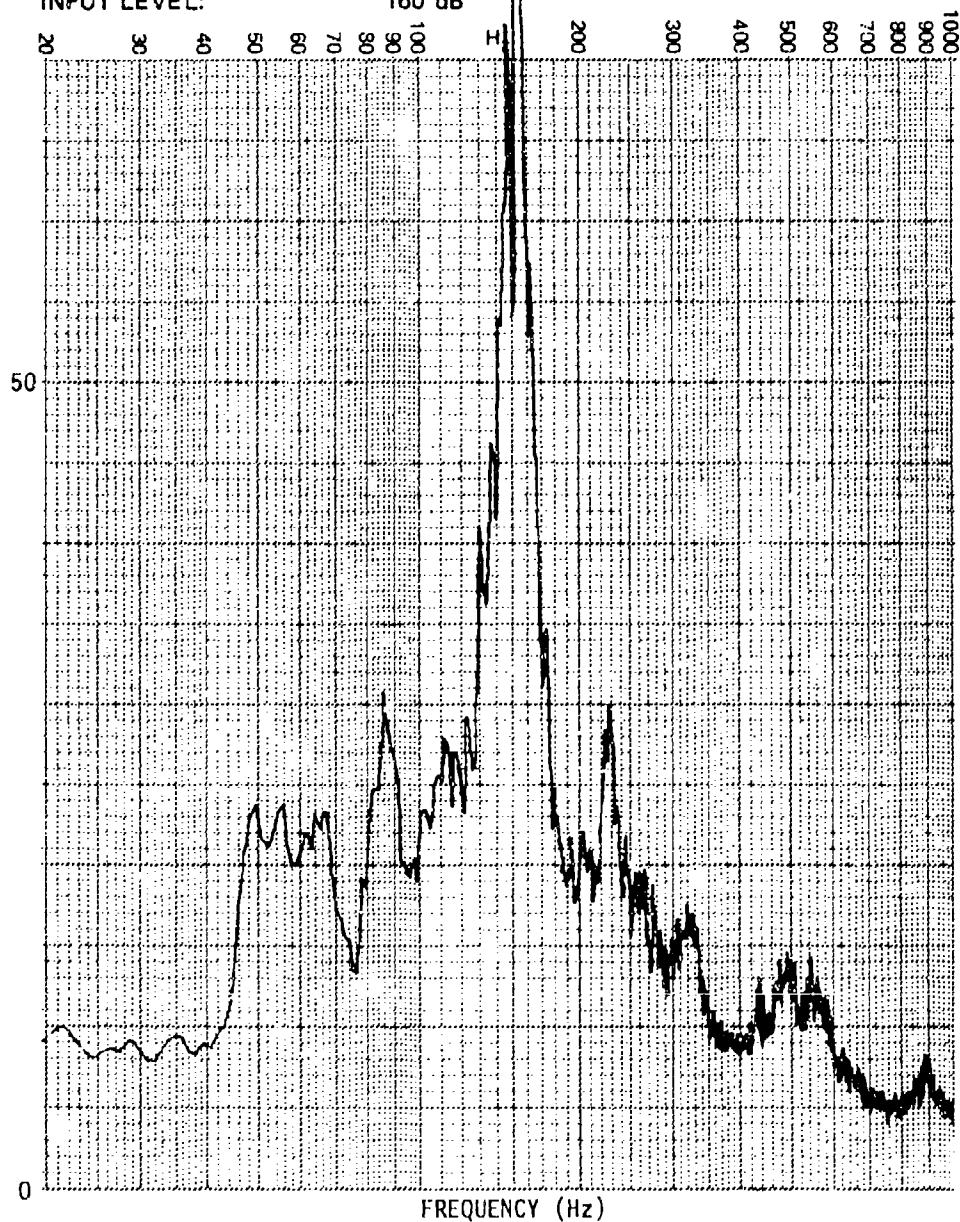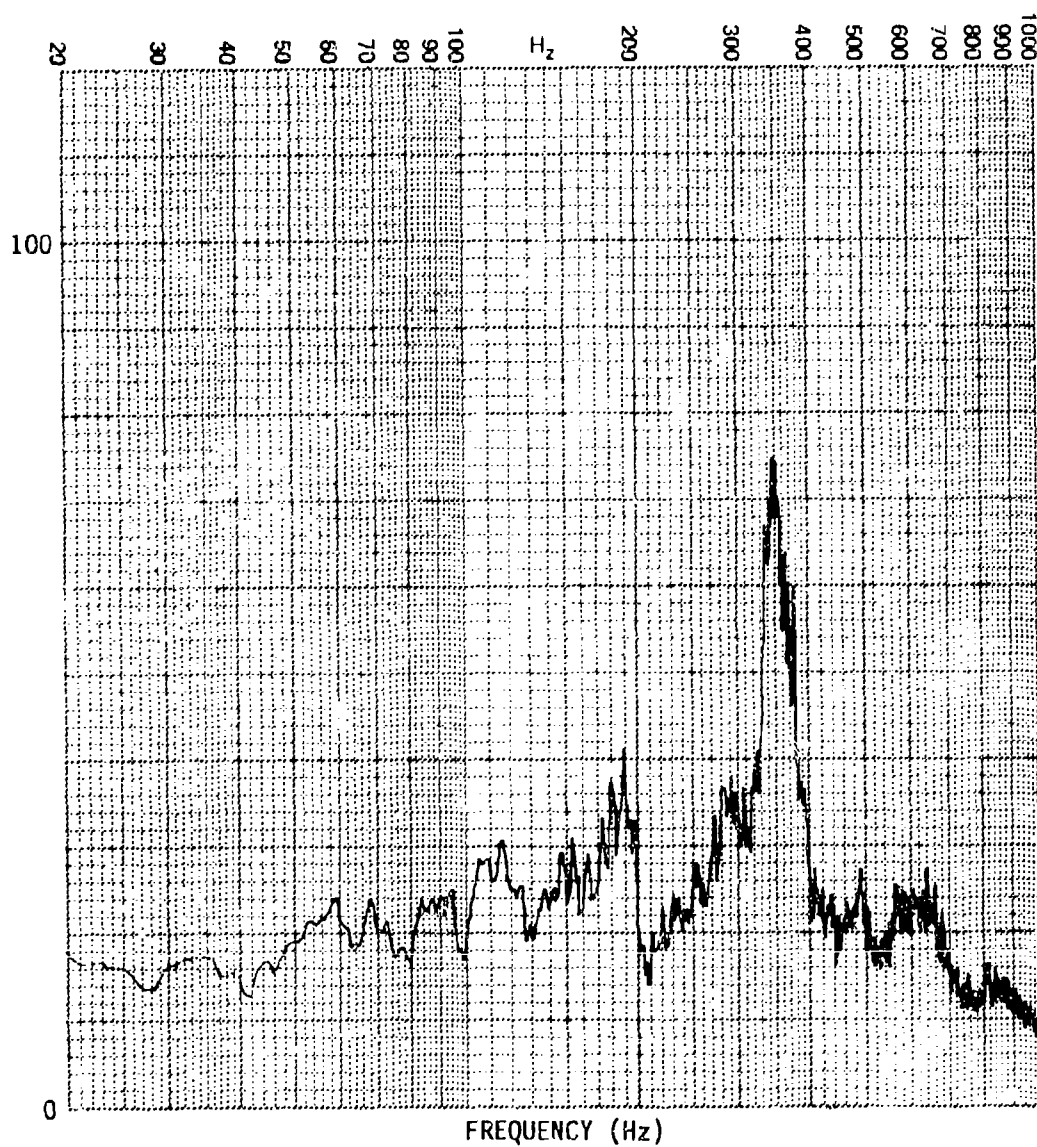
Figure C-12.   Strain Spectrum for Panel a1

C-13

PANEL CONFIGURATION: b2
TRANSDUCER: G10
OVERALL R.M.S. LEVEL:
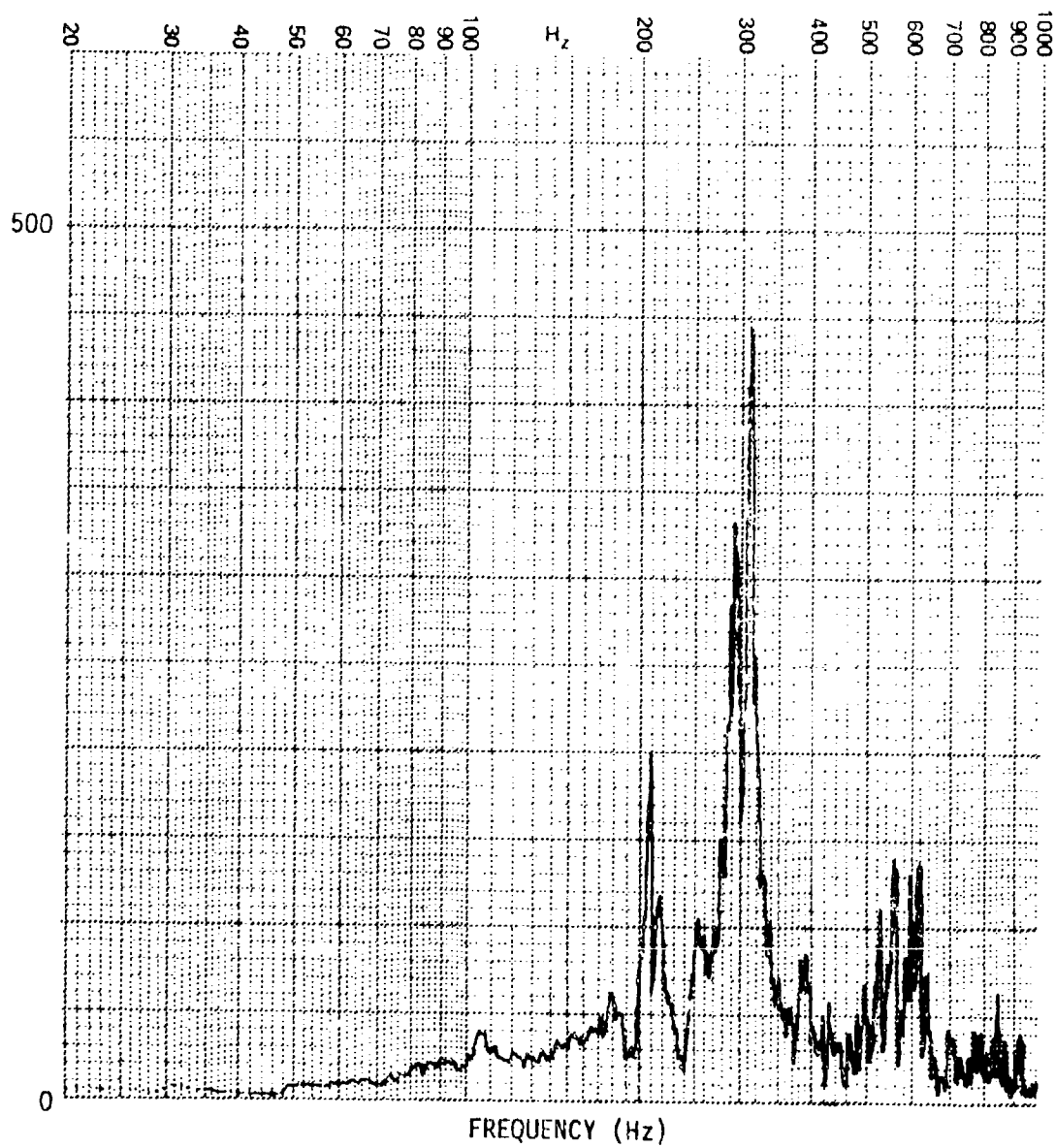INPUT SPECTRUM: SINE
INPUT LEVEL: 130 dB
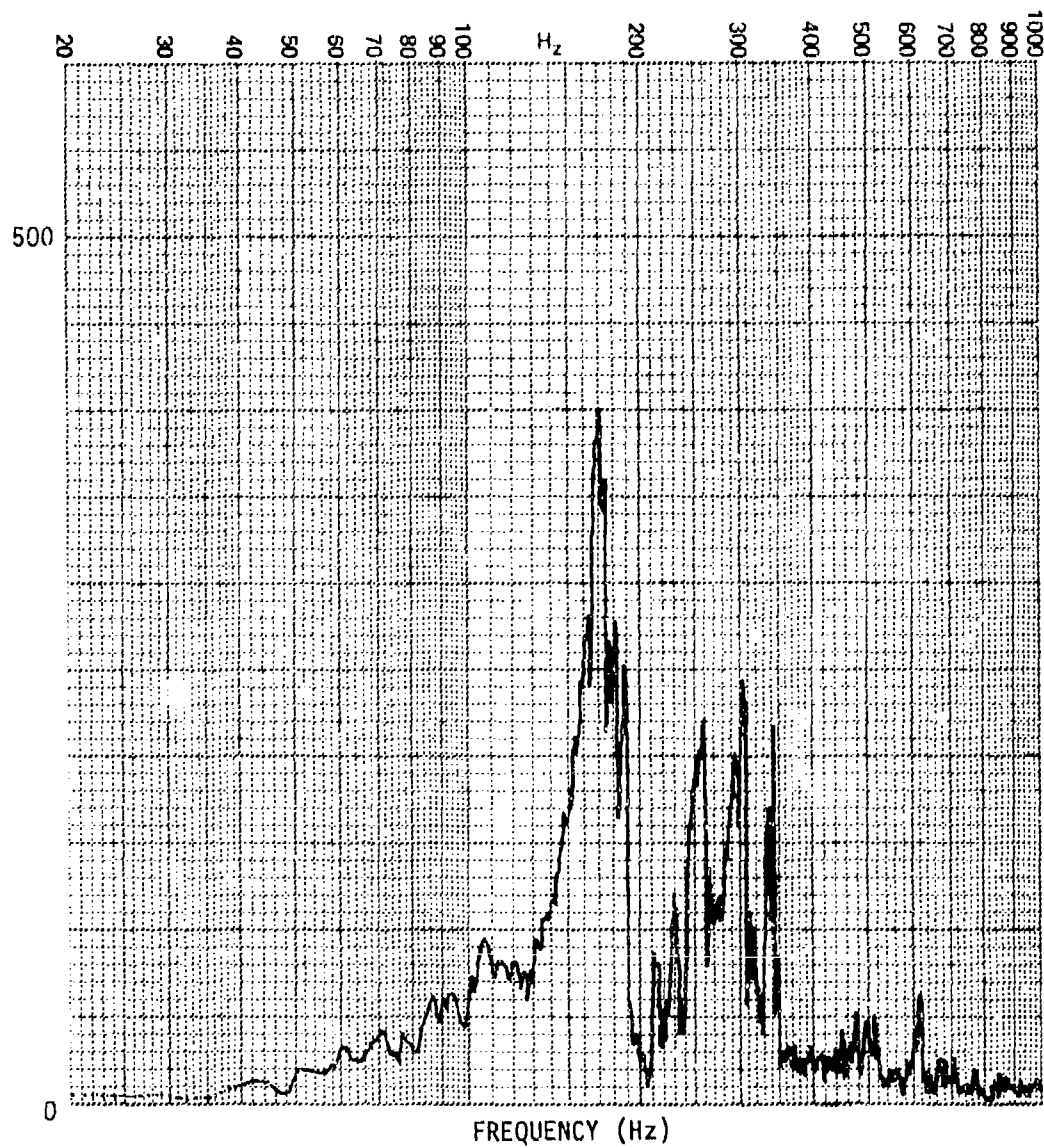
Figure C-13.   Strain Spectrum for Panel b2

C-14

PANEL CONFIGURATION: b2
TRANSDUCER: G10
OVERALL R.M.S. LEVEL: 77.3µe
INPUT SPECTRUM: RANDOM
INPUT LEVEL: 140 dB
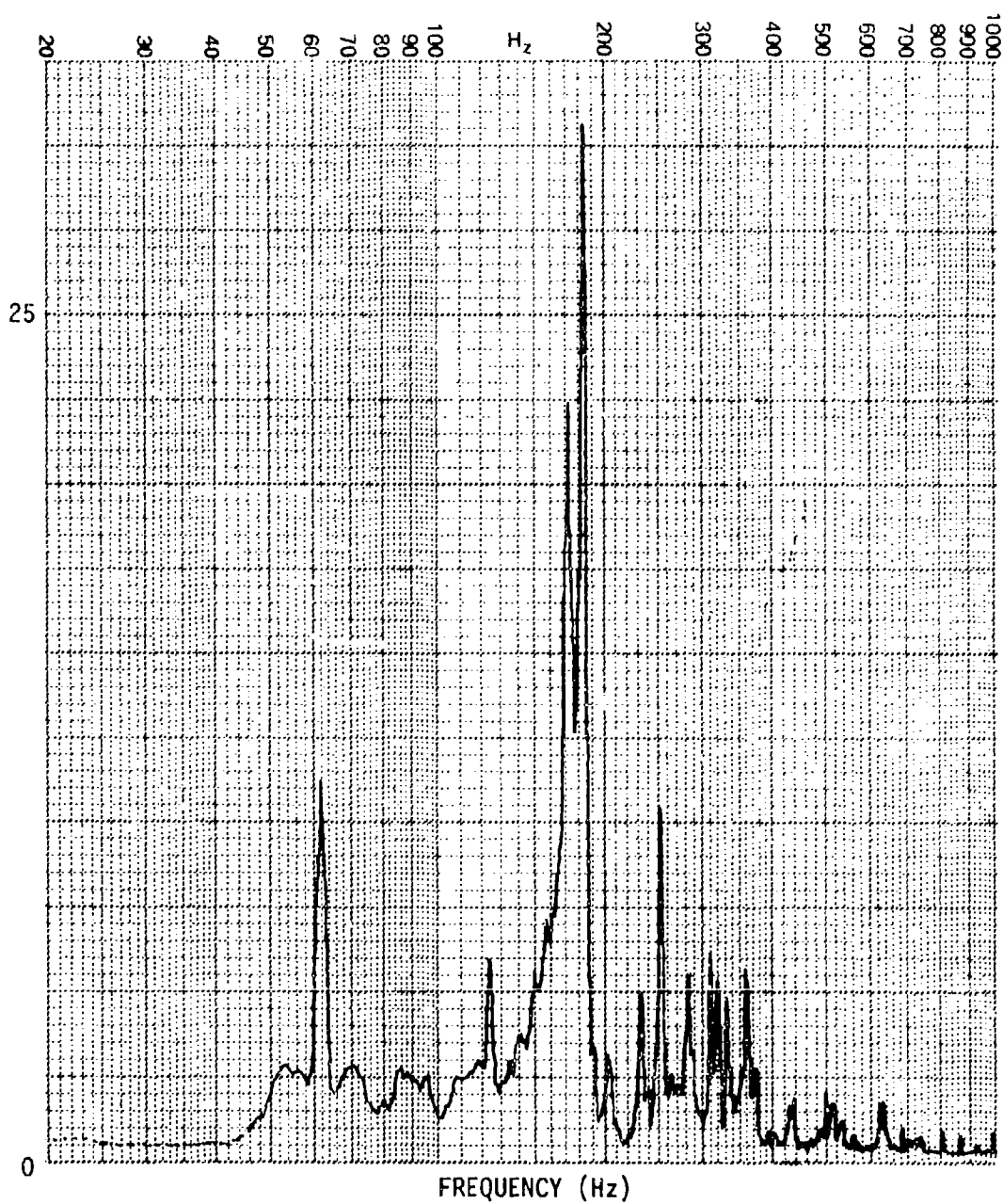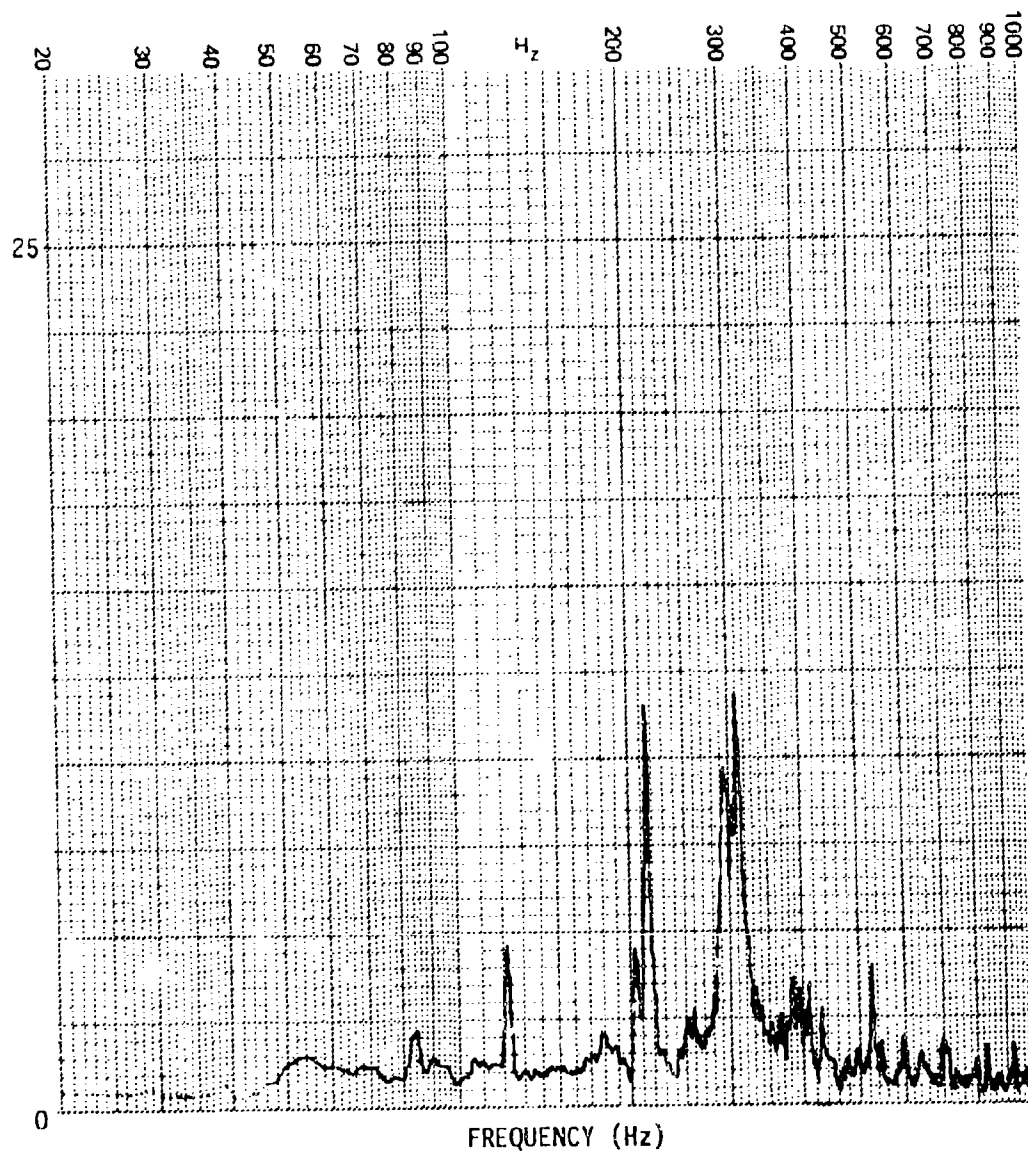

Figure C-14.   Strain Spectrum for Panel b2

C-15

PANEL CONFIGURATION: b2
TRANSDUCER: G10
OVERALL R.M.S. LEVEL: 147.1µε
INPUT SPECTRUM: RANDOM
INPUT LEVEL: 145 dB
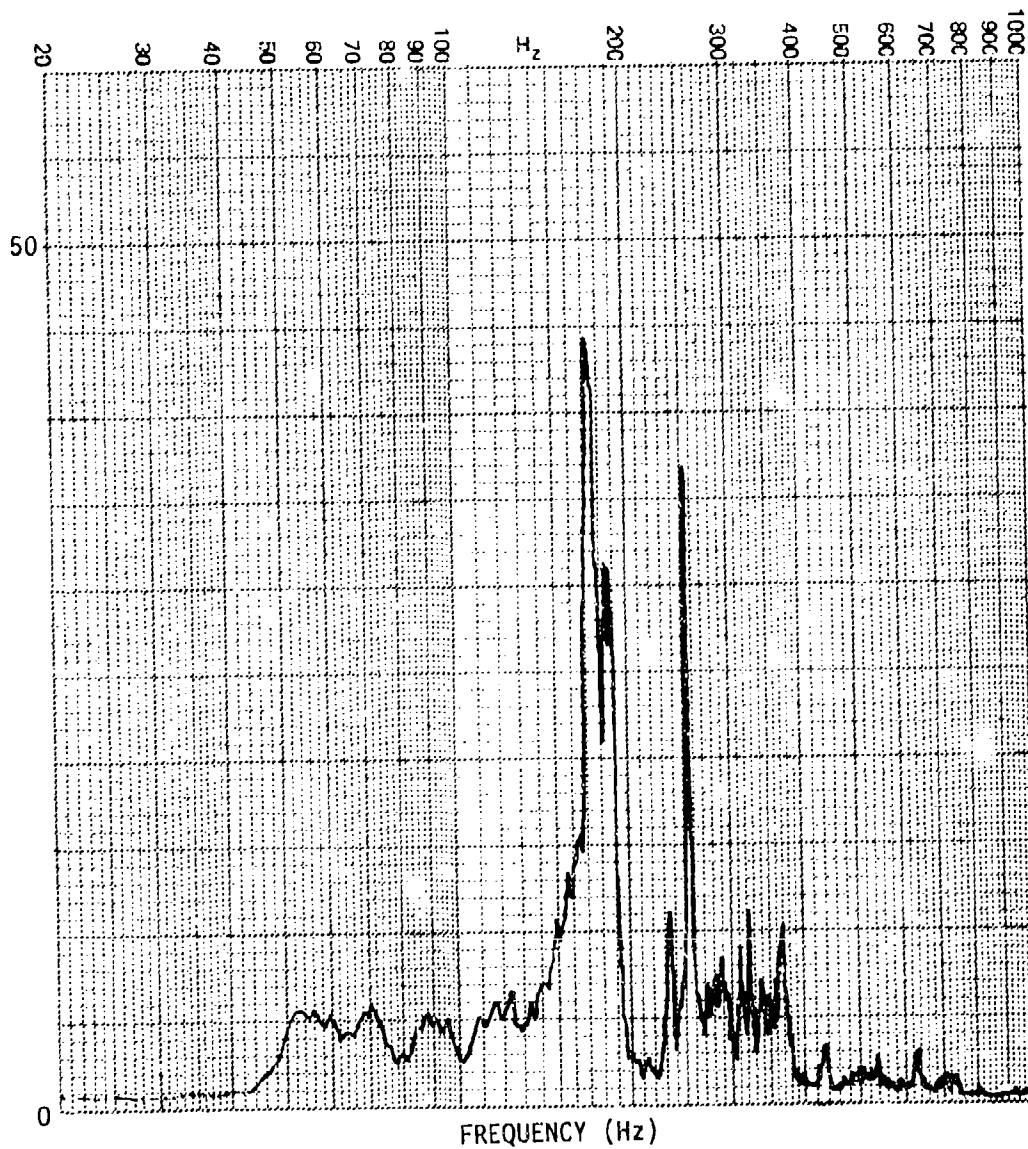
Figure C 15.   Strain Spectrum for Panel b2

C-16

PANEL CONFIGURATION: b2
TRANSDUCER: G10
OVERALL R.M.S. LEVEL: 266.8μe
INPUT SPECTRUM: RANDOM
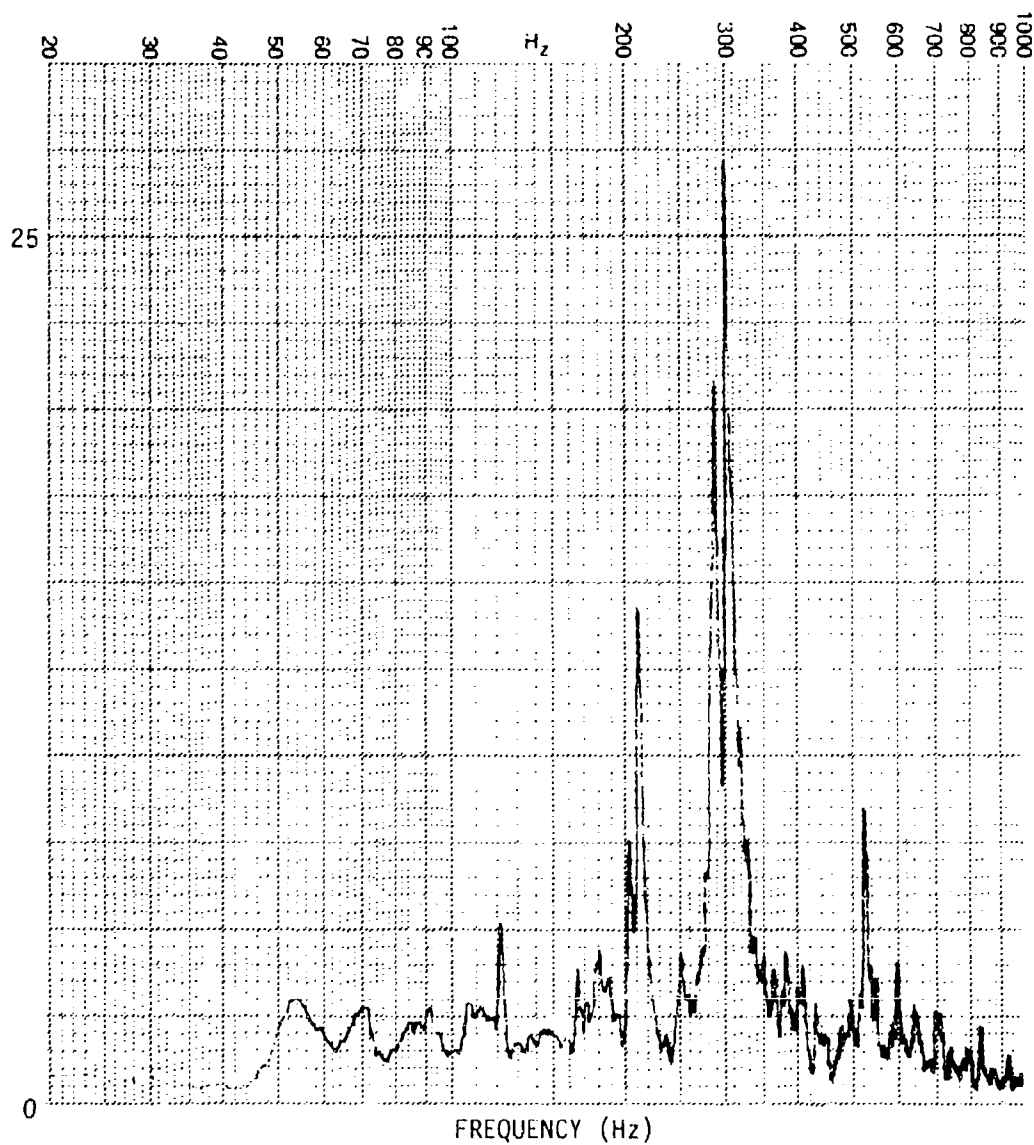INPUT LEVEL: 150 dB
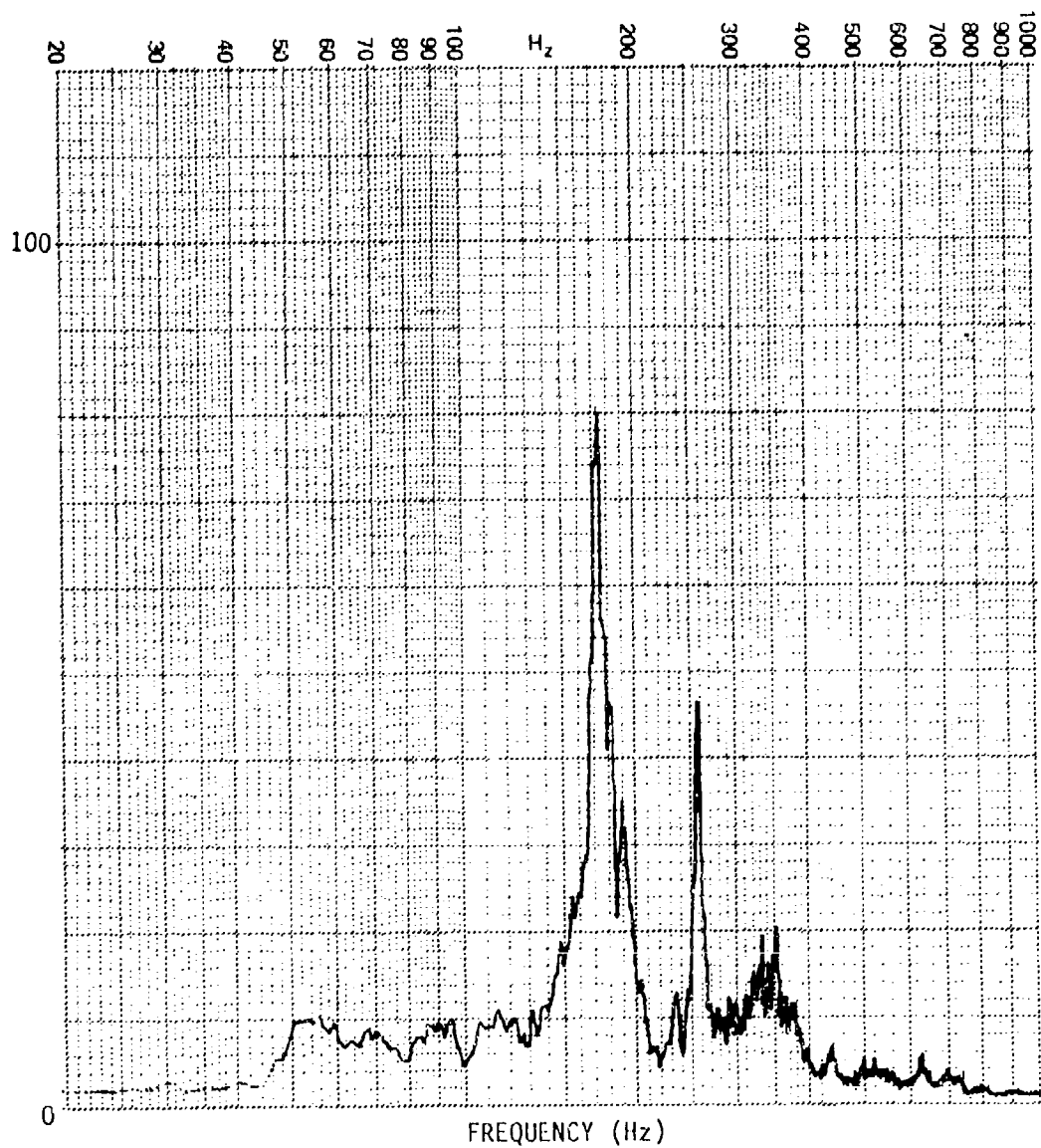
Figure C-16.   Strain Spectrum for Panel b2

C-17

PANEL CONFIGURATION: b2
TRANSDUCER: G10
OVERALL R.M.S. LEVEL: 357.7με
INPUT SPECTRUM: RANDOM
INPUT LEVEL: 155 dB
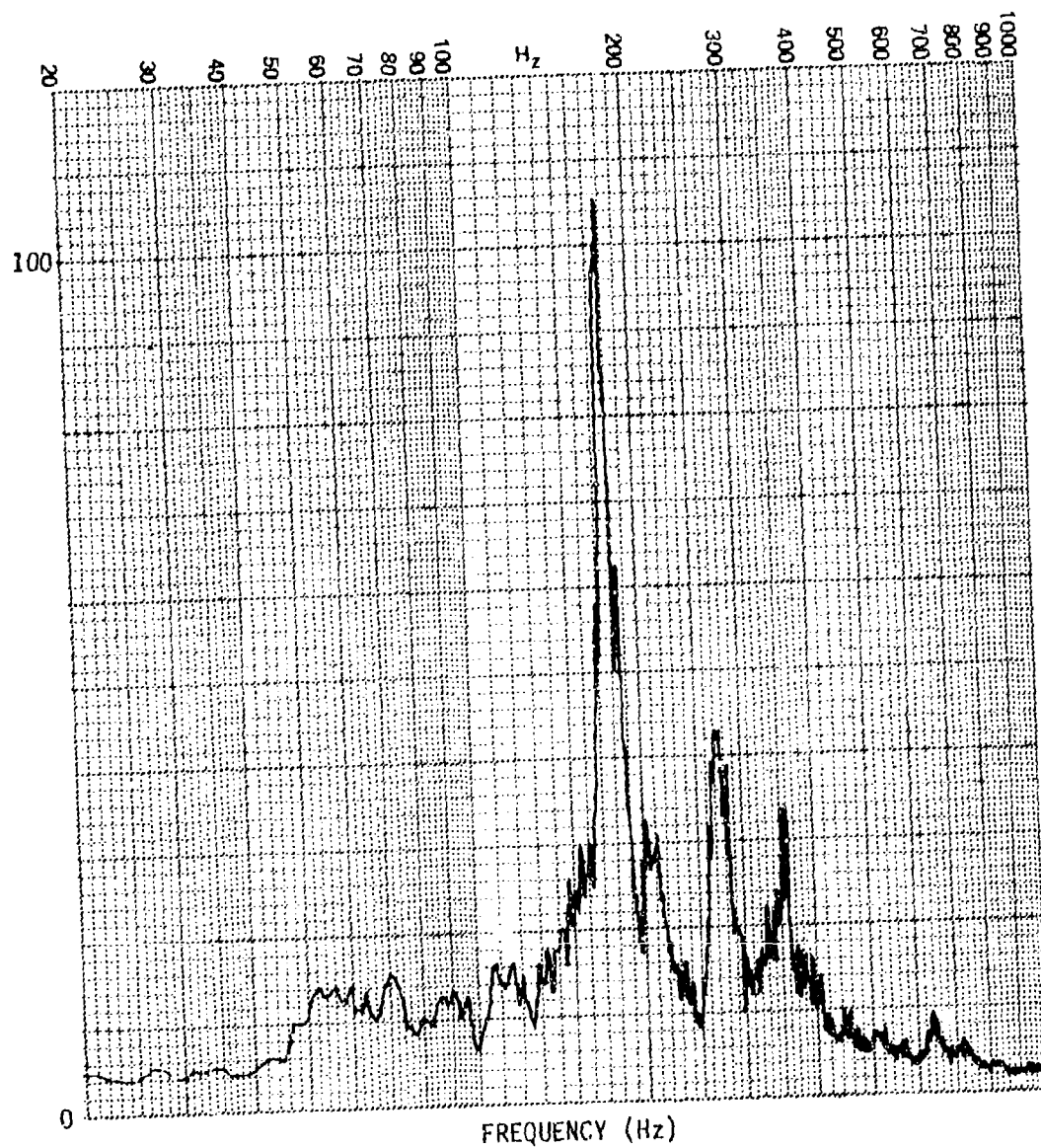
Figure C-17. Strain Spectrum for Panel b2

C-18

PANEL CONFIGURATION: d
TRANSDUCER: G10
OVERALL R.M.S. LEVEL:
INPUT SPECTRUM: SINE
INPUT LEVEL: 130 dB
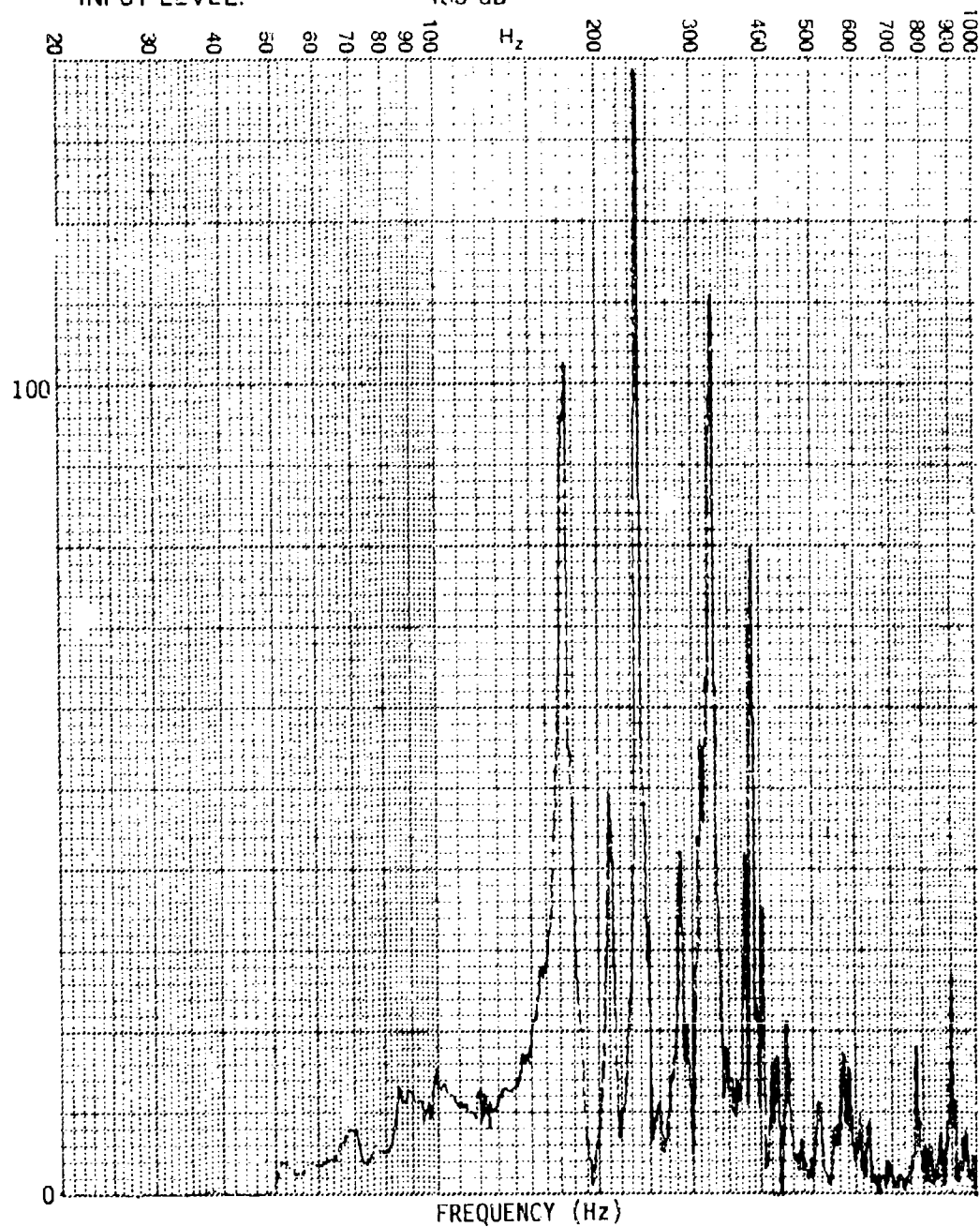
Figure C-18.   Strain Spectrum for Panel d

C-19

PANEL CONFIGURATION: d
TRANSDUCER: G10
OVERALL R.M.S. LEVEL: 33.5 μe
INPUT SPECTRUM   RANDOM
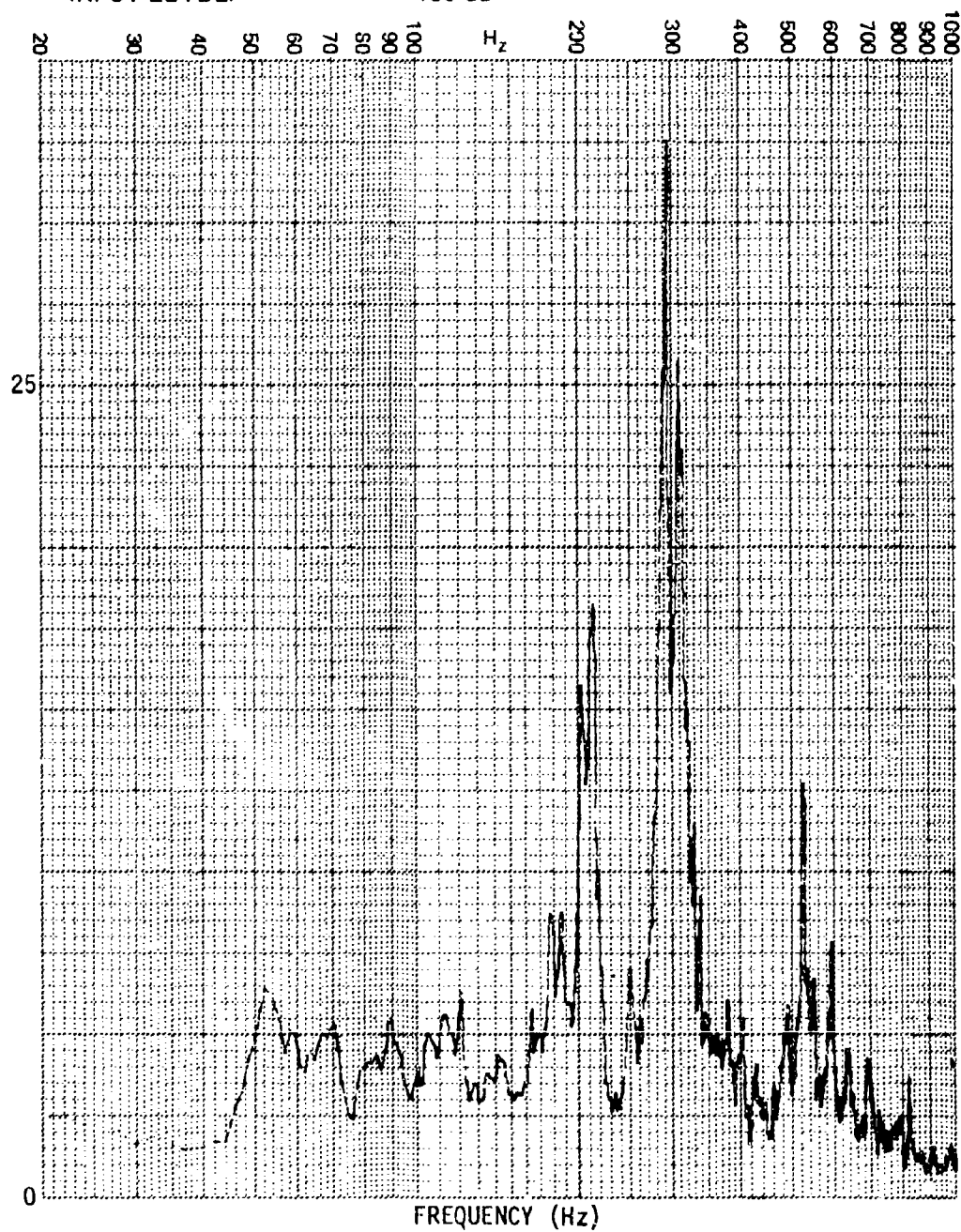INPUT LEVEL: 140 dB
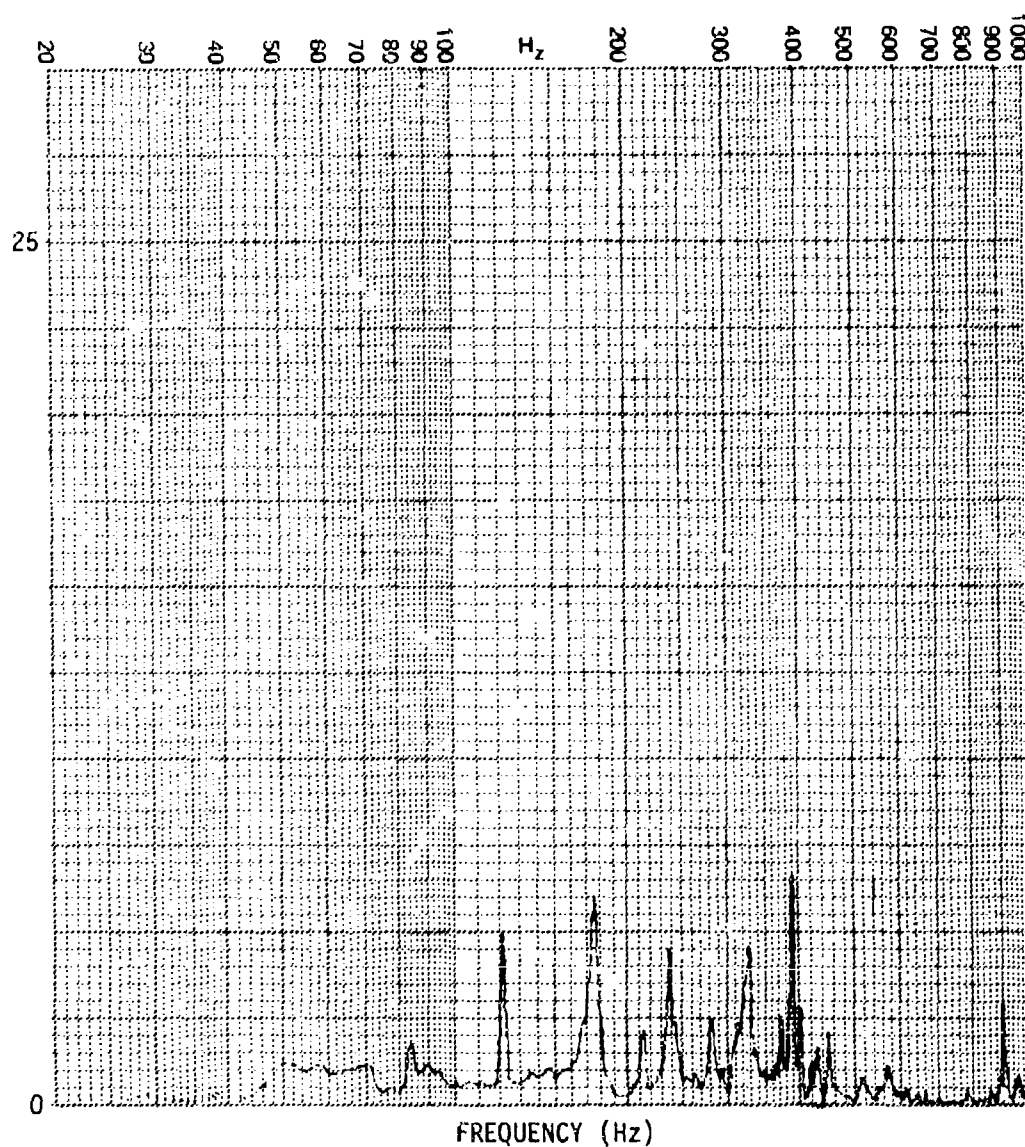
Figure C-19.   Strain Spectrum for Panel d

C-20

PANEL CONFIGURATION: d
TRANSDUCER: G10
OVERALL R.M.S. LEVEL: 56.9μe
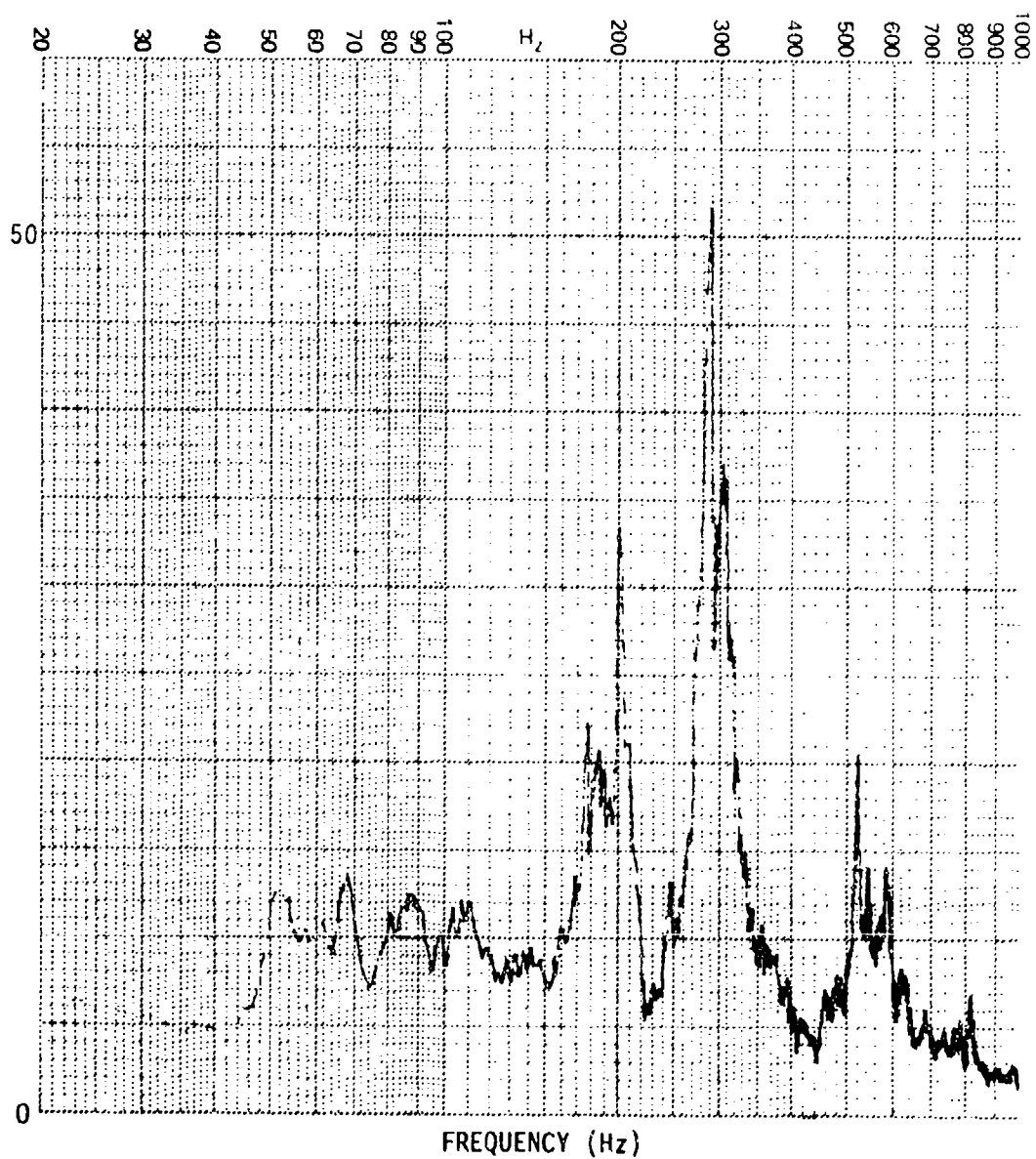INPUT SPECTRUM: RANDOM
INPUT LEVEL: 145 dB
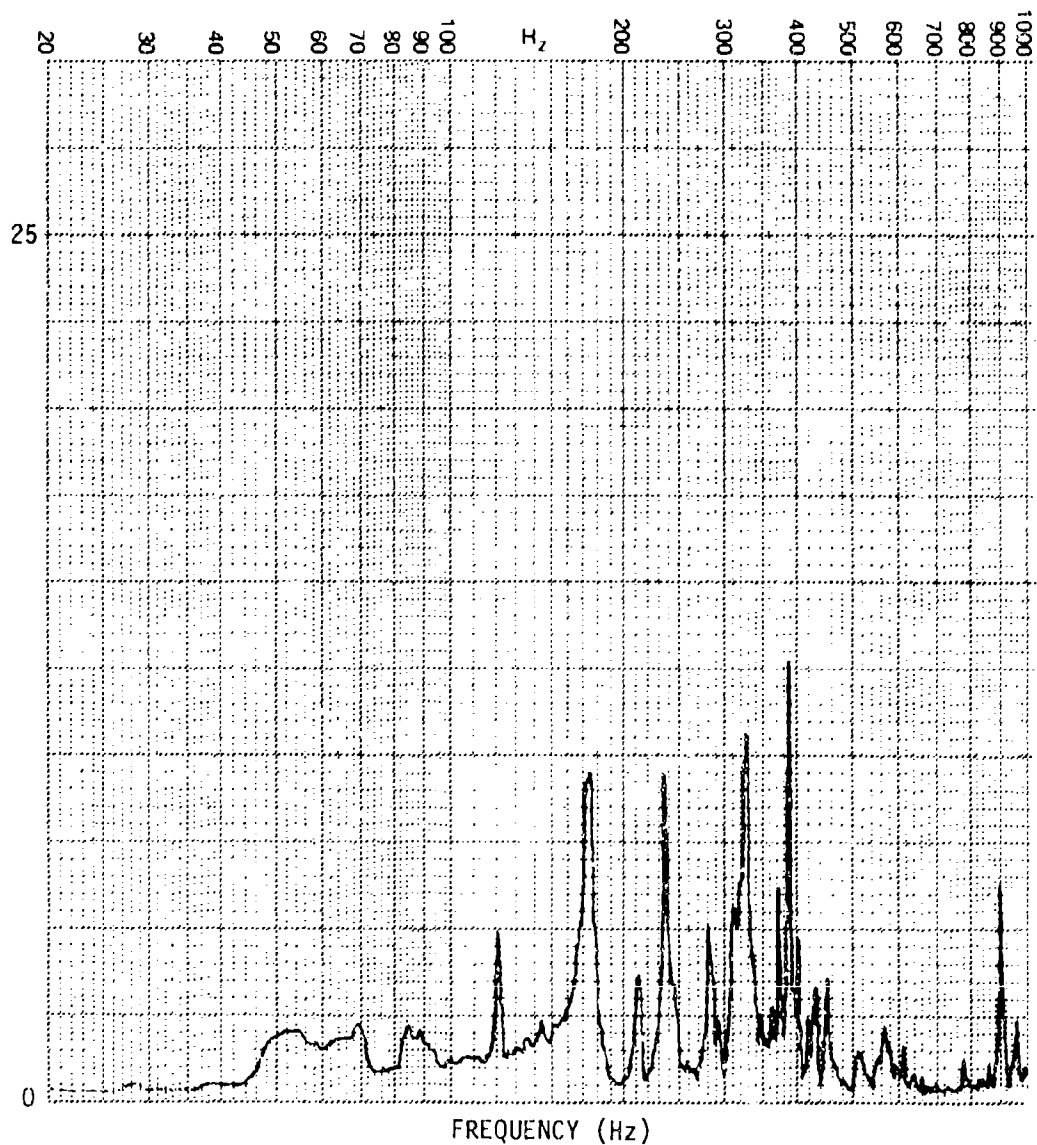
Figure C-20.   Strain Spectrum for Panel d

C-21

PANEL CONFIGURATION: d
TRANSDUCER: G10
OVERALL R.M.S. LEVEL: 101.0μe
INPUT SPECTRUM: RANDOM
INPUT LEVEL: 150 dB
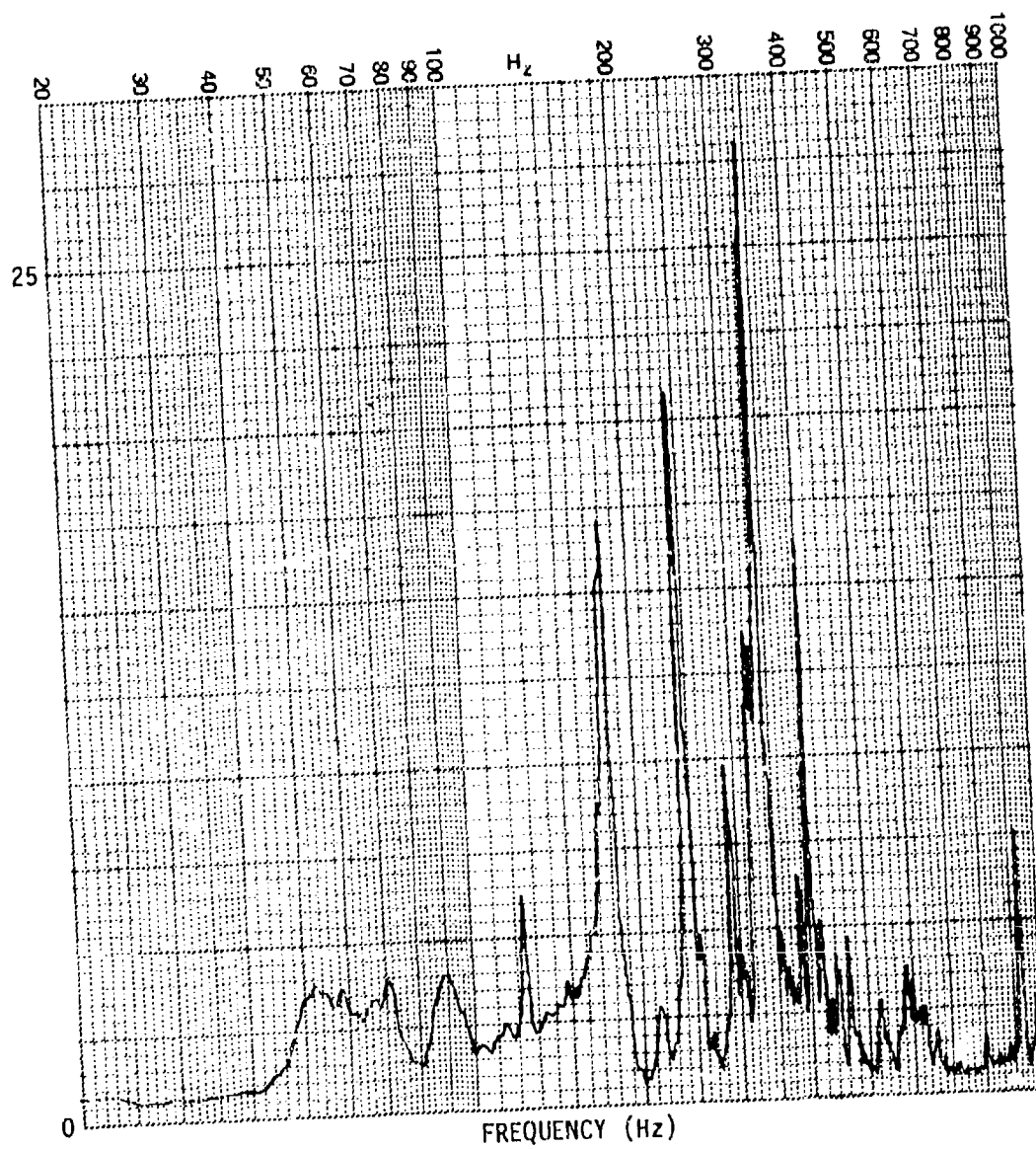
Figure C-21. Strain Spectrum for Panel d

C-22

PANEL CONFIGURATION: d
TRANSDUCER: G10
OVERALL R.M.S. LEVEL: 174.1ᵈᵉ
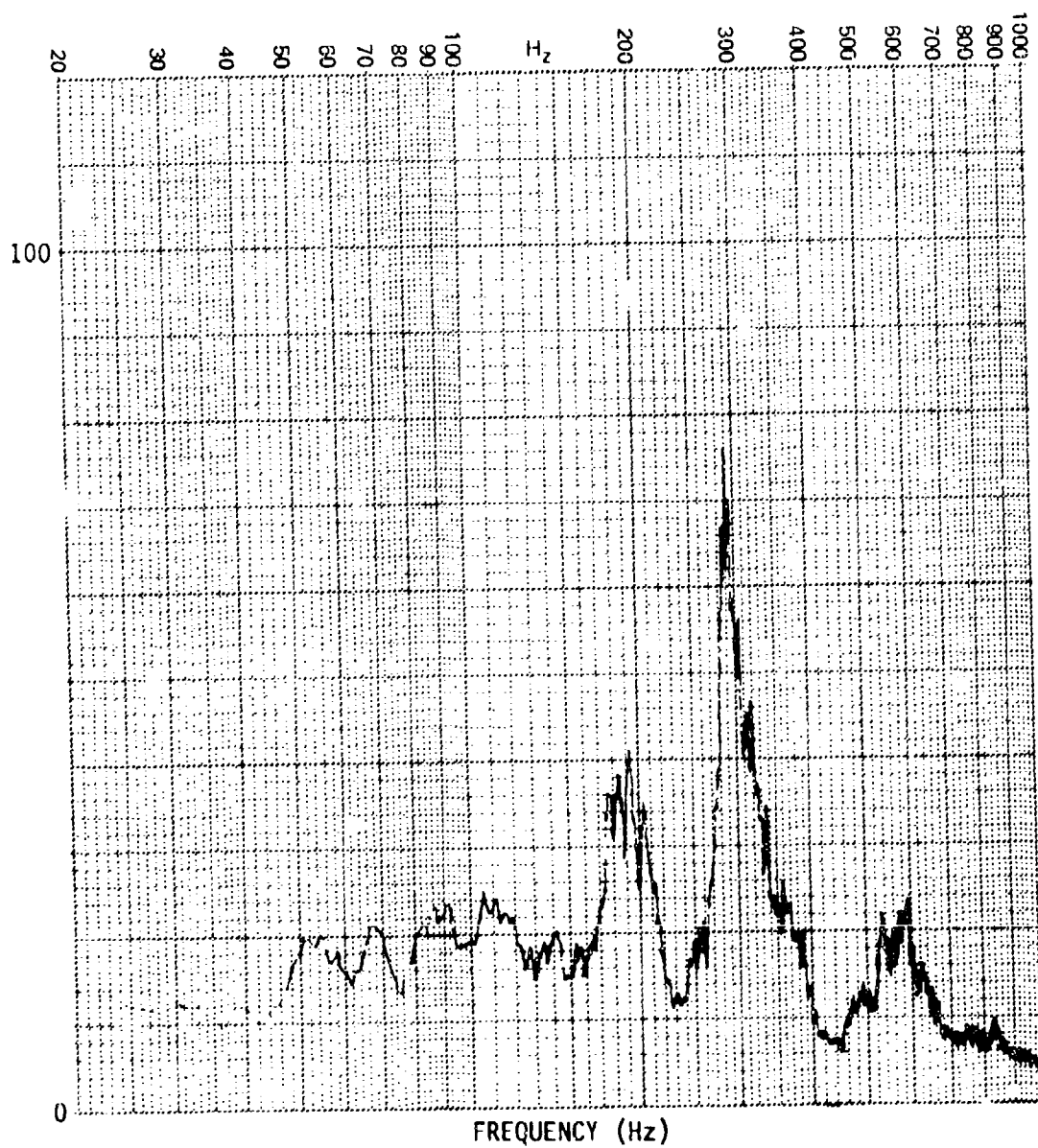INPUT SPECTRUM: RANDOM
INPUT LEVEL: 155 dB

FREQUENCY (Hz)
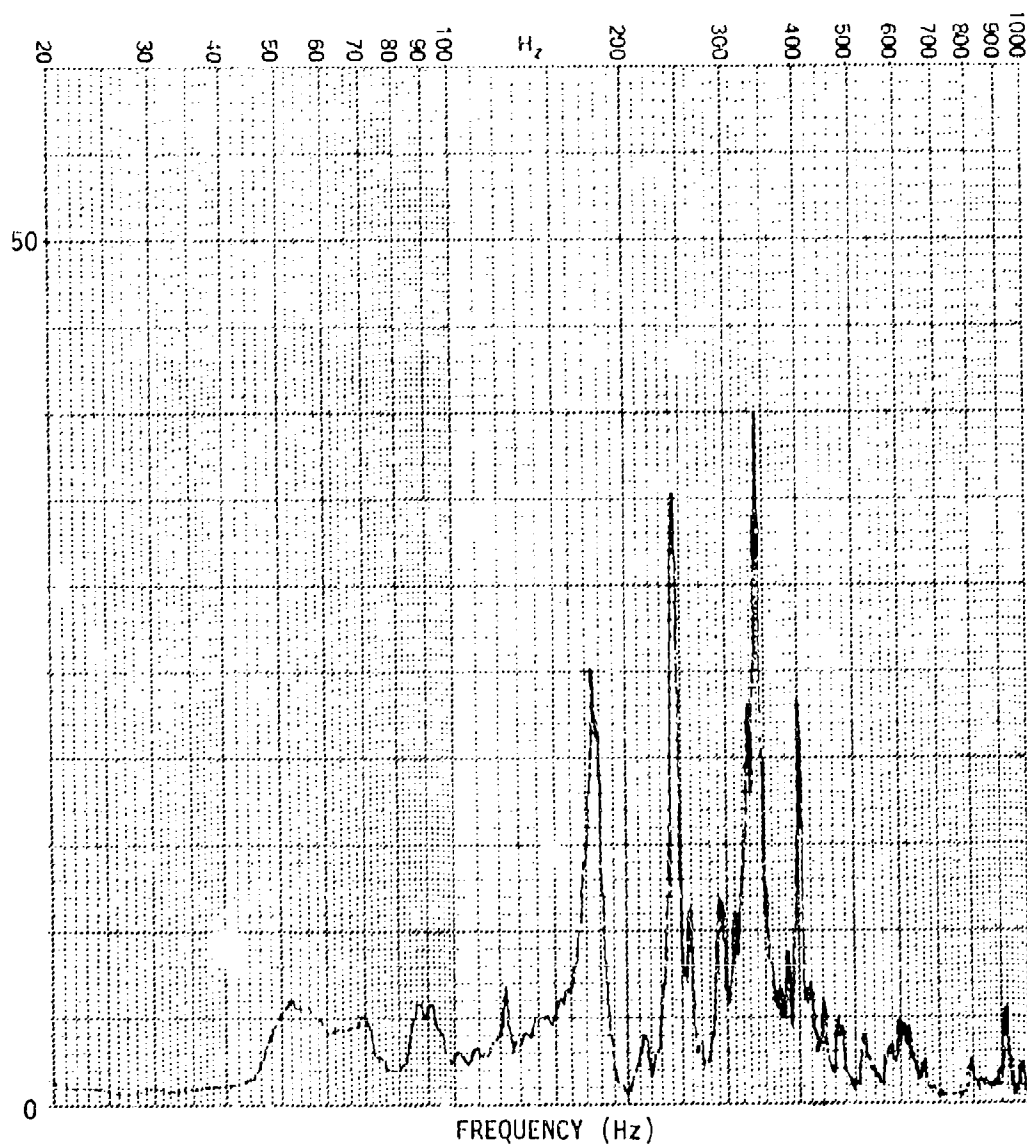
Figure C-22.   Strain Spectrum for Panel d

C-23

PANEL CONFIGURATION: d
TRANSDUCER: G10
OVERALL R.M.S. LEVEL: 274.2 μe
INPUT SPECTRUM: RANDOM
INPUT LEVEL: 160 dB
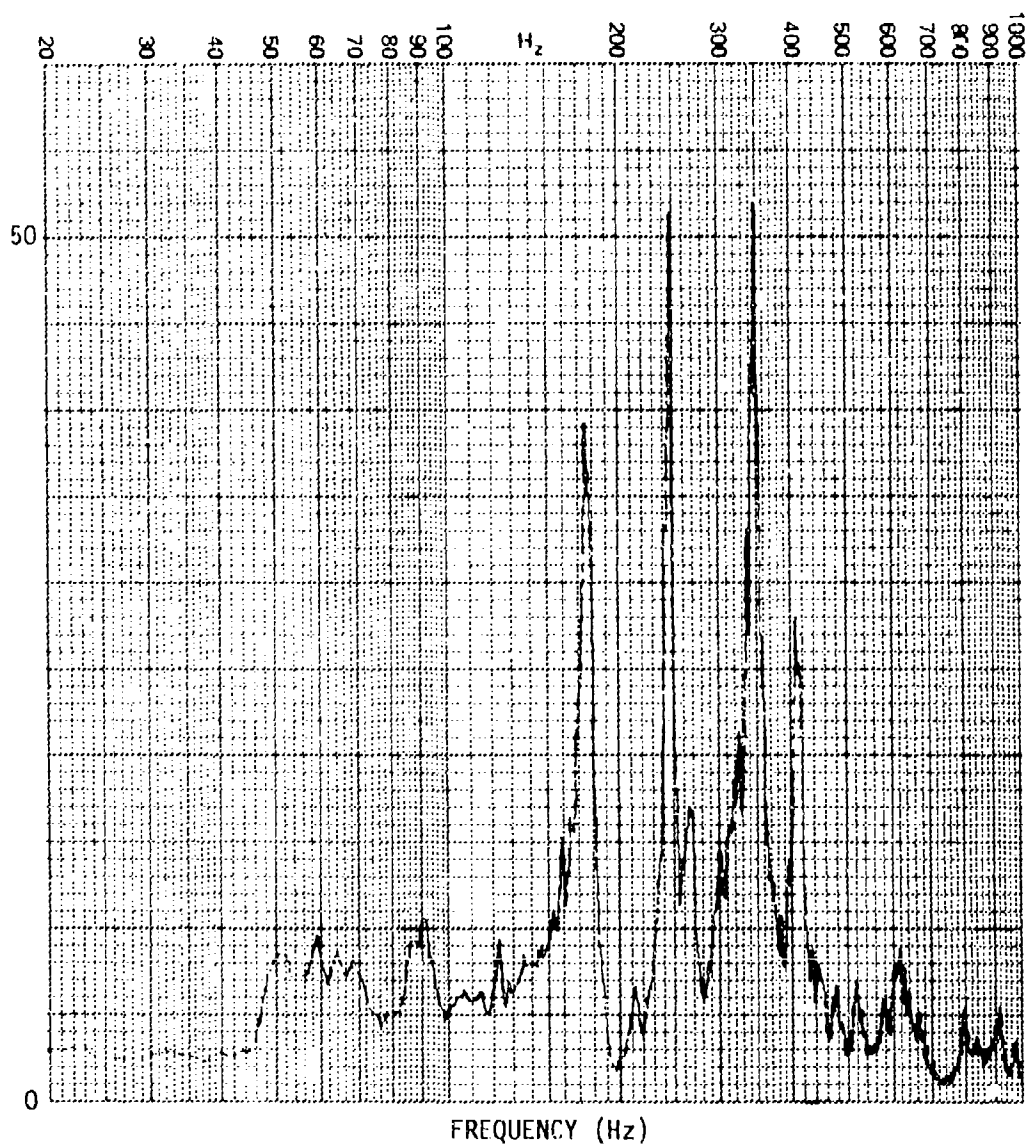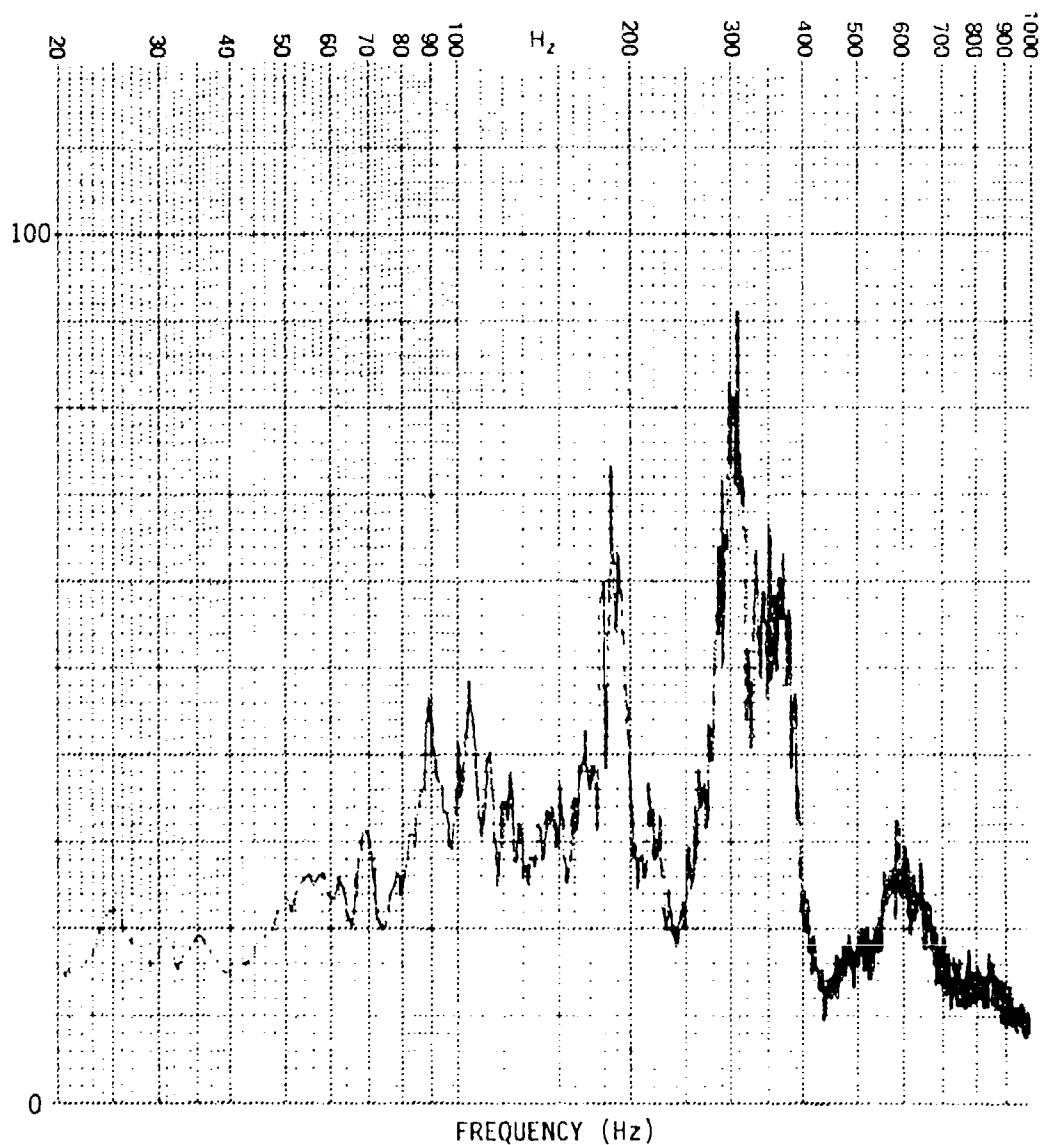

Figure C-23.   Strain Spectrum for Panel d

C-24

PANEL CONFIGURATION: f2
TRANSDUCER: G10
OVERALL R.M.S. LEVEL:
INPUT SPECTRUM: SINE
INPUT LEVEL: 130 dB
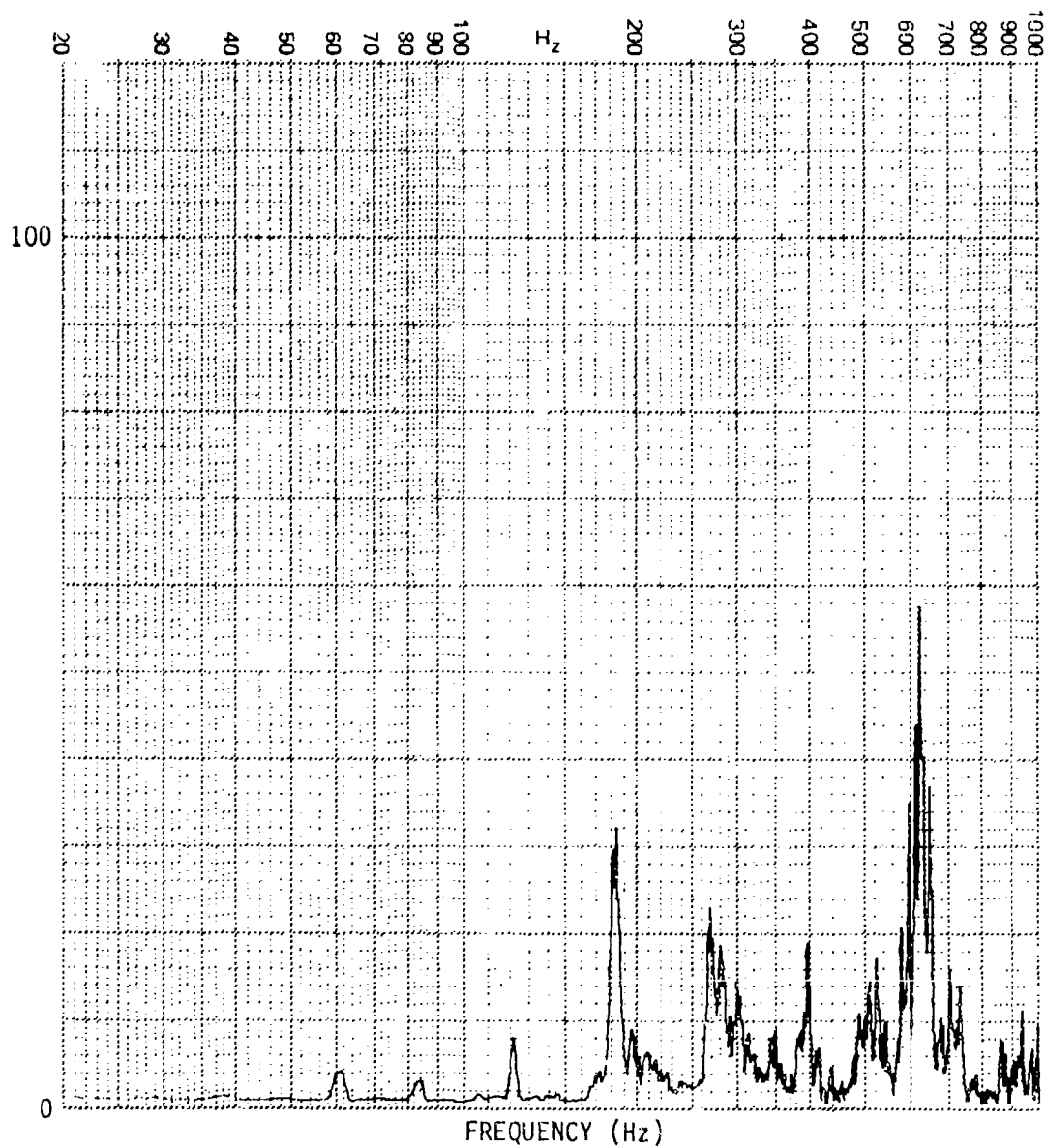
Figure C-24.   Strain Spectrum for Panel f2

C-25

PANEL CONFIGURATION: f2
TRANSDUCER: G10
OVERALL R.M.S. LEVEL: 22.3µe
INPUT SPECTRUM: RANDOM
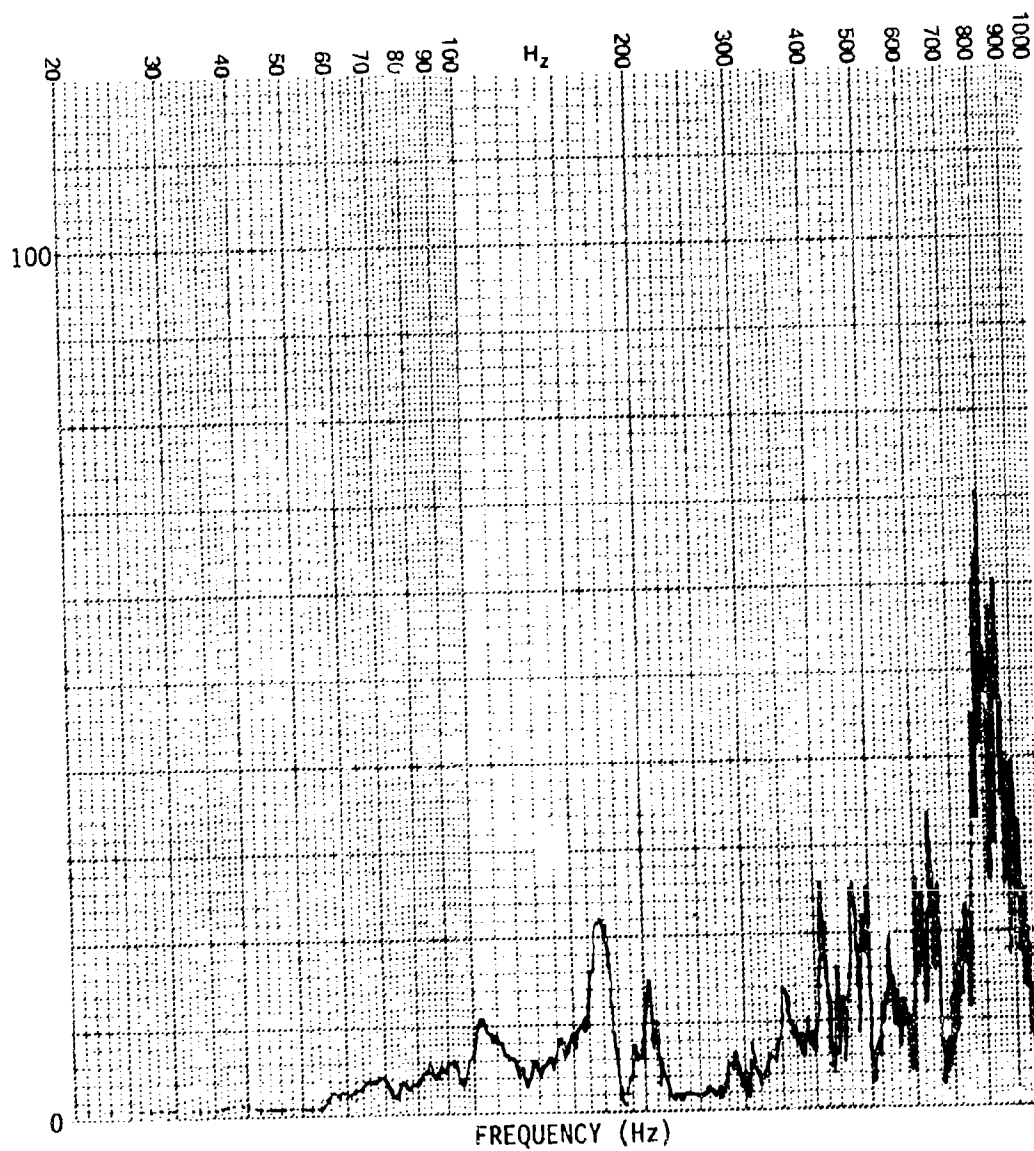INPUT LEVEL: 140 dB
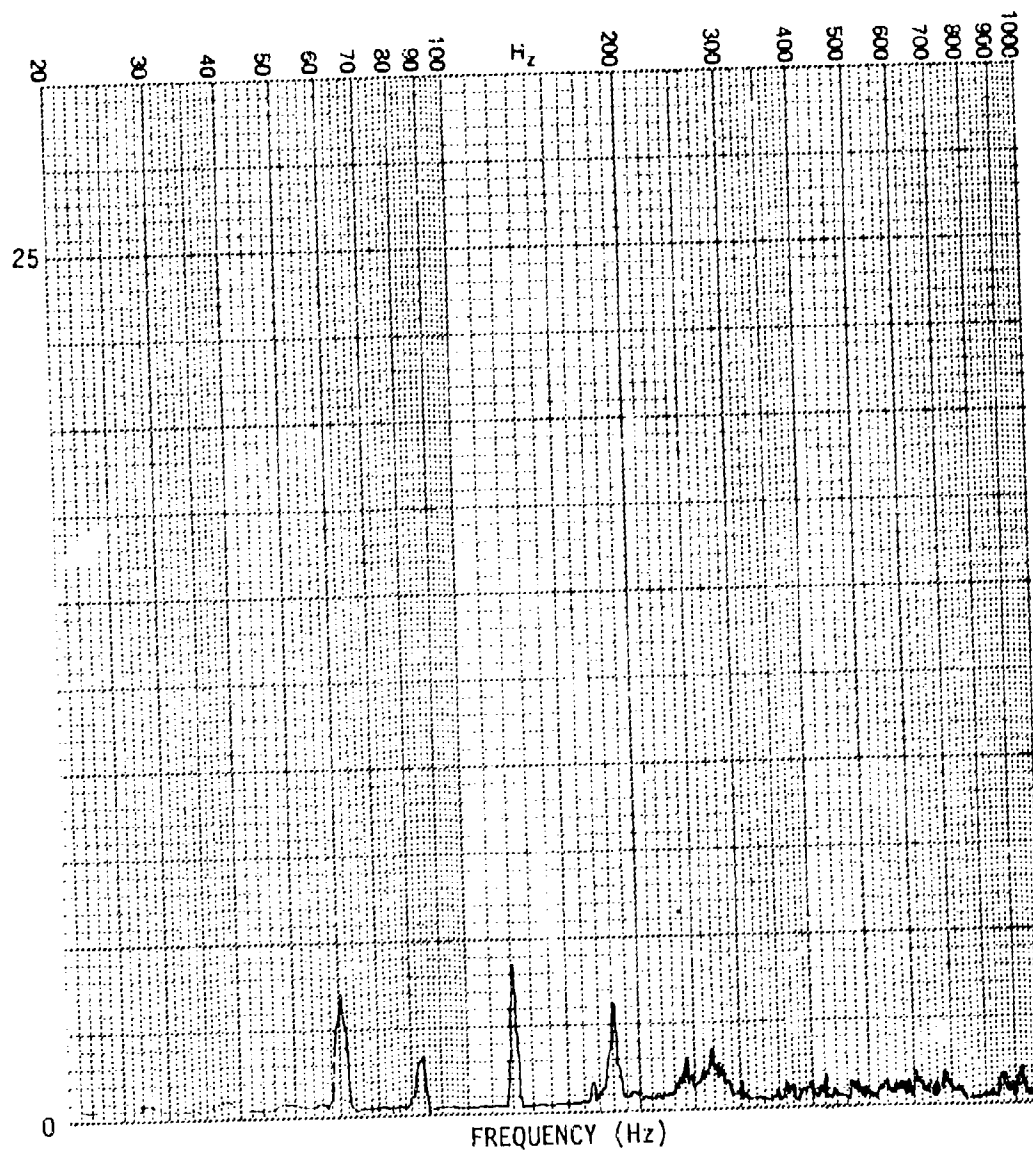
Figure C-25. Strain Spectrum for Panel f2

PANEL CONFIGURATION: f2
TRANSDUCER: G10
OVERALL R.M.S. LEVEL: 30.0μ
INPUT SPECTRUM: RANDOM
INPUT LEVEL: 145 dB
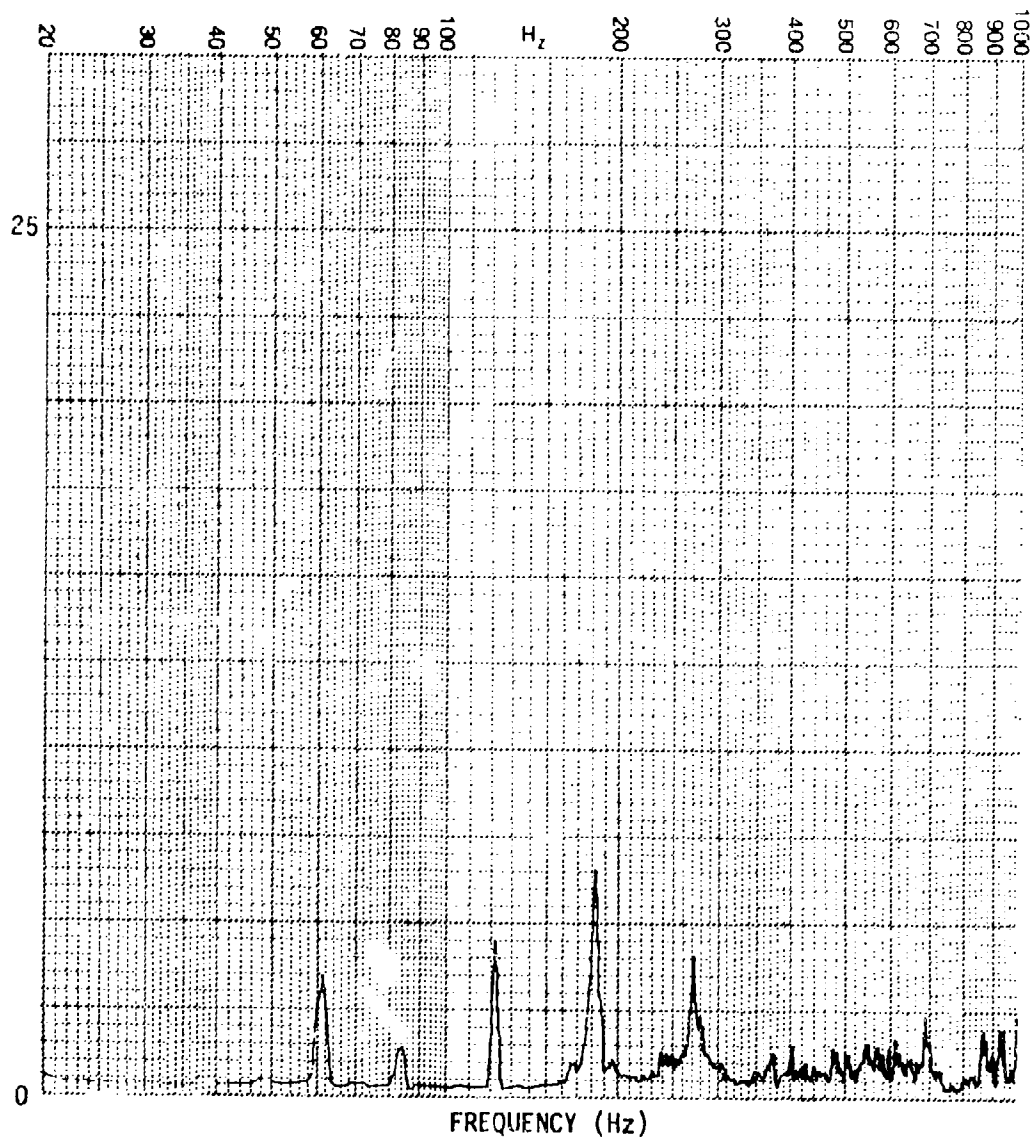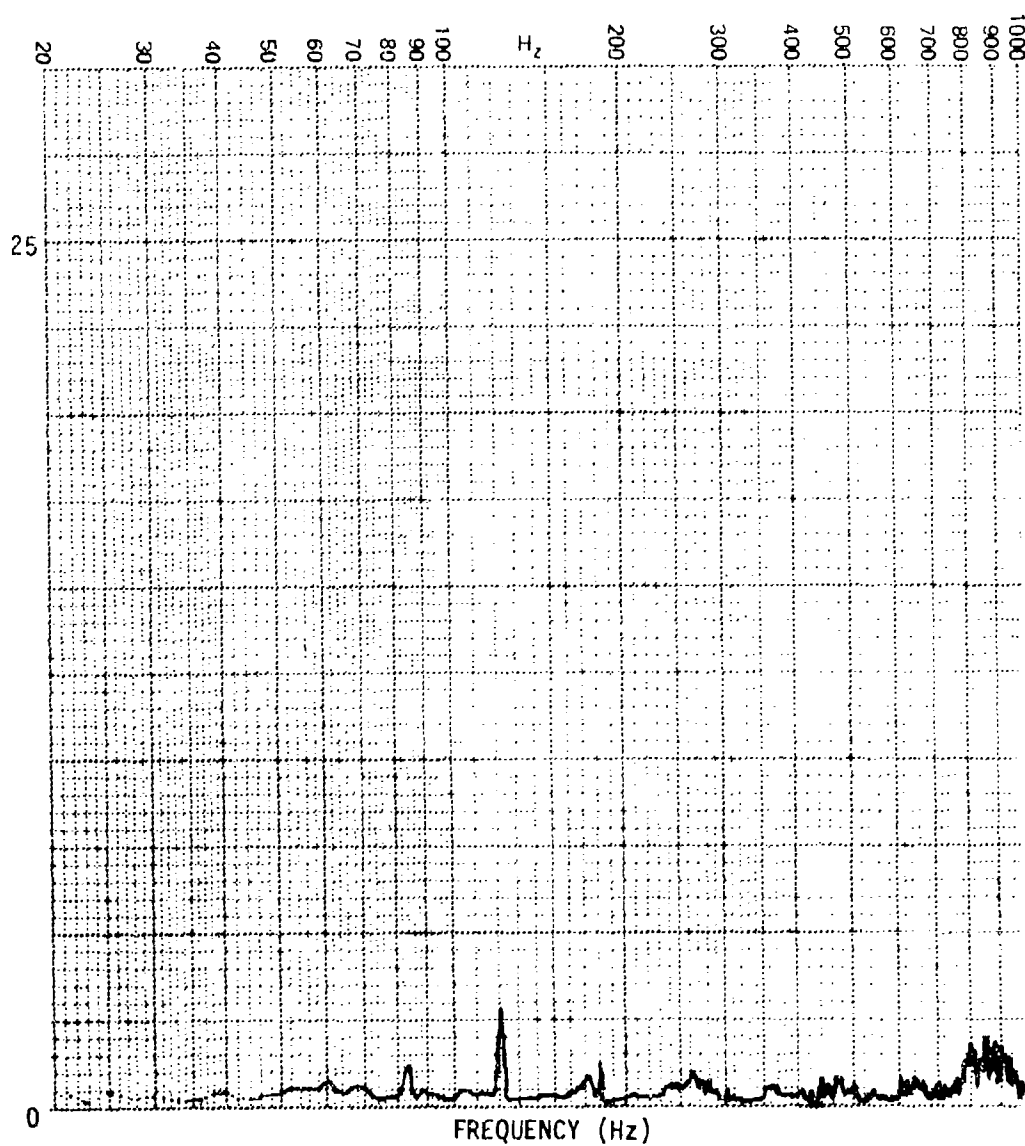

Figure C-26.   Strain Spectrum for Panel f2

C-27

PANEL CONFIGURATION: f2
TRANSDUCER: G10
OVERALL R.M.S. LEVEL: 48.5µe
INPUT SPECTRUM: RANDOM
INPUT LEVEL: 150 dB
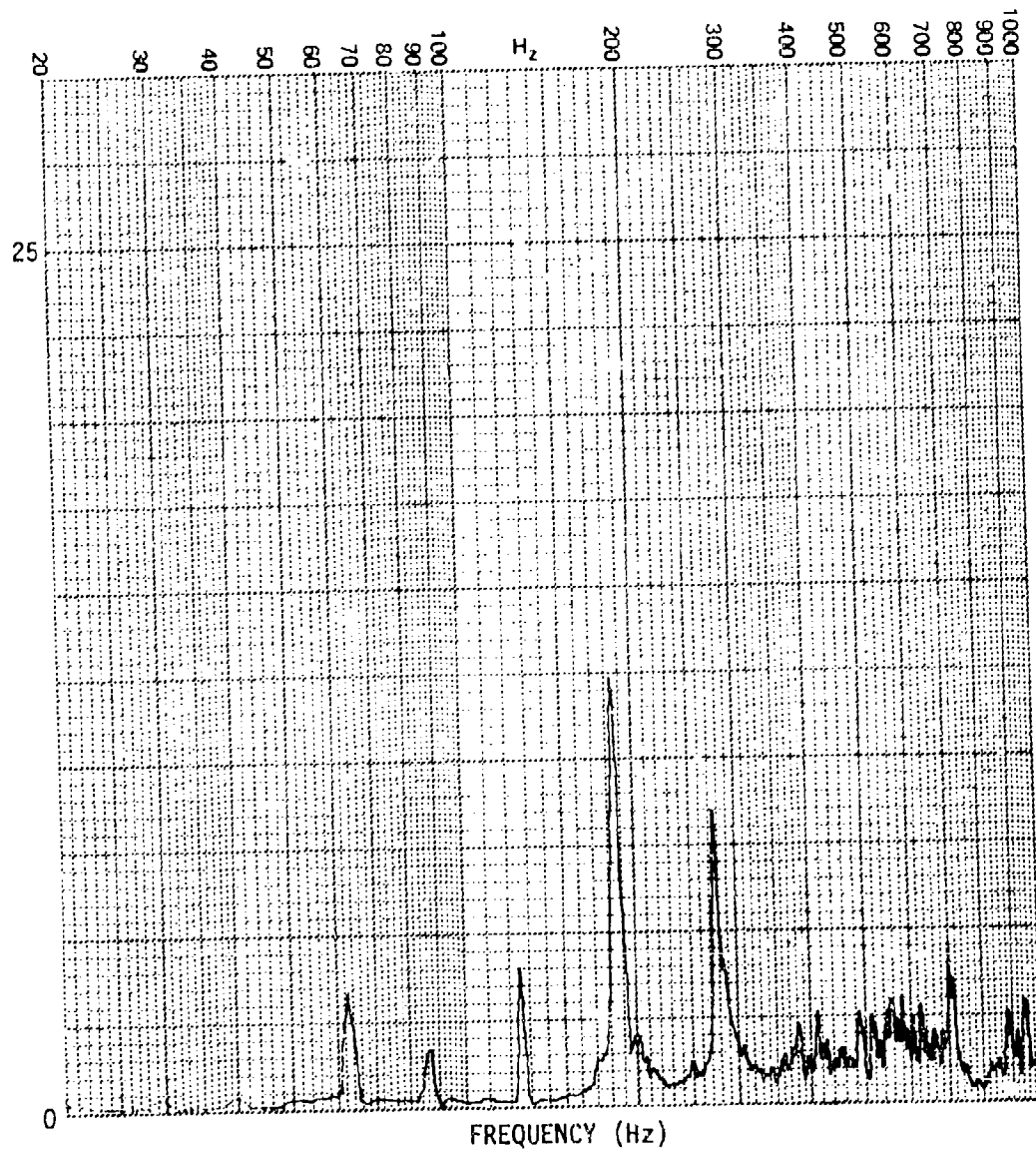
Figure C-27. Strain Spectrum for Panel f2

C-28

PANEL CONFIGURATION: f2
TRANSDUCER: G10
OVERALL R.M.S. LEVEL: 77.6 μe
INPUT SPECTRUM: RANDOM
INPUT LEVEL: 155 dB
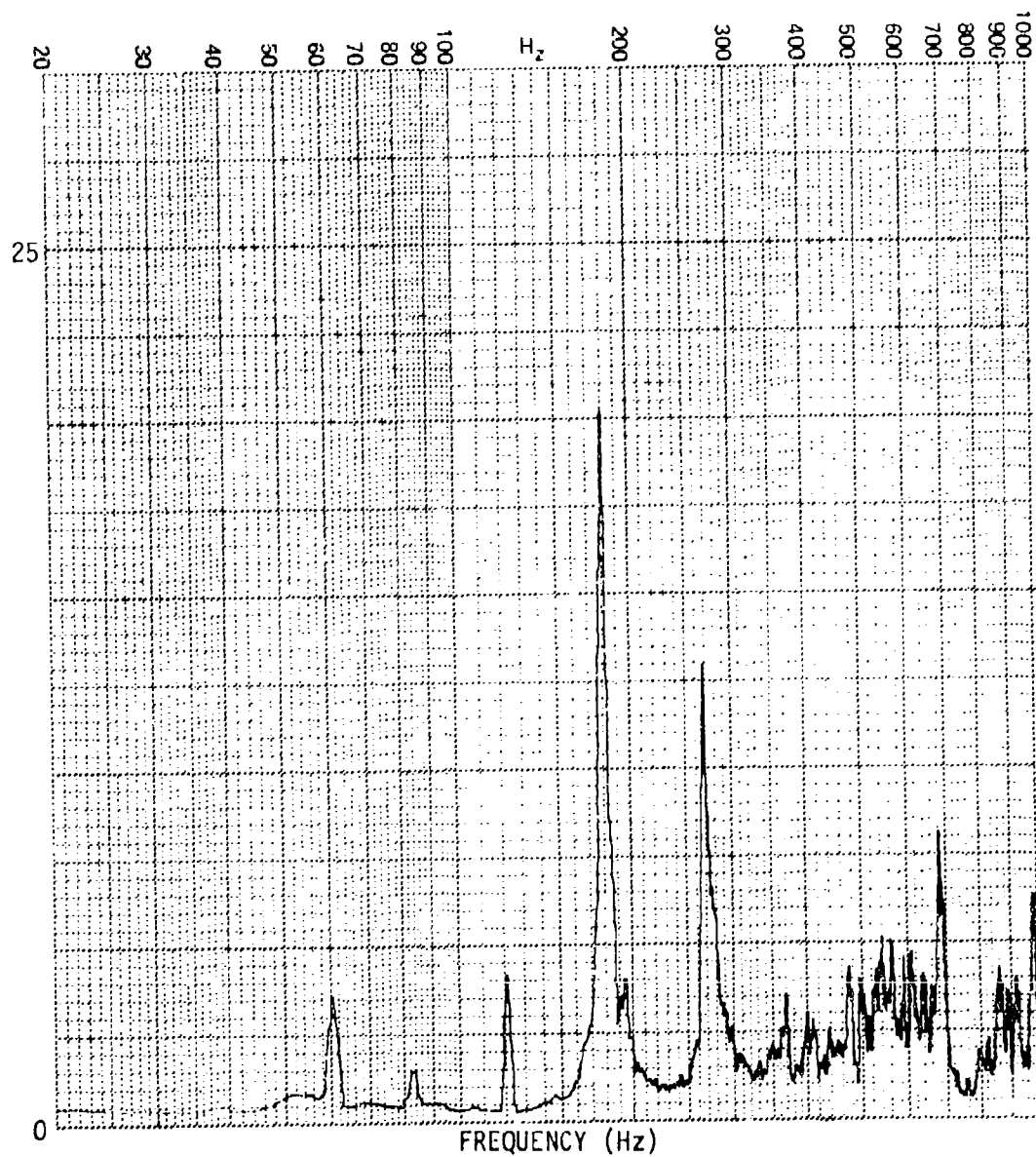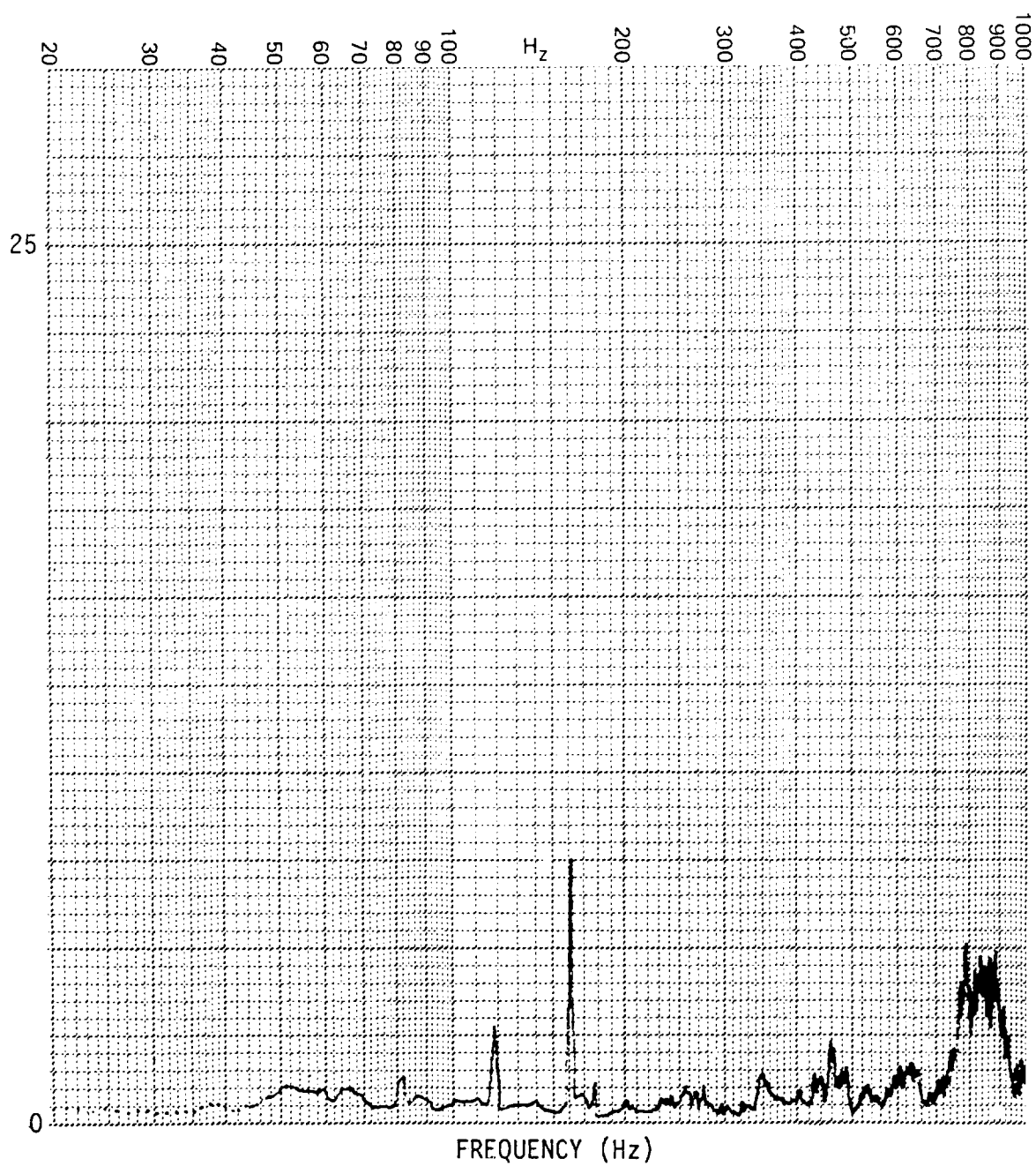

Figure C-28.   Strain Spectrum for Panel f2

C-29

PANEL CONFIGURATION: f2
TRANSDUCER: G10
OVERALL R.M.S. LEVEL: 153.6με
INPUT SPECTRUM: RANDOM
INPUT LEVEL: 160 dB
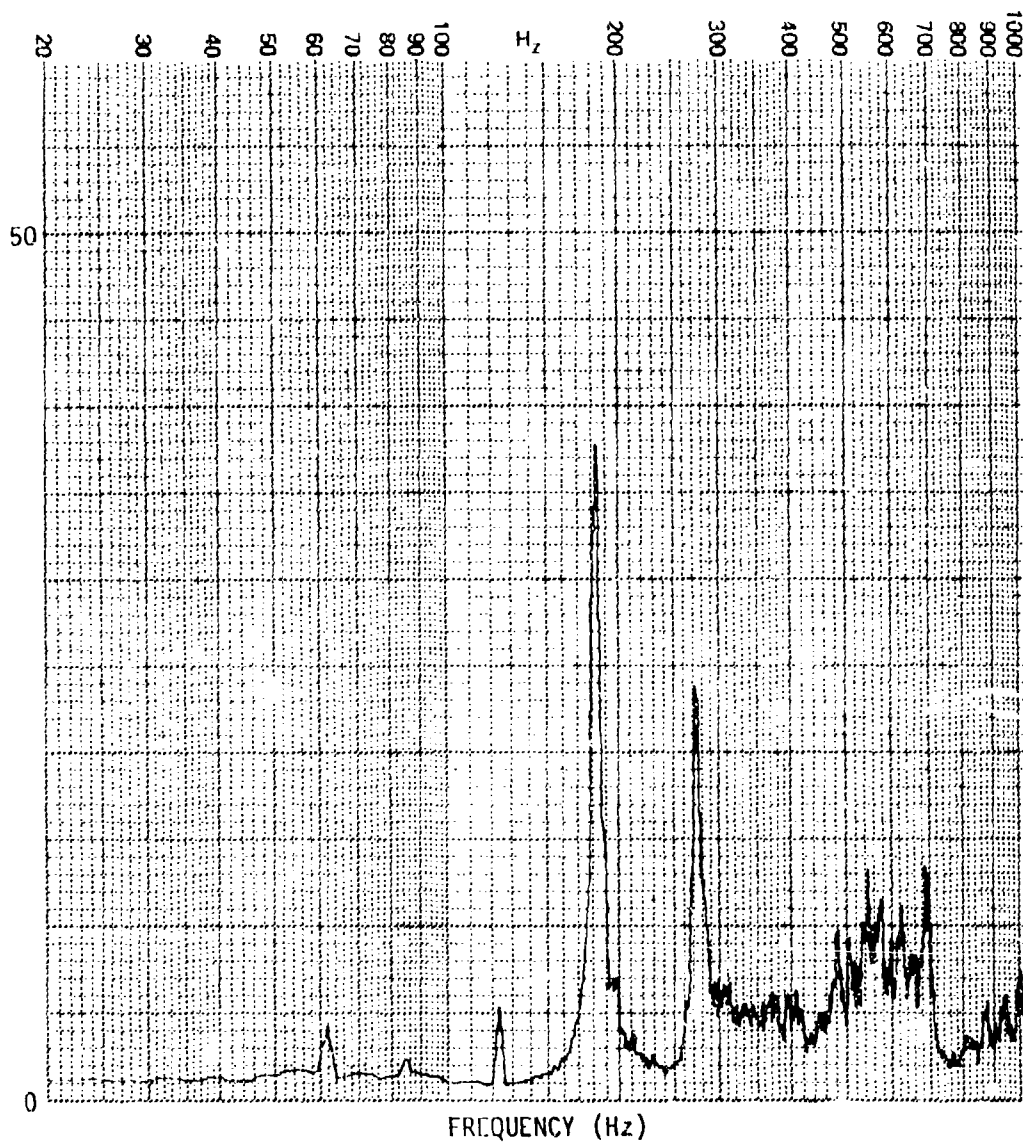
Figure C-29.   Strain Spectrum for Panel f2

PANEL CONFIGURATION: f2
TRANSDUCER: G10
OVERALL R.M.S. LEVEL: 247.4µε
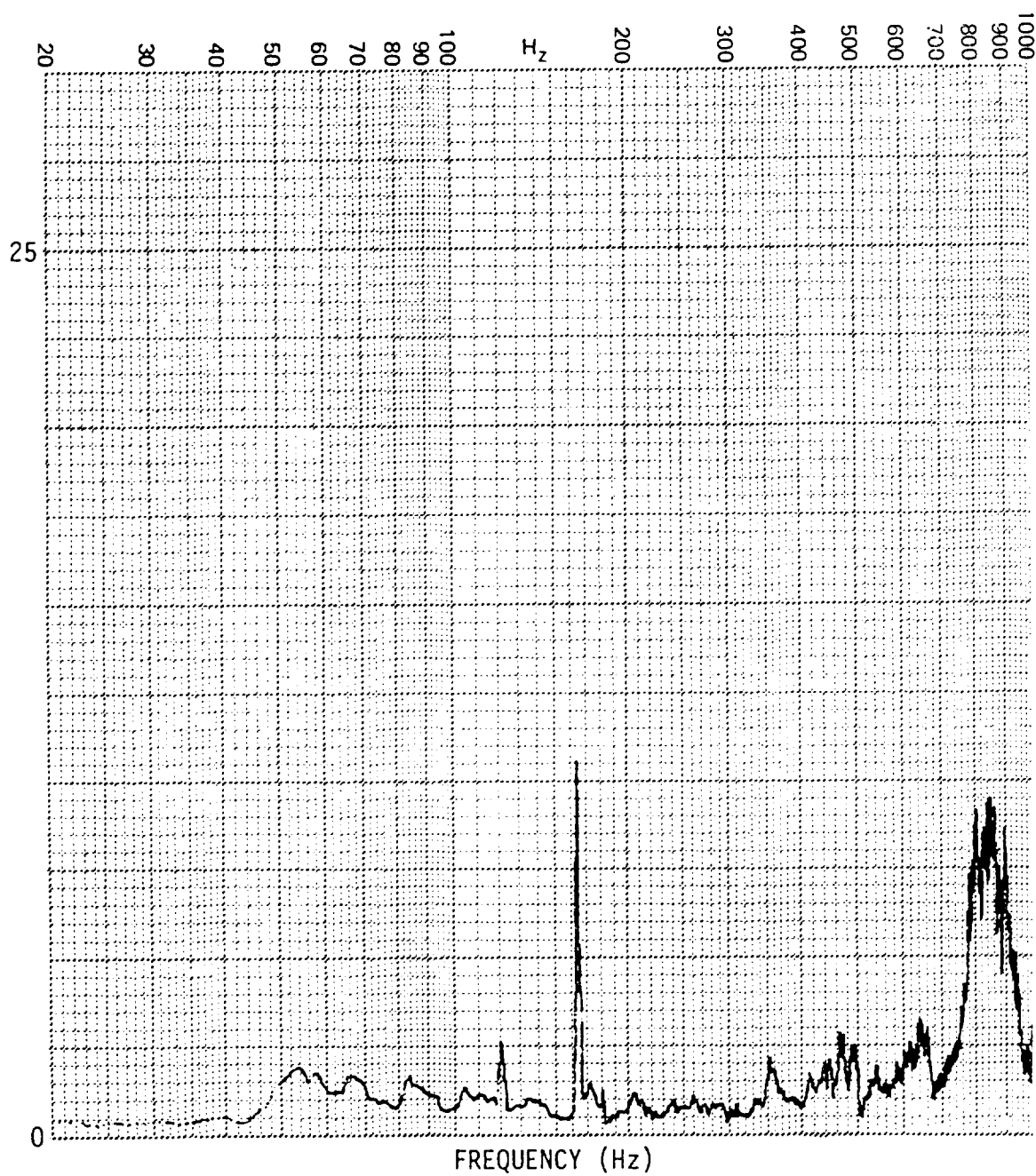INPUT SPECTRUM: RANDOM
INPUT LEVEL: 165 dB
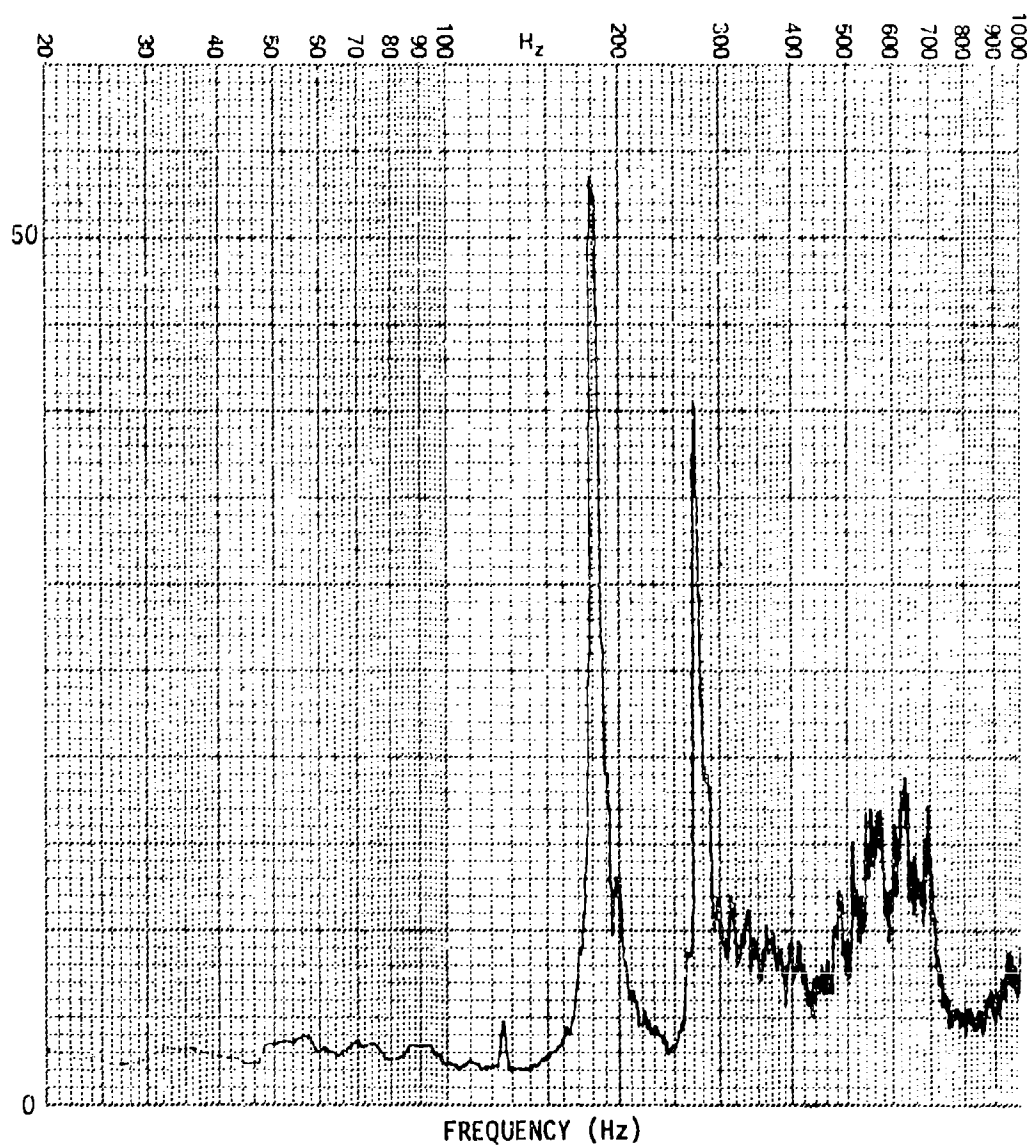
Figure C-30.   Strain Spectrum for Panel f2

C-31

PANEL CONFIGURATION: g2
TRANSDUCER: G10
OVERALL R.M.S. LEVEL:
INPUT SPECTRUM: SINE
INPUT LEVEL: 130 dB

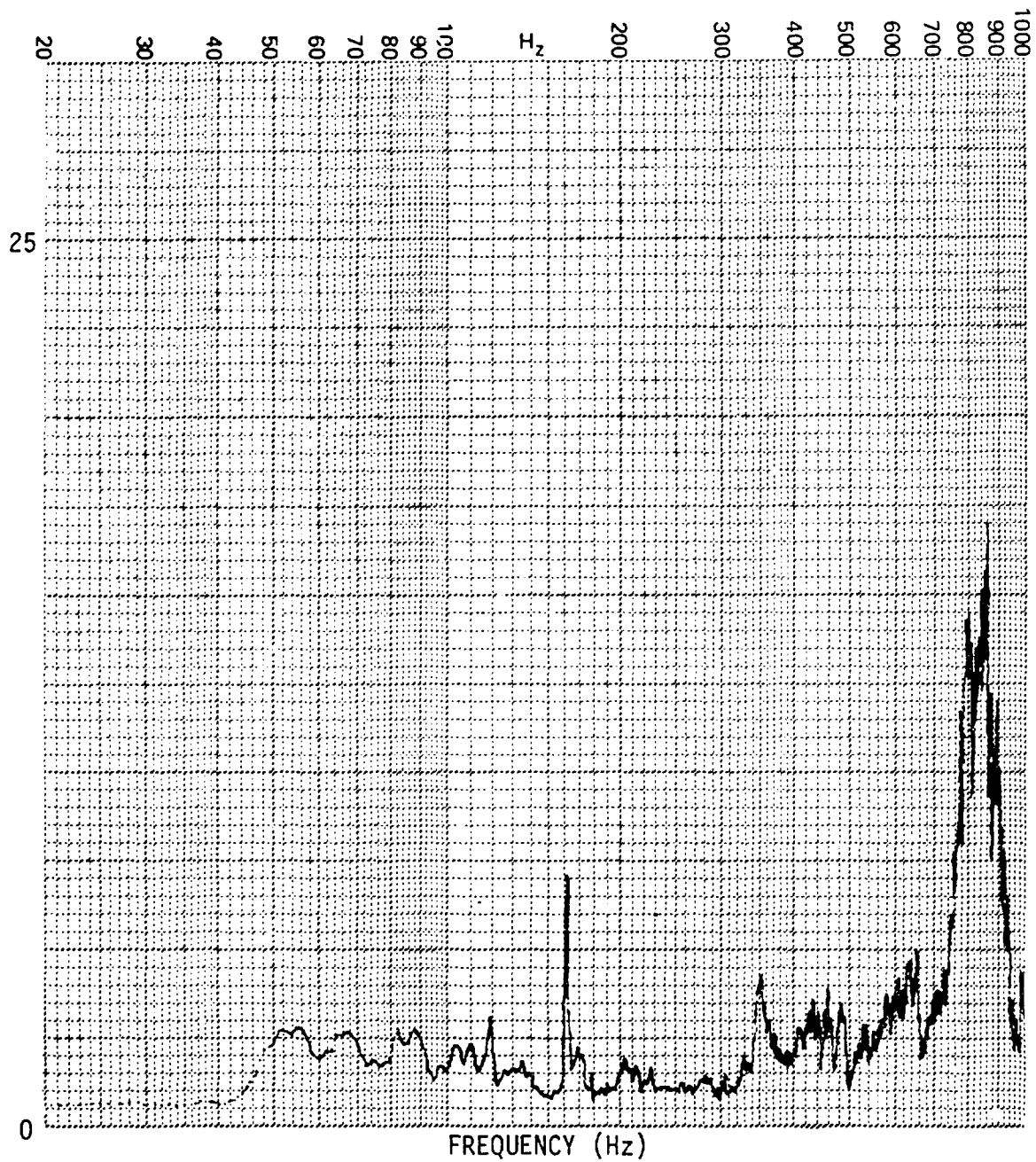
FREQUENCY (Hz)
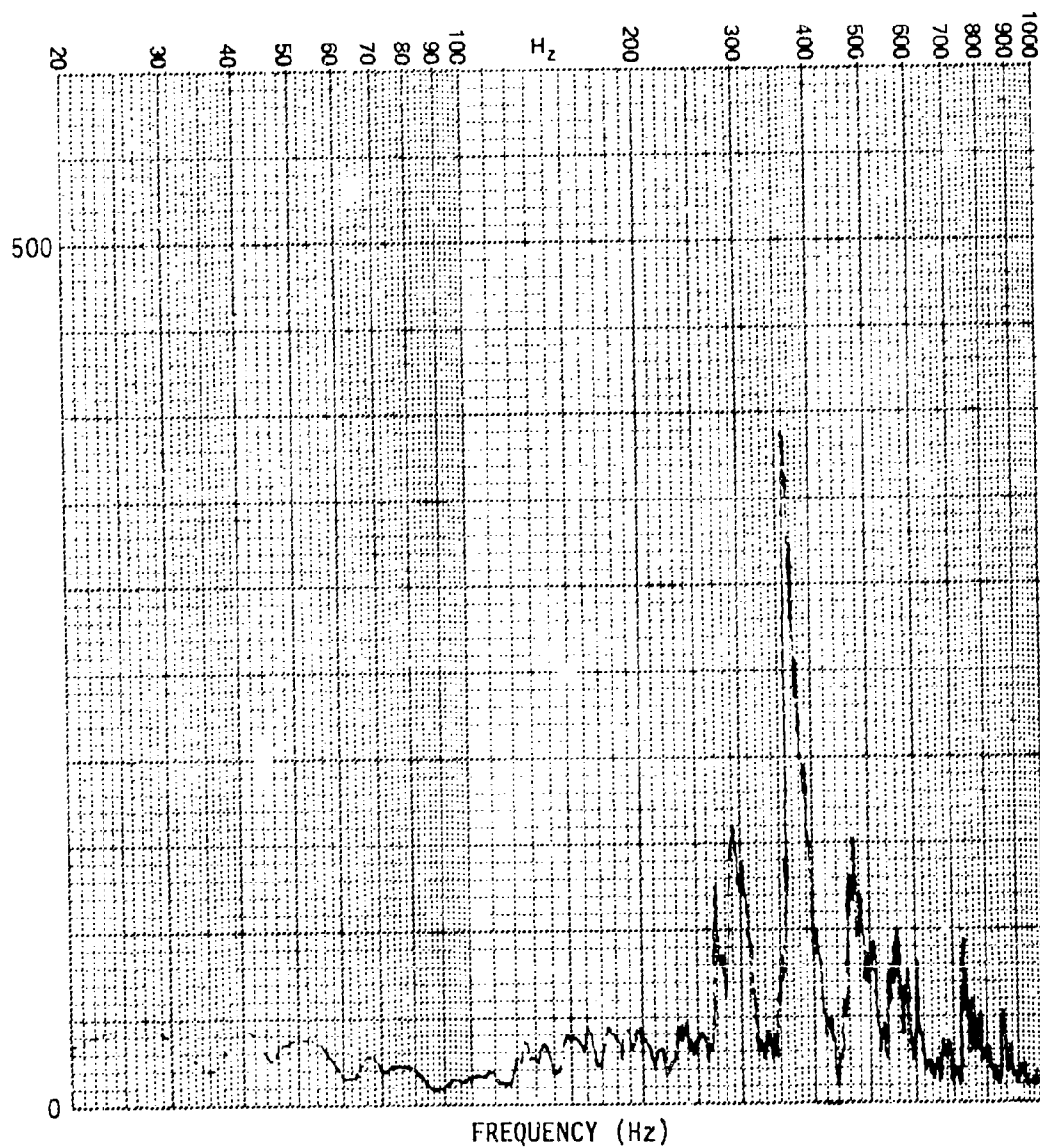
Figure C-31.   Strain Spectrum for Panel g2

PANEL CONFIGURATION: g2
TRANSDUCER: G10
OVERALL R.M.S. LEVEL: 51.0μe
INPUT SPECTRUM: RANDOM
INPUT LEVEL: 140 dB
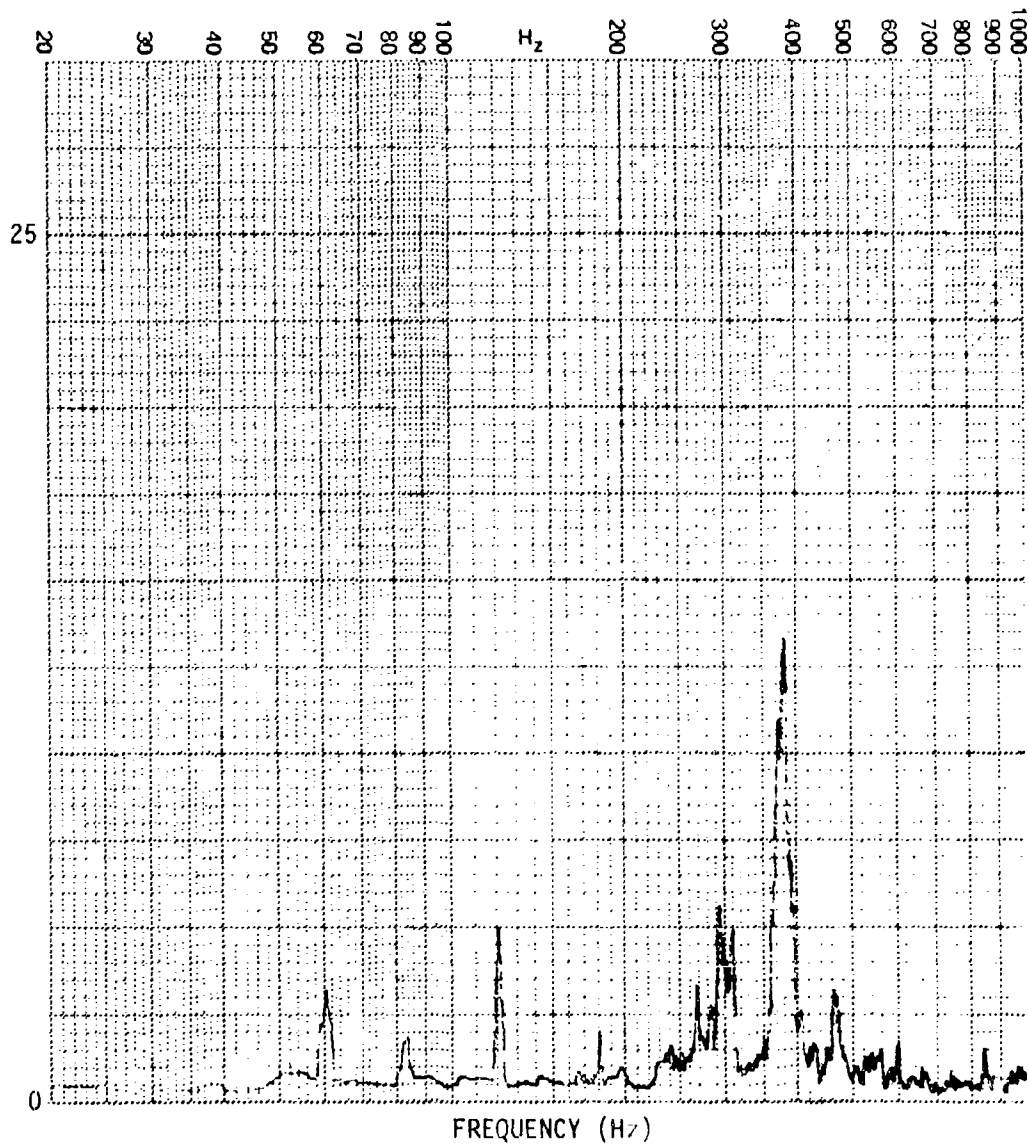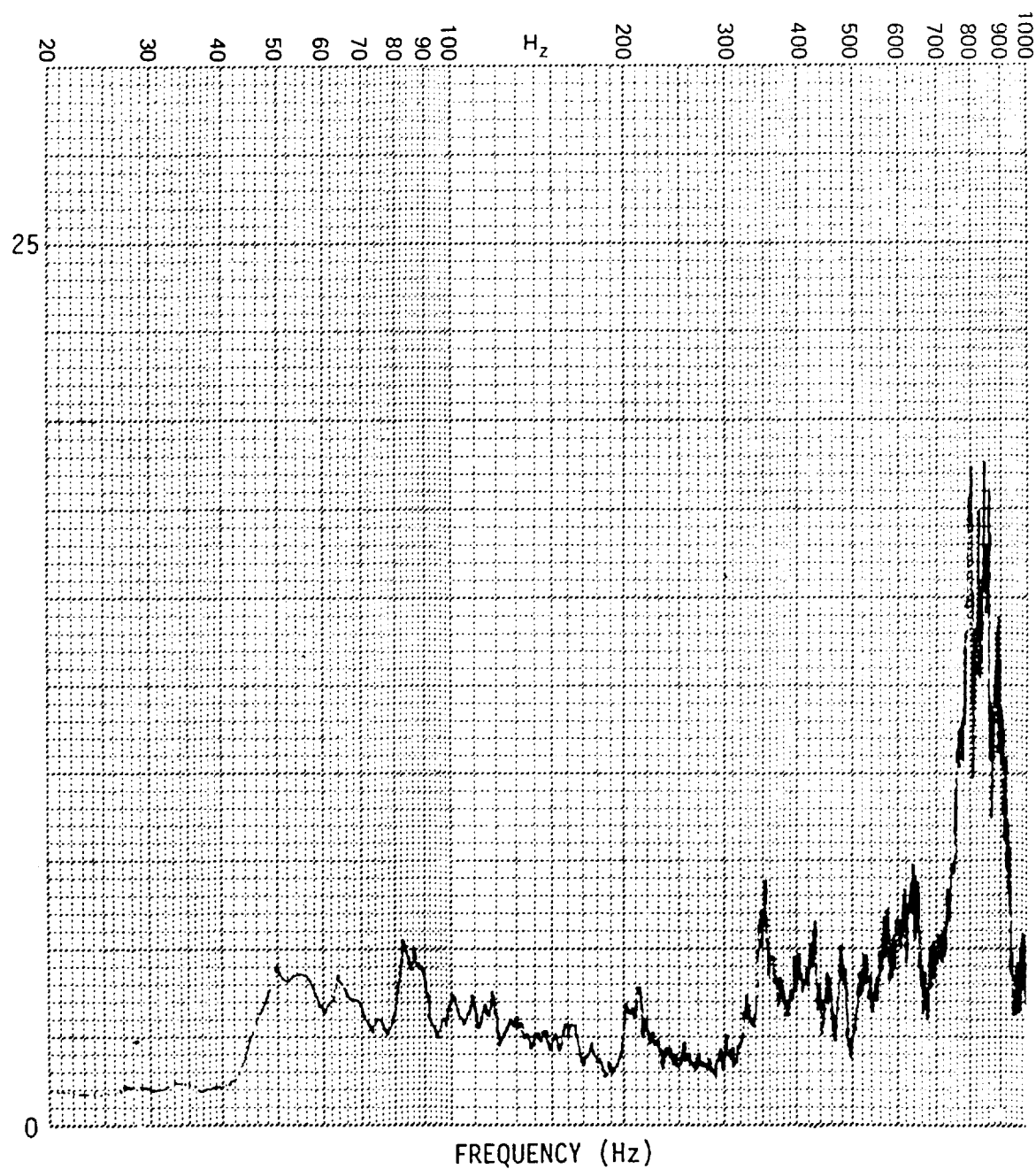

Figure C-32.   Strain Spectrum for Panel g2

C-33

PANEL CONFIGURATION:　　g2
TRANSDUCER:　　　　　　G10
OVERALL R.M.S. LEVEL:　92.9 µe
INPUT SPECTRUM:　　　　RANDOM
INPUT LEVEL:　　　　　　145 dB

Figure C 23   Strain Spectrum for Panel g2

C-3'

PANEL CONFIGURATION: g2
TRANSDUCER: G10
OVERALL R.M.S. LEVEL: 151.4μe
INPUT SPECTRUM: RANDOM
INPUT LEVEL: 150 dB

Figure C-34.   Strain Spectrum for Panel g2

C-35

PANEL CONFIGURATION: g2
TRANSDUCER: G10
OVERALL R.M.S. LEVEL: 250.0ue
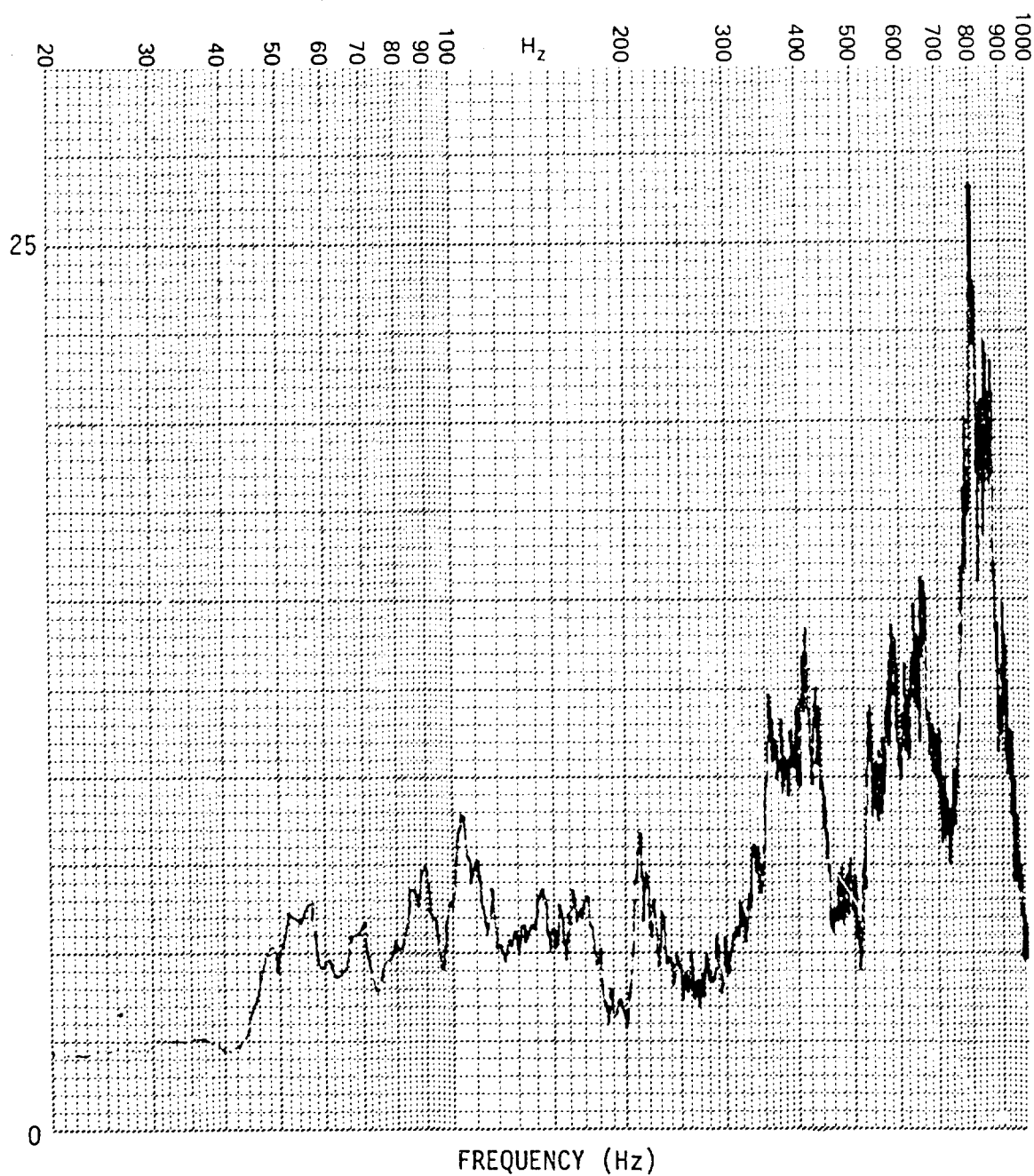INPUT SPECTRUM: RANDOM
INPUT LEVEL: 155 dB

FREQUENCY (Hz)

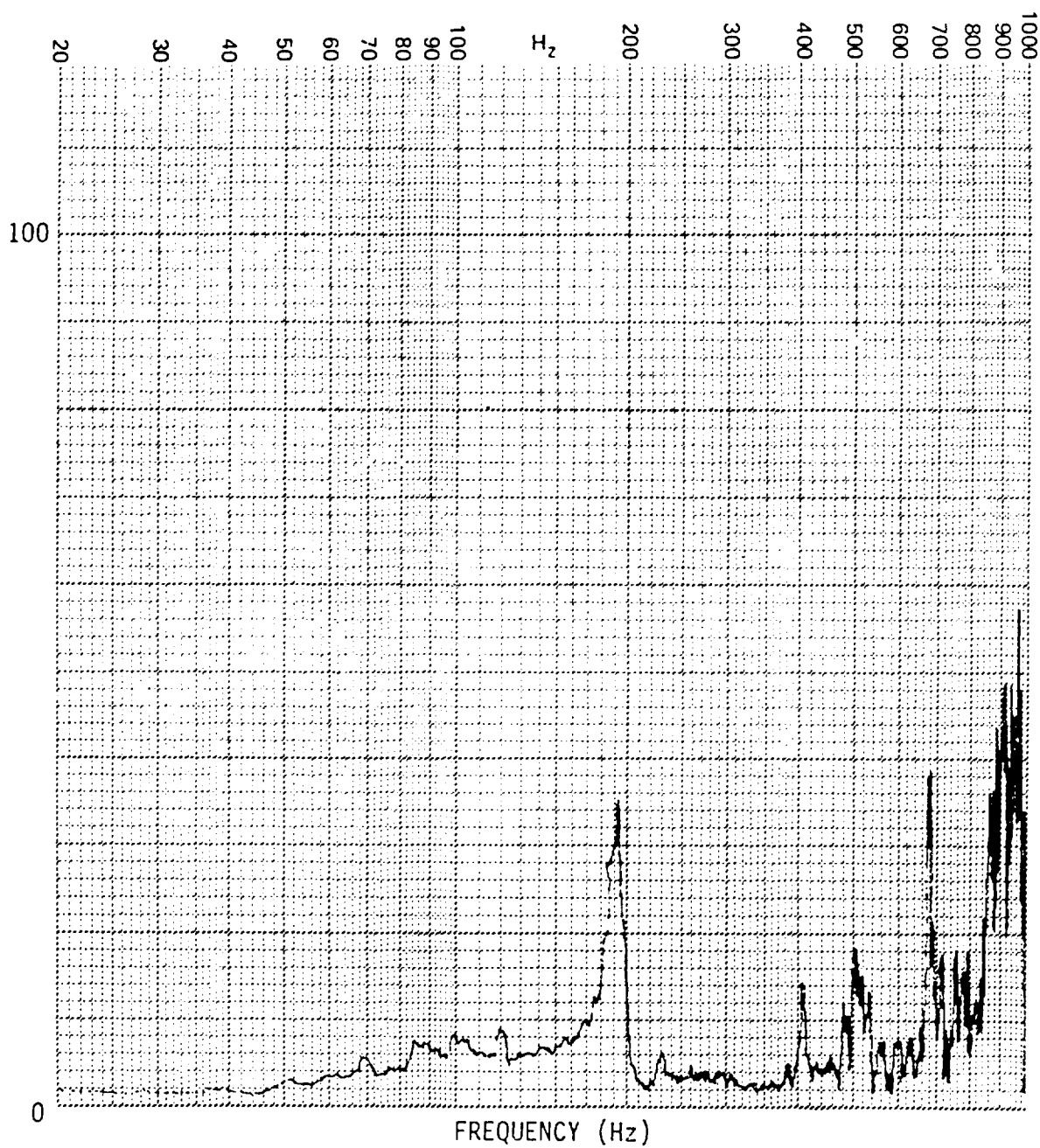Figure C-35.   Strain Spectrum for Panel g2

C-36

PANEL CONFIGURATION: ɳ2
TRANSDUCER: G10
OVERALL R.M.S. LEVEL: 400.1µe
INPUT SPECTRUM: RANDOM
INPUT LEVEL: 160 dB

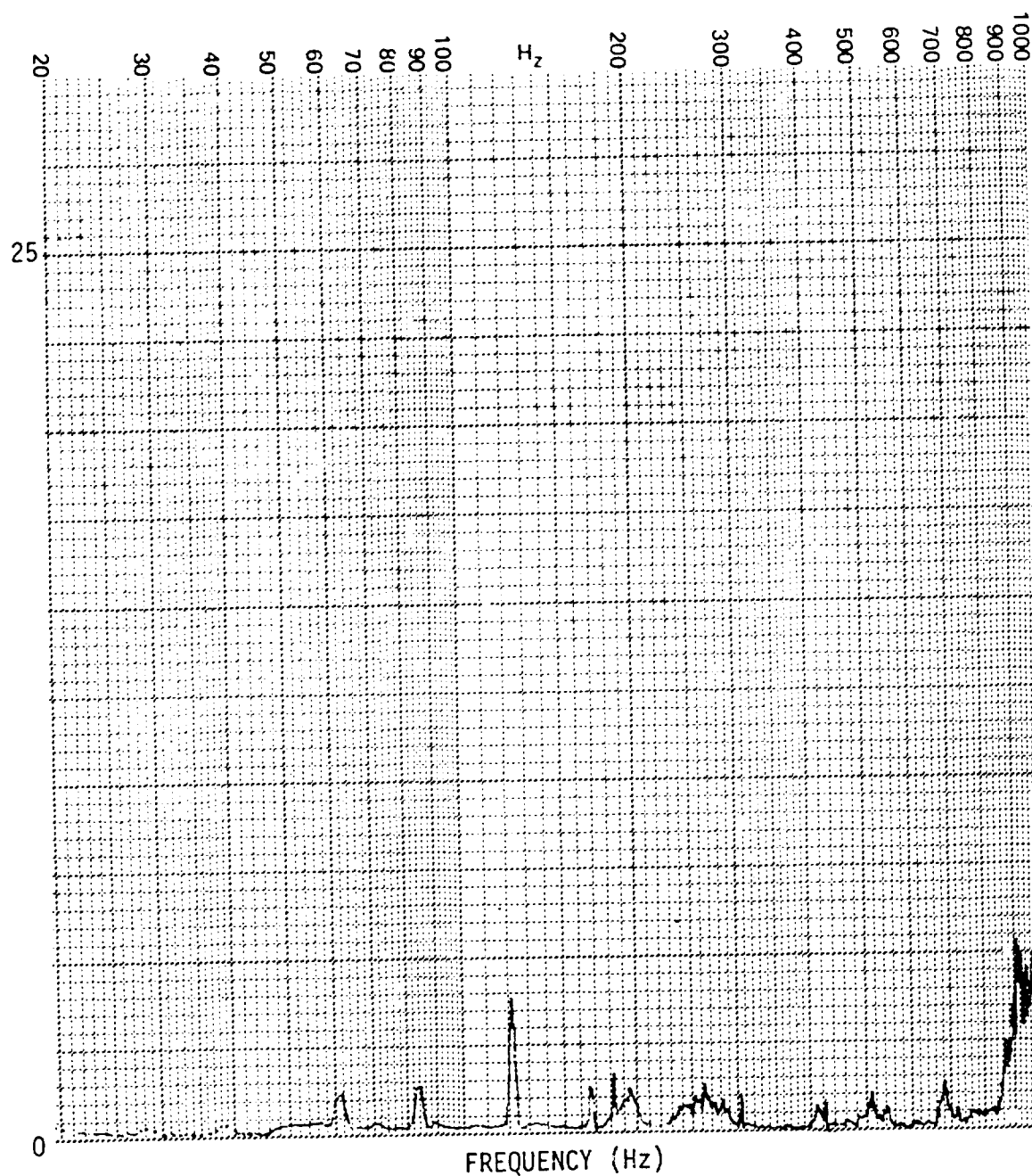
FREQUENCY (Hz)

Figure C-36.   Strain Spectrum for Panel g2

C-37

PANEL CONFIGURATION: g2
TRANSDUCER: G10
OVERALL R.M.S. LEVEL: 595.4 µe
INPUT SPECTRUM: RANDOM
INPUT LEVEL: 165 dB

Figure C-37.   Strain Spectrum for Panel g2

C-38

PANEL CONFIGURATION: h
TRANSDUCER: G10
OVERALL R.M.S. LEVEL:
INPUT SPECTRUM: SINE
INPUT LEVEL: 130 dB

FREQUENCY (Hz)

Figure C-38.   Strain Spectrum for Panel h

C-39

PANEL CONFIGURATION: h
TRANSDUCER: G10
OVERALL R.M.S. LEVEL: 54.1 µe
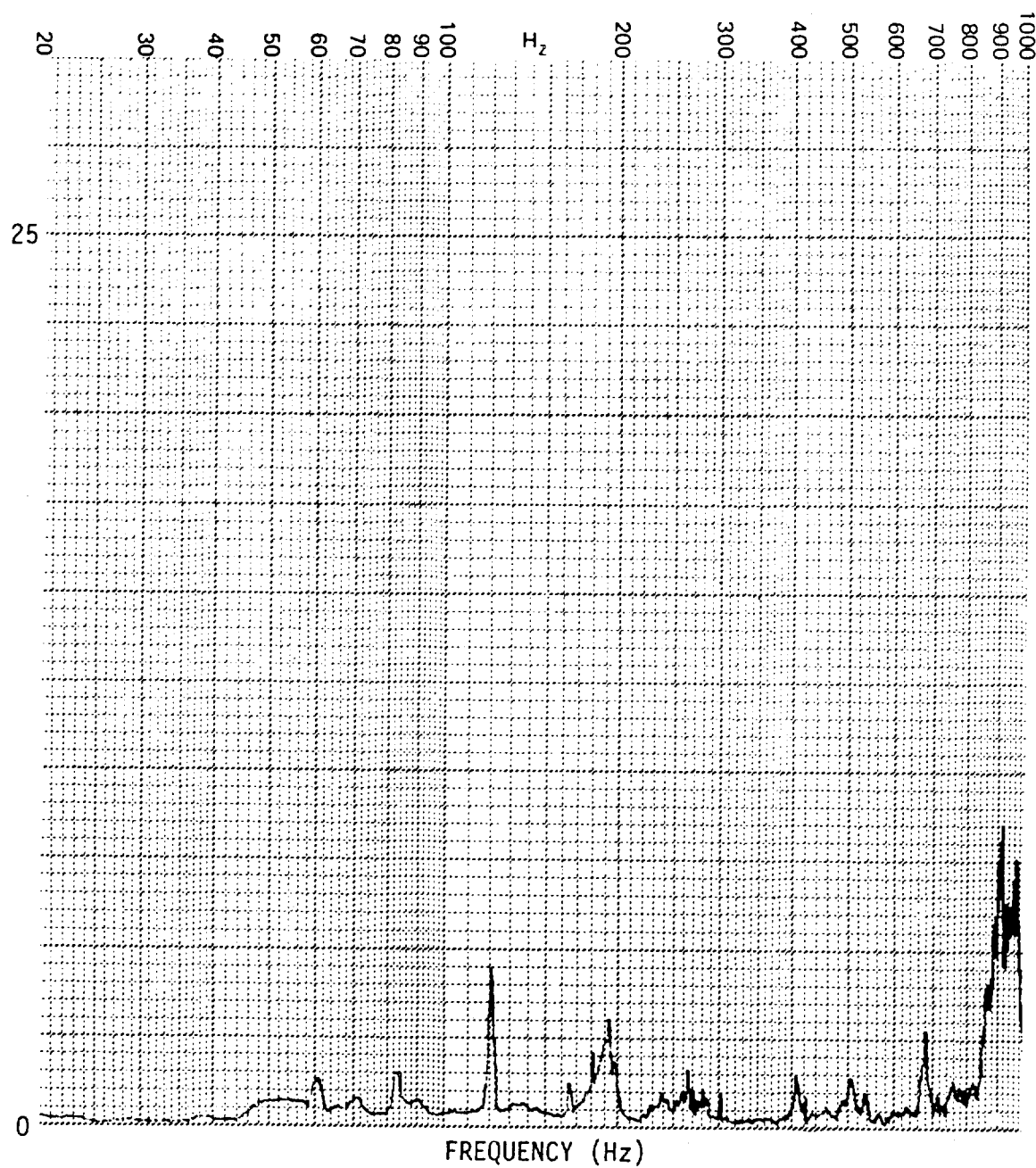INPUT SPECTRUM: RANDOM
INPUT LEVEL: 140 dB

FREQUENCY (Hz)

Figure C-39.   Strain Spectrum for Panel h

C-40

PANEL CONFIGURATION: h
TRANSDUCER: G10
OVERALL R.M.S. LEVEL: 101.1 µe
INPUT SPECTRUM: RANDOM
INPUT LEVEL: 145 dB

Figure C-40.   Strain Spectrum for Panel h

C-41

PANEL CONFIGURATION: h
TRANSDUCER: G10
OVERALL R.M.S. LEVEL: 150.2 μe
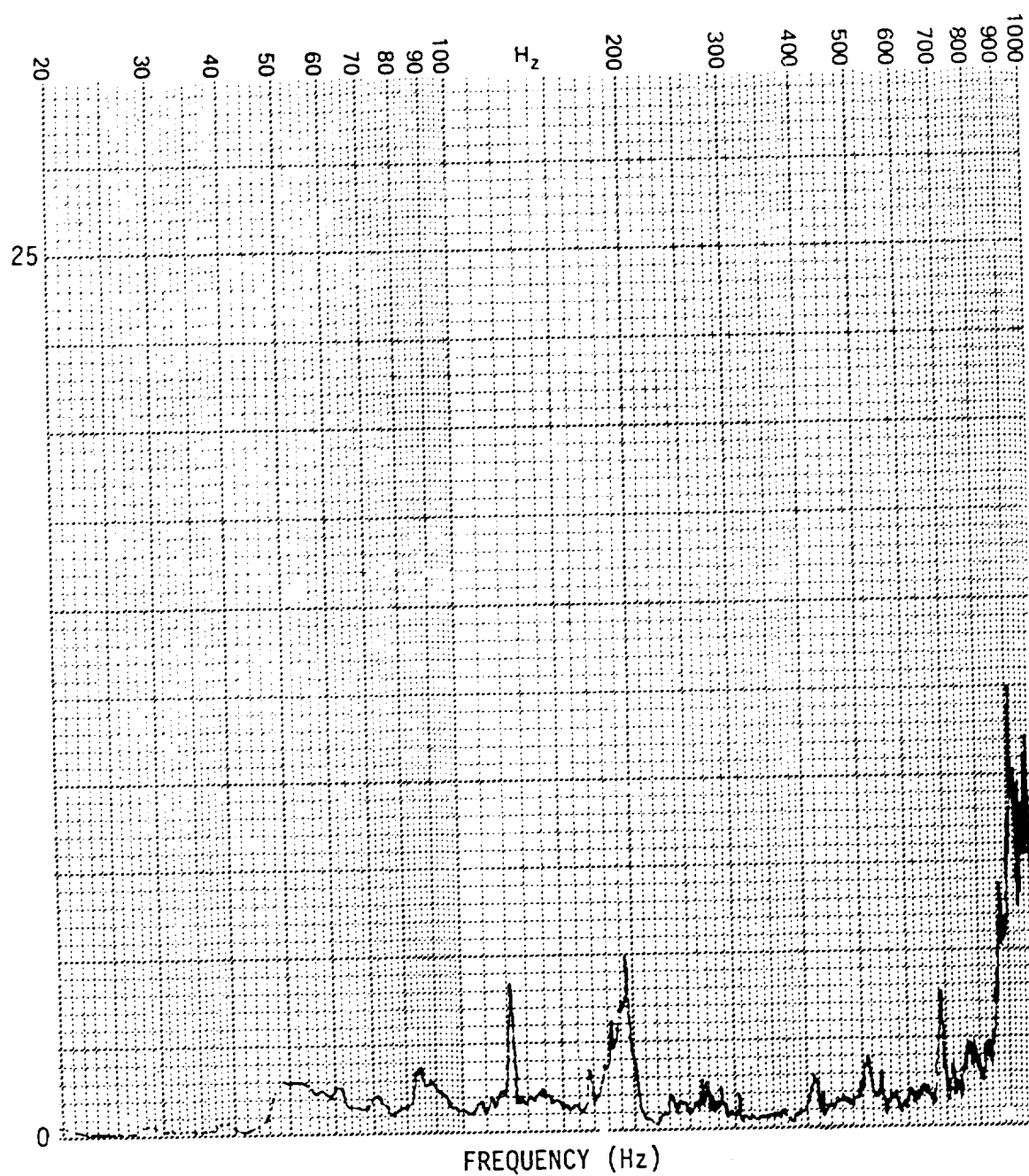INPUT SPECTRUM: RANDOM
INPUT LEVEL: 150 dB

FREQUENCY (Hz)
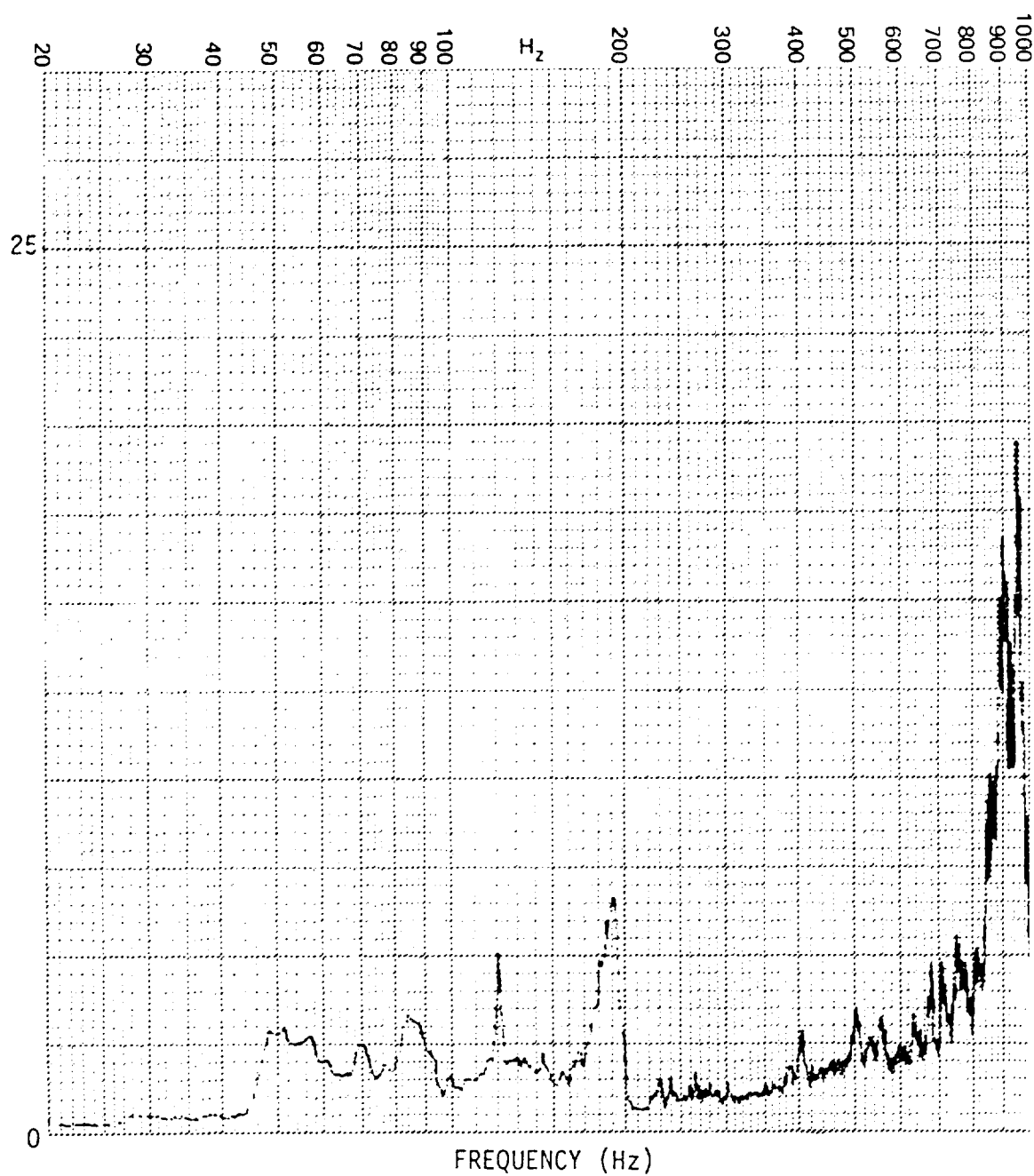
Figure C-41.   Strain Spectrum for Panel h

C-42

PANEL CONFIGURATION: h
TRANSDUCER: G10
OVERALL R.M.S. LEVEL: 285.7 μ∈
INPUT SPECTRUM: RANDOM
INPUT LEVEL: 155 dB

Figure C-42. Strain Spectrum for Panel h

C-43

PANEL CONFIGURATION: h
TRANSDUCER: G10
OVERALL R.M.S. LEVEL: 465.5 μe
INPUT SPECTRUM: RANDOM
INPUT LEVEL: 160 dB

Figure C-43. Strain Spectrum for Panel h

C-44

PANEL CONFIGURATION: h
TRANSDUCER: G10
OVERALL R.M.S. LEVEL: 720.6 με
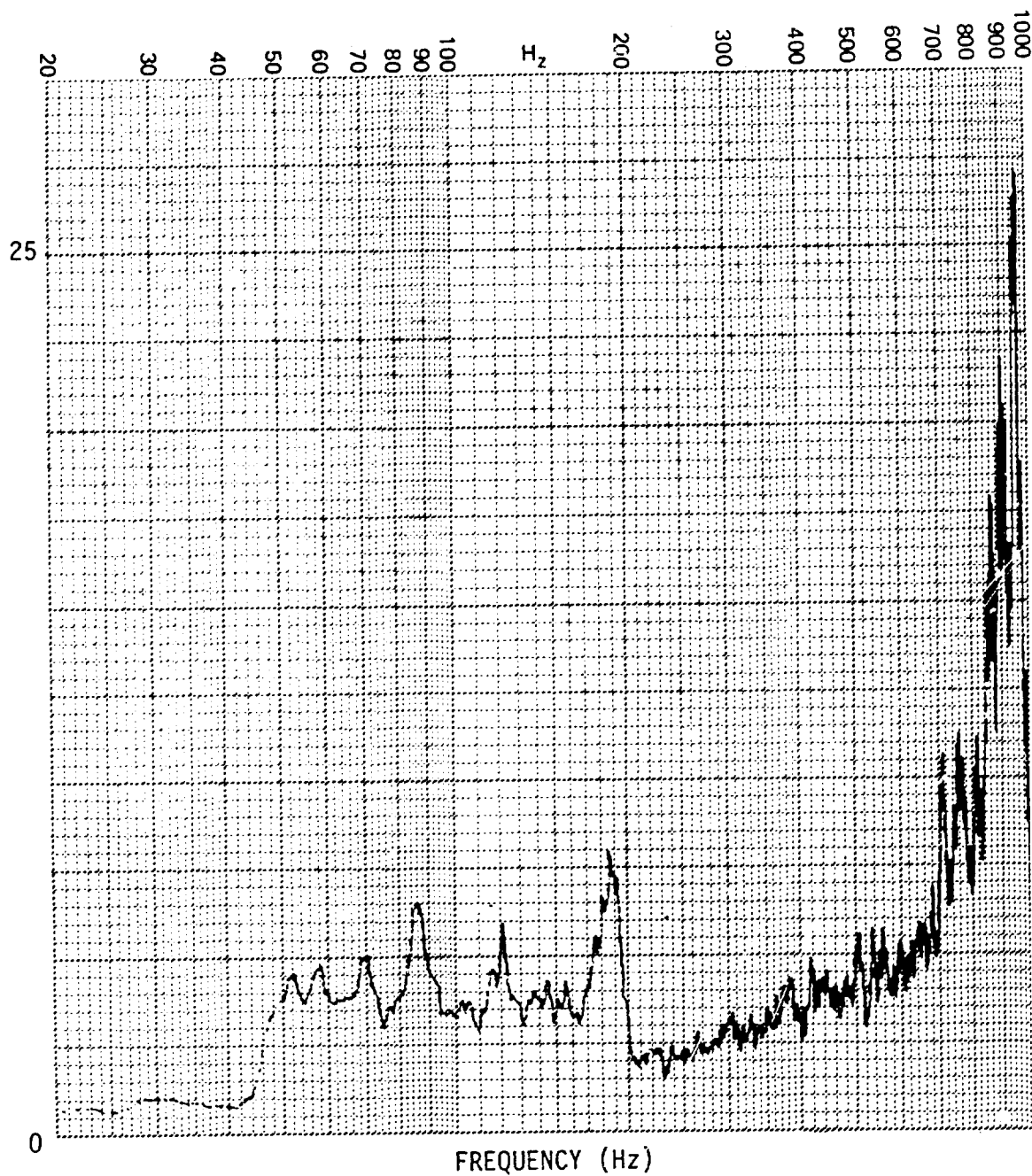INPUT SPECTRUM: RANDOM
INPUT LEVEL: 165 dB
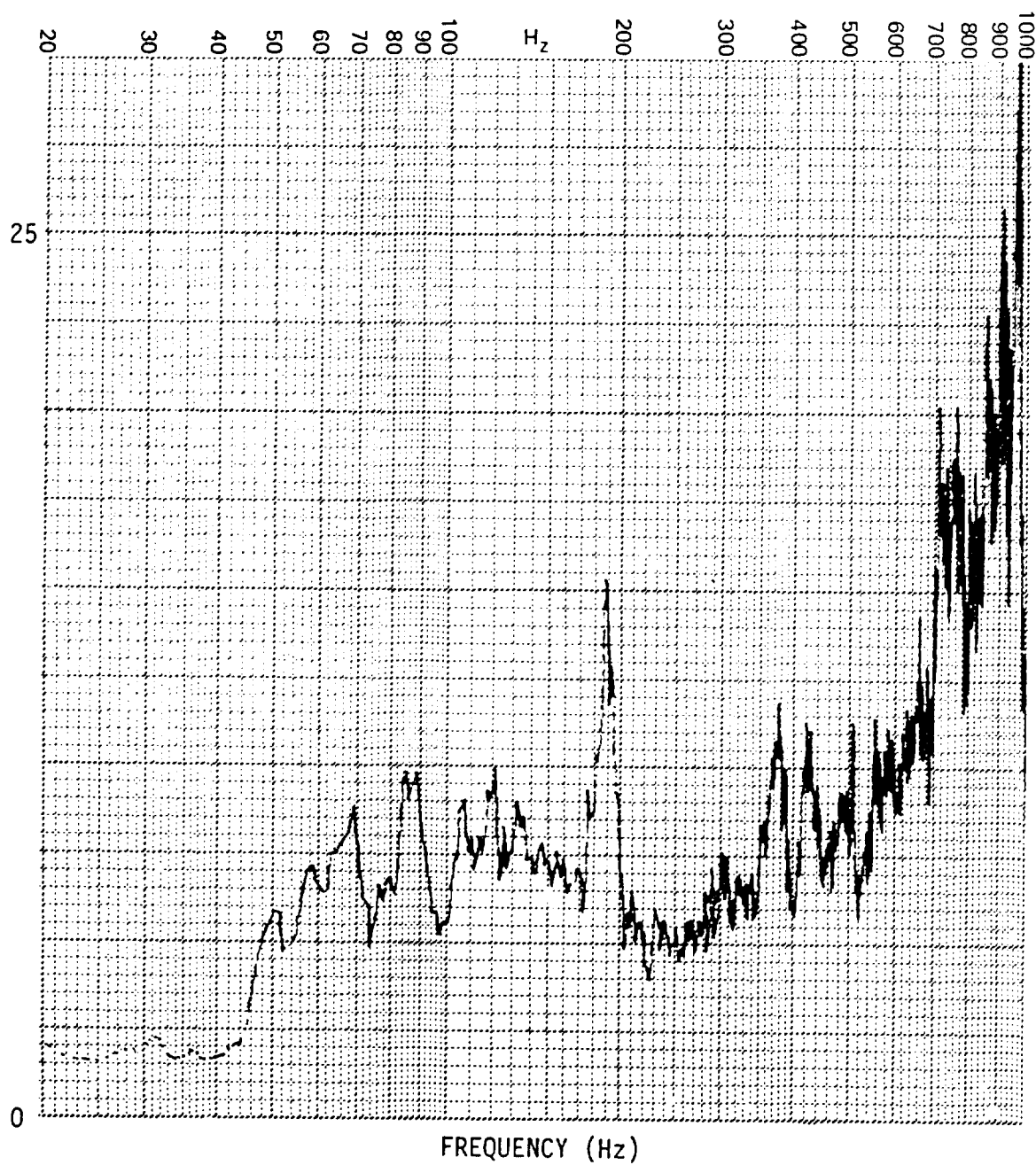

Figure C-44. Strain Spectrum for Panel h

C-45

PANEL CONFIGURATION: i
TRANSDUCER: G10
OVERALL R.M.S. LEVEL:
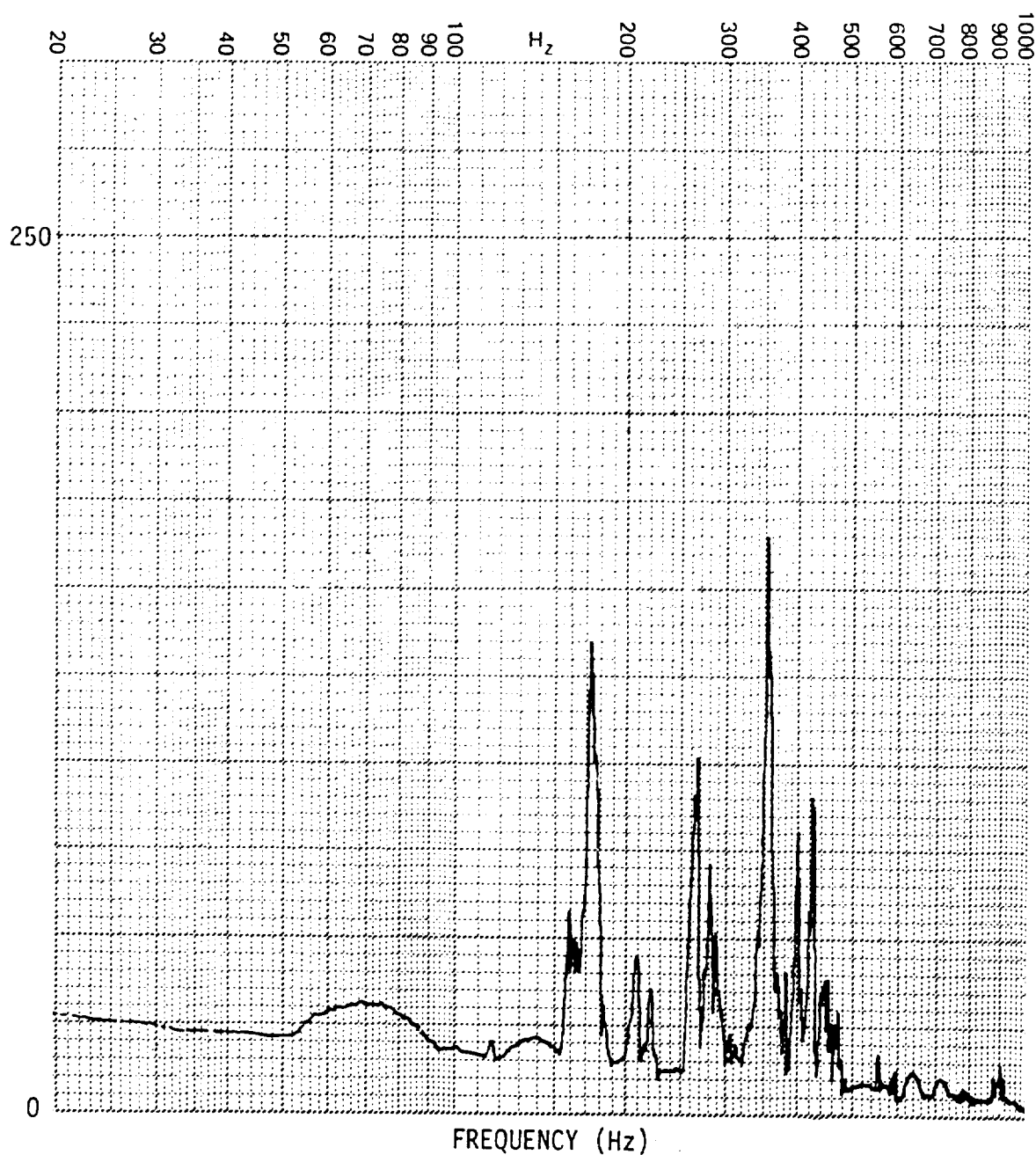INPUT SPECTRUM: SINE
INPUT LEVEL: 130 dB

Figure C-45. Strain Spectrum for Panel i

PANEL CONFIGURATION: i
TRANSDUCER: G10
OVERALL R.M.S. LEVEL: 25.7µϵ
INPUT SPECTRUM: RANDOM
INPUT LEVEL: 140 dB

FREQUENCY (Hz)

Figure C-46.   Strain Spectrum for Panel i

C-47

PANEL CONFIGURATION: i
TRANSDUCER: G10
OVERALL R.M.S. LEVEL: 47.3 μe
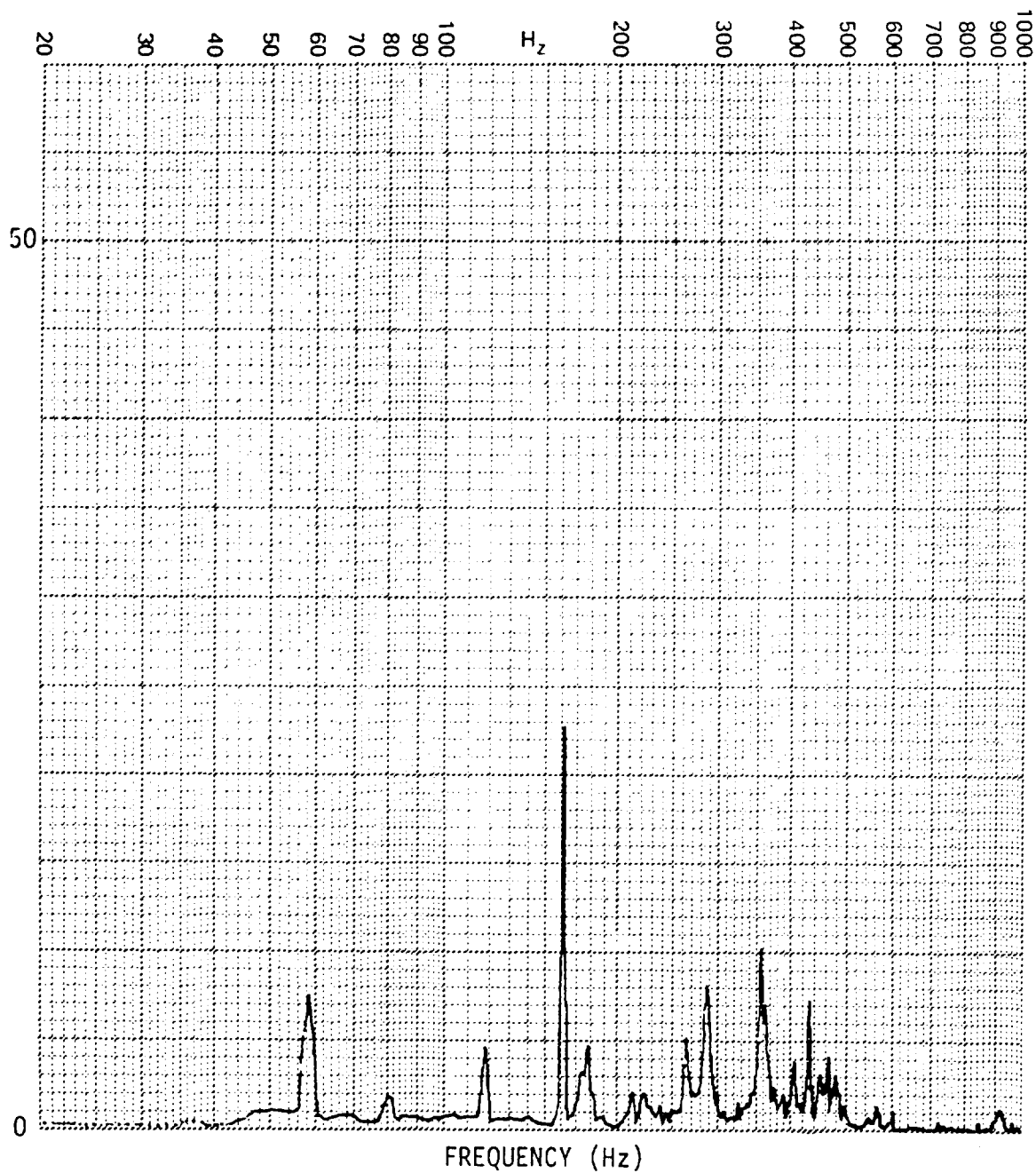INPUT SPECTRUM: RANDOM
INPUT LEVEL: 145 dB

Figure C-47.   Strain Spectrum for Panel i

PANEL CONFIGURATION: i
TRANSDUCER: G10
OVERALL R.M.S. LEVEL: 84.3μe
INPUT SPECTRUM: RANDOM
INPUT LEVEL: 150 dB

Figure C-48.   Strain Spectrum for Panel i

PANEL CONFIGURATION: i
TRANSDUCER: G10
OVERALL R.M.S. LEVEL: 133.1με
INPUT SPECTRUM: RANDOM
INPUT LEVEL: 155 dB

Figure C-49. Strain Spectrum for Panel i

PANEL CONFIGURATION: i
TRANSDUCER: G10
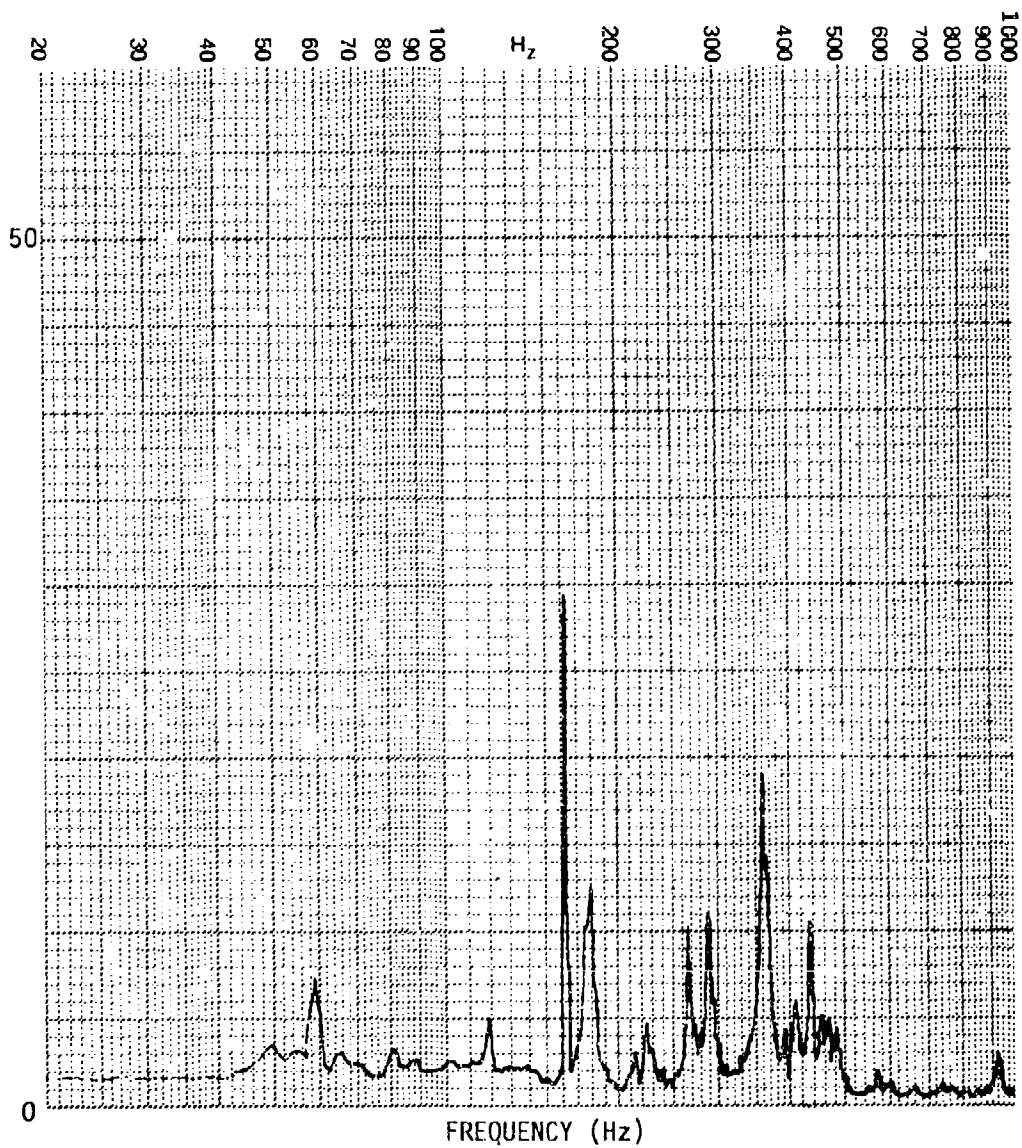OVERALL R.M.S. LEVEL: 168.2 μe
INPUT SPECTRUM: RANDOM
INPUT LEVEL: 160 dB

Figure C-50. Strain Spectrum for Panel i

C-51

PANEL CONFIGURATION: i
TRANSDUCER: G10
OVERALL R.M.S. LEVEL: 256.0 μe
INPUT SPECTRUM: RANDOM
INPUT LEVEL: 165 dB

Figure C-51.   Strain Spectrum for Panel i

PANEL CONFIGURATION: j
TRANSDUCER: G10
OVERALL R.M.S. LEVEL:
INPUT SPECTRUM: SINE
INPUT LEVEL: 130 dB

Figure C-52. Strain Spectrum for Panel j

PANEL CONFIGURATION: j
TRANSDUCER: G10
OVERALL R.M.S. LEVEL: 41.3μe
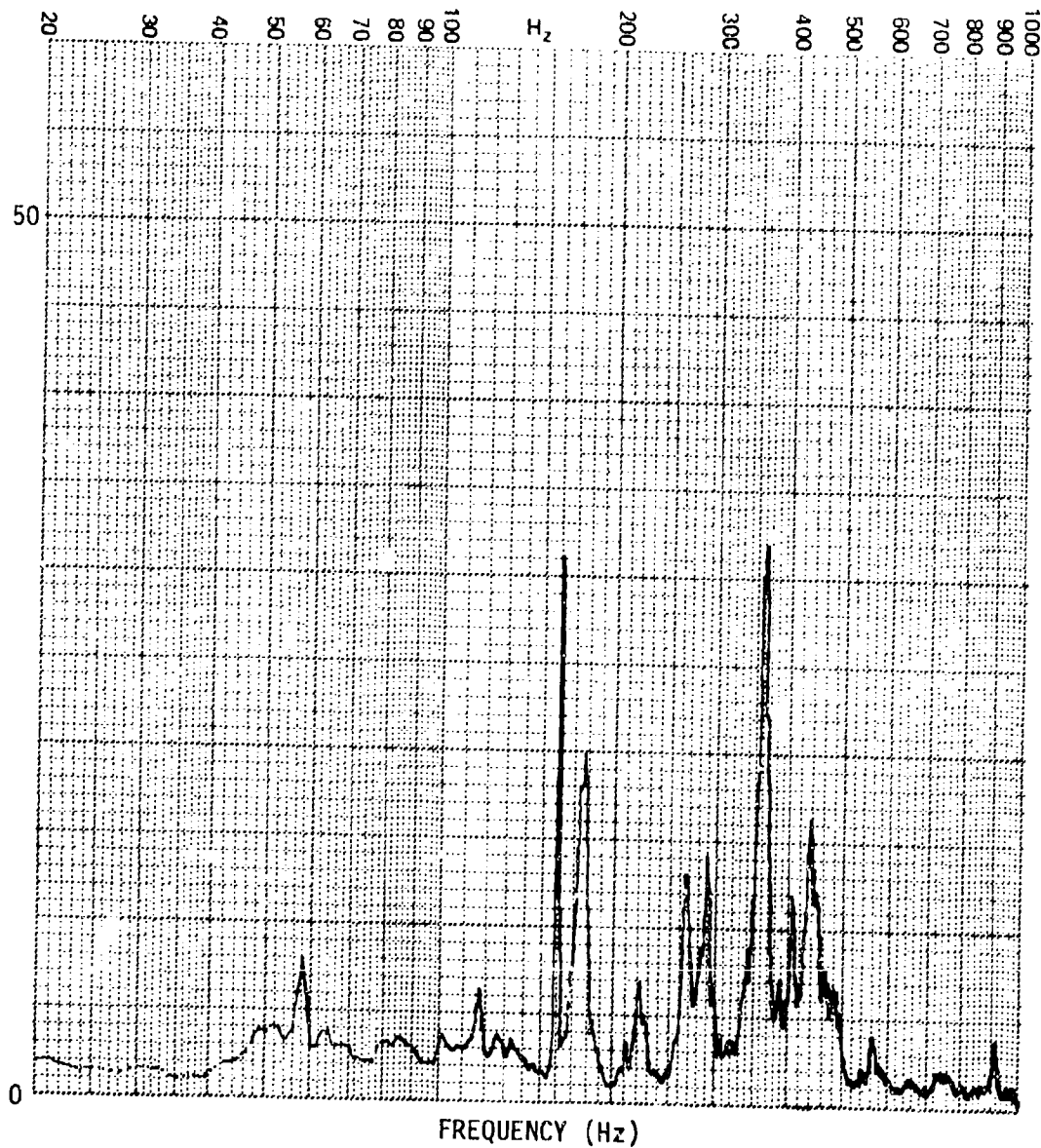INPUT SPECTRUM: RANDOM
INPUT LEVEL: 140 dB
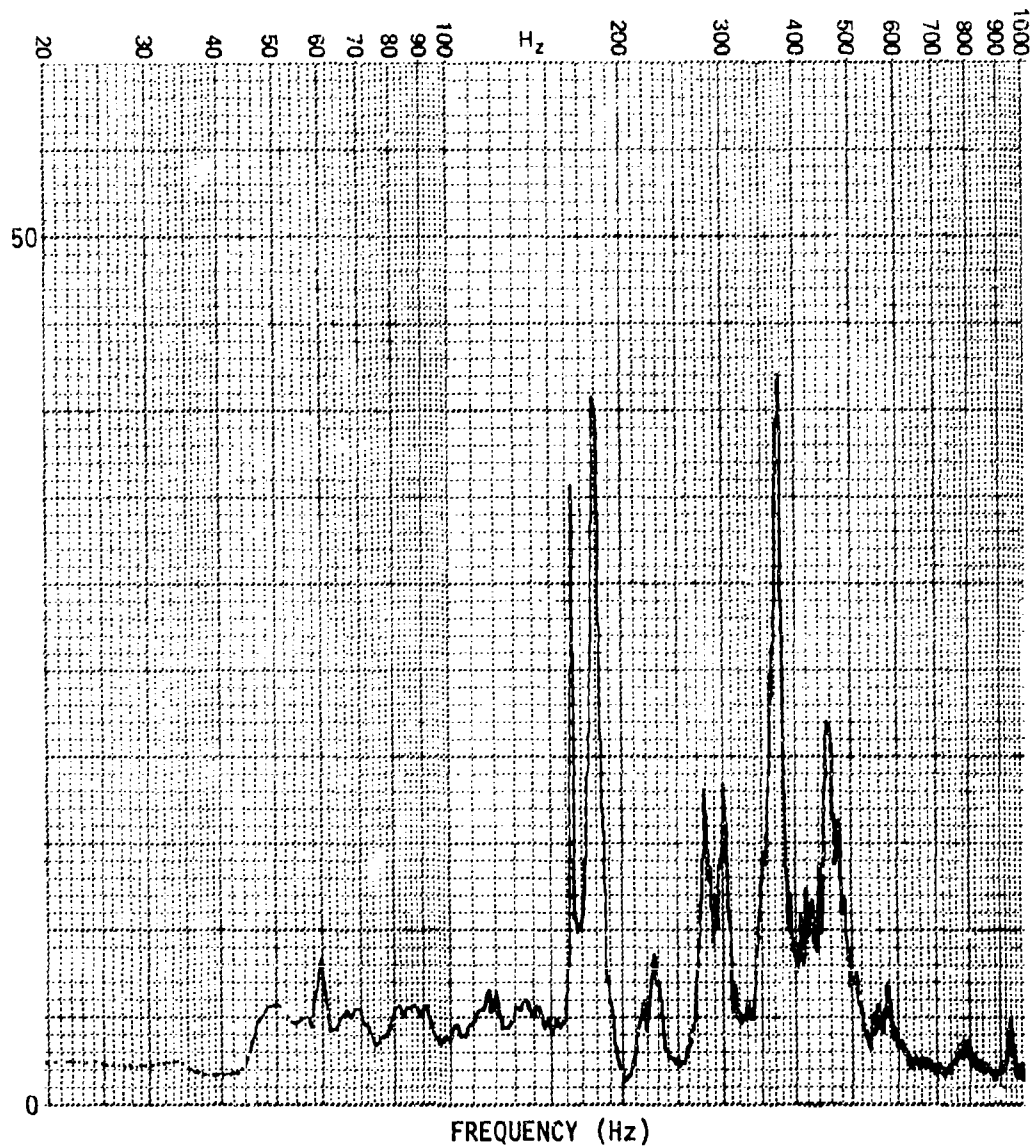

Figure C-53. Strain Spectrum for Panel j

C-54

PANEL CONFIGURATION: j
TRANSDUCER: G10
OVERALL R.M.S. LEVEL: 59.0 μe
INPUT SPECTRUM: RANDOM
INPUT LEVEL: 145 dB

Figure C-54.   Strain Spectrum for Panel j

PANEL CONFIGURATION: j
TRANSDUCER: G10
OVERALL R.M.S. LEVEL: 86.1μe
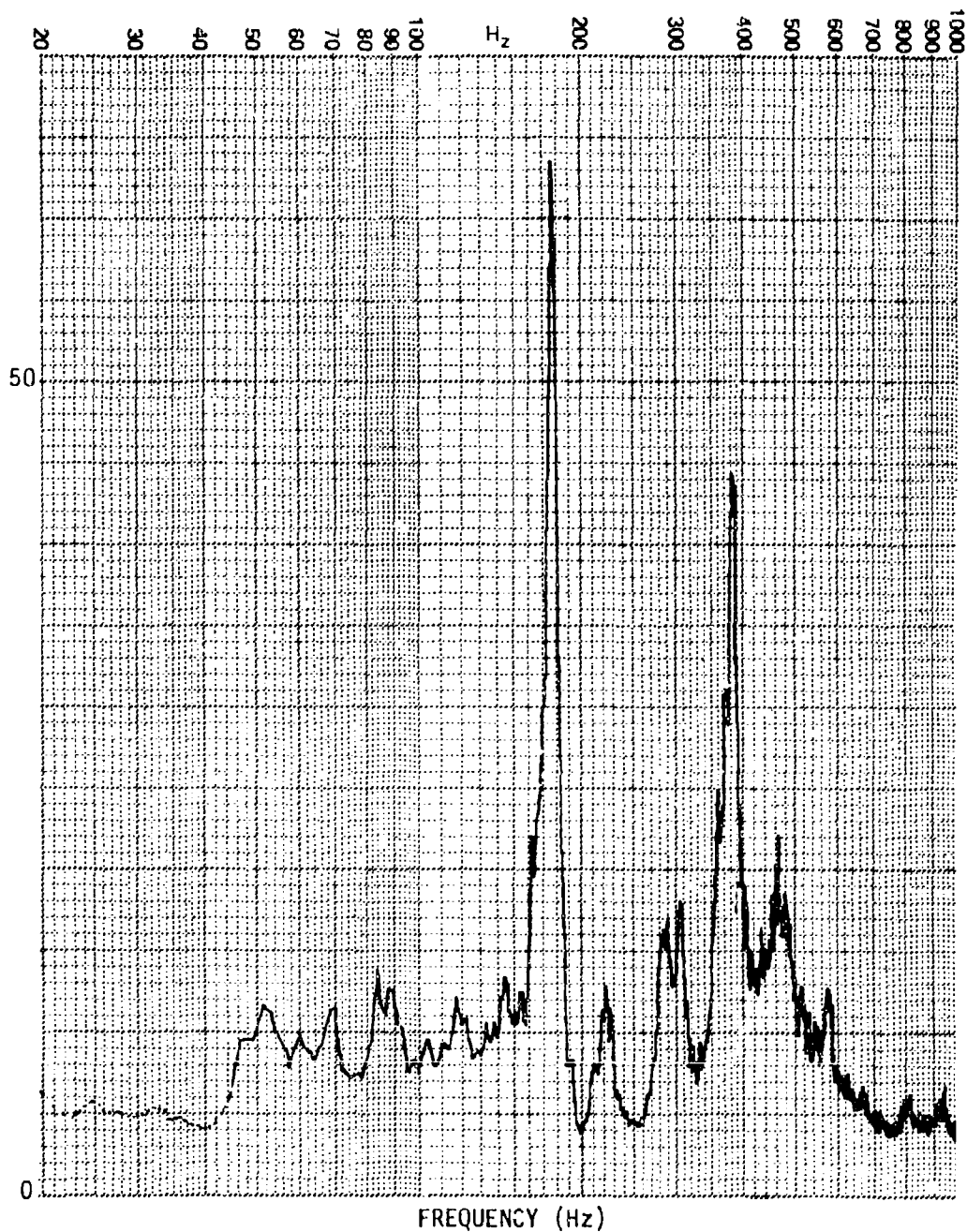INPUT SPECTRUM: RANDOM
INPUT LEVEL: 150 dB

Figure C-55. Strain Spectrum for Panel j

PANEL CONFIGURATION: j
TRANSDUCER: G10
OVERALL R.M.S. LEVEL: 137.3
INPUT SPECTRUM: RANDOM
INPUT LEVEL: 155 dB
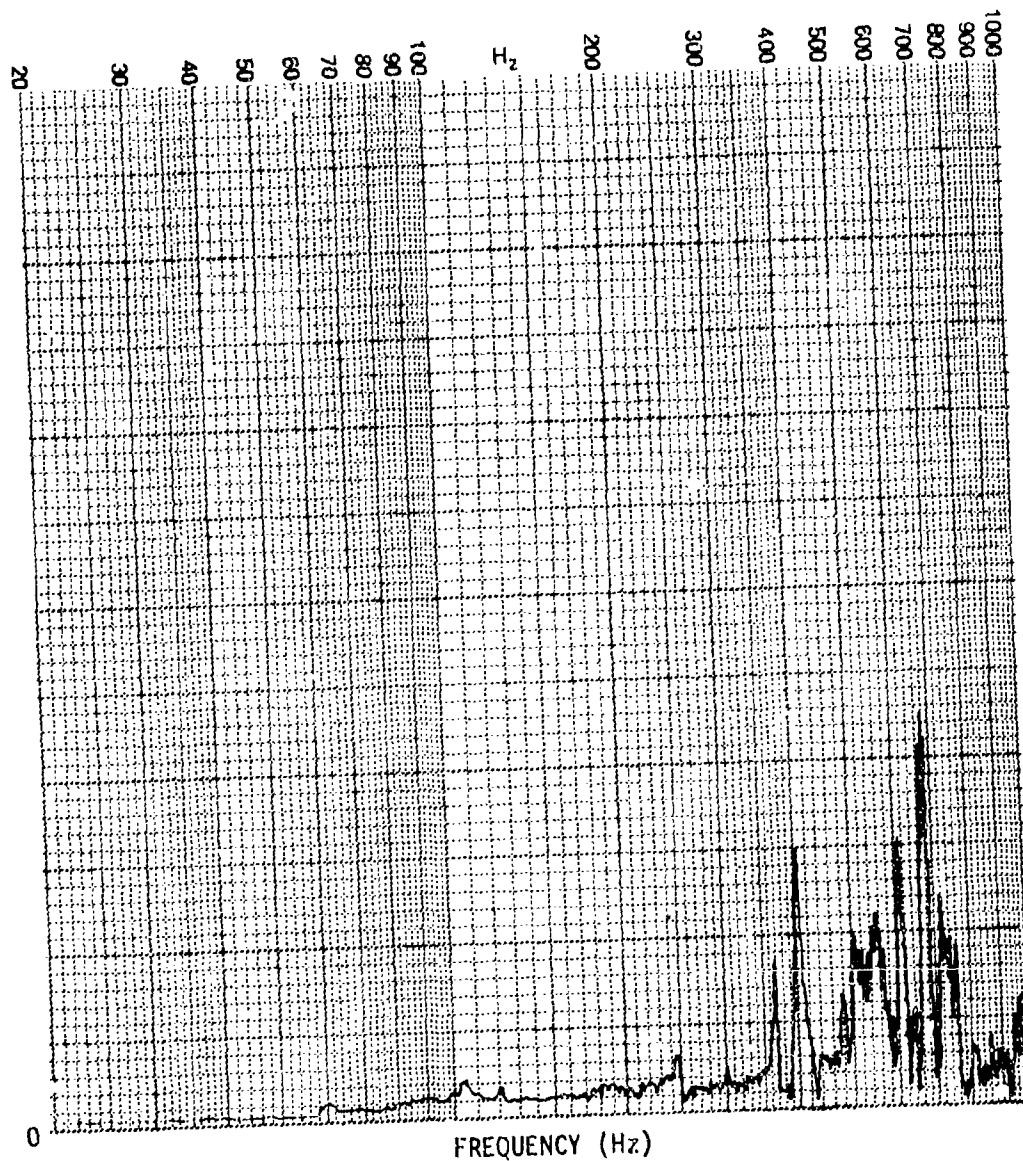

Figure C-56.   Strain Spectrum for Panel j

PANEL CONFIGURATION: j
TRANSDUCER: G10
OVERALL R.M.S. LEVEL: 215.8 μe
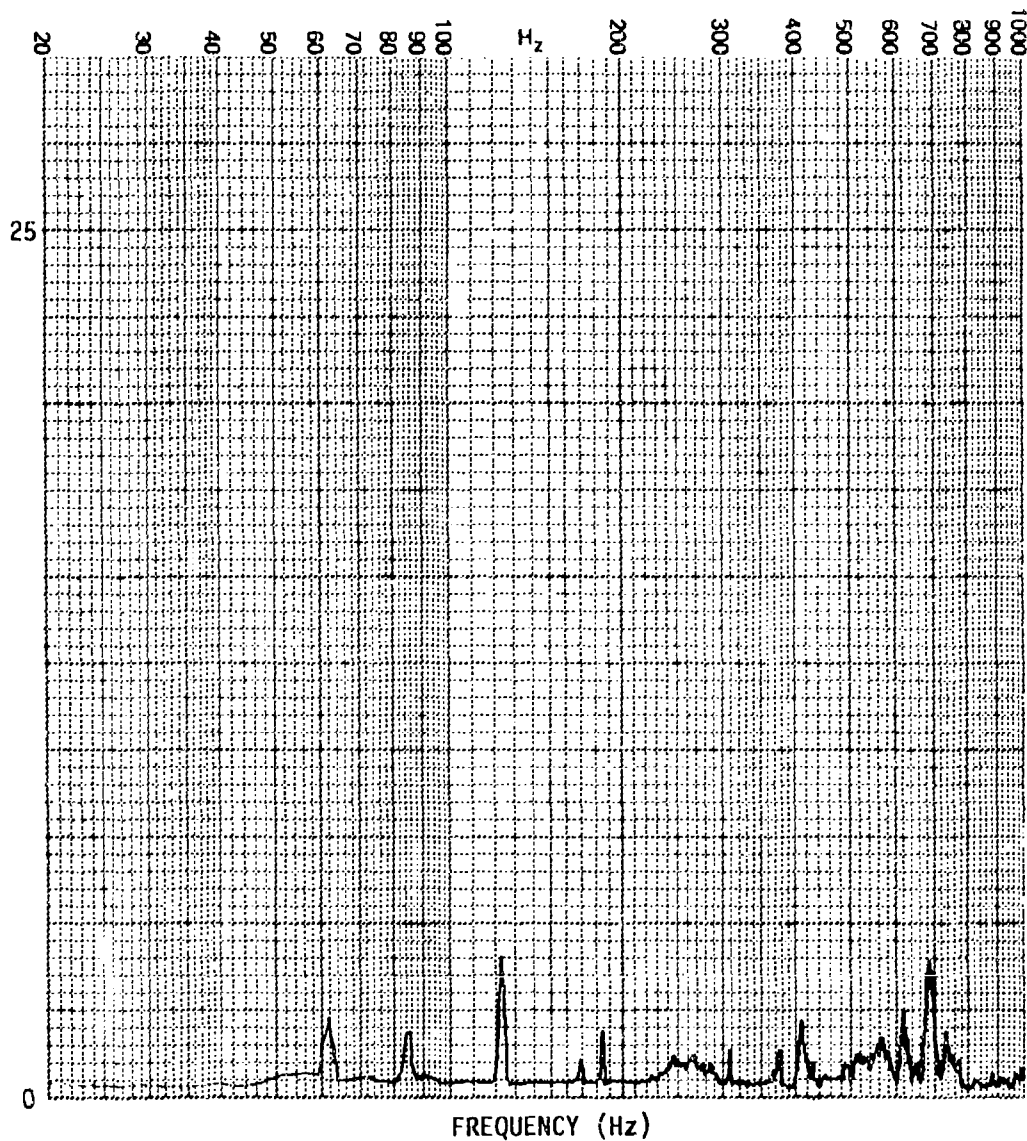INPUT SPECTRUM: RANDOM
INPUT LEVEL: 160 dB

Figure C-57.   Strain Spectrum for Panel j

PANEL CONFIGURATION: j
TRANSDUCER: G10
OVERALL R.M.S. LEVEL: 311.5μe
INPUT SPECTRUM: RANDOM
INPUT LEVEL: 165 dB

Figure C-58. Strain Spectrum for Panel j

PANEL CONFIGURATION: k1
TRANSDUCER: G10
OVERALL R.M.S. LEVEL:
INPUT SPECTRUM: SINE
INPUT LEVEL: 130 dB

Figure C-59.   Strain Spectrum for Panel k1

PANEL CONFIGURATION: k1
TRANSDUCER: G10
OVERALL R.M.S. LEVEL: 50.2 μe
INPUT SPECTRUM: RANDOM
INPUT LEVEL: 140 dB

Figure C-60.   Strain Spectrum for Panel k1

PANEL CONFIGURATION: k1
TRANSDUCER: G10
OVERALL R.M.S. LEVEL: 83.5µe
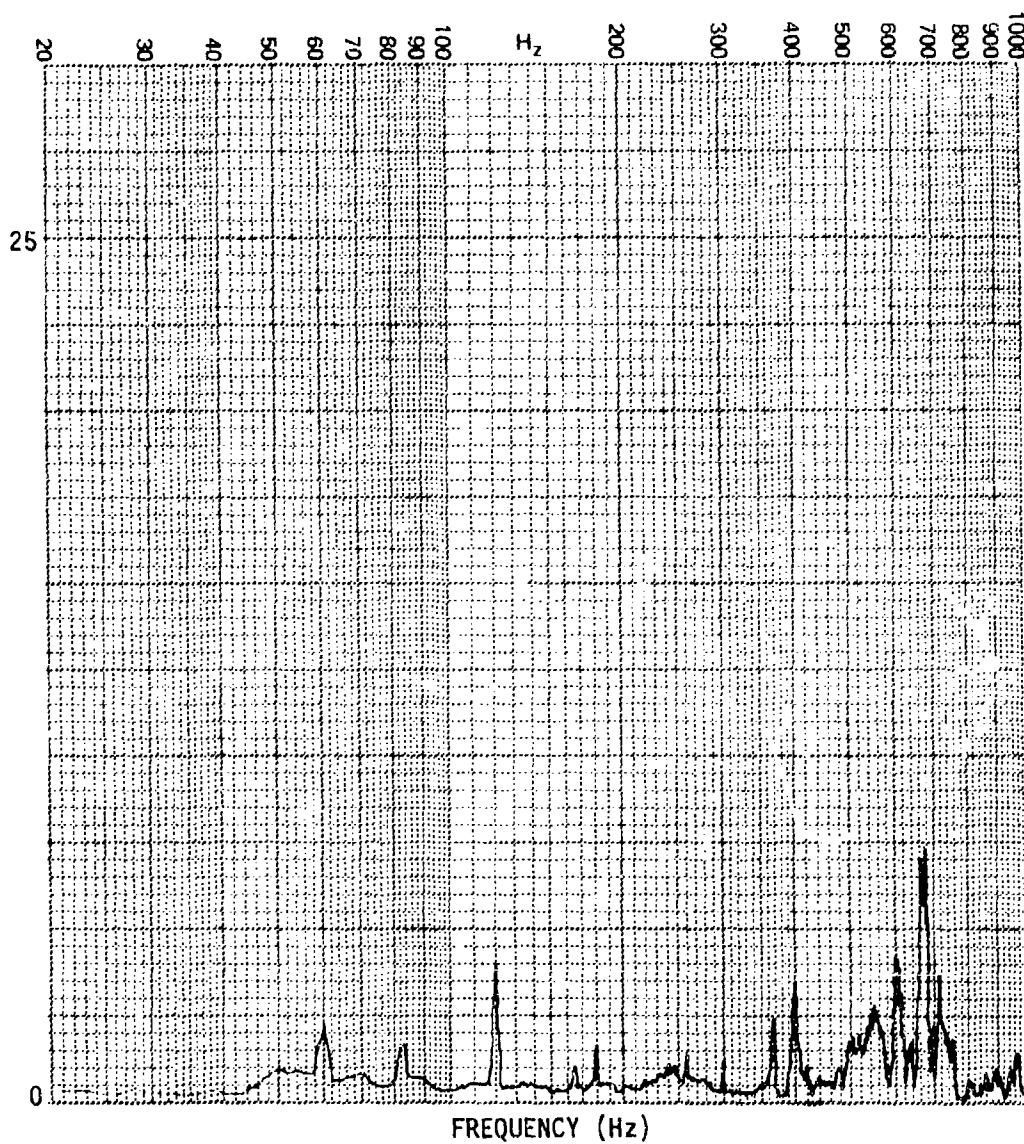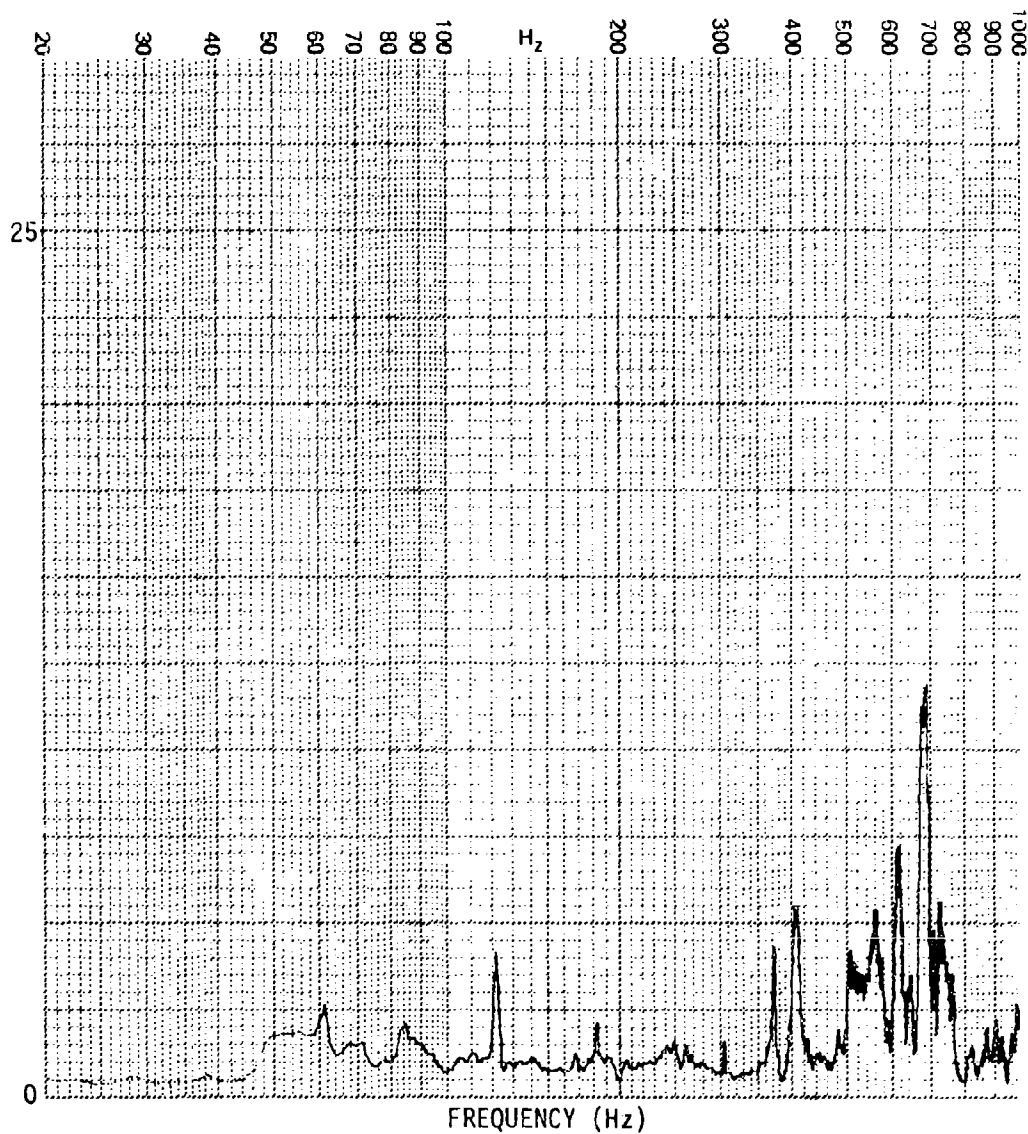INPUT SPECTRUM: RANDOM
INPUT LEVEL: 145 dB

Figure C-61. Strain Spectrum for Panel k1

C-62

PANEL CONFIGURATION: k1
TRANSDUCER: G10
OVERALL R.M.S. LEVEL: 142.4 με
INPUT SPECTRUM: RANDOM
INPUT LEVEL: 150 dB

Figure C-62. Strain Spectrum for Panel k1

PANEL CONFIGURATION: k1
TRANSDUCER: G10
OVERALL R.M.S. LEVEL: 210.7 ue
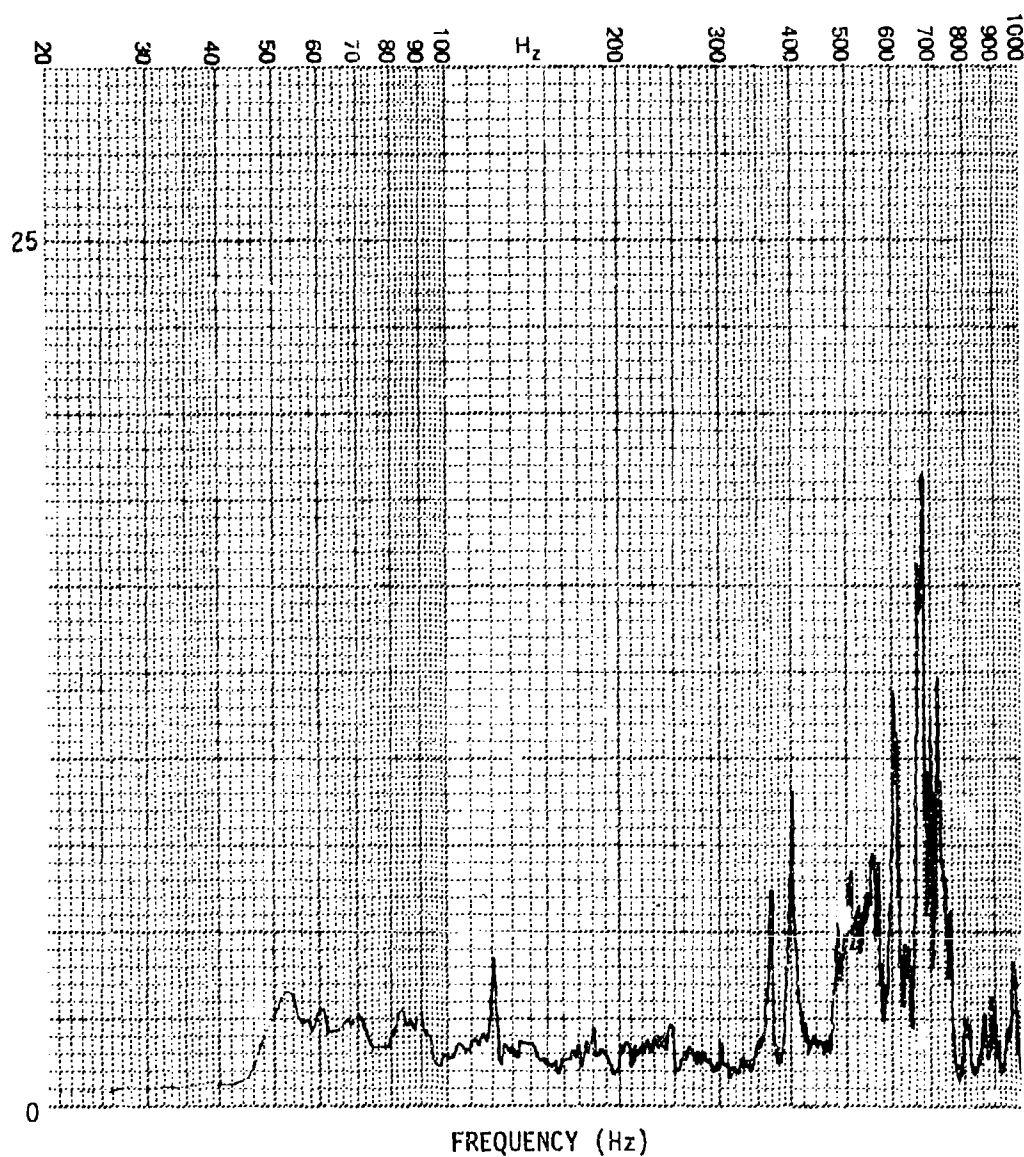INPUT SPECTRUM: RANDOM
INPUT LEVEL: 155 dB

Figure C-63. Strain Spectrum for Panel k1

C-64

PANEL CONFIGURATION: k1
TRANSDUCER: G10
OVERALL R.M.S. LEVEL: 295.0μe
INPUT SPECTRUM: RANDOM
INPUT LEVEL: 160 dB

FREQUENCY (Hz)

Figure C-64. Strain Spectrum for Panel k1

C-65

PANEL CONFIGURATION: I
TRANSDUCER: G10
OVERALL R.M.S. LEVEL:
INPUT SPECTRUM: SINE
INPUT LEVEL: 130 dB
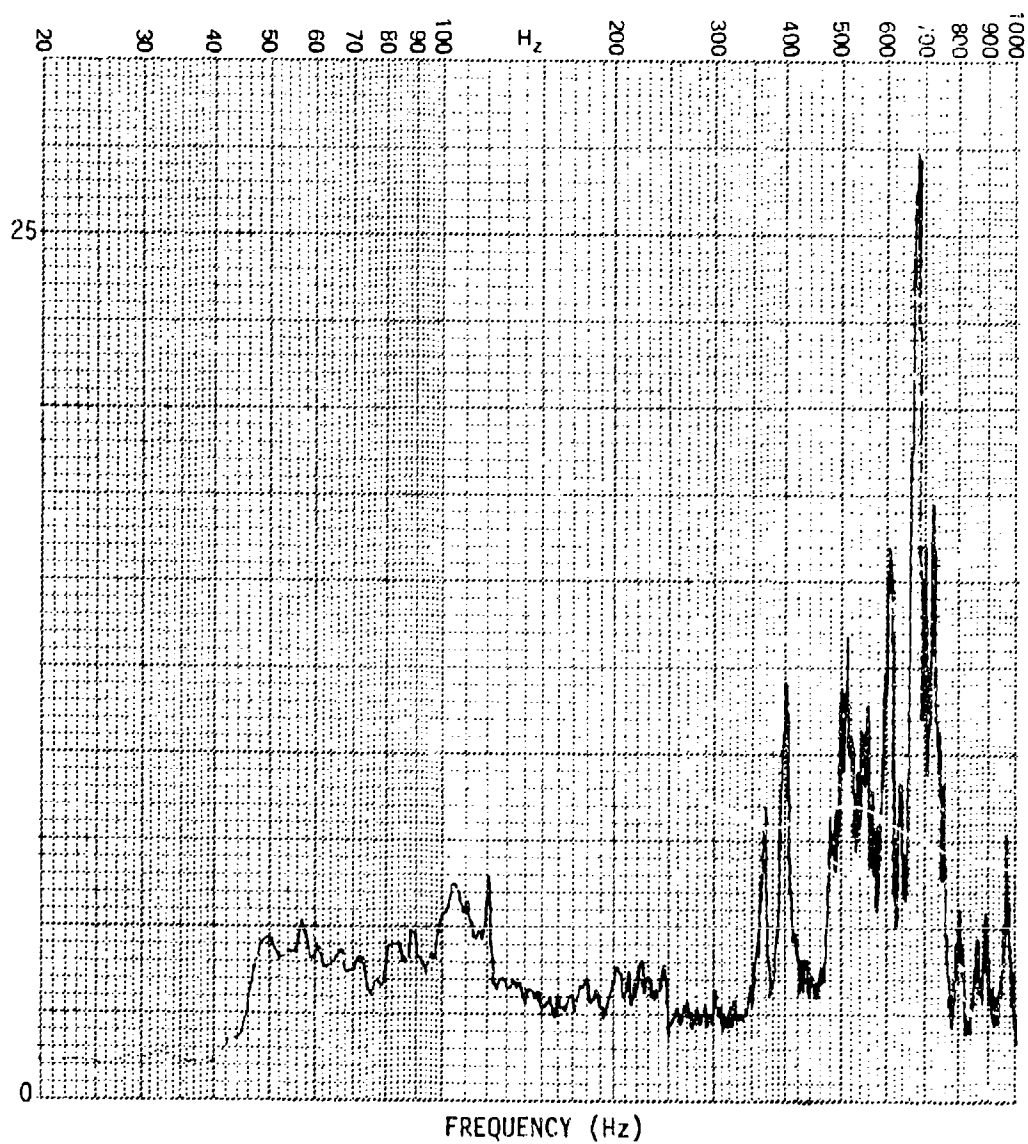

FREQUENCY (Hz)

Figure C-65. Strain Spectrum for Panel 1

PANEL CONFIGURATION: I
TRANSDUCER: G10
OVERALL R.M.S. LEVEL: 28.0μe
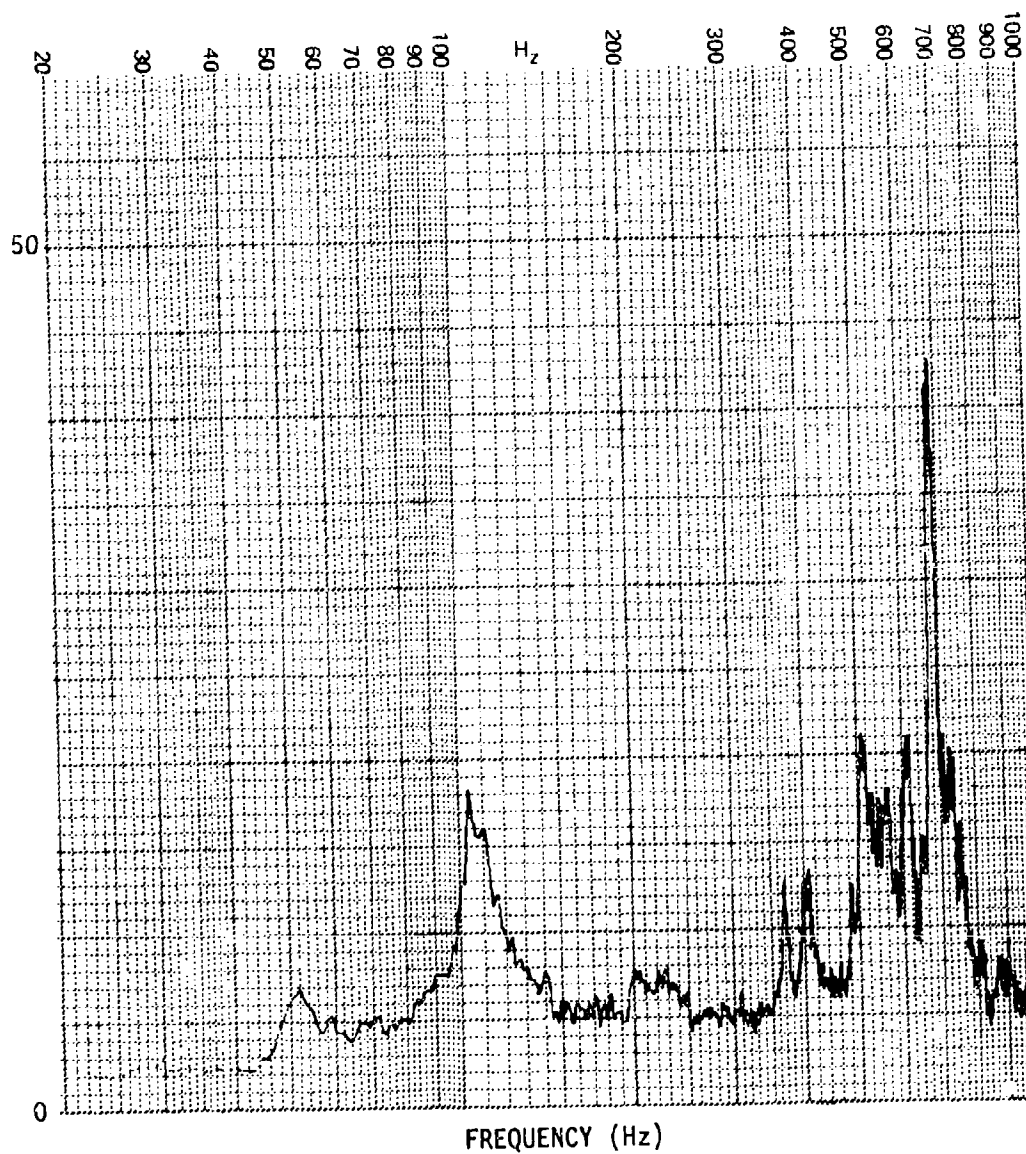INPUT SPECTRUM: RANDOM
INPUT LEVEL: 140 dB

FREQUENCY (Hz)

Figure C-66.   Strain Spectrum for Panel 1

C-67

PANEL CONFIGURATION: I
TRANSDUCER: G10
OVERALL R.M.S. LEVEL: 43.1μe
INPUT SPECTRUM: RANDOM
INPUT LEVEL: 145 dB
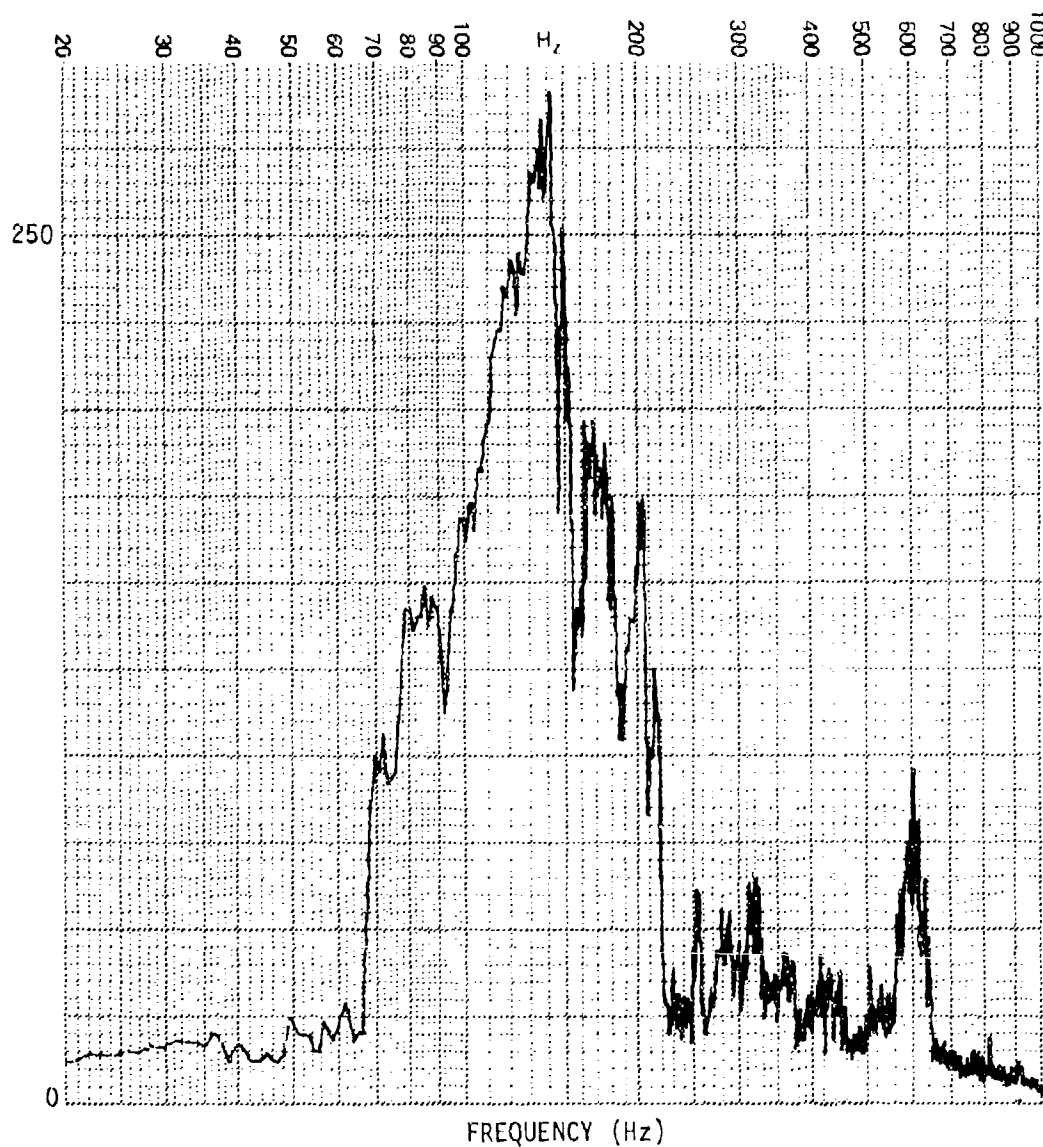

Figure C-67.   Strain Spectrum for Panel 1

C-68

PANEL CONFIGURATION: I
TRANSDUCER: G10
OVERALL R.M.S. LEVEL: 68.3μe
INPUT SPECTRUM: RANDOM
INPUT LEVEL: 150 dB

Figure C-68. Strain Spectrum for Panel 1

C-69

PANEL CONFIGURATION: I
TRANSDUCER: G10
OVERALL R.M.S. LEVEL: 108.8 µe
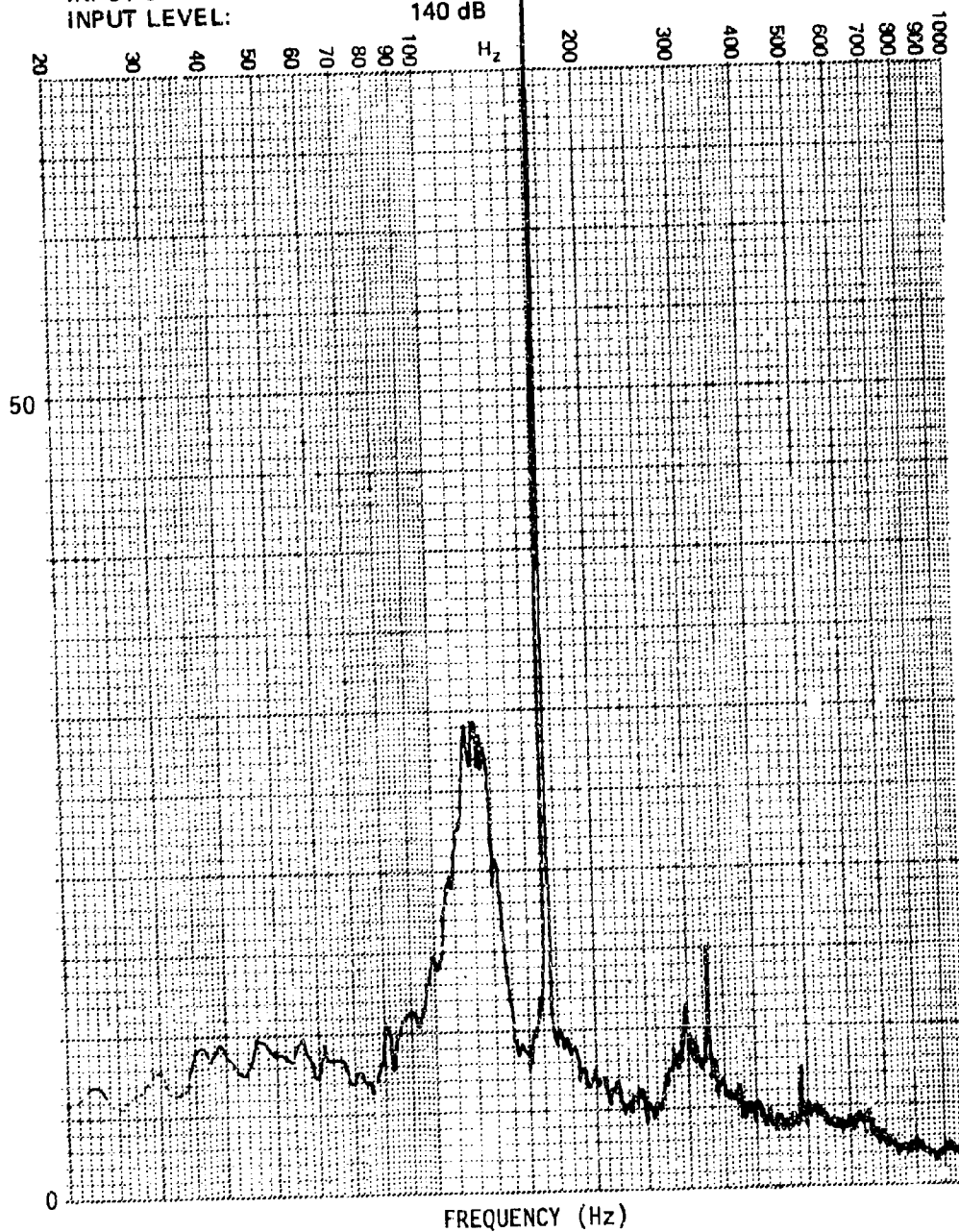INPUT SPECTRUM: RANDOM
INPUT LEVEL: 155 dB

Figure C-69.   Strain Spectrum for Panel 1

C-70

PANEL CONFIGURATION: I
TRANSDUCER: G10
OVERALL R.M.S. LEVEL: 179.3µe
INPUT SPECTRUM: RANDOM
INPUT LEVEL: 160 dB
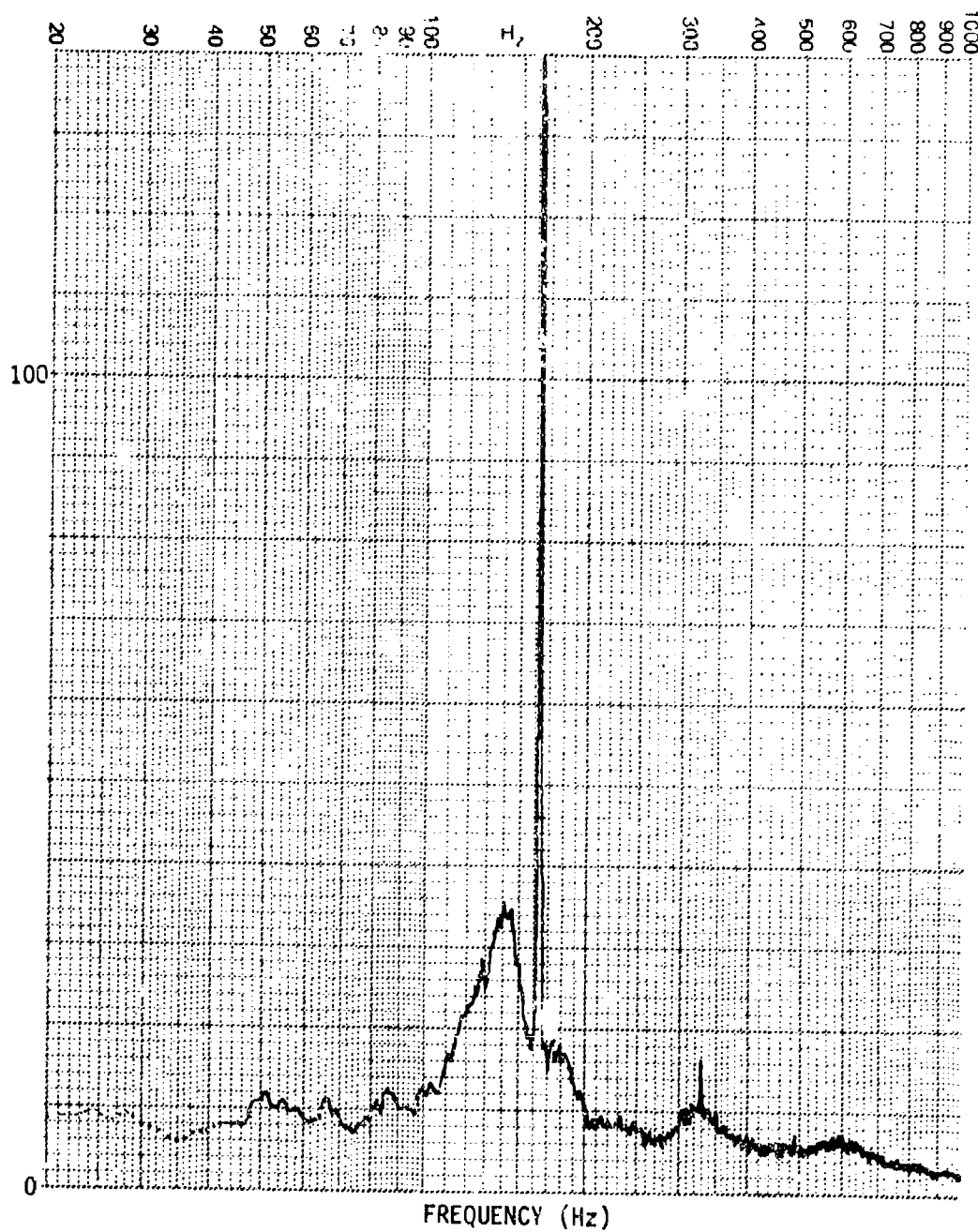

FREQUENCY (Hz)

Figure C-70.   Strain Spectrum for Panel 1

C-71

PANEL CONFIGURATION: I
TRANSDUCER: G10
OVERALL R.M.S. LEVEL: 283.3μe
INPUT SPECTRUM: RANDOM
INPUT LEVEL: 165 dB

Figure C-71. Strain Spectrum for Panel 1

C-72

PANEL CONFIGURATION: n
TRANSDUCER: G10
OVERALL R.M.S. LEVEL:
INPUT SPECTRUM: SINE
INPUT LEVEL: 130 dB

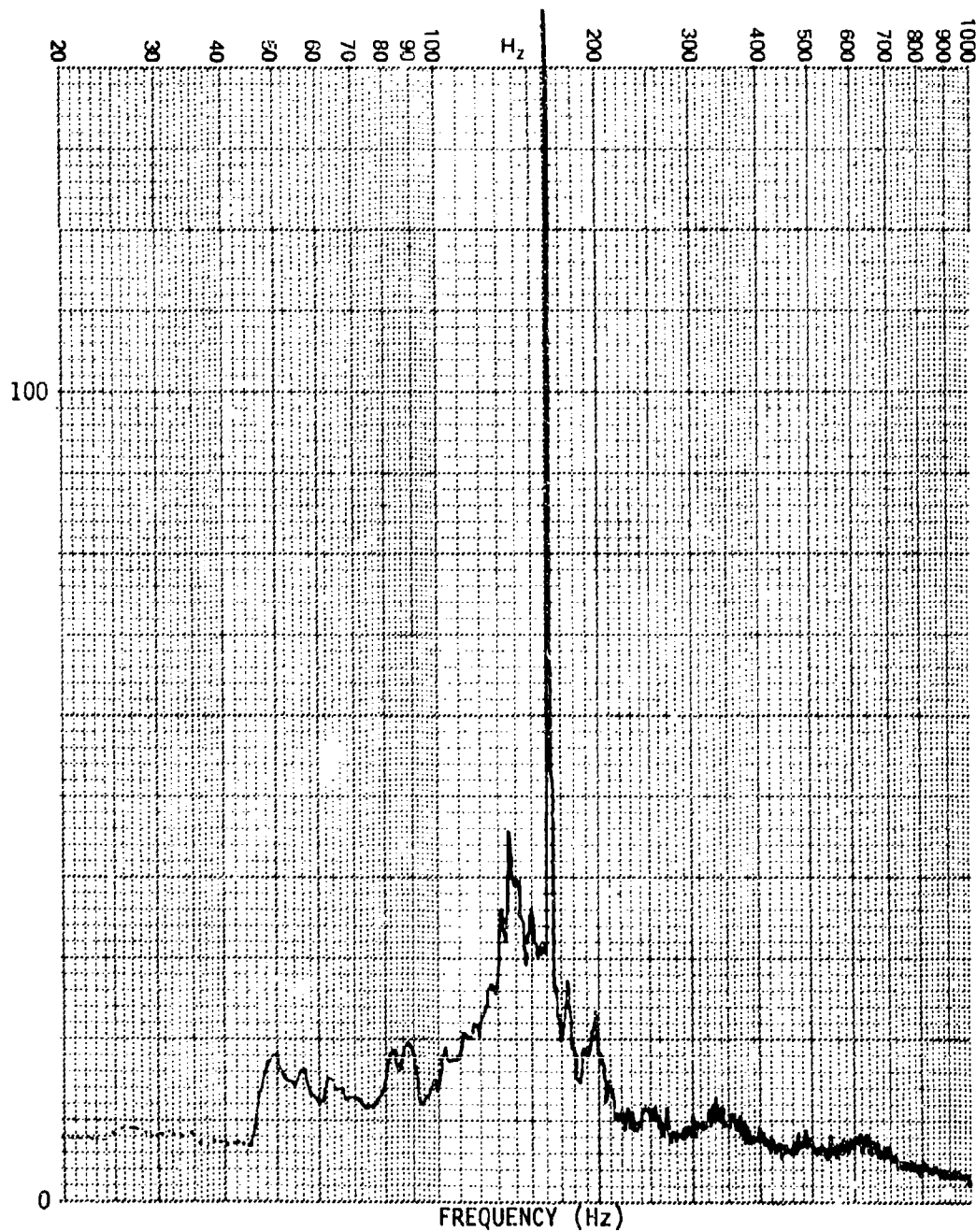FREQUENCY (Hz)

Figure C-72.   Strain Spectrum for Panel n

C-73

FANEL CONFIGURATION: n
TRANSDUCER: G10
OVERALL R.M.S. LEVEL: 186.9µe
INPUT SPECTRUM: RANDOM
INPUT LEVEL: 140 dB

FREQUENCY (Hz)

Figure C-73.   Strain Spectrum for Panel n

PANEL CONFIGURATION: n
TRANSDUCER: G10
OVERALL R.M.S. LEVEL: 265.8 με
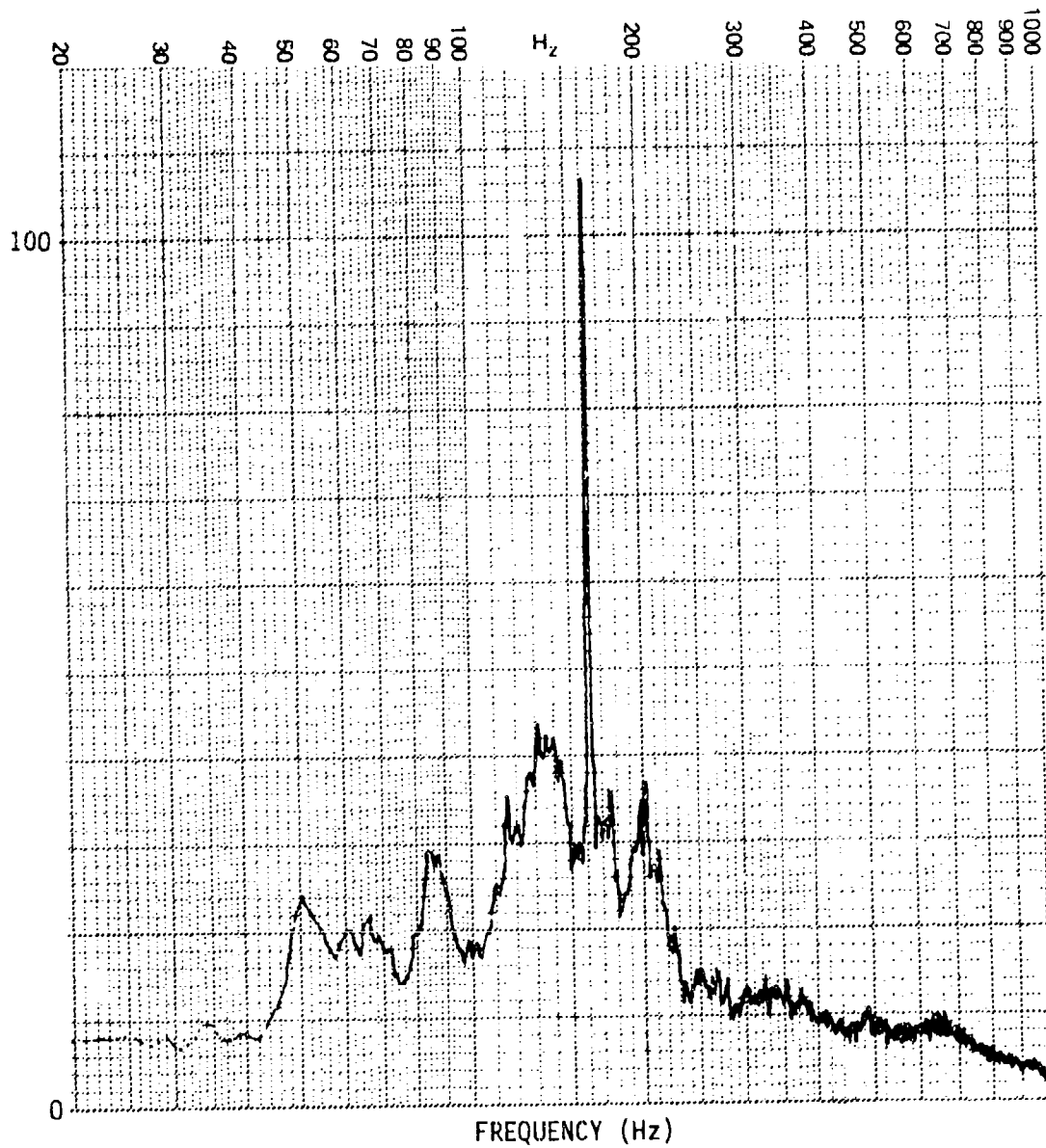INPUT SPECTRUM: RANDOM
INPUT LEVEL: 145 dB

Figure C-74.   Strain Spectrum for Panel n

C-75

PANEL CONFIGURATION: n
TRANSDUCER: G10
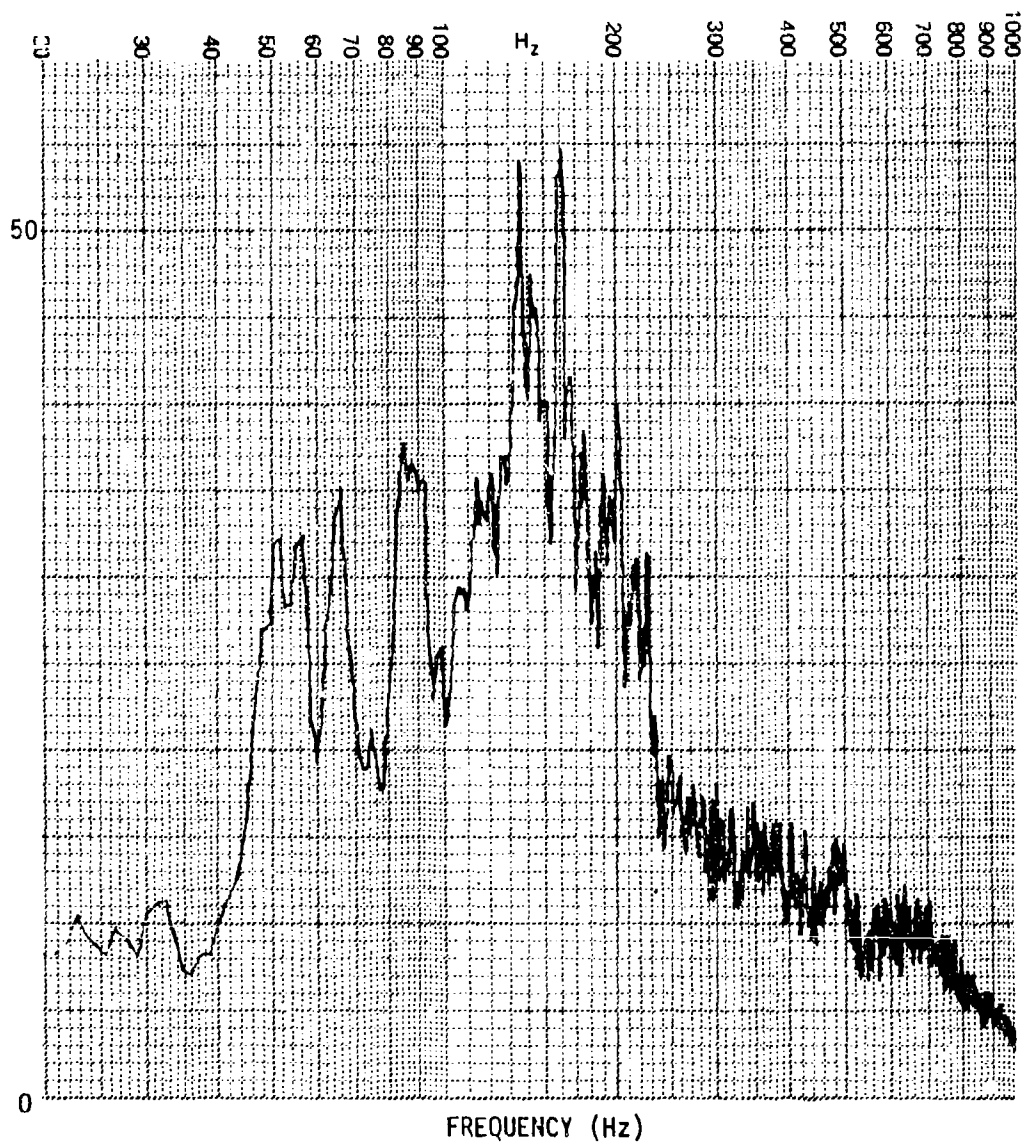OVERALL R.M.S. LEVEL: 307.0μe
INPUT SPECTRUM: RANDOM
INPUT LEVEL: 150 dB

Figure C-75. Strain Spectrum for Panel n

C-76

PANEL CONFIGURATION: n
TRANSDUCER: G10
OVERALL R.M.S. LEVEL: 355.0µe
INPUT SPECTRUM: RANDOM
INPUT LEVEL: 155 dB

Figure C-76.   Strain Spectrum for Panel n

C-77

PANEL CONFIGURATION: n
TRANSDUCER: G10
OVERALL R.M.S. LEVEL: 408.0µe
INPUT SPECTRUM: RANDOM
INPUT LEVEL: 160 dB

Figure C-77.   Strain Spectrum for Panel n

C-78

PANEL CONFIGURATION: p
TRANSDUCER: G10
OVERALL R.M.S. LEVEL:
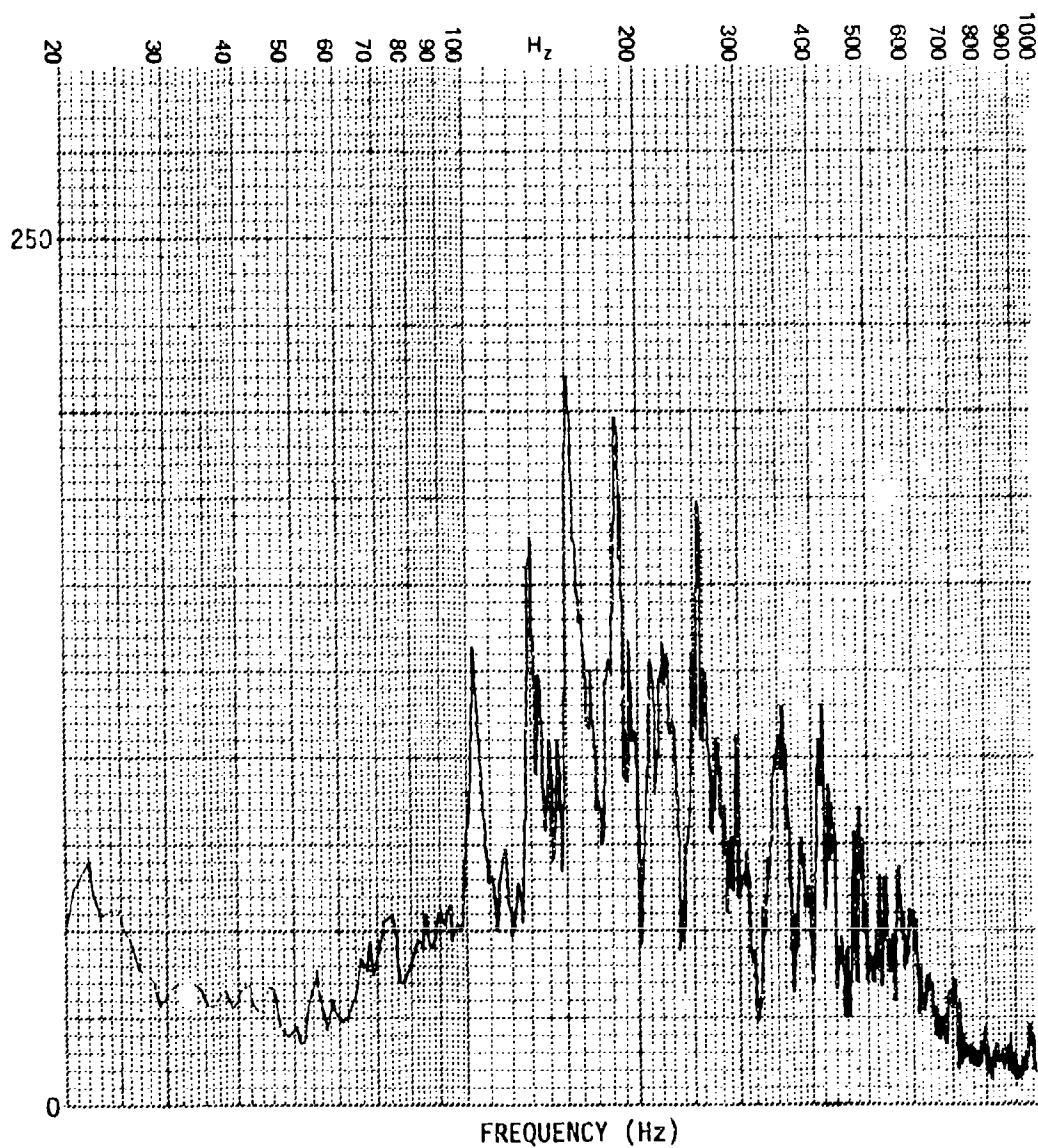INPUT SPECTRUM: SINE
INPUT LEVEL: 130dB

Figure C-78. Strain Spectrum for Panel p

C-79

PANEL CONFIGURATION: p
TRANSDUCER: G10 μe
OVERALL R.M.S. LEVEL: 96.2
INPUT SPECTRUM: RANDOM
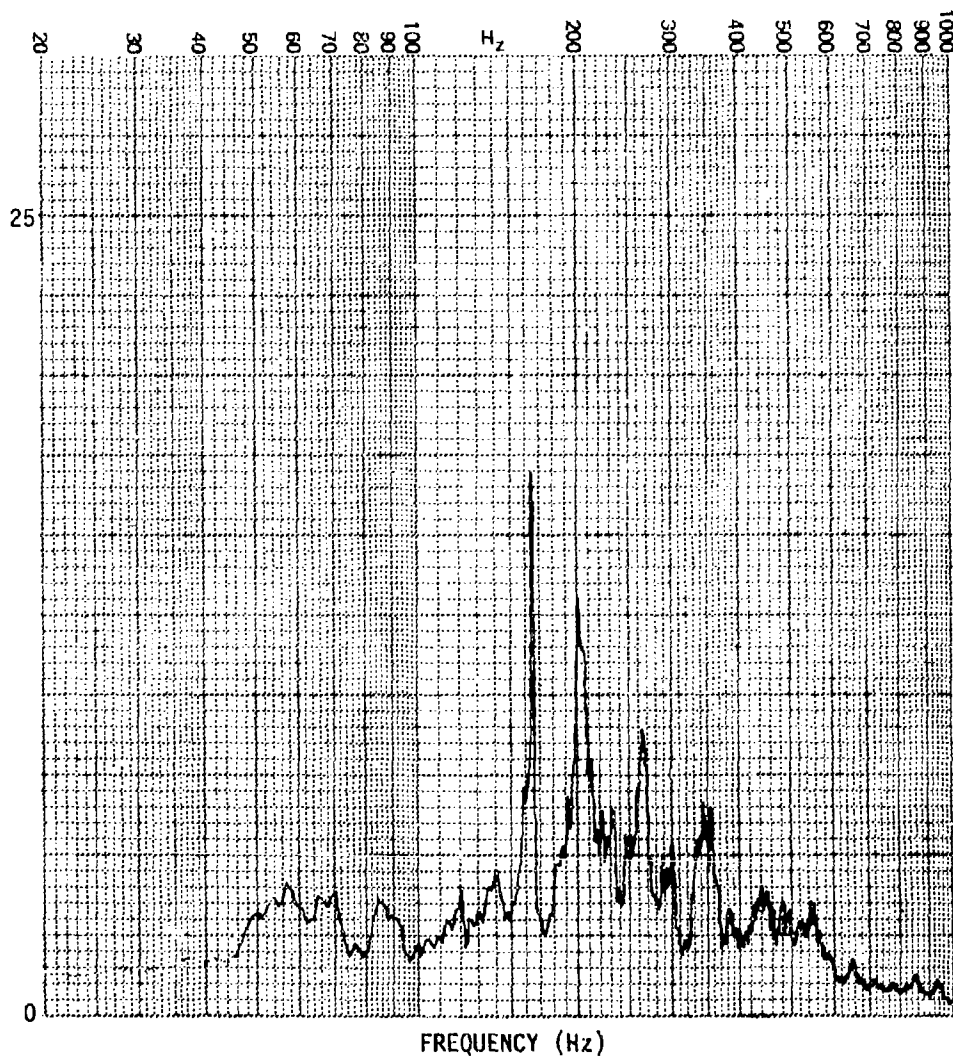INPUT LEVEL: 140 dB

FREQUENCY (Hz)

Figure C-79. Strain Spectrum for Panel p

C-80

PANEL CONFIGURATION: p
TRANSDUCER: G10
OVERALL R.M.S. LEVEL: 115.8μe
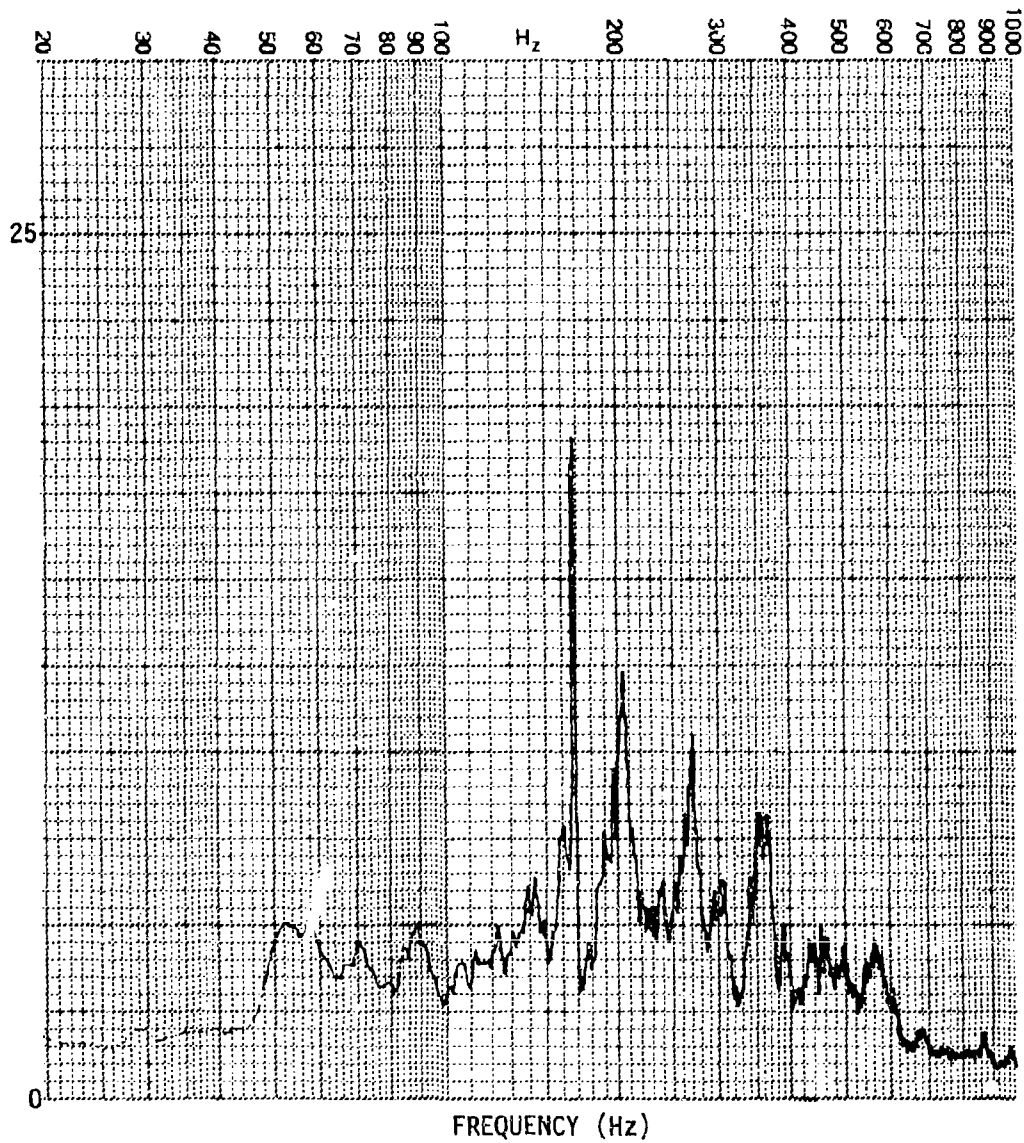INPUT SPECTRUM: RANDOM
INPUT LEVEL: 145 dB

FREQUENCY (Hz)

Figure C-80.   Strain Spectrum for Panel p

C-81

PANEL CONFIGURATION: p
TRANSDUCER: G10
OVERALL R.M.S. LEVEL: 252.7μe
INPUT SPECTRUM: RANDOM
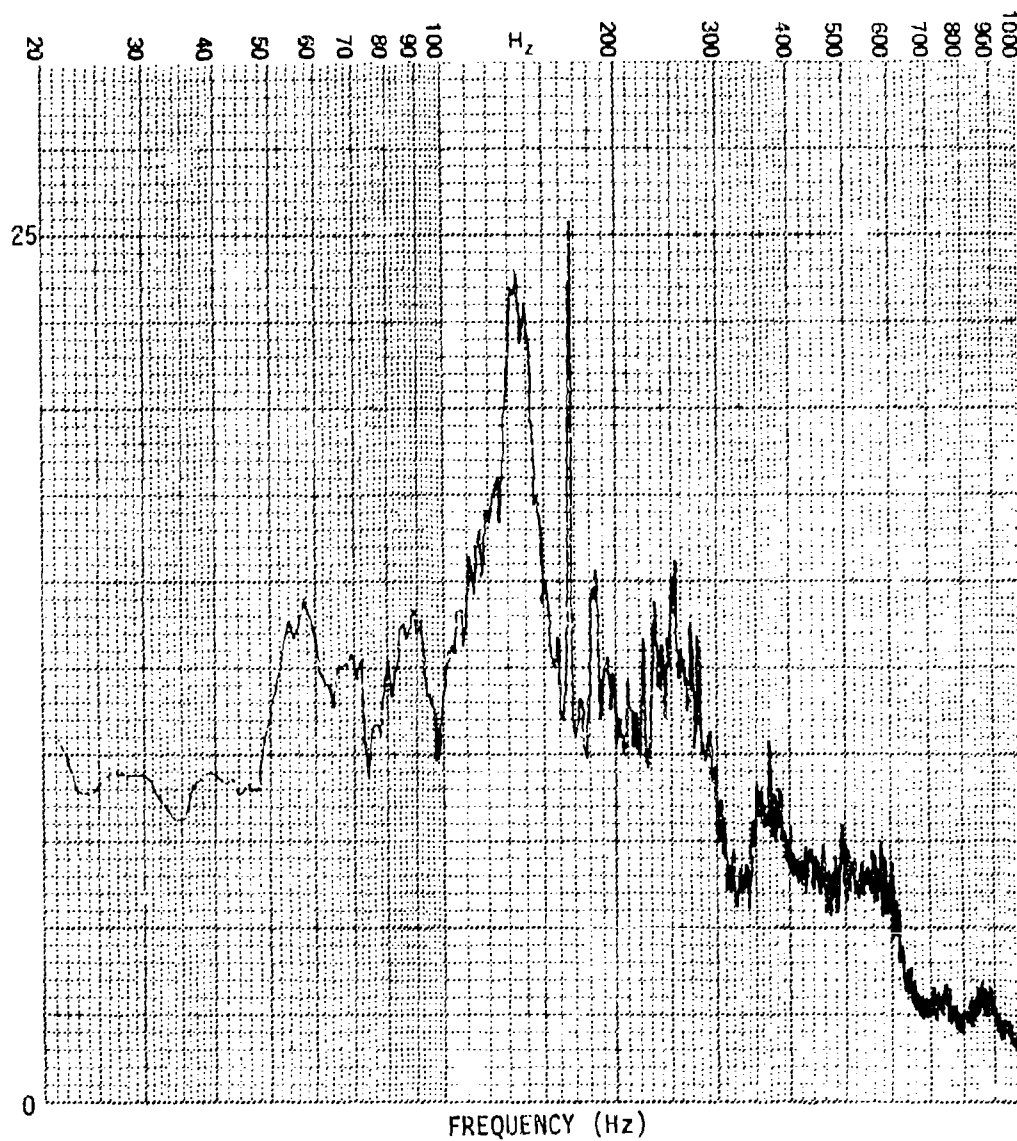INPUT LEVEL: 150 dB

Figure C-81.   Strain Spectrum for Panel p

C-82

PANEL CONFIGURATION: p
TRANSDUCER: G10
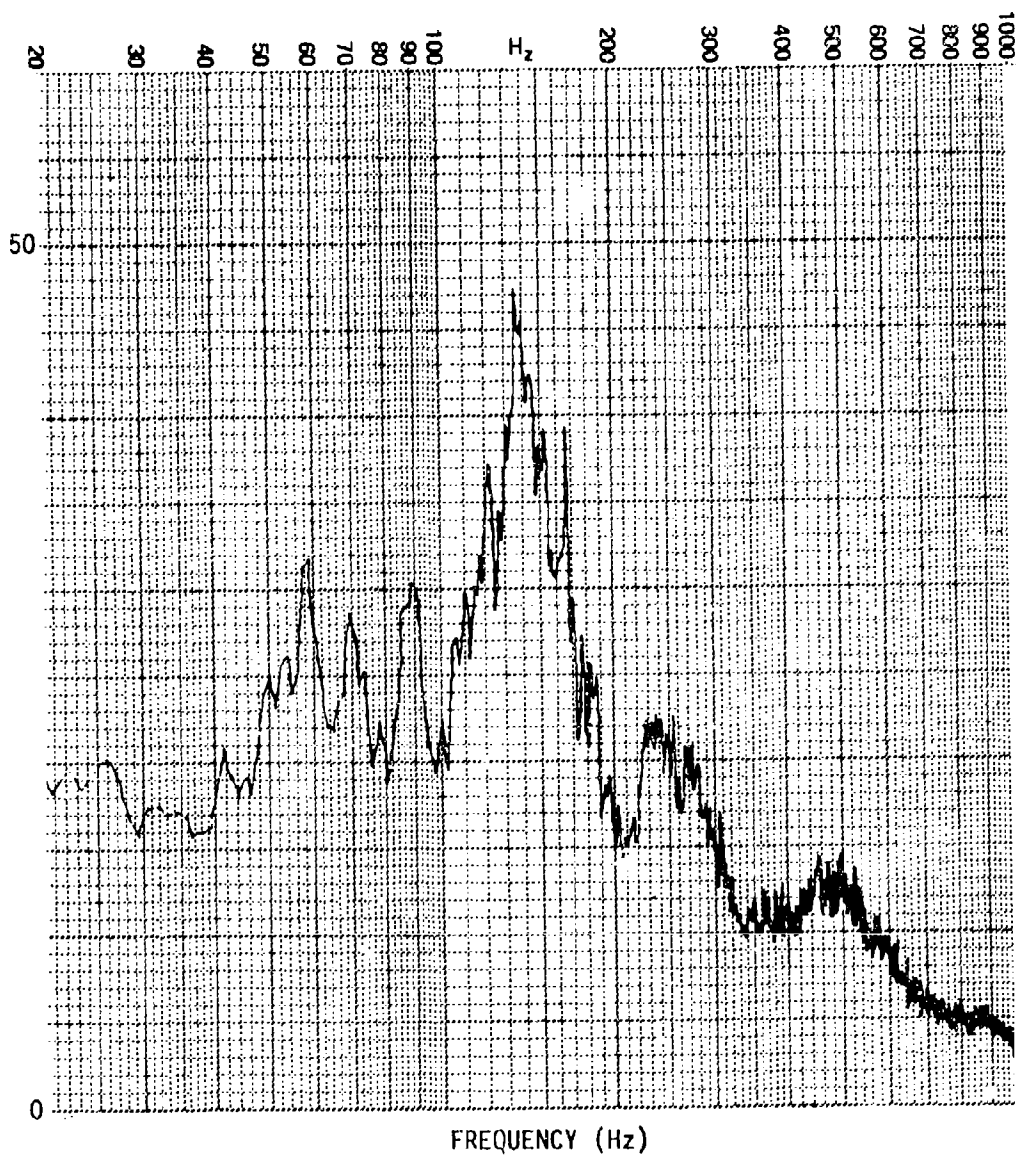OVERALL R.M.S. LEVEL: 455.0 μe
INPUT SPECTRUM: RANDOM
INPUT LEVEL: 155 dB

FREQUENCY (Hz)

Figure C-82.   Strain Spectrum for Panel p

C-83

PANEL CONFIGURATION: q
TRANSDUCER: G10
OVERALL R.M.S. LEVEL:
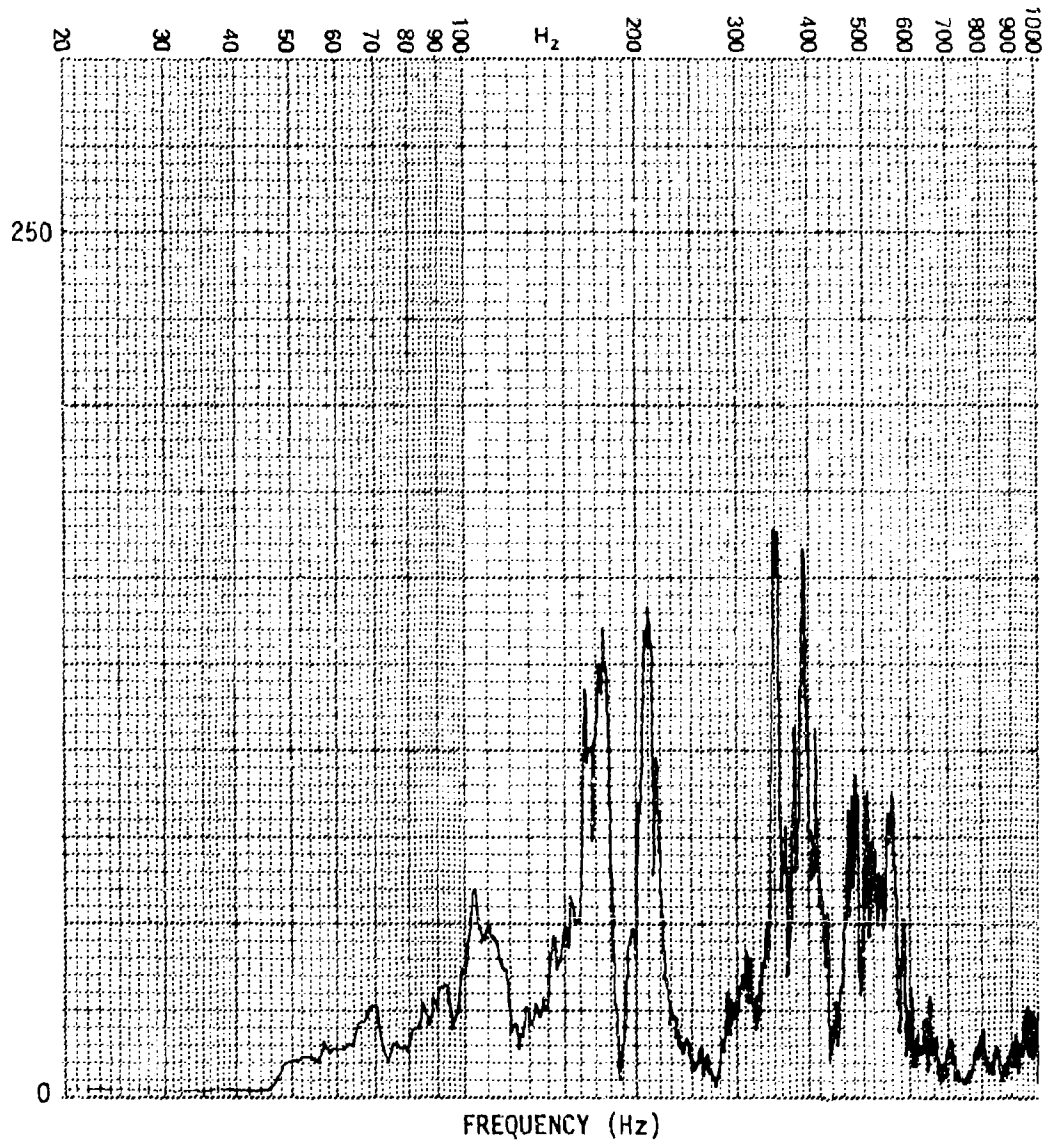INPUT SPECTRUM: SINE
INPUT LEVEL: 130 dB

Figure C-83.   Strain Spectrum for Panel q

PANEL CONFIGURATION: q
TRANSDUCER: G10
OVERALL R.M.S. LEVEL: 57.5µe
INPUT SPECTRUM: RANDOM
INPUT LEVEL: 140 dB

Figure C-84.   Strain Spectrum for Panel q

C-85

PANEL CONFIGURATION: q
TRANSDUCER: G10
OVERALL R.M.S. LEVEL: 92.7μe
INPUT SPECTRUM: RANDOM
INPUT LEVEL: 145 dB
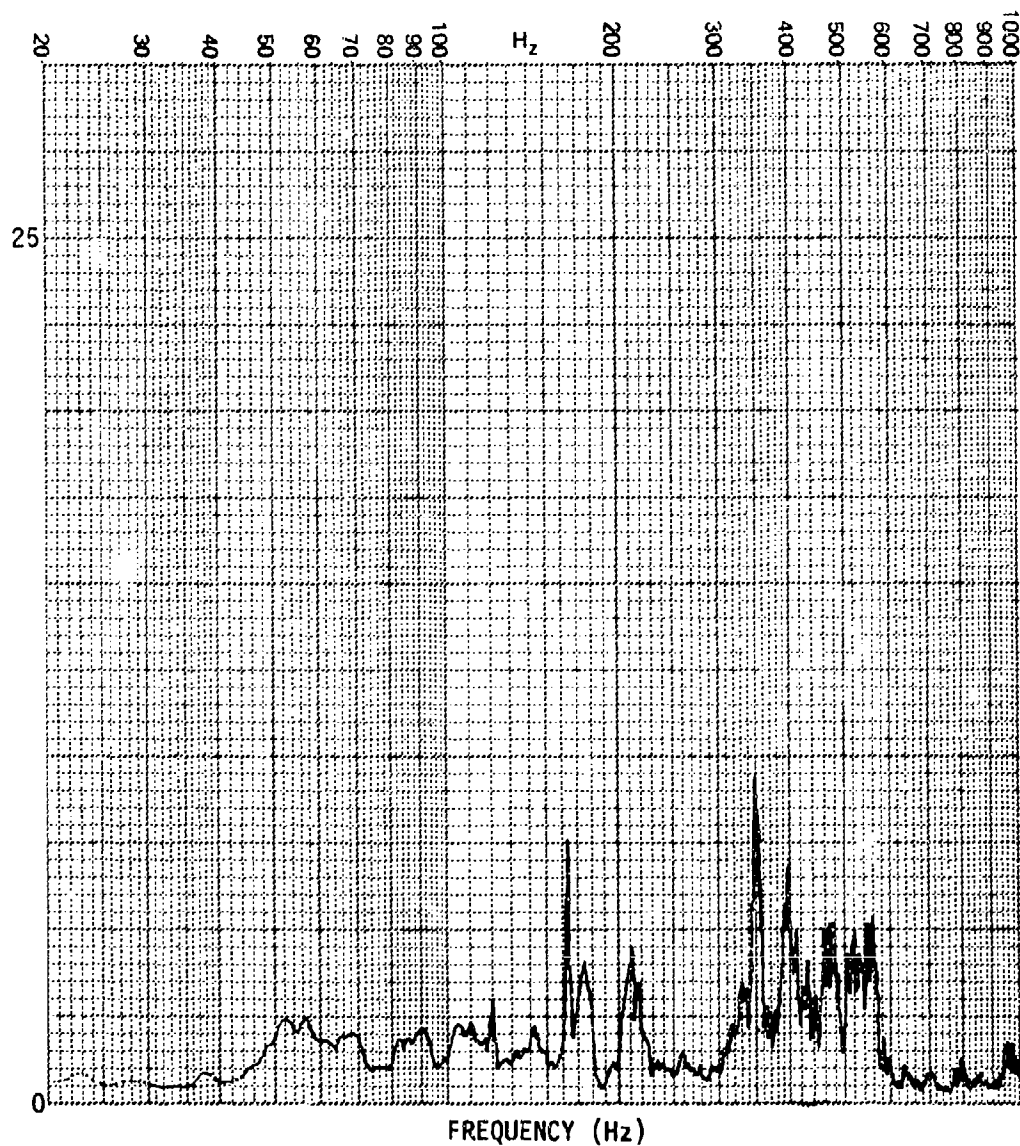

FREQUENCY (Hz)

Figure C-85. Strain Spectrum for Panel q

C-86

PANEL CONFIGURATION: q
TRANSDUCER: G10
OVERALL R.M.S. LEVEL: 141.2μe
INPUT SPECTRUM: RANDOM
INPUT LEVEL: 150 dB

Figure C-86.   Strain Spectrum for Panel q

C-87

PANEL CONFIGURATION: q
TRANSDUCER: G10
OVERALL R.M.S. LEVEL: 201.5ue
INPUT SPECTRUM: RANDOM
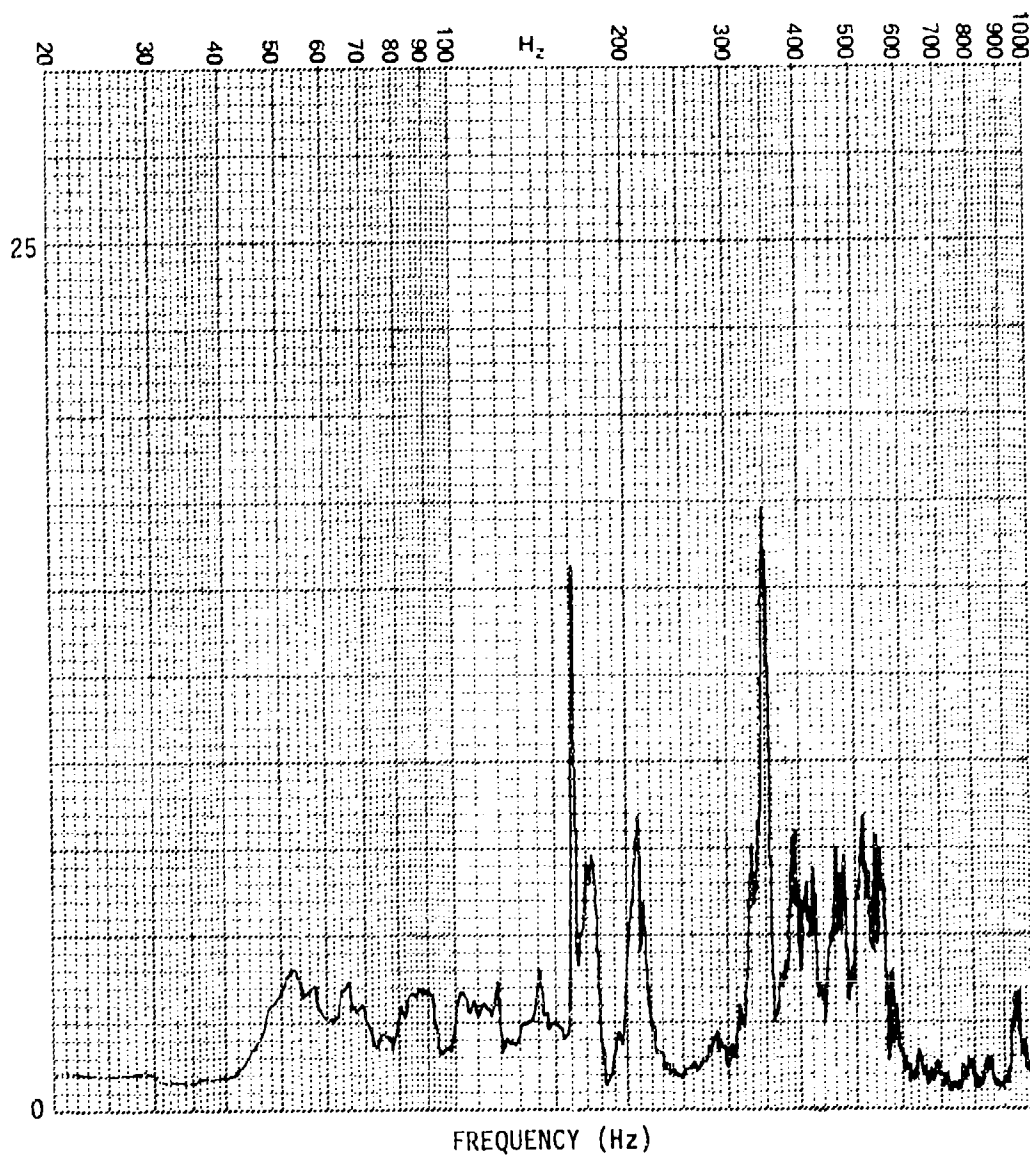INPUT LEVEL: 155 dB

FREQUENCY (Hz)

Figure C-87. Strain Spectrum for Panel q

C-88

PANEL CONFIGURATION: q
TRANSDUCER: G10
OVERALL R.M.S. LEVEL: 312.0μe
INPUT SPECTRUM: RANDOM
INPUT LEVEL: 160 dB

FREQUENCY (Hz)

Figure C-88.   Strain Spectrum for Panel q

C-89

PANEL CONFIGURATION: r
TRANSDUCER: G10
OVERALL R.M.S. LEVEL:
INPUT SPECTRUM: SINE
INPUT LEVEL: 130 dB

Figure C-89.   Strain Spectrum for Panel r

PANEL CONFIGURATION: r
TRANSDUCER: G10
OVERALL R.M.S. LEVEL: 43 8μe
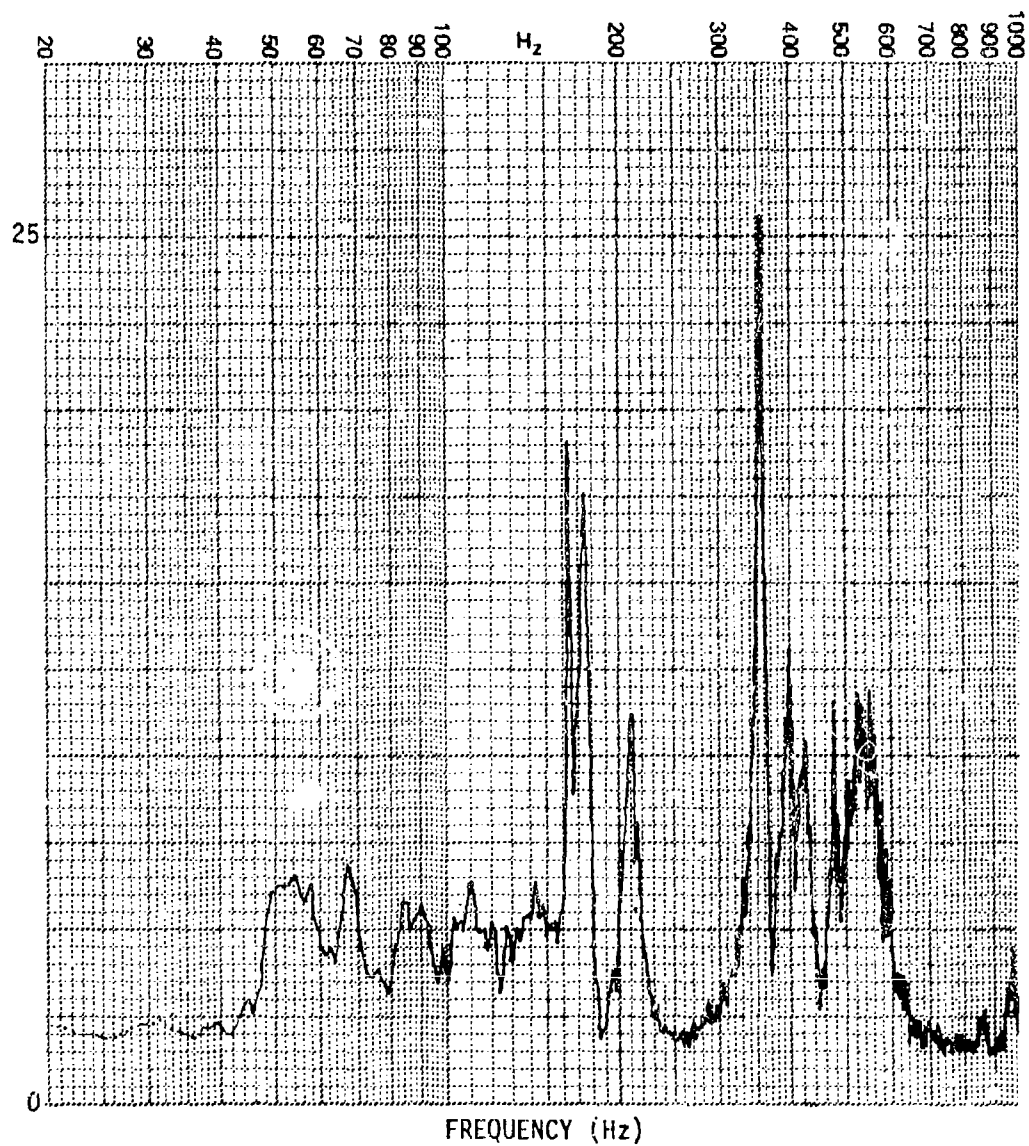INPUT SPECTRUM: RANDOM
INPUT LEVEL: 140 dB

Figure C-90.   Strain Spectrum for Panel r

C-91

PANEL CONFIGURATION: r
TRANSDUCER: G10
OVERALL R.M.S. LEVEL: 61.7 μe
INPUT SPECTRUM: RANDOM
INPUT LEVEL: 145 dB

Figure C-91. Strain Spectrum for Panel r

PANEL CONFIGURATION: r
TRANSDUCER: G10
OVERALL R.M.S. LEVEL: 107.9 µe
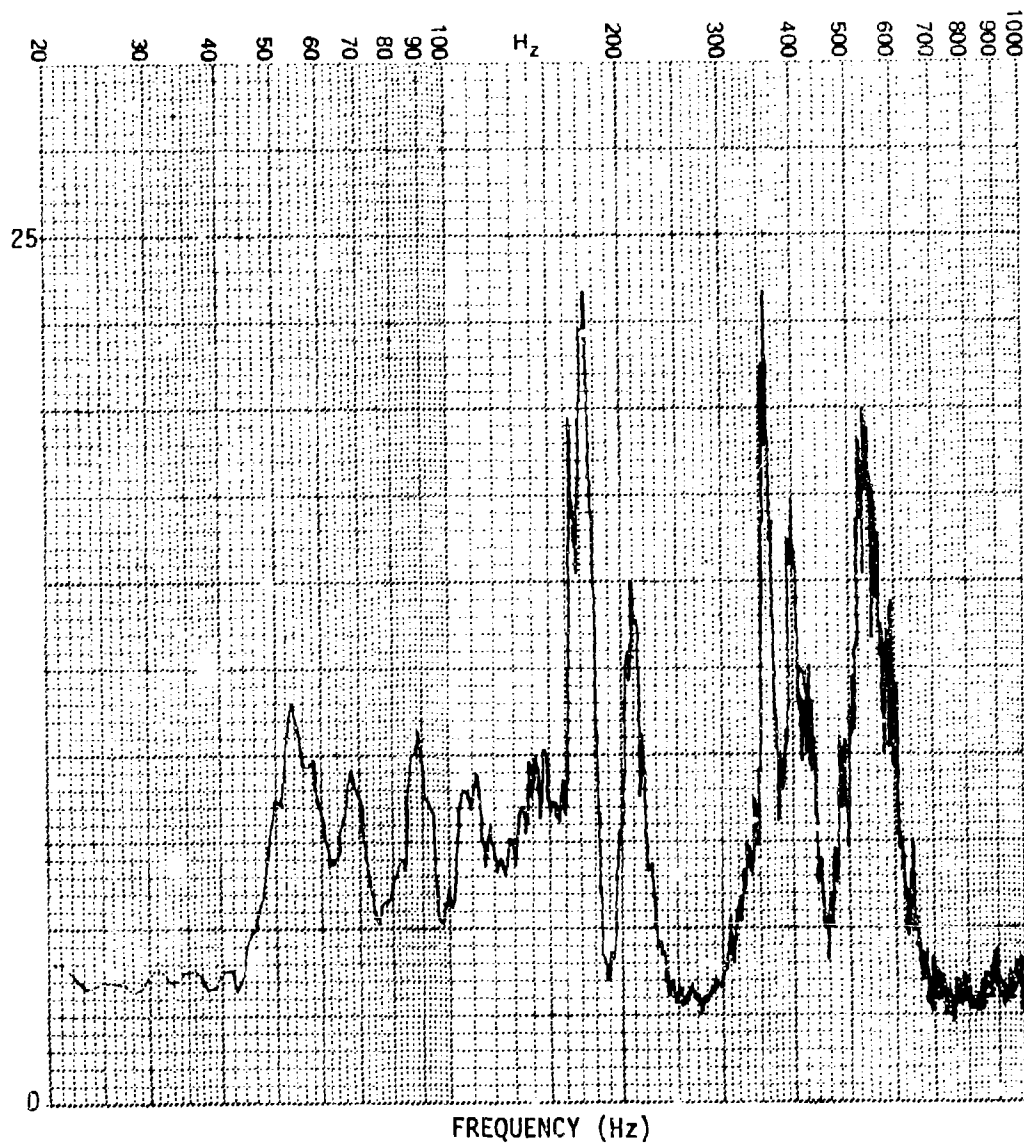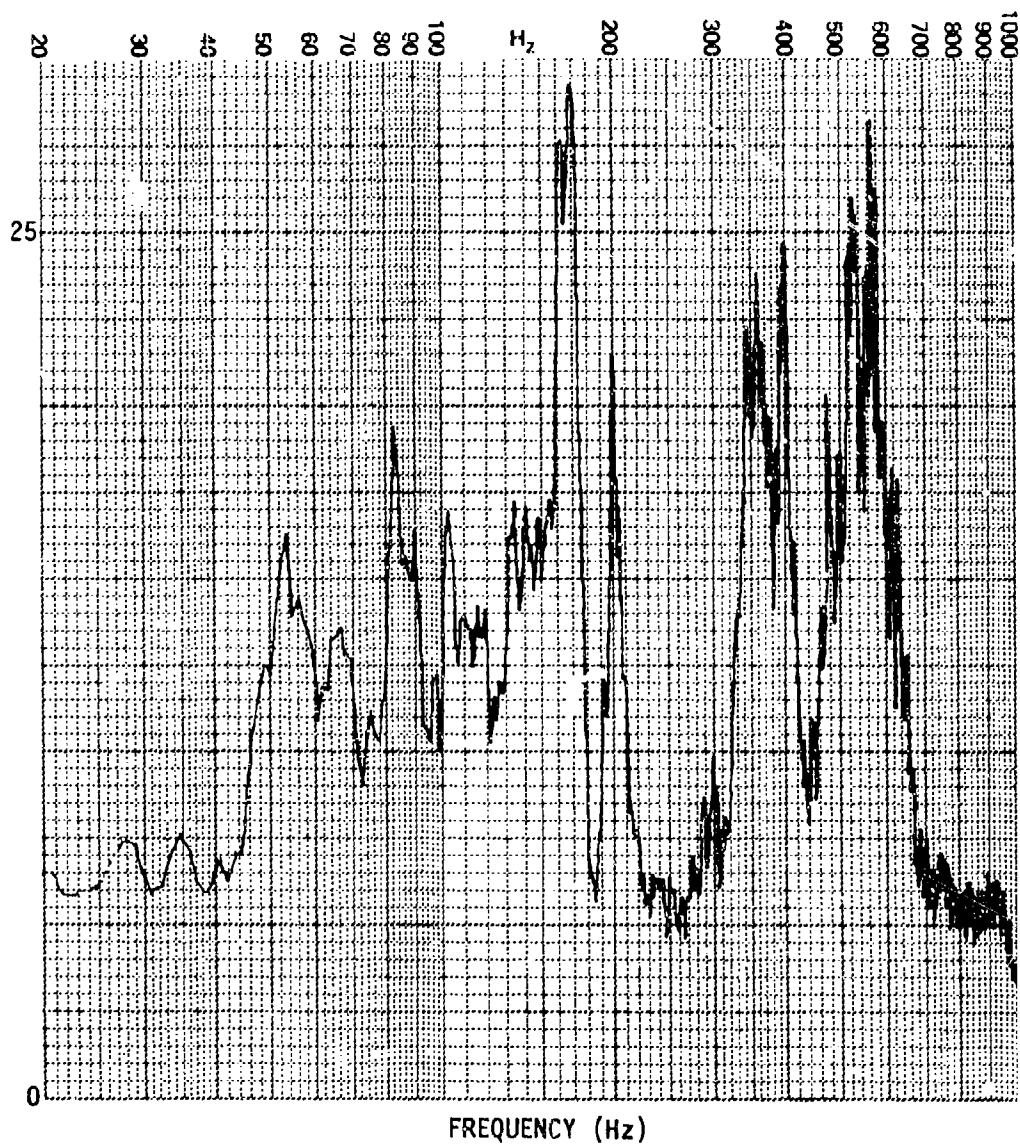INPUT SPECTRUM: RANDOM
INPUT LEVEL: 150 dB

Figure C-92.   Strain Spectrum for Panel r

C-93

PANEL CONFIGURATION: r
TRANSDUCER: G10
OVERALL R.M.S. LEVEL: 159.8 μe
INPUT SPECTRUM: RANDOM
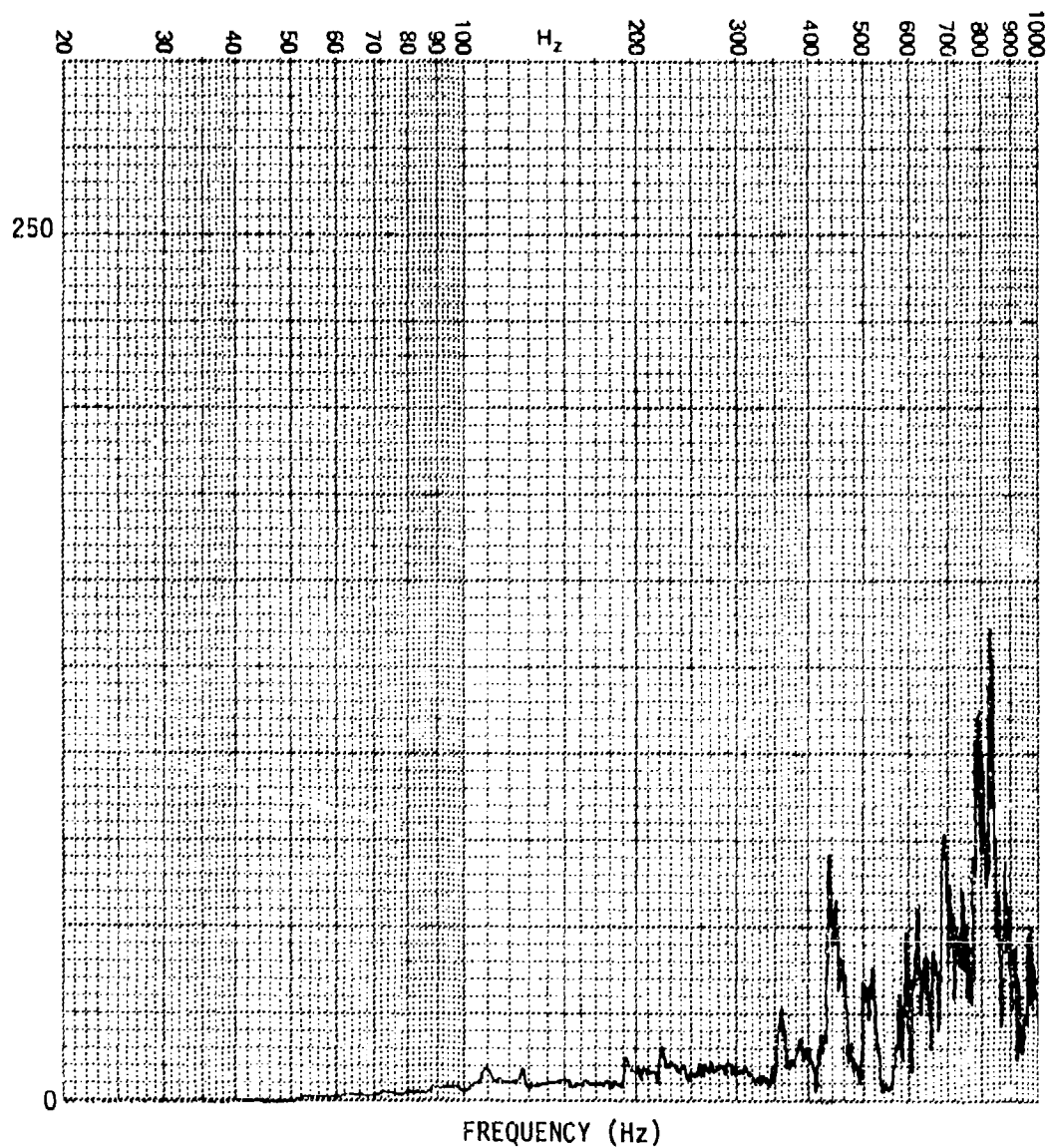INPUT LEVEL: 155 dB

Figure C-93. Strain Spectrum for Panel r

C-94

PANEL CONFIGURATION: r
TRANSDUCER: G10
OVERALL R.M.S. LEVEL: 265.4 μe
INPUT SPECTRUM: RANDOM
INPUT LEVEL: 160 dB

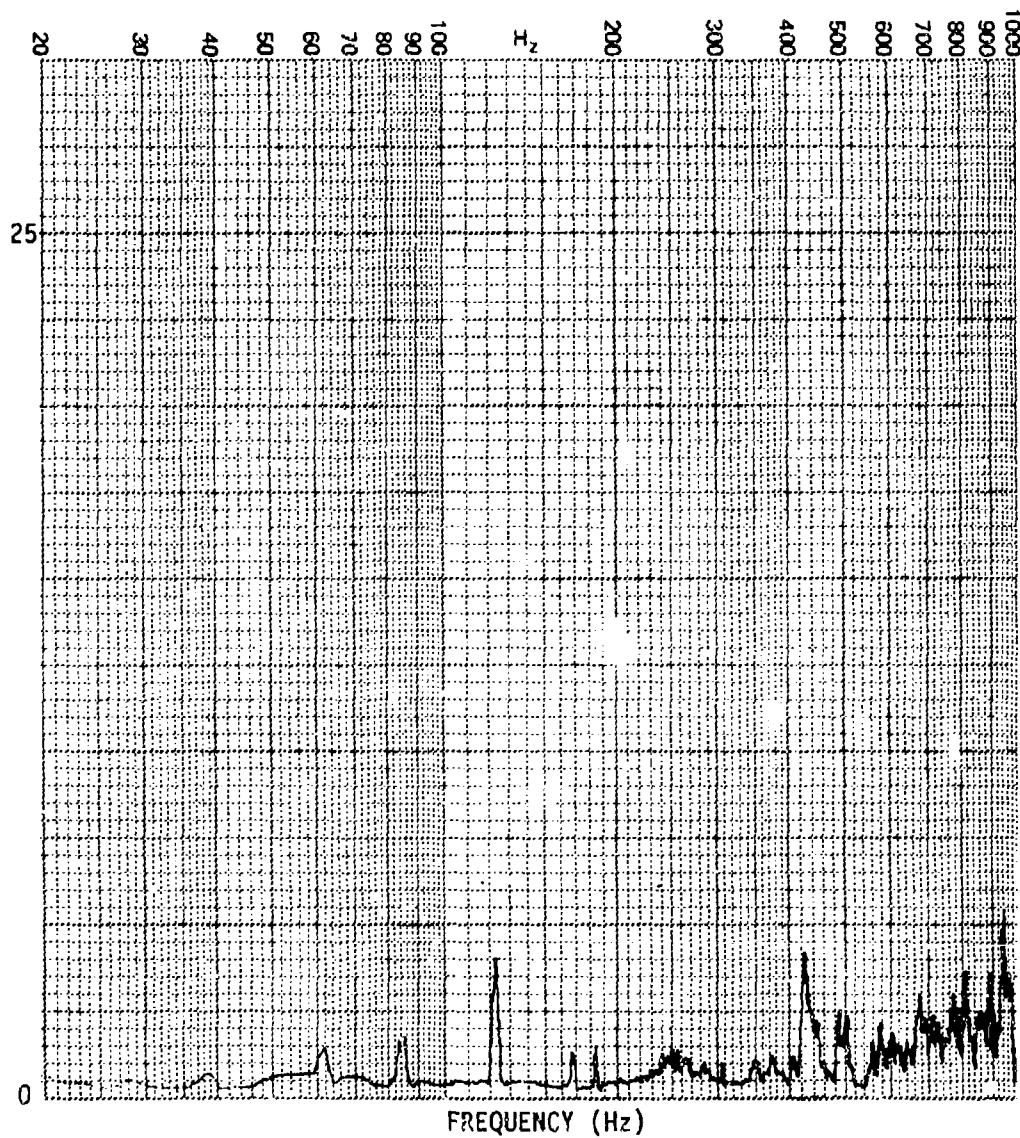
FREQUENCY (Hz)

Figure C-94. Strain Spectrum for Panel r

PANEL CONFIGURATION: r
TRANSDUCER: G10
OVERALL R.M.S. LEVEL: 445.6με
INPUT SPECTRUM: RANDOM
INPUT LEVEL: 165 dB

Figure C-95.   Strain Spectrum for Panel r

C-96

PANEL CONFIGURATION: s
TRANSDUCER: G10
OVERALL R.M.S. LEVEL:
INPUT SPECTRUM: SINE
INPUT LEVEL: 130 dB
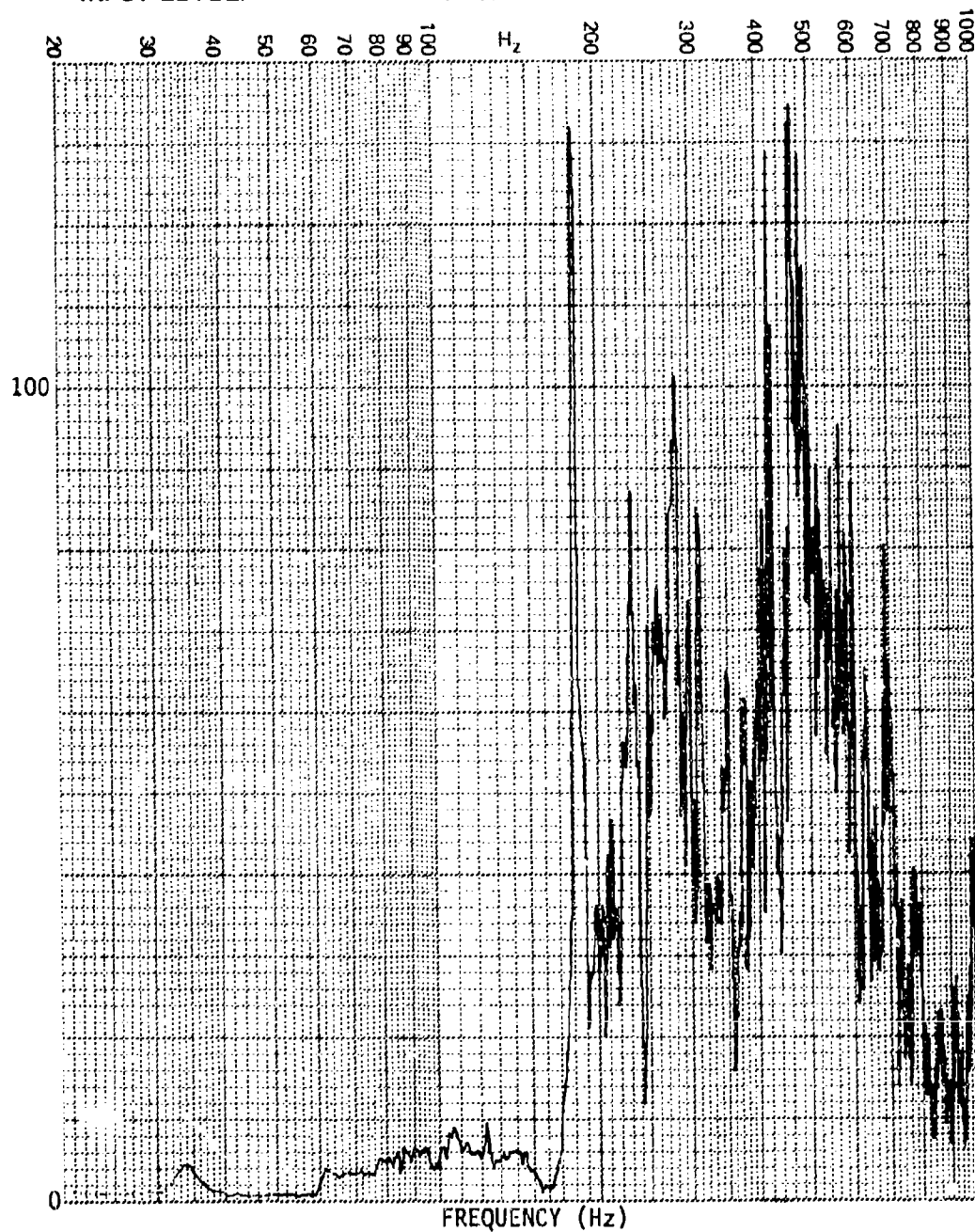
Figure C-96. Strain Spectrum for Panel s

C-97

PANEL CONFIGURATION: s
TRANSDUCER: G10
OVERALL R.M.S. LEVEL: 47.7µe
INPUT SPECTRUM: RANDOM
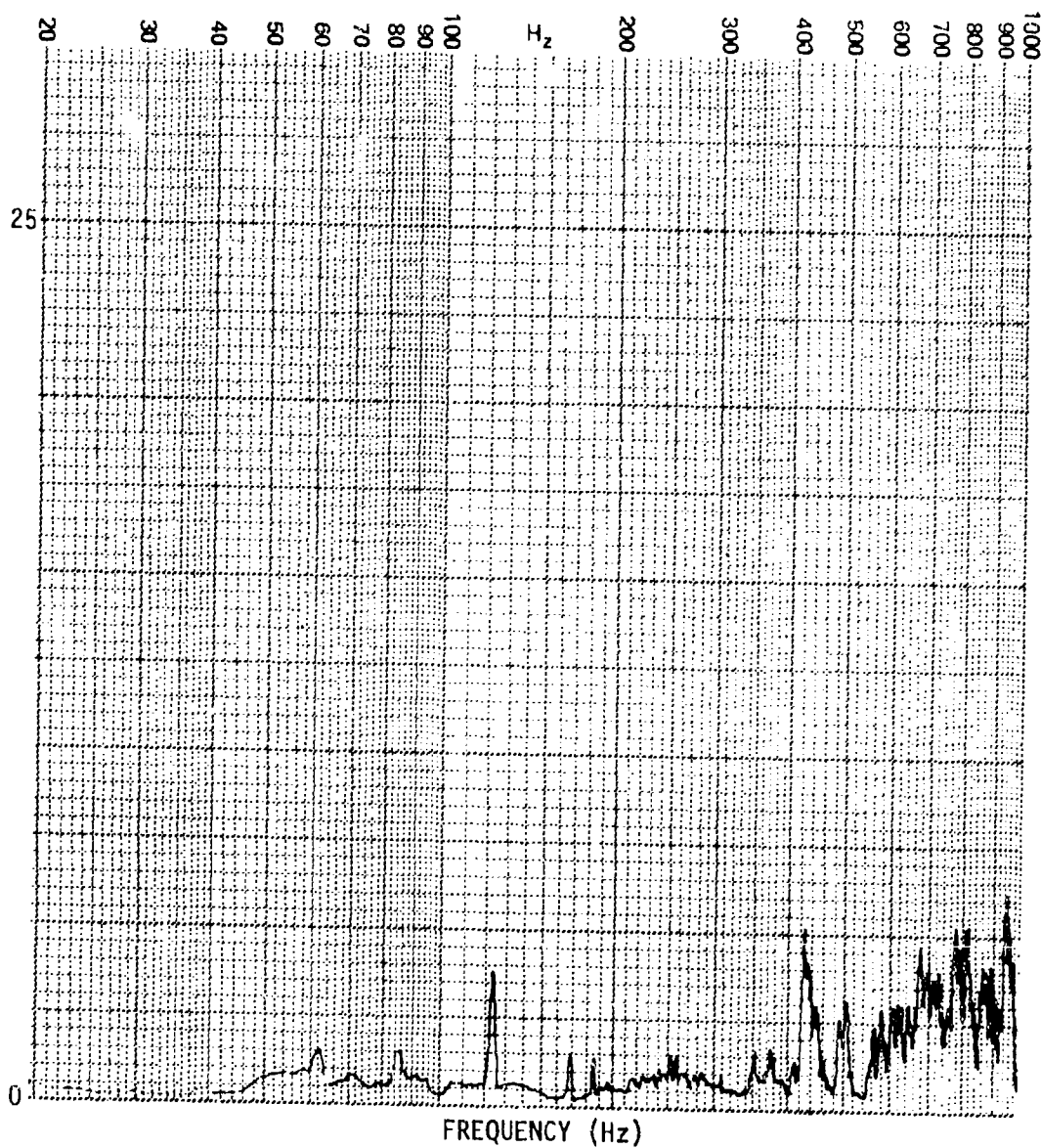INPUT LEVEL: 140 dB
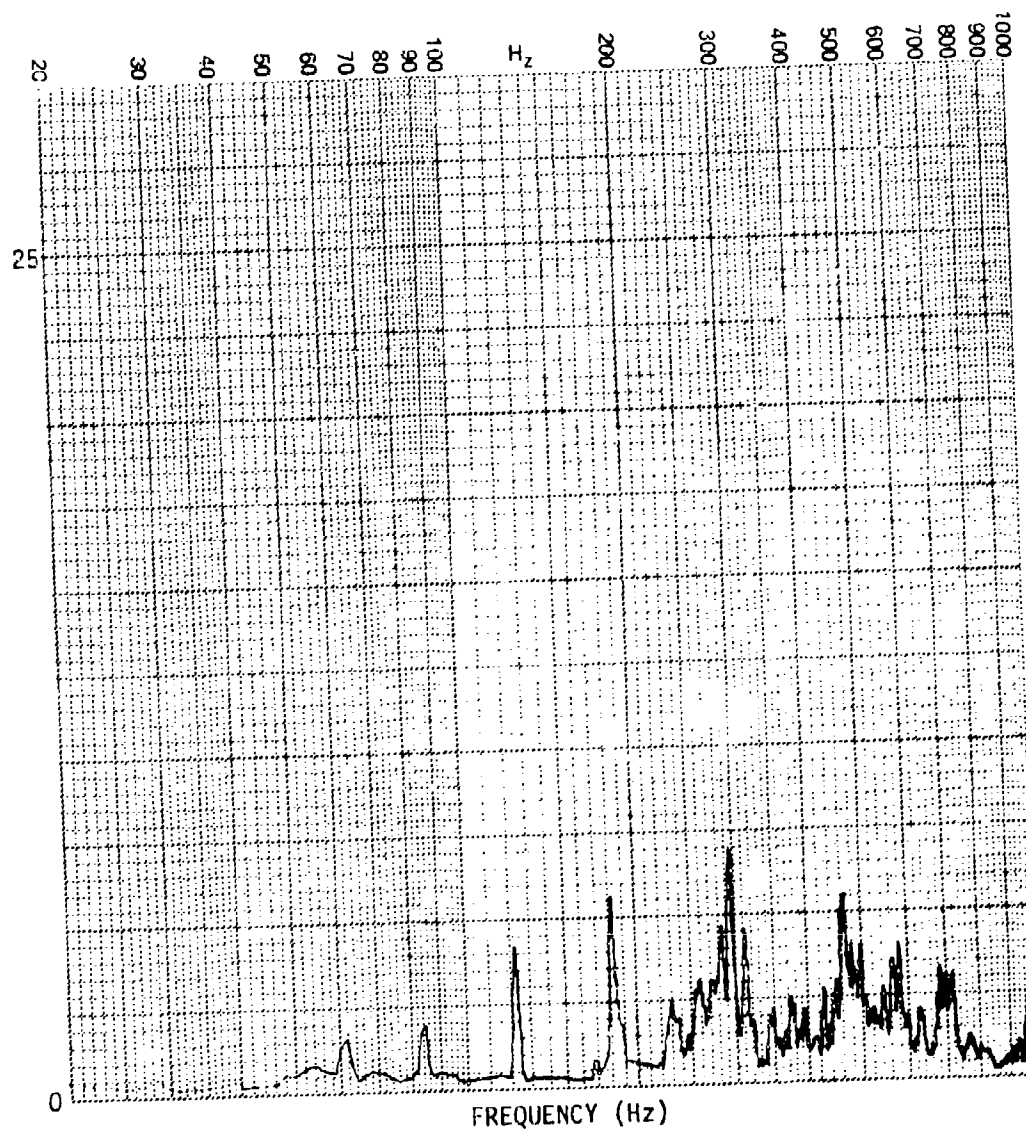
Figure C-97. Strain Spectrum for Panel s

C-98

PANEL CONFIGURATION: s
TRANSDUCER: G10
OVERALL R.M.S. LEVEL: 90.7μe
INPUT SPECTRUM: RANDOM
INPUT LEVEL: 145 dB
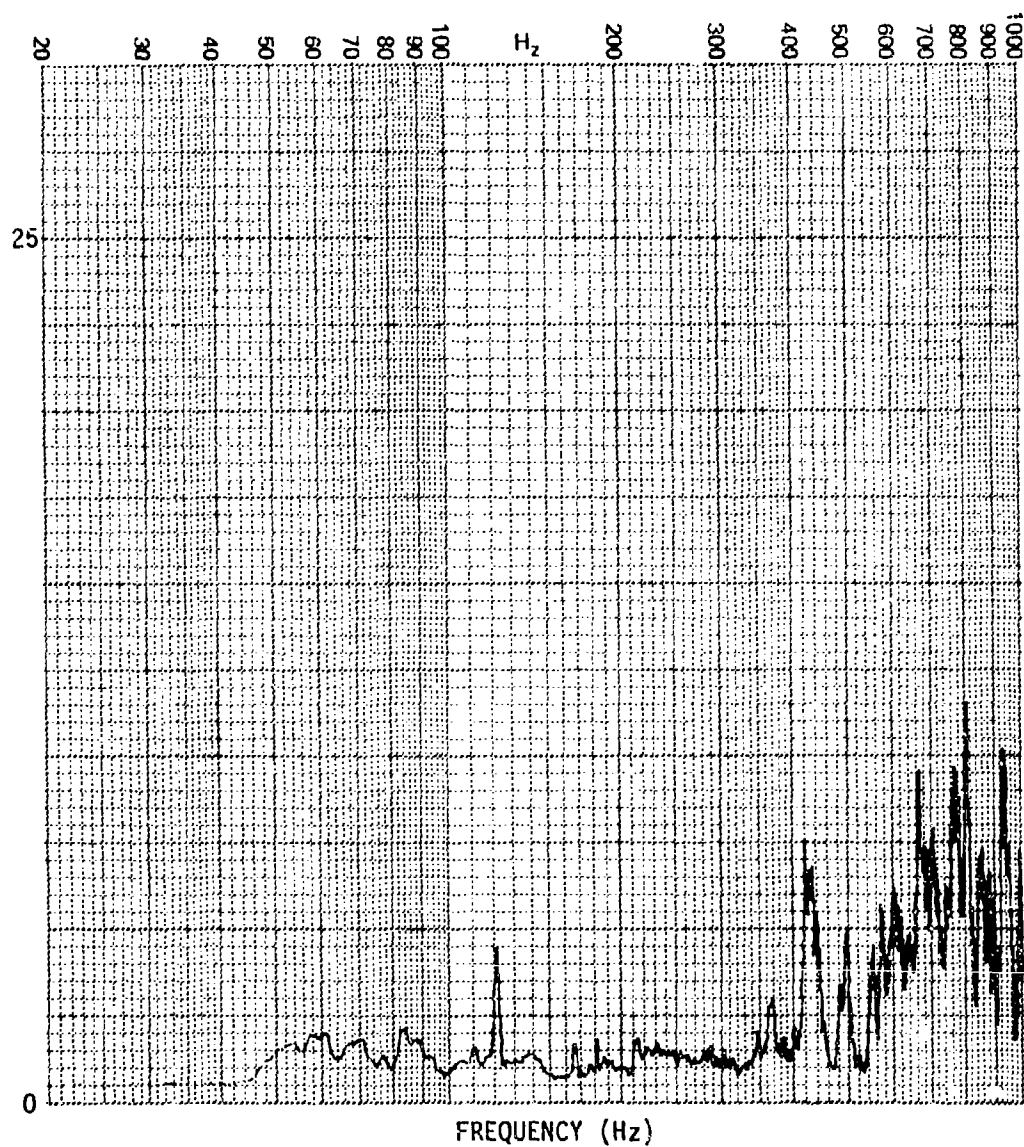

FREQUENCY (Hz)
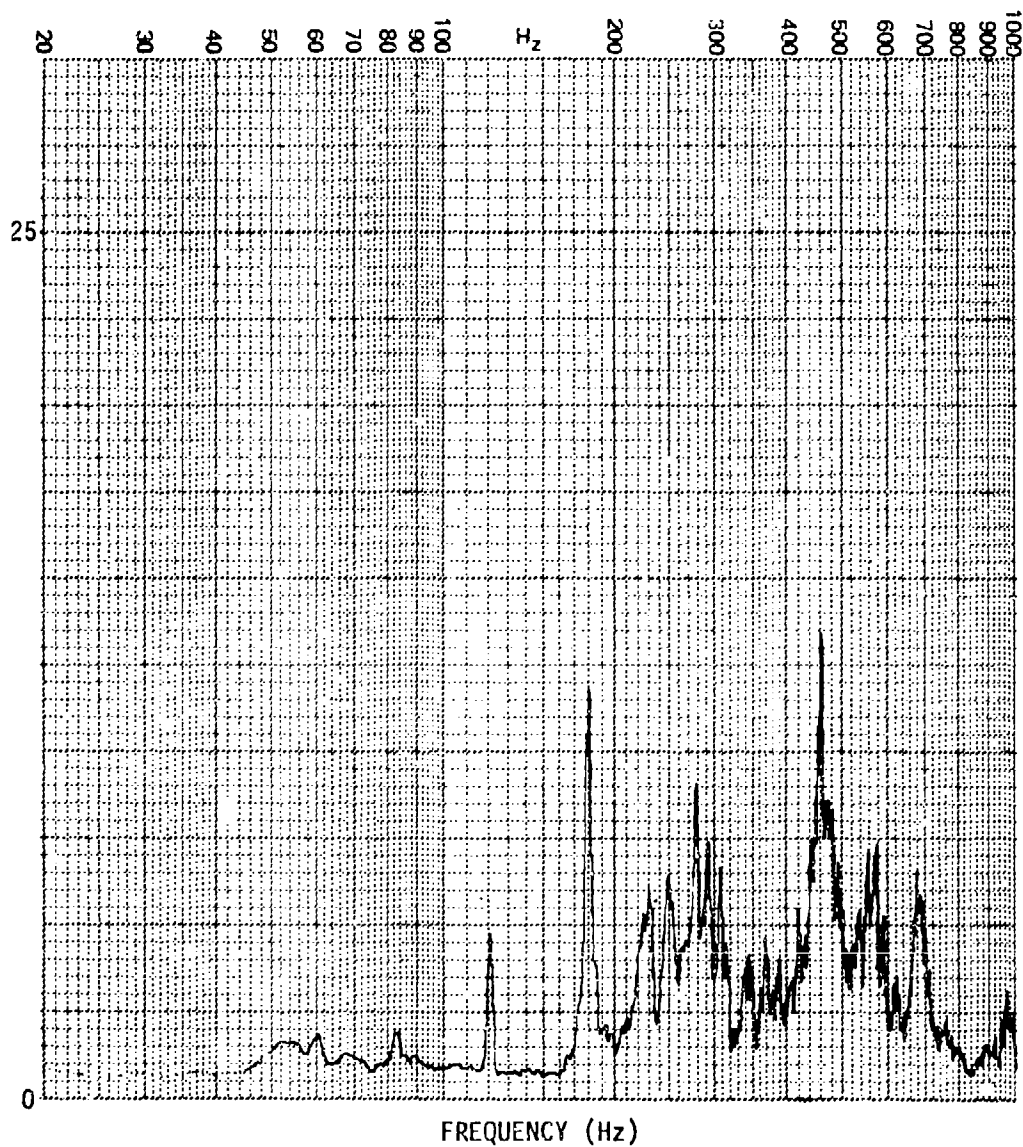
Figure C-98.   Strain Spectrum for Panel s

C-99

PANEL CONFIGURATION: s
TRANSDUCER: G10
OVERALL R.M.S. LEVEL: 149.0µe
INPUT SPECTRUM: RANDOM
INPUT LEVEL: 150 dB

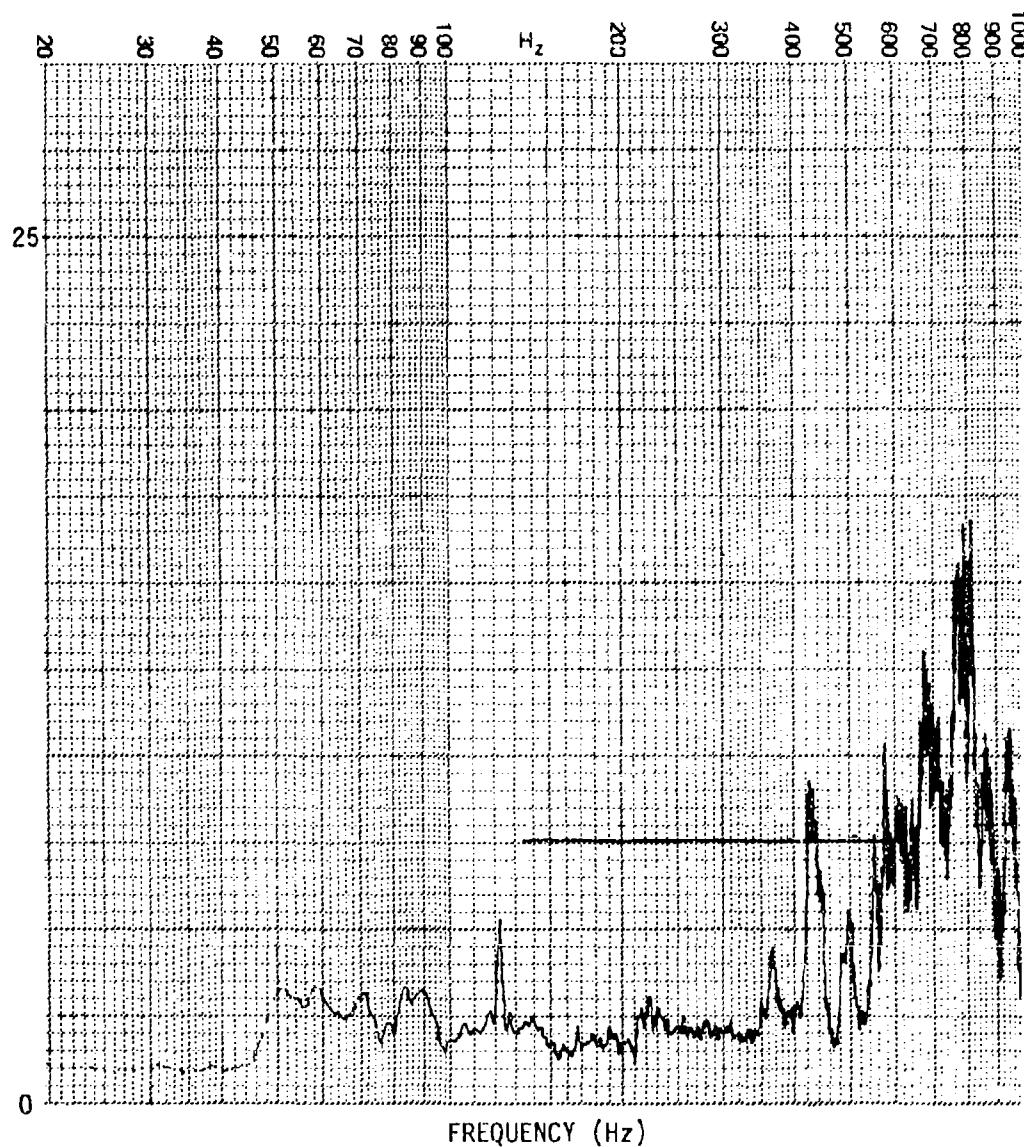

FREQUENCY (Hz)
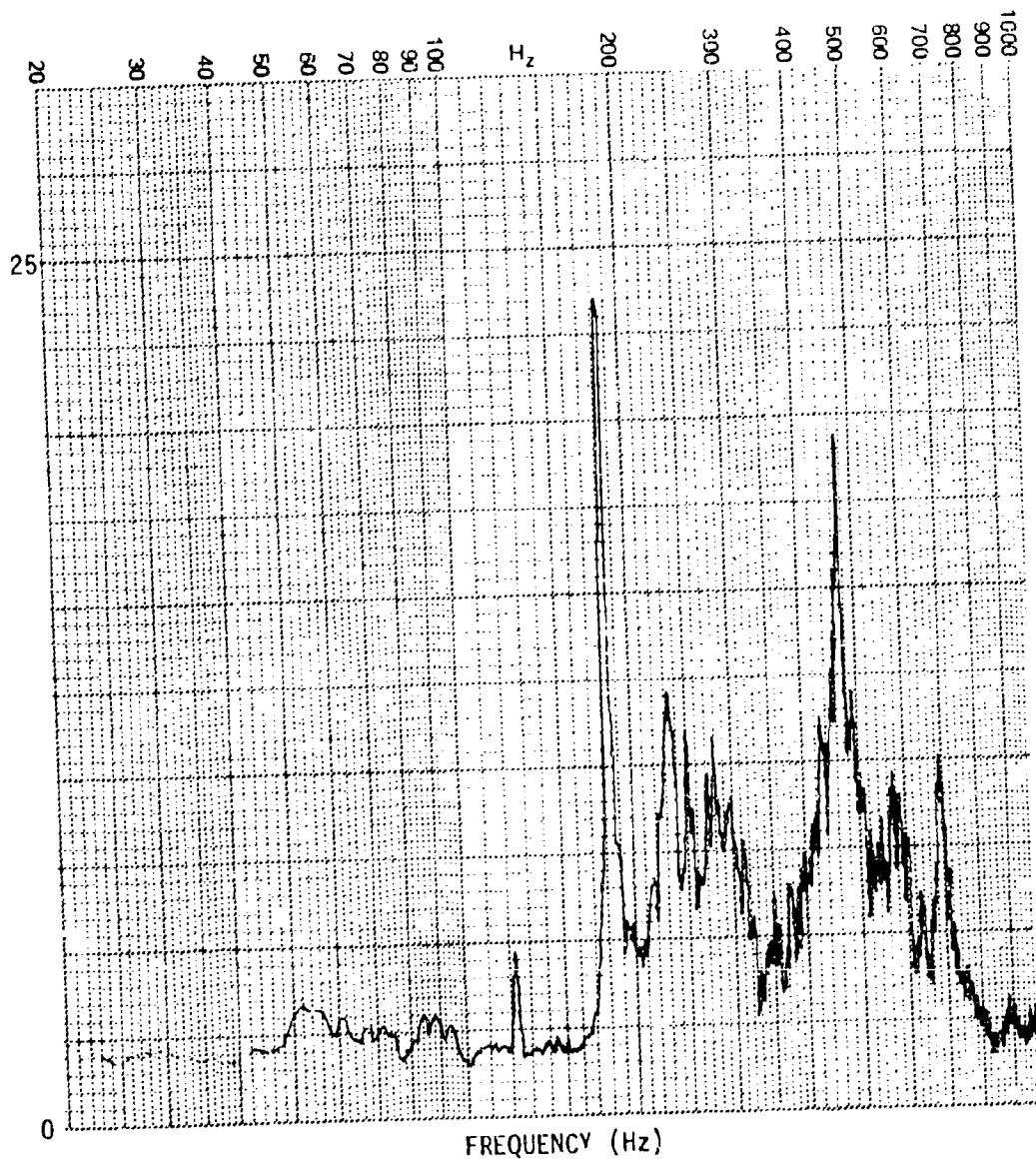
Figure C-99.   Strain Spectrum for Panel s

C-100

PANEL CONFIGURATION: s
TRANSDUCER: G10
OVERALL R.M.S. LEVEL: 261.8μe
INPUT SPECTRUM: RANDOM
INPUT LEVEL: 155 dB
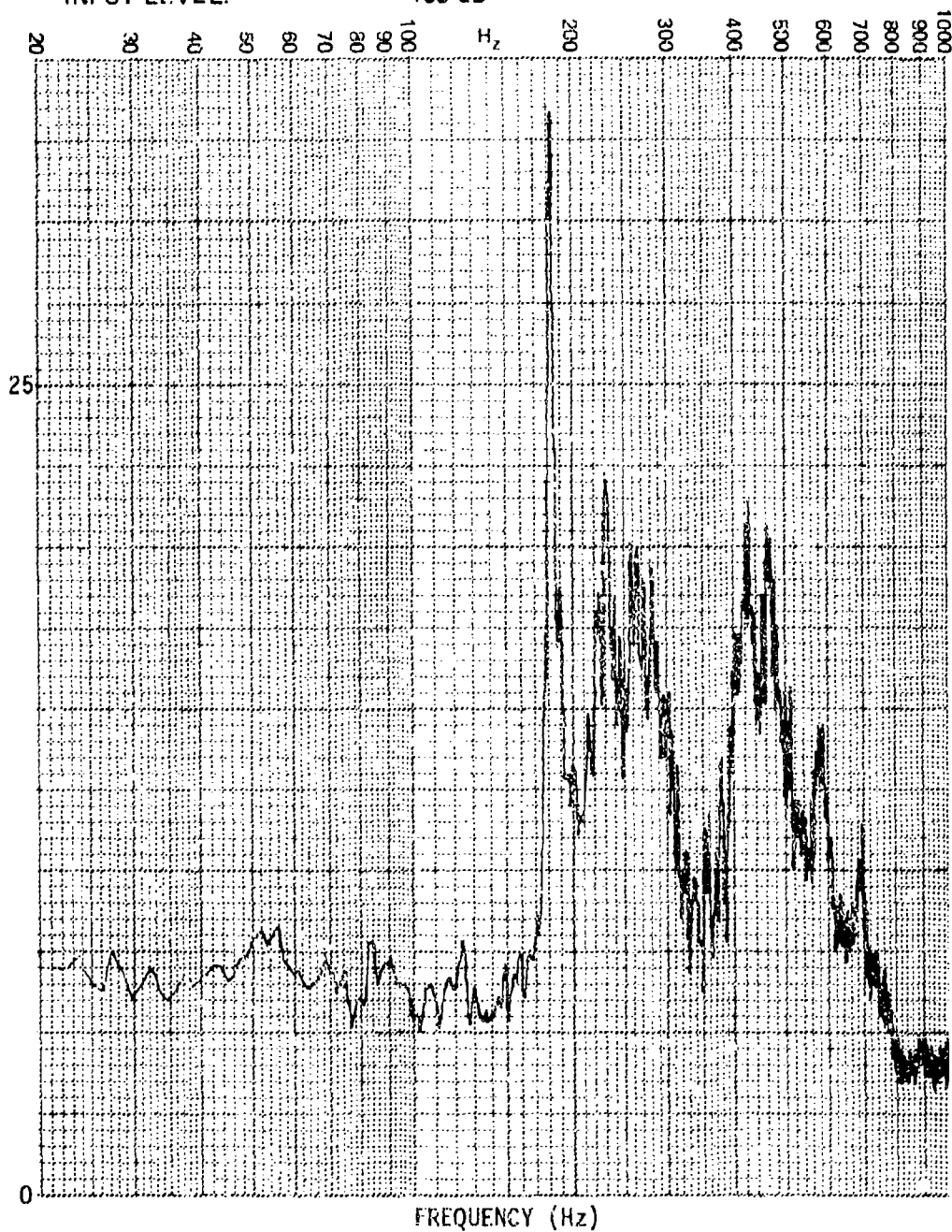
Figure C-100.   Strain Spectrum for Panel s

C-101

PANEL CONFIGURATION: s
TRANSDUCER: G10
OVERALL R.M.S. LEVEL: 444.4µe
INPUT SPECTRUM: RANDOM
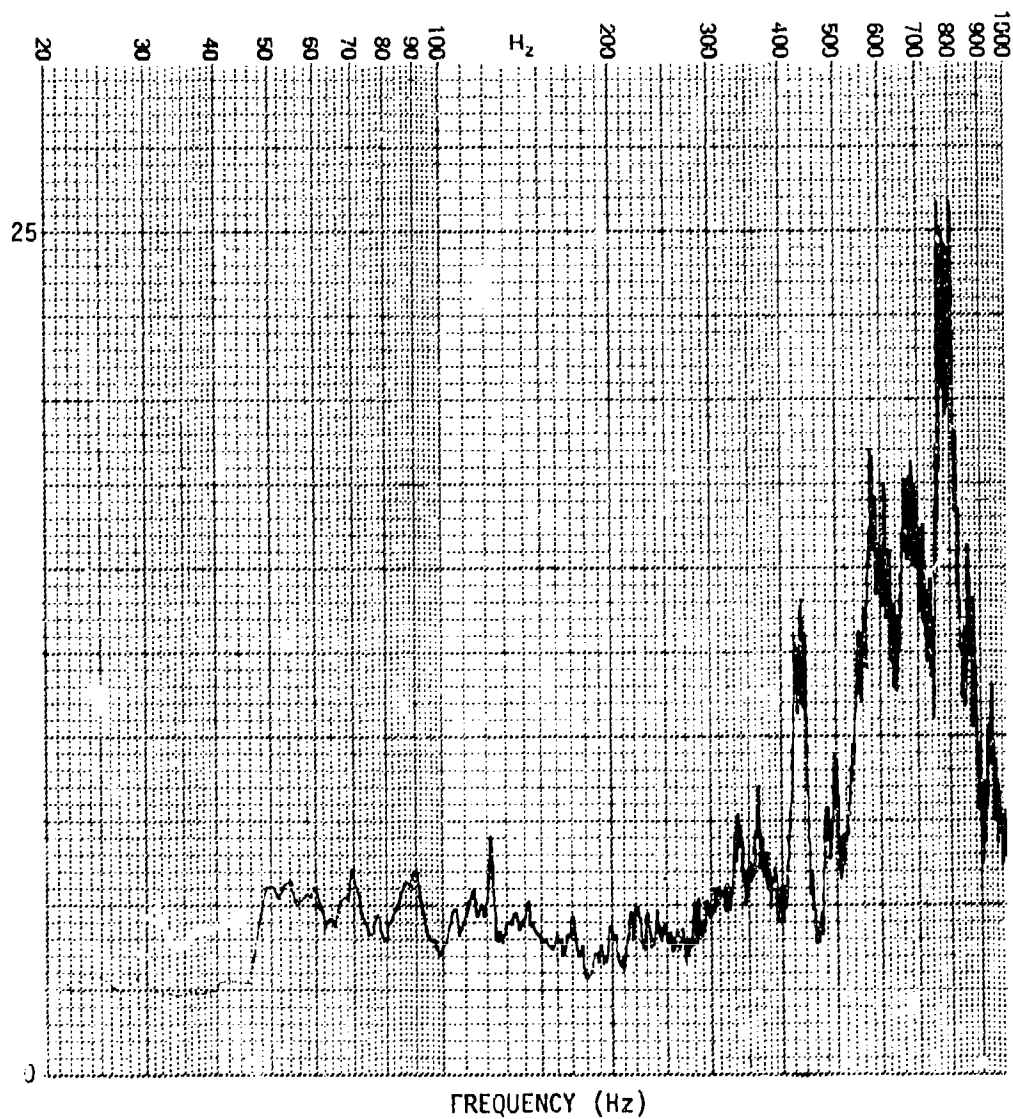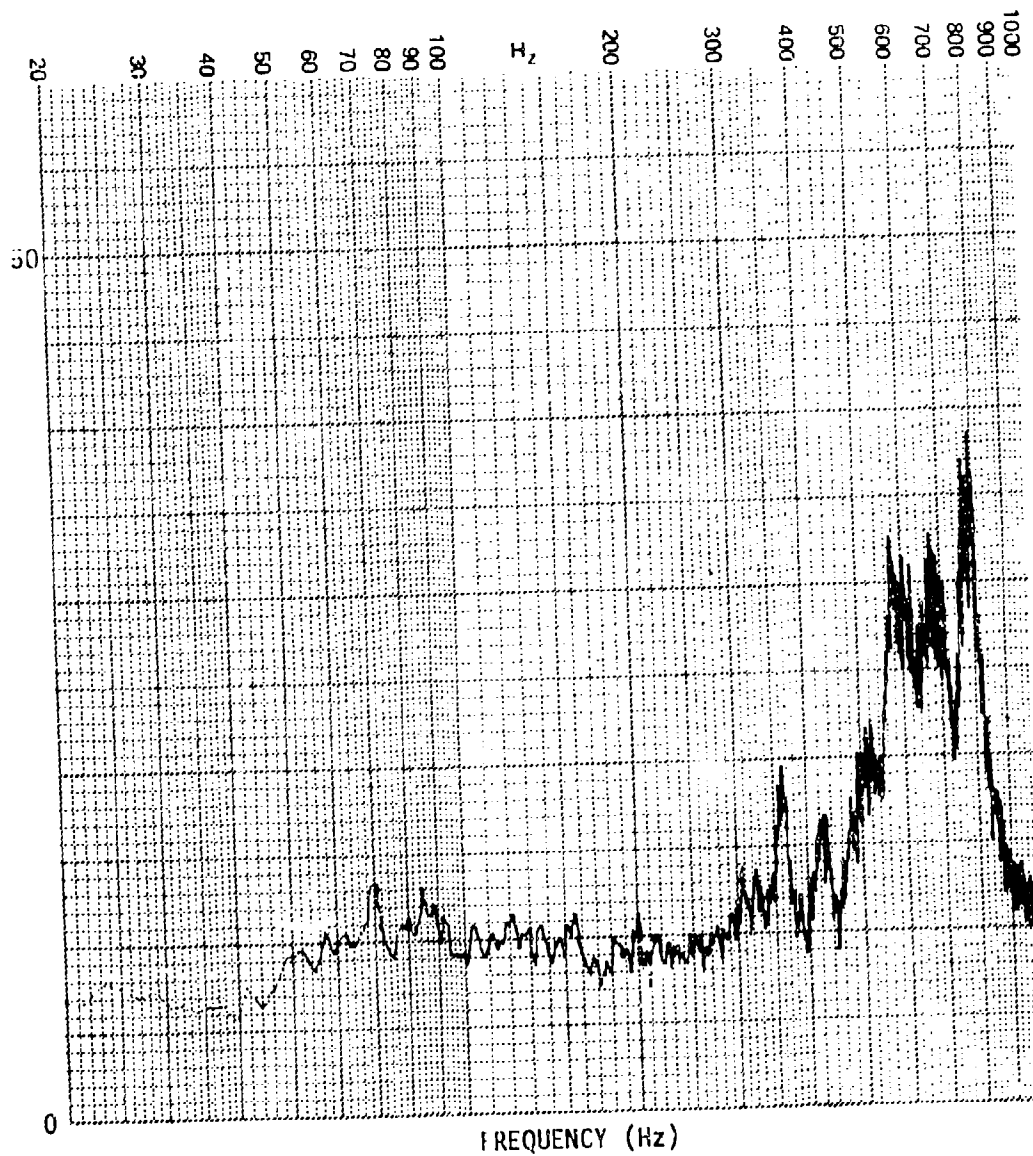INPUT LEVEL: 160 dB

FREQUENCY (Hz)
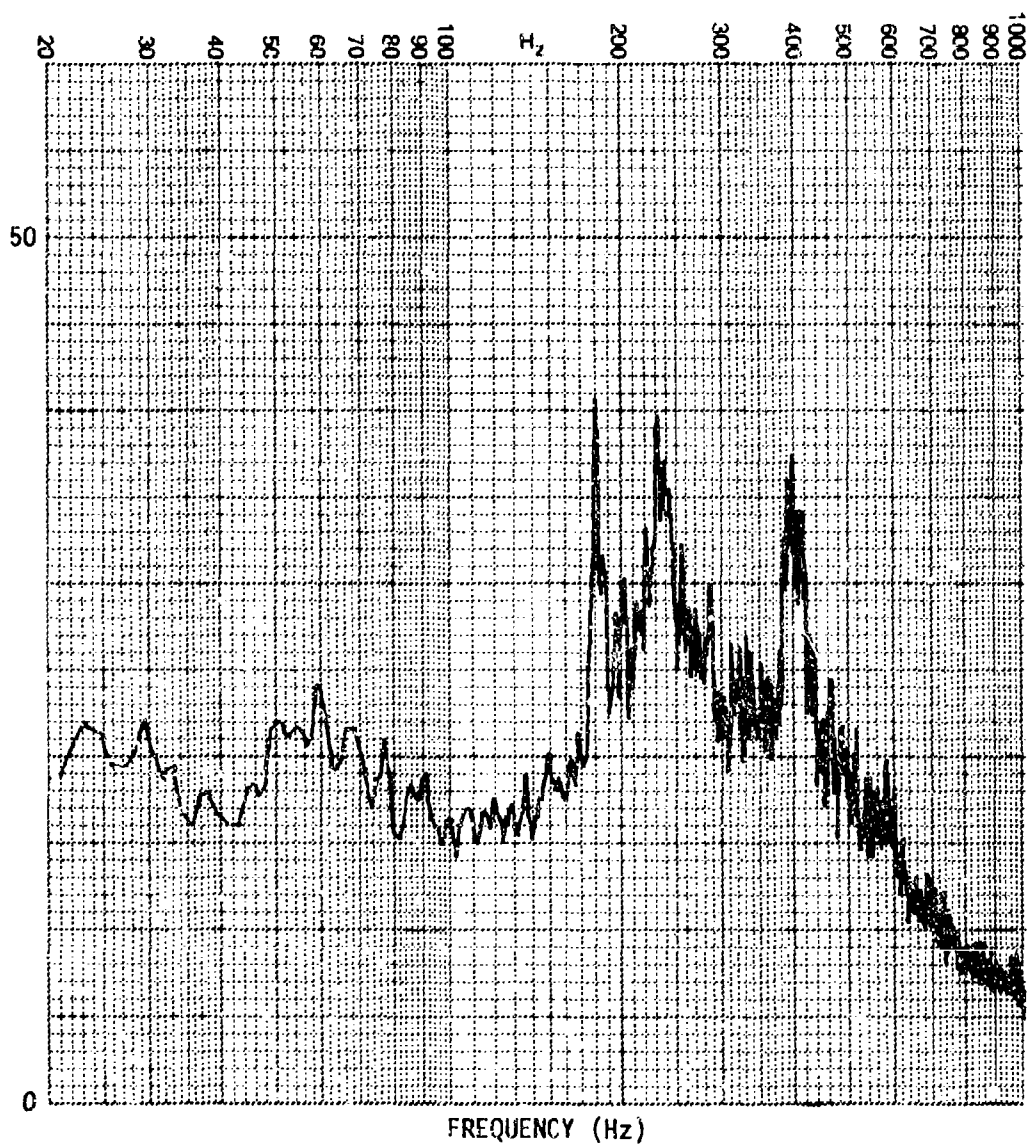
Figure C-101.   Strain Spectrum for Panel

C-102

SUPPLEMENTARY

INFORMATION

ERRATA - March 1989

The following corrections are applicable to AFWAL-TR-80-3019, Sonic Fatigue Design Techniques for Advanced Composite Aircraft Structures.

Delete pages 177 through 186 (paragraphs 5 and 6) and substitute the attached pages 177 through 188.

FLIGHT DYNAMICS LABORATORY
AIR FORCE WRIGHT AERONAUTICAL LABORATORIES
AIR FORCE SYSTEMS COMMAND
WRIGHT-PATTERSON AIR FORCE BASE, OHIO 45433-6553

89 6 01 035

5. DESIGN METHOD

This section contains a semiempirical design method for estimating rms strains and natural frequencies for curves and flat cfrp stiffened-skin panels, subjected to random acoustic loading. The method comprises an equation relating rms strain to panel configuration parameters and overall sound pressure levels, a procedure for estimating the natural frequencies of the fundamental fully-fixed panel mode, and a random fatigue curve for estimating sonic fatigue life.

The method can be directly applied to Z and J section stiffeners and is valid for quasi-isotropic and most orthotropic skin laminates typically used for airplane skin panels. Because the response equation uses overall sound pressure level as the applied load, a technique for utilizing fan noise spectra from high bypass ratio jet engines is also included. A worked example is presented at the end of the section.

Range of Application

The use of regression analysis techniques in developing the strain response equation limits its application to within the following range of panel configuration parameters:

Stiffener spacing: 4 to 8 inches (102 to 204 mm)

Skin laminate thickness: 0.033 to 0.066 inch (0.8 to 1.8 mm)

Stringer laminate thickness: 0.04 to 0.08 inch (1.0 to 1.0 mm)
(1.2 times the skin thickness)

Radius of curvature: flat down to 30 inches (760 mm)

Aspect ratio: 1 to 3 (assumed valid for all values above unity)

177

Within this parameter envelope, the estimated strains showed an average deviation of 9 percent from measured values. A progressive deterioratio of this accuracy can be expected for panel configurations outside the given range. The 90 percent confidence interval for estimated rms strains approximates a ±22 percent variation in accuracy.

CFRP Skin Laminates -- Quasi-isotropic and orthotropic laminates were used in the development of the strain response equation and the fatigue curve. Moderate variations in skin ply orientation and stacking order dc not have a significant effect on the accuracy of this design method.

The following table gives the ply orientation and elastic modulus values for the skin laminates used in this programme:

Table 40. Skin Laminate Ply Orientations
and Elastic Modulus Values
Laminate density $c = 0.055$ lb/in^3
(1,522 Kg/m^3)

PLY ORIENTATION 0° - Transverse to Stringers 90° - Parallel to Stringers	Elastic Modulus			
	(E_y) Transverse to stringers: b - direction		(E_x) Parallel to stringers: a - direction	
	10^6lb/in^2	MN/m^2	10^6lb/in^2	MN/m^2
$(0, \pm 45)_s$	7.5	51,711	3.3	22,753
$(0, \pm 45, 90)_s$	6.7	46,195	6.7	46,195
$(0_2, \pm 45)_s$	9.7	66,879	3.2	22,063
$(0, \pm 45)_{2s}$	7.5	51,711	3.3	22,753
$(0, 90)_s$	9.4	64,811	9.4	64,811

Stiffener Design and Method of Attachment -- The response equation is based on data from skins reinforced with z section stiffeners, adhesively bonded to the skins. However, the equation can be applied to J-stiffened panels by multiplying calculated strains by 0.75. This factor could also be applied to hat section stiffeners.

178

RMS strain levels are not significantly affected by the method of skin-stiffener attachment. Consequently, secondary bonding, co-curing, integral skin-stiffener layup and riveted attachments can be analyzed. The fatigue curve, however, which is based on secondarily bonded stiffeners, may not be valid for the other methods of attachment.

Stiffener cross-section properties should provide for effective panel edge restraint. The upstanding webs of stringers should be attached to intersecting frames in order to provide continuity of stiffness and to prevent the stringers from rotating.

Structural Damping -- The effects of damping have been absorbed into the empirical factors in the strain response equation. The equation is valid for damping ratios in the 0.017 to 0.03 range. The average measured value was 0.025. This range of values may be considered typical for this class of structure. If special damping factors need to be considered, such as the use of damping treatments, highly damped resin systems, discontinuous carbon fibres, etc., then the estimated rms strain should be appropriately factored down. In the absence of alternative relevant data, multiply rms strain by the square root of the ratio (0.025/Actual Damping Ratio).

Nonlinear Response Effects -- Nonlinear response effects have been taken into account to a limited extent, by deriving a lower rate of change in rms strains, with respect to overall sound pressure levels, than is associated with linear response behaviour. These effects have been averaged over the data base and do not take into account individual variations in the degree of nonlinear response characteristics. The degree of nonlinear response approximates to a 7-dB increase in sound pressure level resulting in a doubling of rms strain. Linear behaviour results in a doubling of rms strain for a 6-dB increase in sound pressure level.

Units of Measurement -- The equation for estimating rms strain uses panel width, panel length and skin laminate thickness in non-dimensional form. Consequently, any coherent system of units may be used to estimate rms strains for flat panels. The radius of curvature (R) is expressed in inches, with an alternate expression provided for R in millimetres.

Notation

The following notation is used in this section:

ε_{rms} - RMS strain x 10^6, located at the centre of, and normal to, the longer side of the skin panel

a - length of longer side of panel (frame or longeron spacing)

b - length (arc length) of shorter side of panel (stringer spacing)

t - skin laminate thickness

R - Radius of curvature in the b-direction (inches or mm)

SPL - Overall sound pressure level (dB)

E_y - Youngs modulus for the skin laminate material in the direction of the shorter side of the panel (lb/in^2 or N/m^2). For laminates used in this programme, obtain values from Table 40.

ρ - density of skin laminate material: (lb/in^3) ÷ 386.4 or kg/m^3.

f - fundamental natural frequency of skin panel assuming all edges to be fixed. (Hz)

v   -   velocity parameter for the skin laminate material. Equals $(E_y/\rho)^{1/2} \div 200,000$ when E_y and ρ are expressed in lb and in, and $(E_y/\rho)^{1/2} \div 5,080$ when E_y and ρ are expressed in Kg and m.

Calculation of rms Strain

Equation 25 is used to estimate rms strain:

$$\varepsilon_{rms} = \left(\frac{b}{t}\right)^{4/3} [4 \ \text{Tanh} \ (a/b) - 1] \ 10^{\left(\frac{SPL - 178}{24}\right)} \quad \text{Tanh}\left(\frac{R - 17}{40}\right) \quad (25)$$

where R is in inches.

When R is in metres, the equation is written:

$$\varepsilon_{rms} = \left(\frac{b}{t}\right)^{4/3} [4 \ \text{Tanh} \ (a/b) - 1] \ 10^{\left(\frac{SPL - 178}{24}\right)} \quad \text{Tanh} \left(\frac{R}{10^3} - 0.43\right) \quad (25a)$$

For large radii of curvature, (i.e., R greater than 150 inches or greater than 4,000 mm) the hyperbolic tangent of the radius function is unity, and the equation reduces to the flat panel response equation.

No particular physical significance is attached to the number (178) that is subtracted from the sound pressure level in the exponent of 10, and the equation is valid for both positive and negative exponents.

NOTE 1:   The equations were derived for Z stiffeners. For J stiffeners multiply ε_{rms} by 0.75.

NOTE 2:   The equations are valid for typical damping ratios over the range 0.017 to 0.03. For significantly different damping ratio values multiply ε_{rms} by the square root of the ratio (0.025/actual damping ratio).

NOTE 3:   If a 90% level of confidence is required, then increase the estimated rms strain by 22%.

Calculation of Natural Frequency

$$f = VK \frac{t}{b^2} \qquad (26)$$

where V is defined under Notation and K is obtained from
Figure 64 for given a/b, b, t and R (expressed in the form
b^2 / Rt). Figure 64 is expressed in both British and S.I. units.

Estimation of Sonic Fatigue Life

The estimated sonic fatigue life is obtained by reading the number
of cycles to failure (N) from Figure 65, corresponding to the estimated
rms strain (ε_{rms}). The number of cycles to failure is converted to life
in hours by the relationship ($\frac{N}{3,600f}$), where f is the natural frequency
calculated using Equation 26.

Worked Example

A six-ply skin laminate having a ply orientation of $(0, \pm45)_s$ and
a thickness of 0.033 inch, has an 8-inch stringer spacing, with a panel
length of 12 inches and a radius of curvature of 90 inches. The overall
sound pressure level is 160 dB.

(i) For a = 12 in, b = 8 in, t = 0.033 in, R = 90 in and SPL = 160,
equation 25 gives

$$\varepsilon_{rms} = \left(\frac{8}{0.033}\right)^{4/3} [4\, \text{Tanh}\, \frac{12}{8} -1]\ 10^{\left(\frac{160-178}{24}\right)} \text{Tanh}\left(\frac{90-17}{40}\right)$$

$$= (1,512)(2.62)(0.178)(0.949)$$

$$= \underline{669\ \text{micro-strain}}$$
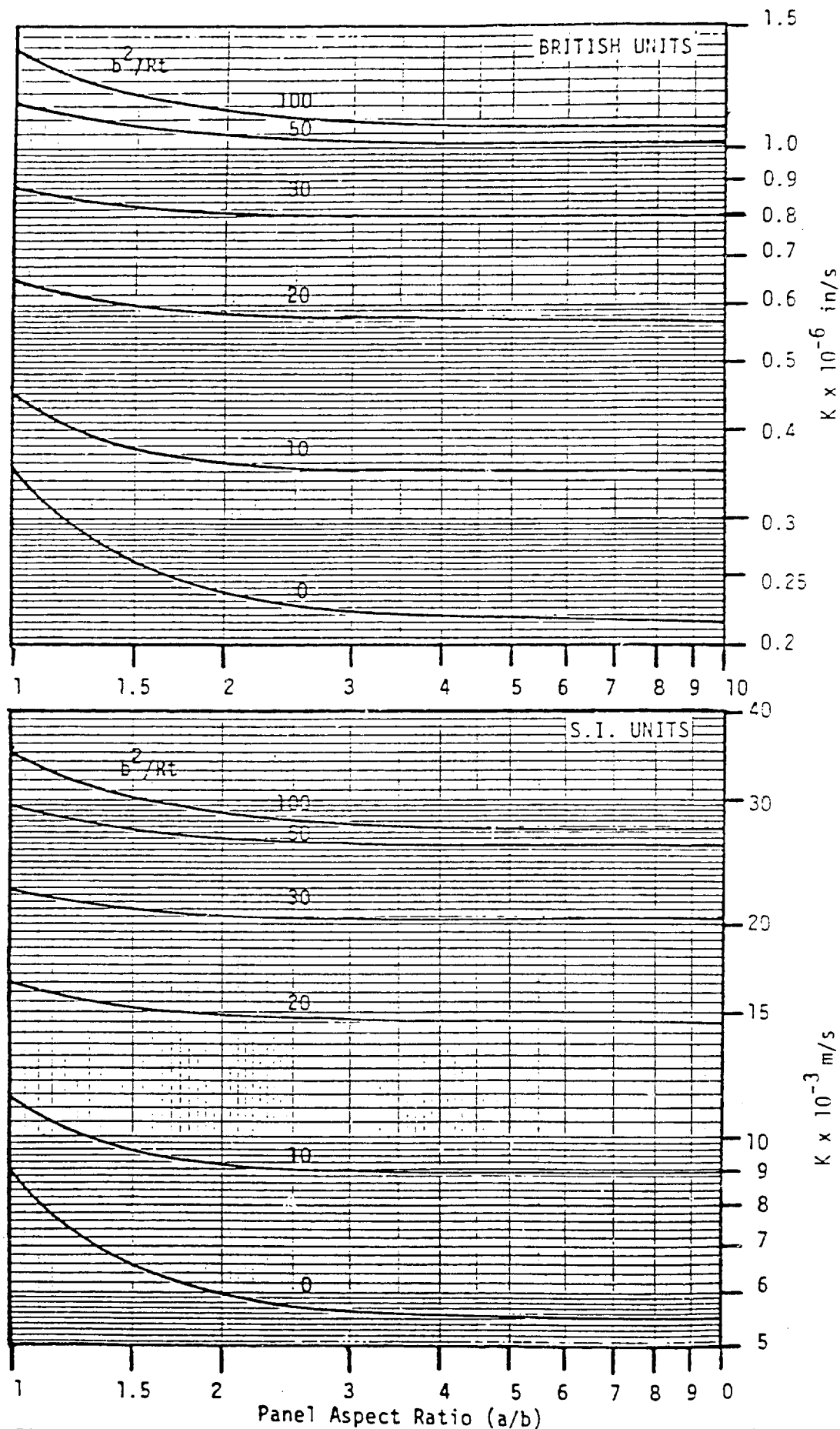
Figure 64. Natural Frequency Nomograph for Panel With Fixed Edges

183
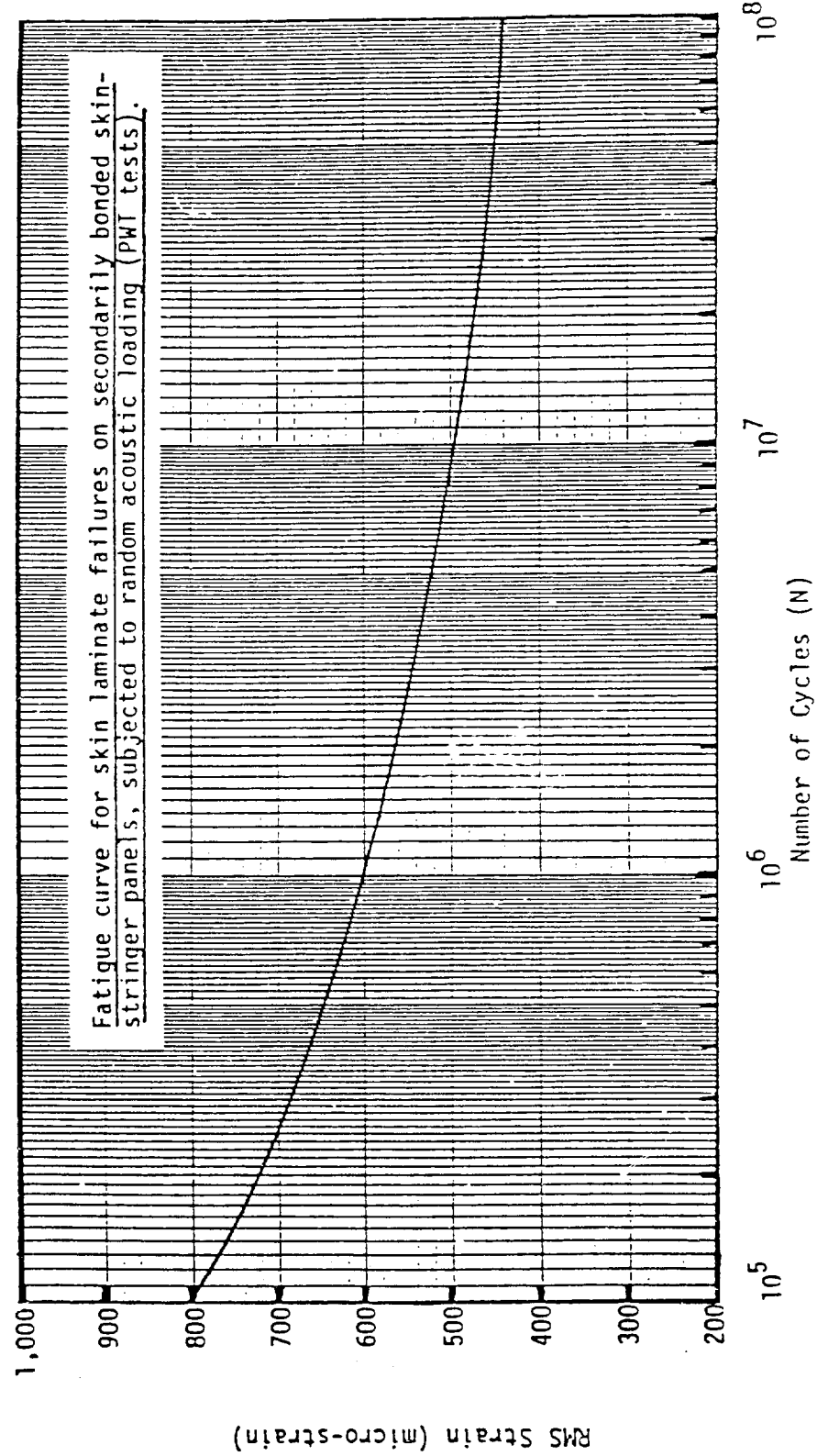
Figure 65. Random Fatigue Curve for CFRP Stiffened-Skin Panels-RMS Strain vs Cycles to Failure

(ii) Natural frequency is estimated from equation 26:

$$f = VK \frac{t}{b^2}$$

$$\text{where } V = \frac{\left(E_y/\rho\right)^{1/2}}{200,000}$$

From Table 40: $E_y = 7.5 \times 10^6$ lb/in

$$\rho = \frac{0.055}{386.4}$$

$$\therefore V = 1.148$$

From Figure 64:

$$\text{For } \frac{b^2}{Rt} = \frac{8^2}{90 \ (0.033)} = 21.5$$

$$\text{and } a/b = 12/8 = 1.5, \text{ then}$$

$$K \times 10^{-6} = 0.6$$
$$\therefore k = 0.6 \times 10^6$$
$$\therefore f = (1.148)(0.6 \times 10^6) \frac{(0.033)}{8^2}$$
$$= \underline{355 \text{ Hz}}$$

(iii) From Figure 65:

Number of cycles to failure for $\varepsilon_{rms} = 669$ is

$N = 3.5 \times 10^6$ cycles

For a frequency of 355 Hz, the estimated sonic fatigue life is

$$\frac{3.5 \times 10^6}{(3,600)(355)}$$
$$= \underline{2.74 \text{ hours}}$$

185

Fan Noise from High Bypass Ratio Jet Engines

The design method presented here utilizes the overall sound
pressure level as the design load. While this is adequate for the broa
band spectra that typify jet exhaust noise, it does not automatically
lend itself to designing for the inlet and fan exit acoustic spectra th
occur due to fan noise on high bypass ratio engines. These spectra oft
have overall sound pressure levels that are dominated by high acoustic
spectrum levels occurring at the fan blade passage frequency and its
next harmonic (typically in the frequency range of 2 to 2.5 KHz and
4 to 5 KHz respectively). These frequencies are above the usual
frequency range of panel resonant response. This, including their
corresponding acoustic spectrum peaks in the overall sound pressure leve
to be used for design purposes, may result in overly conservative design
To deal with this type of acoustic load, the applied overall sound
pressure level should not include these two acoustic spectrum
peaks.

Since design acoustic loads are usually given from 0 to 10,000 Hz in one-
third octave or one-octave band levels, the applied overall sound
pressure level can be obtained by summing these levels up to 10,000 Hz.
The blade passage tone and its next harmonic can be eliminated (if
predominant) by reducing the one-third or one-octave band levels con-
taining these peaks to those levels contained in adjacent frequency
bands. The one-third octave or one-octave levels can then be summed
in the following way:

If the difference (in dB) between two band levels is:

0	1	2	3	4	5	6	7	8	9	10	>10

Then add to the larger level (dB):

3	2.5	2.1	1.8	1.5	1.2	1.0	0.8	0.6	0.5	0.4	0

Example: If there were four bands with the following levels (dB):

140, 134,   139 and 139,   then

difference = 6 dB   difference = 0 dB
add 140 + 1.0   then add 139 + 3
= 141dB   = 142 dB

difference + 1 dB
add 142 + 2.5
= 144.5 dB

186

This 144.5 dB is the overall sound pressure level to be used as the design load.

6. COMPARISONS WITH DESIGN METHODS FOR ALUMINUM PANELS

CFRP skin-stringer structures, of the type evaluated in this programme, are primarily in competition with similarly configured aluminum structures for application on both military and civil airplanes. Cost/weight tradeoffs between cfrp and aluminum structures, having comparable sonic fatigue resistance, are there-fore of interest to potential users of the design method in Section 5. A typical broadband sonic fatigue design load spectrum was used which had an overall sound pressure level of 157 dB and a correspond-ing acoustic spectrum level of 132 dB/Hz in the frequency range of interest. This 25 dB difference between overall and spectrum levels is compatible with the acoustic load in this programme.

The following example problem was used for comparison:

Required life = 10^7 cycles (using a 50% confidence level)

$$b = 8$$
$$a/b = 2$$
$$\zeta = 0.02$$

Calculate required skin thickness.

The following results were obtained:

Riveted Aluminium Skin-Stringer: t = 0.05-in.
Riveted Aluminium Skin-Stringer: t = 0.076-in.
Bonded cfrp Skin-Stringer: t = 0.037-in.

An 8-ply skin laminate having a thickness of 0.044 inch would fall within the 90-percent confidence interval for equation 25.

Since the material density of cfrp is approximately half that of aluminum, the difference in weight between cfrp panels and aluminum panels having comparable sonic fatigue resistance, approaches 2-1/2 to 1.